On the chirally rotated Schrödinger functional with Wilson fermions

D I S S E R T A T I O N

zur Erlangung des akademischen Grades
doctor rerum naturalium
(Dr. rer. nat.)
im Fach Physik

eingereicht an der
Mathematisch-Naturwissenschaftlichen
Fakultät I
Humboldt-Universität zu Berlin

von
Frau Dipl.-Phys. Jenifer González López
geboren am 14.06.1982 in Cacabelos Spanien

Präsident der Humboldt-Universität zu Berlin:
Prof. Dr. Jan-Hendrik Olbertz

Dekan der Mathematisch-Naturwissenschaftlichen
Fakultät I:
Prof. Dr. Andreas Herrmann

Gutachter:

1. Prof. Dr. Michael Müller-Preussker
2. Dr. habil. Karl Jansen
3. Prof. Dr. Giancarlo Rossi

eingereicht am: 25. März 2011

Tag der mündlichen Prüfung: 25. Mai 2011

To my parents
a mis padres

Abstract

There are many phenomena in nature, such as the appearance of hadrons as bound states of quarks and gluons or spontaneous chiral symmetry breaking, which are closely linked to the low energy regime of QCD. From a theoretical point of view, these low energy phenomena can be dealt with only by means of non-perturbative methods. Often, as in the case of quark masses or the strong coupling constant, a non-perturbative renormalization of QCD is required. It is the central goal of this thesis to provide a framework for such a non-perturbative renormalization. For that purpose, we employ a 4-dimensional lattice as a regulator of QCD. As a renormalization scheme, we propose a finite volume Schrödinger functional scheme and here in particular, the chirally rotated Schrödinger functional (χSF).

We first perform analytical studies of the χSF at tree-level of perturbation theory, in the continuum and on the lattice. We study the eigenvalue spectrum of the continuum Dirac operator, equipped with chirally rotated SF boundary conditions, and derive the corresponding quark propagator. We then determine the tree-level quark propagator on the lattice, employing massless Wilson fermions as a regulator of the theory. Beyond tree-level, all studies are performed in the quenched approximation of QCD, as a first, computationally much simpler step to understand the properties of the newly proposed χSF scheme.

One of the main targets of the present work, has been to perform the non-perturbative tuning of the two required coefficients of the χSF scheme, such that a well defined continuum limit can be reached. We demonstrate, as the first main result of this thesis, that the tuning is feasible and that, moreover, physical quantities are insensitive to the particular tuning condition. As in any lattice regularization with SF-like boundary conditions, there are also in the χSF a couple of counterterms at the boundaries, whose coefficients need to be tuned in order to remove the $O(a)$ discretization effects originated at the boundaries. However, besides these boundary $O(a)$ effects, the χSF is expected to be compatible with bulk automatic $O(a)$-improvement. We show here that, indeed, the scaling behavior of physical quantities is consistent with leading $O(a^2)$ discretization effects. This result, furthermore, indicates that the boundary effects do not spoil the $O(a^2)$ scaling behavior of physical observables.

The other most important achievement of this thesis, has been to demonstrate that the χSF scheme, with the here computed tuning coefficients, leads to the correct continuum limit. For this purpose, we have performed universality tests of the continuum limit, at three different values of the renormalization scale and through the computation of several physical quantities of interest. These are the renormalization group invariant mass of the strange quark and the step scaling functions of the pseudo-scalar density and the non-singlet twist-2 operators, O_{12} and O_{44}. The final results in the continuum limit are compared to those obtained using the SF scheme in its standard form, with two different regularizations, standard and clover Wilson fermions. We clearly find an agreement, in the continuum limit, between the results from the χSF and the two regularizations of the standard SF. This agreement is another evidence of the universality of the continuum limit.

The conclusion of these results is that the χSF is a promising scheme to perform non-perturbative renormalizations while maintaining bulk automatic $O(a)$-improvement. This opens the most relevant prospect that the χSF can be safely used in future non-perturbative computations of renormalization factors also beyond the quenched approximation.

Keywords:
Lattice QCD, renormalization, improvement, chiral symmetry

Zusammenfassung

Viele Phänomene in der Natur, wie etwa das Auftreten der Hadronen als gebundene Zustände von Quarks und Gluonen oder die Brechung der chiralen Symmetrie, sind eng verknüpft mit dem Niederenergieverhalten der QCD. Diese Niederenergie-Phänomene können allerdings von der theoretischen Seite her nur mit rein nicht-perturbativen Methoden behandelt werden. Es ist dabei oft der Fall, dass wichtige Größen der QCD, wie die Quarkmassen oder die starke Kopplungskonstante, eine nicht-perturbative Renormierung benötigen. Es ist das zentrale Thema dieser Dissertation, einen Rahmen für solch eine nicht-perturbative Renormierung bereitzustellen. Zu diesem Zweck werden wir ein 4-dimensionales Gitter als eine Regularisierung der QCD verwenden. Als Renormierungsschema schlagen wir vor, das in einem endlichen Volumen definierte Schrödingerfunktional, und hier insbesondere das chiral gedrehte Schrödingerfunktional (chirally rotated, χSF), als Renormierungsschema einzusetzen.

Auf dem Baumgraphenniveau werden wir als ersten Schritt eine analytische Rechnung im Kontinuum und auf dem Gitter durchführen. Dabei werden wir das Eigenwertspektrum des Dirac-Operators mit chiral gedrehten Randbedingungen im Kontinuum betrachten und den entsprechenden Propagator ableiten. Wir werden dann diesen Propagator auf einem Gitter bestimmen, wobei wir masselose Wilson-Fermionen benutzen. Sämtliche Untersuchungen über das Baumgraphenniveau hinaus werden als ersten Schritt in der wesentlich Computerzeit günstigeren Valenzquark-Approximation der QCD durchgeführt, um die Eigenschaften des erst kürzlich vorgeschlagenen χSF, besser zu verstehen.

Eines der Hauptziele ist es dabei, die im χSF benötigten Koeffizienten nicht-perturbativ so einzustellen, dass ein wohl-definierter Kontinuumlimes durchgeführt werden kann. Als ein erstes Hauptresultat dieser Dissertation zeigen wir, dass solch eine Feineinstellung der Parameter des χSF durchführbar ist und dass physikalische Größen nicht sensitiv auf die spezielle Wahl der Bedingung zur Einstellung der Parameter sind. Wie in jeder Gitter-Regularisierung mit SF-artigen Randbedingungen gibt es auch im χSF zwei Gegenterme am Rand, dessen Koeffizienten nicht-perturbativ eingestellt werden müssen, um die $O(a)$-Diskretisierungseffekte, die von den Rändern herrühren, zu kürzen. Allerdings kann erwartet werden, dass neben diesen $O(a)$ Effekten am Rand, das χSF vollständig verträglich mit der $O(a)$-Verbesserung ist. Wir zeigen hier, dass in der Tat das Skalierungsverhalten physikalischer Größen konsistent mit führenden $O(a^2)$ Diskretisierungseffekten ist. Dieses Resultat deutet darüberhinaus darauf hin, dass die Randeffekte das $O(a^2)$ Skalierungsverhalten physikalischer Observablen nicht verletzt.

Das andere, sehr wichtige Ergebnis dieser Arbeit ist der Nachweis, dass das χSF Schema mit den hier berechneten Verbesserungskoeffizienten, zu einem korrekten Kontinuumlimes führt. Zu diesem Zweck haben wir Universalitätstests des Kontinuumlimes durchgführt, wobei wir drei unterschiedliche Werte der Renormierungsskala verwendet und mehrere uns interessierende physikalische Größen berechnet haben. Dies sind die renormierungsgruppeninvariante Masse des Strange-Quarks, sowie die Stufenskalierungsfunktionen (SSF) der pseudoskalaren Dichte und der nicht-singlett, Twist-2 Operatoren O_{12} und O_{44}. Die endgültigen Resultate für diese Observablen werden dann im Kontinuumlimes mit denjenigen verglichen, wie sie mit dem Standard Schrödingerfunktional-Schema erzielt wurden, wobei zwei Regularisierungen, reine Wilson und clover verbesserte Wilson Fermionen verwendet wurden. Die Übereinstimmung der Ergebnisse ist eine weitere Evidenz der Universalität des Kontinuumlimes.

Wir können deshalb den Schluss ziehen, dass das χSF ein viel versprechendes Renormierungsschema darstellt, um eine nicht-perturbative Renormierung vorzunehmen und dabei gleichzeitig die automatische $O(a)$-Verbesserung aufrecht erhalten. Dies eröffnet den sehr wichtigen Ausblick, dass das χSF in zukünftigen nicht-perturbativen Berechnungen von Renormierungskonstanten auch über die Valenzquark-Approximation hinaus eingesetzt werden kann.

Schlagwörter:
Gitter QCD, Renormierung, Verbesserung, Chirale Symmetrie

Contents

1 Introduction **1**

2 QCD on the lattice **5**
2.1 The QCD action . . . 5
2.2 Gauge fields on the lattice . . . 6
2.3 QCD path integral on the lattice . . . 8
2.4 Chiral symmetry . . . 12
2.4.1 Chiral symmetry in the continuum . . . 12
2.4.2 Chiral symmetry and lattice QCD . . . 14
2.5 Continuum limit . . . 15
2.6 Cutoff effects and the Symanzik improvement programme . . . 16
2.7 Fermions on the lattice . . . 19
2.7.1 Naive discretization . . . 20
2.7.2 Wilson fermions . . . 21
2.7.3 Twisted mass Wilson fermions . . . 24

3 Non-perturbative renormalization of QCD **31**
3.1 Ward-Takahashi identities . . . 34
3.2 The Schrödinger functional of QCD . . . 40
3.2.1 The SF on the lattice. Definition . . . 41
3.2.2 The lattice SF and improvement . . . 43
3.3 Non-perturbative renormalization from the SF . . . 44
3.3.1 Renormalized gauge coupling from the SF . . . 45
3.3.2 Hadronic renormalization and matching at low energies . . . 45
3.3.3 Non-perturbative renormalization group. Step scaling function . . . 46
3.3.4 Conversion to the perturbative scheme . . . 47
3.4 Renormalization conditions from the SF. Correlation functions . . . 48
3.5 SF boundary conditions and automatic $O(a)$-improvement . . . 50

4 Chiral rotation of the SF in the continuum **53**
4.1 Definition of the boundary conditions . . . 53
4.1.1 Standard SF boundary conditions . . . 53
4.1.2 χSF boundary conditions . . . 54
4.1.3 γ_5SF boundary conditions . . . 55
4.2 Spectral properties of the Dirac operator . . . 55
4.2.1 Spectral properties: standard SF . . . 55
4.2.2 Spectral properties: χSF . . . 57
4.2.3 Spectral properties: γ_5SF . . . 61
4.3 The quark propagator . . . 64
4.3.1 The quark propagator without boundaries . . . 65
4.3.2 General solution of the homogeneous equation . . . 66
4.3.3 The quark propagator: standard SF . . . 67

4.3.4 The quark propagator: χSF . . . 67
4.3.5 The quark propagator: γ_5SF . . . 69
4.3.6 Chirally rotating the quark propagator with SF boundary conditions . . . 71
4.4 Concluding remarks . . . 72

5 The χSF on the lattice **75**
5.1 The χSF on the lattice in the free theory . . . 75
5.1.1 The free lattice quark propagator with χSF boundary conditions . . . 77
5.2 Renormalizability of the χSF and improvement . . . 80
5.2.1 Counterterm structure in the continuum . . . 82
5.2.2 Counterterm structure on the lattice and tuning parameters . . . 84

6 Non-perturbative tuning of κ and z_f **89**
6.1 Tuning conditions . . . 90
6.2 Tuning strategy . . . 94
6.3 Tuning results . . . 95
6.4 Conclusions on the tuning . . . 102

7 Scaling studies of the χSF **103**
7.1 Scaling analysis in the free theory . . . 103
7.1.1 Continuum limit approach at $z_f = 1$ . . . 105
7.1.2 Continuum limit approach at z_f different from 1 . . . 108
7.2 Scaling analysis in the interacting theory . . . 109
7.2.1 Non-vanishing $\gamma_5\tau^1$-even correlation functions . . . 113
7.2.2 Vanishing $\gamma_5\tau^1$-even correlation functions . . . 114
7.2.3 Vanishing $\gamma_5\tau^1$-odd correlation functions . . . 117
7.3 Conclusions on the scaling analysis . . . 121

8 Computation of Z_{P} and σ_{P} **127**
8.1 Step scaling function of the quark mass . . . 127
8.2 Renormalization prescription of the quark mass . . . 129
8.3 Computation of Z_{P} and Σ_{P} . . . 130
8.4 Computation of σ_{P} . . . 130

9 Computation of the RGI strange quark mass **137**
9.1 The RGI quark mass . . . 137
9.2 Determination of Z_{P} at the matching scale . . . 138
9.3 Determination of the bare reference quark mass . . . 141
9.3.1 Dependence of the pseudo-scalar mass on the quark mass . . . 142
9.3.2 Determination of r_0/a at several beta values . . . 147
9.3.3 Determination of the Kaon mass in lattice units . . . 147
9.3.4 Determination of the reference quark mass in units of r_0 . . . 148
9.4 Determination of the RGI reference mass . . . 149
9.5 Determination of the RGI strange quark mass . . . 151

10 Z-factors and SSFs of twist-2 operators **153**
10.1 Motivation of the twist-2 operators . . . 153
10.2 Twist-2 non-singlet quark operators . . . 155
10.3 SSF and renormalization prescription . . . 158
10.4 Renormalization factors and lattice SSFs . . . 160
10.5 Continuum limit of the SSF . . . 161

10.6 Z-factors at the matching scale and RGI Z-factors . . . 163
10.7 Conclusions on the universality tests . . . 172

11 Topology of the ensembles 173
11.1 Simulation strategy . . . 173
11.2 Discussion of the data . . . 174
11.3 Topology in small volumes . . . 182
11.4 Topology at the matching scale . . . 186

12 Summary and conclusions 187

A Conventions 193
A.1 Index conventions and general notation . . . 193
A.2 Relation Minkowski-Euclidean space . . . 193
A.3 Dirac matrices . . . 194
A.4 Group theory . . . 195
A.5 Lattice derivatives . . . 196
A.5.1 Ordinary lattice derivatives . . . 196
A.5.2 Covariant lattice derivatives . . . 196

B Symmetries 199
B.1 Discrete symmetries . . . 199
B.1.1 Hermiticity and γ_5-hermiticity . . . 199
B.1.2 Charge conjugation, parity and time reversal in the standard basis . . . 199
B.1.3 Charge conjugation, parity and time reversal in the twisted basis . . . 200
B.2 Continuous chiral symmetry with $N_f = 2$ . . . 201
B.2.1 Symmetries in the standard basis . . . 201
B.2.2 Symmetries in the twisted basis . . . 201
B.3 Symmetries of the QCD action . . . 202
B.4 Hermiticity of Wilson-type fermions . . . 203
B.4.1 Standard Wilson fermions . . . 203
B.4.2 Twisted mass Wilson fermions . . . 204

C Useful notions in lattice QCD 207
C.1 Doublers . . . 207
C.2 Exceptional configurations . . . 208
C.2.1 Wilson fermions . . . 208
C.2.2 Twisted mass Wilson fermions . . . 209
C.3 Setting the scale with the static $q\overline{q}$ potential . . . 209
C.4 Symanzik improvement for Wilson-like fermions . . . 210
C.4.1 Improvement of standard Wilson fermions . . . 210
C.4.2 Improvement of twisted mass Wilson fermions . . . 211
C.5 Proof of automatic $O(a)$-improvement . . . 212

D Notes on the tuning 215

E Notes on the scaling analysis. Free theory 227

F Notes on the scaling analysis. Interacting theory 233

G Notes on Z_{P} 247

H Notes on 2-point functions **251**
H.1 Definition of the 2-point functions in SF-like schemes . . . 251
H.1.1 Standard SF formulation . . . 251
H.1.2 χSF formulation . . . 252
H.2 Determination of basic 2-point functions in the χSF . . . 253
H.2.1 Determination of boundary to bulk 2-point functions . . . 253
H.2.2 Determination of boundary to boundary 2-point functions . . . 257
H.3 Correlators of twist-2 operators from the standard SF . . . 260
H.3.1 Particular cases . . . 263
H.4 Rotation of the twist-2 correlators to the twisted basis . . . 266
H.4.1 Rotation of $O^a_{\mu\nu}(x)$ to the twisted basis . . . 266
H.4.2 Rotation of $\mathcal{O}^a$ to the twisted basis . . . 266
H.4.3 Rotation of the 2-point functions to the twisted basis . . . 267
H.5 Correlators of twist-2 operators from the χSF . . . 268

List of Figures **273**

List of Tables **279**

Bibliography **285**

1. Introduction

There are four fundamental interactions in nature; gravitational, electromagnetic, weak and strong. Except gravitation, all other fundamental forces are described by quantum gauge field theories. The theory of the strong force is, at present, Quantum Chromodynamics, QCD [1]. It is a four-dimensional, non-Abelian gauge theory (Yang-Mills [2]), whose gauge group is SU(3). QCD postulates the existence of an additional quantum number in nature, with three degrees of freedom. It is known as the *color* charge and is carried by all strong-interacting fields. The fundamental degrees of freedom of QCD are the matter fields of the theory. These are of fermion nature and, due to Gell-Mann [3] and Zweig [4], are referred to as quark fields or, simply, quarks. Quarks appear in six flavors in nature (up, down, strange, charm, bottom and top). The quanta mediating the interactions between the matter fields, the gauge boson fields, are referred to as gluons. They belong to the Lie algebra of SU(3), while the quark fields are elements of the fundamental representation of the group. Due to the non-Abelian nature of QCD, not only the matter fields but also the gauge bosons carry color quantum numbers. This implies that, besides mediating the interactions between the quark fields, the gauge fields also interact amongst themselves. The way the fields of the theory interact with each other is described by the coupling 'constant' of the theory. In the case of QCD, it is the so called strong coupling constant, α_s. In fact, this coupling is far from being constant, but, instead, it varies with the energy of the process μ. As such, it is usually referred to as the *running* strong coupling constant, and it is more correct to write it as $\alpha_s(\mu)$. In particular, the behavior of $\alpha_s(\mu)$ with respect to the energy makes QCD a very interesting theory although, at the same time, a quite complicated one. The reason is that the coupling constant becomes very large at low energies, large distances, while it decreases towards high energies, short distances. As it is constructed, QCD is expected to provide a description of the strong interaction phenomena in the whole energy range, from small distances much below 1 fm, to large distances of about 1 fm and even larger. In particular, it accommodates at the same time the observed properties of *asymptotic freedom* and *confinement*, directly related to the behavior of $\alpha_s(\mu)$ with μ.

Asymptotic freedom refers to the indirectly observed fact that the strong interaction becomes weaker and weaker with increasing energies, so that the quarks inside the hadrons behave as if they were free particles. This phenomenon was observed in deep inelastic scattering experiments and it can be theoretically described by QCD because it is a non-Abelian gauge theory [5–7]. In fact, an essential ingredient for having asymptotic freedom is the property of the gauge boson fields to interact with each other. As a counter-example, this does not occur in Abelian gauge theories like QED, where the Abelian gauge boson fields, the photons, do not carry electric charge and, thus, do not interact amongst themselves. In particular, opposite to the strong interactions, the strength of the electro-magnetic interaction increases with decreasing distances.

The confinement property of the strong interactions refers to the experimental observation that quarks can not be found as isolated particles but, instead, they are bound in hadronic matter. Theoretically this means that only color singlets exist in nature; color is confined. This property is a phenomenon appearing at low energies, because the strong force increases with increasing distances. Confinement is responsible for, e.g., the spectrum of particles observed in nature, which indeed are all color singlets. As a particular consequence of color confinement, quark masses are not directly accesible to experiment and they can only be determined using experimental results together with theoretical tools.

At sufficiently short distances, where the coupling of the interaction becomes small, it is possible to approximate QCD by a perturbative series in the coupling constant, truncated at a certain order in the perturbative expansion. In fact, such a tool, referred to as perturbation theory, provides a satisfactory description of the high energy phenomena, as it is demonstrated by the very good agreement between the predictions of perturbation theory and the experimental results. However, at low energies perturbation theory ceases to be a proper tool to perform calculations in QCD. The long-distance structure of QCD can only be described by non-perturbative methods. Otherwise, important low-energy physical phenomena, as the mass spectrum and decay constants of experimentally observed particles, or the spontaneous breaking of chiral symmetry, could not be theoretically explained.

Currently, the only available tool to study QCD non-perturbatively from first principles is based on the path integral (PI) evaluation of Green functions. The Green functions describe the propagation of states and contain the whole information of the physical system. The path integral, or functional integral, formalism is a possible way of quantizing a classical theory. It was first introduced in [8] as a new formulation of non-relativistic quantum mechanics, alternative to the already existing pictures of Heisenberg and Schrödinger but still mathematically equivalent to these last two. Thus, which quantization is performed depends on the particular question addressed and the method to be employed to compute physical quantities. Even if first proposed within the quantum mechanical theory, the path integral formulation was later extended to the study of field theories, where it has proven to be very successful. Besides its use in e.g. perturbation theory, in particular, it allows for a non-perturbative treatment of a quantum theory by direct numerical evaluation through the application of Monte Carlo (MC) methods [9]. Such MC methods can be applied if the theory is set up in a four-dimensional Euclidean spacetime lattice with lattice spacing a and with finite volume L^3T. Applied to QCD it is known as *lattice QCD*, LQCD [10] . As a by product, the introduction of the lattice implies an ultraviolet regularization of the theory, whose cutoff is proportional to the inverse of the lattice spacing, $1/a$. Moreover, due to the finite volume also an infrared cutoff is provided. Therefore, to set the theory on the lattice is, by construction, a *non-perturbative* manner of regularizing a quantum field theory, QCD in this case. In fact, lattice QCD provides at the moment the most powerful and successful non-perturbative study of QCD. Additionally, perturbation theory can also be applied on the lattice and the corresponding Feynman rules can be derived.

The fact that QCD is regularized when it is defined on the lattice, is indeed a necessary step in the study of QCD. On short distance scales, the fields of the theory experience large quantum fluctuations which give rise to ultraviolet (UV) divergences. The UV divergences render the theory ill-defined and, in particular, imply that quantum fluctuations contribute to every process at any value of the energy scale. The important observation is that the UV divergences can indeed be cancelled, which is achieved through the renormalization of the parameters of the Lagrangian. As a result, renormalized QCD is a well-defined quantum field theory. However, the first step in the renormalization procedure is to regularize the theory, which, as indicated above, can be achieved, non-perturbatively, defining QCD on the lattice. In this manner, all desired quantities may be computed, since they take finite values at any non-zero value of the lattice spacing a (at finite value of the cutoff). At finite value of the cutoff, however, all quantities depend on the lattice spacing. Thus, in order to provide final answers which can be compared to experimental results, the lattice has to be eventually removed or equivalently, the continuum limit has to be performed, $a \to 0$. Yet, if the continuum limit is performed in a naive way, all previously cancelled infinities will arise again when the lattice spacing is sent to zero. In order to perform the continuum limit in a proper manner a mandatory step is the renormalization of the regularized theory. Only the renormalized theory has a physical meaning and a well-defined continuum limit. In general terms, the renormalization process consists in

rewriting the parameters of the theory in terms of physical quantities which are held fixed while $a \to 0$. The way the theory is renormalized is not unique and several renormalization schemes may be chosen. However, if the non-perturbative properties of QCD are to be described, it is necessary to have a non-perturbative renormalization scheme which is compatible with the lattice formulation of the theory. It is the central goal of the present work to perform a non-perturbative renormalization of QCD using the lattice as a tool to regularize the theory and choosing a proper non-perturbative renormalization scheme.

The chosen renormalization scheme in this thesis belongs to the family of the so called Schrödinger functional (SF) schemes [11]. Here the theory is defined in a finite volume and renormalization takes place through the Schrödinger functional of QCD. These schemes are important because they allow to bridge non-perturbatively a wide range of energies from hadronic scales up to the pure perturbative regime. Therefore it is possible to trace the scale evolution of any scale-dependent quantity with the physical energy scale. In this manner, it is possible to understand up to which energies perturbation theory is reliable and where the non-perturbative effects start to become important. Moreover, in the perturbative regime perturbation theory may be applied within SF schemes and as a result, contact to other perturbative schemes (e.g. $\overline{\text{MS}}$) becomes possible by connecting (matching) the schemes perturbatively. SF renormalization schemes allow to express fundamental QCD quantities such as the Λ parameter or the RGI quark masses in units of some hadronic scale like hadron masses or decay constants, which can be measured in experiments. SF schemes thus allow to solve the problem of scale differences between the hadronic and perturbative regimes, which is a challenge in present computations in QCD.

Initially, the SF scheme was defined and applied in its so called standard formulation which is denoted in this thesis as SF. It has been proposed first for the pure gauge theory in [12–14] and later extended to full QCD in [15–17]. Recently other two formulations of the SF have been proposed. One is the so called chirally rotated Schrödinger functional scheme (χSF) which was first discussed in [18]. The other scheme is what we refer here to as the γ_5-Schrödinger functional (γ_5SF) which was proposed in [19]. The key idea of these two new formulations of the SF resides in the importance of reducing discretization effects when using a lattice as a regulator of QCD.

Over the years it has become one of the challenges for the lattice community to reduce the discretization effects in order to render the final extrapolations to the continuum limit a reliable task. To be concrete, the central goal is to achieve what is commonly denoted as $O(a)$-improvement. This means to eliminate from all physical quantities computed on the lattice any $O(a)$ effects in favor of only leading $O(a^2)$ discretization effects. The pure gauge sector of QCD is free from $O(a)$ effects and it is thus the fermion sector that presents the main problems. Therefore, the major effort goes in finding a proper discretization of fermions on the lattice. Several lattice fermion formulations are available today, each with its own advantages and disadvantages. Amongst the different formulations we are here concerned with Wilson fermions [20]. In this case, $O(a)$ discretization effects are a priori present in physical quantities. The $O(a)$-improvement of the different physical quantities is then achieved by means of the Symanzik improvement programme [21–23]. The improvement programme consists in adding counterterms to the lattice action and interpolating fields, with certain coefficients which are to be non-perturbatively determined such as to cancel the unwanted $O(a)$ effects from any computed quantity. Although it may sound a straightforward task, the non-perturbative determination of improvement coefficients is very demanding. There are cases, however, where the fine tuning of improvement coefficients can be avoided. This is the case when employing a formulation of fermions on the lattice which has the property of automatic $O(a)$-improvement, twisted mass Wilson fermions at maximal twist [24]. Automatic $O(a)$-improvement means that all quantities with a finite continuum limit, i.e. physical quantities, have leading discretization effects of $O(a^2)$, while all

$O(a)$ effects are contained only in those quantities which have a vanishing continuum limit and thus, are not physical.

Here is where the newly proposed SF schemes can make a step forward. While the standard formulation of the SF is incompatible with automatic $O(a)$-improvement in the bulk of the lattice when using standard Wilson fermions as a regulator, the new formulations of the SF are expected to be compatible with automatic $O(a)$-improvement. The γ_5SF scheme is only briefly discussed and analytically studied in the formal continuum theory. We have found certain difficulties [25] which make this formulation not to be the final choice for our calculations. Therefore, the central goal here is to study the χSF scheme. In particular, we are concerned with the demonstration of the validity of the χSF and its applicability in the non-perturbative determination of renormalization constants of different physical observables. The demonstration of validity of the χSF is performed through studies of universality of the continuum limit. To be concrete, we compute several physical quantities using the χSF. We then compare the continuum limit values to those of the same quantities previously determined using the standard formulation of the SF. Since both formulations should be equivalent in the continuum limit, an agreement between the results obtained from both formulations is a numerical evidence of the universality of the continuum limit and, as a consequence, of the validity of the χSF scheme. Such studies are performed in the quenched approximation to QCD, which consists in neglecting the presence of dynamical quarks in favor of only valence quarks. This is an unphysical situation which is, however, a natural first step towards the understanding of the validity of any new development in lattice QCD.

The thesis is organized as follows. In Chap. 2 the main concepts of lattice QCD which are useful in the presentation of our results are reviewed. In Chap. 3 we summarize the key ideas in non-perturbative renormalization and we define the basic notions related to SF schemes. After these two chapters of theoretical discussions we present our first results in Chap. 4. Here we discuss some properties of the χSF and the γ_5SF in the continuum and at tree-level of perturbation theory. Based on [26], we review in Chap. 5 the main theoretical concepts of the χSF formulation and its lattice implementation. Here we also provide an expression for the free quark propagator on the lattice with χSF boundary conditions, as derived in the present work. Later in Chap. 6 the scheme is defined in the massless limit by performing the simultaneous non-perturbative tuning of the quark mass and the boundary coefficient, z_f, to their respective critical values. In Chap. 7 we collect our results in scaling studies of several quantities in their approach to the continuum limit. Chap. 8, Chap. 9 and Chap. 10 are devoted to the studies of universality. For that purpose we have computed several physical quantities. In Chap. 8 we present our results for the step scaling function (SSF) of the pseudo-scalar density, in Chap. 9 we compute the RGI mass of the strange quark and in Chap. 10 we determine the SSFs of the non-singlet twist-2 operators O_{12} and O_{44}. Eventually in Chap. 11 we discuss some topological aspects of our ensembles of gauge configurations. This thesis is closed in Chap. 12 with a brief summary and some concluding remarks.

2. QCD on the lattice

Motivated by the necessity of a lattice regularization in order to describe the long distance properties of QCD, the present chapter is devoted to introduce the main concepts of lattice QCD which will be needed in the subsequent chapters of the present work [1].

Before going into the description of lattice QCD, first the QCD action in the Euclidean continuum theory is introduced in Sec. 2.1. After that, in Sec. 2.2, the gauge fields on the lattice are presented, together with a particular expression for the lattice gauge action. A general form of the lattice QCD action is also given here. At this stage, the path integral on the lattice can be discussed, as well as its numerical evaluation via MC methods in Sec. 2.3. A discussion of chiral symmetry, Sec. 2.4, is also presented. The approach of the lattice theory towards the continuum limit is described in Sec. 2.5 and the Symanzik effective theory, accounting for a description of the discretization effects close to the continuum limit, is covered in Sec. 2.6. Eventually, in Sec. 2.7, the fermion fields and the fermion action on the lattice are introduced.

2.1. The QCD action

In a field theory, the most important cornerstone is the action describing the interactions between the fundamental particles of the theory under consideration. In this section, the QCD action, S^{QCD}, in the continuum and in Euclidean space-time is presented. It can be expressed as the sum of the so called gluon action, $S_{\mathrm{G}}[A]$, and fermion action, $S_{\mathrm{F}}[\psi, \overline{\psi}, A]$, as follows

$$S^{\mathrm{QCD}} = S_{\mathrm{G}}[A] + S_{\mathrm{F}}[\psi, \overline{\psi}, A]\,. \tag{2.1}$$

The fermion action is given by,

$$S_{\mathrm{F}}[\psi, \overline{\psi}, A] = \int \mathrm{d}^4x\; \overline{\psi}(x)\,(\gamma_\mu\, D_\mu + m)\,\psi(x)\,, \tag{2.2}$$

where

$$D_\mu = \partial_\mu + A_\mu(x) \tag{2.3}$$

is the so called covariant derivative. $A_\mu(x)$ represent the massless gauge fields (gluons); they are traceless anti-hermitian 3×3 matrices at each space-time point, x, for a given value of the Lorentz index μ, which belong to the Lie algebra of SU(3), su(3). The gluons are parametrized by eight real-valued fields, $A^a_\mu(x)$, which represent the degrees of freedom, $a = 1, \cdots, 8$, of the corresponding gauge field $A_\mu(x)$ (see App. A.4 and B.3 for additional explanations). The fermion action Eq. (2.2) describes the quark fields and the interactions between quarks and gluons for a single quark flavor of mass m. The full fermionic action is the sum of the fermionic actions of the different flavors (up, down, strange, charm, bottom, top). Matter fields with different flavors differ in their quark masses but have the same coupling to the gauge fields. Thus, the action in Eq. (2.2) is the same for each of the flavors only changing, accordingly, the mass term.

[1] For a recent review of lattice QCD see [27].

The gluonic part of the QCD action,

$$S_{\mathrm{G}}[A] = -\frac{1}{2\,g_0^2}\int \mathrm{d}^4x\ \mathrm{tr}_c\left[F_{\mu\nu}(x)F_{\mu\nu}(x)\right], \tag{2.4}$$

describes the propagation and self-interaction of gluons, gluodynamics. $F_{\mu\nu}(x)$ denotes the field strength tensor defined as

$$\begin{aligned} F_{\mu\nu}(x) &= [D_\mu, D_\nu] \\ &= \partial_\mu A_\nu(x) - \partial_\nu A_\mu(x) + [A_\mu(x), A_\nu(x)] \end{aligned} \tag{2.5}$$

and the trace in Eq. (2.4) is to be taken over the color indices. This color trace accounts for the gauge invariance of the gauge action. Moreover, the sum over the Lorentz indices ensures that the action is a Lorentz scalar, as it should. The self-interactions of gluons come from the non-vanishing value of the last term in Eq. (2.5), due to the non-Abelian nature of the theory. Note that, in order to match the usual notation for the gauge action on the lattice, the bare gauge coupling, g_0, is absorbed in a redefinition of the gauge potentials. The usual expressions may be recovered performing the substitution $\frac{1}{g_0}A_\mu(x) \to A_\mu(x)$.

Through the discussions in this thesis, particular emphasis will be put on the symmetries of QCD. More accurately, in the symmetries of QCD which are broken in the regularization procedure. As it is known, when regularizing a field theory several symmetries may be broken at finite value of the cutoff, which must be recovered when the cutoff is removed. In particular, if a lattice is chosen to regularize a field theory there are certain symmetries of QCD which are always broken; these are *translation* and *rotation* invariance, which become discrete on the lattice. On the contrary, gauge invariance is preserved on the lattice. There are yet other symmetries which might be broken or not depending on the chosen lattice regularization; of particular interest are the discrete QCD symmetries, $\mathcal{C}$, $\mathcal{P}$, $\mathcal{T}$, and the continuous chiral symmetry group, discussed in detail below in Sec. 2.4.

2.2. Gauge fields on the lattice

In the present section, the gauge fields on the lattice are introduced and a particular lattice gauge action is given. On the lattice, the space-time coordinates, x, become discrete, $x = an$, with a being the lattice spacing and n the lattice position. A vector of length a is denoted as $\vec{\mu} = a\hat{\mu}$, with $\hat{\mu}$ an unit vector in direction μ. The fermion fields are denoted $\psi(x)$ and they live on the *sites*, x, of the lattice. The gauge fields on the lattice can not be directly translated from the continuum theory. Instead, they originate from the restriction of having a fermionic *lattice* action which is invariant under local gauge transformations, Eq. (B.26), as it is the case in the continuum theory (cf. App. B.3). Yet, there is an important difference between the continuum and the lattice; while in the continuum the gauge potentials in the Lie algebra of SU(3), $A_\mu(x)$, account for the gauge invariance of the fermionic action, on the lattice this is achieved through the elements of the gauge group SU(3) itself (as first realized by K. Wilson [10]). The group elements are matrices denoted $U_\mu(x)$ and referred to as *link* variables, which have an orientation and connect points on the lattice. The matrices $U_\mu(x)$ are attached to the lattice links, which are the lines connecting the lattice points. Different conventions can be employed to define the orientation of the gauge fields. Defining the link variable, $U_\mu(x)$, as the gauge field connecting the lattice points x and $x + \vec{\mu}$ and oriented from x to $x + \vec{\mu}$, also $U_\mu(x)^\dagger$ can be defined, as the variable on the same link but oriented in the opposite direction. As a consequence, the lattice gauge fields are enforced to transform under the local transformations, $\Omega(x)$, generated

by elements of SU(3) as

$$U_\mu(x) \to U'_\mu(x) = \Omega(x) U_\mu(x) \Omega(x+\vec{\mu})^\dagger \,, \tag{2.6}$$

which automatically implies the transformation

$$U_\mu(x)^\dagger \to U'_\mu(x)^\dagger = \Omega(x+\vec{\mu}) U_\mu(x)^\dagger \Omega(x)^\dagger . \tag{2.7}$$

Following App. A.4, a suitable choice for the link variables is

$$U_\mu(x) = e^{a\, A_\mu(x)} \,. \tag{2.8}$$

The set of all link variables on the lattice, $U \equiv \{U_\mu(x)\}$, is called gauge field configuration.

With such a definition of the link variables, the simplest gauge action which can be constructed on the lattice, while keeping local gauge invariance, was introduced by K. Wilson [10] and it is referred to as the *Wilson gauge action*,

$$S_{\rm G}[U] = \frac{\beta}{N_{\rm c}} \sum_x \sum_{\mu<\nu} \mathrm{Re}\,\mathrm{tr}_c \left[1 - U_{\mu\nu}(x)\right] \,, \quad \beta = \frac{2N_c}{g_0^2} \,. \tag{2.9}$$

N_c denotes the number of colors and β is the so called inverse coupling. $U_{\mu\nu}(x)$ is the plaquette field defined by

$$U_{\mu\nu}(x) = U_\mu(x)\, U_\nu(x+\vec{\mu})\, U_\mu(x+\vec{\nu})^\dagger\, U_\nu(x)^\dagger \,, \tag{2.10}$$

which represents the smallest non-vanishing closed loop on the lattice. This action fulfills the minimal requirements that a lattice action must keep; local gauge invariance, due to the color trace in Eq. (2.9), and a naive continuum limit which agrees with the continuum gauge action given in Eq. (2.4). However, the way of discretizing a theory is not unique. There is the freedom of choosing different lattice actions, with the only restriction that results obtained from different formulations should give the same physical answers. This freedom in the regularization of the theory will be discussed in more detail below when the fermion lattice action is introduced. At the moment, it is enough to keep in mind that there is not an unique way of discretizing the theory on the lattice.

Having defined the gauge fields on the lattice, $U_\mu(x)$, and given a choice for the lattice gauge action, e.g. Eq. (2.9), the full QCD action on the lattice can be written as,

$$S^{\rm QCD}[\psi, \overline{\psi}, U] = S_{\rm G}[U] + S_{\rm F}[\psi, \overline{\psi}, U] \,, \tag{2.11}$$

with $S_{\rm G}$ the pure gauge action defined above in Eq. (2.9) and $S_{\rm F}$ the discretized fermion action. Particular formulations of fermions on the lattice will be described at the end of this chapter in Sec 2.7. At the moment only a general form of the lattice fermion action is considered. The most general expression may be written as follows,

$$S_{\rm F}[\psi, \overline{\psi}, U] = a^4 \sum_x \overline{\psi}(x) \left(D + m_0\right) \psi(x) \,, \tag{2.12}$$

with the sum running over all lattice sites. For later purpose the bare quark mass is denoted as m_0. Such notation will become clear in following sections. D is a particular choice of the massless *lattice* Dirac operator which, at the moment, is left unspecified.

2.3. QCD path integral on the lattice

After having introduced above the lattice QCD action, it is now possible to define the functional integral formalism in lattice QCD. In the functional integral formalism, operators in Hilbert space, $\hat{O}$, become functionals of the classical fields of the theory, $O[\psi, \overline{\psi}, U]$, and vacuum expectation values, $\langle O \rangle$, are represented by integrals of the functionals $O[\psi, \overline{\psi}, U]$ over all possible configurations of the classical fields $(\psi, \overline{\psi}, U)$ as follows

$$\langle O \rangle = \frac{1}{Z} \int \mathcal{D}[\psi]\, \mathcal{D}[\overline{\psi}]\, \mathcal{D}[U]\; e^{-S^{\mathrm{QCD}}[\psi, \overline{\psi}, U]}\; O[\psi, \overline{\psi}, U]\,, \tag{2.13}$$

with the so called partition function

$$Z = \int \mathcal{D}[\psi]\, \mathcal{D}[\overline{\psi}]\, \mathcal{D}[U]\; e^{-S^{\mathrm{QCD}}[\psi, \overline{\psi}, U]}\,, \tag{2.14}$$

and $S^{\mathrm{QCD}}[\psi, \overline{\psi}, U] = S_{\mathrm{F}}[\psi, \overline{\psi}, U] + S_{\mathrm{G}}[U]$ the full QCD action on the lattice. The measures in Eq. (2.13) and Eq. (2.14) are the Grassmann measure

$$\mathcal{D}[\psi]\, \mathcal{D}[\overline{\psi}] = \prod_{x} \prod_{f,\alpha,c} \mathrm{d}\psi^{f}_{\alpha,c}(x)\, \mathrm{d}\overline{\psi}^{f}_{\alpha,c}(x)\,, \tag{2.15}$$

for the fermion, Grassmann, fields and the Haar measure

$$\mathcal{D}[U] = \prod_{x} \prod_{\mu} \mathrm{d}U_{\mu}(x)\,, \tag{2.16}$$

for the gauge fields. The indices f, α and c in Eq. (2.15) denote flavor, Dirac and color indices, respectively. x is the space-time coordinate and the index μ in Eq. (2.16) is a Lorentz index. Both, the Grassmann and Haar measures are gauge invariant. Since also the QCD action, in this case on the lattice, is gauge invariant, it can be deduced that the vacuum expectation value, $\langle O \rangle$, of any *non* gauge-invariant observable is zero.

The final goal is to evaluate the functional integral in Eq. (2.13)-(2.14) numerically using Monte Carlo methods. For that purpose it is necessary to set up the theory in an Euclidean space-time lattice of lattice spacing a and finite volume L^3T. As it can be seen from the functional integral Eq. (2.13), the functionals are weighted with an exponential given by the classical Euclidean QCD action on the lattice, $S^{\mathrm{QCD}}[\psi, \overline{\psi}, U]$, which is also a functional of the classical fields. In virtue of working in Euclidean space, this phase factor has the form of a Boltzmann weight, $e^{-S^{\mathrm{QCD}}} \equiv e^{-\beta H}$, provided the Euclidean lattice QCD action, S^{QCD}, is real and bounded from below. In Euclidean space, therefore, a statistical interpretation of the functional integral is possible and thus, methods of statistical mechanics may be applied to evaluate Eq. (2.13)-(2.14). Note that a statistical interpretation of the functional integral would not be possible in Minkowski space. In this case the exponential would be complex and this would imply an oscillating weight factor lacking of a statistical interpretation. Therefore, to work in Euclidean space is the first requirement towards a numerical evaluation of the functional integral. The way to express the theory in Euclidean space is via a Wick rotation from Minkowski to Euclidean space. (cf. App. A.2). It is worth noting that there exist very strong conditions, the Osterwalder-Schrader conditions, which guarantee that results obtained in Euclidean space-time can be rotated back to Minkowski space, recovering all the physical content of the theory (cf. App. A.2). The requirement of setting the theory on the lattice implies that the continuous Euclidean space-time is replaced by a space-time lattice of spacing a, such that all continuous variables, x, become discrete, $x = an$, with n denoting the lattice points. The discretization of

the space-time implies that all integrals over the space-time points, x, become sums over the lattice poins, n, as follows

$$\int d^4x \longrightarrow a^4 \sum_n . \tag{2.17}$$

If the lattice was infinite, the theory could still not be numerically evaluated because the path integral would have to be performed over an infinite amount of discrete points, n. Therefore, in order to render finite the number of integrations over the fields of the theory ($\psi(an)$, $\overline{\psi}(an)$, $U_\mu(an)$) the lattice volume has to be finite, $V = L^3T$, with N number of points in the spatial directions, $L = aN$, and N_T in the temporal direction, $T = aN_T$. This means that all sums in $n = (n_0, n_1, n_2, n_3)$ are performed only over a finite number of points, N^3N_T, which is restricted to the lattice volume, $\Lambda \equiv \{n_0 = 0, \cdots, N_T - 1\,;\, n_k = 0, \cdots, N - 1\,,\, k = 1, 2, 3\}$, as follows

$$a^4 \sum_n \longrightarrow a^4 \sum_{n\in\Lambda} . \tag{2.18}$$

In order to proceed, a more practical notation is employed in the following. Since the gauge action only depends on the gauge fields, the expectation value of the corresponding observable can be written as follows,

$$\langle O \rangle = \langle\, [O]_{\rm F} \,\rangle_{\rm G} = \frac{1}{Z} \int \mathcal{D}[U]\; e^{-S_{\rm G}[U]}\; Z_{\rm F}[U]\; [O[\psi, \overline{\psi}, U]]_{\rm F} \,. \tag{2.19}$$

In this expression, $\langle\cdot\rangle_{\rm G}$ denotes the expectation value over the gauge fields, while $[\cdot]_{\rm F}$ represents the expectation value over the fermionic variables, on some external gauge field U, which is given by

$$[O]_{\rm F} = \frac{1}{Z_{\rm F}[U]} \int \mathcal{D}[\psi]\, \mathcal{D}[\overline{\psi}]\; e^{-S_{\rm F}[\psi,\overline{\psi},U]}\; O[\psi, \overline{\psi}, U] \,, \tag{2.20}$$

with the fermionic partition function,

$$Z_{\rm F}[U] = \int \mathcal{D}[\psi]\, \mathcal{D}[\overline{\psi}]\; e^{-S_{\rm F}[\psi,\overline{\psi},U]} \,. \tag{2.21}$$

Since fermions appear bilinearly in the QCD action, using the Grassmann algebra it can be shown that, indeed, the fermionic partition function is the determinant of the Dirac operator,

$$Z_{\rm F}[U] = (\det D_m)[U] \,, \tag{2.22}$$

and it is referred to as the *fermion determinant*. In particular here, D_m is the massive Dirac operator on the lattice,

$$D_m = D + m_0 \,. \tag{2.23}$$

But, in order to have a statistical interpretation of the fermionic partition function Eq. (2.22) and, thus, to be able to evaluate it numerically, the determinant of the Dirac operator must fulfill certain requirements. In particular, it must be *real* and *positive*. Yet, such conditions are not always trivial at the lattice level. Therefore, much care has to be taken when discretizing fermions on the lattice in order to realize such conditions, as otherwise the statistical interpretation of the theory is spoiled. For the rest of this discussion it is assumed that D_m is a 'well-behaved' lattice Dirac operator with respect to these conditions.

Given the previous expressions, it can be explained now how the functional integral is numerically evaluated using Monte Carlo techniques. For practical purposes Eq. (2.19) is re-written

in a more convenient way in terms of the determinant of the Dirac operator,

$$\langle O\rangle = \frac{1}{Z}\int \mathcal{D}[U]\, e^{-S_{\rm G}[U]}\, (\det D_m)[U]\, \tilde{O}[U]\,, \quad \tilde{O}[U] \equiv [O[\psi,\overline{\psi},U]]_{\rm F}\,, \tag{2.24}$$

with the partition function

$$Z = \int \mathcal{D}[U]\, e^{-S_{\rm G}[U]}\, (\det D_m)[U]\,. \tag{2.25}$$

The explicit dependence on U emphasizes the fact that once the fermionic contractions are performed, the resulting quantities only depend on the gauge fields U and, thus, only expectation values over the gauge fields remain to be numerically evaluated. Yet, as they are written, the previous integrals can not be directly evaluated using numerical methods. In order to apply Monte Carlo methods it is necessary to first consider a statistical approximation of the integrals in Eq. (2.24)-(2.25).

The way to proceed is the following. First, a sufficiently large number, N, of statistically independent sample gauge configurations, U_i, is generated via MC simulations with a probability distribution density

$$dP(U_i) \sim \mathcal{D}[U_i]\, e^{-S_{\rm G}[U_i]}\, (\det D_m)[U_i]\,. \tag{2.26}$$

This way of generating a sample of gauge configurations is referred to as importance sampling. Then, the corresponding observables, $\tilde{O}$, are evaluated for each configuration in the sample, $\tilde{O}[U_i]$. Eventually, the functional integral Eq. (2.24) is represented by the sample average

$$\langle O\rangle = \frac{1}{N}\sum_{i=1}^{N} \tilde{O}[U_i] + O\Big(\frac{1}{\sqrt{N}}\Big)\,. \tag{2.27}$$

The previous expressions represent the most general case in the evaluation of expectation values in lattice QCD. There are, though, important particular cases of these equations. The simplest one is that of the pure gauge theory. In such an approximation the equations reduce to

$$\langle O\rangle = \frac{1}{Z}\int \mathcal{D}[U]\, e^{-S_{\rm G}[U]}\, O[U]\,, \quad Z = \int \mathcal{D}[U]\, e^{-S_{\rm G}[U]}\,, \tag{2.28}$$

with the probability distribution density only given by the gauge action,

$$dP(U_i) \sim \mathcal{D}[U_i]\, e^{-S_{\rm G}[U_i]}\,, \tag{2.29}$$

and all observables being simplified functionals of only the gauge fields.

The other case to mention is the so called quenched approximation or *quenched QCD*. It consists in considering the theory as having fermion fields only in the valence sector and not in the sea. The valence quarks are the responsible for the quantum numbers of hadrons and are those quarks entering the initial and final states of physical processes. On the contrary, the sea (or dynamical) quarks are those entering the vacuum quark loops, accounting for the creation and annihilation of virtual quark-antiquark pairs. From the point of view of the equations the quenched approximation translates in neglecting the fermion determinant which describes the fermionic vacuum. This reduces Eq. (2.24)-(2.25) to

$$\langle O\rangle = \frac{1}{Z}\int \mathcal{D}[U]\, e^{-S_{\rm G}[U]}\, \tilde{O}[U]\,, \quad Z = \int \mathcal{D}[U]\, e^{-S_{\rm G}[U]}\,, \tag{2.30}$$

with a probability distribution density which is the same as in the pure gauge theory and it is given by Eq. (2.29). In quenched QCD, differently to the pure gauge theory, fermionic

contractions still take place, $\tilde{O}[U]$, which account for the description of the valence sector. Of course, this setup is only an approximation to QCD so it is not expected to describe many of the QCD phenomena on a precise quantitative level. But, it still describes many phenomena up to a very good accuracy, like the ground state of the hadron spectrum of QCD with light quark content. Indeed, this setup has been very important in lattice calculations, since it is computationally much cheaper than the theory with dynamical fermions and it is considered to be the starting point in the study of many new lattice developments. In performing MC simulations there may exist some configurations, exceptional configurations, which give rise to vanishing eigenvalues, zero modes, of the Dirac operator especially towards the region of small quark masses. In the quenched approximation, where the fermion determinant is neglected, the occurrence of such exceptional configurations may become a problem in evaluating the ensemble average Eq. (2.27) (cf. App. C.2 for explanation). Therefore, care has to be taken in quenched QCD with respect to the spectrum of the corresponding lattice Dirac operator.

In contrast to the quenched setup, the full QCD case is referred to as dynamical setup. Most of the dynamical calculations that have taken place up to nowadays were performed with $N_f = 2$ (u, d) and up to $N_f = 3$ (u, d, s) flavors of dynamical quarks, with the light doublet degenerate in mass. To consider up to $N_f = 3$ dynamical quarks has proven to be a very good approximation to dynamical QCD, since the masses of the heavy quarks (c, b, t), almost do not contribute to the dynamics of the sea. Recently, computations with $N_f = 4$ dynamical fermions (u, d, s, c) have already started. The discussion of the heaviest quarks (b, t) goes far beyond the development of the work here presented. For instance, the quark b is studied using heavy-quark effective theories.

For later use, the *generating functional for fermions* is also introduced here,

$$Z_{\mathrm{F}}[\eta,\overline{\eta},U] = \int \mathcal{D}[\psi]\,\mathcal{D}[\overline{\psi}]\; e^{-S_{\mathrm{F}}[\psi,\overline{\psi},U]+(\overline{\eta},\psi)+(\overline{\psi},\eta)}\,, \tag{2.31}$$

with $(\cdot,\cdot)$ the scalar product and $\overline{\eta},\eta$, the 'sources' of the fermion and anti-fermion fields, respectively. Assuming that D_m is not singular, the generating functional may also be written in terms of the fermionic determinant as follows,

$$Z_{\mathrm{F}}[\eta,\overline{\eta},U] = (\det D_m)\, e^{-\overline{\eta}D_m^{-1}\eta}\,. \tag{2.32}$$

From the generating functional for fermions it is possible to obtain the fermionic expectation value of any product of Grassmann fields, by applying the formula

$$[\psi_{i_1}\overline{\psi}_{j_1}\cdots\psi_{i_n}\overline{\psi}_{j_n}]_{\mathrm{F}} = \frac{1}{Z_{\mathrm{F}}[U]}\,\partial_{\eta_{j_1}}\partial_{\overline{\eta}_{i_1}}\cdots\partial_{\eta_{j_n}}\partial_{\overline{\eta}_{i_n}} Z_{\mathrm{F}}[\eta,\overline{\eta},U]\,|_{\eta=\overline{\eta}=0}\,, \tag{2.33}$$

where the fermion/anti-fermion fields, are assumed to be functional derivatives with respect to the source fields, $\overline{\eta}/\eta$. This leads to the so called *Wick's theorem*

$$[\psi_{i_1}\overline{\psi}_{j_1}\cdots\psi_{i_n}\overline{\psi}_{j_n}]_{\mathrm{F}} = (-1)^n \sum_{P(1,2,\ldots,n)} \mathrm{sign}(P)\,(D_m^{-1})_{i_1 j_{P_1}}\cdots(D_m^{-1})_{i_n j_{P_n}}\,. \tag{2.34}$$

Here $\mathrm{sign}(P)$ is the sign of the permutation P and the sum runs over all permutations.

The simplest particular case of this formula is the two-point function, which represents the fermion propagator,

$$[\psi(x)\,\overline{\psi}(y)]_{\mathrm{F}} = \frac{\int \mathcal{D}[\psi]\,\mathcal{D}[\overline{\psi}]\;\psi(x)\overline{\psi}(y)\,e^{-S_{\mathrm{F}}[\psi,\overline{\psi},U]}}{\int \mathcal{D}[\psi]\,\mathcal{D}[\overline{\psi}]\;e^{-S_{\mathrm{F}}[\psi,\overline{\psi},U]}} = D_m^{-1}\,. \tag{2.35}$$

Notation	Symmetry	Transformation
$\mathrm{SU}(N_f)_A$	Chiral (χ)	$\psi \to \exp(\mathrm{i}\,\alpha_i^A\,\gamma_5\,T^i)\,\psi$ $\overline{\psi} \to \overline{\psi}\exp(\mathrm{i}\,\alpha_i^A\,\gamma_5\,T^i)$
$\mathrm{U}(1)_A$	Axial	$\psi \to \exp(\mathrm{i}\,\alpha_0^A\,\gamma_5\,\mathbb{1})\,\psi$ $\overline{\psi} \to \overline{\psi}\exp(\mathrm{i}\,\alpha_0^A\,\gamma_5\,\mathbb{1})$
$\mathrm{SU}(N_f)_V$	Isospin	$\psi \to \exp(\mathrm{i}\,\alpha_i^V\,T^i)\,\psi$ $\overline{\psi} \to \overline{\psi}\exp(-\mathrm{i}\,\alpha_i^V\,T^i)$
$\mathrm{U}(1)_V$	Baryon number	$\psi \to \exp(\mathrm{i}\,\alpha_0^V\,\mathbb{1})\,\psi$ $\overline{\psi} \to \overline{\psi}\exp(-\mathrm{i}\,\alpha_0^V\,\mathbb{1})$

Table 2.1.: Definition of the transformations of the chiral group. Note that, with abuse of notation, we denote here $\mathrm{SU}(N_f)_A$ the non-singlet axial-vector transformations. Such transformations, however, do not have a group structure.

The fermion propagator itself is not a physical observable, since it is not gauge invariant and as such has a vanishing expectation value, $\langle[\psi(x)\,\overline{\psi}(y)]_{\mathrm{F}}\rangle_{\mathrm{G}} = 0$ provided $x \neq y$. It is though important because fermion propagators are the building blocks of any physically important fermionic correlation function.

2.4. Chiral symmetry

Before going into more technical details of lattice QCD and introducing the fermion fields on the lattice, it is important to define and discuss the implications of chiral symmetry [28] in QCD. This is a symmetry of capital importance for the understanding and explanation of many physical phenomena in nature. Moreover, it is one of the main issues to keep in mind when regularizing fermions on the lattice.

2.4.1. Chiral symmetry in the continuum

Classical massless QCD with N_f flavors of quarks has the following chiral symmetry group,

$$\mathrm{SU}(N_f)_L \times \mathrm{SU}(N_f)_R \times \mathrm{U}(1)_V \times \mathrm{U}(1)_A\,. \tag{2.36}$$

In the massless case, left- and right-handed components of the fermion fields transform independently under the $\mathrm{SU}(N_f)$ subgroup of the total chiral group. Here V stays for vector, indicating that the Nöther current associated to this particular transformation is a vector current. In the same way, A stays for axial-vector, denoting the associated axial-vector Nöther current. With abuse of notation, we rewrite here the part $\mathrm{SU}(N_f)$ of the total chiral group given in Eq. (2.36) as follows

$$\mathrm{SU}(N_f)_L \times \mathrm{SU}(N_f)_R \quad \longrightarrow \quad \mathrm{SU}(N_f)_V \times \mathrm{SU}(N_f)_A\,. \tag{2.37}$$

Note that the non-singlet axial-vector transformations, denoted here as $\mathrm{SU}(N_f)_A$, do not have a group structure. We use such group notation in order to discuss the symmetry transformations under the chiral group, of Wilson and twisted mass Wilson fermions, in a more clear manner, as it will be shown below in Sec. 2.7.

Denoting T^i, $i = 1, \cdots, N_f^2 - 1$, the generators of the group $\mathrm{SU}(N_f)$, the transformations of the total chiral group, Eq. (2.36), are summarized in Tab 2.1.

In nature, however, chiral symmetry is broken in several ways. This has important physical implications. In general, a symmetry of the classical action, at the Lagrangian level, can be broken in three different forms; by quantization of the theory, explicitly or spontaneously.

The *explicit breaking* takes place already at the classical level, due to the appearance in the Lagrangian of a term that is not invariant under the transformation considered. The *anomaly* is the consequence of the breaking of a symmetry of the classical theory in the quantization process and it is also an explicit breaking. The *spontaneous breaking* of a symmetry, SSB, takes place when a symmetry of the action is not a symmetry of the ground state of the theory.

In the particular case of QCD, axial symmetry, $\mathrm{U}(1)_A$, is always broken at the quantum level; this is the so-called *axial anomaly*. It is a consequence of the non-invariance of the fermion integration measure under the axial (chiral flavor singlet) transformation. The term which breaks the symmetry is shown to be proportional to the so called topological charge, Q_{top}. This quantity is a property of the gauge fields and it is defined as,

$$Q_{\mathrm{top}} = \int \mathrm{d}^4x \; q(x) \; , \quad q(x) = \frac{1}{32\,\pi^2}\, \epsilon_{\mu\nu\rho\sigma}\, \mathrm{tr}_c \left[F_{\mu\nu}(x)\, F_{\rho\sigma}(x) \right] . \tag{2.38}$$

$F_{\mu\nu}$ is the field strength tensor given in Eq. (2.5) , $q(x)$ the topological charge density and $\epsilon_{\mu\nu\rho\sigma}$ the totally anti-symmetric Levi-Civita tensor.

Therefore, the symmetry group of quantized QCD is at most

$$\mathrm{SU}(N_f)_L \times \mathrm{SU}(N_f)_R \times \mathrm{U}(1)_V \, . \tag{2.39}$$

If a theory with massive fermion fields which are degenerate in mass is considered, the mass term in the action is not invariant under non-singlet axial-vector transformations, usually called *chiral transformations*. Due to the explicit breaking of chiral symmetry by the mass term the left- and right-handed components of the fermion fields mix and there is no $\mathrm{SU}(N_f)_L \times \mathrm{SU}(N_f)_R$ symmetry left anymore. This leaves a theory with a chiral symmetry group

$$\mathrm{SU}(N_f)_V \times \mathrm{U}(1)_V \, . \tag{2.40}$$

If the masses differ for different flavors, non-diagonal mass matrix, the chiral group is still reduced further to the minimal case

$$\mathrm{U}(1)_V^{\,(1)} \times \mathrm{U}(1)_V^{\,(2)} \times \cdots \overset{(N_f-1)}{\times} \mathrm{U}(1)_V \, . \tag{2.41}$$

Note that even in the massless case chiral symmetry is broken, this time spontaneously due to the particular dynamics of QCD. The spontaneous chiral symmetry breaking explains many physical phenomena which could not be understood without it. Amongst them is the smallness of the pion masses, which are the Goldstone bosons of the theory, and the non-degeneracy of the massess of baryonic parity partners. A quantity that indicates the existence of spontaneous symmetry breaking is the *chiral condensate*

$$\langle \overline{\psi}(x) \psi(x) \rangle \, , \tag{2.42}$$

which is the order parameter of chiral symmetry breaking. If the chiral condensate does not vanish in the chiral limit it is because chiral symmetry is spontaneously broken. Note that spontaneous chiral symmetry breaking is possible only in the chiral limit as otherwise the symmetry would be broken explicitly by the mass term. Moreover, a symmetry can be broken spontaneously only in infinite volume. Therefore, when performing calculations in a finite volume, as it is the case of lattice QCD, the infinite volume limit has to be performed before the chiral limit, as otherwise SSB could not be observed. In addition, the spontaneous breaking can only take place in a theory with $N_f \geq 2$ because in the case of $N_f = 1$ the symmetry is already broken explicitly by the anomaly.

For later use, it is written here the equation containing the chiral symmetry realization. At the classical level in the continuum, the massless QCD action is invariant under the transformations of the chiral group, $\mathrm{SU}(N_f)_A$. Such invariance is given by the invariance of the massless Dirac operator, D, under the transformations of the chiral group. Thus, the relation expressing the realization of chiral symmetry in a theory with $N_f = 1$ flavors of quarks is

$$D\,\gamma_5 + \gamma_5\,D = 0 \tag{2.43}$$

and in a theory with $N_f > 1$

$$D\,\gamma_5 T^i + \gamma_5 T^i\,D = 0\,, \quad i = 1 \cdots N_f^2 - 1\,. \tag{2.44}$$

In terms of the quark propagator,

$$D^{-1}\,\gamma_5 + \gamma_5\,D^{-1} = 0\,, \tag{2.45}$$

$$D^{-1}\,\gamma_5 T^i + \gamma_5 T^i\,D^{-1} = 0\,. \tag{2.46}$$

2.4.2. Chiral symmetry and lattice QCD

The realization of chiral symmetry at the lattice level is far from trivial. In particular, all complications concerning chiral symmetry originate in the discretization of the fermion sector of QCD. The complexity in setting fermions on the lattice is summarized by the no-go theorem of Nielsen and Ninomiya [29–31].

Nielsen-Ninomiya no-go theorem:
If D is a translation-invariant lattice Dirac operator and $\tilde{D}(p)$ its Fourier transform, it is impossible to have a lattice Dirac operator that has *simultaneously all* the following properties. (1) *Locality*: $\tilde{D}(p)$ is analytic and periodic in p_μ with period $2\pi/a$. (2) *Small p limit*: $\tilde{D}(p)\,|_{p\sim 0} = \mathrm{i}\,\gamma_\mu\,p_\mu + O(ap^2)$; it is possible to perform an expansion about the poles. (3) *No doublers*: $\tilde{D}(p)$ is invertible for all $p \neq 0$ (module $2\pi/a$). (4) *Continuum chiral symmetry* in the form of Eq. (2.43)-(2.44).

Condition (1) ensures the recovery of point-like locality in the continuum limit and conditions (2) and (3) are required to have a continuum limit of the lattice theory with the correct dispersion relation and number of particles. The theorem implies that chiral symmetry on the lattice can be realized, as stated in the continuum, only at expenses of giving up any of the other three properties. Since, certainly, *locality* and *small p limit* are two properties that should better be kept on the lattice, the problem is mainly concerned with the case of having a lattice theory with chiral symmetry and doublers (cf. App. C.1), or no doublers, yet loose chiral symmetry, in the form of Eq. (2.43)-(2.44). Since having doublers would imply a continuum limit with more particles than there should be, the most natural way to proceed is to have a formulation which breaks chiral symmetry and maintains the properties (1),(2) and (3). This is for instance the case of Wilson fermions [20], as it will be discussed in detail below in Sec. 2.7.

There is still a way, though, of fulfilling all requirements of the no-go theorem but giving up locality *on the lattice*. It is possible to have a lattice Dirac operator which preserves chiral symmetry. In particular, this may occur by considering that the continuum chiral symmetry relation, Eq. (2.43)-(2.44), is accomplished on the lattice only up to cutoff effects [32]. The condition required on the lattice is the so called Ginsparg-Wilson relation [33]. This is referred to as chiral formulation of fermions. It was only ten years after the Ginsparg-Wilson relation was proposed that it was noticed that the lattice Dirac operators of the overlap [34, 35] and fixed point fermions [36] formulations obey this relation.

The maintenance of chiral symmetry on the lattice has many advantages. However, it comes with a technical drawback. Due to the non-locality of the Dirac operator at finite lattice spacing, a numerical evaluation becomes very demanding in this case. From now on, chiral formulations of fermions are not discussed any longer, since such lattice fermions are not used in the course of this thesis. Instead, we will use here Wilson-like fermions (cf. Sec. 2.7).

2.5. Continuum limit

The continuum limit represents the removal of the ultraviolet cutoff imposed in the discretization procedure. In previous sections only the 'naive' continuum limit of the lattice action has been discussed. However, while the classical continuum limit is a necessary condition for a lattice theory to be valid, it is certainly not sufficient; by simply taking the limit $a \to 0$ while keeping fixed all bare parameters of the theory would imply that all initially cancelled divergences would appear again. Instead, the correct way to perform the continuum limit is to allow the bare parameters of the theory to change accordingly, while the lattice spacing is being sent to zero. The way the bare parameters are varied is dictated by enforcing a certain number of physical quantities, as many as the number of bare parameters in the theory, to remain fixed to some specific value, while the lattice spacing is being sent to zero. In this manner the continuum limit is reached while keeping fixed a certain physical situation, which is usually referred to as trajectory of constant physics. This procedure actually represents the renormalization of the theory, treated in detail in Chap. 3. The renormalizability of the theory then ensures that any physical quantity has a finite continuum limit when the lattice spacing is sent to zero along a trajectory of constant physics. There is no restriction in which are the observables chosen to tune the bare parameters. The only requirement is that the chosen trajectory corresponds to a physical situation, which is achieved by tuning the chosen physical quantities such that they take their experimentally known values.

From the renormalization group equations (cf. Sec. 3.3.3) it is deduced that the lattice spacing, a, is a function of the bare coupling, $a(g_0)$, which decreases exponentially for decreasing values of g_0, or equivalently, increasing inverse coupling, β. Such dependence is the so called asymptotic scaling, which implies that the continuum limit, $a \to 0$, is equivalent to the limit $g_0 \to 0$ or $\beta \to \infty$. In the pure gauge theory, the only bare parameter is the gauge coupling and therefore it is the only quantity the lattice spacing depends upon, $a(g_0)$. In quenched QCD, where there are no dynamical quarks, this statement remains true, provided a pure gauge quantity is used to define the trajectory of constant physics [2]. In particular, the quenched approximation is the setup used in this thesis and the physical quantity chosen is the Sommer parameter, r_0 [37], which is a pure gauge quantity. In this particular case a curve parametrizing the dependence of the dimensionless ratio a/r_0 as a function of β was determined for the Wilson gauge action in [38, 39] (cf. App. C.3). From this parametrization it is then possible to compute, for any value of β within the range of validity of the curve, the corresponding value of the lattice spacing in physical units, at the phenomenological value of r_0 which is held fixed, $r_0 = 0.5\,\mathrm{fm}$.

In order to perform the continuum limit of an observable computed on the lattice the first step is to parametrize the dependence of a on β as indicated above. Then the corresponding observable is determined at several values of $a(\beta)$ for larger and larger values of β, while ensuring that the quantities chosen to define a trajectory of constant physics remain fixed. From the obtained results it is possible to determine the dependence of the observable on the lattice spacing close to the continuum limit, in the so called asymptotic region. The study of the dependence of a certain quantity on the lattice spacing is referred to as 'scaling analysis'. From

[2] If the full QCD case was considered, a would also depend on the quark massess, $a(\beta, m)$, which are, generically, denoted here as m.

the scaling behavior of the corresponding observable, the continuum limit, $a \to 0$, can be eventually reached. But, in order to perform the scaling analysis and continuum limit the physical lattice volume, $L^3T = a^4N^3N_T$, has to be large enough to avoid finite size effects [3]. This condition on the volume implies that while the lattice spacing is sent to zero, the number of lattice points increases towards infinite, which is certainly not possible to simulate on the lattice. As a result, all lattice calculations have to be accomplished at a finite value of the lattice spacing and consequently, the continuum limit is only reached via an *extrapolation* to zero lattice spacing. Fortunately, since the computed quantities are known to scale with a certain power in a, which can be determined theoretically, the continuum limit can be reliably performed with only a few values of the lattice spacing. But, in order for the continuum limit to be trustable, the values of the lattice spacing used in the extrapolation should be small enough to ensure that the extrapolated data are close to their continuum values and, therefore, it can be guaranteed that the asymptotic scaling region has been reached. However, the smallness of the lattice spacing is restricted by the number of lattice points which can be simulated in present lattice computations. This number varies depending on the particular case and it is more restricted in dynamical than in quenched simulations, due to the expensive computation of the fermion determinant in the dynamical situation. A cutoff for this number in present lattice simulations and for dynamical Wilson fermions is on the order of N between 32-64, or equivalently, a between (0.08-0.04)fm. In the case of Ginsparg-Wilson fermions simulations become of the order of, at least, 10 times more expensive.

2.6. Cutoff effects and the Symanzik improvement programme

Given a quantity computed on the lattice, its scaling behavior towards the continuum limit is asymptotically governed by its leading discretization effects. The scaling behavior is inherent to the specific lattice formulation and also to the particular observable considered. In the case of the pure gauge theory the leading cutoff effects are of $O(a^2)$ [4]. In the fermion sector, however, there is a broader spectrum of cutoff effects depending on the particular discretization of the Dirac operator. The resulting cutoff effects are in this case directly related to the realization of chiral symmetry on the lattice. Lattice fermion actions which obey the Ginsparg-Wilson relation are affected by only leading $O(a^2)$ discretization effects [40]. If the lattice fermion action violates (lattice) chiral symmetry, the leading cutoff effects are of $O(a)$ [20].

Due to the restriction in the values of the lattice spacing which can be simulated, it is important to have a lattice formulation of fermions with leading $O(a^2)$ discretization effects instead of $O(a)$. Given a certain value of a, a quantity with leading effects proportional to a^2 is parametrically closer to the continuum limit than a quantity which scales with a. In principle this would be achieved using formulations of fermions on the lattice which obey the Ginsparg-Wilson relation. However, these simulations are very demanding for the present computational resources. A computationally cheaper option is to simulate lattice fermions which break chiral symmetry and, thus, are affected by $O(a)$ discretization effects. Fortunately, in virtue of K. Symanzik and its successful improvement programme [21–23], it is possible to cancel the cutoff effects order by order in the lattice spacing in all on-shell [41, 42] quantities. This procedure is referred to as improvement. The Symanzik programme accounts for a description of a lattice theory in terms of a *continuum* local effective theory which, based on the symmetries of the corresponding lattice theory, provides a parametrization of the cutoff effects close to the continuum limit. The

[3] Except in particular cases, where the finite volume is needed. For example, finite-volume renormalization schemes (cf. Chap. 3).

[4] If a theory with boundaries is considered, such statement is not exactly true, as it will be discussed in detail in Chap. 3.

improvement of the theory up to a certain order in a is achieved by adding local counterterms, of the corresponding order in a, to the lattice action and interpolating fields. It is the role of the continuum effective description to teach which are these counterterms that need to be added in their lattice form to the corresponding lattice action and composite fields to be improved. If the improvement programme is applied to cancel the $O(a)$ cutoff effects it is referred to as $O(a)$-improvement.

Any lattice gauge action has leading $O(a^2)$ effects by construction. Therefore, in order to have a lattice QCD action free from $O(a)$-effects it is only necessary to improve the fermion lattice action. Even though, motivated by the reduction of the $O(a^2)$ effects, the Symanzik improvement programme has also been applied to the pure gauge theory at tree-level in [43], giving rise to the so called tree-level Symanzik gauge action, and up to one-loop order in [41], with the resulting Lüscher-Weisz gauge action.

In the fermion sector a typical application of the Symanzik improvement programme is in the case of Wilson fermions (cf. Sec. 2.7.2), with the removal of $O(a)$ discretization effects from the action and physically relevant quantities. This gave rise to a widely used formulation known as improved, or clover, Wilson fermions [42] (cf. Sec. 2.7.2). Assuming a lattice with infinite extent in all directions, $O(a)$-improvement of all on-shell spectral quantities is achieved by only adding one counterterm to the lattice action [42, 44]. However, the main drawback of this formulation arises in the computation of hadronic matrix elements, that is, the on-shell non-spectral observables. In this case, improvement counterterms must be added to most of the interpolating fields [42, 44–46] needed in the computation of such on-shell non-spectral quantities. Yet, the application of the improvement programme can be avoided if a different type of Wilson fermions are used, twisted mass Wilson fermions at maximal twist [24] (cf. Sec. 2.7.3). In this case, all on-shell quantities with a finite continuum limit are $O(a)$-improved without the need of adding any counterterm to the action or interpolating fields; this property is known as *automatic* $O(a)$-improvement and it may be shown using the Symanzik improvement programme. The advantage of having automatic $O(a)$-improvement does not come for free, since this formulation breaks flavor and parity symmetries at finite lattice spacing as it will be discussed in more detail below in Sec. 2.7.3.

The way the improvement programme takes place for particular cases will be presented in the corresponding section when needed. Here, just the main concepts are exposed, together with the most general expressions defining the effective Symanzik theory. The procedure explained in the following is based on the strategy introduced in [44]. The continuum local effective action describing the lattice theory close to the continuum limit has the general form

$$S_{\text{eff}} = S_0 + a\,\mathcal{S}_1 + a^2\,\mathcal{S}_2 + \cdots\,, \tag{2.47}$$

where the leading term, S_0, denotes the target continuum action. All other higher dimensional terms account for the description of the cutoff effects of the lattice theory. They can be seen in the continuum effective theory as operator insertions. In terms of the Lagrangian,

$$L_{\text{eff}}(x) = L_0(x) + a\,\mathcal{L}_1(x) + a^2\,\mathcal{L}_2(x) + \cdots\,, \tag{2.48}$$

the effective action may be rewritten in the form

$$S_{\text{eff}} = \int \mathrm{d}^4x\; L_{\text{eff}}(x)\,. \tag{2.49}$$

$L_0(x)$ is the continuum Lagrangian and the terms $\mathcal{L}_k(x)$, $k > 0$, are linear combinations of local composite fields of energy dimension $4 + k$, in order to match the dimension of the continuum Lagrangian. The key point is that all inserted terms, $\mathcal{L}_k(x)$, must have the same symmetries as

the *lattice* theory to be described.

In order to improve correlation functions of local composite fields, that is, improvement beyond spectral quantities, not only the action but also the local interpolating fields entering the expectation value have to be improved. So, an effective description of the lattice interpolating fields is also needed. Given a renormalized, local, gauge invariant composite field,

$$O_{\mathrm{R}}(x) = Z_{\mathrm{O}}\, O(x)\,, \tag{2.50}$$

where $O(x)$ is the bare field and Z_{O} its corresponding renormalization constant, $O_{\mathrm{R}}(x)$ can be described by the local effective theory as

$$O_{\mathrm{eff}}(x) = O_0(x) + a\,\mathcal{O}_1(x) + a^2\,\mathcal{O}_2(x) + \cdots\,, \tag{2.51}$$

with $a^k\mathcal{O}_k(x)$ $(k > 0)$ having the dimension of $O_0(x)$ and $\mathcal{O}_k(x)$ having the symmetries of the corresponding lattice interpolating field. Therefore, given the vacuum expectation value, on the lattice, of a certain interpolating field, O,

$$\langle \mathbf{O}_{\mathrm{R}} \rangle \equiv \langle O_{\mathrm{R}}(x_1) \cdots O_{\mathrm{R}}(x_n) \rangle\,, \tag{2.52}$$

such expectation value can be described in the effective theory by considering the effective description of the lattice action, Eq. (2.49), and the corresponding local composite fields, Eq. (2.51), entering the definition of O. Only connected n-point functions are considered in the following and it is assumed that O does not mix under renormalization. Considering all x_i different from each other (on-shell quantities), the expectation values in Eq. (2.52) are described in the effective theory and up to $O(a)$ discretization effects as,

$$\langle \mathbf{O} \rangle_{\mathrm{eff}} = \langle \mathbf{O}_0 \rangle_0 - a \int \mathrm{d}^4 y\, \langle \mathbf{O}_0 \mathcal{L}_1(y) \rangle_0 + a\, \langle \mathbf{O}_1 \rangle_0 + O(a^2)\,, \tag{2.53}$$

where $\langle \cdot \rangle_0$ denotes the vacuum expectation value in the continuum, using the continuum action S_0, and

$$\mathbf{O}_0 = O_0(x_1) \cdots O_0(x_n)\,, \tag{2.54}$$

$$\mathbf{O}_1 = \sum_{k=1}^{n} O_0(x_1) \cdots \mathcal{O}_1(x_k) \cdots O_0(x_n)\,. \tag{2.55}$$

In Eq. (2.53), besides the explicit dependence on a also the terms $\mathcal{L}_1(x)$ and $\mathbf{O}_1$ depend implicitly on the lattice spacing. These terms are linear combinations of local composite fields, which are independent on the lattice spacing but whose coefficients depend on a. However, the dependence of the coefficients on the lattice spacing is only logarithmic and as a result it does not spoil the arguments of the improvement programme [44]. Also another remark is to be made at this stage. The integration in the variable y in the second term of the r.h.s. of Eq. (2.53) gives place to divergences at all points $y = x_k$ $(k = 1, \cdots, n)$. This is not a problem since such divergences may be reabsorbed in a redefinition of $\mathcal{O}_1(x)$, in the third term of the r.h.s. of Eq. (2.53).

In order to remove the $O(a)$ effects the next step is to determine all possible local composite fields which can contribute to $\mathcal{L}_1(x)$ and $\mathcal{O}_1(x)$. These are all the possible fields with the dimension of $\mathcal{L}_1(x)$ and $\mathcal{O}_1(x)$, respectively, and which moreover have the symmetries of the *lattice* Lagrangian or interpolating field, on each case. In virtue of the assumption of on-shell improvement, the classical continuum field equations may be applied allowing the elimination of several of these terms and thus reducing the number of contributing cases[5]. Additionally, some

[5]The classical field equations only hold at tree-level. However, the argument to eliminate terms using these equations has been proven to hold beyond tree-level [44].

terms may be reabsorbed by a redefinition of the bare parameters of the theory.

In case the final amount of terms contributing to $\mathcal{L}_1(x)$ and $\mathcal{O}_1(x)$ are, respectively, r and $\overline{r}$, the former can be written as a linear combination of such terms with certain coefficients as

$$\mathcal{L}_1(x) = \sum_{i=1}^{r} \mathbf{c}_i \, \mathcal{L}_1^i(x) \,, \tag{2.56}$$

$$\mathcal{O}_1(x) = \sum_{i=1}^{\overline{r}} \overline{\mathbf{c}}_i \, \mathcal{O}_1^i(x) \,. \tag{2.57}$$

Now that the expressions of all terms needed for on-shell $O(a)$-improvement are known in the continuum effective theory, they just need to be translated to the lattice

$$\mathcal{L}_1(x) \longrightarrow L_1(x) = \sum_{i=1}^{r} c_i \, L_1^i(x) \,, \tag{2.58}$$

$$\mathcal{O}_1(x) \longrightarrow O_1(x) = \sum_{i=1}^{\overline{r}} \overline{c}_i \, O_1^i(x) \,, \tag{2.59}$$

and added to the corresponding lattice action,

$$S_{\mathrm{I}} = S + a^5 \sum_x \sum_{i=1}^{r} c_i \, L_1^i(x) \,, \tag{2.60}$$

and interpolating fields (not yet renormalized),

$$O_{\mathrm{I}}(x) = O(x) + a \sum_{i=1}^{\overline{r}} \overline{c}_i \, O_1^i(x) \,. \tag{2.61}$$

Still, the corresponding coefficients of the counterterms have to be non-perturbatively determined such as to guarantee the cancellation of the $O(a)$ effects. For this, certain conditions have to be imposed and the choice of such conditions depends on each particular case, i.e. the particular lattice action and the observable. Additionally, these coefficients are not constant but instead, they depend on the couplings of the theory. Therefore, they should be determined at each value of the lattice spacing, thus at each value of the bare couplings, in the range where the calculations are to be performed. In most cases it is possible to find a parametrization of the coefficients in terms of the bare parameters, in the range of interest, which allows the knowledge of such coefficients at any value within that range. Usually, this is performed at zero value of the quark mass which renders such determinations mass independent. In this case only a dependence on the gauge coupling is left. The same procedure would apply to remove higher order cutoff effects. However, this would not be practical due to the large amount of counterterms appearing, which increases with the order in the a expansion.

2.7. Fermions on the lattice

The fermion action on the lattice can be written as follows,

$$S_{\mathrm{F}}[\psi, \overline{\psi}, U] = a^4 \sum_x \overline{\psi}(x) \, (D + m_0) \, \psi(x) \,, \tag{2.62}$$

with the sum running over all lattice sites. For later purpose, the bare quark mass is denoted as m_0. D is a particular choice of the massless lattice Dirac operator. As already anticipated in previous sections, amongst the various possibilities it is clearly advantageous to choose D in order to have an $O(a)$-improved lattice theory.

Currently, many different lattice fermion actions are available, each with its advantages and drawbacks, so there is not a 'best' one. Amongst these actions, there is a set whose leading cutoff effects are $O(a^2)$ by definition, called chiral formulations, and other for which an $O(a)$-improvement *a la* Symanzik (cf. Sec. 2.6) is needed, called improved formulations. There is still a third possibility, automatic $O(a)$-improved formulations; these are such that the theory is not $O(a)$-improved, but all relevant physical quantities are improved without the need to compute any improvement coefficient. In the following, several lattice formulations for fermions are presented. Not all existing formulations can be described here, so only those relevant for this thesis are discussed. In particular, all formulations here considered preserve *gauge invariance*, *lattice rotations* and *translations* and *charge conjugation*.

2.7.1. Naive discretization

The simplest and straightforward way of discretizing the fermion fields on the lattice is by means of the so called *naive* discretization. In this case, the lattice Dirac operator takes the same form as in the continuum, $D = \gamma_\mu D_\mu$, but with the covariant derivative, D_μ, translated to the lattice,

$$D_\mu = \frac{1}{2}\Big(\overrightarrow{\nabla}^*_\mu + \overrightarrow{\nabla}_\mu\Big)\,. \tag{2.63}$$

This is the lattice symmetric covariant derivative defined in Eq. (A.28) and recalled here for convenience,

$$\frac{1}{2}\Big(\overrightarrow{\nabla}^*_\mu + \overrightarrow{\nabla}_\mu\Big)\psi(x) = \frac{1}{2a}\left[\,U_\mu(x)\,\psi(x+\vec{\mu}) - U_\mu(x-\vec{\mu})^\dagger\,\psi(x-\vec{\mu})\,\right]. \tag{2.64}$$

The naive continuum limit of the fermionic action can be performed by expanding the gauge link

$$U_\mu(x) = e^{aA_\mu(x)}\,, \tag{2.65}$$

in the small a limit,

$$U_\mu(x) = 1 + aA_\mu(x) + O(a^2)\,. \tag{2.66}$$

In this limit the expression of the continuum fermionic action is recovered. This is the minimal requirement that a lattice formulation of the continuum theory has to fulfill. Therefore, it will not be mentioned again when discussing the rest of the fermionic formulations on the lattice, since it should be automatically understood that they lead to the correct continuum fermion action. In this particular formulation, the continuum and the lattice actions differ only by $O(a^2)$ cutoff effects. This is a consequence of the symmetric form of the lattice covariant derivative, Eq. (2.63). This formulation is however not correct for actual lattice computations due to the presence of *doublers*. These are lattice artifacts which compromise the continuum limit of the theory. They occur because the quark propagator in this particular lattice formulation has 16 poles instead of the single pole at $p = (0,0,0,0)$ present in the continuum theory. The 15 unphysical poles (doublers) remain even after the continuum limit has been performed and therefore need to be removed. For an explicit discussion see App. C.1. The direct consequence of the doubling problem is that the naive formulation, even if $O(a)$-improved, can not be used.

2.7.2. Wilson fermions

The first fermion regularization which accounts for the doubling problem was proposed by K. G. Wilson (1975) [20] and it is known as Wilson action. It consists of the naive lattice Dirac operator plus a new term referred to as the Wilson term. The functionality of the Wilson term is to add a contribution to the mass of the doublers that increases as the continuum limit is approached. This leads, in fact, to infinitely heavy doubler fermions in the continuum limit. In this way the heavy doublers decouple from the theory and only the physical pole remains in the continuum limit.

The Wilson action has the form

$$S_{\mathrm{F}}[\psi,\overline{\psi},U] = a^4 \sum_x \overline{\psi}(x)\,(D_{\mathrm{W}} + m_0)\,\psi(x)\,, \tag{2.67}$$

with the massless Wilson-Dirac operator given by

$$D_{\mathrm{W}} = \sum_\mu \frac{1}{2}\left\{\gamma_\mu\left[\nabla^*_\mu + \nabla_\mu\right] - ar\,\nabla^*_\mu\nabla_\mu\right\}. \tag{2.68}$$

The last term in Eq. (2.68) is the Wilson term. In this expression a is the lattice spacing and $0 < r \leq 1$ is the Wilson parameter. The case $r = 0$ corresponds to the naive fermions. In all calculations presented here this parameter will be set to one, which is the usual choice, so, from now on it will not be written any longer. Note that the Wilson term is a lattice artifact and therefore it vanishes in the naive continuum limit.

In Wilson-type formulations it is common to discuss the theory in terms of the hopping parameter, κ, defined as

$$\kappa = \frac{1}{8 + 2am_0}\,, \tag{2.69}$$

instead of the bare quark mass m_0, in the same fashion as β is used instead of the bare gauge coupling g_0. The hopping parameter was shown [47] to be constrained by the bound

$$|\kappa| < \frac{1}{6}\,, \tag{2.70}$$

if physical positivity is to be preserved. This bound is a consequence of one of the Osterwalder-Schrader conditions [48, 49] (cf. App. A.2). Other important issue is the renormalizability of the regularized theory. It has been demonstrated to all orders in perturbation theory that lattice QCD with Wilson fermions is renormalizable [50–54] and it is assumed that it also holds at the non-perturbative level.

***Discrete symmetries of the Wilson action*:**
The discrete symmetries of the lattice theory with Wilson fermions are the following. γ_5-hermiticity, charge conjugation, $\mathcal{C}$, parity, $\mathcal{P}$, and time reversal, $\mathcal{T}$. In this case, therefore, $\mathcal{CPT}$, $\mathcal{CP}$, $\mathcal{CT}$ and $\mathcal{PT}$ are all symmetries, too. A definition of all these symmetries can be found in App. B.1.

***Chiral (continuous) symmetry*:**
The Wilson action is local, has no doublers and a correct naive continuum limit. Therefore, according to the Nielsen-Ninomiya no-go theorem described in Sec. 2.4.2, chiral symmetry must be broken. Indeed, it is explicitly broken by the Wilson term, which transforms under the chiral group [6] (cf. Tab. 2.1) as a mass term. If $N_f = 2$ flavors of quarks are considered, the

[6] See App. B.2.1 for a definition and description of the continuous transformations of the chiral group with

group generators are $T^a = \tau^a/2$ with $a = 1, 2, 3$ (see App. A.3 and A.4 for notations) and the transformation is [7]

$$\overline{\psi}(x)\,[\,\nabla^*_\mu \nabla_\mu\,]\,\psi(x) \overset{\mathrm{SU(2)}_A}{\longrightarrow} \overline{\psi}(x)\,[\,e^{\mathrm{i}\,\alpha^a_{\mathrm{A}}\,\gamma_5\,\tau^a}\,\nabla^*_\mu \nabla_\mu\,]\,\psi(x)\,. \tag{2.71}$$

This means that the total chiral group for $N_f = 2$ mass-degenerate Wilson fermions is

$$\mathrm{SU(2)}_V \times \mathrm{U(1)}_V\,. \tag{2.72}$$

The breaking of chiral symmetry by the Wilson term implies that the Wilson action is not invariant under chiral symmetry even in the massless limit. This explicit breaking has several 'disturbing' consequences; it has as a direct outcome the appearance of $O(a)$ cutoff effects and moreover, the quark mass acquires an *additive* renormalization besides the usual multiplicative renormalization. In this case, the bare quark mass, m_0, is additively renormalized by the counterterm m_{c} as follows

$$m_{\mathrm{q}} = m_0 - m_{\mathrm{c}}\,. \tag{2.73}$$

The counterterm m_{c} is the so called critical mass or critical line and it is linearly divergent with the inverse of the lattice spacing when $a \to 0$. Taking these considerations into account and assuming a mass-independent renormalization scheme, the bare parameters of the theory are then renormalized as follows

$$g^2_{\mathrm{R}}(\mu) = Z_g(g_0^2, a\mu)\, g_0^2(g_0^2, a)\,, \tag{2.74}$$

$$m_{\mathrm{R}}(\mu) = Z_{\mathrm{m}}(g_0^2, a\mu)\, m_{\mathrm{q}}(g_0^2, a)\,. \tag{2.75}$$

Z is the multiplicative renormalization constant of the corresponding quantity and μ the renormalization scale. No deeper discussion will take place here about renormalization, since Chap. 3 is totally devoted to this topic.

With respect to the lattice artifacts, the $O(a)$ cutoff effects can be removed from all on-shell quantities via the Symanzik improvement programme as sketched in Sec. 2.6. The on-shell improved Wilson action or clover action [42] is obtained by the addition of only one counterterm, the clover or Sheikholeslami-Wohlert term, to the standard Wilson action as

$$S_{\mathrm{F}}[\psi, \overline{\psi}, U] = a^4 \sum_x \overline{\psi}(x)\,(D_{\mathrm{WI}} + m_0)\,\psi(x)\,, \tag{2.76}$$

with the improved Wilson Dirac operator (cf. App. C.4.1)

$$D_{\mathrm{WI}} = \sum_\mu \frac{1}{2}\,\{\gamma_\mu\,[\nabla^*_\mu + \nabla_\mu] - ar\,\nabla^*_\mu \nabla_\mu\} + c_{\mathrm{SW}} \frac{i}{4}\,a \sum_{\mu,\nu}\,\sigma_{\mu\nu}\hat{F}_{\mu\nu}\,. \tag{2.77}$$

The first two terms on the r.h.s. of Eq. (2.77) correspond to the standard Wilson operator defined in Eq. (2.68) and the last one is the clover term. The definition of $\sigma_{\mu\nu}$ is given in Eq. (A.11). The coefficient c_{SW} is the Sheikholeslami-Wohlert coefficient and $\hat{F}_{\mu\nu}(x)$ the field strength tensor on the lattice. The choice of this term [44] is

$$\hat{F}_{\mu\nu}(x) = \frac{1}{8a^2}\,\{Q_{\mu\nu}(x) - Q_{\nu\mu}(x)\}, \tag{2.78}$$

$N_f = 2$.

[7] We remind the reader that $\mathrm{SU(2)}_A$ denotes the non-singlet axial-vector transformations of the chiral group, but it does not imply a group structure. See Sec. 2.4 for discussion.

$$\begin{aligned} Q_{\mu\nu}(x) = & \, U_\mu(x)\, U_\nu(x+\vec{\mu})\, U_\mu(x+\vec{\nu})^\dagger\, U_\nu(x)^\dagger \\ & + U_\nu(x)\, U_\mu(x-\vec{\mu}+\vec{\nu})^\dagger\, U_\nu(x-\vec{\mu})^\dagger\, U_\mu(x-\vec{\mu}) \\ & + U_\mu(x-\vec{\mu})^\dagger\, U_\nu(x-\vec{\mu}-\vec{\nu})^\dagger\, U_\mu(x-\vec{\mu}-\vec{\nu})\, U_\nu(x-\vec{\nu}) \\ & + U_\nu(x-\vec{\nu})^\dagger\, U_\mu(x-\vec{\nu})\, U_\nu(x+\vec{\mu}-\vec{\nu})\, U_\mu(x)^\dagger . \end{aligned} \tag{2.79}$$

Once the lattice action has been discussed, both in the standard and the improved formulations, it is also worth to introduce at this point the local interpolating fields taking part in the definition of different physical observables on the lattice. In particular, only those which are needed in following chapters are discussed here. These are the pseudo-scalar density

$$\mathcal{P}^a(x) = \overline{\psi}(x)\, \gamma_5\, \frac{\tau^a}{2}\, \psi(x)\,, \tag{2.80}$$

the axial-vector current

$$\mathcal{A}^a_\mu(x) = \overline{\psi}(x)\, \gamma_\mu\, \gamma_5\, \frac{\tau^a}{2}\, \psi(x) \tag{2.81}$$

and the vector current

$$\mathcal{V}^a_\mu(x) = \overline{\psi}(x)\, \gamma_\mu\, \frac{\tau^a}{2}\, \psi(x)\,. \tag{2.82}$$

After the application of Symanzik improvement programme to these composite fields [44] [55] (cf. App C.4.1), their on-shell improved version is the following

$$(\mathcal{P}_{\rm I})^a(x) = \mathcal{P}^a(x)\,, \tag{2.83}$$

$$(\mathcal{A}_{\rm I})^a_\mu(x) = \mathcal{A}^a_\mu(x) + a\, c_{\rm A}\, \frac{1}{2}\, (\partial^*_\mu + \partial_\mu)\, \mathcal{P}^a(x)\,, \tag{2.84}$$

$$(\mathcal{V}_{\rm I})^a_\mu(x) = \mathcal{V}^a_\mu(x) + a\, c_{\rm V}\, \frac{1}{2}\, (\partial^*_\nu + \partial_\nu)\, \mathcal{T}^a_{\mu\nu}(x)\,, \tag{2.85}$$

with the tensor field defined as

$$\mathcal{T}^a_{\mu\nu}(x) = {\rm i}\, \overline{\psi}(x)\, \sigma_{\mu\nu}\, \frac{\tau^a}{2}\, \psi(x)\,. \tag{2.86}$$

Always assuming a mass-independent renormalization, in order to keep $O(a)$-improvement the bare parameters of the theory have to be renormalized in the following way [44]

$$\widetilde{g}_0^2 = g_0^2\, (1 + b_{\rm g}\, a m_{\rm q})\,, \tag{2.87}$$

$$\widetilde{m}_{\rm q} = m_{\rm q}\, (1 + b_{\rm m}\, a m_{\rm q})\,, \tag{2.88}$$

with the renormalized coupling and mass given by

$$g^2_{\rm R}(\mu) = Z_g(\widetilde{g}_0^2, a\mu)\, \widetilde{g}_0^2(g_0^2, a)\,, \tag{2.89}$$

$$m_{\rm R}(\mu) = Z_{\rm m}(\widetilde{g}_0^2, a\mu)\, \widetilde{m}_{\rm q}(g_0^2, a)\,. \tag{2.90}$$

The improved density and currents defined in Eq. (2.83), (2.84), (2.85), renormalize as [44]

$$(\mathcal{P}_{\rm R})^a(x) = Z_{\rm P}(\widetilde{g}_0^2, a\mu)\, (1 + b_{\rm P}\, a m_{\rm q})\, \mathcal{P}^a(x)\,, \tag{2.91}$$

$$(\mathcal{A}_{\rm R})^a_\mu(x) = Z_{\rm A}(\widetilde{g}_0^2)\, (1 + b_{\rm A}\, a m_{\rm q})\, (\mathcal{A}_{\rm I})^a_\mu(x)\,, \tag{2.92}$$

$$(\mathcal{V}_{\rm R})^a_\mu(x) = Z_{\rm V}(\widetilde{g}_0^2)\, (1 + b_{\rm V}\, a m_{\rm q})\, (\mathcal{V}_{\rm I})^a_\mu(x)\,. \tag{2.93}$$

The additional renormalization factor of the form $(1 + b\, am_{\rm q})$, which appears in all quantities in the improved theory, is a consequence of the reabsorption of certain $O(a)$ counterterms in the Symanzik expansion, as it is explained in App. C.4.1. Therefore, besides the usual counterterms which have to be non-perturbatively tuned to the appropriate values, also these new counterterms, b, need to be determined [46, 56, 57]. In these expressions, the b coefficients are functions of the redefined coupling, $\widetilde{g}_0$, while the coefficients c_i entering the Symanzik expansion (cf. Eq. (2.60)-(2.61)) are functions of the original bare coupling, g_0. For a more detailed discussion in this topic the reader is referred to [44].

2.7.3. Twisted mass Wilson fermions

Twisted mass Wilson QCD [8] is a lattice regularization using Wilson fermions, whose initial classical continuum action is the so called twisted mass QCD action. The twisted mass *continuum* action for $N_f = 2$ mass degenerate quarks has the form

$$S_{\rm F}[\chi, \overline{\chi}, A] = \int {\rm d}^4x\, \overline{\chi}(x)\, (\gamma_\mu\, D_\mu + m\, e^{{\rm i}\alpha\gamma_5\tau^3})\, \chi(x)\,, \tag{2.94}$$

with τ^3 acting in flavor space and the so called polar mass, m, and the twist angle, α, defined as

$$m = \sqrt{m_{\rm q}^2 + \mu_{\rm q}^2}\,, \qquad \alpha = {\rm atan}(\frac{\mu_{\rm q}}{m_{\rm q}})\,. \tag{2.95}$$

Using these definitions, a more common form to write this action is

$$S_{\rm F}[\chi, \overline{\chi}, A] = \int {\rm d}^4x\, \overline{\chi}(x)\, (\gamma_\mu\, D_\mu + m_{\rm q} + {\rm i}\,\mu_{\rm q}\,\gamma_5\,\tau^3)\, \chi(x)\,. \tag{2.96}$$

The parameter $m_{\rm q}$ is the untwisted quark mass and $\mu_{\rm q}$ the twisted quark mass. In case the rotation angle vanishes, $\alpha = 0$, the polar mass is given only by the untwisted mass, $m_{\rm q}$. In the opposite limit, $\alpha = \pi/2$, all contribution to the polar mass comes only from the twisted mass, $\mu_{\rm q}$; this is the so called *maximal twist* condition.

The twisted mass action is obtained from the standard fermion action, Eq. (2.2), by the non-anomalous continuous axial transformation of the fermion fields

$$\psi(x) = e^{{\rm i}\,\frac{\alpha}{2}\,\gamma_5\,\tau^3}\,\chi(x)\,, \qquad \overline{\psi}(x) = \overline{\chi}(x)\, e^{{\rm i}\,\frac{\alpha}{2}\,\gamma_5\,\tau^3}\,. \tag{2.97}$$

Therefore, the two actions are equivalent in the continuum. They are the same action expressed in two different bases, the so called physical basis $\{\psi, \overline{\psi}\}$ and the twisted basis $\{\chi, \overline{\chi}\}$. This implies that at the continuum classical level standard and twisted mass formulations are the same and thus share all the symmetries.

Before to define the theory on the lattice it is important to make a remark; the statement that QCD and twisted mass QCD are equivalent theories beyond the classical level is not trivial at all. It has been shown above that they are equivalent at the classical level. Yet, in order to demonstrate it at the quantum level, a regularization of both formulations is required which preserves chiral symmetry, in particular, the symmetry relating QCD and twisted mass QCD. In principle, any regularization preserving chiral symmetry may be used to show the equivalence between the two formulations. But if a purely non-perturbative demonstration is to be made, then a lattice regularization has to be chosen. In particular, this equivalence was shown in [60] using Ginsparg-Wilson fermions [9].

[8] Reviews on twisted mass lattice QCD: [58, 59].

[9] There is only one constraint in this demonstration; renormalization has to be such that all multiplicative renormalization constants do not depend on the rotation angle α. This can be achieved employing a mass-

Based on universality arguments, it was also argued in [60] that it is expected that any other regularization of twisted mass will still have the same continuum limit. This statement allows then to employ e.g. Wilson fermions as a regulator of QCD in its twisted mass formulation and to still guarantee the universality of the continuum limit. Twisted mass Wilson fermions is indeed proven to be renormalizable to all orders in perturbation theory and it is moreover unitary, reflection positive and ultra-local (only next-neighbor interactions occur).

The twisted mass Wilson action is obtained by regularizing the twisted mass action, Eq. (2.96), with Wilson fermions and it is given by

$$S_{\mathrm{F}}[\chi,\overline{\chi},U] = a^4 \sum_x \overline{\chi}(x)\,(D_{\mathrm{W}} + m_0 + \mathrm{i}\,\mu_{\mathrm{q}}\,\gamma_5\,\tau^3)\,\chi(x)\,. \tag{2.98}$$

In order to preserve physical positivity, the hopping parameter in the twisted mass Wilson formulation with mass-degenerate quarks[10] obeys the same bound as in the case of standard Wilson fermions, Eq. (2.70). The definition of the hopping parameter in twisted mass is also given by Eq. (2.69), so it is only related to the untwisted quark mass, m_0.

Standard Wilson and twisted mass Wilson fermions are not equivalent at non-zero lattice spacing, since they can not be related by the axial transformation that relates the continuum actions. This is the direct consequence of choosing Wilson fermions as a regulator, because the Wilson term is not invariant under the transformations of the chiral group. Stated differently, standard Wilson and twisted mass Wilson fermions are different regularizations of the same continuum theory and as such, they are expected to behave differently at finite lattice spacing and give the same results only in the continuum limit. In particular, this implies that at finite lattice spacing both formulations do not share all the same symmetries and are affected by different lattice artifacts.

***Discrete symmetries of the twisted mass Wilson action*:**

Twisted mass Wilson fermions obey the following discrete symmetries [11]. γ_5-hermiticity with flavor exchange, charge conjugation, $\mathcal{C}$, and space and time reflections with flavor exchange, $\mathcal{P}_{\mathrm{F}}^{1,2}$ and $\mathcal{T}_{\mathrm{F}}^{1,2}$, respectively. Such subgroups of parity and time reversal may equivalently be seen as space and time reflections with a change of sign of the twisted mass as follows, $\widetilde{\mathcal{P}} \equiv \mathcal{P} \times [\mu_{\mathrm{q}} \to -\mu_{\mathrm{q}}]$ and $\widetilde{\mathcal{T}} \equiv \mathcal{T} \times [\mu_{\mathrm{q}} \to -\mu_{\mathrm{q}}]$, respectively.

It is important to realize, first, that the cutoff effects generated by the breaking of these symmetries are only of $O(a^2)$ and they are numerically well under control [62] and, second, that $\mathcal{PT}$, $\mathcal{C}$ and thus $\mathcal{CPT}$ are still symmetries in this formulation.

***Chiral (continuous) symmetry*:**

In the following, with abuse of notation, we denote $\mathrm{SU}(2)_A^a$ the groups $\mathrm{U}(1)_A$ with generator $\tau^a/2$. The notation $\mathrm{SU}(2)_A^a$ is chosen in order to emphasize the different charge sectors, $a = 1,2,3$. Namely, which of the generators, $\tau^a/2$, of the flavor group enters the corresponding $\mathrm{U}(1)_A$ transformation. The reason for using this notation is that in the following discussion a distinction between the charged ($a = 1,2$) and the neutral ($a = 3$) components has to be made. It is important to keep in mind, though, that such notation does *not* mean that $\mathrm{SU}(2)_A^a$ are SU(2) groups. In fact, they are not. The same notation is employed below when discussing such transformations in the twisted basis. In this last case the transformations are also referred to with an additional subscript denoting the rotation angle, α, which is considered to be maximal

independent renormalization scheme, since α is defined through the mass parameters of the Lagrangian.

[10] The case of adding a non-degenerate heavy doublet [61] will not be discussed in this work. The condition on the hopping parameter for non mass-degenerate twisted mass Wilson quarks has been worked out in [58].

[11] See App. B.1 for a definition and description of the discrete symmetries.

in this case, $\pi/2$. A definition and description of the continuous transformations of the chiral group with $N_f = 2$ in the standard and twisted bases is given in App. B.2. The symmetries in the twisted basis take an unusual form. For a better reading we recall, when needed in the present section, the transformations in the twisted basis.

Due to the use of Wilson fermions as a regulator of the theory, chiral symmetry, as we denoted $\mathrm{SU}(2)_A$ if assuming a theory with $N_f = 2$, is broken by the Wilson term, as it was already explained above in Sec. 2.7.2. There it was also mentioned that the untwisted quark mass, m_0, behaves under the transformations of the chiral group in the same way as the Wilson term. In the present formulation, however, there is an additional mass term, the twisted mass, whose role under chiral transformations differs from the one of the Wilson term. The twisted mass term also breaks chiral symmetry, yet it still remains invariant under the charged sector, which is denoted here as $\mathrm{SU}(2)^{1,2}_A$. Such transformations are as follows,

$$\begin{aligned} \overline{\chi}(x)\,[\mathrm{i}\,\mu_\mathrm{q}\,\gamma_5\,\tau^3]\,\chi(x) \;&\overset{\mathrm{SU}(2)^{1,2}_A}{\longrightarrow}\; \overline{\chi}(x)\,[\mathrm{i}\,\mu_\mathrm{q}\,\gamma_5\,\tau^3]\,\chi(x) \\ &\overset{\mathrm{SU}(2)^{3}_A}{\longrightarrow}\; \overline{\chi}(x)\,[e^{\mathrm{i}\,\alpha^3_\mathrm{A}\,\gamma_5\,\tau^3}\,\mathrm{i}\,\mu_\mathrm{q}\,\gamma_5\,\tau^3]\,\chi(x)\,. \end{aligned} \tag{2.99}$$

Therefore, comparing Eq. (2.99) and Eq. (2.71) it is clear that the twisted mass term and the Wilson term behave 'orthogonally' with respect to the *charged* sector of chiral symmetry. Orthogonally here means that while the twisted mass term remains invariant under the charged transformations the Wilson term does not.

This can also be argued in terms of the twisted symmetries (at maximal twist). In particular, the neutral sector of chiral symmetry takes the usual form,

$$[\mathrm{SU}(2)^3_A]_{\frac{\pi}{2}} : \begin{cases} \chi(x) \;\to\; e^{\mathrm{i}\,\frac{\alpha^3_A}{2}\,\gamma_5\,\tau^3}\,\chi(x) \\ \overline{\chi}(x) \;\to\; \overline{\chi}(x)\,e^{\mathrm{i}\,\frac{\alpha^3_A}{2}\,\gamma_5\,\tau^3} \end{cases} \tag{2.100}$$

while the charged sector rotates to,

$$[\mathrm{SU}(2)^{1,2}_A]_{\frac{\pi}{2}} : \begin{cases} \chi(x) \;\to\; e^{\pm\mathrm{i}\,\frac{\alpha^{1,2}_A}{2}\,\tau^{2,1}}\,\chi(x) \\ \overline{\chi}(x) \;\to\; \overline{\chi}(x)\,e^{\mp\mathrm{i}\,\frac{\alpha^{1,2}_A}{2}\,\tau^{2,1}}\,. \end{cases} \tag{2.101}$$

In this case, the transformations for the Wilson term are

$$\begin{aligned} \overline{\chi}(x)\,[\,\nabla^*_\mu\nabla_\mu\,]\,\chi(x) \;&\overset{[\mathrm{SU}(2)^{1,2}_A]_{\pi/2}}{\longrightarrow}\; \overline{\chi}(x)\,[\,\nabla^*_\mu\nabla_\mu\,]\,\chi(x) \\ &\overset{[\mathrm{SU}(2)^{3}_A]_{\pi/2}}{\longrightarrow}\; \overline{\chi}(x)\,[\,e^{\mathrm{i}\,\alpha^3_\mathrm{A}\,\gamma_5\,\tau^3}\,\nabla^*_\mu\nabla_\mu\,]\,\chi(x)\,, \end{aligned} \tag{2.102}$$

and for the twisted mass term

$$\begin{aligned} \overline{\chi}(x)\,[\mathrm{i}\,\mu_\mathrm{q}\,\gamma_5\,\tau^3]\,\chi(x) \;&\overset{[\mathrm{SU}(2)^{1,2}_A]_{\pi/2}}{\longrightarrow}\; \overline{\chi}(x)\,[e^{\mp\mathrm{i}\,\alpha^{1,2}_\mathrm{A}\,\tau^{2,1}}\,\mathrm{i}\,\mu_\mathrm{q}\,\gamma_5\,\tau^3]\,\chi(x) \\ &\overset{[\mathrm{SU}(2)^{3}_A]_{\pi/2}}{\longrightarrow}\; \overline{\chi}(x)\,[e^{\mathrm{i}\,\alpha^3_\mathrm{A}\,\gamma_5\,\tau^3}\,\mathrm{i}\,\mu_\mathrm{q}\,\gamma_5\,\tau^3]\,\chi(x)\,. \end{aligned} \tag{2.103}$$

In terms of the twisted symmetries, the twisted mass term is not invariant under chiral transformations (Eq. (2.103)) while the Wilson term is still invariant under the transformations of the charged sector (first line of Eq. (2.102)). This again makes evident the orthogonality between the two terms with respect to the charged sector of chiral symmetry. Moreover, an interesting observation is that the twisted mass term transforms in the twisted basis as a standard mass in

the standard basis.

***Isospin (continuous) symmetry*:**
In discussing the isospin transformations, exactly the same notations as in the discussion of chiral symmetry are employed concerning the symmetries in the twisted basis and the different charge sectors of the total isospin group $\mathrm{SU}(2)_V$. As before, a description of all these symmetries and notations can be found in App. B.2.

Differently to what happens in the standard formulation of Wilson fermions, where $\mathrm{SU}(2)_V$ is a symmetry of the theory when mass degenerate quarks are assumed, such symmetry is broken in the lattice theory with twisted mass Wilson fermions. This is due to the presence of the twisted mass term, which is not invariant under the charged transformations of isospin denoted here as $\mathrm{SU}(2)_V^{1,2}$. This is shown by

$$\begin{aligned}\overline{\chi}(x)\,[\mathrm{i}\,\mu_\mathrm{q}\,\gamma_5\,\tau^3]\,\chi(x) \;&\overset{\mathrm{SU}(2)_V^{1,2}}{\longrightarrow}\; \overline{\chi}(x)\,[e^{-\mathrm{i}\,\alpha_\mathrm{V}^{1,2}\,\tau^{1,2}}\,\mathrm{i}\,\mu_\mathrm{q}\,\gamma_5\,\tau^3]\,\chi(x)\\ &\overset{\mathrm{SU}(2)_V^{3}}{\longrightarrow}\; \overline{\chi}(x)\,[\mathrm{i}\,\mu_\mathrm{q}\,\gamma_5\,\tau^3]\,\chi(x)\,.\end{aligned} \tag{2.104}$$

This implies that also with respect to the charged sector of isospin symmetry the twisted mass and Wilson terms behave orthogonally. While the Wilson term is invariant under isospin transformations the twisted mass term is invariant only under the transformations of the neutral sector.

We can argue once more in terms of the twisted symmetries at maximal twist. The transformation in the neutral sector is the same as in the standard case,

$$[\mathrm{SU}(2)_V^3]_{\frac{\pi}{2}}:\begin{cases}\chi(x) \;\to\; e^{\mathrm{i}\,\frac{\alpha_V^a}{2}\,\tau^a}\,\chi(x)\\ \overline{\chi}(x) \;\to\; \overline{\chi}(x)\,e^{-\mathrm{i}\,\frac{\alpha_V^a}{2}\,\tau^a}\end{cases} \tag{2.105}$$

while the transformation for the charged sector takes the form

$$[\mathrm{SU}(2)_V^{1,2}]_{\frac{\pi}{2}}:\begin{cases}\chi(x) \;\to\; e^{\pm\mathrm{i}\,\frac{\alpha_V^{1,2}}{2}\,\gamma_5\,\tau^{2,1}}\,\chi(x)\\ \overline{\chi}(x) \;\to\; \overline{\chi}(x)\,e^{\pm\mathrm{i}\,\frac{\alpha_V^{1,2}}{2}\,\gamma_5\,\tau^{2,1}}\,.\end{cases} \tag{2.106}$$

Using these expressions the Wilson term transforms as

$$\begin{aligned}\overline{\chi}(x)\,[\,\nabla_\mu^*\nabla_\mu\,]\,\chi(x) \;&\overset{[\mathrm{SU}(2)_V^{1,2}]_{\pi/2}}{\longrightarrow}\; \overline{\chi}(x)\,[\,e^{\pm\mathrm{i}\,\alpha_\mathrm{V}^{1,2}\,\gamma_5\,\tau^{2,1}}\,\nabla_\mu^*\nabla_\mu\,]\,\chi(x)\\ &\overset{[\mathrm{SU}(2)_V^{3}]_{\pi/2}}{\longrightarrow}\; \overline{\chi}(x)\,[\,\nabla_\mu^*\nabla_\mu\,]\,\chi(x)\,,\end{aligned} \tag{2.107}$$

and the twisted mass term

$$\begin{aligned}\overline{\chi}(x)\,[\mathrm{i}\,\mu_\mathrm{q}\,\gamma_5\,\tau^3]\,\chi(x) \;&\overset{[\mathrm{SU}(2)_V^{1,2}]_{\pi/2}}{\longrightarrow}\; \overline{\chi}(x)\,[\mathrm{i}\,\mu_\mathrm{q}\,\gamma_5\,\tau^3]\,\chi(x)\\ &\overset{[\mathrm{SU}(2)_V^{3}]_{\pi/2}}{\longrightarrow}\; \overline{\chi}(x)\,[\mathrm{i}\,\mu_\mathrm{q}\,\gamma_5\,\tau^3]\,\chi(x)\,.\end{aligned} \tag{2.108}$$

The twisted mass term is invariant under the twisted isospin transformations (Eq. (2.108)) while the Wilson term is invariant only with respect to the neutral sector (second line of Eq. (2.107)). Again, it is evident that both terms are orthogonal with respect to the charged sector of isospin. Also with respect to isospin symmetry the twisted mass term transforms in the twisted basis as a standard mass (degenerate) term does in the standard basis. An additional comment should be

Standard Wilson	Twisted mass Wilson
Discrete symmetries	
$\mathcal{C}, \mathcal{P}, \mathcal{T}$	$\mathcal{C}, \mathcal{P}_F^{1,2}, \mathcal{T}_F^{1,2}$
$\mathcal{PT}$	$\mathcal{PT}$
$\mathcal{CPT}$	$\mathcal{CPT}$
γ_5-hermiticity	$\gamma_5\tau^{1,2}$-hermiticity
Continuous symmetry group	
$\mathrm{SU}(2)_V \times \mathrm{U}(1)_V$	$\mathrm{SU}(2)_V^3 \times \mathrm{U}(1)_V$

Table 2.2.: Symmetries of Wilson and twisted mass Wilson fermions, with mass degeneracy. For notation and definition of the symmetries see App. B.1 and App. B.2.

made here. From this discussion of isospin symmetry in the twisted basis it is clear that isospin is a symmetry of *continuum* twisted mass QCD. In that case, there is no Wilson term thus no breaking of twisted isospin symmetry takes place. This makes stronger the argumentation that QCD and twisted mass QCD share all the symmetries in the classical continuum theory. Moreover, the same would hold in any regularization which does not break chiral symmetry.

Thus, with respect to standard Wilson fermions, certain discrete symmetries are partially lost, $\mathcal{P}$ and $\mathcal{T}$, and the continuous non-singlet isospin group is also reduced to the group $\mathrm{U}(1)_V$ with generator $\tau^3/2$. All this, assuming a theory with $N_f = 2$ mass degenerate quarks. The relation between the symmetries in these two regularizations of QCD is summarized in Tab. 2.2.

The breaking of parity and isospin symmetries is translated in cutoff effects of $O(a^2)$, which therefore do not spoil automatic $O(a)$-improvement. However, while the cutoff effects originated by the breaking of parity are numerically well under control, the lattice artifacts generated by the breaking of isospin symmetry (e.g. neutral-charged pion splitting at finite lattice spacing) need a special attention. See [62] for a discussion. Other characteristic of this formulation is that it can describe only an even number of quark flavors. Yet, it has still several advantages; the first one is related to the problem of exceptional configurations and it was indeed one of the reasons to introduce the twisted mass term in the QCD action [60, 63–65]. The reason is that the twisted mass provides an IR-cutoff to the theory, so the spectrum of the lattice Dirac operator has a positive bound when working at a finite value of the twisted mass parameter, μ_q, even if very close to the chiral limit. Therefore, no zero modes happen in this formulation and thus quenched simulations can be safely performed (cf. App. C.2). Still, in infinite volume phenomena related to phase transitions may spoil the conclusion that no lower limit for the value of the twisted quark mass exists. This is a very involved subject in itself which is much beyond the purpose of this thesis.

Important publications concerning twisted mass Wilson fermions took place [60, 66, 67] although the main advantage was shown for first time in [24]; when working at *maximal twist* all on-shell quantities with a finite continuum limit are $O(a)$-improved, without the addition of any improvement counterterm to the action and the interpolating fields. This property is referred to as *automatic $O(a)$-improvement*. As a result, using twisted mass Wilson fermions at maximal twist, it is possible to compute quantities on the lattice which have leading $O(a^2)$ discretization effects, as it would be the case of a chiral formulation of fermions, but still maintaining the cheap cost of simulations characteristic of Wilson-type fermions. The condition of maximal twist means to have a quark mass that is fully given by the twisted quark mass, which corresponds to a setup in which the physical untwisted quark mass vanishes. Due to the breaking of chiral symmetry by the Wilson term, the bare untwisted quark mass can not by simply set to zero but, instead, it acquires an additive renormalization. In this situation, the maximal twist condition is achieved via a non-perturbative tuning of the bare untwisted quark mass to some critical value, which

guarantees that the physical untwisted quark mass vanishes. This procedure will be described in very much detail in following chapters. At the moment, it is important to keep in mind that automatic $O(a)$-improvement is realized only at expenses of tuning non-perturbatively *one* parameter (the bare untwisted quark mass) and giving up certain symmetries at non-zero lattice spacing, which are restored in the continuum limit and whose breaking generates lattice artifacts of only $O(a^2)$. All these properties render twisted mass Wilson QCD a valuable regularization of QCD on the lattice. Automatic $O(a)$-improvement of twisted mass Wilson fermions at maximal twist can be shown in several manners [24, 68–70]. A detailed proof is recalled here in App. C.5.

The renormalizability properties of twisted mass lattice QCD are on the same footing as those of standard Wilson QCD (cf. Sec. 2.7.2). The reason behind this statement is that the difference between the two regularizations is the appearance of the twisted mass term in the former case, which does not modify the power counting. From the study of all possible counterterms with the symmetries of the lattice action (twisted mass Wilson) which have dimension less or equal four it is deduced that in a mass-independent renormalization scheme the bare parameters renormalize as

$$g_{\mathrm{R}}^2(\mu) = Z_{\mathrm{g}}(\widetilde{g}_0^2, a\mu)\, \widetilde{g}_0^2(g_0^2, a)\,, \tag{2.109}$$

$$m_{\mathrm{R}}(\mu) = Z_{\mathrm{m}}(\widetilde{g}_0^2, a\mu)\, \widetilde{m}_{\mathrm{q}}(g_0^2, a)\,, \tag{2.110}$$

$$\mu_{\mathrm{R}}(\mu) = Z_{\mu}(\widetilde{g}_0^2, a\mu)\, \widetilde{\mu}_{\mathrm{q}}(g_0^2, a)\,. \tag{2.111}$$

Like with standard Wilson fermions, in order to have $O(a)$-improvement with a renormalization scheme which is mass-independent a rescaling of the bare parameters is needed

$$\widetilde{g}_0^2 = g_0^2\,(1 + b_{\mathrm{g}}\, a m_{\mathrm{q}})\,, \tag{2.112}$$

$$\widetilde{m}_{\mathrm{q}} = m_{\mathrm{q}}\,(1 + b_{\mathrm{m}}\, a m_{\mathrm{q}}) \,+\, \widetilde{b}_{\mathrm{m}}\, a\mu_{\mathrm{q}}^2\,, \tag{2.113}$$

$$\widetilde{\mu}_{\mathrm{q}} = \mu_{\mathrm{q}}\,(1 + b_{\mu}\, a m_{\mathrm{q}})\,. \tag{2.114}$$

Here, m_{q} is the additively renormalized bare quark mass characteristic of Wilson formulations and defined in Eq. (2.73). On the contrary, the twisted mass renormalizes only multiplicatively.

In case of working *at maximal twist* all the renormalization terms of the type $(1 + b\, a m_{\mathrm{q}})$ are absent from any quantity. This is because in this limit m_{q} assumes a zero value up to $O(a)$ effects. Thus

$$\widetilde{g}_0^2 = g_0^2 \,+\, O(a^2)\,, \tag{2.115}$$

$$\widetilde{m}_{\mathrm{q}} = m_{\mathrm{q}} \,+\, \widetilde{b}_{\mathrm{m}}\, a\mu_{\mathrm{q}}^2 \,+\, O(a^2)\,, \tag{2.116}$$

$$\widetilde{\mu}_{\mathrm{q}} = \mu_{\mathrm{q}} \,+\, O(a^2)\,. \tag{2.117}$$

The only remaining improvement coefficient, $\widetilde{b}_{\mathrm{m}}$, has been proven to be redundant [67]. This means that an important advantage is achieved if using twisted mass fermions at maximal twist. In this case no improvement counterterm takes place and the renormalization of the parameters and interpolating fields of the theory can be defined as usual,

$$\begin{aligned} g_{\mathrm{R}}^2(\mu) &= Z_{\mathrm{g}}(g_0^2, a\mu)\, g_0^2(g_0^2, a)\,, \\ m_{\mathrm{R}}(\mu) &= Z_{\mathrm{m}}(g_0^2, a\mu)\, m_{\mathrm{q}}(g_0^2, a)\,, \\ \mu_{\mathrm{R}}(\mu) &= Z_{\mu}(g_0^2, a\mu)\, \mu_{\mathrm{q}}(g_0^2, a)\,. \end{aligned} \tag{2.118}$$

Concerning the interpolating fields, some explanation is needed [12]. The interpolating fields in

[12] Fields in the physical basis are always denoted with calligraphic style and fields in the twisted basis are denoted

the twisted basis take exactly the same form as in the physical basis, but keeping in mind that these are fields in the twisted basis. These definitions are for the chiral multiplet of densities,

$$P^a(x) = \overline{\chi}(x)\,\gamma_5\,\frac{\tau^a}{2}\,\chi(x)\,, \tag{2.119}$$

$$S^0(x) = \overline{\chi}(x)\chi(x)\,, \tag{2.120}$$

and the chiral multiplet of currents,

$$A^a_\mu(x) = \overline{\chi}(x)\,\gamma_\mu\,\gamma_5\,\frac{\tau^a}{2}\,\chi(x)\,, \tag{2.121}$$

$$V^a_\mu(x) = \overline{\chi}(x)\,\gamma_\mu\,\frac{\tau^a}{2}\,\chi(x)\,. \tag{2.122}$$

Now, from the non-singlet axial rotation relating twisted mass and standard QCD the interpolating fields in one basis can be related to the fiels in the other basis. The relation is such that the fields in one basis are written as linear combinations of fields of the same chiral multiplet in the other basis. This happens as follows for the multiplet of densities,

$$\mathcal{P}^a = \overline{\psi}(x)\,\gamma_5\,\frac{\tau^a}{2}\,\psi(x) \;=\; \begin{cases} P^a & (a=1,2)\,, \\ \cos(\alpha)\,P^3 + \mathrm{i}\sin(\alpha)\,\frac{1}{2}\,S^0 & (a=3)\,, \end{cases} \tag{2.123}$$

$$\mathcal{S}^0 = \overline{\psi}(x)\psi(x) = \cos(\alpha)\,S^0 + 2\mathrm{i}\sin(\alpha)\,P^3\,, \tag{2.124}$$

and for the multiplet of currents,

$$\mathcal{A}^a_\mu = \overline{\psi}(x)\,\gamma_\mu\,\gamma_5\,\frac{\tau^a}{2}\,\psi(x) \;=\; \begin{cases} \cos(\alpha)\,A^a_\mu + \epsilon^{3ab}\sin(\alpha)\,V^b_\mu & (a=1,2)\,, \\ A^3_\mu & (a=3)\,, \end{cases} \tag{2.125}$$

$$\mathcal{V}^a_\mu = \overline{\psi}(x)\,\gamma_\mu\,\frac{\tau^a}{2}\,\psi(x) \;=\; \begin{cases} \cos(\alpha)\,V^a_\mu + \epsilon^{3ab}\sin(\alpha)\,A^b_\mu & (a=1,2)\,, \\ V^3_\mu & (a=3)\,. \end{cases} \tag{2.126}$$

In the case of twisted mass at maximal twist, where automatic $O(a)$-improvement is at work, the renormalization of the interpolating fields is as follows,

$$(P_{\mathrm{R}})^a(x) = Z_{\mathrm{P}}(g_0^2, a\mu)\,(P^a(x) + \delta^{a3}\,\mu_{\mathrm{q}} c_{\mathrm{P}} a^{-2})\,, \tag{2.127}$$

$$(S_{\mathrm{R}})^0(x) = Z_{\mathrm{S}}(g_0^2, a\mu)\,S^0(x)\,, \tag{2.128}$$

$$(A_{\mathrm{R}})^a_\mu(x) = Z_{\mathrm{A}}(g_0^2)\,A^a_\mu(x)\,, \tag{2.129}$$

$$(V_{\mathrm{R}})^a_\mu(x) = Z_{\mathrm{V}}(g_0^2)\,V^a_\mu(x)\,. \tag{2.130}$$

Through this chapter, the renormalization of QCD has been discussed only formally and no mention of any specific renormalization scheme has been made so far. In the following chapters the renormalization of QCD is discussed in detail. In particular, the case of a mass-independent non-perturbative renormalization scheme will be treated. The interest goes in finding a renormalization scheme which is suitable to renormalize bare quantities computed using twisted mass Wilson fermions at maximal twist. It is clear that the minimal requirement is that such a renormalization scheme preserves the property of automatic $O(a)$-improvement.

with normal letters.

3. Non-perturbative renormalization of QCD

QCD is the quantum field theory which describes the strong interactions. On short distance scales, the fields of the theory experience large quantum fluctuations, which give rise to ultraviolet (UV) divergences. The UV divergences render the theory ill-defined and, in particular, imply that quantum fluctuations contribute to every process at any value of the energy scale. The important observation is that the UV divergences can be cancelled, so that QCD remains well-defined. The cancellation of the UV divergences is achieved through a renormalization of the parameters of the Lagrangian and it is referred to as UV-renormalization.

A necessary first step in the renormalization of the theory is the introduction of an UV-regulator. As discussed in Chap. 2, we have chosen a lattice regularization, which allows for a non-perturbative treatment of QCD. In lattice QCD, the theory is regularized imposing an upper cutoff, Λ, to the momenta, which is proportional to the inverse of the lattice spacing, $\Lambda = \pi/a$. The cutoff implies that the theory remains finite at any value of the momenta below the cutoff. This allows the computation of physical quantities, in the regularized theory, which are functions of the cutoff and take finite values. However, in order to make contact to experimental results first the cutoff has to be removed. In lattice terminology, the continuum limit has to be performed (cf. Sec. 2.5). Yet, before to perform the continuum limit, the parameters of the Lagrangian have to be renormalized, as otherwise divergences appear in several physical quantities, which render the theory unphysical.

Initially, QCD is defined in terms of the bare fields and the bare couplings appearing in the Lagrangian; the bare gauge coupling g_0, the bare quark masses m_0^i and the bare matter fields ψ. Conceptually, what renormalization does is to cancel the divergences of the theory by an adjustment of the parameters in the Lagrangian. It relates the bare couplings and fields to their so called renormalized counterparts, which are well-defined quantities. Therefore, after renormalization takes place, all physical quantities remain finite and the continuum limit can be performed, obtaining a well defined physical answer which can be directly compared to experimental results. A priori, many renormalized quantities depend on the renormalization scale μ. The way scale-dependent quantities depend on the renormalization scale is described by the renormalization group (cf. Sec. 3.3.3). Additionally, due to the introduction of a regulator, scale-independent renormalizations of certain quantities might be required. This corresponds to the renormalization of certain finite bare functions of the cutoff which do not diverge when the cutoff is removed. Finite-renormalizations arise as a consequence of the breaking of symmetries of the quantum continuum theory by the regularization. In particular in this thesis we are only concerned with the problem of scale-dependent renormalizations.

The choice of the renormalization procedure is not unique. In particular, the description of the non-perturbative regime of QCD provided by lattice QCD is something which should not be lost in the renormalization procedure, therefore, it is very important to find a proper *non-perturbative renormalization* scheme. In addition, the scheme should be such that perturbation theory may also be applied. This would make possible the determination of the fundamental parameters of QCD, the Λ-parameter and the RGI quark masses M, as well as the renormalization of composite operators, which can then be related to other more common renormalization schemes, e.g. $\overline{\text{MS}}$, allowing for a direct comparison to experimental results. In general, for perturbation theory to be applicable the energy scale should be large enough, $\mu \sim 10\,\text{GeV}$. Such an energy scale is, however, rather difficult to realize on the lattice. The first limitation is that the value of the

cutoff should be large enough compared to the energy scale,

$$\mu \ll 1/a\,, \tag{3.1}$$

in order to guarantee sufficiently small discretization effects and thus, a reliable extrapolation to the continuum limit. The second restriction is that the physical size of the lattice, L, has to be large enough to avoid finite size effects. This restriction is given typically by the confinement scale (cf. App. C.3, Eq. (C.13)) in pure gauge theories,

$$L \gg \sigma^{-1/2} \sim 2.5\,\mathrm{GeV}^{-1} \sim 0.5\,\mathrm{fm} \tag{3.2}$$

and by the inverse pion mass in full QCD,

$$L \gg m_\pi^{-1} \sim 7\,\mathrm{GeV}^{-1} \sim 1.4\,\mathrm{fm}\,. \tag{3.3}$$

Considering μ to take a value in the perturbative regime, the previous conditions summarize as follows for the pure gauge theory,

$$L \gg 2.5\,\mathrm{GeV}^{-1} \gg \frac{1}{\mu} \sim 0.1\,\mathrm{GeV}^{-1} \gg a \tag{3.4}$$

and for full QCD,

$$L \gg 7\,\mathrm{GeV}^{-1} \gg \frac{1}{\mu} \sim 0.1\,\mathrm{GeV}^{-1} \gg a\,. \tag{3.5}$$

These relations require simulations with a number of lattice points of the order $N \gg 25$ (pure gauge) or $N \gg 70$ (full QCD), which is certainly not possible with the present computational resources, at least when considering full QCD. As a result, in order to simulate reasonable lattices, $N \sim 32 - 64$, while keeping finite size effects under control, the lattice spacing has to be restricted to the order of $(0.08 - 0.04)\,\mathrm{fm}$ (equivalent to $L \sim 2.5\,\mathrm{fm} \sim 12.7\,\mathrm{GeV}^{-1}$), which automatically induces a more constrained upper cutoff in the energy scale which can be reached if the requirement of a reliable continuum limit is to be kept. On the other hand, for too small values of the energy scale non-perturbative effects might become important and therefore, it becomes questionable whether a safe contact to perturbation theory can be made. Fortunately, as it will be discussed below, there are certain non-perturbatively defined renormalization schemes bypassing the problem of scale differences on the lattice.

There are several non-perturbative renormalization schemes which can be applied in lattice QCD. Hadronic schemes are typically used in lattice computations but these are related to the low energy range of QCD. Consequently, such schemes do not allow to bridge all the energy range up to the perturbative region. For this last purpose, *finite volume* schemes [11] are a possible choice. They are not the only possibility, but is the only case considered in this work. Finite volume schemes are very useful in lattice QCD and allow naturally to make contact to perturbation theory; they allow to bridge a wide range of energies from hadronic scales up to the pure perturbative regime overcoming the problem of scale differences contained in Eq. (3.4)-(3.5). As a result, the scale evolution of any scale-dependent quantity can be traced between two energy regions far apart and therefore, an understanding of how the transition between perturbative and non-perturbative regimes takes place becomes possible. It gives information of, for instance, up to which energies perturbation theory is reliable and where the non-perturbative effects start to become important. The reason this evolution is feasible is because finite volume schemes identify the physical size of the system L (which can be considered as a finite size effect) with the renormalization scale μ as follows,

$$\mu = 1/L\,. \tag{3.6}$$

In this manner, the energy is increased towards the perturbative regime by decreasing L. This reduction of L is performed in a number of finite steps. Each step is small enough such that it does not imply large scale differences and moreover, the condition to have small discretization errors is relaxed to $L/a \gg 1$ at each step; since L is to be kept fixed, the condition $L/a \gg 1$ corresponds to being close to the continuum limit. Once the perturbative regime is reached, perturbation theory can be safely applied and contact to other perturbative schemes can be made.

The utility of connecting low to high energies becomes transparent if the scheme is used on a lattice. At low energies the lattice spacing can be expressed in physical units using hadronic observables determined experimentally. This procedure is called 'to set the scale' and it will be discussed in Sec. 3.3.2 in the context of hadronic scheme renormalization. At high energies one can perform a matching to other renormalization schemes, like the $\overline{\mathrm{MS}}$, which are amenable to a direct comparison with experimental results. As a result, finite volume schemes act as intermediate schemes that provide a direct relation between non-perturbative hadronic observables and other intrinsically perturbative schemes which are usually adopted to parametrize experimental data. These techniques are referred to as finite size techniques and are summarized in Fig. 3.1. Amongst important applications of these techniques are the determination of the fundamental

	INFINITE VOLUME		FINITE VOLUME
PT:	$\mu \sim 10\,\mathrm{GeV} \sim (0.02\,\mathrm{fm})^{-1}$	$\overset{\text{conversion}}{\longleftarrow}$	Λ_{SF}, M
			$\uparrow$
			$\uparrow$ Perturbative evolution
			$\uparrow$
			$\mathrm{SF}(\mu = s^n/L_{\max})$
			$\uparrow$
			$\uparrow$ Non-perturbative evolution
			$\uparrow$
			$\mathrm{SF}(\mu = s/L_{\max})$
			$\uparrow$
HS:	$L_{\max} \sim 0.5\,\mathrm{fm} \sim (0.4\,\mathrm{GeV})^{-1}$	$\overset{\text{matching}}{\longrightarrow}$	$\mathrm{SF}(\mu = 1/L_{\max})$

Figure 3.1.: The strategy for a non-perturbative renormalization via the SF. The scaling factor 's' is typically chosen to be s=2.

parameters of QCD (the Λ-parameter and the RGI quark masses M) which can be obtained from the knowledge of the scale dependence of the running coupling, $\alpha(\mu)$, and of the running quark masses $\overline{m}(\mu)$. These techniques can be also applied to the renormalization of composite operators arising in the application of the OPE (operator product expansion). A detailed explanation on how these techniques are applied is given below in Sec. 3.3.

For finite volume schemes to be useful in practical applications, the renormalization conditions defined through the scheme must fulfill the following requirements; small statistical uncertainty when computed in MC simulations, small discretization errors and a perturbative expansion such that an early contact to the numerical data can be made at not too small couplings. Moreover, it is desirable that the renormalization scheme maintains gauge invariance and, when improvement is at work, also respects on-shell improvement. A priori, there are many ways of defining

finite volume schemes. A particular kind of finite volume schemes which enjoy all the previous requirements are the so called Schrödinger functional (SF) schemes [12] (cf. Sec. 3.2). Within these schemes renormalization takes place through the Schrödinger functional of QCD which, in its *standard* form, has been proposed first in [12–14] for the pure gauge theory and extended to full QCD in [15–17]. It has been successfully applied mainly by the ALPHA collaboration but also by other groups, e.g. [71–74]. We will discuss later the precise formulation of the Schrödinger functional and explain in detail how it is applied for a non-perturbative renormalization of QCD on the lattice. In this work, the standard form is denoted as SF in order to distinguish it from two other more recent formulations of such schemes. One is the so called *chirally rotated Schrödinger functional* scheme, which is denoted as χSF and has been discussed first in [18]. The other is here referred to as γ_5-*Schrödinger functional* (γ_5SF) which was introduced in [19]. The main purpose of these new formulations is to have a SF-like renormalization scheme which can be applied to the computation of renormalization constants of bare quantities obtained using twisted mass Wilson fermions at maximal twist (cf. Sec. 2.7.3) and with the main target to maintain automatic $O(a)$-improvement in the renormalization procedure. Even if the γ_5SF is briefly discussed and analytically studied in this thesis, the central goal is to study the χSF scheme, for reasons that will become clear later. In particular, the study is concerned with the applicability of the χSF in the computation of renormalization constants of physical observables and the demonstration of the validity of the χSF, by comparing the continuum limit of physical quantities obtained from the SF and the χSF schemes. The results here presented have been computed only in the quenched approximation (cf. Sec. 2.3), since this is a natural first step towards the understanding of the validity of a new development on the lattice.

The chapter is structured as follows. In Sec. 3.1, the Ward-Takahashi identities are discussed. In Sec. 3.2 we describe the Schrödinger functional (SF) and its use as a non-perturbative renormalization scheme. In Sec. 3.4 it is discussed how correlation functions are defined within the SF. The chapter is concluded in Sec. 3.5 with the motivation of the chirally rotated SF (χSF).

3.1. Ward-Takahashi identities

The Ward-Takahashi or Ward identities (WI) are identities between correlation functions. The WI originate from transformations of the fields integrated over in the path integral and express the behavior of the path integral under such transformations of the fields. They are the quantum counterparts of the Nöther conservation laws in classical field theory and remain valid after the renormalization of the theory. In particular, the WI indicate whether a symmetry is broken or not.

Considering continuum QCD with $N_f = 2$ flavors of quarks and given an interpolating field O, its vacuum expectation value is given by the path integral (cf. Sec. 2.3)

$$\langle O \rangle = \frac{1}{Z} \int \mathcal{D}[\psi, \overline{\psi}, A]\; O[\psi, \overline{\psi}, A]\; e^{-S[\psi, \overline{\psi}, A]} \tag{3.7}$$

with the partition function

$$Z = \int \mathcal{D}[\psi, \overline{\psi}, A]\; e^{-S[\psi, \overline{\psi}, A]}\,. \tag{3.8}$$

If the quark fields experience an -at this point yet unspecified- infinitesimal transformation as follows,

$$\psi \to \psi' = \psi + \delta\psi\,, \quad \overline{\psi} \to \overline{\psi}' = \overline{\psi} + \delta\overline{\psi}\,, \tag{3.9}$$

the resulting variation of the expectation value $\langle O \rangle$ given in Eq. (3.7) can be expressed as follows

$$\langle O \rangle \to \langle O \rangle' = \langle O \rangle + \langle \delta O \rangle - \langle O\, \delta S \rangle + \langle O\, \delta J \rangle\,. \tag{3.10}$$

Here, $\langle \delta O \rangle$ corresponds to the variation of the interpolating field, $\langle O\, \delta S \rangle$ results from the variation of the action and $\langle O\, \delta J \rangle$ from the variation of the Jacobian J. The Jacobian accounts for the change in the Grassmann integration measure

$$\mathcal{D}[\psi', \overline{\psi}'] = J\, \mathcal{D}[\psi, \overline{\psi}]\,, \tag{3.11}$$

and can be written, using the properties of the determinant, as $J = 1 + \delta J$. Imposing invariance of $\langle O \rangle$ under the transformation, $\langle O \rangle' = \langle O \rangle$, Eq. (3.10) reduces to

$$\langle \delta O \rangle = \langle O\, \delta S \rangle - \langle O\, \delta J \rangle\,. \tag{3.12}$$

If the corresponding transformation is non-anomalous ($\delta J = 0$)[1] the invariance of the path integral is expressed via the WI

$$\langle \delta O \rangle = \langle O\, \delta S \rangle\,. \tag{3.13}$$

This relation is important since it allows to express expectation values of transformed interpolating fields in terms of expectation values of variations of the action under that transformation. Therefore, it is crucial to know how the action, S, transforms under a given infinitesimal transformation of the quark fields according to Eq. (3.9). Considering a local transformation, the variation, δ, of the fields, $\psi, \overline{\psi}$, has the general form

$$\delta\psi = \mathrm{i}\,\omega(x)\, T\, \psi\,, \quad \delta\overline{\psi} = \overline{\psi}\, \mathrm{i}\,\omega(x)\, \hat{T}\,, \tag{3.14}$$

with $\omega(x)$ the transformation parameter. $\omega(x)$ is assumed to have support in a space-time region $\mathcal{R}$, with boundary $\partial\mathcal{R}$, and to vanish in a smooth way outside $\mathcal{R}$. $T, \hat{T}$ is a particular combination of Dirac and Pauli matrices encoding the structure of the transformations.

Under these considerations, the variation of the fermion action is [2]

$$\delta S_{\mathrm{F}} = \mathrm{i} \int_{\mathcal{R}} \mathrm{d}^4x\, \overline{\psi}(x) \left[\Big(\partial_\mu \omega(x) \Big)\, \gamma_\mu\, T + \omega(x)\, (\gamma_\mu\, T + \hat{T}\, \gamma_\mu)\, D_\mu(x) + \omega(x)\, (m\, T + \hat{T}\, m) \right] \psi(x)\,, \tag{3.15}$$

where m is the mass term which, at the moment, may have any general form. Using integration by parts and considering the condition of vanishing $\omega(x)$ outside the integration region $\mathcal{R}$, the previous expression reduces to

$$\begin{aligned} \delta S_{\mathrm{F}} = \mathrm{i} \int_{\mathcal{R}} \mathrm{d}^4x\, \omega(x) \Big[& - \partial_\mu \Big(\overline{\psi}(x)\, \gamma_\mu\, T\, \psi(x) \Big) \\ & + \overline{\psi}(x) \left[(\gamma_\mu\, T + \hat{T}\, \gamma_\mu)\, D_\mu(x) + (m\, T + \hat{T}\, m) \right] \psi(x) \Big]\,. \end{aligned} \tag{3.16}$$

As it will be shown below, all transformations considered in this work are characterized by

$$\gamma_\mu\, T + \hat{T}\, \gamma_\mu = 0\,. \tag{3.17}$$

This simplifies the variation of the action, Eq. (3.16), to the final form,

$$\delta S_{\mathrm{F}} = \mathrm{i} \int_{\mathcal{R}} \mathrm{d}^4x\, \omega(x) \Big[- \partial_\mu \Big(\overline{\psi}(x)\, \gamma_\mu\, T\, \psi(x) \Big) + \overline{\psi}(x) \Big(m\, T + \hat{T}\, m \Big)\, \psi(x) \Big]\,. \tag{3.18}$$

Once the variation of the action is known, particular cases of the relation Eq. (3.13) can be studied depending on the choice of the interpolator O and the considered transformation. If the

[1] This happens e.g. when the transformation matrix T is traceless, because $\delta J \sim \mathrm{tr}(T)$.

[2] Note that under the transformations of the fermion fields the gauge action stays invariant.

interpolating field is chosen to be the identity, $O = 1$, Eq. (3.13) reduces to

$$\langle \delta S \rangle = 0 \,, \tag{3.19}$$

from which the Nöther conservation laws can be derived. Another very interesting choice is the case of having $O = O_{\rm ext}$, that is, the interpolator has support only outside the integration region $\mathcal{R}$. In this case, the l.h.s. of Eq. (3.13) vanishes and the relation reduces to the simpler and commonly used WI

$$\langle \delta S \, O_{\rm ext} \rangle = 0 \,. \tag{3.20}$$

On the lattice, WI of the form of Eq. (3.20), in their lattice version, are extensively used. This is the only type of WI which is considered in this thesis.

In the following, we will discuss particular cases of the WI given in Eq. (3.20). Inserting now Eq. (3.18) into Eq. (3.20), the most general form of the expectation value, Eq. (3.20), under all the previous conditions is

$$\mathrm{i} \int_{\mathcal{R}} \mathrm{d}^4x \; \omega(x) \left\langle \Big[- \partial_\mu \Big(\overline{\psi}(x) \, \gamma_\mu \, T \, \psi(x) \Big) + \overline{\psi}(x) \, \Big(m \, T + \hat{T} \, m \Big) \, \psi(x) \Big] \, O_{\rm ext} \right\rangle = 0 \,. \tag{3.21}$$

Since this equation should hold for any $\omega(x)$, the WI associated to the transformation is obtained

$$\left\langle \Big[\partial_\mu \Big(\overline{\psi}(x) \, \gamma_\mu \, T \, \psi(x) \Big) \Big] O_{\rm ext} \right\rangle = \left\langle \Big[\overline{\psi}(x) \, \Big(m \, T + \hat{T} \, m \Big) \, \psi(x) \Big] O_{\rm ext} \right\rangle , \tag{3.22}$$

which is valid provided the field $O_{\rm ext}$ is not located at the space-time point x.

Eq. (3.22) can now be written for the specific cases of interest in this thesis. Such are the non-singlet vector and axial-vector transformations,

$$T_{\rm V} = \frac{\tau^a}{2} = -\hat{T}_{\rm V} \,, \tag{3.23}$$

$$T_{\rm A} = \gamma_5 \, \frac{\tau^a}{2} = \hat{T}_{\rm A} \,, \tag{3.24}$$

which give rise, respectively, to the PCVC WI,

$$\left\langle \Big[\partial_\mu \Big(\overline{\psi}(x) \, \gamma_\mu \frac{\tau^a}{2} \, \psi(x) \Big) \Big] O_{\rm ext} \right\rangle = \left\langle \overline{\psi}(x) \, \Big[m, \frac{\tau^a}{2} \Big] \, \psi(x) \, O_{\rm ext} \right\rangle , \tag{3.25}$$

and the PCAC WI,

$$\left\langle \Big[\partial_\mu \Big(\overline{\psi}(x) \, \gamma_\mu \gamma_5 \frac{\tau^a}{2} \, \psi(x) \Big) \Big] O_{\rm ext} \right\rangle = \left\langle \overline{\psi}(x) \, \Big\{ m, \gamma_5 \frac{\tau^a}{2} \Big\} \, \psi(x) \, O_{\rm ext} \right\rangle . \tag{3.26}$$

For later purposes, two possible cases are considered here. The first is QCD in the *standard* basis, $\{\psi, \overline{\psi}\}$, with $m = m_{\rm q} 1_{\rm f}$ the standard mass term, which is proportional to the identity matrix in flavor space and it describes two mass-degenerate quark flavors. In this setup, the mass term commutes with both transformations, vector and axial-vector. This implies a conserved vector current, $\mathcal{V}^a_\mu(x)$, as expressed by the resulting non-singlet vector WI (VWI),

$$\langle \partial_\mu \mathcal{V}^a_\mu(x) \, O_{\rm ext} \rangle = 0 \,, \tag{3.27}$$

and a partially conserved axial current as it is shown by the non-singlet axial-vector WI (AWI),

$$\langle \partial_\mu \mathcal{A}^a_\mu(x) \, O_{\rm ext} \rangle = 2 m_{\rm q} \, \langle \mathcal{P}^a(x) \, O_{\rm ext} \rangle \,. \tag{3.28}$$

From the AWI it is deduced that for a vanishing quark mass the non-singlet axial-vector current is also conserved.

The second setup is to consider *twisted mass* QCD in the twisted basis $\{\chi, \overline{\chi}\}$, where the mass term for a general rotation angle, α, is the sum of the standard and twisted mass terms, $m_{\rm q} 1_{\rm f} + {\rm i}\mu_{\rm q}\gamma_5\tau^3$. Now, both currents are only partially conserved due to the presence of the twisted mass term. The PCVC WI is,

$$\left\langle \partial_\mu V_\mu^a(x)\, O_{\rm ext}\right\rangle = -2\mu_{\rm q}\,\epsilon^{3ab}\left\langle P^b(x)\, O_{\rm ext}\right\rangle, \tag{3.29}$$

which contains the explicit breaking of isospin symmetry by the twisted mass term and the PCAC relation,

$$\left\langle \partial_\mu A_\mu^a(x)\, O_{\rm ext}\right\rangle = 2m_{\rm q}\left\langle P^a(x)\, O_{\rm ext}\right\rangle + {\rm i}\mu_{\rm q}\,\delta^{3a}\left\langle S^0(x)\, O_{\rm ext}\right\rangle. \tag{3.30}$$

As in the standard basis, in the chiral limit both currents are conserved. For a description of the two bases and detailed definitions of the currents and densities in both bases see Sec. 2.7.2 and Sec. 2.7.3. Note that we continue using the calligraphic notation for the fields in the standard basis and the normal letters for the fields in the twisted basis.

All this discussion has been carried out in the continuum quantized theory and no mention of the regularization was made so far. The WI have a physical meaning only in the renormalized theory and indeed, the renormalization process needs a regularization of the theory beforehand. A problem may arise at this point, since any regularization of a quantum field theory breaks certain symmetries in the regularization procedure. It directly implies that some WI do not hold at a finite value of the cutoff. In principle, this is not a problem because the corresponding violation of a certain WI is only driven by cutoff effects which are expected to vanish in the continuum limit, after the interpolating fields entering the WI have been properly renormalized. Additionally, the regulator must be such that it is able to reproduce the anomalies of the quantized theory and to guarantee such anomalies to survive after the removal of the cutoff.

Let us start assuming that a regularization has been found which does not break isospin neither axial chiral symmetries. In this case, it is always possible to find a vector and an axial-vector current such that the VWI and AWI defined above in the continuum, hold exactly in the regularized theory. Moreover, the isospin conservation would guarantee that the vector current is protected against renormalization and all members of an isospin multiplet renormalize equally (have the same renormalization constant). The conservation of chiral symmetry would tell that the axial current is also protected against renormalization and that all members of the chiral multiplet also renormalize in the same way. Indeed, the conclusions drawn are that $Z_{\rm V} = Z_{\rm A} = 1$ and $Z_{\rm S}/Z_{\rm P} = 1$. Under these conditions it is possible to define, for instance, renormalized quark masses from the previous AWI and VWI. In standard QCD, the multiplicatively renormalized quark mass $m_{\rm R}$ can be defined through the renormalized version of Eq. (3.28) as follows,

$$m_{\rm R} = Z_{\rm P}^{-1}\, m_{\rm q}\,, \qquad m_{\rm q} \equiv \frac{\left\langle \partial_\mu \mathcal{A}_\mu^a(x)\, O_{\rm ext}\right\rangle}{2\left\langle \mathcal{P}^a(x)\, O_{\rm ext}\right\rangle}. \tag{3.31}$$

In the case of twisted mass, the following renormalizations would hold,

$$\mu_{\rm R} = Z_{\rm P}^{-1}\,\mu_{\rm q}\,, \qquad \mu_{\rm q} \equiv \frac{\left\langle \partial_\mu V_\mu^a(x)\, O_{\rm ext}\right\rangle}{2\left\langle P^b(x)\, O_{\rm ext}\right\rangle}, \quad a,b = 1,2 \text{ and } a \neq b\,, \tag{3.32}$$

$$m_{\rm R} = Z_{\rm P}^{-1}\, m_{\rm q}\,, \qquad m_{\rm q} \equiv \frac{\left\langle \partial_\mu A_\mu^a(x)\, O_{\rm ext}\right\rangle}{2\left\langle P^a(x)\, O_{\rm ext}\right\rangle}, \quad a = 1,2\,. \tag{3.33}$$

The information obtained from Eq. (3.31)-Eq. (3.33) is that, given a discretization of fermions which preserves chiral symmetry, quark masses renormalize exactly as in the continuum theory; multiplicatively and through the scale-dependent renormalization constant of the pseudo-scalar density, Z_{P}, or equivalently Z_{S}. Moreover, due to the multiplicative renormalizability of the quark masses, the theory may be defined at any value of the quark masses by simply setting the bare quark mass parameters, m_{q} and μ_{q}, to the chosen values.

Yet in this thesis, the regularization employed is lattice QCD with *Wilson-like fermions* (cf. Sec. 2.7.2, Sec. 2.7.3). As already explained, at finite lattice spacing Wilson-like fermions *break chiral symmetry*. The breaking effects are expected to go away in the continuum limit of the theory after renormalization. However, at non-zero lattice spacing the WI described above, Eq. (3.27)-(3.28) in the standard basis or Eq. (3.29)-(3.30) in the twisted basis, are expected to hold after renormalization of the theory only up to cutoff effects. The leading cutoff effects are expected to be of $O(a^n)$, with $n = 1$ in the unimproved theory and $n = 2$ in the improved case. Thus, the lattice relations are, in standard Wilson QCD,

$$\langle \widetilde{\partial}_\mu (\mathcal{V}_{\mathrm{R}})^a_\mu(x)\, O_{\mathrm{ext}} \rangle = O(a^n)\,, \tag{3.34}$$

$$\langle \widetilde{\partial}_\mu (\mathcal{A}_{\mathrm{R}})^a_\mu(x)\, O_{\mathrm{ext}} \rangle = 2m_{\mathrm{R}} \langle (\mathcal{P}_{\mathrm{R}})^a(x)\, O_{\mathrm{ext}} \rangle + O(a^n)\,, \tag{3.35}$$

and, in twisted mass Wilson QCD,

$$\langle \widetilde{\partial}_\mu (V_{\mathrm{R}})^a_\mu(x)\, O_{\mathrm{ext}} \rangle = -2\mu_{\mathrm{R}}\, \epsilon^{3ab} \langle (P_{\mathrm{R}})^b(x)\, O_{\mathrm{ext}} \rangle + O(a^n)\,, \tag{3.36}$$

$$\langle \widetilde{\partial}_\mu (A_{\mathrm{R}})^a_\mu(x)\, O_{\mathrm{ext}} \rangle = 2m_{\mathrm{R}} \langle (P_{\mathrm{R}})^a(x)\, O_{\mathrm{ext}} \rangle + \mathrm{i}\mu_{\mathrm{R}}\, \delta^{3a} \langle (S_{\mathrm{R}})^0(x)\, O_{\mathrm{ext}} \rangle + O(a^n)\,. \tag{3.37}$$

Here $\widetilde{\partial}_\mu$ denotes the symmetric ordinary derivative on the lattice defined in Eq. (A.21).

As first discussed in the remarkable paper [75], the breaking of chiral symmetry by the Wilson term has several direct consequences in this context. One is the *additive quark mass renormalization*,

$$m_{\mathrm{q}} = m_0 - m_{\mathrm{c}}\,, \tag{3.38}$$

with the critical mass, m_{c}, linearly divergent with the inverse of the lattice spacing when $a \to 0$. The breaking of chiral symmetry also gives rise to a *finite renormalization* of the non-singlet vector current, the non-singlet axial-vector current and the ratio of the scale-dependent renormalization constants of the chiral densities,

$$(\mathcal{V}_{\mathrm{R}})^a_\mu = Z_{\mathrm{V}}(g_0)\, \mathcal{V}^a_\mu\,, \qquad Z_{\mathrm{V}}(g_0) = 1 + Z^{(1)}_{\mathrm{V}} g_0^2 + O(g_0^4)\,, \tag{3.39}$$

$$(\mathcal{A}_{\mathrm{R}})^a_\mu = Z_{\mathrm{A}}(g_0)\, \mathcal{A}^a_\mu\,, \qquad Z_{\mathrm{A}}(g_0) = 1 + Z^{(1)}_{\mathrm{A}} g_0^2 + O(g_0^4)\,, \tag{3.40}$$

$$Z_{\mathrm{S}}/Z_{\mathrm{P}} = 1 + \mathrm{C}(g_0)\,. \tag{3.41}$$

In addition, *mixing* of operators may occur which can lead to further additive and finite renormalizations. The same holds for the currents in the twisted basis. These facts make evident how important the AWI is in formulations which break chiral symmetry. In particular, as it was proposed in [75], the AWI can be used to determine the scale-independent renormalization constants, Z_{A} and Z_{V}, and the additive quark mass renormalization. Stated differently, the AWI can be utilized to restore the broken chiral symmetry up to cutoff effects. The same reasoning holds for any other broken symmetry and its corresponding WI. Since $O(a)$-effects are also a consequence of the breaking of chiral symmetry by Wilson fermions, the AWI can likewise be employed in the non-perturbative determination of the improvement coefficients by e.g. demanding the AWI of the improved axial current to hold up to cutoff effects of $O(a^2)$. In the particular case of this thesis there is no need to determine improvement coefficients because we

only consider formulations which preserve automatic $O(a)$-improvement. Moreover, in our setup there is no need to perform finite renormalizations, as it will become clear below. Therefore, we also do not have to compute any scale-independent renormalization factor.

In our case we will make use of the AWI in the restoration of chiral symmetry by defining the theory with Wilson fermions in the massless limit, $m_{\rm q} = 0$. This is what we are after since our final goal is to have a mass-independent renormalization scheme. In this case, the chiral limit, $m_{\rm q} = 0$, corresponds to determine the critical line $m_0 = m_{\rm c}$. Such determination is far from trivial. It requires a non-perturbative tuning of m_0 to its critical value m_c at each value of the bare coupling g_0. The tuning can be achieved through the PCAC relation as follows. A bare standard quark mass, $m_{\rm q}$, may be defined to be the PCAC mass, $m_{\rm PCAC}$, through

$$m_{\rm PCAC} \equiv \frac{\langle \widetilde{\partial}_\mu \mathcal{A}^a_\mu(x)\, O_{\rm ext}\rangle}{2\,\langle \mathcal{P}^a(x)\, O_{\rm ext}\rangle}\,. \tag{3.42}$$

The PCAC mass is imposed to vanish at non-zero lattice spacing, which implies a restoration of chiral symmetry at every value of the lattice spacing and thus, in the continuum limit. A detailed description on how the tuning is performed will be given in Chap. 6.

The treatment above assumed that a direct translation of the WI from the continuum to the lattice is allowed, keeping in mind that the lattice identities only hold up to cutoff effects. However, it might look strange that, for instance, the VWI does not hold exactly on the lattice given the fact that isospin symmetry is not broken by the Wilson term. It is indeed true that the vector current is a Nöther current at finite lattice spacing and thus the VWI holds exactly. Yet, the Nöther current does not take the form of the vector current in the continuum,

$$\mathcal{V}^a_\mu(x) = \overline{\psi}(x)\,\gamma_\mu \frac{\tau^a}{2}\,\psi(x) \tag{3.43}$$

but, instead, a lattice version of it. It is the so called point-splitted vector current which, for standard Wilson fermions is given as,

$$\widetilde{\mathcal{V}}^a_\mu(x) = \frac{1}{2}\Big\{\overline{\psi}(x)\,(\gamma_\mu - 1)\frac{\tau^a}{2}\,U_\mu(x)\,\psi(x+\vec{\mu}) + \overline{\psi}(x+\vec{\mu})\,(\gamma_\mu + 1)\frac{\tau^a}{2}\,U_\mu(x)^\dagger\,\psi(x)\Big\}\,. \tag{3.44}$$

The same relations hold for twisted mass Wilson fermions, but expressed in the twisted basis, $\{\chi, \overline{\chi}\}$. Such a current is derived from the non-singlet vector variation of the *lattice* action, together with a final redefinition of $\mathcal{V}^a_\mu(x)$ which removes the contribution from the chirally breaking Wilson term. In practice, either using the continuum-like relations or the point-splitted ones is equally correct. The difference is that using the continuum-like expressions is computationally cheaper but it has the disadvantage of an additional finite renormalization of the vector current, $Z_{\rm V}(g_0)$. The axial-vector current on the lattice is determined similarly, from a non-singlet axial variation of the *lattice* action. In this case, however, the explicit breaking of chiral symmetry by the Wilson term can not be reabsorbed in the redefinition of the axial current and it goes away only in the continuum limit. Therefore, no conserved axial current exists at finite lattice spacing even in the chiral limit and $Z_{\rm A}(g_0)$ needs to be computed in any case. If a singlet axial variation of the lattice action is performed, the axial anomaly is reproduced by the corresponding variation of the Wilson term.

In this section we have discussed the case of twisted mass fermions in parallel to the standard setup. The reason is that we intend to define the mass-independent renormalization scheme in order to eventually renormalize quantities computed from twisted mass Wilson fermions at maximal twist. In particular, amongst other observables, we are interested in computing the renormalized quark mass. At maximal twist, the quark mass is fully given by the twisted mass,

μ_q, which, different to the standard mass, renormalizes only multiplicatively. Its renormalization properties may be deduced from the PCVC relation, Eq. (3.36), together with Eq. (3.39). A priori, from these relations it can be understood that the twisted quark mass renormalizes through the scale-dependent renormalization factor, Z_P, and the scale-independent renormalization factor Z_V. However, in terms of the point-splitted vector current, $\widetilde{V}^a_\mu(x)$, the VWI given in Eq. (3.29), holds exactly even at non-zero lattice spacing,

$$\langle \widetilde{\partial}_\mu \widetilde{V}^a_\mu(x)\, O_{\rm ext}\rangle = -2\mu_q\, \epsilon^{3ab} \langle P^b(x)\, O_{\rm ext}\rangle\,. \tag{3.45}$$

As a result, from Eq. (3.45) and the fact that $\widetilde{V}^a_\mu(x)$ does not need to be renormalized, it is possible to define the renormalized twisted quark mass, μ_R, as follows

$$\mu_R = Z_P^{-1}\,\mu_q\,, \qquad \mu_q \equiv \frac{\langle \widetilde{\partial}_\mu \widetilde{V}^a_\mu(x)\, O_{\rm ext}\rangle}{2\,\langle P^b(x)\, O_{\rm ext}\rangle}\,, \quad a,b=1,2 \text{ and } a\neq b\,, \tag{3.46}$$

which shows that, as in the continuum (cf. Eq. (3.32)), μ_q renormalizes only through Z_P[3]. We want to emphasize, though, that our ultimate goal will not be the computation of the bare quantities from twisted mass but, instead, the determination of the corresponding renormalization factors using the mass-independent renormalization scheme.

There is still a last issue which has not been discussed so far. In order to probe all these relations, $O_{\rm ext}$ has to be properly chosen in each case. Indeed, different choices of $O_{\rm ext}$ allow to probe the corresponding WI in several manners. This is discussed in more detail below in Sec. 3.4.

3.2. The Schrödinger functional of QCD

The Schrödinger functional (SF) of QCD [12, 15, 16] is the gauge invariant functional integral for QCD on a hyper-cylinder where the fields satisfy L-periodic boundary conditions in the spatial directions and Dirichlet boundary conditions at the Euclidean times 0 and T. The Schrödinger functional is a general concept of continuum QCD which is non-perturbatively defined. It has been shown to be very successful when used as a renormalization scheme of lattice QCD [73, 76, 77] but it can also be used with any other regulator of QCD, since the Schrödinger functional is regularization independent. Moreover, it may be applied both, non-perturbatively and in perturbation theory. Because of the Dirichlet boundary conditions in the time direction, the SF can be defined at exactly zero quark mass, thus allowing a mass-independent renormalization. As it will be shown below in more detail, the renormalized gauge coupling can be directly defined through the SF of QCD. Moreover, due to the possibility of applying finite size techniques the SF has become very important in lattice QCD. It was implemented for first time on the lattice in the pure gauge theory; a definition of the gauge coupling was given and the running of the coupling with the renormalization scale was studied. The implementation of the SF on the lattice beyond the pure gauge theory is, however, not a straightforward issue. Initially, the implementation using Wilson-type fermions was worked out. Afterwards, the SF has been formulated also with other kind of lattice fermions[4].

Since the SF is defined in a finite volume with boundaries, care has to be taken when considering its renormalizability; due to the presence of the boundary conditions, additional divergences might appear from boundary terms at $x_0 = 0$ and $x_0 = T$, which could render meaningless a

[3] For a more detailed discussion on the twisted mass setup with Wilson fermions, in the present context, the reader is referred to [60].

[4] In any case, in this work we are only interested in Wilson-type formulations.

theory defined through the SF. In the ϕ^4-theory the renormalizability of the SF has been proven to all orders in perturbation theory by Symanzik in [21]. He showed that the SF stays finite after the renormalization of the couplings of the theory and the addition of a finite number of boundary counter terms with $d \leq 3$ (local composite fields integrated at the boundaries). Symanzik conjectured that this should also be true in the renormalization of the SF of any quantum field theory of $d = 4$, thus in particular QCD. A proof for QCD to all orders in perturbation is however still missing. Yet, the renormalization of the SF has been demonstrated up to 2-loops in [78, 79] for the pure gauge theory and up to 1-loop in [15, 16] for QCD. Numerical studies [13, 14, 80] also suport the validity of the conjecture. Moreover, in the case of the pure gauge theory no boundary counterterms exist; only the renormalization of the gauge coupling is needed for the SF to be renormalized. The same is not true in full QCD, where boundary counterterms are needed to renormalize the SF [15, 16]. These boundary counterterms amount to a multiplicative renormalization of the boundary quark fields (cf. Eq. (3.51)-(3.52)). Therefore, the SF of full QCD is renormalized after the renormalization of the gauge coupling, the quark masses and the boundary quark fields.

In the use of the SF as a finite size scheme, the renormalization scale of the theory, μ, is identified with the finite size of the system, $1/L$, as already stated above in Eq. (3.6), provided L is the only scale of the theory. To achieve this requirement all dimensionful external parameters entering the renormalization conditions have to be rescaled with the appropriate powers of L. In particular, if the volume of the 4-dimensional space-time is as usual, L^3T, the time extent of the system, T, also has to be rescaled in terms of L. The usual choice, and the one chosen through this work is to set $T = L$.

3.2.1. The SF on the lattice. Definition

Considering the Euclidean four dimensional space-time lattice in a finite volume, L^3T, with periodic boundary conditions in the spatial directions and Dirichlet boundary conditions in the time direction, the space-time becomes a discretized finite-volume hyper-cylinder as shown in Fig. 3.2[5]. All fields of the theory also fulfill these boundary conditions.

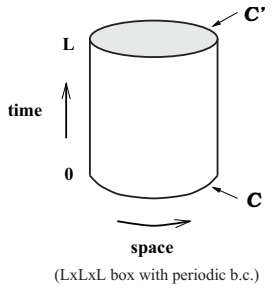

Figure 3.2.: Schrödinger functional boundary conditions.

On the lattice, the temporal gauge links, $U_0(x)$, are defined for all lattice points, x, satisfying $0 \leq x_0 < T$. The L-periodicity in the spatial directions is given for the gauge fields, $U_\mu(x)$, by

$$U_\mu(x + L\hat{k}) = U_\mu(x) \tag{3.47}$$

and for the matter fields $\psi(x), \overline{\psi}(x)$,

$$\psi(x + L\hat{k}) = \psi(x)\,, \qquad \overline{\psi}(x + L\hat{k}) = \overline{\psi}(x)\,. \tag{3.48}$$

[5]Fig. 3.2 has been taken from [81], which is a good reference for an introduction to non-perturbative renormalization.

In the temporal direction, the boundary conditions of the spatial gauge links are,

$$U_k(x)|_{x_0=0} = W_k(\vec{x}) = e^{a\,C_k(\vec{x})}\,, \tag{3.49}$$

$$U_k(x)|_{x_0=T} = W'_k(\vec{x}) = e^{a\,C'_k(\vec{x})}\,. \tag{3.50}$$

C_k, C'_k are classical gauge potentials defining the boundary conditions in the continuum formulation of the SF and the definition above guarantees that the boundary fields on the lattice, W_k, W'_k, become the classical gauge potentials in the continuum limit, thus, recovering the continuum SF. The classical gauge potentials are 3×3, traceless, anti-hermitian matrices which, when different from zero, induce a background field. The induced background field is useful in many applications, e.g. in the definition of the gauge coupling constant (cf. Sec. 3.3.1) or when applying perturbation theory. However, for all purposes in this work, no background field is needed and the gauge potentials are set to zero, $C_k = C'_k = 0$.

The fermion fields satisfy the following inhomogeneous boundary conditions,

$$P_+\,\psi(x)|_{x_0=0} = \rho(\vec{x}) \qquad P_-\,\psi(x)|_{x_0=T} = \rho'(\vec{x}) \tag{3.51}$$

$$\overline{\psi}(x)\,P_-|_{x_0=0} = \overline{\rho}(\vec{x}) \qquad \overline{\psi}(x)\,P_+|_{x_0=T} = \overline{\rho}'(\vec{x}) \tag{3.52}$$

with the parity projector defined as

$$P_\pm = \frac{1}{2}\,(1 \pm \gamma_0)\,. \tag{3.53}$$

The projector implies that only *half* of the components of the quark fields are fixed at the boundaries. This is enough to have a unique solution of the Dirac equation because the Dirac operator is a first order differential operator.

It is common to define the 'boundary fields',

$$\zeta(\vec{x}) = \frac{\delta}{\delta\overline{\rho}(\vec{x})} \qquad \overline{\zeta}(\vec{x}) = -\,\frac{\delta}{\delta\rho(\vec{x})} \tag{3.54}$$

$$\zeta'(\vec{x}) = \frac{\delta}{\delta\overline{\rho}'(\vec{x})} \qquad \overline{\zeta}'(\vec{x}) = -\,\frac{\delta}{\delta\rho'(\vec{x})}\,, \tag{3.55}$$

which play an important role when constructing correlation functions (cf. Sec. 3.4).

Another possibility to define the fermionic boundary conditions is to use the homogeneous Dirichlet boundary conditions [82],

$$P_+\,\psi(x)|_{x_0=0} = 0 \qquad P_-\,\psi(x)|_{x_0=T} = 0 \tag{3.56}$$

$$\overline{\psi}(x)\,P_-|_{x_0=0} = 0 \qquad \overline{\psi}(x)\,P_+|_{x_0=T} = 0 \tag{3.57}$$

with the non-zero components of the quark fields directly introduced as

$$P_-\,\psi(x)|_{x_0=0} = \zeta(\vec{x}) \qquad P_+\,\psi(x)|_{x_0=T} = \zeta'(\vec{x}) \tag{3.58}$$

$$\overline{\psi}(x)\,P_+|_{x_0=0} = \overline{\zeta}(\vec{x}) \qquad \overline{\psi}(x)\,P_-|_{x_0=T} = \overline{\zeta}'(\vec{x})\,. \tag{3.59}$$

Since the space-time is restricted to the finite-volume hyper-cylinder defined by the SF boundary conditions, the sum in the space-time variable, x, in the corresponding action is thus restricted to such finite SF volume. However, it is possible to express the action with SF boundary conditions as a sum over all space-time points, without any restriction concerning the finite volume. To this end, the fields are defined at all space-time points considering that outside the SF volume all gauge links are set to the identity and all fermion fields are set to zero (padding with

zeroes [44]).

The pure lattice gauge action is then given by [14]

$$S_{\mathrm{G}}[U] = \frac{2}{g_0^2} \sum_x \sum_{\mu<\nu} w(p) \,\mathrm{Re}\,\mathrm{tr}_c \left[1 - U_{\mu\nu}(x)\right], \tag{3.60}$$

where $U_{\mu\nu}(x)$ is the plaquette defined in Eq. (2.10) and the sum is performed over all space-time points, x. This is the Wilson gauge action of Eq. (2.9) weighted with the weight factors $w(p)$ which take the values

$$w(p) = \begin{cases} \frac{1}{2} & \text{for spatial plaquettes at } x_0 = 0 \text{ or } x_0 = T\,, \\ 1 & \text{for all other plaquettes}\,. \end{cases} \tag{3.61}$$

The lattice fermion action is [15, 16]

$$S_{\mathrm{F}}[\psi, \overline{\psi}, U] = a^4 \sum_x \overline{\psi}(x) \left(D_{\mathrm{W}} + m_0\right) \psi(x)\,, \tag{3.62}$$

with the massless Wilson-Dirac operator, D_{W}, as defined in Eq. (2.68) and the sum running also over all space-time points.

The SF of QCD on the lattice can now be properly defined. The Schrödinger functional of QCD is the gauge invariant Euclidean functional of the classical boundary fields,

$$\mathcal{Z}[\overline{\rho}', \rho', C'; \overline{\rho}, \rho, C] = \int \mathcal{D}[\psi]\, \mathcal{D}[\overline{\psi}]\, \mathcal{D}[U]\; e^{-S^{\mathrm{QCD}}[\psi, \overline{\psi}, U]}\,. \tag{3.63}$$

The Haar measure is as defined in Eq. (2.16) and the Grassmann measure in Eq. (2.15). The lattice QCD action, $S^{\mathrm{QCD}}[\psi, \overline{\psi}, U]$, is the sum of Eq. (3.60) and Eq. (3.62). The lattice SF (Eq. (3.63)) is invariant under arbitrary gauge transformations of the boundary fields and it is still a functional of only the continuum boundary fields.

3.2.2. The lattice SF and improvement

A drawback of the SF is that the Dirichlet boundary conditions in the time direction induce *boundary cutoff effects* of $O(a)$ in both, the pure gauge and the fermion actions. These effects are not due to the breaking of any symmetry of the continuum theory by the regulator. Instead, they appear as a result of insertions of local operators of $d = 4$ integrated at the time boundaries, which are allowed by the symmetries of the theory. These $O(a)$ effects are present in any lattice regularization with SF boundary conditions, either if chiral symmetry is preserved by the discretization or not. Consequently, even improved formulations have uncanceled *boundary* $O(a)$-effects in the presence of SF boundary conditions.

According to the necessity of $O(a)$-improvement on the lattice, the application of Symanzik programme is required [83, 84]. For the improvement of the gauge action, Eq. (3.60), two boundary counter terms are necessary. They amount to the substitution of the weight factor $w(p)$ defined in Eq. (3.61) by

$$w(p) = \begin{cases} \frac{1}{2} c_s(g_0) & \text{for spatial plaquettes at } x_0 = 0 \text{ or } x_0 = T\,, \\ c_t(g_0) & \text{for time-like plaquettes attached to a boundary plane}\,, \\ 1 & \text{for all other plaquettes}\,. \end{cases} \tag{3.64}$$

The coefficients $c_s(g_0)$ and $c_t(g_0)$ should be tuned in order to guarantee $O(a)$-improvement. It is not possible to perform a non-perturbative determination, for which these coefficients are

only known up to a certain order in perturbation theory,

$$c_s(g_0) = c_s^{(0)} + c_s^{(1)}\, g_0^2 + O(g_0^4)\,, \tag{3.65}$$

$$c_t(g_0) = c_t^{(0)} + c_t^{(1)}\, g_0^2 + O(g_0^4)\,, \tag{3.66}$$

with

$$c_{s,t}^{(k)} = \sum_{l=0}^{k} c_{s,t}^{(k,l)}\, N_f^l\,. \tag{3.67}$$

c_s is only known at tree-level of perturbation theory. This coefficient is not needed if either $C_k = C_k' = 0$ or only constant abelian background fields, W and W', are considered. This is so because in this case the contribution to the action of the spatial plaquettes at the boundaries vanishes. The expression of c_t is known up to two loops for $N_f = 0$. The one loop determination was done in [14] and extended to two loop in [85, 86]

$$c_s(g_0) = 1 + O(g_0^2)\,, \tag{3.68}$$

$$c_t(g_0) = 1 - 0.089\, g_0^2 - 0.030\, g_0^4 + O(g_0^6)\,. \tag{3.69}$$

All computations in this thesis are performed with the 2-loop value of c_t. In this case, the boundary cutoff effects coming from the gauge action are reduced to $O(ag_0^6)$.

In the case of the fermion action, besides the usual bulk improvement giving rise to the improved Wilson-Dirac operator, as explained in detail in Sec. 2.7.2 and defined in Eq. (2.76)-(2.77), also two boundary counterterms are inevitable with coefficients denoted as $\widetilde{c}_{s,t}$. They obey the same type of expansion in terms of the bare gauge coupling as $c_{s,t}$. The knowledge of $\widetilde{c}_s$ is not needed, because it does not contribute to the lattice action neither to the correlation functions of interest here. Concerning $\widetilde{c}_t$, it is known up to 1-loop order [87]. In the quenched approximation these coefficients take the values

$$\widetilde{c}_s(g_0) = 1 + O(g_0^2)\,, \tag{3.70}$$

$$\widetilde{c}_t(g_0) = 1 - 0.018\, g_0^2 + O(g_0^4)\,. \tag{3.71}$$

In the massless limit the boundary effects originating from the fermion action are reduced to $O(ag_0^4)$. For this thesis, however, the fermionic boundary coefficients are not relevant at all. The reason is that for the calculations of this thesis we will actually not use the fermion action just described. Yet, continuum limit results obtained with this improved action are used for universality tests of our setup, which is the reason why it has been introduced here.

3.3. Non-perturbative renormalization from the SF

In this section it is explained how non-perturbative renormalization takes place using SF-like schemes; it will be described how SF-schemes account for the matching between any perturbative renormalization scheme (usually the $\overline{\text{MS}}$) and some hadronic scheme (HS). In this way, quantities determined at short distances using the chosen perturbative scheme are eventually expressed in units of a low energy scale of the theory.

The process of non-perturbative renormalization using a finite size scheme, the SF here, takes place in three main steps; (1) hadronic renormalization and matching at low energies with the finite size scheme, (2) non-perturbative evolution to high energies through the finite size scheme and computation of renormalization group invariant (RGI) quantities, (3) conversion to a desired perturbative scheme. These steps are summarized in Fig. 3.1.

In the following discussion, even if not mentioned explicitly, the quenched approximation is

assumed. The explanation of the non-perturbative renormalization strategy [81, 88] is restricted to the case of the gauge coupling but it is similarly applied to any other running quantity, i.e. the running quark masses and renormalization factors.

3.3.1. Renormalized gauge coupling from the SF

In the pure gauge theory or in the quenched approximation, a renormalized gauge coupling, $\overline{g}(\mu)$, can be defined from the Schrödinger functional [12, 14] as follows

$$\overline{g}^2(\mu) = k\,\langle \frac{\partial S_G}{\partial \eta}\rangle_{\eta=0}\,, \qquad \mu = 1/L\,. \tag{3.72}$$

In this expression, $S_{\rm G}$ is the pure gauge action and k is a proportionality constant guaranteeing that at lowest order of perturbation theory $\overline{g}^2 = g_0^2$. The parameter η is a consequence of the particular boundary conditions in the time direction chosen for the gauge fields [14], $C_k(\eta), C'_k(\eta)$. The exact definition of the coupling is not relevant for the discussions in this thesis, thus, a discussion concerning this topic is omitted. What is important is that the coupling is defined in terms of a local quantity, $\langle \frac{\partial S_G}{\partial \eta}\rangle$, which is easy to evaluate using MC methods. This observable is moreover not affected by large fluctuations thus providing a very accurate answer. In order to define the coupling in this way, all dimensionful quantities have to be rescaled in terms of L, such that L remains the only external scale upon which the renormalized coupling depends.

With the usual notation, the running coupling is rewritten as

$$\alpha(\mu) = \frac{\overline{g}^2(\mu)}{4\pi}\,, \qquad \mu = 1/L\,. \tag{3.73}$$

3.3.2. Hadronic renormalization and matching at low energies

At low energies renormalization commonly takes place in a hadronic scheme. The scheme is defined by choosing a number of physical observables which do not need to be renormalized, e.g. hadron masses, that are held fixed to their experimentally known values. All quantities computed on the lattice are then expressed in units of the observables chosen to define the hadronic scheme, which thus serve to *set the scale*. Since in this thesis the quenched approximation is considered, the Sommer parameter [37], r_0, is a good choice (cf. App. C.3).

The *matching at low energies* is the process of relating the HS with the intermediate finite-volume scheme, the SF in this case. It consists in expressing the scale, L, of the finite-volume scheme in units of the hadronic scale, r_0, at some energy value where it is possible to compute accurately both r_0 and the renormalized coupling. Assuming this happens in a point where the renormalized coupling $\overline{g}^2$ takes the value u_0, the matching point L is defined as

$$L = L_{\rm max} \quad \text{such that} \quad \overline{g}^2 = u_0\,. \tag{3.74}$$

Once the matching point is defined the matching at low energies is performed by determining the ratio $L_{\rm max}/r_0$. It is done in basically two steps. On the one hand the ratio a/r_0 is computed at several values of β [38, 39]. On the other hand, at the same values of β the ratio $L_{\rm max}/a$ is computed. This last step is done by determining $\overline{g}^2(L)$ at several values of L/a, for each β, and interpolating to the value of $L/a = L_{\rm max}/a$ such that $\overline{g}^2(L_{\rm max}) = u_0$. This procedure leads to the relation

$$\frac{L_{\rm max}}{r_0} = \Big(\frac{L_{\rm max}}{a}\Big)\Big(\frac{a}{r_0}\Big)\,, \tag{3.75}$$

which can be eventually extrapolated to the continuum limit giving the final answer

$$L_{\max}/r_0 = \text{final value}\,. \tag{3.76}$$

3.3.3. Non-perturbative renormalization group. Step scaling function

The renormalization group (RG) equation of a scale-dependent quantity describes the dependence of the corresponding renormalized quantity on the renormalization scale, $\mu = 1/L$. In the case of the gauge coupling, its dependence on the renormalization scale is dictated by the Callan-Symanzik β-function as follows

$$\beta(\overline{g}) = -L\,\frac{\partial \overline{g}}{\partial L}\,. \tag{3.77}$$

If the exact expression of the β-function was known the integration of the Callan-Symanzik equation could be performed exactly. Thus, given an initial value for the renormalized coupling, $\overline{g}^2(L)$, at a certain scale L, the integrated form of the β-function would tell which is the value of the renormalized coupling at the scale $L' = sL$, $\overline{g}^2(sL)$, where s is some chosen scale factor. This integrated form of the β-function is the so called step scaling function (SSF) and it is usually denoted as $\sigma(s, \overline{g}^2(L))$. These lines can be summarized by the following expressions

$$\overline{g}^2(sL) = \sigma(s, \overline{g}^2(L))\,, \qquad \int_{\overline{g}^2(L)}^{\sigma(s,\overline{g}^2(L))} \frac{d\overline{g}}{\beta(\overline{g})} = -\int_L^{sL} \frac{dL}{L} = -\ln(s)\,. \tag{3.78}$$

However, the β-function is only known perturbatively up to a certain order in perturbation theory. In the limit of small renormalized coupling it has the expansion

$$\beta(\overline{g}) \overset{\overline{g}\to 0}{\sim} -\overline{g}^3 \sum_{n=0}^{\infty} b_n\, \overline{g}^{2n}\,, \tag{3.79}$$

with the renormalization scheme-independent coefficients

$$b_0 = \frac{1}{(4\pi)^2}\,(11 - \frac{2}{3}N_f)\,, \quad b_1 = \frac{1}{(4\pi)^4}\,(102 - \frac{38}{3}N_f)\,, \tag{3.80}$$

and the rest of the coefficients in the expansion being dependent on the chosen definition of the renormalized coupling, or equivalently, on the renormalization scheme. Therefore, an explicit analytic expression for the step scaling function can only be obtained in a perturbative way and up to a certain order. It is done by substitution of Eq. (3.79) into Eq. (3.77) up to the corresponding order of perturbation theory and then performing the integration.

Yet, on the lattice, to reach the energies where the perturbative formulae can be applied is a challenge. It is at this point where the SF-scheme makes a step forward, accounting for the energy evolution of the renormalized coupling, defined in Eq. (3.72), from hadronic scales up to the pure perturbative regime. This is achieved by solving Eq. (3.78) *numerically* in a non-perturbative way using Monte Carlo methods. In this manner a purely non-perturbative determination of the SSF is obtained at any desired scale $\mu = 1/L$.

Only an additional consideration has to be made at this point. Since the SSF is determined on the lattice, discretization effects are present. Therefore, the SSF computed on the lattice differs from the continuum SSF by cutoff effects and it depends on the details of the chosen lattice action. In the continuum limit, however, the SSF is a finite well defined quantity which is independent on the regulator. The continuum SSF only depends on the renormalization scheme and the value of the renormalization scale. The lattice step scaling function is usually denoted

as Σ. It can be then written as

$$\Sigma(s, \overline{g}^2(L), a/L) = \overline{g}^2(sL)\,, \tag{3.81}$$

and it must then satisfy

$$\Sigma(s, \overline{g}^2(L), 0) = \sigma(s, \overline{g}^2(L))\,. \tag{3.82}$$

As a consequence, in order to calculate the evolution of the continuum SSF, σ, from low to high energies, first the lattice SSF, Σ, has to be extrapolated to the continuum limit. The continuum extrapolation, $a/L \to 0$, is performed at each fixed value of the renormalization scale, $1/L$.

To evolve one step of size s in the energy scale from a higher to a lower energy, $L \to sL$, the following steps have to be performed: to fix the number of lattice points, L/a. At this fixed value of L/a the bare coupling is tuned such that $\overline{g}^2(L)$ takes a chosen value u (renormalization). Keeping fixed the value of g_0 (thus a) the renormalized coupling is computed at scale sL, $\overline{g}^2(sL)$ (evolution), obtaining thus $\Sigma(s, u, a/L)$. All these steps are repeated at several values of L/a and the continuum limit, $a/L \to 0$, of Σ is performed. At this point, the continuum SSF, $\sigma(s, u)$, which describes the evolution of the renormalized coupling from a scale L to sL is known.

This procedure can be repeated K-times, starting at some value of L in the perturbative region and going down in energies to the matching scale, $s^K L = L_{\max}$. From these data, a parametrization of σ as a function of $\overline{g}(L)$ can be obtained. Afterwards, given the chosen initial value of the renormalized coupling, $\overline{g}^2(L_{\max}) = u_0$, at the matching scale (cf. Eq. (3.74)) the evolution can be traced up to high energies from the curve using the recursive relation

$$u_k = \sigma(u_{k+1})\,, \quad k = 0, 1, 2, \dots\,, \tag{3.83}$$

with the definition $u_k = \overline{g}(s^{-k} L_{\max})$.

3.3.4. Conversion to the perturbative scheme

Once the perturbative region has been reached, perturbation theory can be applied within the SF scheme and the usual quantities in perturbation theory may be computed. For $N_f = 0$ the expansion of the β function in the SF scheme is known up to three loops. The first two coefficients, b_0 and b_1, are universal. The three-loop coefficient, b_2, has been determined in [85]. Up to two loops, the analytic expression for the asymptotic solution of Eq. (3.77) is given by,

$$\overline{g}^2(\mu) \overset{\mu\to\infty}{\sim} \frac{1}{b_0 \ln(\mu^2/\Lambda^2)} - \frac{b_1 \ln[\ln(\mu^2/\Lambda^2)]}{b_0^3\,[\ln(\mu^2/\Lambda^2)]^2} + O\Big(\frac{\{\ln[\ln(\mu^2/\Lambda^2)]\}^2}{[\ln(\mu^2/\Lambda^2)]^3}\Big)\,. \tag{3.84}$$

The renormalization scale, μ, is here $\mu = 1/L$. Λ is the integration constant, which is scale-independent and scheme-dependent. Together with the RGI quark masses, it is one of the so called fundamental parameters of QCD. The exact expression defining the RGI Λ-parameter is

$$\Lambda = \mu\,(b_0 \overline{g}^2)^{-b_1/(2b_0^2)}\, e^{-1/(2b_0\overline{g}^2)} \exp\Big\{ -\int_0^{\overline{g}} \mathrm{d}x\, \Big[\frac{1}{\beta(x)} + \frac{1}{b_0 x^3} - \frac{b_1}{b_0^2 x}\Big]\Big\}\,. \tag{3.85}$$

From this equation the value of Λ may be perturbatively determined in the SF scheme in units of $L_{\max}$. It has been done up to 3-loop accuracy [79, 85, 89]. Using Eq. (3.76), the $\Lambda_{\rm SF}$ is re-expressed in units of the hadronic scale, $\Lambda_{\rm SF}/r_0$. The subscript SF emphasizes the fact that the Λ-parameter is a scheme-dependent quantity (differently from the RGI quark masses which are scheme-independent).

At this stage, the *conversion to the perturbative scheme* can be performed. In order to find the exact relation between Λ in both schemes, first, a 1-loop computation of the relation between

$\alpha(\mu)$ in both schemes is needed [13, 14]. This is because the change of the Λ-parameter from a scheme, $S1$, to any other scheme, $S2$, is established by the relation

$$\Lambda_{\mathrm{S1}} = \Lambda_{\mathrm{S2}}\, e^{c^{(1)}/b_0}\,, \tag{3.86}$$

with $c^{(1)}$ the 1-loop coefficient relating the renormalized running coupling constants in both schemes. In particular, for $N_f = 0$ the conversion from Λ_{SF} to $\Lambda_{\overline{\mathrm{MS}}}$ gives the exact relation

$$\Lambda_{\overline{\mathrm{MS}}}/\Lambda_{\mathrm{SF}} = 2.049 \tag{3.87}$$

and the expression of $\Lambda_{\overline{\mathrm{MS}}}$ in units of the hadronic scale is finally obtained,

$$\Lambda_{\overline{\mathrm{MS}}} = 0.636(54)/r_0\,, \tag{3.88}$$

without any reference to the intermediate finite-volume scheme. This is the final solution to the non-perturbative renormalization problem.

Using the typical value of $r_0 = 0.5\,\mathrm{fm}$, the conversion to physical units is performed [90],

$$\Lambda_{\overline{\mathrm{MS}}} = (251 \pm 21)\,\mathrm{MeV}\,. \tag{3.89}$$

Yet, due to the uncertainty in r_0 the solid result is Eq. (3.88). Now that $\Lambda_{\overline{\mathrm{MS}}}$ is known in units of r_0, Eq. (3.85) can be solved perturbatively within the $\overline{\mathrm{MS}}$-scheme and thereby the running coupling in this scheme may be expressed in units of the hadronic scale r_0.

The renormalization of the quark mass and any other quantity may be computed in analogy to the case of the gauge coupling, as it will be shown in following chapters.

3.4. Renormalization conditions from the SF. Correlation functions

Renormalization conditions are generically imposed through relations between correlation functions. Depending on the particular observable to be renormalized, different correlation functions enter the renormalization condition. In general, the correlation functions considered are of the form

$$\langle O(x)\, \mathcal{O}_{\mathrm{ext}} \rangle\,. \tag{3.90}$$

$O(x)$ is an interpolating field chosen according to the particular quantity to be renormalized. On the contrary, many different choices of the external field, $\mathcal{O}_{\mathrm{ext}}$, may be used to probe the same correlation function, provided $\mathcal{O}_{\mathrm{ext}}$ is not defined at x.

In principle, all dependence of the functional integral on the boundary fields $C, C', \rho, \rho', \overline{\rho}, \overline{\rho}'$, is contained in the action, while typical interpolating fields involve only dynamical fields in the bulk of the lattice away from the boundaries. However, it is possible to define interpolating fields which contain derivatives with respect to the boundary fermion fields. These are usually referred to as *boundary operators*. The boundary operators have the effect to insert in the functional integral dynamical variables close to the boundaries of the lattice.

Given a particular Dirac and flavor structure, Γ, a boundary operator $\mathcal{O}$ with zero momentum at $x_0 = 0$ may be defined,

$$\mathcal{O} = -a^6 \sum_{\vec{y},\vec{z}} \frac{\delta}{\delta\rho(\vec{y})}\, \Gamma\, \frac{\delta}{\delta\overline{\rho}(\vec{z})}\,, \tag{3.91}$$

and the corresponding operator $\mathcal{O}'$ at $x_0 = T$,

$$\mathcal{O}' = -a^6 \sum_{\vec{y},\vec{z}} \frac{\delta}{\delta\rho'(\vec{y})}\, \Gamma\, \frac{\delta}{\delta\overline{\rho}'(\vec{z})}\,. \tag{3.92}$$

From Eq. (3.54)-(3.55) it is visible the relation between the derivatives and the quark and antiquark fields near the boundaries. Applying such relations, Eq. (3.91) and Eq. (3.92) are rewritten in the more common form,

$$\mathcal{O} = a^6 \sum_{\vec{y},\vec{z}} \overline{\zeta}(\vec{y})\, \Gamma\, \zeta(\vec{z})\,, \tag{3.93}$$

$$\mathcal{O}' = a^6 \sum_{\vec{y},\vec{z}} \overline{\zeta}'(\vec{y})\, \Gamma\, \zeta'(\vec{z})\,. \tag{3.94}$$

Using the previous definitions and considering $O(x)$ to be a bulk interpolating field, a correlation function boundary to bulk can be defined as follows

$$\langle O(x)\, \mathcal{O} \rangle = \Big\{ \frac{1}{\mathcal{Z}} \int \mathcal{D}[\psi]\, \mathcal{D}[\overline{\psi}]\, D[U]\; O(x)\, \mathcal{O}\, e^{-S^{\rm QCD}[\psi,\overline{\psi},U]} \Big\}_{\overline{\rho}'=\rho'=\overline{\rho}=\rho=0}\,, \tag{3.95}$$

and the same holds for the other boundary at T. Also correlation functions boundary to boundary (from $x_0 = 0$ to $x_0 = T$) can be defined in the same way,

$$\langle \mathcal{O}'\, \mathcal{O} \rangle = \Big\{ \frac{1}{\mathcal{Z}} \int \mathcal{D}[\psi]\, \mathcal{D}[\overline{\psi}]\, D[U]\; \mathcal{O}'\, \mathcal{O}\, e^{-S^{\rm QCD}[\psi,\overline{\psi},U]} \Big\}_{\overline{\rho}'=\rho'=\overline{\rho}=\rho=0}\,. \tag{3.96}$$

Eq. (3.95) is proportional to the probability amplitude that a pair quark-antiquark is created at $x_0 = 0$ with zero spatial momentum and propagates into the lattice until the point x where it is annihilated. Eq. (3.96) is proportional to the probability amplitude that a pair quark-antiquark is created at $x_0 = 0$ with zero spatial momentum and propagates into the lattice until the other time boundary $x_0 = T$ where it is annihilated [6]. Boundary to bulk correlation functions are usually normalized by the boundary to boundary correlation functions in order to cancel out the multiplicative renormalization of the quark boundary fields.

It is discussed at the end of App. A.5.2 that there exists the possibility of choosing, instead of periodic boundary conditions (PBC) [7], the so called generalized PBC or twisted BC. In the same appendix, it is also explained that the choice of such boundary conditions is equivalent to having PBC but with certain phase factors entering the definitions of the lattice derivatives. These phase factors are of the form,

$$\lambda_\mu = e^{\mathrm{i}\, a\, \theta_\mu / L}\,, \qquad \theta_0 = 0\,, \quad -\pi < \theta_k \leq \pi\,, \tag{3.97}$$

with θ_k parameters which can be freely chosen. PBC are recovered in case all θ_k are set to zero and the phase factors go away in the infinite volume limit. It was noticed in [44, 91] that these type of boundary conditions may be used within the SF scheme to probe the theory; different choices of the parameters θ_k give rise to *different* definitions of the renormalization scheme. All calculations performed in this thesis imply PBC in the spatial directions, with the phase factors, Eq. (3.97), directly entering the lattice derivatives, as shown in App. A.5.2. In particular, several choices of the parameters θ_k will be considered in order to define different renormalization conditions.

[6] These two types of correlation functions, Eq. (3.95)-(3.96), are not the only correlation functions which can be defined but are the cases we are interested in here.

[7] Discussing the SF periodic boundary conditions always refer to the spatial directions.

3.5. SF boundary conditions and automatic $O(a)$-improvement

This chapter will be closed with a discussion of the realization of automatic $O(a)$-improvement, in a lattice theory with massless Wilson fermions and SF boundary conditions. It is an issue of central importance, if a non-perturbative mass-independent SF-type scheme is to be considered in the renormalization of quantities computed using twisted mass Wilson fermions at maximal twist (cf. Sec. 2.7.3).

At this point, it should already be clear why to use a SF-like scheme is desirable on the lattice. Another important reason to mention is the presence of a lower positive bound in the spectrum of the Dirac operator, which is provided by the Dirichlet boundary conditions in the time direction. It has been proven at tree-level of perturbation theory [15] that such a bound is proportional to the inverse of the time extent of the system [8], $\lambda_{\min} \sim 1/T$. Thus, *no zero modes* can appear in the presence of SF boundary conditions and the theory can be safely defined in the chiral limit i.e. at exactly zero value of the quark masses. Therefore, SF schemes are a natural candidate to carry out a mass-independent renormalization on the lattice.

If a particular regularization is chosen in the large scale simulations, from which the bare quantities are obtained, the corresponding renormalization scheme must be defined through the *same* regulator. Here, we are interested in defining a non-perturbative and mass-independent SF renormalization scheme for twisted mass fermions at maximal twist and Wilson gauge action. Thus, renormalization is also performed using the Wilson gauge action and twisted mass Wilson fermions at maximal twist. The definition of the SF in the gauge sector with Wilson gauge action has been discussed in detail in Sec. 3.2. The fermion sector is however more involved and it is what occupies the discussion in the present section and following chapters.

As detailed above in previous sections, the SF scheme with massless Wilson fermions has been and is extensively used, in its unimproved and improved formulations, as a renormalization scheme of bare quantities computed from large volume simulations using, respectively, unimproved or improved Wilson fermions (cf. Sec. 2.7.2, 3.2.2). Since, at zero quark mass Wilson and twisted mass Wilson formulations are exactly equivalent, the SF with *massless* unimproved (standard) Wilson fermions can be equally used as a renormalization scheme for twisted mass Wilson fermions. Note, however, that the SF in its improved (clover) formulation could not be used to renormalize twisted mass Wilson or unimproved Wilson fermions, because clover is a different regularization even in the chiral limit.

When discussing twisted mass Wilson fermions (cf. Sec. 2.7.3), it has been emphasized the property of automatic $O(a)$-improvement [24], which is realized when working at the condition of maximal twist. This condition is guaranteed with a proper tuning of the untwisted quark mass to its critical value, as discussed in Sec. 2.7.3 and Sec. 3.1. (See App. C.5 for a detailed proof of automatic $O(a)$-improvement). Clearly, the property of automatic $O(a)$-improvement should not be lost in the renormalization of the theory. Therefore, it is important to understand whether this property, of twisted mass Wilson fermions at maximal twist, is maintained after renormalization through the SF scheme with massless Wilson fermions. Note that, talking of automatic $O(a)$-improvement when using a formulation with SF boundaries, always refers to the bulk of the lattice, since boundary improvement counterterms are always present in any formulation of the theory with SF-like boundary conditions.

In fact, it can be shown [18, 26, 59] that the standard Schrödinger functional (or SF) boundary conditions, defined in Eq. (3.56)-(3.57), spoil the property of automatic $O(a)$-improvement which, otherwise, massless Wilson fermions would enjoy in a finite volume (cf. App. C.5). The reason is that the SF boundary conditions, Eq. (3.56)-(3.57), break chiral symmetry. In par-

[8] There is no proof beyond tree-level. Yet, according to the numerical studies, this argument is expected to hold in the interacting theory provided the size of the system is small enough.

ticular, the SF projectors, $P_\pm$, defined above in Eq. (3.53), do not commute with the chiral transformation $\mathcal{R}_5$, defined as

$$\psi(x) \longrightarrow \mathrm{i}\gamma_5\,\psi(x)\,, \quad \overline{\psi}(x) \longrightarrow \overline{\psi}(x)\,\mathrm{i}\gamma_5\,. \tag{3.98}$$

Instead, they behave as follows,

$$P_\pm\,\gamma_5 = \gamma_5\,P_\mp\,, \tag{3.99}$$

which implies that the transformed fields,

$$\psi'(x) = \mathrm{i}\gamma_5\,\psi(x)\,, \quad \overline{\psi}'(x) = \overline{\psi}(x)\,\mathrm{i}\gamma_5\,, \tag{3.100}$$

satisfy the complementary boundary conditions,

$$P_-\,\psi'(x)|_{x_0=0} = 0 \qquad\qquad P_+\,\psi'(x)|_{x_0=T} = 0 \tag{3.101}$$

$$\overline{\psi}'(x)\,P_+|_{x_0=0} = 0 \qquad\qquad \overline{\psi}'(x)\,P_-|_{x_0=T} = 0\,. \tag{3.102}$$

As a result, $\mathcal{R}_5$ is not anymore a symmetry of the theory, already at the *continuum* level.

According to the arguments given in App. C.5, the invariance of the massless continuum theory under chiral symmetry, $\mathcal{R}_5$, is the basis for automatic $O(a)$-improvement to hold at the level of the discretized theory. This implies that no automatic $O(a)$-improvement can take place for massless Wilson fermions with *standard* SF boundary conditions. Consequently, it is necessary to add and compute improvement counterterms to the action in the *bulk* and to the interpolating fields, which are otherwise avoided when automatic $O(a)$-improvement is at work (boundary counterterms are always present in any formulation with SF-like boundaries).

Yet, a solution to this problem has been proposed in [18, 26, 59]. Stefan Sint argued that bulk automatic $O(a)$-improvement of massless Wilson fermions in a finite volume and having SF-like boundary conditions can be maintained. This is possible if there exists a transformation which is a symmetry of the massless continuum theory without boundaries, that leaves invariant the homogeneous SF boundary conditions and which is broken by the Wilson term. It is also possible if a different formulation of the homogeneous SF boundary conditions is found, which stay invariant under the corresponding symmetry transformation. The suggestion in [26] was to consider a flavor doublet of quarks and to use the transformation $\mathcal{R}_5^{1,2}$, which is just $\mathcal{R}_5$ augmented with a flavor structure. $\mathcal{R}_5^{1,2}$ is still a symmetry of the massless continuum action and it is explicitly broken by the Wilson term. Its definition is the following,

$$\chi(x) \xrightarrow{\mathcal{R}_5^{1,2}} \mathrm{i}\gamma_5\tau^{1,2}\,\chi(x)\,, \quad \overline{\chi}(x) \xrightarrow{\mathcal{R}_5^{1,2}} \overline{\chi}(x)\,\mathrm{i}\gamma_5\tau^{1,2}\,. \tag{3.103}$$

Using $\mathcal{R}_5^{1,2}$, automatic $O(a)$-improvement can be shown in the same way as with $\mathcal{R}_5$ (cf. App. C.5).

For the fermionic SF boundary conditions, two possibilities were proposed in [26] which remain invariant under $\mathcal{R}_5^{1,2}$. A first choice could be to keep the standard boundary conditions augmented with a flavor structure, by changing the projectors to

$$\widetilde{P}_\pm = \frac{1}{2}\,(1 \pm \gamma_0\tau^3)\,. \tag{3.104}$$

The second possibility consists in using different projectors, $\widetilde{Q}_\pm$, defined as follows

$$\widetilde{Q}_\pm = \frac{1}{2}\,(1 \pm \mathrm{i}\gamma_0\gamma_5\tau^3)\,. \tag{3.105}$$

While both boundary conditions, resulting from these projectors, are in principle a valid choice, only the ones given by the projectors of Eq. (3.105) have been studied so far [25, 26, 92, 93]. The reason is that no lattice action has been found which fulfills the boundary conditions with the projectors defined in Eq. (3.104). Concerning the boundary conditions arising from the projectors $\widetilde{Q}_{\pm}$, they can be obtained, in the continuum theory, from the standard (homogeneous) SF boundary conditions, Eq. (3.56)-(3.57), by a non-anomalous axial transformation of the fermion fields as given in Eq. (2.97). They are referred to as *chirally rotated* SF (χSF) boundary conditions and can be seen as the standard SF boundary conditions in a different basis, the twisted basis $\{\chi(x), \overline{\chi}(x)\}$. As it will be discussed in detail in Chap. 4, the resulting boundary conditions satisfied by the fermion fields in the continuum are

$$\widetilde{Q}_{+}\,\chi(x)|_{x_0=0} = 0 \qquad \widetilde{Q}_{-}\,\chi(x)|_{x_0=T} = 0 \tag{3.106}$$

$$\overline{\chi}(x)\,\widetilde{Q}_{+}|_{x_0=0} = 0 \qquad \overline{\chi}(x)\,\widetilde{Q}_{-}|_{x_0=T} = 0\,. \tag{3.107}$$

In the same way as between twisted mass and standard fermions, there is a dictionary relating correlation functions in both bases. The relation between the χSF and the SF boundary conditions in the continuum theory is what makes the χSF boundary conditions so interesting with respect to the ones obtained from the projectors in Eq. (3.104); the fact the SF and χSF are related by a change of basis in the continuum implies that both formulations are exactly equivalent.

There has been another proposal, which also attempts to solve the problem of automatic $O(a)$-improvement of massless Wilson fermions in a finite volume with SF boundary conditions. In [19] R. Frezzotti and G.C. Rossi suggested still a different type of SF boundary conditions. This formulation is denoted throughout this thesis as γ_5SF, in order to distinguish it from the SF and χSF formulations. The authors of [19] suggest to keep $\mathcal{R}_5$ as the symmetry employed to argue automatic $O(a)$-improvement, but to use different projectors which remain invariant under $\mathcal{R}_5$. A flavor doublet is also assumed in this formulation. The boundary conditions are in this case[9],

$$\widetilde{\Pi}_{+}\,\phi(x)|_{x_0=0} = 0 \qquad \widetilde{\Pi}_{-}\,\phi(x)|_{x_0=T} = 0 \tag{3.108}$$

$$\overline{\phi}(x)\,\widetilde{\Pi}_{-}|_{x_0=0} = 0 \qquad \overline{\phi}(x)\,\widetilde{\Pi}_{+}|_{x_0=T} = 0 \tag{3.109}$$

with the projectors,

$$\widetilde{\Pi}_{\pm} = \frac{1}{2}\left(1 \pm \gamma_5 \tau^3\right). \tag{3.110}$$

In the course of this thesis, we have performed an analytical study and comparison in the free continuum theory of both formulations, χSF and γ_5SF [25], which is presented in Chap. 4. As it will be shown in Chap. 4, we have found certain problems in the γ_5SF formulation. Therefore, only studies from the χSF formulation have been carried out at the non-perturbative level both, from the pure theoretical point of view [18, 25, 26, 59] and numerically on the lattice [92, 93], in the quenched approximation. All our analytical and numerical results are collected in following chapters.

[9] Note that a different notation from the one in [19] is used in the definition of the projectors. A 'tilde' has been added, following the notation in [26], to denote the presence of a flavor structure. The cases without 'tilde' will refer to the single flavor case.

4. Chiral rotation of the SF in the continuum

At the end of the previous chapter, the necessity of having a Schrödinger functional renormalization scheme with *chirally rotated* Dirichlet boundary conditions in time direction was stressed. In this case, bulk automatic $O(a)$-improvement is expected to be preserved on the lattice with massless Wilson fermions and SF-like boundary conditions. Two proposals appeared in the literature within this context, the χSF [18, 26, 59] (cf. Eq. (3.106)-(3.107)) and the γ_5SF [19] (cf. Eq. (3.108)-(3.109)).

In order to understand which of the two chiral formulations of the SF we wanted to use as renormalization scheme, our first step was to analyze the *continuum target theory* at tree-level of perturbation theory in both formulations. In particular, we investigated [25] the *spectral properties* and the *quark propagators* which derive from the two proposals. In this chapter, the results of that study are presented with the corresponding conclusion why we eventually use one scheme and not the other.

In Sec. 4.1 we collect the three different types of SF boundary conditions that have been proposed. We present our results on the study of the eigenvalue spectrum in Sec. 4.2 and the quark propagators in Sec. 4.3. The chapter is closed in Sec. 4.4 with a discussion of the obtained results and a conclusion on which SF scheme is to be used.

4.1. Definition of the boundary conditions

The aim of this section is to recall the expressions of the three types of SF boundary conditions introduced in the previous chapter, in order to make clear the discussion of the spectrum and quark propagator in following sections.

4.1.1. Standard SF boundary conditions

The homogeneous standard SF boundary conditions [15, 82] were introduced in Sec. 3.2.1. For convenience they are recalled here and given by the equations,

$$P_+\,\psi(x)|_{x_0=0} = 0 \qquad\qquad P_-\,\psi(x)|_{x_0=T} = 0 \quad \text{via } \mathcal{T} \tag{4.1}$$

$$\overline{\psi}(x)\,P_-|_{x_0=0} = 0 \quad \text{via } \mathcal{C} \qquad\qquad \overline{\psi}(x)\,P_+|_{x_0=T} = 0 \quad \text{via } \mathcal{T} \text{ and } \mathcal{C} \tag{4.2}$$

with the projectors,

$$P_\pm = \frac{1}{2}\,(1 \pm \gamma_0)\ . \tag{4.3}$$

The boundary conditions on the non-vanishing components are,

$$P_-\,\psi(x)|_{x_0=0} = \zeta(\vec{x}) \qquad\qquad P_+\,\psi(x)|_{x_0=T} = \zeta'(\vec{x}) \tag{4.4}$$

$$\overline{\psi}(x)\,P_+|_{x_0=0} = \overline{\zeta}(\vec{x}) \qquad\qquad \overline{\psi}(x)\,P_-|_{x_0=T} = \overline{\zeta}'(\vec{x})\,. \tag{4.5}$$

The boundary conditions have been supplemented with the comments 'via $\mathcal{C}$ or $\mathcal{T}$'. This notation means that these boundary conditions are obtained from the ones of the quark field $\psi(x)$ at $x_0 = 0$ using the transformations[1] $\mathcal{C}$ and/or $\mathcal{T}$, which are charge conjugation and time

[1] For definitions of the symmetries see App. B.1.

reversal, respectively. These transformation symmetries are important for the discussions below, since they, together with parity, $\mathcal{P}$, are the discrete symmetries of QCD even in a finite volume with SF boundary conditions.

4.1.2. χSF boundary conditions

In the continuum, the χSF boundary conditions can be obtained from the homogeneous standard SF boundary conditions via the non-singlet axial transformation defined in Eq. (2.97), at maximal twist $\alpha = \pi/2$. This was already mentioned at the end of the last chapter but it is shown here explicitly. Applying such a rotation to the quark and anti-quark fields, for a general rotation angle α, the boundary conditions take the form,

$$\widetilde{P}_+(\alpha)\,\chi(x)|_{x_0=0} = 0 \qquad \widetilde{P}_-(\alpha)\,\chi(x)|_{x_0=T} = 0 \tag{4.6}$$

$$\overline{\chi}(x)\gamma_0\,\widetilde{P}_-(\alpha)|_{x_0=0} = 0 \qquad \overline{\chi}(x)\gamma_0\,\widetilde{P}_+(\alpha)|_{x_0=T} = 0 \tag{4.7}$$

with the projectors

$$\widetilde{P}_\pm(\alpha) = \frac{1}{2}\left(1 \pm \gamma_0\, e^{\mathrm{i}\alpha\gamma_5\tau^3}\right). \tag{4.8}$$

The boundary conditions on the non-vanishing components are defined by identifying them with the fermionic boundary fields as follows,

$$\widetilde{P}_-(\alpha)\,\chi(x)|_{x_0=0} = \zeta(\vec{x}) \qquad \widetilde{P}_+(\alpha)\,\chi(x)|_{x_0=T} = \zeta'(\vec{x}) \tag{4.9}$$

$$\overline{\chi}(x)\,\widetilde{P}_+(-\alpha)|_{x_0=0} = \overline{\zeta}(\vec{x}) \qquad \overline{\chi}(x)\,\widetilde{P}_-(-\alpha)|_{x_0=T} = \overline{\zeta}'(\vec{x})\,. \tag{4.10}$$

If the maximal twist condition is chosen, $\alpha = \frac{\pi}{2}$, the χSF boundary conditions are obtained,

$$\widetilde{Q}_+\,\chi(x)|_{x_0=0} = 0 \qquad \widetilde{Q}_-\,\chi(x)|_{x_0=T} = 0 \quad \text{via } \mathcal{T}_{\pi/2} \tag{4.11}$$

$$\overline{\chi}(x)\,\widetilde{Q}_+|_{x_0=0} = 0 \quad \text{via } \mathcal{C} \qquad \overline{\chi}(x)\,\widetilde{Q}_-|_{x_0=T} = 0 \quad \text{via } \mathcal{T}_{\pi/2} \text{ and } \mathcal{C} \tag{4.12}$$

with projectors

$$\widetilde{Q}_\pm \equiv \widetilde{P}_\pm(\pi/2) = \frac{1}{2}\left(1 \pm \mathrm{i}\gamma_0\gamma_5\tau^3\right). \tag{4.13}$$

The boundary conditions on the non-vanishing components are,

$$\widetilde{Q}_-\,\chi(x)|_{x_0=0} = \zeta(\vec{x}) \qquad \widetilde{Q}_+\,\chi(x)|_{x_0=T} = \zeta'(\vec{x}) \tag{4.14}$$

$$\overline{\chi}(x)\,\widetilde{Q}_-|_{x_0=0} = \overline{\zeta}(\vec{x}) \qquad \overline{\chi}(x)\,\widetilde{Q}_+|_{x_0=T} = \overline{\zeta}'(\vec{x})\,. \tag{4.15}$$

It is important to notice the correspondence between the relation SF-χSF and QCD-tmQCD. The discrete symmetries of the SF are the same as those of QCD while the discrete symmetries of the χSF correspond to the ones of tmQCD at maximal twist. In fact, these symmetries are not different at all in both formulations, they are just expressed in a different basis. Therefore, in the continuum, the SF and the χSF share all the symmetries[2].

[2] See App. B for a definition of all these symmetries.

4.1.3. γ_5SF boundary conditions

The γ_5SF boundary conditions proposed in [19] are

$$\widetilde{\Pi}_+\phi(x)|_{x_0=0} = 0 \qquad \widetilde{\Pi}_-\phi(x)|_{x_0=T} = 0 \quad \text{via } \mathcal{T} \tag{4.16}$$

$$\overline{\phi}(x)\widetilde{\Pi}_-|_{x_0=0} = 0 \quad \text{via } \mathcal{C}_F^{1,2} \qquad \overline{\phi}(x)\widetilde{\Pi}_+|_{x_0=T} = 0 \quad \text{via } \mathcal{T} \text{ and } \mathcal{C}_F^{1,2} \tag{4.17}$$

with the projectors

$$\widetilde{\Pi}_\pm = \frac{1}{2}\left(1 \pm \gamma_5\tau^3\right) . \tag{4.18}$$

The boundary conditions in Eq. (4.16)-(4.17) can not be brought to the standard ones by any transformation of the quark fields in the continuum theory. This observation is already a warning. The fact that the boundary conditions are different already at the continuum level, might lead to difficulties to check universality once the system is put on the lattice.

Moreover, although $\mathcal{CPT}$ is still a symmetry of this formulation, the discrete symmetries [3] separately are in this case, $\mathcal{C}_F^{1,2}$, $\mathcal{P}_F^{1,2}$, $\mathcal{T}$. These symmetries are different from the discrete symmetries of both the SF and the χSF. At first sight this is not a reason to dismiss such boundary conditions but, as it will be discussed below, some problems arise due to the particular symmetries of this formulation which, already in the continuum, do not agree with the symmetries of QCD.

4.2. Spectral properties of the Dirac operator

We present here our analysis of the spectral properties of the Dirac operator. We studied the eigenvalues of the *free* Dirac operator in the *continuum* theory for the two new formulations of the SF boundary conditions, the χSF and the γ_5SF. For this analysis we followed closely the study of [15] for the standard formulation of the SF. Concerning the standard SF, only the main results are collected here and the reader is referred to the literature for a more comprehensive discussion. It is well known that in the standard formulation the eigenvalue spectrum of the Dirac operator has a gap. Such a gap is of capital importance if the theory is to be eventually studied on the lattice, where the numerical inversion of the Dirac operator is required. In the massless limit, the Dirac operator may have zero modes which cause problems in the numerical inversion. In particular, the massless theory has to be considered if a mass independent renormalization scheme is to be defined, as it is our case in this thesis. Therefore, the main interest of this section is to find out whether the newly proposed SF formulations retain the gap in the eigenvalue spectrum at tree-level of perturbation theory.

4.2.1. Spectral properties: standard SF

The Dirac operator, D, in the free continuum theory is given as

$$D = \gamma_\mu\partial_\mu + m\,, \tag{4.19}$$

where m is the usual mass term in continuum QCD.

Due to the presence of the SF boundary conditions, ψ and $\overline{\psi}^\dagger$ (see [15] for unexplained notations) belong to different vector spaces. This generates an ill-defined eigenvalue problem of the Dirac operator D. As it was argued in [15], the ellipticity[4] of the operators D and $D^\dagger$

[3] See App. B.1 for definitions of the symmetries.

[4] An operator is elliptic if the principal symbol of the operator does not vanish when its argument is non zero. In our case the principal symbol is given by $i\gamma_\mu p_\mu$, which vanishes only when $p_\mu = 0$.

guarantees the existence of a first order elliptic boundary value problem with the operator $\mathcal{D}$ defined by

$$\mathcal{D} \equiv \begin{pmatrix} 0 & D^\dagger \\ D & 0 \end{pmatrix} ,$$

which is an hermitian operator acting in a linear space $\mathcal{H}$ with projectors

$$\widetilde{P}_\pm = \frac{1}{2}\left(1 \pm \gamma_0 \tau^3\right), \tag{4.20}$$

and fields $\Psi(x)$, two-components vectors in $\mathcal{H}$,

$$\Psi(x) = \begin{pmatrix} \psi(x) \\ \overline{\psi}^\dagger(x) \end{pmatrix} .$$

This allows to write down the action as a quadratic form[5] and to have a well defined eigenvalue problem, provided the complementary components of the quark fields satisfy Neumann boundary conditions as follows,

$$(\partial_0 - m)\, \widetilde{P}_-\, \Psi(x)|_{x_0=0} = 0\,, \qquad (\partial_0 + m)\, \widetilde{P}_+\, \Psi(x)|_{x_0=T} = 0\,, \tag{4.21}$$

or equivalently,

$$(\partial_0 - m)\, P_-\, \psi(x)|_{x_0=0} = 0 \qquad (\partial_0 + m)\, P_+\, \psi(x)|_{x_0=T} = 0 \tag{4.22}$$

$$\overline{\psi}(x)\, P_+\, (\partial_0 + m)|_{x_0=0} = 0 \qquad \overline{\psi}(x)\, P_-\, (\partial_0 - m)|_{x_0=T} = 0\,. \tag{4.23}$$

With the additional boundary conditions it is possible to solve the eigenvalue problem of $\mathcal{D}^2$

$$\mathcal{D}^2 = \begin{pmatrix} D^\dagger D & 0 \\ 0 & D D^\dagger \end{pmatrix} ,$$

which is a second order boundary value problem with half of the components of the quark fields satisfying Dirichlet-type boundary conditions (cf. Eq. (4.1)-(4.2)) and the other half obeying Neumann-type boundary conditions (cf. Eq. (4.22)-(4.23)). The solution to this problem provides the solution to the eigenvalue problem for the operator $D^\dagger D$. This is enough to scrutinize the properties of the spectrum of the Dirac operator with boundaries, because the propagator can be written as $D^{-1} = (D^\dagger D)^{-1} D^\dagger$. Thereby, it is sufficient to study the eigenvalue spectrum and eigenfunctions of $\mathcal{D}^2$, which is a diagonal problem in Dirac space and therefore easier to solve than the problem for $\mathcal{D}$ itself.

The presence of the Neumann boundary conditions fixes the values of the frequency, p_0, which has to satisfy

$$\tan\left(p_0\, T\right) = -\,\frac{p_0}{m}. \tag{4.24}$$

This equation originates as a consequence of the boundary conditions in the time direction and it implicitly defines the discrete eigenvalue spectrum.

Since the discrete spatial momenta are given by $\vec{p} = 2\pi\vec{n}/L$, the eigenvalues of $\mathcal{D}^2$ can be written as

$$\lambda_n^2 = p_0^2 + (\frac{2\pi\vec{n}}{L})^2 + m^2\,, \qquad \vec{n} = (n_1, n_2, n_3), \quad n_{i=1,2,3} \in \mathcal{Z}\,. \tag{4.25}$$

Therefore, due to the boundary conditions the problem has a discrete spectrum with eigenvalues

[5] The quadratic dependence of the action on the quark fields guarantees the existence of stationary points of the action, thus, the existence of a classical solution.

which are all non-negative. Indeed, it can be seen that these eigenvalues are all *strictly positive* at finite T, whenever the mass is not infinitely negative [15].

In particular, in the massless limit the minimum eigenvalue is given by

$$\lambda_0^2(m=0) = \left(\frac{\pi}{2\mathrm{T}}\right)^2 . \tag{4.26}$$

It is clear from this equation how the bound in the spectrum originates from the boundary conditions in the time direction, since it is the time extent of the system, T, which provides the spectral gap. The existence of this bound is a crucial point if a mass independent scheme is to be defined on the lattice, where the numerical inversion of $D^\dagger D$ is required in the massless limit.

4.2.2. Spectral properties: χSF

In the χSF setup a two flavor theory is considered. In a similar way as it was done for the SF, a linear space $\mathcal{H}$ can be constructed as a direct sum of two pre-Hilbert spaces[6], each of them corresponding to one flavor. We denote the two flavors as $u(x)$ and $d(x)$ and consider them to satisfy the χSF boundary conditions given, respectively, by

$$Q_+\, u(x)|_{x_0=0} = 0 \qquad Q_-\, u(x)|_{x_0=T} = 0 \tag{4.27}$$

$$\overline{u}(x)\, Q_+|_{x_0=0} = 0 \qquad \overline{u}(x)\, Q_-|_{x_0=T} = 0 \tag{4.28}$$

and

$$Q_-\, d(x)|_{x_0=0} = 0 \qquad Q_+\, d(x)|_{x_0=T} = 0 \tag{4.29}$$

$$\overline{d}(x)\, Q_-|_{x_0=0} = 0 \qquad \overline{d}(x)\, Q_+|_{x_0=T} = 0\,, \tag{4.30}$$

where the projectors are defined as follows

$$Q_\pm = \frac{1}{2}\left(1 \pm \mathrm{i}\gamma_0\gamma_5\right) . \tag{4.31}$$

As in the standard case, the boundary conditions define two different pre-Hilbert spaces, given by the expressions

$$\mathcal{H}_u \equiv \{u(x) : Q_+\, u(x)|_{x_0=0} = 0\,, \quad Q_-\, u(x)|_{x_0=T} = 0\} \ , \tag{4.32}$$

$$\mathcal{H}_d \equiv \{d(x) : Q_-\, d(x)|_{x_0=0} = 0\,, \quad Q_+\, d(x)|_{x_0=T} = 0\} \ , \tag{4.33}$$

with inner product

$$(u_1, u_2)_{\mathcal{H}_u} \equiv \int_0^L \mathrm{d}^3x \int_0^T \mathrm{d}x_0\, u_1^\dagger(x) u_2(x) \tag{4.34}$$

and the corresponding equation for $d(x)$. Due to the boundaries, $\overline{u}(x)$ defines $\overline{u}^\dagger(x) \in \mathcal{H}_u$ and $\overline{d}(x)$ defines $\overline{d}^\dagger(x) \in \mathcal{H}_d$.

For later purposes, we decided to study the continuum Dirac operator with a general twisted mass term, $m_\mathrm{q} + \mathrm{i}\mu_\mathrm{q}\gamma_5\tau^3$. The Dirac operator can be defined separately for the two quark flavors,

[6] An inner product space, also called pre-Hilbert space, is a vector space of arbitrary dimension with additional structure given by the inner product. Its completion with respect to the metric induced by the inner product is a Hilbert space.

with D_u acting on $u(x)$ and D_d acting on $d(x)$,

$$D_u = \gamma_\mu \partial_\mu + m_\mathrm{q} + \mathrm{i}\mu_\mathrm{q}\gamma_5 = \gamma_5 D_d^\dagger \gamma_5 \,, \tag{4.35}$$

$$D_d = \gamma_\mu \partial_\mu + m_\mathrm{q} - \mathrm{i}\mu_\mathrm{q}\gamma_5 = \gamma_5 D_u^\dagger \gamma_5 \,. \tag{4.36}$$

The two-flavor fermion action is the sum of the actions of the two flavors separately,

$$S_\mathrm{F} = S_\mathrm{F}^u \left[\overline{u}, u\right] + S_\mathrm{F}^d \left[\overline{d}, d\right] \tag{4.37}$$

with

$$S_\mathrm{F}^u \left[\overline{u}, u\right] = \int_0^L \mathrm{d}^3 x \int_0^T \mathrm{d}x_0 \, \overline{u}(x) \, D_u \, u(x) \tag{4.38}$$

$$S_\mathrm{F}^d \left[\overline{d}, d\right] = \int_0^L \mathrm{d}^3 x \int_0^T \mathrm{d}x_0 \, \overline{d}(x) \, D_d \, d(x) \,. \tag{4.39}$$

First of all, in order to be able to write down the fermion action, for each flavor, as a quadratic form,

$$S_\mathrm{F}^u \left[\overline{u}, u\right] = \left(\overline{u}^\dagger, D_u u\right)_{\mathcal{H}_u} = \left(D_u^\dagger \overline{u}^\dagger, u\right)_{\mathcal{H}_u} \,, \tag{4.40}$$

$$S_\mathrm{F}^d \left[\overline{d}, d\right] = \left(\overline{d}^\dagger, D_d d\right)_{\mathcal{H}_d} = \left(D_d^\dagger \overline{d}^\dagger, d\right)_{\mathcal{H}_d} \,, \tag{4.41}$$

thus guaranteeing the existence of a classical solution, it must be imposed that the Dirac operators for each flavor act as follows in the pre-Hilbert spaces,

$$D_u : \, \mathcal{H}_u \longmapsto \mathcal{H}_u \,, \qquad D_u^\dagger : \, \mathcal{H}_u \longmapsto \mathcal{H}_u \,, \tag{4.42}$$

$$D_d : \, \mathcal{H}_d \longmapsto \mathcal{H}_d \,, \qquad D_d^\dagger : \, \mathcal{H}_d \longmapsto \mathcal{H}_d \,, \tag{4.43}$$

which is equivalent to demand that

$$D_u \, u(x) \in \mathcal{H}_u \qquad D_d \, d(x) \in \mathcal{H}_d \,. \tag{4.44}$$

These conditions already guarantee a well defined eigenvalue problem for each flavor separately. That is, $u(x)$ and $D_u \, u(x)$ belong to the same space $\mathcal{H}_u$ and $d(x)$ and $D_d \, d(x)$ are both in $\mathcal{H}_d$. Therefore, contrary to the standard SF, for the χSF it is not strictly necessary to define a two-term linear space to have a well defined eigenvalue problem. Nevertheless, a two flavor structure is needed to construct a lattice operator using orbifolding techniques [18]. For this reason, from now on the two flavor structure is kept, having in mind that for the purposes of this particular discussion it is not really needed.

In order to write down all the expressions as a two-flavor structure, we define spinors with two flavor components as

$$\chi(x) \equiv \begin{pmatrix} u(x) \\ d(x) \end{pmatrix}$$

and a Dirac operator with a two flavor structure, which acts on $\chi(x)$, given by

$$D \equiv \gamma_\mu \partial_\mu + m_\mathrm{q} + \mathrm{i}\mu_\mathrm{q}\gamma_5 \tau^3 = \begin{pmatrix} D_u & 0 \\ 0 & D_d \end{pmatrix} \,,$$

with the two-flavor fermion action,

$$S_{\mathrm{F}}\left[\overline{\chi},\chi\right] = \int_0^L \mathrm{d}^3x \int_0^T \mathrm{d}x_0\, \overline{\chi}(x)\, D\, \chi(x)\,. \tag{4.45}$$

This is just the twisted mass fermionic action in the free continuum theory, with the Dirac operator D being the twisted mass free Dirac operator. The projectors $Q_\pm$ can be substituted by defining projectors, $\widetilde{Q}_\pm$, which account for the flavor structure. These are indeed the χSF projectos defined above in Eq. (4.13). In this way it becomes possible to construct a linear space $\mathcal{H}$,

$$\mathcal{H} \equiv \mathcal{H}_u \oplus \mathcal{H}_d = \left\{\chi(x) : \widetilde{Q}_+\, \chi(x)|_{x_0=0} = 0\,, \quad \widetilde{Q}_-\, \chi(x)|_{x_0=T} = 0\right\}\,. \tag{4.46}$$

D is then an elliptic operator which entails a well-defined eigenvalue problem and for $m_{\mathrm{q}} = 0$ (maximal twist) is anti-hermitian. Its action on smooth functions of $\mathcal{H}$ is such that

$$D:\ \mathcal{H} \longmapsto \mathcal{H}\,. \tag{4.47}$$

The fermion action can be written as a quadratic form in the linear space $\mathcal{H}$

$$S_{\mathrm{F}}\left[\overline{\chi},\chi\right] = \left(\overline{\chi}^\dagger, D\chi\right)_{\mathcal{H}} = \left(D^\dagger\overline{\chi}^\dagger, \chi\right)_{\mathcal{H}}\,. \tag{4.48}$$

As it was the case in the standard SF setup, the conditions on D_u and D_d given by Eq. (4.44) determine Neumann boundary conditions for the complementary components of the quark fields and these are given by

$$(\partial_0 - \mu_{\mathrm{q}})\, \widetilde{Q}_-\, \chi(x)|_{x_0=0} = 0\,, \quad (\partial_0 + \mu_{\mathrm{q}})\, \widetilde{Q}_+\, \chi(x)|_{x_0=T} = 0\,. \tag{4.49}$$

It is interesting to note here that this boundary conditions have the same structure as in the standard case but now, all the dependence on the mass term is given by the twisted mass. The consequences of this fact are presented in the following paragraphs.

The operator

$$D^\dagger D = \begin{pmatrix} D_u^\dagger D_u & 0 \\ 0 & D_d^\dagger D_d \end{pmatrix}$$

defines, as D, an elliptic boundary value problem which is of second order in this case and can be solved in virtue of the additional boundary conditions on the complementary components of the quark fields. For the same reasons as in the standard formulation, we are interested in solving the second order eigenvalue problem defined by the operator $D^\dagger D$, which also acts on the smooth functions $\chi(x)$.

To study the spectrum of the operator $D^\dagger D$, which is diagonal in Dirac and flavor spaces, it is rewritten in the form

$$D^\dagger D = \begin{pmatrix} \left(-\partial_\mu^2 + m_{\mathrm{q}}^2 + \mu_{\mathrm{q}}^2\right) & 0 \\ 0 & \left(-\partial_\mu^2 + m_{\mathrm{q}}^2 + \mu_{\mathrm{q}}^2\right) \end{pmatrix}\,.$$

Because of the periodic boundary conditions in the spatial directions, we can consider the problem in the time-momentum representation

$$\chi(x) = \frac{1}{L^3} \sum_{\vec{p}} e^{\mathrm{i}\vec{p}\vec{x}}\, \chi(x_0, \vec{p})\,, \tag{4.50}$$

thus the operator $D^\dagger D$ acts as follows

$$D^\dagger D\,\chi(x) = \frac{1}{L^3}\sum_{\vec{p}} e^{\mathrm{i}\vec{p}\vec{x}} \begin{pmatrix} \left(-\partial_0^2 + \vec{p}^2 + m_{\mathrm{q}}^2 + \mu_{\mathrm{q}}^2\right) & 0 \\ 0 & \left(-\partial_0^2 + \vec{p}^2 + m_{\mathrm{q}}^2 + \mu_{\mathrm{q}}^2\right) \end{pmatrix} \chi(x_0,\vec{p})\,.$$

$\chi(x)$ (or $\chi(x_0,\vec{p})$) is a vector with eight components $\chi(x)_l$ ($\chi(x_0,\vec{p})_l$). Due to the diagonal structure of $D^\dagger D$ we can consider the eigenvalue problem on each component separately as

$$\left(-\partial_0^2 + \vec{p}^2 + m_{\mathrm{q}}^2 + \mu_{\mathrm{q}}^2\right)\chi(x_0,\vec{p})_l = \lambda^2\,\chi(x_0,\vec{p})_l\,, \qquad l = 1,\ldots,8 \tag{4.51}$$

with either the boundary conditions

$$\chi(0,\vec{p})_l = 0\,, \quad \chi'(T,\vec{p})_l + \mu_{\mathrm{q}}\,\chi(T,\vec{p})_l = 0\,, \tag{4.52}$$

in case $\chi(x_0,\vec{p})_l$ belongs to the subspace defined by $\widetilde{Q}_+$, or

$$\chi(T,\vec{p})_l = 0\,, \quad \chi'(0,\vec{p})_l - \mu_{\mathrm{q}}\,\chi(0,\vec{p})_l = 0\,, \tag{4.53}$$

if $\chi(x_0,\vec{p})_l$ belongs to the subspace defined by $\widetilde{Q}_-$. In these equations, the primes denote partial derivatives with respect to time.

We are dealing with exactly the same equations as in [15] for the case of standard SF boundary conditions but with two important differences. First of all, the role played by the standard mass term, m, appearing in the Neumann boundary conditions in the standard case, is now played by the twisted quark mass μ_{q}. Secondly, we are now solving the equations for the functions χ_l, belonging to the subspaces generated by either $\widetilde{Q}_+$ or $\widetilde{Q}_-$ and not, as before, $\widetilde{P}_\pm$. Indeed, note that the meaning of $\widetilde{Q}_\pm$ is different from the one of $\widetilde{P}_\pm$. The solution of the problem whose eigenfunctions belong to $\widetilde{Q}_+$ determines the + components of the u quark fields and the − components of the d quark fields. The problem for the eigenfunctions belonging to $\widetilde{Q}_-$ determines the other components. However, in the standard case the subspace defined by $\widetilde{P}_+$ defines the plus and minus components of ψ and $\overline{\psi}^\dagger$, respectively, and the other way around for the subspace of $\widetilde{P}_-$.

The eigenvalue equation, Eq. (4.51), is the equation of a harmonic oscillator with frequency, p_0,

$$p_0^2 \equiv \lambda^2 - \vec{p}^2 - m_{\mathrm{q}}^2 - \mu_{\mathrm{q}}^2\,, \tag{4.54}$$

whose eigenfunctions are of the kind

$$\chi(x_0,\vec{p})_l = A\,\sin\left(p_0 x_0 + \Phi\right)\,. \tag{4.55}$$

A is the amplitude determined by the normalization condition and Φ the initial phase determined by the boundary conditions.

If $p_0 = 0$ there is a solution only if $\mu_q = -1/T$. In this particular case the eigenfunctions take the form

$$\chi(x_0,\vec{p})_l = Ax_0 + B \tag{4.56}$$

where again, A is determined by the normalization condition and the integration constant B by the boundary conditions.

If $\chi(x_0,\vec{p})_l$ belongs to the subspace defined by $\widetilde{Q}_+$ then,

$$\chi(x_0,\vec{p})_l = A\,\sin\left(p_0 x_0\right)\,, \qquad p_0 \neq 0\,, \tag{4.57}$$

$$\chi(x_0,\vec{p})_l = Ax_0\,, \qquad p_0 = 0\,,\ \mu_{\mathrm{q}} = -1/T\,, \tag{4.58}$$

while for $\chi(x_0,\vec{p})_l$ belonging to the subspace defined by $\widetilde{Q}_-$,

$$\chi(x_0,\vec{p})_l = A\,\sin\left(p_0\,(x_0-T)\right)\,, \qquad p_0 \neq 0\,, \tag{4.59}$$

$$\chi(x_0,\vec{p})_l = A(x_0-T)\,, \qquad p_0 = 0,\ \mu_{\rm q} = -1/T\,. \tag{4.60}$$

The Neumann boundary conditions fix the values of the frequency, p_0, which has to satisfy in both subspaces the same equation

$$\tan\left(p_0\,T\right) = -\,\frac{p_0}{\mu_{\rm q}}\,. \tag{4.61}$$

Eq. (4.61) is the same equation obtained in the standard case, Eq. (4.24), but with the twisted mass instead of the standard quark mass. This condition on p_0 is then a consequence of the χSF boundary conditions introduced here.

The eigenvalues of $D^\dagger D$ are

$$\lambda_n^2 = p_0^2 + (\frac{2\pi\vec{n}}{L})^2 + \mu_{\rm q}^2 + m_{\rm q}^2\,, \qquad \vec{n} = (n_1,n_2,n_3), \quad n_{i=1,2,3} \in \mathcal{Z}\,, \tag{4.62}$$

with p_0 determined by Eq. (4.61). From Eq. (4.61) it is clear that the possible values of p_0 do not depend on the standard mass, but only on the twisted mass in the same way they depend on the standard mass with standard boundary conditions. Looking at Eq. (4.62) it can be seen that the only effect of the untwisted mass term is to lift the eigenvalues similarly to an external shift in the momenta.

As a conclusion, the chirally rotated boundary conditions proposed in [18] define a boundary value problem for the second order differential operator $D^\dagger D$, which has a discrete and positive spectrum with a minimum eigenvalue that in the limit of zero twisted mass is given by

$$\lambda_0^2(\mu_{\rm q}=0) = \left(\frac{\pi}{2T}\right)^2 + m_{\rm q}^2\,. \tag{4.63}$$

It is important to notice that only at maximal twist ($m_{\rm q} = 0$) or in the chiral limit the eigenvalues have exactly the same form as with the standard SF. This equivalence was expected, because the χSF is obtained from a maximal twist rotation of the SF [7], which, in the continuum, is a simple change of variables.

A last comment should be made on the reason why the standard and twisted masses exchange roles in the two formulations. The reason is that the standard mass behaves with respect to the chiral group in the same way as the standard SF boundary conditions. Equally, the twisted mass term behaves in the same way as the chirally rotated SF boundary conditions. Moreover, the twisted mass term is orthogonal, with respect to the chiral group, to the standard SF boundary conditions and the same relation holds between the standard mass term and the χSF boundary conditions.

4.2.3. Spectral properties: γ_5SF

Also in this section a two flavor theory is considered. We construct, in the same way as above, a linear space which is a direct sum of the two pre-Hilbert spaces that correspond to each flavor. The two flavors are represented by the fields $u(x)$ and $d(x)$ satisfying the γ_5SF boundary

[7] This relation can be also seen when we consider the quark propagator with χSF b.c. and a general mass term.

conditions proposed in [19] and given, respectively, by the following equations

$$\Pi_+ u(x)|_{x_0=0} = 0 \qquad \Pi_- u(x)|_{x_0=T} = 0 \tag{4.64}$$
$$\overline{u}(x)\,\Pi_-|_{x_0=0} = 0 \qquad \overline{u}(x)\,\Pi_+|_{x_0=T} = 0 \tag{4.65}$$

$$\Pi_- d(x)|_{x_0=0} = 0 \qquad \Pi_+ d(x)|_{x_0=T} = 0 \tag{4.66}$$
$$\overline{d}(x)\Pi_+|_{x_0=0} = 0 \qquad \overline{d}(x)\Pi_-|_{x_0=T} = 0 \tag{4.67}$$

where the projectors are,

$$\Pi_\pm = \frac{1}{2}\,(1 \pm \gamma_5)\ . \tag{4.68}$$

Two different pre-Hilbert spaces can be defined,

$$\mathcal{H}_u \equiv \{u(x) : \Pi_+\, u(x)|_{x_0=0} = 0\,, \quad \Pi_-\, u(x)|_{x_0=T} = 0\}\ , \tag{4.69}$$
$$\mathcal{H}_d \equiv \{d(x) :\ \Pi_-\, d(x)|_{x_0=0} = 0\,, \quad \Pi_+\, d(x)|_{x_0=T} = 0\}\ , \tag{4.70}$$

with inner product as given in Eq. (4.34). The fermion fields are such that $u(x) \in \mathcal{H}_u$ and $d(x) \in \mathcal{H}_d$ and, due to the boundaries, $\overline{u}(x)$ defines $\overline{u}^\dagger(x) \in \mathcal{H}_d$ and $\overline{d}(x)$ defines $\overline{d}^\dagger(x) \in \mathcal{H}_u$.

We also consider here the continuum Dirac operator with a general mass term, with the definitions given in Eq. (4.35)-(4.36) and the two-flavor fermion action of Eq. (4.37)-(4.38)-(4.39).

In order to write down the fermion action for each flavor as a quadratic form,

$$S_{\rm F}^u\,[\overline{u}, u] = \left(\overline{u}^\dagger, D_u u\right)_{\mathcal{H}_d} = \left(D_u^\dagger \overline{u}^\dagger, u\right)_{\mathcal{H}_u}\ , \tag{4.71}$$
$$S_{\rm F}^d\,\left[\overline{d}, d\right] = \left(\overline{d}^\dagger, D_d d\right)_{\mathcal{H}_u} = \left(D_d^\dagger \overline{d}^\dagger, d\right)_{\mathcal{H}_d}\ , \tag{4.72}$$

the Dirac operators for the two flavors must act as follows

$$D_u :\ \mathcal{H}_u \longmapsto \mathcal{H}_d\,, \qquad D_u^\dagger :\ \mathcal{H}_d \longmapsto \mathcal{H}_u\,, \tag{4.73}$$
$$D_d :\ \mathcal{H}_d \longmapsto \mathcal{H}_u\,, \qquad D_d^\dagger :\ \mathcal{H}_u \longmapsto \mathcal{H}_d\,, \tag{4.74}$$

which is equivalent to

$$D_u\, u(x) \in \mathcal{H}_d \qquad D_d\, d(x) \in \mathcal{H}_u\,. \tag{4.75}$$

Note that due to these conditions the eigenvalue problem for D_u and D_d is, as in the standard case, ill-defined. Again, in order to write down everything in the two-components notation we define spinors with two flavor components,

$$\phi(x) \equiv \begin{pmatrix} u(x) \\ d(x) \end{pmatrix}$$

and a Dirac operator which acts on $\phi(x)$ given by

$$D \equiv \begin{pmatrix} 0 & D_d \\ D_u & 0 \end{pmatrix}\ .$$

Considering also projectors describing the flavor structure, $\widetilde{\Pi}_\pm$, they turn out to be the γ_5SF

projectors defined in Eq. (4.18). Then the linear space $\mathcal{H}$ can be defined such that

$$\mathcal{H} \equiv \mathcal{H}_u \oplus \mathcal{H}_d = \left\{ \phi(x) : \widetilde{\Pi}_+ \, \phi(x)|_{x_0=0} = 0 \,, \quad \widetilde{\Pi}_- \, \phi(x)|_{x_0=T} = 0 \right\} \tag{4.76}$$

and D is an operator which is anti-hermitian in the massless limit and acts as follows

$$D : \; \mathcal{H} \longmapsto \mathcal{H} \,. \tag{4.77}$$

The eigenvalue problem is now well defined. Yet, contrary to what happens in the standard and chirally rotated formulations, the conditions for D_u and D_d given by Eq. (4.75) do *not* imply Neumann boundary conditions for the complementary components of the quark fields. In fact, in this case we obtain the following boundary conditions,

$$\left(m_{\rm q} + i\mu_{\rm q}\gamma_5\tau^3 \right) \widetilde{\Pi}_- \phi(x)|_{x_0=0} = 0 \,, \qquad \left(m_{\rm q} + i\mu_{\rm q}\gamma_5\tau^3 \right) \widetilde{\Pi}_+ \phi(x)|_{x_0=T} = 0 \,. \tag{4.78}$$

These equations have a solution only if either the complete mass term vanishes or the complementary components of the quark fields also satisfy homogeneous Dirichlet boundary conditions. The second case would correspond to an eigenfunction which vanishes everywhere and therefore it is certainly not what we are looking for. It leaves us with the conclusion that this problem could have a non-trivial solution only in the chiral limit, where the previous equations are satisfied automatically. But in this case, there would not be any additional boundary conditions for the complementary components of the quark fields, which is however necessary to solve the second order differential eigenvalue equation for the operator $D^\dagger D$. Moreover, these equations would lead to the same conclusion independently of the form of the mass term. Such a result is a consequence of the fact that there is no distinction between the normal (γ_0) and the tangential (γ_k) components of the fields at the time boundaries ($x_0 = 0, T$) with respect to the projectors here considered, since these last do not contain γ_0 in this formulation.

There is still a further remark which concerns the form of the action. The action can be written as

$$S_{\rm F} = \int_0^L {\rm d}^3x \int_0^T {\rm d}x_0 \, (\overline{d}, \overline{u}) D (u, d)^{\rm T} . \tag{4.79}$$

This unnatural structure of the action is related to the fact that the boundary conditions for the $(\overline{d}, \overline{u})$ fields are not related to the ones for the (u, d) fields through the charge conjugation transformation defined in Eq. (B.7). This issue is treated in more detail below when discussing the quark propagator in Sec. 4.3.5.

We may still write the operator $D^\dagger D$ corresponding to these boundary conditions,

$$D^\dagger D = \begin{pmatrix} D_d^\dagger D_u & 0 \\ 0 & D_u^\dagger D_d \end{pmatrix} .$$

From our previous analysis we are led to study the spectrum of the operator $D^\dagger D$ only in the massless limit. $D^\dagger D$ is a diagonal operator in Dirac and flavor spaces and it is given by

$$D^\dagger D = \begin{pmatrix} -\partial_\mu^2 & 0 \\ 0 & -\partial_\mu^2 \end{pmatrix} .$$

In the time-momentum representation the operator $D^\dagger D$ acts as follows

$$D^\dagger D \, \phi(x) = \frac{1}{L^3} \sum_{\vec{p}} e^{{\rm i}\vec{p}\vec{x}} \begin{pmatrix} (-\partial_0^2 + \vec{p}^2) & 0 \\ 0 & (-\partial_0^2 + \vec{p}^2) \end{pmatrix} \phi(x_0, \vec{p}).$$

As in the previous cases, $\phi(x)$ (or $\phi(x_0,\vec{p})$) is a vector with eight components $\phi(x)_l$ ($\phi(x_0,\vec{p})_l$), and due to the diagonal structure of $D^\dagger D$ we can consider the eigenvalue problem on each component separately as

$$\left(-\partial_0^2+\vec{p}^2\right)\,\phi(x_0,\vec{p})_l=\lambda^2\,\phi(x_0,\vec{p})_l \qquad l=1,\ldots,8 \tag{4.80}$$

with either the boundary conditions

$$\phi(0,\vec{p})_l=0\,, \tag{4.81}$$

in case $\phi(x_0,\vec{p})_l$ belongs to the subspace defined by $\widetilde{\Pi}_+$, or

$$\phi(T,\vec{p})_l=0\,, \tag{4.82}$$

if $\phi(x_0,\vec{p})_l$ belongs to the subspace defined by $\widetilde{\Pi}_-$. Again, the eigenvalue Eq. (4.80) is a harmonic oscillator of frequency $p_0^2=\lambda^2-\vec{p}^2$ and eigenfunctions

$$\phi(x_0,\vec{p})_l=A\,\sin\left(p_0x_0\right)\,, \qquad p_0\neq 0\,, \tag{4.83}$$

in case $\phi(x_0,\vec{p})_l$ belongs to the subspace defined by $\widetilde{\Pi}_+$, while

$$\phi(x_0,\vec{p})_l=A\,\sin\left(p_0\left(x_0-T\right)\right)\,, \qquad p_0\neq 0\,, \tag{4.84}$$

if $\phi(x_0,\vec{p})_l$ belongs to the subspace defined by $\widetilde{\Pi}_-$.

However, due to the lack of additional boundary conditions for the complementary components, there is *no restriction* on the possible values of p_0. The important point to note is that this is a direct *consequence* of the chosen *boundary conditions*. We conclude that the eigenvalue problem with γ_5SF boundary conditions has either the trivial solution, if the mass is different from zero, or infinite solutions, in the chiral limit.

4.3. The quark propagator

In this section, our results on the determination of the quark propagator in the free continuum theory for the χSF and γ_5SF formulations are collected. As in the case of the eigenvalue problem, also the main results concerning the standard formulation are presented. We are interested in obtaining the expression in the time-momentum representation.

Denoting $S\left(x,y\right)$ the free quark propagator with the chosen boundary conditions, the problem to be solved is

$$\left(D+M\right)\,S\left(x,y\right)=\delta^4\left(x-y\right)\,, \qquad 0<x_0,y_0<T\,, \tag{4.85}$$

with $S\left(x,y\right)$ satisfying some boundary conditions at $x_0=0$ and $x_0=T$ which are dictated by the boundary conditions imposed on the quark fields. $\delta^4\left(x-y\right)$ is the four-dimensional space-time delta function. In order not to obscure the aim of the study in this section, the Dirac, flavor and color structure is not explicitly written. D denotes the massless continuum Dirac operator in the free theory,

$$D=\gamma_\mu\partial_\mu^x\,, \tag{4.86}$$

and M is some general mass term which is left unspecified at the moment.

In order to solve this problem with boundaries the usual way to proceed is the following. The solution to this problem, $S(x,y)$, can be expressed as the difference of two terms,

$$S\left(x,y\right)=S_\infty\left(x,y\right)-\psi\left(x,y\right)\,. \tag{4.87}$$

$S_\infty(x,y)$ is a particular solution of the inhomogeneous equation, Eq. (4.85), in the theory without boundaries. The second term, $\psi(x,y)$, represents a general solution of the homogeneous equation with certain coefficients which remain unknown. Such coefficients are determined by imposing $S(x,y)$ to satisfy the corresponding boundary conditions which, in fact, only affect $\psi(x,y)$ but not $S_\infty(x,y)$. This gives a particular solution of the homogeneous equation and as a consequence of $S(x,y)$ itself. Therefore, to obtain the quark propagator with prescribed boundary values, the standard technique is to first compute the solution of the inhomogeneous Dirac equation without boundaries and then to add a suitable solution of the homogeneous equation.

4.3.1. The quark propagator without boundaries

Since $S_\infty(x,y)$ does not feel the boundaries [8] its expression is common to all the cases. Thus, before discussing any particular formulation, $S_\infty(x,y)$ is determined by solving the equation,

$$(D+M)\; S_\infty(x,y) = \delta^4(x-y)\;, \qquad \forall\, x_0, y_0\,. \tag{4.88}$$

Considering the Fourier transform, the quark propagator can be written as

$$S_\infty(x,y) = \frac{1}{L^3}\sum_{\vec{p}} e^{\mathrm{i}\vec{p}(\vec{x}-\vec{y})}\, S_\infty(x_0-y_0;\vec{p})\;, \tag{4.89}$$

with

$$S_\infty(x_0-y_0;\vec{p}) \equiv \int_{-\infty}^{+\infty}\frac{\mathrm{d}p_0}{2\pi}\, e^{\mathrm{i}p_0(x_0-y_0)}\, S_\infty(p_0,\vec{p})\;. \tag{4.90}$$

$S_\infty(p_0,\vec{p})$ can be obtained from Eq. (4.88) and has the form[9]

$$S_\infty(p_0,\vec{p}) = \frac{-\mathrm{i}\gamma_\mu p_\mu + M^\dagger}{p^2 + M^\dagger M}\,. \tag{4.91}$$

The integral required by Eq. (4.90) can be performed at this point. Using the residues method, the final expression can be cast in the form

$$S_\infty(x,y) = (D^\dagger + M^\dagger) G_\infty(x,y)\;, \tag{4.92}$$

where

$$G_\infty(x,y) = \frac{1}{L^3}\sum_{\vec{p}} e^{i\vec{p}(\vec{x}-\vec{y})}\,\frac{1}{2\omega(\vec{p})}\mathrm{e}^{-\omega(\vec{p})|x_0-y_0|}\,. \tag{4.93}$$

The function $\omega(\vec{p})$ is the energy,

$$\pm\,\mathrm{i}p_0 = \mp\omega(\vec{p})\,, \qquad \omega(\vec{p}) \equiv \sqrt{\vec{p}^2 + M^\dagger M}\,. \tag{4.94}$$

The aim of the following sections is to find a suitable solution of the homogeneous Dirac equation and therefore $S(x_0,y_0;\vec{p})$ itself, when different SF boundary conditions are imposed on the quark fields. The quark propagator with χSF boundary conditions will be also computed in an alternative way, by performing an axial rotation of the quark propagator with SF boundary conditions. In the very next section, the general solution of the homogeneous equation is determined for the quark propagator and in the following sections the particular forms for the

[8] Periodic boundary conditions in the spatial directions are assumed. By abuse of language, 'boundary conditions' refer to the boundary conditions in the 'time-direction'. Whenever a reference to the boundary conditions in the spatial directions is needed it will be made explicit.

[9] The following notation is used: $p^2 = p_\mu p_\mu$ and $\vec{p}^2 = p_k p_k$, with Einstein convention.

three cases of boundary conditions considered here will be given.

4.3.2. General solution of the homogeneous equation

In order to find a general solution of the homogeneous equation, the following equation has to be solved for $\psi(x,y)$,

$$(D+M)\;\psi\,(x,y)=0\,, \tag{4.95}$$

and the most general form of such a solution is,

$$\begin{aligned}\psi\,(x,y)&=\frac{1}{L^3}\sum_{\vec{p}}e^{\mathrm{i}\vec{p}(\vec{x}-\vec{y})}\,\psi(x_0-y_0;\vec{p})\,,\\ \psi(x_0-y_0;\vec{p})&=\sum_{\alpha=1}^{2}\{a^\alpha(\vec{p})\otimes u^\alpha(\vec{p})\,e^{-\omega(\vec{p})(x_0-y_0)}+b^\alpha(-\vec{p})\otimes v^\alpha(-\vec{p})\,e^{\omega(\vec{p})(x_0-y_0)}\}\,.\end{aligned} \tag{4.96}$$

In this expression α denotes the spin. The energy, $\omega(\vec{p})$, is assumed to take non-negative values, $\omega(\vec{p})\geq 0$ and it is defined in Eq. (4.94). The functions $u^\alpha(\vec{p})$ and $v^\alpha(\vec{p})$, of dimension 4×1, are eigenstates of the operator $\mathrm{i}\gamma_\mu p_\mu$ with eigenvalues $-M$ and $+M$, respectively. That is, they are solutions of the equations

$$[\mathrm{i}\gamma_\mu p_\mu+M]\,u^\alpha(\vec{p})=0\,, \tag{4.97}$$

$$[\mathrm{i}\gamma_\mu p_\mu-M]\,v^\alpha(\vec{p})=0\,, \tag{4.98}$$

and as such, they satisfy the relations,

$$u^\alpha(\vec{p})^\dagger u^\beta(\vec{p})=2\omega(\vec{p})\delta^{\alpha\beta}\,, \tag{4.99}$$

$$v^\alpha(\vec{p})^\dagger v^\beta(\vec{p})=2\omega(\vec{p})\delta^{\alpha\beta}\,, \tag{4.100}$$

$$u^\alpha(\vec{p})^\dagger v^\beta(-\vec{p})=0\quad\forall\,\alpha,\beta\,. \tag{4.101}$$

Possible solutions to Eq. (4.97)-(4.98) are,

$$u^\alpha(\vec{p})=A^\alpha(\vec{p})\,[\mathrm{i}\gamma_\mu p_\mu-M]\,u^\alpha(\vec{0})\,, \tag{4.102}$$

$$v^\alpha(\vec{p})=B^\alpha(\vec{p})\,[\mathrm{i}\gamma_\mu p_\mu+M]\,v^\alpha(\vec{0})\,, \tag{4.103}$$

with the zero-momentum spinors, $u^\alpha(\vec{0})$ and $v^\alpha(\vec{0})$, being solutions of

$$[1-\gamma_0]\,u^\alpha(\vec{0})=0\,, \tag{4.104}$$

$$[1+\gamma_0]\,v^\alpha(\vec{0})=0\,. \tag{4.105}$$

$a^\alpha(\vec{p})$ and $b^\alpha(-\vec{p})$ are coefficients of dimension 1×4 which are unknown a priori. Such coefficients are determined when a particular solution of Eq. (4.95) is to be found, meaning in our case, when particular boundary conditions are imposed. In any case, a general form of these coefficients can be determined in terms of $\psi(x_0-y_0;\vec{p})$, by making use of Eq. (4.99)-(4.101). Such coefficients are then,

$$a^\alpha(\vec{p})=\frac{1}{2\omega(\vec{p})}\,\overline{u}^\alpha(\vec{p})\,\gamma_0\,\psi(x_0-y_0;\vec{p})|_{x_0-y_0=0}\,,\quad\alpha=1,2\,, \tag{4.106}$$

$$b^\alpha(\vec{p})=\frac{1}{2\omega(\vec{p})}\,\overline{v}^\alpha(\vec{p})\,\gamma_0\,\psi(x_0-y_0;-\vec{p})|_{x_0-y_0=0}\,,\quad\alpha=1,2\,. \tag{4.107}$$

The tensor product, $\otimes$, in Eq. (4.96) ensures that $\psi(x,y)$ is a 4×4 matrix.

At this stage, writing the quark propagator $S(x,y)$ as stated in Eq. (4.87), the most general solution of the inhomogeneous equation is already known. Thus, the only step left is to impose the corresponding boundary conditions on this quark propagator. After that, a particular expression for a and b is known and therefore the particular expression for $S(x,y)$. In the following sections, particular solutions are found for SF, χSF and γ_5SF boundary conditions.

4.3.3. The quark propagator: standard SF

Due to the boundary conditions on the matter fields, Eq. (4.1)-(4.2), the quark propagator in the theory with SF boundary conditions is a solution of the equations

$$(D+M)\; S^{\mathrm{SF}}(x,y) = \delta^4(x-y)\;, \qquad 0<x_0,y_0<T\,, \tag{4.108}$$

$$P_+\, S^{\mathrm{SF}}(x,y)|_{x_0=0} = 0\,, \qquad P_-\, S^{\mathrm{SF}}(x,y)|_{x_0=T} = 0\,. \tag{4.109}$$

Additionally, the quark propagator obtained from such equations must satisfy the boundary conditions when the corresponding projectors are applied on the right side,

$$S^{\mathrm{SF}}(x,y)\, P_-|_{y_0=0} = 0\,, \qquad S^{\mathrm{SF}}(x,y)\, P_+|_{y_0=T} = 0\,. \tag{4.110}$$

As shown in [87], a unique and non-trivial solution exists for Eq. (4.108)-(4.109) and an expression for $S^{\mathrm{SF}}(x,y)$ was also given in this reference. This solution moreover satisfies, as it should, the boundary conditions specified in Eq. (4.110). The main results of that derivation are summarized here. After some algebra and considering a standard mass term, $M=m$, the final expression of the propagator reads

$$S^{\mathrm{SF}}(x,y) = (D^\dagger + m)\, G^{\mathrm{SF}}(x,y)\;, \tag{4.111}$$

where

$$\begin{aligned} G^{\mathrm{SF}}(x,y) = \frac{1}{L^3}\sum_{\vec{p}} e^{\mathrm{i}\vec{p}(\vec{x}-\vec{y})}\, \frac{1}{2\omega(\vec{p})R(p)} \Big[& (m+\omega(\vec{p}))\, \mathrm{e}^{-\omega(\vec{p})|x_0-y_0|} \\ & + (m-\omega(\vec{p}))\, \mathrm{e}^{-\omega(\vec{p})(2T-|x_0-y_0|)} \\ & - (m-\gamma_0\omega(\vec{p}))\, \mathrm{e}^{-\omega(\vec{p})(x_0+y_0)} \\ & - (m+\gamma_0\omega(\vec{p}))\, \mathrm{e}^{-\omega(\vec{p})(2T-x_0-y_0)} \Big]\,, \end{aligned} \tag{4.112}$$

$$R(p) \equiv [\omega(\vec{p})+m] + [\omega(\vec{p})-m]\; e^{-2\omega(\vec{p})T}\,, \tag{4.113}$$

$$M^\dagger M = m^2 \qquad \Longrightarrow \qquad \omega(\vec{p}) = \sqrt{\vec{p}^2+m^2}\,. \tag{4.114}$$

4.3.4. The quark propagator: χSF

The quark propagator in the theory with χSF boundary conditions, Eq. (4.11)-(4.12), is obtained from

$$(D+M)\; S^{\chi\mathrm{SF}}(x,y) = \delta^4(x-y)\;, \qquad 0<x_0,y_0<T\,, \tag{4.115}$$

$$\widetilde{Q}_+\, S^{\chi\mathrm{SF}}(x,y)|_{x_0=0} = 0\,, \qquad \widetilde{Q}_-\, S^{\chi\mathrm{SF}}(x,y)|_{x_0=T} = 0\,. \tag{4.116}$$

The solution of these equations must also verify the conditions when projectors are applied on the right side

$$S^{\chi\mathrm{SF}}(x,y)\,\widetilde{Q}_+|_{y_0=0}=0\,,\qquad S^{\chi\mathrm{SF}}(x,y)\,\widetilde{Q}_-|_{y_0=T}=0\,. \tag{4.117}$$

In order to find a solution of Eq. (4.115)-(4.116), we have proceeded in a similar manner as it was done for the SF in [87]. The way to go on, is then to consider the general solution and to impose the conditions of Eq. (4.116). After that, a unique solution of the equation for the quark propagator with χSF boundary conditions is obtained. Even if finally interested in defining a massless theory, where the form of the mass term is in principle not relevant, we have decided to study the quark propagator with χSF boundary conditions considering a general twisted mass term.

The mass term can be written

$$M=m\,e^{\mathrm{i}\alpha\gamma_5\tau^3}\,, \tag{4.118}$$

or in the form

$$M=m_{\mathrm{q}}+\mathrm{i}\mu_{\mathrm{q}}\gamma_5\tau^3\,, \tag{4.119}$$

if we define, as usually in the twisted mass notation,

$$m_{\mathrm{q}}\equiv m\cos(\alpha)\qquad \mu_{\mathrm{q}}\equiv m\sin(\alpha)\,. \tag{4.120}$$

In this case, the expression for the quark propagator is given by

$$S^{\chi\mathrm{SF}}\,(x,y)=(D^\dagger+M^\dagger)\,G^{\chi\mathrm{SF}}\,(x,y)\;, \tag{4.121}$$

with

$$\begin{aligned}G^{\chi\mathrm{SF}}\,(x,y)=\frac{1}{L^3}\sum_{\vec{p}}\,e^{\mathrm{i}\vec{p}(\vec{x}-\vec{y})}\,\frac{1}{2\omega(\vec{p})R(p)}\Big[&\,(\mu_{\mathrm{q}}+\omega(\vec{p}))\;\mathrm{e}^{-\omega(\vec{p})|x_0-y_0|}\\&+(\mu_{\mathrm{q}}-\omega(\vec{p}))\;\mathrm{e}^{-\omega(\vec{p})(2T-|x_0-y_0|)}\\&-\Big(\mu_{\mathrm{q}}+\mathrm{i}\gamma_0\gamma_5\tau^3\omega(\vec{p})\Big)\;\mathrm{e}^{-\omega(\vec{p})(x_0+y_0)}\\&-\Big(\mu_{\mathrm{q}}-\mathrm{i}\gamma_0\gamma_5\tau^3\omega(\vec{p})\Big)\;\mathrm{e}^{-\omega(\vec{p})(2T-x_0-y_0)}\Big]\,.\end{aligned} \tag{4.122}$$

Here, the dependence of $R(p)$ on the mass is only through the twisted mass parameter,

$$R(p)=[\omega(\vec{p})+\mu_{\mathrm{q}}]+[\omega(\vec{p})-\mu_{\mathrm{q}}]\;e^{-2\omega(\vec{p})T} \tag{4.123}$$

and

$$M^\dagger M=m_{\mathrm{q}}^2+\mu_{\mathrm{q}}^2\qquad\Longrightarrow\qquad\omega(\vec{p})=\sqrt{\vec{p}^{\,2}+m_{\mathrm{q}}^2+\mu_{\mathrm{q}}^2}\,. \tag{4.124}$$

Therefore, as in the standard formulation, we have also found an unique and non-trivial expression for the quark propagator when the quark fields satisfy χSF boundary conditions and with a general twisted mass term. From that solution particular cases of the mass term can be considered. For later discussion we give these expressions for a standard mass term and for a maximally twisted mass term.

If the mass term is the *standard* one,

$$S^{\chi\mathrm{SF}}\,(x,y)=(D^\dagger+m_{\mathrm{q}})\,G^{\chi\mathrm{SF}}\,(x,y)\;, \tag{4.125}$$

with

$$G^{\chi\mathrm{SF}}(x,y) = \frac{1}{L^3}\sum_{\vec{p}} e^{\mathrm{i}\vec{p}(\vec{x}-\vec{y})}\,\frac{1}{2\omega(\vec{p})D(p)}\Big[\,\mathrm{e}^{-\omega(\vec{p})|x_0-y_0|} - \mathrm{e}^{-\omega(\vec{p})(2T-|x_0-y_0|)} - \mathrm{i}\gamma_0\gamma_5\tau^3\mathrm{e}^{-\omega(\vec{p})(x_0+y_0)} + \mathrm{i}\gamma_0\gamma_5\tau^3\mathrm{e}^{-\omega(\vec{p})(2T-x_0-y_0)}\Big]\,, \tag{4.126}$$

where we have defined

$$D(p) \equiv 1 + e^{-2\omega(\vec{p})T}\,, \tag{4.127}$$

and

$$M^\dagger M = m_{\mathrm{q}}^2 \qquad \Longrightarrow \qquad \omega(\vec{p}) = \sqrt{\vec{p}^2 + m_{\mathrm{q}}^2}\,. \tag{4.128}$$

In case we choose a *maximally twisted* mass term then the expression would be

$$S^{\chi\mathrm{SF}}(x,y) = (D^\dagger - \mathrm{i}\mu_{\mathrm{q}}\gamma_5\tau^3)\,G^{\chi\mathrm{SF}}(x,y)\;, \tag{4.129}$$

where

$$G^{\chi\mathrm{SF}}(x,y) = \frac{1}{L^3}\sum_{\vec{p}} e^{\mathrm{i}\vec{p}(\vec{x}-\vec{y})}\,\frac{1}{2\omega(\vec{p})R(p)}\Big[\,(\mu_{\mathrm{q}}+\omega(\vec{p}))\;\mathrm{e}^{-\omega(\vec{p})|x_0-y_0|} + (\mu_{\mathrm{q}}-\omega(\vec{p}))\;\mathrm{e}^{-\omega(\vec{p})(2T-|x_0-y_0|)} - \Big(\mu_{\mathrm{q}}+\mathrm{i}\gamma_0\gamma_5\tau^3\omega(\vec{p})\Big)\;\mathrm{e}^{-\omega(\vec{p})(x_0+y_0)} - \Big(\mu_{\mathrm{q}}-i\gamma_0\gamma_5\tau^3\omega(\vec{p})\Big)\;\mathrm{e}^{-\omega(\vec{p})(2T-x_0-y_0)}\Big]\,, \tag{4.130}$$

with $R(p)$ as defined above in Eq. (4.123), but with the energy given now by

$$M^\dagger M = \mu_{\mathrm{q}}^2 \qquad \Longrightarrow \qquad \omega(\vec{p}) = \sqrt{\vec{p}^2 + \mu_{\mathrm{q}}^2}\,. \tag{4.131}$$

4.3.5. The quark propagator: γ_5SF

The equations for the quark propagator when the fermion fields satisfy the boundary conditions given in Eq. (4.16)-(4.17) are

$$(D+M)\;S^{\gamma_5\mathrm{SF}}(x,y) = \delta^4(x-y)\;, \qquad 0 < x_0, y_0 < T\,, \tag{4.132}$$

$$\widetilde{\Pi}_+\,S^{\gamma_5\mathrm{SF}}(x,y)|_{x_0=0} = 0\,, \qquad \widetilde{\Pi}_-\,S^{\gamma_5\mathrm{SF}}(x,y)|_{x_0=T} = 0\,. \tag{4.133}$$

The breaking of parity symmetry by these boundary conditions gives place to a quark propagator with more terms than in the two previous cases, together with a more lengthy algebra to find such a solution. Nevertheless, a solution may still be found which can be cast in the form

$$S^{\gamma_5\mathrm{SF}}(x,y) = (D^\dagger + m)\,G^{\gamma_5\mathrm{SF}}(x,y)\;, \tag{4.134}$$

with

$$
\begin{aligned}
G^{\gamma_5\mathrm{SF}}(x,y) = & \frac{1}{L^3}\sum_{\vec{p}} e^{\mathrm{i}\vec{p}(\vec{x}-\vec{y})}\,\frac{1}{2\omega(\vec{p})F(p)}\times \\
& \left\{\left[1-2\left(\frac{m}{2\omega(\vec{p})}\right)^2\right]\mathrm{e}^{-\omega(\vec{p})|x_0-y_0|}+\left(\frac{m}{2\omega(\vec{p})}\right)\mathrm{e}^{\omega(\vec{p})(2T-|x_0-y_0|)}\right. \\
& -\left[\widetilde{\Pi}_+-\left(\frac{m}{2\omega(\vec{p})}\right)^2-\left(\frac{m}{2\omega(\vec{p})}\right)\gamma_0\gamma_5\tau^3\right]\mathrm{e}^{-\omega(\vec{p})(x_0-y_0)} \\
& -\left[\widetilde{\Pi}_--\left(\frac{m}{2\omega(\vec{p})}\right)^2+\left(\frac{m}{2\omega(\vec{p})}\right)\gamma_0\gamma_5\tau^3\right]\mathrm{e}^{\omega(\vec{p})(x_0-y_0)} \\
& -\left[\left(\frac{m}{2\omega(\vec{p})}\right)\gamma_0\widetilde{\Pi}_+-\left(\frac{m}{2\omega(\vec{p})}\right)^2\right]\mathrm{e}^{-\omega(\vec{p})(x_0+y_0)} \\
& -\left[\left(\frac{m}{2\omega(\vec{p})}\right)\gamma_0\widetilde{\Pi}_++\left(\frac{m}{2\omega(\vec{p})}\right)^2\right]\mathrm{e}^{\omega(\vec{p})(x_0+y_0)} \\
& +\left[\left(\frac{m}{2\omega(\vec{p})}\right)\gamma_0\widetilde{\Pi}_-+\left(\frac{m}{2\omega(\vec{p})}\right)^2\right]\mathrm{e}^{-\omega(\vec{p})(2T-x_0-y_0)} \\
& \left.+\left[\left(\frac{m}{2\omega(\vec{p})}\right)\gamma_0\widetilde{\Pi}_--\left(\frac{m}{2\omega(\vec{p})}\right)^2\right]\mathrm{e}^{\omega(\vec{p})(2T-x_0+y_0)}\right\},
\end{aligned}
\tag{4.135}
$$

where we define

$$
F(p)\equiv 1+\left(\frac{m}{\omega(\vec{p})}\right)^2\cosh^2\left(\omega(\vec{p})T\right)\,. \tag{4.136}
$$

However, this quark propagator does *not* satisfy the corresponding boundary conditions when the projectors are applied on the right side, namely,

$$
S^{\gamma_5\mathrm{SF}}(x,y)\,\widetilde{\Pi}_-|_{y_0=0}\neq 0\,,\qquad S^{\gamma_5\mathrm{SF}}(x,y)\,\widetilde{\Pi}_+|_{y_0=T}\neq 0\,. \tag{4.137}
$$

This means that the *only solution* for the quark propagator with quark fields obeying γ_5SF boundary conditions is the *trivial* one.

Indeed, the non-trivial solution of the quark propagator in Eq. (4.135) satisfies different boundary conditions on the right side. The new boundary conditions are obtained from the ones in Eq. (4.133) using charge conjugation and take the form,

$$
S^{\gamma_5\mathrm{SF}}(x,y)\,\widetilde{\Pi}_+|_{y_0=0}=0\,,\qquad S^{\gamma_5\mathrm{SF}}(x,y)\,\widetilde{\Pi}_-|_{y_0=T}=0\,. \tag{4.138}
$$

These new boundary conditions on the quark propagator correspond to the following boundary conditions on the anti-quark fields,

$$
\overline{\phi}(x)\,\widetilde{\Pi}_+|_{x_0=0}=0\,,\qquad \overline{\phi}(x)\,\widetilde{\Pi}_-|_{x_0=T}=0\,, \tag{4.139}
$$

which induces a theory with boundaries which violates $\mathcal{P}$ and $\mathcal{CPT}$.

To conclude, continuum QCD in the free case with the original γ_5SF boundary conditions has a quark propagator which vanishes everywhere. A non vanishing solution can only be found changing the boundary conditions, such that charge conjugation symmetry is preserved by the new boundary conditions. Given the fact that the γ_5SF formulation violates parity and preserves time reversal, the result would be a QCD theory with boundaries which violates $\mathcal{CPT}$. We remark that for the χSF boundary conditions of [26] the situation is different. It is sufficient

to consider parity and time-reversal symmetries in the twisted basis to see that they actually preserve separately $\mathcal{C}$, $\mathcal{P}$ and $\mathcal{T}$.

Through this section we have also kept a (standard) mass term until the end. This does not modify our conclusions here but, considering our results obtained in Sec. 4.2.3, this study could only make sense if the mass term is set to zero.

4.3.6. Chirally rotating the quark propagator with SF boundary conditions

The aim of this section is to show that in the free continuum theory the propagators with SF and χSF boundary conditions are related by a chiral rotation, so one expression can be brought into the other without any ambiguity. This indeed implies that both boundary conditions lead to the same theory at tree-level in the continuum.

The starting point is the quark propagator with SF boundary conditions derived in Sec. 4.3.3,

$$S^{\mathrm{SF}}(x,y) = \langle \psi(x)\overline{\psi}(y)\rangle \,. \tag{4.140}$$

Performing the axial transformation, Eq. (2.97), of the quark fields, $\{\psi,\overline{\psi}\}$, which brings them to the twisted basis, $\{\chi,\overline{\chi}\}$, an expression of the quark propagator with SF boundary conditions in the twisted basis is obtained,

$$S^{\mathrm{SF}}(x,y) = e^{\mathrm{i}\frac{\alpha}{2}\gamma_5\tau^3}\,\langle \chi(x)\overline{\chi}(y)\rangle\, e^{\mathrm{i}\frac{\alpha}{2}\gamma_5\tau^3}\,. \tag{4.141}$$

Therefore, the quark propagator in the twisted basis, which is denoted in the following as $S^{\alpha}(x,y)$ for a general rotation angle α, can be obtained from the propagator obeying the SF boundary conditions by simply performing the rotation

$$S^{\alpha}(x,y) = \langle \chi(x)\overline{\chi}(y)\rangle = e^{-\mathrm{i}\frac{\alpha}{2}\gamma_5\tau^3}\, S^{\mathrm{SF}}(x,y)\, e^{-\mathrm{i}\frac{\alpha}{2}\gamma_5\tau^3}\,, \tag{4.142}$$

with $S^{\mathrm{SF}}(x,y)$ given by Eq. (4.111)-(4.112).

After some calculations and considering the polar mass, M, defined in Eq. (4.118)-(4.119) and the twisted and untwisted quark masses, Eq. (4.120), we obtain

$$S^{\alpha}\,(x,y) = (D^{\dagger}+M^{\dagger})\,G^{\alpha}\,(x,y)\;, \tag{4.143}$$

with

$$\begin{aligned} G^{\alpha}\,(x,y) = \frac{1}{L^3}\sum_{\vec{p}} e^{\mathrm{i}\vec{p}(\vec{x}-\vec{y})}\,\frac{1}{2\omega(\vec{p})R(p)}\times \\ \Big[\Big(\sqrt{m_{\mathrm{q}}^2+\mu_{\mathrm{q}}^2}+\omega(\vec{p})\Big)\;\mathrm{e}^{-\omega(\vec{p})|x_0-y_0|} \\ +\Big(\sqrt{m_{\mathrm{q}}^2+\mu_{\mathrm{q}}^2}-\omega(\vec{p})\Big)\;\mathrm{e}^{-\omega(\vec{p})(2T-|x_0-y_0|)} \\ -\Big(\sqrt{m_{\mathrm{q}}^2+\mu_{\mathrm{q}}^2}-\gamma_0\omega(\vec{p})e^{-\mathrm{i}\alpha\gamma_5\tau^3}\Big)\;\mathrm{e}^{-\omega(\vec{p})(x_0+y_0)} \\ -\Big(\sqrt{m_{\mathrm{q}}^2+\mu_{\mathrm{q}}^2}+\gamma_0\omega(\vec{p})e^{-\mathrm{i}\alpha\gamma_5\tau^3}\Big)\;\mathrm{e}^{-\omega(\vec{p})(2T-x_0-y_0)}\Big]\,, \end{aligned} \tag{4.144}$$

and

$$R(p) \equiv \Big[\omega(\vec{p})+\sqrt{m_{\mathrm{q}}^2+\mu_{\mathrm{q}}^2}\Big]+\Big[\omega(\vec{p})-\sqrt{m_{\mathrm{q}}^2+\mu_{\mathrm{q}}^2}\Big]\;e^{-2\omega(\vec{p})T}\,, \tag{4.145}$$

$$\omega(\vec{p}) = \sqrt{\vec{p}^{\,2}+m_{\mathrm{q}}^2+\mu_{\mathrm{q}}^2}\,. \tag{4.146}$$

Eq. (4.143)-(4.146), obtained by performing the rotation of the quark propagator obeying

SF boundary conditions for a general angle α, correspond to the quark propagator that would be obtained by imposing on the quark fields chirally rotated boundary conditions with general angle α of the form given in Eq. (4.6)-(4.7), provided the mass term is twisted with the same angle α as the boundaries or that a zero mass setup is chosen.

At maximal twist, $\alpha = \frac{\pi}{2}$, the expression exactly corresponds to Eq. (4.129)-(4.131) for the quark propagator obtained in section 4.3.4, where χSF boundary conditons were considered with a maximally twisted mass term. That is, the quark propagator with χSF boundary conditions can be obtained, in the continuum theory, by 'maximally twisting' the quark propagator with SF boundary conditions in the way

$$S^{\chi\mathrm{SF}}(x,y) = e^{-\mathrm{i}\frac{\pi}{4}\gamma_5\tau^3}\, S^{\mathrm{SF}}(x,y)\, e^{-\mathrm{i}\frac{\pi}{4}\gamma_5\tau^3}\,, \tag{4.147}$$

provided the mass term also rotates. Therefore, the two theories are equivalent if also the mass term is rotated accordingly. In particular, there is no ambiguity if working at zero quark mass, as it will be the case of this thesis, where a massless renormalization scheme is considered.

4.4. Concluding remarks

We have analyzed fundamental aspects of two different ways of implementing Schrödinger functional boundary conditions in the free continuum theory; these are the eigenvalue spectrum and the quark propagator. For comparison, we have recalled the main results already known from the standard formulation of the SF. For the chirally rotated SF boundary conditions, in analogy to the standard SF boundaries, we have found that the QCD spectrum is well defined and a positive lower bound can be found for the minimal eigenvalue even in the massless theory. We have also found the explicit analytic expression for the quark propagator. With the γ_5SF boundary conditions, we have noticed that the eigenvalue problem has either a trivial solution or, in the massless case, infinite solutions. The reason is the lack of additional conditions on the normal derivatives of the fields at the boundaries. This result is a consequence of the fact that there is no distinction between the normal (γ_0) and the tangential (γ_k) components of the fields at the time boundaries with respect to the projectors here considered. For the quark propagator we find a similar pattern; in order to satisfy all the boundary conditions, the quark propagator has to vanish. We still found an analytic expression for the quark propagator, which satisfies the boundary conditions with the projectors applied on the left (induced by the conditions on ϕ), but which does not satisfy the ones with the projectors applied on the right side (induced by the conditions on $\overline{\phi}$). We showed that this quark propagator actually satisfies different boundary conditions on the right side, which are obtained from the ones on the left via charge conjugation. Therefore, a non vanishing solution can only be found changing the boundary conditions, such that charge conjugation is a preserved symmetry amongst the boundary conditions. Yet, given the fact that the γ_5SF boundary conditions violate parity and preserve time reversal, this would correspond to a theory which violates $\mathcal{P}$ and $\mathcal{CPT}$.

It is important to emphasize that for the χSF boundary conditions the situation is different. It is enough to consider parity and time-reversal symmetries in the twisted basis to see that they actually preserve separately $\mathcal{C}$, $\mathcal{P}$ and $\mathcal{T}$. If one is interested in the lattice formulation of the χSF with Wilson fermions, then the Wilson term will certainly break the twisted parity $\mathcal{P}_{\frac{\pi}{2}}$ and twisted time reversal $\mathcal{T}_{\frac{\pi}{2}}$, pretty much in the same spirit of what happens in infinite volume for twisted mass QCD. Though, separately $\mathcal{C}$ and $\mathcal{PT}$, and thus $\mathcal{CPT}$, remain symmetries of the lattice theory with Wilson fermions.

Our conclusion is that the standard and χSF boundary conditions are a sound definition of QCD with SF boundaries, while the γ_5SF formulation has still issues which need to be

further investigated. Based on these results we have decided to only investigate further the χSF formulation, whose discussion occupies the rest of this thesis.

5. The χSF on the lattice

From our study in the free continuum theory described in Chap. 4, we have concluded to use the chirally rotated Schrödinger functional, χSF, as renormalization scheme. Indeed, from pure continuum considerations this formulation of the SF seems to provide a perfectly well defined theory. However, this can not be guaranteed until studies beyond the free continuum theory are performed. In particular, it is a priori not clear how the χSF boundary conditions can be implemented on the lattice or even if they can at all. Also the renormalizability properties of this formulation should be understood.

A theoretical study of the validity of the χSF scheme has been performed by S. Sint, with the corresponding results recently published in [26]. From this study it can be concluded that from the theoretical point of view, the χSF does not show any particular problem which invalidates its use. Indeed, it seems to be a promising renormalization scheme which is totally equivalent to the standard SF in the continuum limit of the renormalized theory. All these theoretical arguments, however, need a numerical check which confirms that the χSF can be eventually used in numerical simulations. Particularly, it is important to first understand if a lattice implementation is feasible in practice and, in case it is, whether results obtained from this formulation lead to a well defined continuum limit. Of course, a check of automatic $O(a)$-improvement in the bulk of the lattice is also required, since the χSF formulation is expected to respect bulk automatic $O(a)$-improvement. The study and understanding of all these issues are the central goal of this thesis and several physical observables have been computed to test the χSF. To be concrete, we have considered the step scaling functions (SSF) of the pseudo-scalar density and the non-singlet twist-2 operators, O_{12} and O_{44}, as well as the RGI mass of the strange quark. All these studies have been performed for several physical conditions, ranging from the purely perturbative down to hadronic scales.

Most of our results are contained in following chapters. The interest of the present one is to introduce the reader to the main concepts of the χSF on the lattice. Even if a very detailed description of such theoretical arguments can be found in [26], still the main results are collected here. All these concepts will be important in the following presentation of our numerical results. In Sec. 5.1, the implementation of the χSF on the lattice in the free theory is described, together with our analytical derivation of the free lattice quark propagator. Sec. 5.2 is devoted to the discussion of the renormalizability and improvement of the lattice theory with χSF boundary conditions.

5.1. The χSF on the lattice in the free theory

On the lattice, boundary conditions arise dynamically from the structure of the lattice action near the boundaries and they can not be simply imposed as in the continuum [82]. In some cases, in order to have the desired boundary conditions in the continuum limit, the lattice action has to be modified near the boundaries. The form of the lattice action near the boundaries can be determined in several ways. In the case of the χSF boundary conditions the correct lattice action has been obtained using orbifold techniques [26, 94]. What orbifold does is to define the action of the *lattice* Dirac operator near the time boundaries, such that in the free lattice theory the desired boundary conditions are obtained.

In [26], three different versions of the orbifold construction have been proposed. These lead to lattice actions which differ by cutoff effects at finite lattice spacing. The three constructions are based on different choices of the orbifold reflection. One case refers to a *site* reflection about the time slice $x_0 = 0$. The other two cases are *link* reflections about the points $x_0 = \pm a/2$, respectively. We study the case corresponding to the construction based on the link reflection about the point $x_0 = -a/2$, which is referred to as 'orbifold reflection with an $O(a)$ offset'. In this case, the dynamical fermion fields are all those in the interval $0 \leq x_0 \leq T$. This is distinct to what happens in the standard setup, where the fields integrated over are all those in the interval $0 < x_0 < T$, while the fermion fields are fixed at the boundaries, $x_0 = 0$ and $x_0 = T$.

If a theory with Wilson quarks is assumed in infinite volume, the orbifold construction with $O(a)$ offset gives rise to the two-flavor lattice fermion action with χSF boundary conditions,

$$S_{\mathrm{F}} = a^4 \sum_{x_0=0}^{T} \sum_{\vec{x}} \overline{\chi}(x) \left(\mathcal{D}_{\mathrm{W}} + m_0\right) \chi(x) \,. \tag{5.1}$$

In this expression, the massless Wilson-Dirac operator with boundaries is given by

$$a\mathcal{D}_{\mathrm{W}}\,\chi(x) = \begin{cases} -U_0(x)P_-\chi(x+\vec{0}) + (K + \mathrm{i}\gamma_5\tau^3 P_-)\,\chi(x) & \text{if } x_0 = 0\,, \\ aD_{\mathrm{W}}\,\chi(x) & \text{if } 0 < x_0 < T\,, \\ (K + \mathrm{i}\gamma_5\tau^3 P_+)\,\chi(x) - U_0(x-\vec{0})^\dagger P_+\chi(x-\vec{0}) & \text{if } x_0 = T\,, \end{cases} \tag{5.2}$$

satisfying, as the twisted mass operator, the hermiticity property,

$$\tau^{1,2}\gamma_5\,\mathcal{D}_{\mathrm{W}}\,\gamma_5\,\tau^{1,2} = \mathcal{D}_{\mathrm{W}}^\dagger \,. \tag{5.3}$$

D_{W} is the massless Wilson operator defined in Eq. (2.68). It may be written as

$$aD_{\mathrm{W}}\,\chi(x) = -U_0(x)P_-\chi(x+\vec{0}) + K\chi(x) - U_0(x-\vec{0})^\dagger P_+\chi(x-\vec{0})\,, \tag{5.4}$$

with K the dimensionless time-diagonal kernel of the Wilson-Dirac operator,

$$K = 1 + \sum_{k=1}^{3} \frac{a}{2}\left\{\gamma_k\left[\nabla_k^* + \nabla_k\right] - a\,\nabla_k^*\nabla_k\right\}. \tag{5.5}$$

The boundary conditions obtained from this construction agree with the desired boundary conditions in the continuum only up to cutoff effects of $O(a)$ and they are of the form,

$$\widetilde{Q}_+\left(1 - \frac{1}{2}a\partial_0^*\right)\chi(x)|_{x_0=0} = 0 \qquad \widetilde{Q}_-\left(1 + \frac{1}{2}a\partial_0\right)\chi(x)|_{x_0=T} = 0 \tag{5.6}$$

$$\overline{\chi}(x)\,\widetilde{Q}_+\left(1 - \frac{1}{2}a\overleftarrow{\partial}_0^*\right)|_{x_0=0} = 0 \qquad \overline{\chi}(x)\,\widetilde{Q}_-\left(1 + \frac{1}{2}a\overleftarrow{\partial}_0\right)|_{x_0=T} = 0\,. \tag{5.7}$$

The projectors $\widetilde{Q}_\pm$ are the χSF projectors in the continuum theory, already defined in previous chapters. In fact, such disagreement between the lattice and the continuum boundary conditions is a consequence of the particular orbifold construction. While the one with a site reflection about the point $x_0 = 0$ gives rise to exactly the same boundary conditions as in the continuum theory, the orbifold constructions based on link reflections define boundary conditions which are displaced by cutoff effects with respect to the continuum ones. This is because in these last cases the reflection points, $x_0 = \pm a/2$, can not be reached on the lattice, where only positions at integer multiples of the lattice spacing, a, are allowed. In the construction chosen here, for instance, the boundary conditions with the continuum structure are satisfied at $x_0 = -a/2, T + a/2$, instead

of at $x_0 = 0, T$. But, since these points can not be reached on the lattice, such conditions are shifted to $x_0 = 0, T$, thus generating the $O(a)$ terms in Eq. (5.6)-(5.7).

It has also been shown in [26] that, as in the continuum theory, the spectrum of the hermitian lattice operator, $\gamma_5\tau^1\mathcal{D}_{\rm W}$, is bounded from below with a non-vanishing minimum eigenvalue which in the massless case is given by,

$$|\lambda_0| = \frac{2}{a}\left|\sin\left(\frac{a\pi}{4(\mathrm{T}+a)}\right)\right| \quad \stackrel{a=0}{\longrightarrow} \quad \frac{\pi}{2\mathrm{T}}\,. \tag{5.8}$$

In fact, the eigenvalue spectrum coincides with the one in the continuum theory in the limit $a \to 0$.

It is worth to mention at this point the role of the quark mass. As it can be seen from the expression of the action in Eq. (5.1), a standard mass term has been considered. The reason is that we are eventually interested in having a massless theory with Wilson fermions in the bulk. In this case, allowing for a twisted mass term is totally irrelevant. On the contrary, the standard mass term must be kept. As discussed in Chap. 3, due to the breaking of chiral symmetry by the Wilson term, the standard quark mass gets an additive renormalization and as a consequence it can not be simply set to zero in the massless limit. Instead, it needs a non-perturbative tuning to its critical value, thus ensuring the physical quark mass to vanish.

The lattice theory at tree-level is now defined. Before to consider the implications of interactions it is worth to finish this section presenting our analytical derivation of the quark propagator on the lattice at tree-level of perturbation theory.

5.1.1. The free lattice quark propagator with χSF boundary conditions

In this section we obtain the analytical expression of the quark propagator on the lattice and at tree-level of perturbation theory, when χSF boundary conditions are imposed on the quark fields. As in the continuum theory (cf. Sec. 4.3), we are interested in obtaining the expression in the time-momentum representation. The procedure to obtain the quark propagator when the quark fields are subject to certain boundary conditions is exactly the same as in the continuum. We refer the reader to Sec. 4.3 for a detailed explanation and collect here only the main results of such a derivation.

The aim here is to determine $S\,(x_0, y_0; \vec{p})$, when the orbifold construction with an $O(a)$ offset, as explained above, is considered. In this case, as it can be seen in Eq. (5.2), the massless lattice Dirac operator coincides with the massless Wilson operator in the bulk of the lattice, $a \leq x_0 \leq T - a$, and it is modified at the time boundaries, $x_0 = 0$ and $x_0 = T$, due to the presence of the boundary conditions, Eq. (5.6)-(5.7). Let us denote $S\,(x, y)$ the lattice free quark propagator with the chosen boundary conditions. The problem we want to solve is then

$$(D_{\rm W} + m_0)\; S\,(x, y) = a^{-4}\,\delta_{x,y} \qquad 0 < x_0 < T\,, \tag{5.9}$$

$$\widetilde{Q}_+\left(1 - \frac{a}{2}\partial_0^*\right) S(x, y)|_{x_0=0} = 0 \qquad \widetilde{Q}_-\left(1 + \frac{a}{2}\partial_0\right) S(x, y)|_{x_0=T} = 0\,. \tag{5.10}$$

$\delta_{x,y}$ is the dimensionless Kronecker delta and D_W denotes the massless Wilson-Dirac operator defined in Eq. (2.68) and recalled here for convenience,

$$D_{\rm W} = \sum_\mu \frac{1}{2}\left\{\gamma_\mu\left[\nabla_\mu^* + \nabla_\mu\right] - ar\,\nabla_\mu^*\nabla_\mu\right\}\,. \tag{5.11}$$

The covariant derivatives are as defined in App. A.5.2, but with the gauge links set to one because we are treating the free theory in this section. We also allow now for the phase factor,

θ_μ, entering the definitions of the lattice derivatives. Here, only a standard mass term, m_0, is considered, since the final purpose is to have a zero mass setup.

Proceeding as we did in the free continuum theory, we apply the standard technique. First, the solution, $S_\infty(x,y)$, of the inhomogeneous Dirac equation for infinite time extent is computed as described by the equation,

$$(D_{\mathrm{W}} + m_0)\; S_\infty(x,y) = a^{-4}\delta_{x,y} \qquad \forall\, x_0, y_0\,. \tag{5.12}$$

Then, a suitable solution, $\psi(x,y)$, of the homogeneous equation,

$$(D_{\mathrm{W}} + m_0)\; \psi(x,y) = 0\,, \tag{5.13}$$

is subtracted,

$$S(x,y) = S_\infty(x,y) - \psi(x,y)\;, \tag{5.14}$$

whose particular form will be determined by the specific boundary conditions which $S(x,y)$ satisfies at $x_0 = 0$ and $x_0 = T$. In this case, the χSF boundary conditions with $O(a)$-offset.

We assume in the following that $0 < y_0 < T$. In order to obtain the expression of the propagator in the time-momentum representation we make use of the Fourier transform in the spatial directions. This is possible thanks to translation invariance in such directions. In this case, the quark propagator may be written as,

$$S(x,y) = \frac{1}{L^3}\sum_{\vec{p}} e^{i\vec{p}(\vec{x}-\vec{y})}\, S(x_0, y_0; \vec{p})\;, \tag{5.15}$$

where

$$S(x_0, y_0; \vec{p}) = S_\infty(x_0 - y_0; \vec{p}) - \psi(x_0, y_0; \vec{p})\;, \tag{5.16}$$

with the definition

$$S_\infty(x_0 - y_0; \vec{p}) \equiv \int_{-\frac{\pi}{a}}^{+\frac{\pi}{a}} \frac{dp_0}{2\pi}\, e^{ip_0(x_0-y_0)}\, S_\infty(p_0, \vec{p})\;. \tag{5.17}$$

The expression of $S_\infty(p_0, \vec{p})$ has the form

$$S_\infty(p_0, \vec{p}) = \frac{-i\gamma_\mu \mathring{p}_\mu^+ + \mathcal{M}(p^+)}{(\mathring{p}^+)^2 + \mathcal{M}(p^+)^2}\;, \tag{5.18}$$

with the definitions

$$p_\mu^\pm = p_\mu \pm \theta_\mu/L\,, \qquad \theta_0 = 0\,, \tag{5.19}$$

$$\mathring{p}_\mu^\pm = \frac{1}{a}\sin\left(a p_\mu^\pm\right)\;, \qquad \mathcal{M}(p^\pm) = m_0 + \frac{1}{2}a\hat{p}_\mu^{\pm\,2}\,, \qquad \hat{p}_\mu^\pm = \frac{2}{a}\sin\left(\frac{a p_\mu^\pm}{2}\right)\;. \tag{5.20}$$

Using the residues method, the final expression for S_∞ in the time-momentum representation is

$$\begin{aligned} S_\infty(x_0 - y_0; \vec{p}) =& \frac{e^{-\omega(\vec{p}^+)(x_0-y_0)}}{2\mathring{\omega}(\vec{p}^+)A(\vec{p}^+)}\left[+\mathring{\omega}(\vec{p}^+)\gamma_0 - i\mathring{p}_k^+\gamma_k + \mathcal{M}(p^+)\right]\theta(x_0 - y_0) \\ &+ \frac{e^{+\omega(\vec{p}^+)(x_0-y_0)}}{2\mathring{\omega}(\vec{p}^+)A(\vec{p}^+)}\left[-\mathring{\omega}(\vec{p}^+)\gamma_0 - i\mathring{p}_k^+\gamma_k + \mathcal{M}(p^+)\right]\theta(y_0 - x_0) \\ &+ \frac{1}{2\mathring{\omega}(\vec{p}^+)A(\vec{p}^+)}\left[-i\mathring{p}_k^+\gamma_k + m_0 + \frac{a}{2}\hat{p}_k^{+2} + \frac{1}{a}\left(1 - e^{-a\omega(\vec{p}^+)}\right)\right]\delta(x_0 - y_0)\;. \end{aligned} \tag{5.21}$$

We have used the function $\theta(x)$ defined to be $\theta(x) = 1$ if $x > 0$ and zero otherwise. The function $\omega(\vec{p}^{+})$, such that $p_0 = i\omega(\vec{p}^{+})$, is given by

$$\sinh\left[\frac{a}{2}\omega\left(\vec{p}^{\pm}\right)\right] = \left\{\frac{a^2\mathring{p}_k^{\pm\,2} + \left(A(\vec{p}^{\pm}) - 1\right)^2}{4A(\vec{p}^{\pm})}\right\}^{1/2} , \tag{5.22}$$

and

$$\mathring{\omega}(p^{\pm}) \equiv -i\mathring{p}_0^{\pm} = \frac{1}{a}\sinh\left[a\omega(\vec{p}^{\pm})\right] , \tag{5.23}$$

$$A\left(\vec{p}^{\pm}\right) \equiv 1 + a\left(m_0 + \frac{a}{2}\hat{p}_k^{\pm\,2}\right) . \tag{5.24}$$

The next step is to find the form of $\psi\left(x_0, y_0; \vec{p}\right)$ and therefore $S\left(x_0, y_0; \vec{p}\right)$. Considering the plane wave expansion of $\psi(x, y)$,

$$\psi\left(x, y\right) = \frac{1}{L^3}\sum_{\vec{p}} e^{i\vec{p}(\vec{x}-\vec{y})}\,\psi\left(x_0, y_0; \vec{p}\right) , \tag{5.25}$$

a general solution for $\psi\left(x_0, y_0; \vec{p}\right)$ is obtained, which for the χSF boundary conditions here considered takes the particular form

$$\begin{aligned}\psi\left(x_0, y_0; \vec{p}\right) = {} & \frac{e^{-\omega(\vec{p}^{+})(x_0 - y_0 + 2(T+a))}}{2\mathring{\omega}(\vec{p}^{+})A(\vec{p}^{+})D(p^{+})}\left[+\mathring{\omega}(\vec{p}^{+})\gamma_0 - i\mathring{p}_k^{+}\gamma_k + \mathcal{M}(p^{+})\right]\times \\ & \left[1 + i\gamma_0\gamma_5\tau^3\, e^{a\omega(\vec{p}^{+})}e^{2\omega(\vec{p}^{+})(T-y_0)}\right] \\ & + \frac{e^{+\omega(\vec{p}^{+})(x_0 - y_0 - 2(T+a))}}{2\mathring{\omega}(\vec{p}^{+})A(\vec{p}^{+})D(p^{+})}\left[-\mathring{\omega}(\vec{p}^{+})\gamma_0 - i\mathring{p}_k^{+}\gamma_k + \mathcal{M}(p^{+})\right]\times \\ & \left[1 - i\gamma_0\gamma_5\tau^3\, e^{a\omega(\vec{p}^{+})}e^{2\omega(\vec{p}^{+})y_0}\right] ,\end{aligned} \tag{5.26}$$

where we have defined

$$D(p^{\pm}) \equiv 1 + e^{-2\omega(\vec{p}^{\pm})(T+a)} . \tag{5.27}$$

From the previous results, we can give the final expression of the quark propagator. In order to write it in a compact form, we consider the relation,

$$S\left(x, y\right) = \left(D_{\mathrm{W}}^{\dagger} + m_0\right) G\left(x, y\right) , \tag{5.28}$$

with

$$G\left(x, y\right) = \frac{1}{L^3}\sum_{\vec{p}} e^{i\vec{p}(\vec{x}-\vec{y})}\, G\left(x_0, y_0; \vec{p}\right) , \tag{5.29}$$

where

$$\begin{aligned}G\left(x_0, y_0; \vec{p}\right) = \frac{1}{2\mathring{\omega}(\vec{p}^{+})A(\vec{p}^{+})D(p^{+})}\Big\{ & e^{-\omega(\vec{p}^{+})|x_0 - y_0|} - e^{-\omega(\vec{p}^{+})(2(T+a) - |x_0 - y_0|)} \\ & - i\gamma_0\gamma_5\tau^3 e^{-\omega(\vec{p}^{+})(x_0 + y_0 + a)} \\ & + i\gamma_0\gamma_5\tau^3 e^{-\omega(\vec{p}^{+})(2(T+a) - (x_0 + y_0 + a))}\Big\} .\end{aligned} \tag{5.30}$$

Note that, simply performing the difference of the expressions in Eq. (5.21) and Eq. (5.26), we directly obtain the more explicit expression, $S\left(x_0, y_0; \vec{p}\right)$. Equivalently, it can be obtained acting with the Dirac operator in $G\left(x, y\right)$, as indicated above in Eq. (5.28), with the corresponding

expression of $G\,(x,y)$, defined in Eq. (5.29)-Eq. (5.30). In either case, the result is the following,

$$\begin{aligned} S\,(x_0,y_0;\vec{p}) =& \frac{1}{2\mathring{\omega}(\vec{p}^{+})A(\vec{p}^{+})D(p^{+})}\Big\{ \\ & e^{-\omega(\vec{p}^{+})(x_0-y_0)}\left[\mathring{\omega}(\vec{p}^{+})\gamma_0 - i\mathring{p}_k^{+}\gamma_k + \mathcal{M}(p^{+})\right]\Big\{\theta(x_0-y_0)\,D(p^{+}) \\ & -\left[1+i\gamma_0\gamma_5\tau^3 e^{a\omega(\vec{p}^{+})}e^{2\omega(\vec{p}^{+})(T-y_0)}\right]\,(D(p^{+})-1)\Big\} \\ & +e^{\omega(\vec{p}^{+})(x_0-y_0)}\left[-\mathring{\omega}(\vec{p}^{+})\gamma_0 - i\mathring{p}_k^{+}\gamma_k + \mathcal{M}(p^{+})\right]\Big\{\theta(y_0-x_0)\,D(p^{+}) \\ & -\left[1-i\gamma_0\gamma_5\tau^3 e^{a\omega(\vec{p}^{+})}e^{2\omega(\vec{p}^{+})y_0}\right]\,(D(p^{+})-1)\Big\} \\ & +\left[-i\mathring{p}_k^{+}\gamma_k + m_0 + \frac{a}{2}\hat{p}_k^{+\,2} + \frac{1}{a}\left(1-e^{-a\omega(\vec{p}^{+})}\right)\right]\,D(p^{+})\,\delta(x_0-y_0)\,\Big\}\,. \end{aligned} \tag{5.31}$$

An important consideration to be made here is that the obtained expression for the quark propagator also satisfies, as it should, the corresponding boundary conditions on the right side,

$$S(x,y)\widetilde{Q}_{+}\left(1-\frac{a}{2}\overleftarrow{\partial}_0^{*}\right)|_{y_0=0}=0 \qquad S(x,y)\widetilde{Q}_{-}\left(1+\frac{a}{2}\overleftarrow{\partial}_0\right)|_{y_0=T}=0\,. \tag{5.32}$$

To conclude this section we would like to mention that the analytical expression of the lattice quark propagator, derived in this thesis and presented in this section, has been numerically cross-checked with the propagator obtained from a numerical inversion of the free lattice Dirac operator given in Eq. (5.2) and also with the corresponding propagator in [26].

5.2. Renormalizability of the χSF and improvement

After the lattice theory with desired boundary conditions has been defined in the free case, the next step is to study the renormalization properties of such a theory. In order to do so, an analysis of the *lattice* symmetries is required, that provides an understanding about the possible counterterms appearing in the renormalization procedure. A priori, those will be not only bulk but also boundary counterterms. In order to understand the renormalization properties, it is necessary to determine all counterterms of dimension $d \leq 4$ in bulk and $d \leq 3$ at the boundaries, which are generated by the interactions. For $O(a)$ improvement via the Symanzik programme the same holds but considering operators of $d = 5$ in the bulk and $d = 4$ at the boundaries. As already said, the symmetries of the lattice theory with massless Wilson fermions and χSF boundary conditions are the same as those of twisted mass Wilson fermions (cf. Sec. 2.7.3). The only exceptions are the space-time symmetries mixing spatial and time directions, since in SF formulations the spatial and temporal components are clearly different. Amongst the symmetries shared with twisted mass are, spatial lattice rotations, charge conjugation, $\mathcal{C}$, space and time reflections with flavor exchange, $\mathcal{P}_{\mathrm{F}}^{1,2}$, $\mathcal{T}_{\mathrm{F}}^{1,2}$, global $U(1)$ vector rotations with generator $\tau^3/2$, and γ_5-hermiticity with flavor exchange (cf. Eq. (5.3)).

The bulk counterterms allowed by these symmetries are exactly the same as in infinite volume and have already been discussed in Chap. 2 and Chap. 3, when Wilson-like fermions were described. Concerning renormalization, the only bulk counterterm is the critical mass, m_c, which accounts for the additive renormalization of the standard bare quark mass, m_0. Such counterterm is a relevant operator, linearly divergent with the inverse of the lattice spacing when $a \to 0$. For $O(a)$-improvement there is also only one counterterm in the bulk of the lattice. This is the clover term, which is an irrelevant operator of mass dimension 5. Both counterterms appear due to the explicit breaking of chiral symmetry by the regularization,

by the Wilson term in this case. In Chap. 2 and Chap. 3, it has also been argued that the clover term is not needed for $O(a)$-improvement if massless Wilson fermions with χSF boundary conditions are considered, because it only modifies the relevant correlation functions at $O(a^2)$. In this case, bulk improvement should be automatic possibly after the tuning of some *boundary* counterterms. Therefore, in the *bulk* we are left with *no* $O(a)$-improvement counterterm and with only the additive renormalization of the quark mass.

In the same way, taking into account the symmetries of the *lattice* theory, a classification of all allowed *boundary* counterterms of mass dimension up to $d = 4$ can be made. No counterterm divergent with the lattice spacing, $d < 3$, is allowed at the boundaries. So, for renormalization and $O(a)$-improvement, it is enough to list the possible boundary counterterms which are marginal, $d = 3$, and irrelevant with $d = 4$. Namely, all $O(1)$ and $O(a)$ counterterms, respectively.

There are three operators of energy dimension 3,

$$\mathcal{O}_1 = \overline{\chi}(x)\,\gamma_0\widetilde{Q}_+\,\chi(x) - \overline{\chi}(x)\,\gamma_0\widetilde{Q}_-\,\chi(x) = \overline{\chi}(x)\,\mathrm{i}\gamma_5\tau^3\,\chi(x)\,, \tag{5.33}$$

$$\mathcal{O}_2 = \overline{\chi}(x)\,\widetilde{Q}_+\,\chi(x)\,, \tag{5.34}$$

$$\mathcal{O}_3 = \overline{\chi}(x)\,\widetilde{Q}_-\,\chi(x)\,, \tag{5.35}$$

and eight operators of dimension 4,

$$\mathcal{O}_4 = \overline{\chi}(x)\,\widetilde{Q}_+\gamma_k D_k\,\chi(x) - \overline{\chi}(x)\,\overleftarrow{D}_k\gamma_k\widetilde{Q}_+\,\chi(x)\,, \tag{5.36}$$

$$\mathcal{O}_5 = \overline{\chi}(x)\,\widetilde{Q}_-\gamma_k D_k\,\chi(x) - \overline{\chi}(x)\,\overleftarrow{D}_k\gamma_k\widetilde{Q}_-\,\chi(x)\,, \tag{5.37}$$

$$\mathcal{O}_6 = \overline{\chi}(x)\,\widetilde{Q}_+\gamma_0 D_0\,\chi(x) - \overline{\chi}(x)\,\overleftarrow{D}_0\gamma_0\widetilde{Q}_+\,\chi(x)\,, \tag{5.38}$$

$$\mathcal{O}_7 = \overline{\chi}(x)\,\widetilde{Q}_-\gamma_0 D_0\,\chi(x) - \overline{\chi}(x)\,\overleftarrow{D}_0\gamma_0\widetilde{Q}_-\,\chi(x)\,, \tag{5.39}$$

$$\mathcal{O}_8 = \overline{\chi}(x)\,\widetilde{Q}_+ D_0\,\chi(x) + \overline{\chi}(x)\,\overleftarrow{D}_0\widetilde{Q}_+\,\chi(x)\,, \tag{5.40}$$

$$\mathcal{O}_9 = \overline{\chi}(x)\,\widetilde{Q}_- D_0\,\chi(x) + \overline{\chi}(x)\,\overleftarrow{D}_0\widetilde{Q}_-\,\chi(x)\,, \tag{5.41}$$

$$\mathcal{O}_{10} = \overline{\chi}(x)\,\widetilde{Q}_+\gamma_0\gamma_k D_k\,\chi(x) + \overline{\chi}(x)\,\overleftarrow{D}_k\gamma_k\gamma_0\widetilde{Q}_+\,\chi(x)\,, \tag{5.42}$$

$$\mathcal{O}_{11} = \overline{\chi}(x)\,\widetilde{Q}_-\gamma_0\gamma_k D_k\,\chi(x) + \overline{\chi}(x)\,\overleftarrow{D}_k\gamma_k\gamma_0\widetilde{Q}_-\,\chi(x)\,. \tag{5.43}$$

As usual, the number of improvement counterterms needed for on-shell improvement might be reduced by using the classical equations of motion,

$$\not{D}\chi(x) = 0\,, \qquad \overline{\chi}(x)\,\overleftarrow{\not{D}} = 0\,, \tag{5.44}$$

where $\not{D} = \gamma_\mu D_\mu$. In this case, the following relations hold,

$$\mathcal{O}_4 + \mathcal{O}_6 = 0\,, \tag{5.45}$$

$$\mathcal{O}_5 + \mathcal{O}_7 = 0\,, \tag{5.46}$$

$$\mathcal{O}_8 + \mathcal{O}_{10} = 0\,, \tag{5.47}$$

$$\mathcal{O}_9 + \mathcal{O}_{11} = 0\,. \tag{5.48}$$

$$\tag{5.49}$$

Since total derivatives do not contribute to the action there is an additional relation,

$$\mathcal{O}_{10} - \mathcal{O}_{11} = \partial_k\left(\overline{\chi}(x)\,\gamma_k\,\mathrm{i}\gamma_5\tau^3\,\chi(x)\right). \tag{5.50}$$

Therefore, from considering the previous five relations, Eq. (5.45)-(5.50), only three out of

eight $O(a)$ improvement counterterms are needed at the boundaries, which have to be added to the lattice action with their corresponding improvement coefficients. In summary, only six boundary counterterms have to be considered for the renormalizability and $O(a)$ improvement of the theory with massless Wilson fermions in the bulk and χSF boundary conditions. Three of them are renormalization counterterms, Eq. (5.33)-(5.35), and the other three are improvement counterterms, Eq. (5.36)-(5.37)-(5.42).

Once all possible boundary counterterms are known, the next step is to understand how they have to be eventually added to the lattice action and operators to be renormalized and improved. The renormalizability properties of a theory with boundaries are best understood if inhomogeneous boundary conditions are considered. This is so because in such a case the generating functional for fermions might be used to directly derive the counterterm structure of the action and all two-point functions, as it is done, for instance, in the standard formulation of the SF [87]. But, unfortunately, an orbifold construction of the lattice theory, as it is the case here, can only implement homogeneous boundary conditions. There is, though, a possible way out; the renormalization and improvement structure may be found out from the formal continuum theory, where inhomogeneous χSF boundary conditions may be imposed without any problem. After that, such knowledge can be carried over to the lattice formulation. We present the discussion in the continuum in Sec. 5.2.1 and the lattice implementation is left to Sec. 5.2.2.

5.2.1. Counterterm structure in the continuum

In general, correlation functions can be derived from the generating functional for fermions, Eq. (2.31)-(2.32), as described in Sec. 2.3. This is done by identifying the fermion and anti-fermion fields, $\{\chi, \overline{\chi}\}$, with functional derivatives with respect to the source fields. In particular, they are defined as follows,

$$\chi(x) \leftrightarrow \frac{\delta}{\delta\overline{\eta}(x)}\,, \qquad \overline{\chi}(x) \leftrightarrow -\frac{\delta}{\delta\eta(x)}\,, \tag{5.51}$$

with η and $\overline{\eta}$ the sources of the anti-fermion and fermion fields, respectively. If a theory with boundary conditions is considered, Eq. (5.51) represents the definition of the quark fields in the interior of the space-time volume, away from the boundaries. In this case, a distinction between bulk and boundary fields is needed. As discussed in Sec. 3.4, in the theory with *inhomogeneous* boundary conditions the boundary fields may also be treated in a similar manner as the fields in the bulk. Namely, the quark and anti-quark fields at the boundaries are not anymore defined as operator insertions, but instead, they are functional derivatives with respect to the boundary sources of the quark and anti-quark fields. These sources are given by the inhomogeneous boundary conditions. In our particular case, we consider the continuum theory with inhomogeneous χSF boundary conditions,

$$\widetilde{Q}_+\,\chi(x)|_{x_0=0} = \rho(\vec{x}) \qquad \widetilde{Q}_-\,\chi(x)|_{x_0=T} = \rho'(\vec{x}) \tag{5.52}$$

$$\overline{\chi}(x)\,\widetilde{Q}_+|_{x_0=0} = \overline{\rho}(\vec{x}) \qquad \overline{\chi}(x)\,\widetilde{Q}_-|_{x_0=T} = \overline{\rho}'(\vec{x}) \tag{5.53}$$

where the 'boundary fields' at $x_0 = 0$, $\{\zeta, \overline{\zeta}\}$, and at $x_0 = T$, $\{\zeta', \overline{\zeta}'\}$, are defined through,

$$\zeta(\vec{x}) \leftrightarrow -\frac{\delta}{\delta[\overline{\rho}(\vec{x})\gamma_0]}\,, \qquad \overline{\zeta}(\vec{x}) \leftrightarrow -\frac{\delta}{\delta[\gamma_0\rho(\vec{x})]}\,, \tag{5.54}$$

$$\zeta'(\vec{x}) \leftrightarrow \frac{\delta}{\delta[\overline{\rho}'(\vec{x})\gamma_0]}\,, \qquad \overline{\zeta}'(\vec{x}) \leftrightarrow \frac{\delta}{\delta[\gamma_0\rho'(\vec{x})]}\,. \tag{5.55}$$

As a result, from these definitions the fermionic expectation value of any operator O, which may contain derivatives with respect to the source fields in the bulk and/or at the boundaries, can be computed from,

$$[O]_{\mathrm{F}} = \Big\{ \frac{1}{\mathcal{Z}_{\mathrm{F}}} O\, \mathcal{Z}_{\mathrm{F}} \Big\}_{\overline{\rho}=\cdots=\eta=0} , \tag{5.56}$$

as explained in Sec. 2.3. Here the generating functional for fermions is defined as follows,

$$\mathcal{Z}_{\mathrm{F}}[\rho,\overline{\rho};\rho',\overline{\rho}';\eta,\overline{\eta}] = \int \mathcal{D}[\chi,\overline{\chi}]\; e^{-S_{\mathrm{F}}^{\mathrm{cont}}[\chi,\overline{\chi},A]+(\overline{\eta},\chi)+(\overline{\chi},\eta)} , \tag{5.57}$$

with the fermion action in the massless continuum theory with inhomogeneous χSF boundary conditions given as

$$\begin{aligned} S_{\mathrm{F}}^{\mathrm{cont}}[\chi,\overline{\chi},A] = {} & \frac{1}{2}\int_0^T \mathrm{d}x_0 \int_0^L \mathrm{d}^3\vec{x}\; \overline{\chi}(x) \overleftrightarrow{\not{D}}\, \chi(x) \\ & - \frac{1}{2}\int_0^L \mathrm{d}^3\vec{x}\; [\overline{\chi}(x)\, \mathrm{i}\gamma_5\tau^3\, \chi(x)]_{x_0=0} - \frac{1}{2}\int_0^L \mathrm{d}^3\vec{x}\; [\overline{\chi}(x)\, \mathrm{i}\gamma_5\tau^3\, \chi(x)]_{x_0=T} \end{aligned} \tag{5.58}$$

and the symmetric expression

$$\overleftrightarrow{\not{D}} = \overrightarrow{\not{D}} + \overleftarrow{\not{D}} . \tag{5.59}$$

From the generating functional in Eq. (5.57) with action Eq. (5.58), all possible two-point functions can be derived. The two-point functions are important because they are the building blocks of any other correlation function. They are derived by applying Eq. (5.56), with O an operator containing different combinations of derivatives with respect to the source fields in the bulk and/or at the boundaries. However, while the generating functional of Eq. (5.57) only depends on the source fields in the bulk through the exponential of $(\overline{\eta},\chi)+(\overline{\chi},\eta)$, all dependence on the boundary source fields is contained in the fermion action, Eq. (5.58). Therefore, for the derivation of such correlation functions it is best to rewrite the generating functional in a different way. In particular, in terms of the classical fields $\{\chi_{\mathrm{cl}},\overline{\chi}_{\mathrm{cl}}\}$. This can be achieved by writing the matter fields, $\{\chi,\overline{\chi}\}$, as the sum of the classical fields, satisfying the inhomogeneous χSF boundary conditions, and the quantum fluctuations, usually denoted as $\{v,\overline{v}\}$ and satisfying homogeneous χSF boundary conditions. This is the usual technique applied in the standard formulation of the SF. In the χSF formulation, such generating functional may then be rewritten as [26],

$$\ln\mathcal{Z}_{\mathrm{F}} = \ln\mathcal{Z}_{\mathrm{F},0} - S_{\mathrm{F}}^{\mathrm{cont}}[\chi_{\mathrm{cl}},\overline{\chi}_{\mathrm{cl}},A] + (\overline{\eta},S\eta) + (\overline{\eta},\chi_{\mathrm{cl}}) + (\overline{\chi}_{\mathrm{cl}},\eta) , \tag{5.60}$$

with

$$\mathcal{Z}_{\mathrm{F},0} = \mathcal{Z}_{\mathrm{F}}[0,0;0,0;0,0] , \qquad (S\eta)(x) = \int \mathrm{d}^4y\; S(x,y)\eta(y) , \tag{5.61}$$

and the fermion action of the classical fields,

$$\begin{aligned} S_{\mathrm{F}}^{\mathrm{cont}}[\chi_{\mathrm{cl}},\overline{\chi}_{\mathrm{cl}},A] = \int \mathrm{d}^3\vec{x}\,\mathrm{d}^3\vec{y}\; \Big[& \overline{\rho}(\vec{x})\,\gamma_0\widetilde{Q}_- S(0,\vec{x};0,\vec{y})\widetilde{Q}_-\gamma_0\,\rho(\vec{y}) \\ & -\overline{\rho}(\vec{x})\,\gamma_0\widetilde{Q}_- S(0,\vec{x};T,\vec{y})\widetilde{Q}_+\gamma_0\,\rho'(\vec{y}) \\ & -\overline{\rho}'(\vec{x})\,\gamma_0\widetilde{Q}_+ S(T,\vec{x};0,\vec{y})\widetilde{Q}_-\gamma_0\,\rho(\vec{y}) \\ & +\overline{\rho}'(\vec{x})\,\gamma_0\widetilde{Q}_+ S(T,\vec{x};T,\vec{y})\widetilde{Q}_+\gamma_0\,\rho'(\vec{y}) \Big] . \end{aligned} \tag{5.62}$$

$S(x,y)$ is the fermion propagator in the continuum, with χSF boundary conditions and immerse in the external gauge field A_μ.

From such expressions all two-point functions may be eventually derived and they are given

by,

$$[\chi(x)\overline{\chi}(y)]_{\mathrm{F}} = S(x,y)\,, \tag{5.63}$$
$$[\chi(x)\overline{\zeta}(\vec{y})]_{\mathrm{F}} = S(x;0,\vec{y})\,\widetilde{Q}_-\,, \tag{5.64}$$
$$[\chi(x)\overline{\zeta}'(\vec{y})]_{\mathrm{F}} = S(x;T,\vec{y})\,\widetilde{Q}_+\,, \tag{5.65}$$
$$[\zeta(\vec{x})\overline{\chi}(y)]_{\mathrm{F}} = \widetilde{Q}_-\,S(0,\vec{x};y)\,, \tag{5.66}$$
$$[\zeta'(\vec{x})\overline{\chi}(y)]_{\mathrm{F}} = \widetilde{Q}_+\,S(T,\vec{x};y)\,, \tag{5.67}$$
$$[\zeta(\vec{x})\overline{\zeta}(\vec{y})]_{\mathrm{F}} = \widetilde{Q}_-\,S(0,\vec{x};0,\vec{y})\,\widetilde{Q}_-\,, \tag{5.68}$$
$$[\zeta(\vec{x})\overline{\zeta}'(\vec{y})]_{\mathrm{F}} = \widetilde{Q}_-\,S(0,\vec{x};T,\vec{y})\,\widetilde{Q}_+\,, \tag{5.69}$$
$$[\zeta'(\vec{x})\overline{\zeta}(\vec{y})]_{\mathrm{F}} = \widetilde{Q}_+\,S(T,\vec{x};0,\vec{y})\,\widetilde{Q}_-\,, \tag{5.70}$$
$$[\zeta'(\vec{x})\overline{\zeta}'(\vec{y})]_{\mathrm{F}} = \widetilde{Q}_+\,S(T,\vec{x};T,\vec{y})\,\widetilde{Q}_+\,. \tag{5.71}$$

The counterterm action in the continuum theory can now be determined. It has been shown above that the counterterm basis at the boundaries is made of the operators $\mathcal{O}_{1-5}$ and $\mathcal{O}_{10}$ inserted at both boundaries, $x_0 = 0$ and $x_0 = T$. Considering such counterterm basis and using time reflection symmetry, the counterterm action in the continuum, $S_{\mathrm{F}}^{\mathrm{c.t.}}$, takes the form,

$$\begin{aligned} S_{\mathrm{F}}^{\mathrm{c.t.}} = &\int_0^L \mathrm{d}^3\vec{x}\,[c_1\mathcal{O}_1 + c_2\mathcal{O}_2 + c_3\mathcal{O}_3 + ac_4\mathcal{O}_4 + ac_5\mathcal{O}_5 + ac_{10}\mathcal{O}_{10}]_{x_0=0} \\ &+ \int_0^L \mathrm{d}^3\vec{x}\,[c_1\mathcal{O}_1 + c_2\mathcal{O}_3 + c_3\mathcal{O}_2 + ac_4\mathcal{O}_5 + ac_5\mathcal{O}_4 - ac_{10}\mathcal{O}_{10}]_{x_0=T}\,, \end{aligned} \tag{5.72}$$

with the total fermion continuum action given as [1]

$$S_{\mathrm{F}}^{\mathrm{total}} = S_{\mathrm{F}}^{\mathrm{cont}} + S_{\mathrm{F}}^{\mathrm{c.t.}}\,. \tag{5.73}$$

As in the standard SF, O_1 is a logarithmically divergent counterterm which can be reabsorbed in a multiplicative renormalization of the quark boundary fields, $\zeta, \overline{\zeta}, \zeta', \overline{\zeta}'$. This renormalization constant does not need to be determined if correlation functions involving the boundary quark fields are normalized by correlation functions boundary-to-boundary, as explained in Sec. 3.4, because these ratios cancel the renormalization of the boundary fields. This is the case in all results here presented, so no mention of such renormalizations is made in the following.

From the total expression of the action and using the generating functional for fermions as indicated above, also the counterterm structure of all two-point functions can be derived in the continuum. In order not to have a too lengthly discussion and since we are eventually interested in the lattice formulation of all these expressions, the continuum two-point functions are not discussed here and we refer the reader to the literature [26] for further insights in the topic. As already anticipated, the counterterm structure in the continuum theory specifies how renormalization and $O(a)$-improvement counterterms arise at the lattice level. The lattice expressions are presented in the following section.

5.2.2. Counterterm structure on the lattice and tuning parameters

Once the counterterm structure of the action and two-point functions is understood in the continuum theory, such knowledge can be directly applied to define the lattice theory. At the lattice level, however, *homogeneous* boundary conditions are considered. Therefore, besides

[1] Note that we do not include the bulk improvement counterterm to the action (clover term), because it has been already argued that this term only modifies the $O(a^2)$ effects of the theory with χSF boundaries.

translating all fields to their lattice counterparts, also the particularization to zero boundary fields should be made. In this case, only the terms O_3 and O_5 contribute at $x_0 = 0$, while only O_2 and O_4 do not vanish at $x_0 = T$. This has the advantage that the expressions can be simplified by considering the sums $O_2 + O_3$ and $O_4 + O_5$ at the two boundaries, with certain renormalization and improvement coefficients, respectively. With this considerations, the theory discussed in the previous sections is parametrized on the lattice as follows. The lattice Dirac operator is given by,

$$\mathcal{D}_{\mathrm{W}}^{\mathrm{total}} = \mathcal{D}_{\mathrm{W}} + \delta\mathcal{D}_{\mathrm{W}}\,, \tag{5.74}$$

with $\mathcal{D}_{\mathrm{W}}$ given above in Eq. (5.2) and the counterterm operator, $\delta\mathcal{D}_{\mathrm{W}}$, defined as

$$\delta\mathcal{D}_{\mathrm{W}} = (\delta_{x_0,0} + \delta_{x_0,T})\left[(z_f - 1) + (d_s - 1)\, a\mathbf{D}_s\right], \tag{5.75}$$

with

$$\mathbf{D}_s = \frac{1}{2}\,\gamma_k\,(\nabla_k^* + \nabla_k)\,, \qquad \overleftarrow{\mathbf{D}}_s = \frac{1}{2}\,(\overleftarrow{\nabla}_k^* + \overleftarrow{\nabla}_k)\,\gamma_k\,. \tag{5.76}$$

The parameter z_f is the coefficient of the term $O_2 + O_3$ and d_s is the coefficient of $O_4 + O_5$. While the improvement coefficient, d_s, has an analogue in the standard SF formulation, $\widetilde{c}_t$, the renormalization coefficient, z_f, does not. It is new with respect to the standard formulation and if properly determined, it accounts for a restoration of the broken parity and flavor symmetries, or equivalently, $\gamma_5\tau^1$ if seen in the twisted basis. Thus, with respect to the standard SF, only one additional counterterm to the fermion action is required *at the boundaries*. These two counterterms, which enter directly the expression of the Dirac operator, do therefore contribute to all correlation functions. Thus, even if they are only insertions at the boundaries, they also affect the physics in the bulk of the lattice.

Using the following definitions for the parallel transported boundary-to-boundary propagators,

$$\overline{S}(0,\vec{x};0,\vec{y}) \equiv U_0(0,\vec{x})\,S(a,\vec{x};a,\vec{y})\,U_0(0,\vec{y})^\dagger\,, \tag{5.77}$$
$$\overline{S}(0,\vec{x};T,\vec{y}) \equiv U_0(0,\vec{x})\,S(a,\vec{x};T-a,\vec{y})\,U_0(T-a,\vec{y})\,, \tag{5.78}$$
$$\overline{S}(T,\vec{x};0,\vec{y}) \equiv U_0(T-a,\vec{x})^\dagger\,S(T-a,\vec{x};a,\vec{y})\,U_0(0,\vec{y})^\dagger\,, \tag{5.79}$$
$$\overline{S}(T,\vec{x};T,\vec{y}) \equiv U_0(T-a,\vec{x})^\dagger\,S(T-a,\vec{x};T-a,\vec{y})\,U_0(T-a,\vec{y})\,, \tag{5.80}$$

the basic two-point functions on the lattice with χSF boundary conditions take the form

$$[\chi(x)\overline{\chi}(y)]_{\mathrm{F}} = S(x,y)\,, \tag{5.81}$$
$$[\chi(x)\overline{\zeta}(\vec{y})]_{\mathrm{F}} = S(x;a,\vec{y})\,U_0(0,\vec{y})^\dagger\,(1 - \overline{d}_s a\overleftarrow{\mathbf{D}}_s)\,\widetilde{Q}_-\,, \tag{5.82}$$
$$[\chi(x)\overline{\zeta}'(\vec{y})]_{\mathrm{F}} = S(x;T-a,\vec{y})\,U_0(T-a,\vec{y})\,(1 - \overline{d}_s a\overleftarrow{\mathbf{D}}_s)\,\widetilde{Q}_+\,, \tag{5.83}$$
$$[\zeta(\vec{x})\overline{\chi}(y)]_{\mathrm{F}} = \widetilde{Q}_-\,(1 + \overline{d}_s a\mathbf{D}_s)\,U_0(0,\vec{x})\,S(a,\vec{x};y)\,, \tag{5.84}$$
$$[\zeta'(\vec{x})\overline{\chi}(y)]_{\mathrm{F}} = \widetilde{Q}_+\,(1 + \overline{d}_s a\mathbf{D}_s)\,U_0(T-a,\vec{x})^\dagger\,S(T-a,\vec{x};y)\,, \tag{5.85}$$
$$[\zeta(\vec{x})\overline{\zeta}(\vec{y})]_{\mathrm{F}} = \widetilde{Q}_-\,(1 + \overline{d}_s a\mathbf{D}_s)\,[\overline{S}(0,\vec{x};0,\vec{y}) - (\widetilde{z}_f + \widetilde{d}_s a\mathbf{D}_s)\,\delta(\vec{x}-\vec{y})]\,(1 - \overline{d}_s a\overleftarrow{\mathbf{D}}_s)\,\widetilde{Q}_-\,, \tag{5.86}$$
$$[\zeta(\vec{x})\overline{\zeta}'(\vec{y})]_{\mathrm{F}} = \widetilde{Q}_-\,(1 + \overline{d}_s a\mathbf{D}_s)\,\overline{S}(0,\vec{x};T,\vec{y})\,(1 - \overline{d}_s a\overleftarrow{\mathbf{D}}_s)\,\widetilde{Q}_+\,, \tag{5.87}$$
$$[\zeta'(\vec{x})\overline{\zeta}(\vec{y})]_{\mathrm{F}} = \widetilde{Q}_+\,(1 + \overline{d}_s a\mathbf{D}_s)\,\overline{S}(T,\vec{x};0,\vec{y})\,(1 - \overline{d}_s a\overleftarrow{\mathbf{D}}_s)\,\widetilde{Q}_-\,, \tag{5.88}$$
$$[\zeta'(\vec{x})\overline{\zeta}'(\vec{y})]_{\mathrm{F}} = \widetilde{Q}_+\,(1 + \overline{d}_s a\mathbf{D}_s)\,[\overline{S}(T,\vec{x};T,\vec{y}) - (\widetilde{z}_f + \widetilde{d}_s a\mathbf{D}_s)\,\delta(\vec{x}-\vec{y})]\,(1 - \overline{d}_s a\overleftarrow{\mathbf{D}}_s)\,\widetilde{Q}_+\,. \tag{5.89}$$

In these expressions, $\widetilde{d}_s$ has a counterpart, $\widetilde{c}_s$, in the standard setup. However, $\widetilde{z}_f$ and $\overline{d}_s$ do not. These last two, as z_f, are a consequence of the breaking of $\gamma_5\tau^1$-symmetry by the

regularization. $\widetilde{z}_f$ and $\widetilde{d}_s$ only contribute if spatial contact terms arise, as it is guaranteed by the delta function in the spatial coordinates. Such correlation functions may be avoided, so these coefficients are totally irrelevant here. Also $\overline{d}_s$ does not need to be determined. The reason is that it is the improvement coefficient of a $\gamma_5\tau^1$-odd operator, thus leading a contribution of only $O(a^2)$ effects in even correlation functions and therefore of no importance for $O(a)$-improvement. As a result, the relevant two-point functions up to $O(a^2)$ corrections turn out to be,

$$[\chi(x)\overline{\chi}(y)]_{\mathrm{F}} = S(x,y)\,, \tag{5.90}$$

$$[\chi(x)\overline{\zeta}(\vec{y})]_{\mathrm{F}} = S(x;a,\vec{y})\,U_0(0,\vec{y})^\dagger\,\widetilde{Q}_-\,, \tag{5.91}$$

$$[\chi(x)\overline{\zeta}'(\vec{y})]_{\mathrm{F}} = S(x;T-a,\vec{y})\,U_0(T-a,\vec{y})\,\widetilde{Q}_+\,, \tag{5.92}$$

$$[\zeta(\vec{x})\overline{\chi}(y)]_{\mathrm{F}} = \widetilde{Q}_-\,U_0(0,\vec{x})\,S(a,\vec{x};y)\,, \tag{5.93}$$

$$[\zeta'(\vec{x})\overline{\chi}(y)]_{\mathrm{F}} = \widetilde{Q}_+\,U_0(T-a,\vec{x})^\dagger\,S(T-a,\vec{x};y)\,, \tag{5.94}$$

$$[\zeta(\vec{x})\overline{\zeta}(\vec{y})]_{\mathrm{F}} = \widetilde{Q}_-\,U_0(0,\vec{x})\,S(a,\vec{x};a,\vec{y})\,U_0(0,\vec{y})^\dagger\,\widetilde{Q}_-\,, \qquad \vec{x}\neq\vec{y}\,, \tag{5.95}$$

$$[\zeta(\vec{x})\overline{\zeta}'(\vec{y})]_{\mathrm{F}} = \widetilde{Q}_-\,U_0(0,\vec{x})\,S(a,\vec{x};T-a,\vec{y})\,U_0(T-a,\vec{y})\,\widetilde{Q}_+\,, \tag{5.96}$$

$$[\zeta'(\vec{x})\overline{\zeta}(\vec{y})]_{\mathrm{F}} = \widetilde{Q}_+\,U_0(T-a,\vec{x})^\dagger\,S(T-a,\vec{x};a,\vec{y})\,U_0(0,\vec{y})^\dagger\,\widetilde{Q}_-\,, \tag{5.97}$$

$$[\zeta'(\vec{x})\overline{\zeta}'(\vec{y})]_{\mathrm{F}} = \widetilde{Q}_+\,U_0(T-a,\vec{x})^\dagger\,S(T-a,\vec{x};T-a,\vec{y})\,U_0(T-a,\vec{y})\,\widetilde{Q}_+\,, \qquad \vec{x}\neq\vec{y}\,. \tag{5.98}$$

The result is that although all two-point functions are implicitly affected by the counterterms to the Dirac operator, with coefficients z_f and d_s, these two are the only boundary counter terms required for the two-point functions of interest.

The conclusion is that, concerning boundary counterterms, it is enough to determine two boundary coefficients. The improvement coefficient d_s, for a boundary $O(a)$-improvement of all physical correlation functions, and the renormalization coefficient z_f, for a restoration of the broken symmetry, $\gamma_5\tau^1$, by the regularization. The tuning of z_f is equivalent to a renormalization of the rotation angle, α, such that the correct boundary conditions are recovered in the continuum limit. This is because the symmetry, $\gamma_5\tau^1$, protecting the rotation angle at maximal twist, $\alpha=\pi/2$, is broken at finite lattice spacing. This allows the interactions to rotate the angle away from $\pi/2$ thus giving rise to the wrong boundary conditions. By properly tuning z_f, the correct angle is ensured to happen at finite lattice spacing and as a result, also in the continuum limit. Thus, a proper tuning of z_f ensures the correct continuum limit of the theory. Since $\gamma_5\tau^1$ is a symmetry of the massless continuum theory, which is only broken in the regularization procedure, z_f accounts for a finite renormalization. That is, it obeys the form,

$$z_f(g_0) = z_f^{(0)} + z_f^{(1)}\,g_0^2 + O(g_0^4)\,, \tag{5.99}$$

with all coefficients in the expansion being finite. The improvement coefficient, d_s, obeys the same kind of expansion in the bare gauge coupling,

$$d_s(g_0) = d_s^{(0)} + d_s^{(1)}\,g_0^2 + O(g_0^4)\,. \tag{5.100}$$

In perturbation theory, only the tree-level values of these coefficients are known at present. z_f is not needed at tree-level on the lattice, which is equivalent to say that its tree-level value is $z_f^{(0)}=1$. This value has been obtained by a direct comparison of the free quark propagator in the continuum (cf. Eq. (4.121)) and the continuum limit of the analytical expression for the free lattice quark propagator (cf. Eq. (5.31)). However, if the offset setup is chosen in the orbifold construction, as it is our case here, d_s is already needed at tree-level in order to cancel boundary $O(a)$ effects. The correct value is in this case $d_s^{(0)}=1/2$. We have determined this value from

a numerical inspection of the free quark propagator on the lattice, obtained from the numerical inversion of the operator in Eq. (5.74). In fact, this result agrees with the one obtained in [26].

The knowledge of d_s^0 guarantees boundary cutoff effects of at most $O(ag_0^2)$. However, a determination beyond tree-level would be very desirable. Like in the standard SF, a perturbative determination of d_s should be enough in the cancellation of boundary effects. As a counter example, a perturbative determination of z_f is clearly not enough. The reason is that z_f is the coefficient of a marginal operator, thus accounting for the renormalization of the theory. If z_f is not determined non-perturbatively, the continuum limit might be compromised giving rise to the wrong continuum theory. In addition, since $\gamma_5\tau^1$-symmetry would not be properly restored in this case, no bulk automatic $O(a)$-improvement would take place. A non-perturbative determination of z_f is then mandatory. Its determination can be carried out by imposing suitable $\gamma_5\tau^1$-odd correlation functions to vanish. This is similar to what is done in the tuning of the bare standard quark mass to its critical value, when imposing a chiral symmetry violating correlation function to vanish, e.g. the PCAC mass. Since the renormalization conditions are not unique, different determinations of z_f are expected to differ by $O(a)$ effects, which should only affect even correlation functions up to $O(a^2)$. This is similar to what happens with the standard quark mass, whose intrinsic $O(a)$ effects only affect physical quantities at $O(a^2)$. In fact, in this work both, m_0 and z_f have to be tuned non-perturbatively and simultaneously if a massless renormalization scheme with χSF boundary conditions is to be defined. All this procedure will be presented in following chapters and it is one of the main topics of this thesis. In particular, it is very important to understand whether this 'combined' tuning is feasible at all, as otherwise no practical application of the χSF scheme would be possible.

The important conclusion of the above discussion is that even if, with respect to the standard formulation of the SF, there is an additional boundary coefficient, z_f, which has to be non-perturbatively determined, this is enough to guarantee a correct continuum limit of the theory and bulk automatic $O(a)$-improvement up to boundary effects of at most $O(ag_0^2)$, since the boundary coefficients, d_s and c_t, are only known in perturbation theory. Therefore, besides the boundary improvement counterterms to the action, d_s and c_t, no improvement counterterms need to be added to any $\gamma_5\tau^1$-even quantity, which are in fact the only physically relevant observables. All this is true assuming that the quark mass is also properly tuned to its critical value, $m_0 \to m_c$. It is our task in following chapters to demonstrate the statements made here. For that purpose, the 2-loop value of c_t (cf. Sec. 3.2.2) and the tree-level value of d_s are used in all our calculations, while a simultaneous non-perturbative tuning of m_0 and z_f is needed before the computation of any physical quantity. The explanation of the tuning procedure that we have preformed is presented in the next chapter together with the corresponding results for the critical values of the coefficients, m_c and z_f^c.

6. Non-perturbative tuning of κ and z_f

From pure theoretical arguments, it may be concluded that the χSF formulation with massless Wilson fermions in the bulk leads to a suitable non-perturbative renormalization scheme. In particular, the χSF scheme is expected to have a well defined continuum limit, in which it should be equivalent to the standard formulation of the SF. This is true after the non-perturbative tuning of only *two* parameters, which are functions of the bare gauge coupling, g_0. These are the bare quark mass, m_0, and the boundary coefficient, z_f. The bare quark mass needs to be tuned to its critical value, m_c, in order to have a massless scheme. The tuning of the coefficient z_f to its critical value, z_f^c, is required in order to recover the correct boundary conditions in the continuum and thus, the right continuum limit. These arguments are equivalent to saying that the tuning of these coefficients is required in order to restore the symmetries of the continuum theory which are broken at finite lattice spacing by the regulator; the tuning of m_0 restores chiral symmetry and the tuning of z_f restores parity and flavor symmetries. Moreover, after the proper determination of m_c, z_f^c and the two boundary improvement coefficients to the action, c_t and d_s, bulk automatic $O(a)$-improvement is expected to hold. This means that without any improvement counterterm to the action in the bulk and to the interpolating fields, all physical quantities have leading $O(a^2)$ discretization effects. In practice, only a perturbative determination of the boundary improvement coefficients, c_t and d_s, is available. While c_t is known up to 2-loops (cf. Sec. 3.2.2 for a detailed explanation and references), thus reducing the boundary effects to $O(ag_0^6)$, the boundary effects coming from d_s are still of $O(ag_0^2)$, since only the tree-level value of d_s is known at present. Therefore, in this situation automatic improvement is expected to hold only up to boundary effects of at most $O(ag_0^2)$. It is then important for us to understand how large are these boundary effects coming from d_s and whether they compromise the $O(a^2)$ scaling behavior of physical observables, in their approach to the continuum limit. Scaling analysis of physical quantities will be performed in all following chapters. Here we are only concerned with the non-perturbative tuning of m_0 and z_f.

The critical mass, m_c, is linearly divergent with the inverse of the lattice spacing, when $a \to 0$. It is the coefficient of a relevant counterterm of dimension 3 in the bulk of the lattice and it enters the lattice action as follows,

$$\delta S_m = a^4 \sum_x \delta\mathcal{L}_m\,, \qquad \delta\mathcal{L}_m = m_c\,\overline{\chi}(x)\chi(x)\,. \tag{6.1}$$

z_f is a finite coefficient at the boundaries which enters the lattice action in the form,

$$\delta S_z = a^3 \sum_{\vec{x}} \delta\mathcal{L}_z\,, \qquad \delta\mathcal{L}_z = (z_f - 1)\left\{\overline{\chi}(x)\chi(x)|_{x_0=0} + \overline{\chi}(x)\chi(x)|_{x_0=T}\right\}. \tag{6.2}$$

d_s is the coefficient of an irrelevant boundary operator of dimension 4,

$$\delta S_d = a^3 \sum_{\vec{x}} \delta\mathcal{L}_d\,, \qquad \delta\mathcal{L}_d = (d_s - 1)\left\{\overline{\chi}(x)a\mathbf{D}_s\chi(x)|_{x_0=0} + \overline{\chi}(x)a\mathbf{D}_s\chi(x)|_{x_0=T}\right\}, \tag{6.3}$$

$$\mathbf{D}_s = \frac{1}{2}\,\gamma_k\,(\nabla_k^* + \nabla_k)\,. \tag{6.4}$$

Such kind of counterterm, Eq. (6.3), is inherent to SF formulations, chirally rotated or not, and it can not be avoided in any formulation of the SF on the lattice, independently on the lattice action adopted. For this kind of coefficients a perturbative determination is enough, in practice, in the cancellation of boundary $O(a)$ effects, as it has been argued for its equivalent in the standard formulation of the SF, the coefficient $\tilde{c}_t$ (cf. Sec. 3.2.2). Of the same kind is the aforementioned coefficient c_t, which is the coefficient of an irrelevant boundary counterterm to the lattice gauge action (cf. Sec. 3.2.2). Note that, in principle, we could also add the clover counterterm to the action, which is a dimension 5 operator in the bulk. However, since within the χSF scheme this term should only modify the $O(a^2)$ effects of $\gamma_5\tau^1$-even observables, the clover term is avoided in all our studies.

All these theoretical expectations is what we want to demonstrate in this thesis. For that purpose, before computing any physical observable the first thing to do is to setup the scheme; this means to tune all the parameters mentioned above to their critical values. At present, only the tree-level value of d_s is known in perturbation theory and it is the value used in all calculations in this thesis. For c_t, we employ the 2-loop value [85, 86], $c_t(g_0) = 1 - 0.089\, g_0^2 - 0.030\, g_0^4$. Here we are concerned with the non-perturbative tuning of the other two coefficients, m_0 and z_f. This is in principle not an easy task, since both of them enter the renormalization of the theory; they must be tuned simultaneously and in a non-perturbative manner. From now on, as it is usually done, all discussions will take place in terms of the inverse mass, κ, instead of m_0. The hopping parameter, κ, was introduced earlier in Eq. (2.69) and it is recalled here for a better readability,

$$\kappa = \frac{1}{8 + 2am_0}\,. \tag{6.5}$$

Due to the potential complications which may arise in the tuning procedure we first performed some studies at tree-level of perturbation theory. In particular, we tested several tuning strategies. The preferred one, as it emerged from our tree-level investigation, was applied in the interacting theory at the non-perturbative level [93]. Besides the particular selection of the tuning strategy also a tuning condition has to be chosen. The tuning condition is not unique. Different definitions are expected to give rise to critical values of the parameters which differ amongst themselves by discretization effects. In particular, in order to see the variations in z_f^c when changing the tuning condition we have used here several $\gamma_5\tau^1$-odd quantities in the determination of z_f^c. We will show that, as expected, various definitions of z_f^c lead to values of z_f^c which differ from each other by $O(a)$ cutoff effects.

Scaling tests and checks of universality of the continuum limit, using the χSF scheme, are presented in following chapters. Here we constrain the discussion to only the tuning of κ and z_f, since this subject is already rather technic. In Sec. 6.1, we summarize the requirements needed to tune κ and z_f and we define all different tuning conditions which have been used in this thesis. In Sec. 6.2, we explain the strategy of the combined tuning. Here, only a particular choice of tuning condition for z_f is used. Later in Sec. 6.3 we show the results of the tuning for all different tuning conditions employed. We discuss the results and draw our conclusions in Sec. 6.4

6.1. Tuning conditions

The non-perturbative determination of κ_c and z_f^c requires imposing conditions at finite lattice spacing that ensure the restoration of the expected symmetries in the continuum limit: twisted parity and twisted flavor symmetries (cf. App. B.1.3-B.2.2) which, at finite lattice spacing are broken by the Wilson term. Moreover, these conditions should be imposed at each lattice spacing while fixing a suitable renormalized quantity. In this work, we keep the renormalized SF

T/L	d_s	p_1	p_2	p_3	θ_A	θ_B	$\overline{x}_0$	$\overline{y}_0$
1	0.5	0.0	0.0	0.0	0.0	0.5	T/2	3T/4

Table 6.1.: Fixed parameters during the tuning.

coupling, $\overline{g}$, fixed. This is equivalent to fixing the physical size of the box, L. Since all physical quantities scale with the renormalization scale, L, fixing L ensures that all physical quantities remain fixed, as well. In particular here, we choose $T = L$. Also other parameters are held fixed during all our calculations in this thesis. These are d_s, which is set to its tree-level value, $d_s^{(0)}$, and the spatial momenta, $\vec{p}$, which are set to zero. In the spatial directions, periodic boundary conditions up to a phase are assumed, whose phase dependence is parametrized by the angles $\vec{\theta} = (\theta_1, \theta_2, \theta_3)$. During the tuning procedure, these angles are used in order to define unlike tuning conditions. To be concrete, we choose the symmetric case, $\theta_k = \theta$ $(k = 1, 2, 3)$ and two values of θ are used, $\theta_A = 0$ and $\theta_B = 0.5$. The choices of fixed parameters are summarized in Tab. 6.1.

Before specifying the tuning conditions, we define the correlation functions which are needed within our tuning procedure. In particular, we will employ boundary to bulk correlation functions which, moreover, only involve the boundary at $x_0 = 0$. For this purpose, the first thing we need is to define the boundary operators. Given the boundary quark fields at $x_0 = 0$,

$$\zeta(\vec{x}) = U_0(0, \vec{x})\chi(a, \vec{x}) \qquad \overline{\zeta}(\vec{x}) = \overline{\chi}(a, \vec{x})U_0(0, \vec{x})^\dagger \,, \tag{6.6}$$

we define, generically, the boundary interpolating fields at $x_0 = 0$ as

$$\widetilde{\mathcal{O}}^a_\pm = a^6 \sum_{\vec{y},\vec{z}} \overline{\zeta}(\vec{y})\Gamma_{\widetilde{\mathrm{O}}}\widetilde{Q}_\pm\zeta(\vec{z}) \,. \tag{6.7}$$

In this expression, $\widetilde{Q}_\pm$ are the χSF projectors defined in previous chapters. $\Gamma_{\widetilde{\mathrm{O}}}$ contains the flavor and Dirac structure of an operator of type $\widetilde{O}$ which, in our particular cases, correspond to a pseudo-scalar density and an axial-vector current,

$$\widetilde{\mathcal{P}}^a_\pm = a^6 \sum_{\vec{y},\vec{z}} \overline{\zeta}(\vec{y})\gamma_5 \frac{\tau^a}{2}\widetilde{Q}_\pm\zeta(\vec{z}) \,, \tag{6.8a}$$

$$\widetilde{\mathcal{A}}^a_{\mu\pm} = a^6 \sum_{\vec{y},\vec{z}} \overline{\zeta}(\vec{y})\gamma_\mu\gamma_5 \frac{\tau^a}{2}\widetilde{Q}_\pm\zeta(\vec{z}) \,. \tag{6.8b}$$

At this point, there is a difference in the notation with respect to the SF formulation. In the SF, differently from our convention, the projectors are included in the definition of the boundary fields, $\zeta, \overline{\zeta}$, and do not appear explicitly in the definition of the boundary operators.

Considering the previous definitions of the boundary interpolating fields, we may introduce now our notation for the boundary to bulk correlation functions. Given a bulk operator, $X^a(x)$, the type of correlation functions that we consider here are the following,

$$g^{ab}_{\mathrm{X}_\pm}(x_0, \theta) = -\frac{a^3}{L^3}\sum_{\vec{x}} \langle X^a(x)\widetilde{\mathcal{P}}^b_\pm \rangle \,, \tag{6.9a}$$

$$\overline{g}^{ab}_{\mathrm{X}_\pm}(x_0, \theta) = -\frac{a^3}{L^3}\sum_{\vec{x}} \langle X^a(x)\widetilde{\mathcal{A}}^b_{\mu\pm} \rangle \,. \tag{6.9b}$$

For the tuning we used only the particular cases,

$$g^{ab}_{\mathrm{P}_\pm}(x_0,\theta) = -\frac{a^3}{L^3}\sum_{\vec{x}}\langle P^a(x)\widetilde{\mathcal{P}}^b_\pm\rangle\,, \tag{6.10a}$$

$$g^{ab}_{\mathrm{A}_{\mu\pm}}(x_0,\theta) = -\frac{a^3}{L^3}\sum_{\vec{x}}\langle A^a_\mu(x)\widetilde{\mathcal{P}}^b_\pm\rangle\,, \tag{6.10b}$$

$$\overline{g}^{ab}_{\mathrm{V}_{\mu\pm}}(x_0,\theta) = -\frac{a^3}{L^3}\sum_{\vec{x}}\langle V^a_\mu(x)\widetilde{\mathcal{A}}^b_{\mu\pm}\rangle\,. \tag{6.10c}$$

There is also a difference here with respect to the standard SF. While in the SF formulation these correlation functions are denoted f_{X}, they are denoted here g_{X}. The reason is that the g_{X} are correlators in the χ-basis, while the f_{X} refer to the standard basis. The superscripts, a, b, denote the flavor index. The subscripts X, of the form g_{X}, indicate the corresponding operator inserted in the bulk of the lattice. Three bulk operators are considered here; the pseudo-scalar density, $P^a(x)$, and the axial-vector and vector currents, $A^a_\mu(x)$, $V^a_\mu(x)$. In the previous expressions, the χSF projectors, $\widetilde{Q}_\pm$, are the responsible for the subscript $\pm$ in the correlation functions, depending on whether one or the other projector is chosen. Due to the particular χSF boundary conditions, cf. Eq. (4.11)-(4.12), all correlation functions defined through $\widetilde{Q}_+$ at $x_0 = 0$ should vanish in the continuum limit and, at finite lattice spacing, only up to cutoff effects [1]. Therefore, such kind of correlation functions will be used only later on to perform checks on the correct implementation of the boundary conditions. In order to impose the tuning conditions, only correlation functions defined through $\widetilde{Q}_-$ are considered. Note that here we only provide the definitions of the two-point functions. In order not to obscure the discussion of the tuning, we refer the reader to App. H for a detailed treatment of these correlation functions.

As last consideration before going into the details of the particular tuning conditions, we also need to define the correlation function,

$$G^{ab}_{\mathrm{A}_{\mu\pm}}(x_0,y_0;\theta,\theta') \equiv (g_{\mathrm{I}})^{ab}_{\mathrm{A}_{\mu\pm}}(x_0,\theta) - s(x_0,\theta)\,\frac{(g_{\mathrm{I}})^{ab}_{\mathrm{A}_{\mu\pm}}(y_0,\theta) - (g_{\mathrm{I}})^{ab}_{\mathrm{A}_{\mu\pm}}(y_0,\theta')}{s(y_0,\theta) - s(y_0,\theta')}\,. \tag{6.11}$$

The notation is the following. Let us consider the improved axial current,

$$(A_{\mathrm{I}})^a_\mu(x) = A^a_\mu(x) + a\,c_{\mathrm{A}}\,\widetilde{\partial}_\mu\,P^a(x)\,, \tag{6.12}$$

where the derivative on the lattice, $\widetilde{\partial}_\mu$, is defined to be the symmetric derivative,

$$\widetilde{\partial}_\mu \equiv \frac{1}{2}\,(\partial^*_\mu + \partial_\mu)\,, \tag{6.13}$$

with the definition of the partial derivatives on the lattice given in App. A.5.1. The correlation function $(g_{\mathrm{I}})^{ab}_{\mathrm{A}_{\mu\pm}}(x_0,\theta)$ is defined as

$$(g_{\mathrm{I}})^{ab}_{\mathrm{A}_{\mu\pm}}(x_0,\theta) = -\frac{a^3}{L^3}\sum_{\vec{x}}\langle (A_{\mathrm{I}})^a_\mu(x)\widetilde{\mathcal{P}}^b_\pm\rangle\,. \tag{6.14}$$

This is just the equivalent of Eq. (6.10b), where the expression of the improved axial current is used instead of the unimproved one. Eq. (6.14) may be rewritten in terms of Eq. (6.10a) and

[1] The same holds for $\widetilde{Q}_-$ at $x_0 = T$. However, we do not consider here such correlation functions.

Eq. (6.10b) as follows,

$$(g_{\mathrm{I}})^{ab}_{\mathrm{A}_{\mu\pm}}(x_0,\theta) = g^{ab}_{\mathrm{A}_{\mu\pm}}(x_0,\theta) + c_{\mathrm{A}}\, s(x_0,\theta)\,, \qquad s(x_0,\theta) \equiv a\,\widetilde{\partial}_\mu\, g^{ab}_{\mathrm{P}_\pm}(x_0,\theta)\,. \tag{6.15}$$

By substitution of Eq. (6.15) into Eq. (6.11), the last can be cast in a more explicit manner,

$$\begin{aligned} G^{ab}_{\mathrm{A}_{\mu\pm}}(x_0,y_0;\theta,\theta') = {} & g^{ab}_{\mathrm{A}_{\mu\pm}}(x_0,\theta) \\ & - [g^{ab}_{\mathrm{A}_{\mu\pm}}(y_0,\theta) - g^{ab}_{\mathrm{A}_{\mu\pm}}(y_0,\theta')]\, \frac{\widetilde{\partial}_\mu g^{ab}_{\mathrm{P}_\pm}(x_0,\theta)}{\widetilde{\partial}_\mu g^{ab}_{\mathrm{P}_\pm}(y_0,\theta) - \widetilde{\partial}_\mu g^{ab}_{\mathrm{P}_\pm}(y_0,\theta')}\,. \end{aligned} \tag{6.16}$$

This expression is independent on the improvement coefficient of the axial current, c_{A}, and it indicates that, $G^{ab}_{\mathrm{A}_{\mu\pm}}(x_0,y_0;\theta,\theta')$ is $g^{ab}_{\mathrm{A}_{\mu\pm}}(x_0,\theta)$ up to cutoff effects of leading $O(a)$. Therefore, this is just a modification of $g^{ab}_{\mathrm{A}_{\mu\pm}}(x_0,\theta)$ up to cutoff effects.

As already anticipated, imposing distinct symmetry restoration conditions would give rise to different values of κ_c and z_f^c due to cutoff effects. Therefore, it is important to study the sensitivity of κ and z_f to the particular definitions in order to better understand the intrinsic uncertainty in the determination of these counterterms. In fact, κ does not show any special behavior in the χSF setup with respect to other formulations with Wilson fermions. Thus, only one condition has been investigated for κ. On the contrary, as it will be shown later, there is a large sensitivity on the choice of the tuning condition used to determine z_f^c. Therefore, we have concentrated our efforts in the investigation of different tuning conditions for z_f, where we have studied seven different possibilities, which we denote from (1) to (7). Note that even if different tuning conditions have been used to define z_f^c, the tuning strategy is always the same (cf. Sec. 6.2).

To tune κ to its critical value we adopt the standard procedure of imposing a vanishing PCAC mass. To be concrete, it is defined here as,

$$m_{\mathrm{PCAC}} \equiv \frac{\widetilde{\partial}_0 g^{11}_{\mathrm{A}_{0-}}(\overline{x}_0,\theta_A)}{2g^{11}_{\mathrm{P}_-}(\overline{x}_0,\theta_A)}\,. \tag{6.17}$$

To tune z_f we require a $\gamma_5\tau^1$-odd correlation function to vanish. The correlation functions (from (1) to (7)) that we have used to tune z_f are the following,

$$(1) \equiv g_{\mathrm{A}_{0-}} \equiv g^{11}_{\mathrm{A}_{0-}}(\overline{x}_0,\theta_A)\,, \tag{6.18a}$$

$$(2) \equiv g'_{\mathrm{A}_{0-}} \equiv g^{11}_{\mathrm{A}_{0-}}(\overline{x}_0,\theta_B)\,, \tag{6.18b}$$

$$(3) \equiv g^{\mathrm{diff}}_{\mathrm{A}_{0-}} \equiv g_{\mathrm{A}_{0-}} - g'_{\mathrm{A}_{0-}}\,, \tag{6.18c}$$

$$(4) \equiv \overline{g}_{\mathrm{V}_{k-}} \equiv \frac{1}{3}\sum_{k=1}^{3} \overline{g}^{12}_{\mathrm{V}_{k-}}(\overline{x}_0,\theta_A)\,, \tag{6.18d}$$

$$(5) \equiv \overline{g}'_{\mathrm{V}_{k-}} \equiv \frac{1}{3}\sum_{k=1}^{3} \overline{g}^{12}_{\mathrm{V}_{k-}}(\overline{x}_0,\theta_B)\,, \tag{6.18e}$$

$$(6) \equiv \overline{g}^{\mathrm{diff}}_{\mathrm{V}_{k-}} \equiv \overline{g}_{\mathrm{V}_{k-}} - \overline{g}'_{\mathrm{V}_{k-}}\,, \tag{6.18f}$$

$$(7) \equiv G_{\mathrm{A}} \equiv G^{11}_{\mathrm{A}_{0-}}(\overline{x}_0,\overline{y}_0;\theta_A,\theta_B)\,. \tag{6.18g}$$

The values of the parameters used in the definitions Eq. (6.17) and Eq. (6.18) can by read off from Tab. 6.1. In all these conditions, the particular combinations of interpolating fields with their corresponding Dirac and flavor indices are chosen such that the resulting correlation function is non-vanishing by definition. That is, the correlation functions should not violate any symmetry

of the lattice theory. Moreover, they have to be chosen such as to violate chiral symmetry, in the case of the $m_{\rm PCAC}$, or $\gamma_5\tau^1$-symmetry, in case of the conditions (1)-(7). Eq. (6.17) and the conditions (1)-(6) are obtained directly from the definitions in Eq. (6.10) with the corresponding substitutions. The condition (7) is obtained from Eq. (6.11), also with the corresponding substitutions. The idea to use the correlation function as defined in Eq. (6.11) has its origin in [91], although the definition given there is slightly different from the one we have chosen and the purpose was also not the same. The reason for us to choose such a correlation function here is to have an additional condition for the tuning of z_f, since the purpose is to investigate several tuning conditions which differ amongst themselves by $O(a)$ effects. This allows to study the sensitivity of z_f on the choice of the tuning condition, but also to test the universality of the continuum limit.

In this work, as it is the usual choice in SF schemes, we have defined the correlation functions in the middle of the time-extent of the lattice, $x_0 = T/2$. The only exception here is the condition (7), which involves two time slices. There the choice is $x_0 = T/2$ and $y_0 = 3T/4$. The reason for all such choices is to keep as far away as possible from the boundaries, thus avoiding boundary effects, and, in case of (7), keeping the two time-slices as far as possible from each other, while still staying away from the boundaries. A last remark concerning our particular choices of tuning conditions is to be made here. In order to restore the symmetries of the theory, we impose the different symmetry-violating correlation functions to vanish at finite lattice spacing. In principle, a better choice would be to consider that the corresponding correlation function takes its tree-level value at non-zero lattice spacing. However, from our initial studies at tree-level of perturbation theory (cf. Chap. 7), we have seen that such effects are very small and they do not cause changes in our final results.

Amongst all these conditions for the tuning of z_f, we have done a separate analysis with a different set of parameters using only method (1) (see Tab. D.1, Tab. D.2 and Tab. D.3). This situation corresponds to the results presented in [93], where we first explained our tuning strategy at the non-perturbative level. This separate analysis has been useful to check the tuning procedure. Results obtained by this analysis are labelled here as obtained with method (1*). In order to render the explanation of the tuning strategy as clear as possible, we restrict ourselves in the next section, Sec. 6.2, to only the cases treated in [93]. Later, in Sec. 6.3, we explain extensively all our results for the different tuning conditions and physical situations.

6.2. Tuning strategy

In order to check the practicality of tuning κ and z_f non-perturbatively, we have performed the tuning at three values of the renormalization scale $\mu = 1/L$, corresponding to a hadronic ($\overline{g}^2$ fixed with $L = 1.436\, r_0$), an intermediate ($\overline{g}^2 = 2.4484$) and a perturbative ($\overline{g}^2 = 0.9944$) scale. The results at these three points are summarized in Tab. 6.2.

We now explain the procedure that we have used to perform the tuning. With this purpose, we show examples for the smallest lattice, $L/a = 8$, of our most difficult point which is the hadronic scale. The values of β used are given in Tab. 6.2 and are taken from [97]. The tuning is performed in several steps. First, we calculate $m_{\rm PCAC}$ and $g_{\rm A_{0-}}$ at four values of z_f, and for each value of z_f, we use four values of κ, thus giving 16 pairs of κ and z_f. This allows us to determine $g_{\rm A_{0-}}$ as a function of $m_{\rm PCAC}$ for each value of z_f, as illustrated in Fig. 6.1. For each value of z_f, we perform a linear interpolation of $g_{\rm A_{0-}}$ in terms of $m_{\rm PCAC}$ to the point $m_{\rm PCAC} = 0$. This determines the values of $g_{\rm A_{0-}}$ at $m_{\rm PCAC} = 0$, denoted $g^*_{\rm A_{0-}}$, for each of the four values of z_f, as shown in Fig. 6.2. These data are presented in Tab. D.11. The corresponding data for the intermediate and perturbative scales are collected in Tab. D.13 and Tab. D.15, respectively. We now interpolate these values of $g^*_{\rm A_{0-}}$ as a function of z_f to the point of vanishing $g^*_{\rm A_{0-}}$,

L/a	β	z_f^c (χSF)	κ_c (χSF)	κ_c (SF)
Tuning at a hadronic scale, $\mu \sim 300$MeV				
8	6.0219	1.8090 (32)	0.153530 (24)	0.153371 (10)
10	6.1628	1.7920 (30)	0.152134 (17)	0.152012 (7)
12	6.2885	1.7664 (51)	0.150815 (22)	0.150752 (10)
16	6.4956	1.7212 (83)	0.148945 (25)	0.148876 (13)
Tuning at an intermediate scale, $\mu \sim 1$GeV				
8	7.0197	1.5467 (15)	0.144501 (13)	0.144454 (7)
12	7.3551	1.5126 (23)	0.143113 (12)	0.143113 (6)
16	7.6101	1.4942 (37)	0.142112 (13)	0.142107 (6)
Tuning at a perturbative scale, $\mu \sim 30$GeV				
8	10.3000	1.29730 (67)	0.1354609 (54)	0.135457 (5)
12	10.6086	1.2954 (11)	0.1351758 (56)	0.135160 (4)
16	10.8910	1.2858 (15)	0.1348440 (61)	0.134849 (6)

Table 6.2.: Results from the tuning at a hadronic, intermediate and perturbative scale. We give the critical values, z_f^c and κ_c, calculated in this work for the χSF. These results have been obtained using method (1*) (see Tab. D.1, Tab. D.2 and Tab. D.3). For reference, we also give κ_c for the SF [73, 95, 96].

thus, giving us the critical value z_f^c. These data are presented in Tab. D.12. For the other two couplings, the data are shown in Tab. D.14 and Tab. D.16.

Next we determine κ_c. Using the same 16 pairs of κ and z_f, we calculate m_{PCAC} as a function of κ for each z_f. This is shown in Fig. 6.3. Note that m_{PCAC} has a very mild dependence on z_f, so the four curves at fixed z_f are nearly indistinguishable. Interpolating in κ to the point of vanishing PCAC mass, κ^*, we obtain the values of κ^* at each z_f. The corresponding data are summarized in Tab. D.11 and, for the other two scales, in Tab. D.13 and Tab. D.15. The resulting values of κ^* as a function of z_f are shown in Fig. 6.4. We now interpolate these results in z_f to the previously determined value of z_f^c, thus determining the value of κ_c. These results may be read off from Tab. D.12, Tab. D.14 and Tab. D.16 for the three scales, respectively.

A key observation of this work is the mild dependence of m_{PCAC} on z_f, at least in the region near κ_c and z_f^c. This can be easily seen in Fig. 6.3. The consequence of this is clear in Fig. 6.4: the determination of κ_c also has a weak dependence on z_f^c and the errors of both are relatively independent. If this behaviour persists with calculations including dynamical quark degrees of freedom, it could ease the numerical effort necessary to perform the tuning, thus reducing the number of required simulations.

6.3. Tuning results

With the strategy discussed in Sec. 6.2, we have performed the tuning of κ and z_f using m_{PCAC} in Eq. (6.17) and the conditions (1)-(7) defined in Eq. (6.18). The tuning has been performed for five fixed values of the renormalized gauge coupling, $\overline{g}(L)$, which correspond to five values of the physical energy scale, $1/L$. In particular, the physical scale ranges from the purely non-perturbative to the perturbative regime and 14 values of β have been considered within that range. For better clarity, the tuning points are summarized in Tab. 6.3. The notation in this table is the following. 'Scale' refers to the physical scale, namely, the fixed value of the renormalized gauge coupling. We have denoted the five scales as 'NP', 'I', 'P', '2P' and 'PP', from the hadronic to the most perturbative scale. NP corresponds to $L = 1.436\, r_0$, I to $\overline{g}^2 = 2.4484$ and P to $\overline{g}^2 = 0.9944$. For 2P and PP we have not determined the gauge coupling

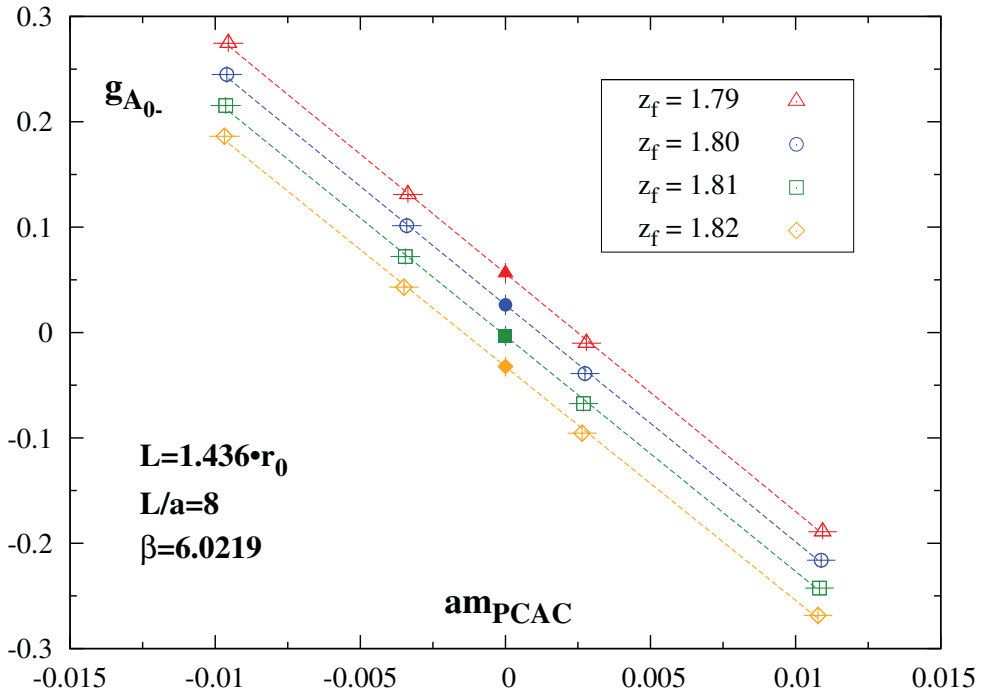

Figure 6.1.: $g_{\mathrm{A}_{0-}}$ vs. am_{PCAC} at four values of z_f (open symbols). All fits are linear in am_{PCAC}. The values of $g_{\mathrm{A}_{0-}}$ at $am_{\mathrm{PCAC}} = 0$, denoted $g^*_{\mathrm{A}_{0-}}$, are also plotted (filled symbols). See data in Tab. D.11.

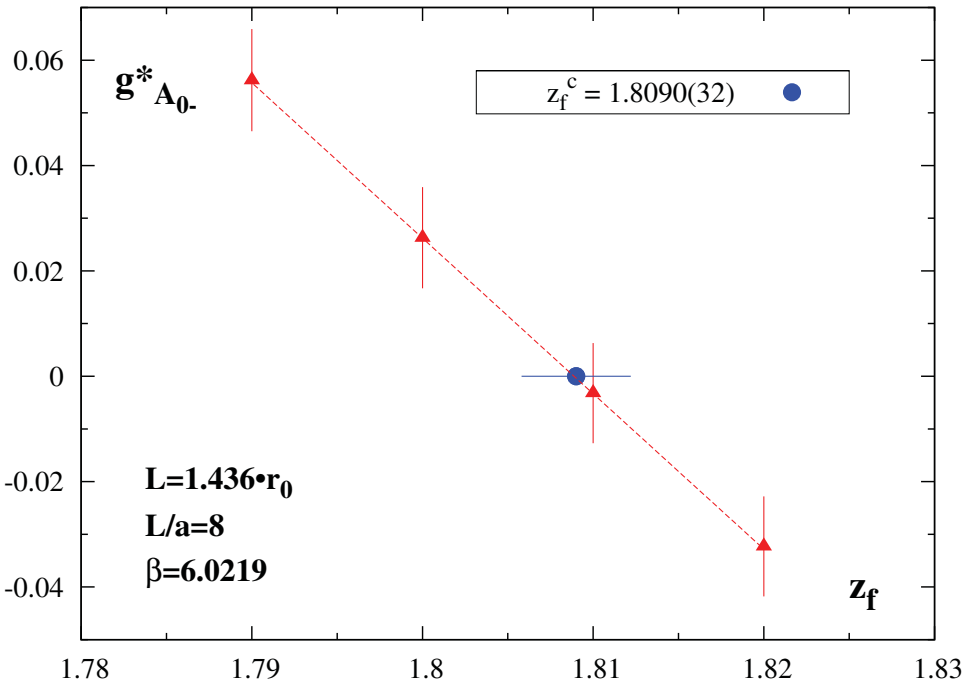

Figure 6.2.: $g^*_{\mathrm{A}_{0-}}$ vs. z_f (red). The fit is linear in z_f. The value of z_f^c, $z_f(g^*_{\mathrm{A}_{0-}} = 0)$, is also plotted (blue). See data in Tab. D.12.

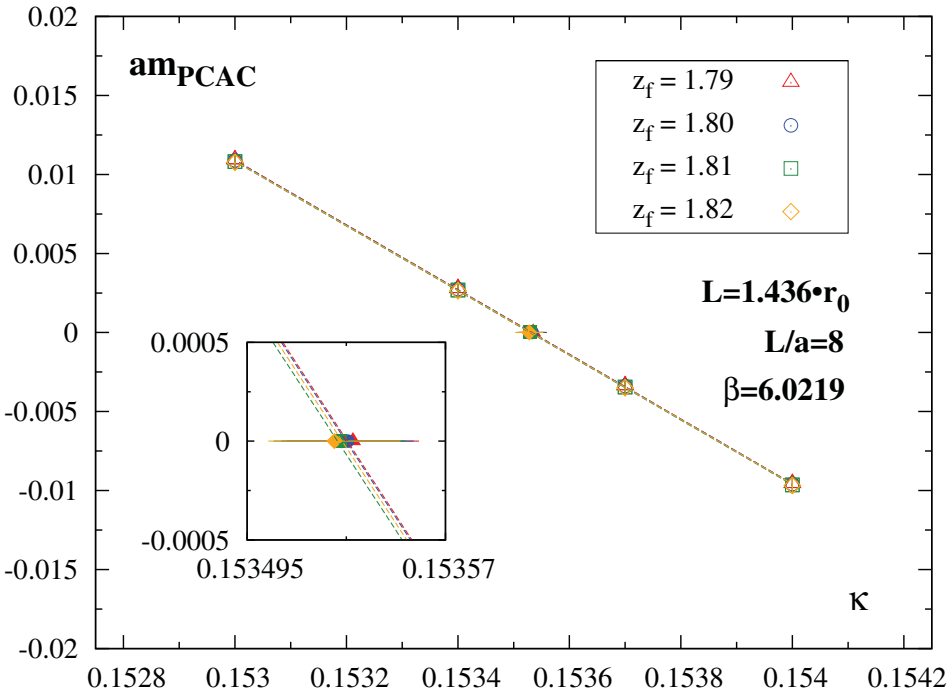

Figure 6.3.: am_{PCAC} vs. κ at four values of z_f (open symbols). All fits are linear in κ. The values of κ at $am_{\mathrm{PCAC}} = 0$, denoted κ^*, are also plotted (filled symbols). See data in Tab. D.11.

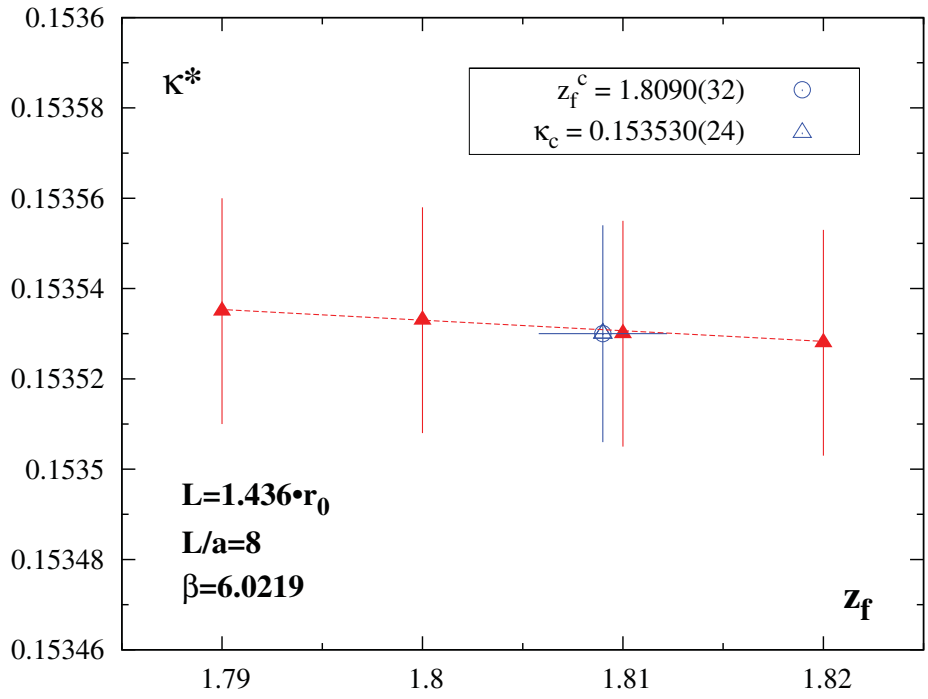

Figure 6.4.: κ^* vs. z_f (red). The fit is linear in z_f. The value of z_f^c (cf. Fig. 6.2) and of κ_c, defined as $\kappa^*(z_f = z_f^c)$, are also plotted (blue). See data in Tab. D.12.

Scale	L/a	β	Name	Results
$L = 1.436\, r_0$	8	6.0219	NP	Tab. D.6
	10	6.1628		
	12	6.2885		
	16	6.4956		
	20	6.6790		
	24	6.8187		
$\overline{g}^2 = 2.4484$	8	7.0197	I	Tab. D.7
	12	7.3551		
	16	7.6101		
$\overline{g}^2 = 0.9944$	8	10.3000	P	Tab. D.8
	12	10.6086		
	16	10.8910		
	16	12.0000	2P	Tab. D.9
	16	24.0000	PP	Tab. D.10

Table 6.3.: Summary of all the points where the tuning was performed. The references in the last column correspond to the tables where all results are presented.

explicitly. These two scales have been considered in order to study the dependence of z_f on g_0, for small values of g_0, thinking of a future perturbative determination of z_f, for which the knowledge of the renormalized coupling is not necessary. In the last column of the table, there are the references to the tables where the results, corresponding to each scale, are presented. Such tables are Tab. D.6-Tab. D.10. For a better comparison of all methods we added 2 summary tables, one for z_f^c and other for κ_c, which contain all the critical values obtained using all the tuning conditions. These are Tab. D.17 and Tab. D.18 for κ_c and z_f^c, respectively. We also present tables showing the values used as guess for z_f and κ, at each of the points where the tuning was performed. In these same tables, the column labelled '$N_{\rm conf}$' represents the number of configurations used in the computation of all observables at the corresponding point. These are Tab. D.1 to Tab. D.5.

During the tuning, we have used several combinations of the number of values of κ and z_f taken as a guess. As indicated in Sec. 6.2, the usual choice is to use 4 values of κ and 4 values of z_f. However, there are cases where we have used, instead, 5 values of z_f and/or 2 values of κ. In particular, we have used 2 values of κ at all the β values where we also performed the separate tuning using (1*). The reason is that, relying on the very weak dependence of κ and z_f on each other, as it was shown above in Fig. 6.3-Fig. 6.4, we expected the value of κ_c not to change appreciably even if z_f^c would vary visibly from one method to another. Therefore, we considered that the value of κ_c obtained using (1*) was already a very accurate guess on where the critical value of κ should be using all the other conditions. In fact, these expectations were later confirmed from our results of κ_c, which, from one method to another, are the same within statistical errors. Actually, in most cases κ_c did not change in any digit between any of the methods employed in the determination of z_f^c (cf. Tab. D.17). On the contrary, changes in z_f^c between the different methods are particularly manifest. This may be seen better in Tab. D.18. Here we can see how, in most cases, z_f^c does not agree within errors from one method to another. This behavior becomes stronger at lower energies, i.e. for decreasing values of β. Even if z_f^c does not agree from one method to another, the differences are expected to be only $O(a)$ discretization effects and, as such, should vanish in the continuum limit linearly in the lattice spacing. Our results confirm this expectation. In order to see this behavior, we have performed the continuum limit of differences in z_f^c, as determined from different methods, at the

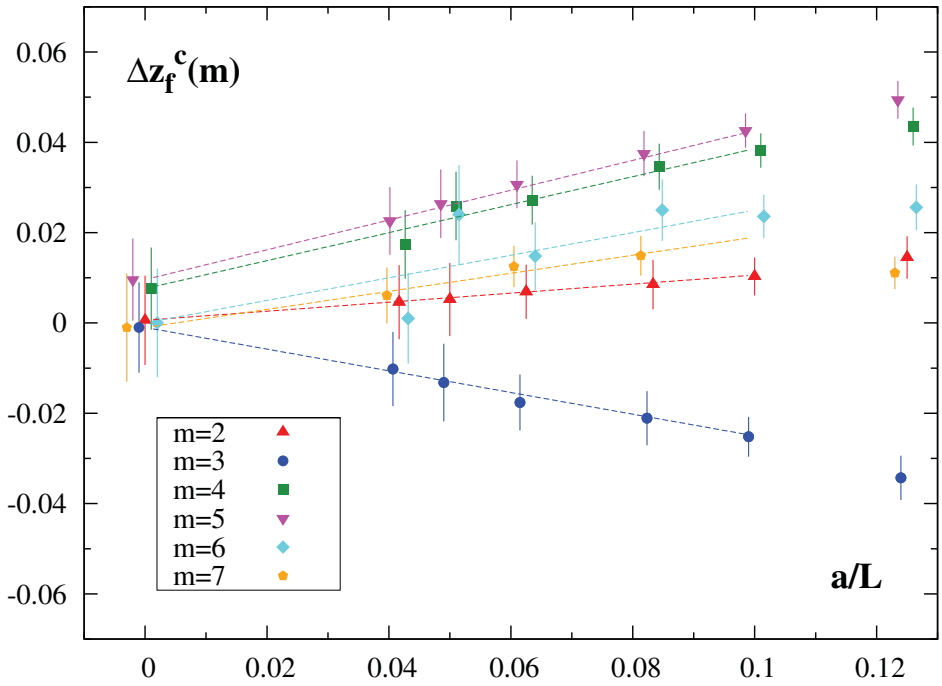

Figure 6.5.: Differences of z_f^c, $\Delta z_f^c(m)$, as determined from different methods (cf. Eq. (6.19)). The differences are always $z_f^c(1)$ minus $z_f^c(m)$, determined from any other method $m = 2 \ldots 7$. The data are presented in Tab. D.19. All extrapolations to the continuum limit are linear in a/L and the point $L/a = 8$ is excluded from all the fits. The results from the fits are presented in Tab. D.20. The points have been plotted slightly displaced from each other amongst the different methods.

lowest value of the renormalization scale. In particular, the data correspond to the differences

$$\Delta z_f^c(m) = z_f^c(1) - z_f^c(m)\,, \quad m = 2, 3, 4, 5, 6, 7\,. \tag{6.19}$$

That is, differences between method 1 and all other methods. The data for $\Delta z_f^c(m)$ are presented in Tab. D.19 for all the methods and the corresponding fits to the continuum limit are shown in Tab. D.20. We have performed linear fits in a/L and the point $L/a = 8$ has been excluded from all the fits. The data for $\Delta z_f^c(m)$, together with the extrapolation to the continuum limit are plotted in Fig. 6.5. From this analysis we can conclude that the differences in z_f^c from different methods are only cutoff effects of $O(a)$, as expected, which vanish in the continuum limit. This result may be considered as an additional test of the universality of the continuum limit. Since different choices of z_f^c give rise to different regularizations of the theory, an agreement in the continuum limit between the different definitions of z_f^c is another evidence of the universality of the continuum limit. Moreover, discrepancies of $O(a)$ between different values of z_f^c, should affect physical observables, at most, at $O(a^2)$. This expectation will be confirmed in the following chapter, where we analyze the dependence of several quantities on the particular tuning condition.

6.4. Conclusions on the tuning

We have presented the results of the non-perturbative tuning of κ and z_f for the χSF, at several physical scales and for a range of lattice spacings, using 7 different definitions of z_f^c. This demonstrates that the tuning of these two coefficients is indeed feasible, at least in the quenched approximation. Moreover, we observe that the tuning of z_f and κ are nearly independent. This observation is important, keeping in mind dynamical fermion simulations; if this behaviour persists with dynamical calculations, it may ease the numerical effort necessary to perform the tuning, thus reducing the number of required simulations. We have also shown that even if z_f^c differs from one method to another at finite values of the cutoff, such differences are only $O(a)$ discretization effects, as expected theoretically. These discrepancies vanish in the continuum limit, giving rise to another numerical evidence of the universality of the continuum limit.

Note that, even with non-improved Wilson fermions in the bulk, κ and z_f are the only parameters that must be non-perturbatively tuned within the χSF setup, in order to guarantee *bulk* automatic $O(a)$-improvement. This eliminates the need for the bulk counterterm to the action, $c_{\rm sw}$, and for the many operator improvement coefficients necessary in the SF. The *boundary* improvement coefficients, c_t and d_s, are still required in this formulation, as in any lattice regularization with SF-like boundary conditions. However, for the boundary improvement coefficients, a perturbative determination is expected to be enough in the cancellation of $O(a)$ discretization effects.

Our task in following chapters is, therefore, to perform tests on the continuum limit of this formulation, studying the universality of the continuum limit, and to check that bulk automatic $O(a)$-improvement holds, up to possible boundary discretization effects. The universality tests are performed by reproducing a variety of quantities already computed using the SF in its standard setup. To be concrete, we compute the renormalization constant of the pseudo-scalar density, $Z_{\rm P}$, and the continuum limit of its SSF, $\sigma_{\rm P}$, in Chap. 8. In Chap. 9, we present our determination of the RGI mass of the strange quark, $M_{\rm s}$ and in Chap. 10 we determine the continuum limit of the SSFs of the non-singlet twist-2 operators, O_{12} and O_{44}. We perform in the following chapter, Chap. 7, scaling studies of several correlation functions, as determined from values of z_f^c obtained using the seven tuning conditions discussed in the present chapter. These studies are relevant in the understanding on how the $O(a)$ uncertainties in the determination of z_f^c affect physical quantities, whose continuum limit should be independent on the particular definition of the critical parameters, z_f^c in this case. We also present in Chap. 7 tests of the χSF at tree-level of perturbation theory.

7. Scaling studies of the χSF

In this chapter we present scaling studies of several quantities in their approach to the continuum limit. We show results in the free theory and in the interacting case.

The tree-level results are presented in Sec. 7.1. In Sec. 7.1.1 we study the norm of the quark propagator, which is a quantity without a definite $\gamma_5\tau^1$-symmetry, that is, it is not even or odd under a $\gamma_5\tau^1$ transformation. Here, we also analyze the behavior of a $\gamma_5\tau^1$-even quantity, constructed as the norm of the propagator minus its hermitian conjugate. With these studies we demonstrate that both, the quark propagator and the $\gamma_5\tau^1$-even combination, are $O(a)$-improved in the massless free quark theory if the correct tree-level values of the parameters, $\kappa^{(0)} = 1/8$, $z_f^{(0)} = 1$ and $d_s^{(0)} = 1/2$, are chosen. We also show that both of them agree in the continuum limit with their corresponding continuum counterparts, which have been derived analytically. In Sec. 7.1.2 we perform checks of the dependence of the quark propagator on z_f, when z_f is varied away from its critical value at tree-level, $z_f^{(0)} = 1$. With this study we wanted to understand how an uncertainty in the tree-level value of z_f^c is reflected in the determination of physical quantities. The reason is that the tuning of z_f, at each value of the lattice spacing, has been performed by imposing a certain $\gamma_5\tau^1$-odd quantity to vanish (cf. Chap. 6), thus implying a restoration of $\gamma_5\tau^1$-symmetry in the continuum limit. This is so because in the massless continuum theory $\gamma_5\tau^1$ is a symmetry and therefore $\gamma_5\tau^1$-odd quantities should vanish exactly. However, at finite lattice spacing $\gamma_5\tau^1$-odd quantities vanish only up to discretization effects of $O(a)$. Therefore, in order to assure that z_f^c approaches exactly one in the limit $g_0 \to 0$, in principle, the tuning conditions should be imposed such that the corresponding $\gamma_5\tau^1$-odd quantity takes its tree-level value (instead of zero), at each value of the lattice spacing where the tuning is performed. Yet, we have found that imposing the $\gamma_5\tau^1$-odd quantities to take their value in the continuum (to vanish) does not change the scaling behavior of physical observables at tree-level and, moreover, it does not affect the critical values of z_f in the interacting theory.

The results in the interacting theory are presented in Sec. 7.2. Here, we study the approach towards the continuum limit of several correlation functions for different values of z_f^c, as determined from the methods (1) to (7) in Chap. 6. For these studies, we analyzed different types of correlation functions which we classify in three groups. The first kind, Sec. 7.2.1, corresponds to those observables which do not vanish in the continuum limit and are $\gamma_5\tau^1$-even, thus expected to be automatic $O(a)$-improved in the bulk of the lattice. These are e.g. $g^{11}_{\mathrm{P}_-}$, $g^{12}_{\mathrm{V}_{0-}}$ and g^{11}_{I}. The second case, Sec. 7.2.2, are the quantities which are $\gamma_5\tau^1$-even but do vanish in the continuum limit if the correct boundary conditions are recovered. Examples are $g^{11}_{\mathrm{P}_+}$ and $g^{12}_{\mathrm{V}_{0+}}$. The last type, Sec. 7.2.3, corresponds to the $\gamma_5\tau^1$-odd correlation functions. These are not improved and should vanish in the continuum limit up to $O(a)$ discretization effects. They are, for instance, $g^{11}_{\mathrm{A}_{0-}}$ and $\overline{g}^{12}_{\mathrm{V}_{k-}}$. With this analysis we demonstrate that physical observables are not affected by different choices in the definition of z_f^c. Moreover, we show that $\gamma_5\tau^1$-symmetry is restored in the continuum limit.

7.1. Scaling analysis in the free theory

We present here our results of the scaling analysis at tree-level of perturbation theory. We have chosen as an 'observable' the free quark propagator on the lattice, which we denote $S(x, y)$. In

the interacting theory the expectation value of the quark propagator vanishes because it is *non* gauge-invariant, thus, it is not an observable in itself. However, this is not so in the free case where the quark propagator is a suitable quantity to study.

In the evaluation of the quark propagator the main ingredient is the Dirac operator. On the lattice, the numerical inversion of the Dirac operator provides the quark propagator. We thus start recalling the expressions of the Dirac operator on the lattice with χSF boundaries, as introduced in previous chapters. At tree-level, the total Dirac operator is given as

$$a\mathcal{D}_{\mathrm{W}}^{\mathrm{total}}\,\chi(x) = \begin{cases} -P_-\chi(x+\vec{0}) + \left[K + \mathrm{i}\gamma_5\tau^3 P_- + (z_f-1) + (d_s-1)a\mathbf{D}_s\right]\chi(x) & x_0 = 0\,, \\ aD_{\mathrm{W}}\,\chi(x) & 0 < x_0 < T\,, \\ \left[K + \mathrm{i}\gamma_5\tau^3 P_+ + (z_f-1) + (d_s-1)a\mathbf{D}_s\right]\chi(x) - P_+\chi(x-\vec{0}) & x_0 = T\,, \end{cases} \tag{7.1}$$

where the gauge links have been set to one with respect to Eq. (5.2). This is the Dirac operator given as the sum of the original operator, Eq. (5.2), plus the counterterm operator, Eq. (5.75).

In our numerical evaluation of the quark propagator in the free theory we have first determined analytically the Dirac operator in the time-momentum representation and then numerically inverted this last expresion. In order to find the expression in the time-momentum representation, we perform a Fourier transform of the quark fields, only in the spatial directions, and act with $\mathcal{D}_{\mathrm{W}}^{\mathrm{total}}$ on the Fourier transformed field. In this case, the form of the Dirac operator is

$$a\widetilde{\mathcal{D}}_{\mathrm{W}}^{\mathrm{total}} = \begin{cases} -P_-\delta_{y_0,x_0+a} + \widetilde{K} + \left[\mathrm{i}\gamma_5\tau^3 P_- + (z_f-1) + a\,(d_s-1)\,\mathrm{i}\gamma_k\mathring{p}_k^+\right]\delta_{y_0,x_0} & x_0 = 0\,, \\ a\widetilde{D}_{\mathrm{W}} & 0 < x_0 < T\,, \\ \widetilde{K} + \left[\mathrm{i}\gamma_5\tau^3 P_+ + (z_f-1) + a\,(d_s-1)\,\mathrm{i}\gamma_k\mathring{p}_k^+\right]\delta_{y_0,x_0} - P_+\delta_{y_0,x_0-a} & x_0 = T\,. \end{cases} \tag{7.2}$$

$\widetilde{K}$ is the dimensionless time-diagonal kernel of the Wilson-Dirac operator in the time-momentum representation,

$$\widetilde{K} \equiv K(x_0,y_0;\vec{p}) = \left[\frac{1}{2\kappa} - \frac{1}{2}\sum_{k=1}^{3}\left\{(1-\gamma_k)\,e^{\mathrm{i}ap_k^+} + (1+\gamma_k)\,e^{-\mathrm{i}ap_k^+}\right\}\right]\delta_{y_0,x_0}\,, \tag{7.3}$$

which may equally be expressed as,

$$K(x_0,y_0;\vec{p}) = \left[\left(\frac{1}{2\kappa} - 3\right) + \frac{1}{2}\sum_{k=1}^{3}\left\{\gamma_k 2\mathrm{i}a\mathring{p}_k^+ + a^2\hat{p}_k^{+2}\right\}\right]\delta_{y_0,x_0}\,. \tag{7.4}$$

In terms of $K(x_0,y_0;\vec{p})$, the Wilson operator in the time-momentum representation takes the form,

$$a\widetilde{D}_{\mathrm{W}} \equiv aD_{\mathrm{W}}(x_0,y_0;\vec{p}) = -P_-\delta_{y_0,x_0+a} + K(x_0,y_0;\vec{p}) - P_+\delta_{y_0,x_0-a}\,. \tag{7.5}$$

The momentum p_μ^+ is defined in Eq. (5.19) while $\mathring{p}_\mu^+$ and $\hat{p}_\mu^+$ are given in Eq. (5.20). These equations are rewritten here for convenience,

$$p_\mu^\pm = p_\mu \pm \theta_\mu/L\,, \qquad \theta_0 = 0\,, \tag{7.6}$$

$$\mathring{p}_\mu^\pm = \frac{1}{a}\sin\left(ap_\mu^\pm\right)\,, \qquad \hat{p}_\mu^\pm = \frac{2}{a}\sin\left(\frac{ap_\mu^\pm}{2}\right)\,. \tag{7.7}$$

In the following tree-level tests the momenta $\vec{p}$ are always set to zero, $\vec{p} = (0,0,0)$, and all contribution to the spatial momenta $\vec{p}^{+}$ comes only from $\vec{\theta}$. Choosing different values of the parameters θ_k, we can probe the system in several manners. Here, we present results for three different choices: $\vec{\theta} = (1,1,1), (1,1,0), (1,0,0)$. Concerning the rest of the parameters, κ and d_s are set to their critical tree-level values, $\kappa^{(0)} = 1/8$ and $d_s^{(0)} = 1/2$. z_f will take its tree-level value, $z_f^{(0)} = 1$, in Sec. 7.1.1 but it will be set away from one in Sec. 7.1.2. In all calculations, $T = L$.

Note that no tuning is required at tree-level; the parameters just need to be set to their analytically known critical values. As discussed in Chap. 5, d_s has to be considered already at tree-level if boundary $O(a)$ effects are to be cancelled. This might look surprising because the massless free quark Schrödinger functional is $O(a)$-improved in the standard formulation [87]. In the χSF, d_s is needed at tree-level due to our particular choice of the orbifold construction, although this is not a problem; it only has to be kept in mind that d_s needs to be set to its correct value in the free case.

7.1.1. Continuum limit approach at $z_f = 1$

We discuss here our results of the scaling studies in the free theory, when the critical tree-level values of all the parameters are chosen. We study two quantities. One is the norm of the quark propagator, $||S(x_0, y_0; \vec{p}^{+})||$ (with an explicit definition of the norm $||\cdot||$ given below). It does not have a definite $\gamma_5\tau^1$-symmetry and therefore, it is a priori not expected to be automatic $O(a)$-improved. The other quantity is defined as the norm of the quark propagator minus its hermitian conjugate, $||(S - S^{\dagger})(x_0, y_0; \vec{p}^{+})||$, and it is $\gamma_5\tau^1$-even. Both quantities are expressed in the time-momentum representation and are evaluated at fixed time slices, x_0 and y_0, and at fixed values of $\vec{\theta}$. These observables are matrices with Dirac, flavor and time indices [1]. Since the time is fixed, the resulting matrix has only Dirac and flavor structure. In this case, the norm is defined as follows,

$$||S|| = \frac{1}{N}\sqrt{\sum_{i,j=0}^{N-1}\Big\{\mathrm{Re}(S_{ij})^2 + \mathrm{Im}(S_{ij})^2\Big\}} \qquad N = N_d N_f\,. \tag{7.8}$$

The aim of this study is, on the one hand, to show that the $O(a)$ cutoff effects are absent in $\gamma_5\tau^1$-even quantities and, on the other hand, to demonstrate the universality of the continuum limit at tree-level of perturbation theory. For that purpose we computed these two observables, $||S(x_0, y_0; \vec{p}^{+})||$ and $||(S - S^{\dagger})(x_0, y_0; \vec{p}^{+})||$, at several values of $\vec{\theta}$ and for different times slices. In order to perform the scaling analysis towards the continuum limit, for each physical situation, the quantities have been evaluated at several values of the lattice spacing ranging in $L/a = 4, 8, 16, 32, 64$. The results for $||S||$ are presented in Tab. E.1, Tab. E.3 and Tab. E.5, for the $\vec{\theta}$ values $(1,1,1)$, $(1,1,0)$ and $(1,0,0)$, respectively. The same holds for $||S - S^{\dagger}||$, but in Tab. E.2, Tab. E.4 and Tab. E.6. In all these tables, the expressions (aT, bT) denote the propagation points (x_0, y_0), with T the physical time-extent of the lattice which is chosen to be $T = L$.

From the data in the previous tables we have performed the continuum limit of both quantities, $||S||$ and $||S - S^{\dagger}||$. For both quantities, we have analyzed two different ways of approaching the continuum limit, depending on the fitting functions considered. In particular, we consider fits of the form

$$f_A = a_0 + a_1\Big(\frac{a}{L}\Big)^2 + a_2\Big(\frac{a}{L}\Big)^4 \tag{7.9}$$

[1] Note that at tree-level the Dirac operator is diagonal in color.

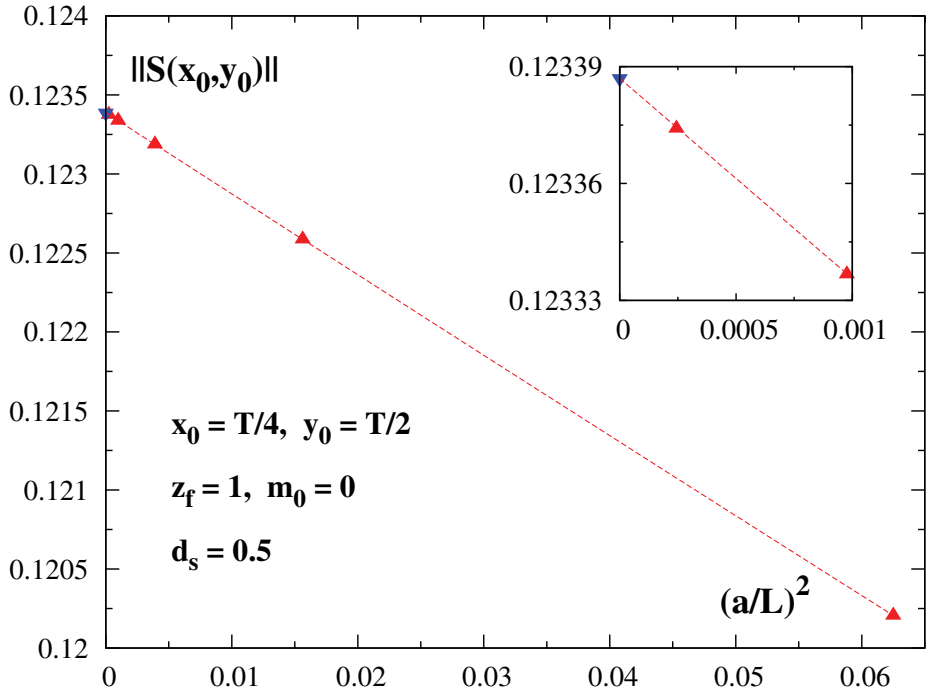

Figure 7.1.: Continuum limit of the norm of the quark propagator, $S(x_0, y_0)$, at fixed time slices $(x_0, y_0) = (T/4, T/2)$ and fixed $\vec{\theta} = (1, 0, 0)$. Fit: $y = a_0 + a_1\left(\frac{a}{L}\right)^2 + a_2\left(\frac{a}{L}\right)^4$ (cf. Tab. E.7). All parameters are set to their critical values at tree-level of perturbation theory. The blue point represents the value in the continuum limit, as obtained from the fit.

and

$$f_B = b_0 + b_1\left(\frac{a}{L}\right) + b_2\left(\frac{a}{L}\right)^2. \tag{7.10}$$

Since the behavior for different $\vec{\theta}$ values is similar in all cases, we present the continuum extrapolation results only for $\vec{\theta} = (1, 0, 0)$. Such results are summarized in Tab. E.7 and Tab. E.8 for $||S||$ and in Tab. E.9 and Tab. E.10 for $||S - S^\dagger||$. The data in Tab. E.5 and Tab. E.6, together with the results from the fits, Tab. E.7 and Tab. E.9, are plotted in Fig. 7.1 and Fig. 7.2, respectively, for the time slices $(x_0 = T/4, y_0 = T/2)$.

In all aforementioned tables we have added a row with the label 'cont'. The numbers in these rows correspond to the direct evaluation of the analytical expression of the quark propagator in the continuum, as obtained in Sec. 4.3.4. Thus, we can perform a direct comparison between the continuum limit values, obtained via the extrapolation of the lattice data, and the continuum values, obtained by evaluating the exact continuum expression of the corresponding quantity. We recall at this point that we have also evaluated the analytical expression of the quark propagator on the lattice, in the time-momentum representation, as derived in Sec. 5.1.1. These numbers agree in all digits with the ones obtained via the inversion of the lattice Dirac operator, which represents a cross-check of the results here presented.

From all these analysis we can conclude that both, the norm of S and the norm of $S - S^\dagger$

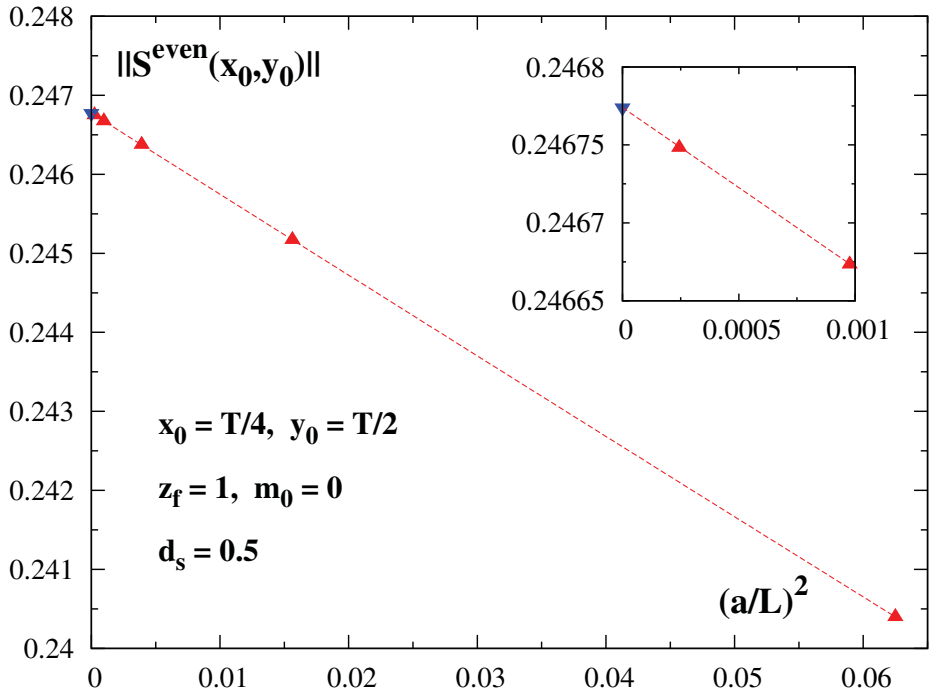

Figure 7.2.: Continuum limit of the norm of the even operator, $S^{\text{even}}(x_0, y_0) \equiv (S - S^\dagger)(x_0, y_0)$, at fixed time slices $(x_0, y_0) = (T/4, T/2)$ and fixed $\vec{\theta} = (1, 0, 0)$. Fit: $y = a_0 + a_1\left(\frac{a}{L}\right)^2 + a_2\left(\frac{a}{L}\right)^4$ (cf. Tab. E.9). All parameters are set to their critical values at tree-level of perturbation theory. The blue point represents the value in the continuum limit, as obtained from the fit.

are $O(a)$-improved in the free theory, for any choice of the kinematical parameters and for any given time slice. This can be seen from the small values taken by the coefficient of the $O(a)$, b_1, in Tab. E.8 and Tab. E.10. Moreover, from Tab. E.7 and Tab. E.9, we deduce that the $O(a^4)$ are small compared to the $O(a^2)$. We can then state that, if the critical values of κ, z_f and d_s are chosen at tree-level, not only $\gamma_5\tau^1$-even quantities are $O(a)$-improved but, in fact, the free quark χSF itself is $O(a)$-improved. Additionally, the continuum limit of each quantity agrees exactly with the corresponding value obtained from the analytical continuum expression. This can be seen in Tab. E.7, Tab. E.9 and also in Fig. 7.1, Fig. 7.2. Therefore, since the standard SF and the χSF are equivalent in the continuum (cf. Chap. 4), the universality of the continuum limit at tree-level is numerically corroborated, using the χSF scheme.

7.1.2. Continuum limit approach at z_f different from 1

In this section we analyze, at tree-level of perturbation theory, the situation when z_f is chosen to be different from one at tree-level[2].

Let us first recall the main concepts necessary in the discussion of our results. In the massless continuum theory with χSF boundary conditions, $\gamma_5\tau^1$ is a symmetry. This implies that all $\gamma_5\tau^1$-odd quantities vanish exactly. On the lattice with Wilson fermions, $\gamma_5\tau^1$-symmetry is broken by the Wilson term and, as a result, $\gamma_5\tau^1$ is not a symmetry of the lattice theory. In the present context this implies that, on the lattice, $\gamma_5\tau^1$-odd quantities, $g^{\rm odd}_{\rm latt}$, vanish only up to discretization effects. In addition, the lattice symmetries allow a dimension 3 boundary counterterm with coefficient z_f, whose tree-level value is $z_f^{(0)} = 1$. As discussed in detail in Chap. 6, beyond tree-level z_f requires to be non-perturbatively tuned to its critical value, z_f^c, at each value of the lattice spacing, in order to restore $\gamma_5\tau^1$-symmetry in the continuum limit. The definition of z_f^c given in Chap. 6 is to impose a $\gamma_5\tau^1$-symmetry violating correlation function to vanish, $g^{\rm odd}_{\rm latt} = 0$, for each value of L/a at which the tuning is performed. However, $g^{\rm odd}_{\rm latt}$ does not vanish at tree-level of perturbation theory on the lattice, even if $z_f^{(0)} = 1$. A priori, this implies that the previous definition of z_f^c would give rise to a value of $z_f^{(0)}$ different from one in the limit $g_0 \to 0$. In order to assure that $z_f^{(0)} = 1$ in the limit $g_0 \to 0$, the chosen tuning condition should be that the $\gamma_5\tau^1$-odd correlation function takes its correct value at tree-level, $g^{\rm odd}_{\rm latt} = (g^{\rm odd}_{\rm latt})^{(0)}$. Based on this discussion, we show in the following that the choice $g^{\rm odd}_{\rm latt} = 0$ is perfectly justified.

From the results of the non-perturbative tuning of z_f discussed in Chap. 6, we can see that only changes in $g^{\rm odd}_{\rm latt}$ of $O(10^{-2})$ or larger cause visible changes in the values of z_f. This may be seen, for instance, in Fig. 6.2 and Tab. D.12, from the values of the slope $dg^{\rm odd}_{\rm latt}/dz_f$. On the other hand, due to the tuning procedure that we first performed in the free theory, we have learned that $(g^{\rm odd}_{\rm latt})^{(0)} \sim O(10^{-5})$. These results mean that the tree-level values of $g^{\rm odd}_{\rm latt}$ are negligible in the interacting theory, with respect to changes in z_f, which automatically justifies the choice $g^{\rm odd}_{\rm latt} = 0$ in the definition of z_f^c.

As a second result of this section, we show in the following that variations of $O(10^{-5})$ in the tree-level values of the $\gamma_5\tau^1$-odd quantities do not affect the continuum limit of observables at tree-level and do not spoil automatic $O(a)$-improvement. From the initial tuning at tree-level, we know that changes of $O(10^{-5})$ in $(g^{\rm odd}_{\rm latt})^{(0)}$ correspond to changes in $z_f^{(0)}$ of $O(10^{-3})$. Therefore, we are particularly interested in seeing what happens to the observables for changes of z_f of $O(10^{-3})$. For that purpose we have analyzed the behavior of the quark propagator, $||S(x_0, y_0; \vec{p}^{+})||$, towards the continuum limit, as a function of z_f when z_f is chosen away from its critical tree-level value, while keeping all other parameters fixed. In particular, we show here

[2]The author thanks Rainer Sommer for suggesting this study.

results for $(x_0, y_0) = (T/4, T/2)$ and $\vec{\theta} = (1, 1, 1)$. These results are presented in Tab. E.11 and Tab. E.12. The difference between the two tables is the way the scan in z_f is performed.

Tab. E.12 corresponds to a finer scan in z_f with differences from the value $z_f = 1$ of at most $O(10^{-3})$. All data in this table have been fitted according to the curve,

$$f'_A = a_0 + a_1\Big(\frac{a}{L}\Big)^2 . \tag{7.11}$$

The results from the fits are also summarized in Tab. E.12. The data together with the fitting curves are plotted in Fig. 7.3. From this study we can conclude that an uncertainty in z_f of $O(10^{-3})$, at tree-level, does not modify the continuum limit of physical quantities and it does not spoil automatic $O(a)$-improvement.

Tab. E.11 corresponds to a wider range of values of z_f, differing from $z_f = 1$ even up to $O(10^{-1})$. For the data in this table we have performed two kinds of fits. A first fit of the type in Eq. (7.11) and a second fit of the form,

$$f'_B = b_0 + b_1\Big(\frac{a}{L}\Big) + b_2\Big(\frac{a}{L}\Big)^2 + b_3\Big(\frac{a}{L}\Big)^3 . \tag{7.12}$$

The results of the fits are presented in Tab. E.11. The data with the fitting curves are plotted in Fig. 7.4 for the fits of the type in Eq. (7.11) and in Fig. 7.5 for the fits of the type in Eq. (7.12). From these results we can conclude that, for changes in z_f larger than $O(10^{-2})$, $O(a)$ effects already become important and the continuum limit is compromised if these $O(a)$ effects are not taken into account.

The outcome of this study is the following. Either imposing tuning conditions by setting to zero the $\gamma_5\tau^1$-odd quantities used to define z_f^c, or setting such quantities to their correct tree-level values at finite lattice spacing, does not affect observables in the free theory and it does not influence the values of z_f^c in the interacting case. This result thus justifies our procedure for the tuning of z_f^c in Chap. 6.

7.2. Scaling analysis in the interacting theory

In the present section, we show our results of the scaling analysis of several correlation functions, which have been computed using the values of the critical parameters, κ_c and z_f^c, as determined from all the 7 conditions defined in Chap. 6. We have carried out these studies at all the β values at which the tuning has been performed. In Chap. 6 we have shown that different definitions of z_f^c lead to critical values of z_f which differ from each other by cutoff effects of $O(a)$. With the scaling study here presented, we demonstrate that these discrepancies in z_f^c do not influence the continuum limit value of physical observables. This is a very important result since the continuum limit should be independent on the particular definition of the critical parameters. Furthermore, we will show that all physically relevant quantities, when determined from the different values of z_f^c, agree within statistical errors already at finite lattice spacing, even at the coarsest lattices. This agreement holds even at the matching scale with the hadronic scheme, where cutoff effects are expected to be larger. Indeed, the agreement at non-zero lattice spacing indicates that the discretization effects are very small.

In order to analyze the different correlation functions we have classified them in three types. The first, Sec. 7.2.1, are those $\gamma_5\tau^1$-even correlation functions which have a non-vanishing continuum limit. These are the only quantities which have a physical meaning and, moreover, are expected to be automatic $O(a)$-improved (up to boundary effects), provided κ and z_f are correctly tuned to their critical values. The second kind, Sec. 7.2.2, are those $\gamma_5\tau^1$-even correlation functions which vanish in the continuum limit, because of the boundary conditions. The last

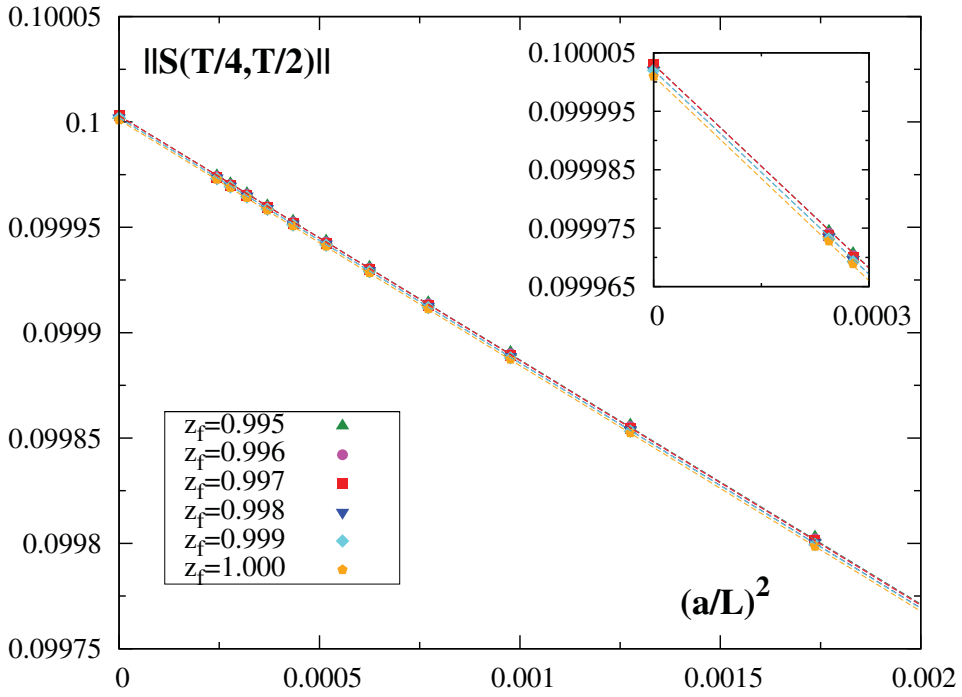

Figure 7.3.: Continuum limit of the norm of the quark propagator, $S(x_0, y_0)$, at fixed time slices $(x_0, y_0) = (T/4, T/2)$ and fixed $\vec{\theta} = (1, 1, 1)$. The parameters m_0 and d_s are set to their critical tree-level values, while several values of z_f are considered. The range in the values of z_f is $[0.995, 1.000]$. All fits are of the form: $y = a_0 + a_1\left(\frac{a}{L}\right)^2$ (cf. Tab. E.12).

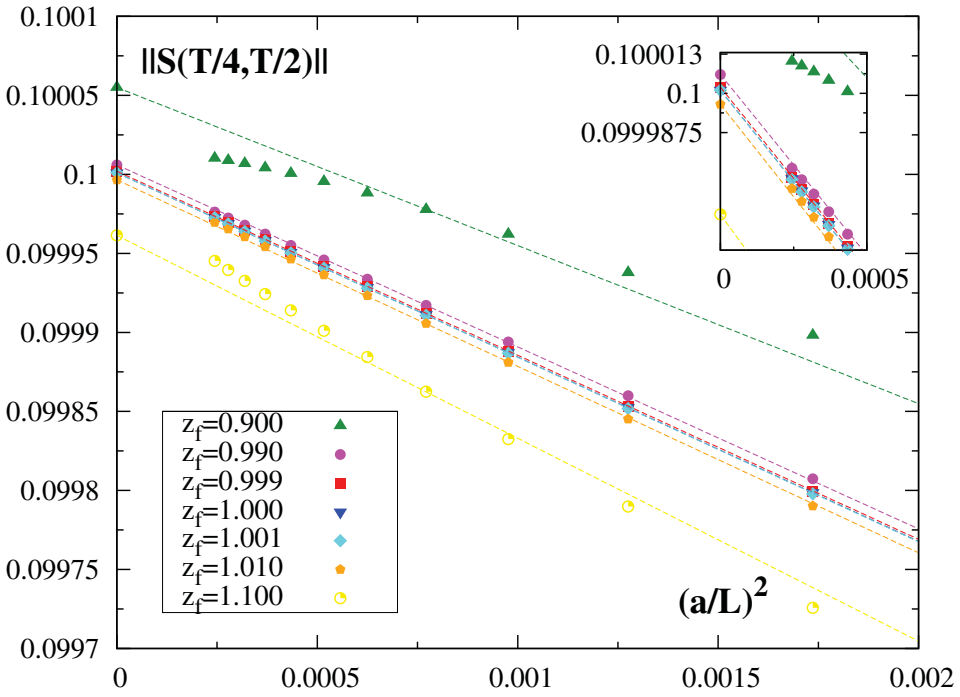

Figure 7.4.: Same caption as in Fig. 7.3, except that in the present plot the chosen range of z_f is wider than in Fig. 7.3. The range in the values of z_f is now $[0.900, 1.100]$. All fits are of the form: $y = a_0 + a_1 \left(\frac{a}{L}\right)^2$ (cf. Tab. E.11).

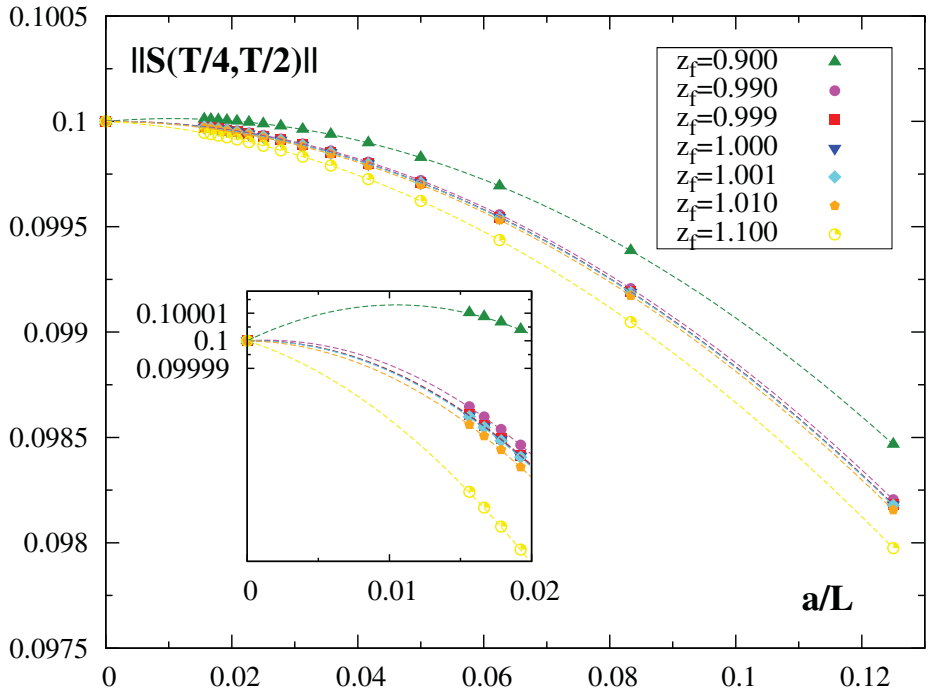

Figure 7.5.: Same caption as in Fig. 7.4, except that the fits performed in the present plot are of the form: $y = b_0 + b_1\left(\frac{a}{L}\right) + b_2\left(\frac{a}{L}\right)^2 + b_3\left(\frac{a}{L}\right)^3$ (cf. Tab. E.11).

type, Sec. 7.2.3, are $\gamma_5\tau^1$-odd quantities. They should vanish in the continuum limit up to $O(a)$ cutoff effects if $\gamma_5\tau^1$-symmetry is restored in the continuum limit.

These 3 kinds of correlation functions have been obtained from the definitions of the boundary to bulk correlation functions given in Eq. (6.10), which we recall here for convenience,

$$g^{ab}_{\mathrm{P}_\pm}(x_0,\theta) = -\frac{a^3}{L^3}\sum_{\vec{x}}\langle P^a(x)\widetilde{\mathcal{P}}^b_\pm\rangle\,, \tag{7.13a}$$

$$g^{ab}_{\mathrm{A}_{\mu\pm}}(x_0,\theta) = -\frac{a^3}{L^3}\sum_{\vec{x}}\langle A^a_\mu(x)\widetilde{\mathcal{P}}^b_\pm\rangle\,, \tag{7.13b}$$

$$\overline{g}^{ab}_{\mathrm{V}_{\mu\pm}}(x_0,\theta) = -\frac{a^3}{L^3}\sum_{\vec{x}}\langle V^a_\mu(x)\widetilde{\mathcal{A}}^b_{\mu\pm}\rangle\,. \tag{7.13c}$$

For unexplained notations in this section, the reader is referred to Sec. 6.1 of the previous chapter and to App. H, where the two-point functions are discussed in very much detail. With suitable combinations of the Dirac and flavor indices in Eq. (7.13), we can define correlation functions which are either even or odd under $\gamma_5\tau^1$ transformations. Moreover, all correlation functions with the + sign should vanish in the continuum limit because of the boundary conditions, independently on symmetry considerations. On the contrary, all those with the − sign are a priori different from zero, unless any symmetry requires them to vanish. These arguments imply that the physical correlation functions are those $\gamma_5\tau^1$-even with the − sign. The second type are the $\gamma_5\tau^1$-even with the + sign and the third type are the $\gamma_5\tau^1$-odd, amongst which we consider here only those with the − sign.

As discussed in Sec. 3.4, correlation functions boundary to bulk are normalized with certain boundary to boundary correlation functions in order to cancel the renormalization of the boundary quark fields. In particular in this work, only one such correlation function boundary to boundary is considered. It is the equivalent of f_1 [98] in the standard SF and it is defined as,

$$g_1^{ab}(\theta) = -\frac{1}{L^6}\,\langle\widetilde{\mathcal{P}'}^a_+\widetilde{\mathcal{P}}^b_-\rangle\,. \tag{7.14}$$

Note that the combination of signs in Eq. (7.14) is the only possibility for g_1^{ab} not to vanish in the continuum limit, according to the boundary conditions satisfied in the continuum.

In following sections we show the results obtained for these three types of correlation functions in several particular cases and draw the corresponding conclusions.

7.2.1. Non-vanishing $\gamma_5\tau^1$-even correlation functions

The $\gamma_5\tau^1$-even correlation functions, determined at the values of κ_c and z_f^c obtained from the tuning conditions (1) to (7), are collected in Tab. F.1-Tab. F.10. In Tab. F.1-Tab. F.5 we show results at $\vec{\theta} = (0,0,0)$. In Tab. F.6-Tab. F.10 results for $\vec{\theta} = (0.5,0.5,0.5)$ are collected. The observables that we present in these tables are $g^{11}_{\mathrm{P}_-}$, $g^{12}_{\mathrm{V}_{0-}}$ and g_1^{11}, according to the definitions given above in Eq. (7.13) and Eq. (7.14). In Tab. G.1-Tab. G.5 we show the corresponding results for the renormalization constant of the pseudo-scalar density, Z_{P}, computed only at $\vec{\theta} = (0.5,0.5,0.5)$. Concerning Z_{P}, its definition will be discussed in detail in the next chapter. Here, we just mention that it is a $\gamma_5\tau^1$-even quantity defined through $g^{11}_{\mathrm{P}_-}$ and g_1^{11}. The determination of all these quantities from the methods (1) to (7) has been performed via interpolations to κ_c and z_f^c [3]. On the contrary, for the observables computed from the method (1*) (cf. Tab. 6.2), new simulations were performed at κ_c and z_f^c, so no interpolations were needed. The data from

[3] The same holds for all quantities presented in this thesis only if the definitions (1) to (7) are considered.

(1*), computed at $\vec{\theta} = (0.5, 0.5, 0.5)$, are presented in Tab. F.6-Tab. F.8 for the correlation functions and in Tab. G.1-Tab. G.3 for $Z_{\rm P}$ [4].

From the data presented in all the previous tables we can conclude the following. At the 14 values of β that we have analyzed, all non-vanishing $\gamma_5\tau^1$-even quantities do not depend on the definition of z_f^c, within statistical errors. This holds for any of the values of the kinematical parameters that we have investigated. Examples at the matching scale, $L = 1.436\, r_0$, are shown in Fig. 7.6 for $g^{11}_{\rm P_-}$ at $\vec{\theta} = (0, 0, 0)$ and in Fig. 7.7 for $g^{12}_{\rm V_{0-}}$ at $\vec{\theta} = (0.5, 0.5, 0.5)$. Moreover, quantities obtained via an interpolation of the data do agree within errors with those obtained by means of new simulations performed at the critical values of κ and z_f. A consequence of the agreement between all the methods at each value of the lattice spacing is that the continuum limit of each of these quantities is the same independently on the particular definition of z_f^c, given a particular choice of the kinematical parameters. As expected, a quantity which is computed at two different values of $\vec{\theta}$, while keeping all other parameters fixed, does not lead to the same value at finite lattice spacing, neither in the continuum limit. Different values of $\vec{\theta}$ give rise to different renormalization conditions. Therefore, when performing universality tests of the continuum limit, comparing the χSF with respect to the SF, the observables to be compared must be computed at the same values of all kinematical variables; in particular, at the same values of $\vec{\theta}$.

The continuum limit approach of the $\gamma_5\tau^1$-even correlation functions is not addressed here. The reason is that these quantities need to be renormalized and thus, only the scaling analysis of the corresponding renormalized quantity is meaningful. We compute renormalized quantities and SSFs in following chapters. These are the observables that we will use to study the behavior towards the continuum limit.

7.2.2. Vanishing $\gamma_5\tau^1$-even correlation functions

We present here results for the $\gamma_5\tau^1$-even correlation functions which should vanish in the continuum limit. They do not vanish because of symmetry arguments. Instead, they vanish due to the particular form of the χSF boundary conditions, provided the correct boundary conditions are recovered in the continuum limit. The results are collected in Tab. F.1-Tab. F.10. We show results for $\vec{\theta} = (0, 0, 0)$ and $\vec{\theta} = (0.5, 0.5, 0.5)$ in Tab. F.1-Tab. F.5 and Tab. F.6-Tab. F.10, respectively. The cases we present here correspond to $g^{11}_{\rm P_+}$, $g^{12}_{\rm V_{0+}}$.

From these data we see that there is no agreement between the different methods at finite lattice spacing. Yet, this is not worrisome while there is agreement in the continuum limit. These are quantities that vanish in the continuum limit and take very small values already at finite lattice spacing. Therefore, the $O(a)$ uncertainties in z_f may lead to significant cutoff effects in these quantities. Nevertheless, we can see that towards the continuum limit the results from different methods approach each other. This is an indication that all methods may converge in the continuum limit. Indeed, there is a numerical evidence that $g^{11}_{\rm P_+}$ and $g^{12}_{\rm V_{0+}}$ decrease towards the continuum limit for all the methods, although, we have not yet found a pattern. In particular, it is not clear at the moment whether the scaling behavior towards the continuum limit may be affected by $O(a)$ effects, at least at the values of the lattice spacing at which we have performed our simulations. For that purpose we have studied these quantities as a function of $(a/L)^2$ and also as a function of a/L. This can be seen e.g. in Fig. 7.8 and Fig. 7.9 for $g^{11}_{\rm P_+}$ for $\vec{\theta} = (0, 0, 0)$ and $\vec{\theta} = (0.5, 0.5, 0.5)$, respectively, and in Fig. 7.10 and Fig. 7.11 for $g^{12}_{\rm V_{0+}}$. All these plots correspond to the matching scale, which is the value of the coupling at which the cutoff effects are stronger. As stated above, it is not clear at the moment how these quantities

[4] From method (1*) we have also determined the correlation functions and $Z_{\rm P}$ at $\vec{\theta} = (1, 0, 0)$. Only the data for $Z_{\rm P}$ will be discussed in this case, but this discussion is left to the next chapter.

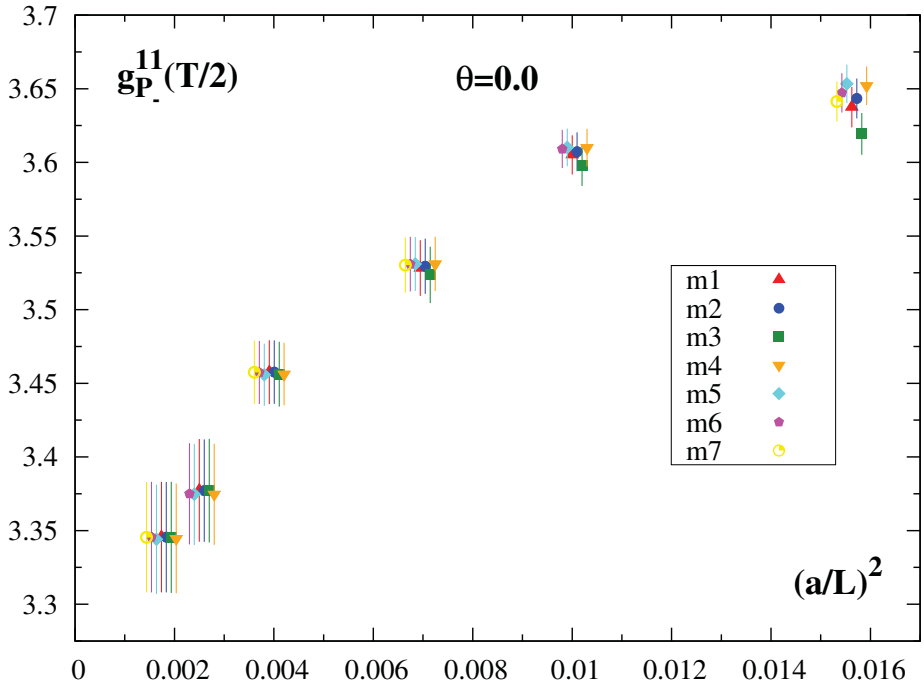

Figure 7.6.: Comparison between different tuning conditions using the $\gamma_5\tau^1$-even quantity $g^{11}_{\mathrm{P\_}}$. Scale NP and $\vec{\theta} = (0,0,0)$. Data for all methods (1) to (7) are presented (cf. Tab. F.1). No continuum limit is performed, since this quantity takes a finite value in the continuum limit only after renormalization. Instead, the purpose of the plot is to compare the results from the different tuning conditions at non-zero lattice spacing. The data from the different methods have been plotted slightly displaced from each other.

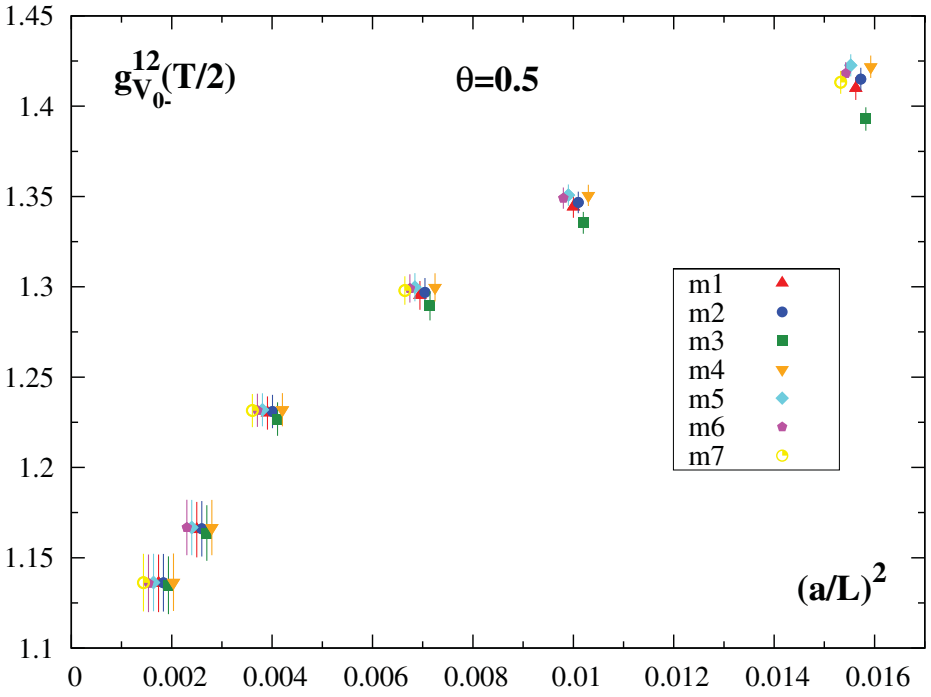

Figure 7.7.: Comparison between different tuning conditions using the $\gamma_5\tau^1$-even quantity $g^{12}_{\mathrm{V}_{0-}}$. Scale NP and $\vec{\theta} = (0.5, 0.5, 0.5)$. Data for all methods (1) to (7) are presented (cf. Tab. F.6). No continuum limit is performed, since this quantity takes a finite value in the continuum limit only after renormalization. Instead, the purpose of the plot is to compare the results from the different tuning conditions at non-zero lattice spacing. The data from the different methods have been plotted slightly displaced from each other.

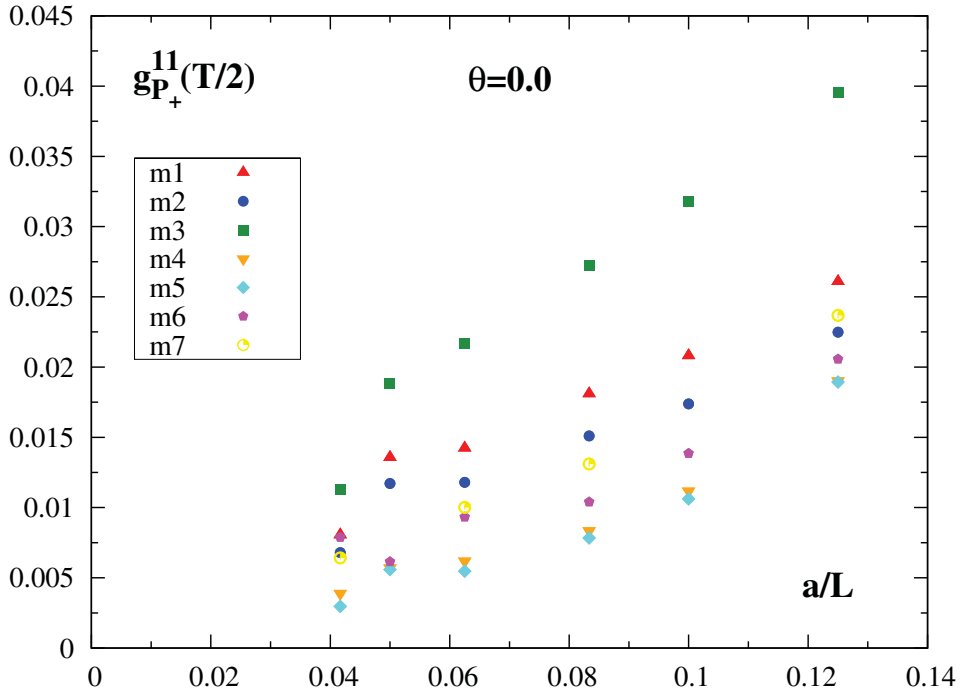

Figure 7.8.: Approach to the continuum limit of the $\gamma_5\tau^1$-even quantity $g^{11}_{\mathrm{P}_+}$. Scale NP and $\vec{\theta} = (0,0,0)$. Data for all methods (1) to (7) are presented (cf. Tab. F.1). $g^{11}_{\mathrm{P}_+}$ is plotted here as a function of a/L.

approach the continuum limit and further investigations are required, if possible, at values of the lattice spacing closer to the continuum limit. In this case, also a determination of d_s beyond the tree approximation would be very desirable, since it may be helpful to better understand how the continuum limit is approached.

7.2.3. Vanishing $\gamma_5\tau^1$-odd correlation functions

We treat here the case of $\gamma_5\tau^1$-odd correlation functions. Amongst all the $\gamma_5\tau^1$-odd correlation functions, we choose only those which do not vanish due to the boundary conditions but only because of symmetry considerations. Results are presented in Tab. F.11-Tab. F.20. In particular, we show the data for $g^{11}_{\mathrm{A}_{0-}}$ and $\overline{g}^{12}_{\mathrm{V}_{k-}}$, which are the quantities that have been used to define the tuning conditions. These quantities are also determined at $\vec{\theta} = (0,0,0)$ and $\vec{\theta} = (0.5,0.5,0.5)$ and the corresponding data are shown, respectively, in Tab. F.11-Tab. F.15 and Tab. F.16-Tab. F.20.

Although results from different definitions of z^c_f do not coincide at finite lattice spacing, all methods converge towards the continuum limit. As expected, the continuum limit is approached linearly in the lattice spacing, because $\gamma_5\tau^1$-odd quantities are not automatic $O(a)$-improved; quantities derived from all methods do converge to zero in the continuum limit with leading $O(a)$ discretization effects. This is a strong evidence that $\gamma_5\tau^1$-symmetry is restored in the continuum limit. We have plotted the continuum limit approach for $g^{11}_{\mathrm{A}_{0-}}$ in Fig. 7.12-Fig. 7.13

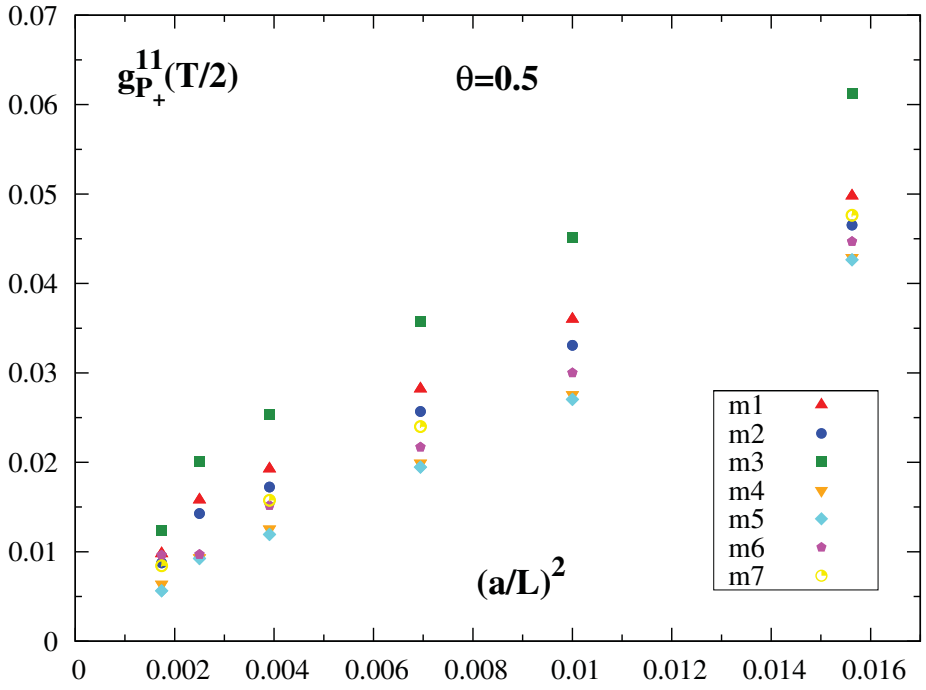

Figure 7.9.: Approach to the continuum limit of the $\gamma_5\tau^1$-even quantity $g^{11}_{\mathrm{P}_+}$. Scale NP and $\vec{\theta} = (0.5, 0.5, 0.5)$. Data for all methods (1) to (7) are presented (cf. Tab. F.6). $g^{11}_{\mathrm{P}_+}$ is plotted as a function of $(a/L)^2$.

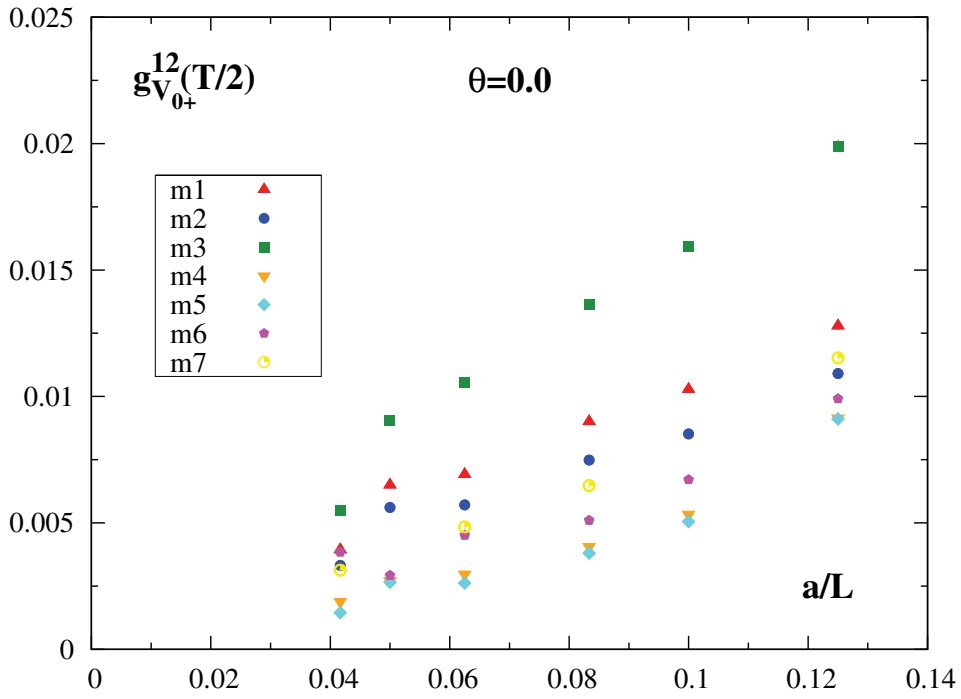

Figure 7.10.: Same caption as in Fig. 7.8, except that we plot in this case the $\gamma_5\tau^1$-even quantity $g^{12}_{V_{0+}}$.

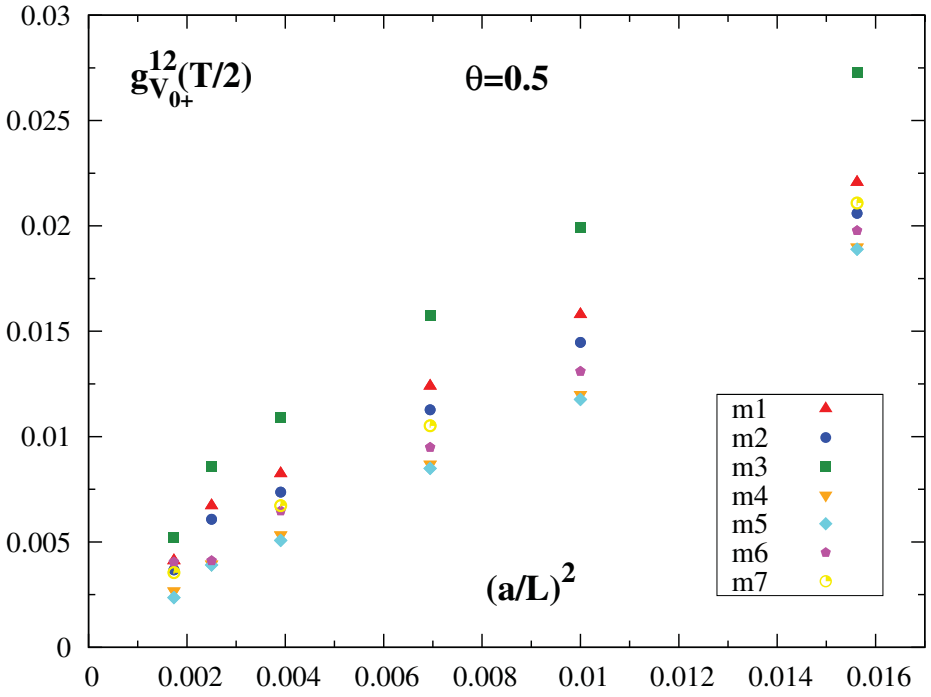

Figure 7.11.: Same caption as in Fig. 7.9, except that we plot in this case the $\gamma_5\tau^1$-even quantity $g^{12}_{\mathrm{V}_{0+}}$.

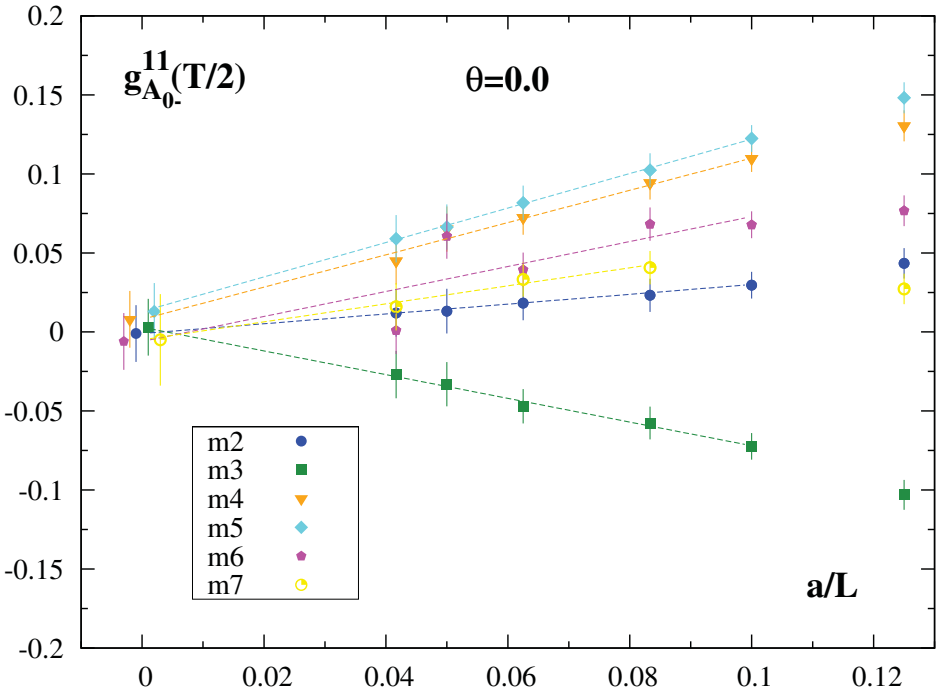

Figure 7.12.: Extrapolation to the continuum limit of the $\gamma_5\tau^1$-odd quantity $g^{11}_{\mathrm{A}_{0-}}$. Scale NP and $\vec{\theta} = (0,0,0)$. Data for methods (2) to (7) are presented (cf. Tab. F.11). The fits are all linear in a/L (cf. Tab. F.21). The point $L/a = 8$ has been excluded from all the fits. We show the data for all tuning conditions except condition (1) because it corresponds to imposing $g^{11}_{\mathrm{A}_{0-}} = 0$. The continuum limit values obtained from the different tuning conditions have been plotted slightly displaced from each other.

for $\vec{\theta} = (0,0,0)$ and $\vec{\theta} = (0.5,0.5,0.5)$, respectively and the same for $\overline{g}^{12}_{\mathrm{V}_{k-}}$ in Fig. 7.14-Fig. 7.15. These plots correspond to our most non-perturbative point, $L = 1.436\,r_0$, which is the case where the cutoff effects are stronger. The data shown in the previous plots have been fitted with a linear fit in a/L,

$$f = b_0 + b_1\Big(\frac{a}{L}\Big)\,. \tag{7.15}$$

We have not considered the point $L/a = 8$ in the fits. The results from the fits are summarized in Tab. F.21 for $g^{11}_{\mathrm{A}_{0-}}$ and in Tab. F.22 for $\overline{g}^{12}_{\mathrm{V}_{k-}}$.

7.3. Conclusions on the scaling analysis

From our studies of the χSF presented in this chapter we have derived several conclusions. The first one is that the massless free quark χSF is $O(a)$-improved provided the boundary coefficient, d_s, is set to its correct tree-level value. Moreover, the quantities computed within the χSF in the tree approximation take the expected values in the continuum limit; this is a numerical evidence of the universality of the continuum limit in the free theory, using the χSF scheme. With these tree-level studies, we have also shown that it is justified to impose tuning conditions,

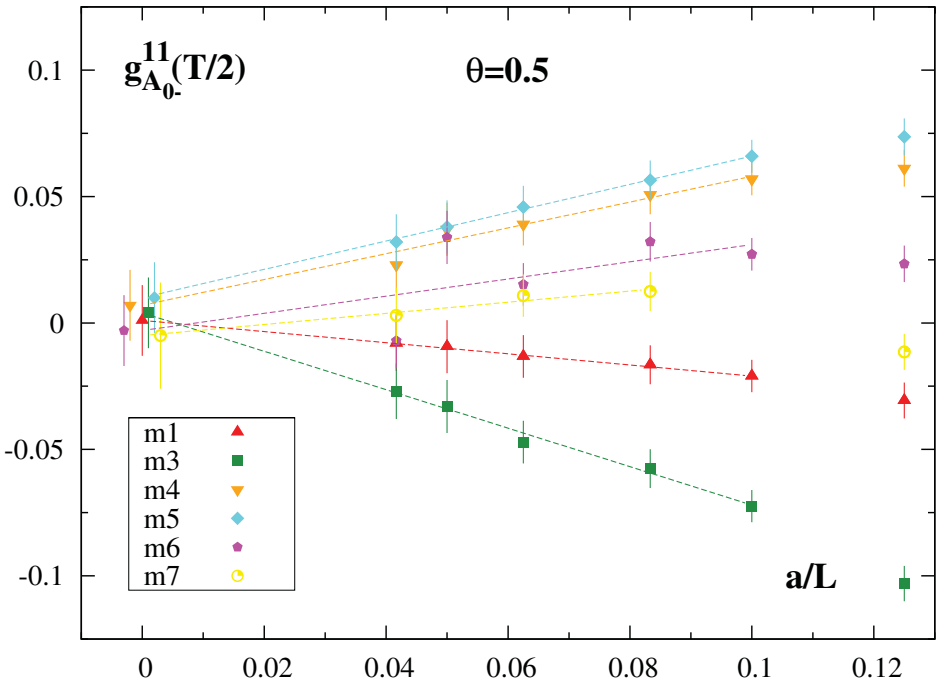

Figure 7.13.: Extrapolation to the continuum limit of the $\gamma_5\tau^1$-odd quantity $g^{11}_{\mathrm{A}_{0-}}$. Scale NP and $\vec{\theta} = (0.5, 0.5, 0.5)$. Data for methods (1) and (3) to (7) are presented (cf. Tab. F.16). The fits are all linear in a/L (cf. Tab. F.21). The point $L/a = 8$ has been excluded from all the fits. We show the data for all tuning conditions except condition (2) because it corresponds to imposing $g^{11}_{\mathrm{A}_{0-}} = 0$. The continuum limit values obtained from the different tuning conditions have been plotted slightly displaced from each other.

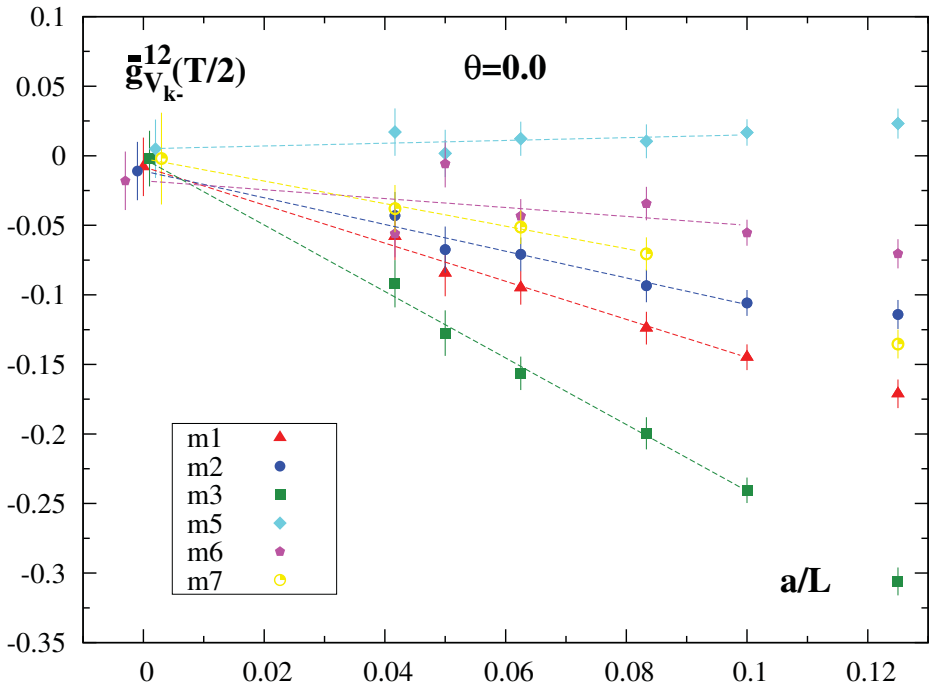

Figure 7.14.: Extrapolation to the continuum limit of the $\gamma_5\tau^1$-odd quantity $\overline{g}^{12}_{V_{k-}}$. Scale NP and $\vec{\theta} = (0,0,0)$. Data for methods (1) to (3) and (5) to (7) are presented (cf. Tab. F.11). The fits are all linear in a/L (cf. Tab. F.22). The point $L/a = 8$ has been excluded from all the fits. We show the data for all tuning conditions except condition (4) because it corresponds to imposing $\overline{g}^{12}_{V_{k-}} = 0$. The continuum limit values obtained from the different tuning conditions have been plotted slightly displaced from each other.

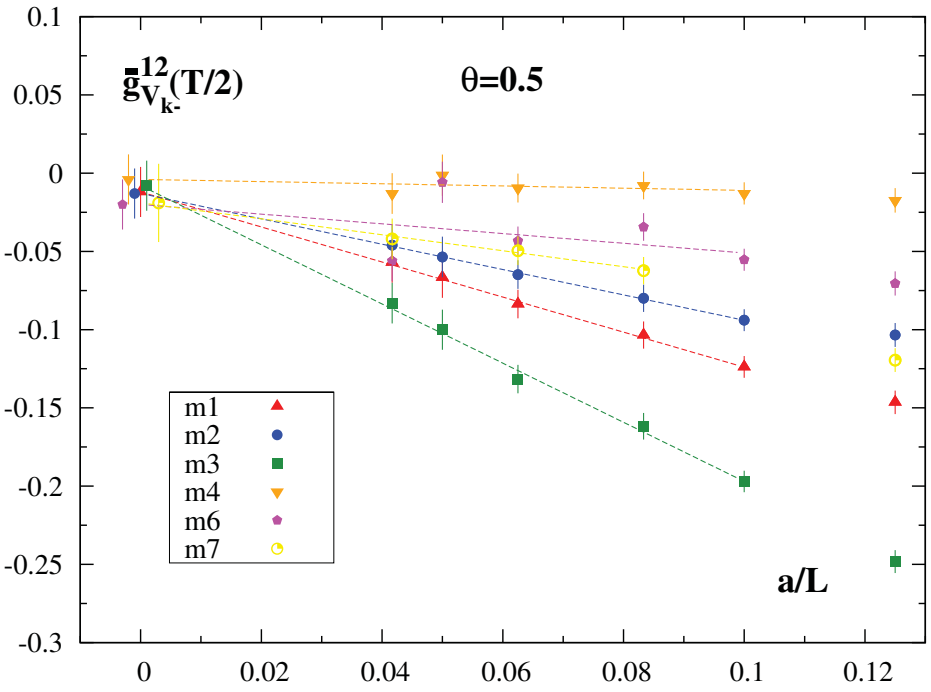

Figure 7.15.: Extrapolation to the continuum limit of the $\gamma_5\tau^1$-odd quantity $\overline{g}^{12}_{\mathrm{V}_{k-}}$. Scale NP and $\vec{\theta} = (0.5, 0.5, 0.5)$. Data for methods (1) to (4) and (6) to (7) are presented (cf. Tab. F.16). The fits are all linear in a/L (cf. Tab. F.22). The point $L/a = 8$ has been excluded from all the fits. We show the data for all tuning conditions except condition (5) because it corresponds to imposing $\overline{g}^{12}_{\mathrm{V}_{k-}} = 0$. The continuum limit values obtained from the different tuning conditions have been plotted slightly displaced from each other.

at each value of the lattice spacing, by assuming the $\gamma_5\tau^1$-odd correlation functions, used in the definition of z_f^c, to take their correct value in the continuum.

From the analysis in the interacting theory, we learned that all quantities which should vanish in the continuum limit, either by boundary conditions or symmetry arguments, have a very strong dependence on z_f^c. Concerning the quantities which vanish due to boundary conditions, we see that they decrease towards the continuum limit, independently on the chosen tuning condition, and, when computed from different values of z_f^c, the spread in the results tends to vanish in the continuum limit approach. Yet, we have not found how exactly the continuum limit is reached and further investigations are still required for these quantities. A vanishing value is a numerical evidence that, indeed, the correct boundary conditions are recovered in the continuum. At the moment, there is though little doubt that the correct boundary conditions are recovered. From the universality tests which are presented in following chapters, using the χSF formulation, we show that the χSF gives rise to the correct continuum limit, which is a strong hint that the correct boundary conditions are recovered in the continuum limit.

In the case of those correlation functions which vanish due to symmetry arguments, we have shown that they go to zero in the continuum limit with leading $O(a)$ discretization effects for all the tuning conditions, as expected. This is a numerical evidence of the restoration of $\gamma_5\tau^1$-symmetry in the continuum limit and the independence of the continuum limit values on the particular tuning condition. This result is another indication that the correct boundary conditions are recovered in the continuum limit.

All quantities with a finite continuum limit i.e. the only physically relevant quantities, do agree within statistical errors, from one method to tune z_f to another, already at non-zero lattice spacing, at any of the 14 values of β that we have considered. This result is very encouraging; although we can not make a general statement about all possible physical observables, our expectation is that other physical quantities, different from the ones studied in the course of this thesis, will behave in the same manner. These results are another indication of the universality of the continuum limit. In addition, the fact that the values agree already at non-zero lattice spacing, indicates that the discretization effects are rather small in physically relevant observables computed using the χSF formulation.

8. Computation of Z_{P} and σ_{P}

In the present and following chapters we check the continuum limit of the χSF renormalization scheme, through universality tests of the continuum limit. We have argued that both formulations, SF and χSF, are related by a change of basis in the continuum, at least on the classical level. Therefore, at the classical level both formulations are exactly equivalent, just expressed in a different basis. This equivalence is expected to hold at the quantum level in the continuum limit, independently on the chosen regularization scheme. This means that, given a certain value of the renormalization scale, $1/L$, and the kinematical variables, e.g. $\vec{\theta}$, a physical quantity computed using the χSF or the SF should take the same value in the continuum limit, independently on the regularization employed; *universality* should hold. Therefore, in order to test the universality of the continuum limit, we compute certain observables within the χSF formulation and perform the corresponding continuum limit. Once the continuum limit has been taken, we compare the continuum limit values to those of the same quantity obtained using the SF. As we will show in the present and following chapters, the results obtained from both formulations do agree in the continuum limit. We will show the agreement between the SF and the χSF for different observables and for several combinations of the values of the renormalization scale and the renormalization prescription. Such results are, therefore, a demonstration of the correctness of the continuum limit of the χSF renormalization scheme and, consequently, of its applicability in the determination of renormalization factors.

Good candidates to perform universality tests are the step scaling functions (SSFs) of scale-dependent observables. The SSF, σ_{O}, of a certain scale-dependent observable, $O(L)$, describes the behavior of $O(L)$ under changes in the value of the renormalization scale, $1/L$. The reason SSFs are good candidates to perform universality tests is that they are finite quantities which depend upon the renormalization scheme and the chosen renormalization prescription, but which do not depend on the particular regularization. At finite value of the cutoff, SSFs are still regularization-dependent yet, after the removal of the cutoff they should be independent on the regulator.

In this chapter we present our results in the computation of the SSF of the quark mass, using the χSF scheme, at two values of the renormalization scale, $1/L$. We compare our continuum limit results with the ones obtained using the SF with two different regularizations, standard and improved Wilson fermions. The chapter is structured as follows. In Sec. 8.1 we define the SSF of the quark mass, as derived from the RG equations. In Sec. 8.2 a renormalization prescription for the quark mass is given. Here we define the renormalization factor of the pseudo-scalar density, Z_{P}, and its SSF. The results for Z_{P} and the SSF on the lattice, Σ_{P}, are presented in Sec. 8.3. We show the continuum limit results for the SSF, σ_{P}, in Sec. 8.4. Here we also compare the obtained values to those using the SF formulation.

8.1. Step scaling function of the quark mass

Following the procedure indicated in Sec. 3.3.3 for the case of the gauge coupling constant, we define here the SSF of the quark mass and the corresponding RGI quark mass, using the RG equations. Variations of the renormalized quark mass, $\overline{m}(L)$, under changes in the renormaliza-

tion scale, $1/L$, are described by the coefficient $\tau(\overline{g}(L))$ of the RG equations as follows

$$L\,\frac{\partial\overline{m}(L)}{\partial L} = -\,\tau(\overline{g}(L))\,\overline{m}(L)\,. \tag{8.1}$$

This equation describes any of the quark flavors, due to the independence of the scheme on the mass. The integrated form of Eq. (8.1) reads as follows,

$$\overline{m}(sL) = \sigma_{\rm m}(s,\overline{g}^2(L))\,\overline{m}(L)\,, \qquad \sigma_{\rm m}(s,\overline{g}^2(L)) = \exp\left\{\int_{\overline{g}(L)}^{\overline{g}(sL)} dg\,\frac{\tau(g)}{\beta(g)}\right\}. \tag{8.2}$$

In this expression, β is the Callan-Symanzik β-function describing the changes in the gauge coupling, $\overline{g}(L)$, with the renormalization scale. It has been defined and discussed in Sec. 3.3.3. As the β-function, the τ-function is only known perturbatively. Its asymptotic expansion is given as,

$$\tau(\overline{g}) \overset{\overline{g}\to 0}{\sim} -\overline{g}^2 \sum_{n=0}^{\infty} d_n\,\overline{g}^{2n}\,. \tag{8.3}$$

The first coefficient in the expansion,

$$d_0 = \frac{8}{(4\pi)^2}\,, \tag{8.4}$$

is renormalization-scheme-independent while all other higher order coefficients are scheme-dependent.

The exact expression defining the RGI quark mass is

$$M = \overline{m}\,(2b_0\overline{g}^2)^{-d_0/(2b_0)}\exp\left\{-\int_0^{\overline{g}} {\rm d}g\,\left[\frac{\tau(g)}{\beta(g)} - \frac{d_0}{b_0 g}\right]\right\}. \tag{8.5}$$

The RGI quark mass is not only scale-independent but also scheme-independent. Therefore, using this relation with the corresponding β- and τ-functions and the running coupling and quark mass, the result given in one scheme or another should be exactly the same. This implies, for instance, that once M has been determined from a particular computation, the value of the running quark mass, $\overline{m}(L)$, can be obtained from that value of M in any desired renormalization scheme and at any value of the renormalization scale. In particular, this provides the standard procedure to transform lattice results to the $\overline{\rm MS}$-scheme.

We will come back to the issue of the RGI quark mass in Chap. 9. In the present chapter, we are concerned with the SSF of the quark mass, $\sigma_{\rm m}(s,\overline{g}^2(L))$, as defined above in Eq. (8.2). The SSF of the quark mass provides the evolution of the renormalized quark mass, $\overline{m}(L)$, from a value of the renormalization scale $1/L$ to the value $1/sL$, where s is a certain scale factor.

According to the discussion in Chap. 3, we are interested in the renormalization of the twisted quark mass. In Sec. 3.1 it was argued that a running twisted quark mass, $\overline{\mu}(L)$, may be defined through the PCVC relation. This implies that the twisted quark mass is renormalized multiplicatively through the inverse of the renormalization factor of the pseudo-scalar density, $Z_{\rm P}$, in the following way

$$\overline{\mu}(L) = Z_\mu(g_0,L)\,\mu(g_0)\,, \qquad Z_\mu(g_0,L) = Z_{\rm P}^{-1}(g_0,L)\,. \tag{8.6}$$

Therefore, the SSF of the quark mass, as defined in Eq. (8.2), is just the inverse SSF of the

pseudo-scalar density, $\sigma_{\rm P}(s,\overline{g}^2(L))$, which is defined as,

$$\sigma_{\rm P}(s,\overline{g}^2(L)) = \frac{Z_{\rm P}(g_0,sL)}{Z_{\rm P}(g_0,L)}\,. \tag{8.7}$$

Stated differently; if $\sigma_{\rm m}(s,\overline{g}^2(L))$ describes the evolution of the quark mass from a scale L to another scale L', then $\sigma_{\rm P}(s,\overline{g}^2(L))$ describes the corresponding evolution from L' to L. In the following, all discussion will take place in terms of only $Z_{\rm P}(g_0,L)$ and $\sigma_{\rm P}(s,\overline{g}^2(L))$.

The computation of the SSF of the pseudo-scalar density is performed in a similar way as in the case of the running coupling. Indeed, given any running observable, its SSF can always be defined through the renormalization group and numerically evaluated using the finite size techniques, as it has been explained in the case of the running gauge coupling in Chap. 3. A fact to be aware of is that, for the computation of the SSF of any observable, it is always needed the previous knowledge of the SSF of the gauge coupling. In this work, where the quenched setup is chosen and the gauge action is the SF gauge action given in Sec. 3.2.2, there is no need in recomputing the renormalized gauge coupling and its corresponding SSF. These are already known from previous publications [96] for a very wide range of energies. If a different gauge action and/or dynamical fermions are included, the gauge coupling would need to be recomputed within the new setup.

8.2. Renormalization prescription of the quark mass

We can now describe the chosen renormalization prescription for the quark mass. The definition and discussion of the SSF in the previous section was performed in the continuum theory. However, we have to consider that we use a lattice as a regulator and therefore, lattice artifacts must be taken into account. In this case, the renormalized twisted quark mass, $\overline{\mu}(L)$, is given as

$$\overline{\mu}(L) = \lim_{a\to 0} Z_{\rm P}^{-1}(g_0,L/a)\,\mu(g_0)\,, \tag{8.8}$$

with $\mu(g_0)$ the bare twisted quark mass and a the lattice spacing. The chosen renormalization condition for the pseudo-scalar density in the χSF scheme is the following,

$$Z_{\rm P}(g_0,L/a) = c(\theta,a/L)\,\frac{\sqrt{g_1(\theta)}}{g_{\rm P}(L/2,\theta)}\Big|_{m=0}\,. \tag{8.9}$$

In this expression, $m=0$ indicates that the renormalization condition is imposed at zero quark mass. In our case, Wilson fermions, this means at the critical value of the bare quark mass, $m_0 = m_c$, as determined from the tuning in Chap. 6. The factor $c(\theta,a/L)$ is chosen such that $Z_{\rm P}$ takes the correct value at tree-level, $Z_{\rm P}(0,L/a)=1$. Therefore it is defined as

$$c(\theta,a/L) \equiv \frac{g_{\rm P}(L/2,\theta)}{\sqrt{g_1(\theta)}}\Big|^{\rm tree}_{m_0=0}\,. \tag{8.10}$$

The two-point functions entering the definition of $Z_{\rm P}$ have already been discussed in Chap. 6 and Chap. 7 and a more detailed treatment can be found in App. H. They are recalled here for a better reading of the present section,

$$g_{\rm P}(x_0,\theta) \equiv g^{11}_{\rm P_-}(x_0,\theta) = -\frac{a^3}{L^3}\sum_{\vec{x}}\langle P^1(x)\widetilde{\mathcal{P}}^1_-\rangle \tag{8.11}$$

and

$$g_1(\theta) \equiv g_1^{11}(\theta) = -\frac{1}{L^6}\,\langle \widetilde{\mathcal{P}'}^1_+ \widetilde{\mathcal{P}}^1_- \rangle\,. \tag{8.12}$$

In order to determine the renormalization prescription completely, a value of θ has to be chosen. In particular, we consider here two cases, $\vec{\theta} = (0.5, 0.5, 0.5)$ and $\vec{\theta} = (1, 0, 0)$.

Given a fixed value of the renormalization scale, defined through $\overline{g}^2(L) = u$, and a fixed value of the lattice spacing, L/a, the lattice SSF of the quark mass, defined in the chiral limit, is given as

$$\Sigma_{\rm P}(s, u, a/L) = \frac{Z_{\rm P}(g_0, sL/a)}{Z_{\rm P}(g_0, L/a)}\Big|_{m=0,\,\overline{g}^2(L)=u}\,. \tag{8.13}$$

In the continuum limit, the SSF is finite and takes the value

$$\sigma_{\rm P}(s, u) = \lim_{a\to 0} \Sigma_{\rm P}(s, u, a/L) = \frac{\overline{\mu}(L)}{\overline{\mu}(sL)}\Big|_{\overline{g}^2(L)=u}\,, \tag{8.14}$$

with $\overline{\mu}(L)$ the renormalized running quark mass at a given scale $1/L$.

8.3. Computation of $Z_{\rm P}$ and $\Sigma_{\rm P}$

From the definition of the SSF, Eq. (8.13), it is understood that in order to compute the SSF at a certain value of the renormalization scale, $1/L$, the Z-factor needs to be evaluated both at L and sL, for a fixed value of the lattice spacing. In particular here we always use $s = 2$. This means that, for a fixed value of a (equivalently β), simulations have to be performed at a certain value of $L/a = N$ (single lattices) and also at $2L/a = 2N$ (double lattices). In such computations, the values of all parameters, e.g. κ_c and z_f^c, are the same at L and $2L$ for a fixed value of the lattice spacing, since such parameters only depend on the bare coupling and are, therefore, RG invariant. This is important because it implies that the tuning of the parameters only needs to be performed at the 'single' and hence smaller lattices. Otherwise, the tuning would turn out to be computationally very expensive.

We summarize the results for $Z_{\rm P}$ in Tab. 8.1, at $\vec{\theta} = (0.5, 0.5, 0.5)$ and $\vec{\theta} = (1, 0, 0)$. Results at three different values of the renormalization scale are presented; the hadronic scale $L = 1.436\, r_0$, the intermediate scale $\overline{g}^2 = 2.4484$ and the perturbative scale $\overline{g}^2 = 0.9944$. The computation of the SSF will take place at only the intermediate and the perturbative scales. At the hadronic (matching) scale we do not compute the SSF but instead, the renormalized quark mass as it will be discussed in the following chapter. All results presented in the present and following chapters have been obtained using the critical values of the parameters, κ_c and z_f^c, as determined from the tuning condition (1*) (cf. Chap. 6).

From the data in Tab. 8.1 we have computed the SSF on the lattice, for each lattice spacing at the intermediate and perturbative scales. The results are presented in Tab. 8.2 for $\vec{\theta} = (0.5, 0.5, 0.5)$ and Tab. 8.3 for $\vec{\theta} = (1, 0, 0)$. In Tab. 8.2 we also show the results obtained from the SF with improved and standard Wilson fermions as taken from [96]. These data are presented in columns 3 and 4 and denoted 'Clover' and 'Wilson', respectively.

8.4. Computation of $\sigma_{\rm P}$

In this section we present our results of the extrapolation to the continuum limit of the lattice SSF. The type of fit used to perform the continuum limit is linear in $(a/L)^2$ for the χSF and SF with $c_{\rm SW}$,

$$y = c_0 + c_1\Big(\frac{a}{L}\Big)^2 \tag{8.15}$$

		$\vec{\theta} = (0.5, 0.5, 0.5)$		$\vec{\theta} = (1, 0, 0)$	
L/a	β	$Z_{\mathrm{P}}(g_0, L/a)$	$Z_{\mathrm{P}}(g_0, 2L/a)$	$Z_{\mathrm{P}}(g_0, L/a)$	$Z_{\mathrm{P}}(g_0, 2L/a)$
Hadronic scale: $L = 1.436\, r_0$					
8	6.0219	0.5385 (12)		0.5432 (12)	
10	6.1628	0.5264 (12)		0.5310 (12)	
12	6.2885	0.5272 (16)		0.5321 (17)	
16	6.4956	0.5187 (22)		0.5245 (21)	
Intermediate scale: $\bar{g}^2 = 2.4484$					
8	7.0197	0.68509 (95)	0.6199 (14)	0.68850 (93)	0.6241 (13)
12	7.3551	0.6735 (13)	0.6082 (19)	0.6788 (12)	0.6142 (21)
16	7.6101	0.6672 (16)	0.5991 (22)	0.6737 (16)	0.6015 (22)
Perturbative scale: $\bar{g}^2 = 0.9944$					
8	10.3000	0.82689 (56)	0.80129 (84)	0.83007 (58)	0.80358 (84)
12	10.6086	0.81651 (88)	0.78549 (84)	0.81924 (82)	0.79008 (80)
16	10.8910	0.8110 (10)	0.7820 (14)	0.8136 (11)	0.7802 (15)

Table 8.1.: Renormalization factors of the pseudo-scalar density, Z_{P}, at $\vec{\theta} = (0.5, 0.5, 0.5)$ and $\vec{\theta} = (1, 0, 0)$. Results are shown for the χSF with standard Wilson fermions at three values of the renormalization scale and for several values of the lattice spacing.

$\Sigma_{\mathrm{P}}(2, u, a/L)$			
L/a	χSF	SF (Clover)	SF (Wilson)
Intermediate scale: $\bar{g}^2 = 2.4484$			
8	0.9048 (23)	0.8945 (23)	0.8993 (20)
12	0.9030 (33)	0.8908 (23)	0.8924 (30)
16	0.8980 (39)	0.8998 (25)	0.9036 (32)
Perturbative scale: $\bar{g}^2 = 0.9944$			
8	0.9690 (12)	0.9633 (14)	0.9641 (12)
12	0.9620 (15)	0.9599 (19)	0.9632 (17)
16	0.9643 (22)	0.9622 (20)	0.9652 (22)

Table 8.2.: SSF of the pseudo-scalar density at finite lattice spacing, $\Sigma_{\mathrm{P}}(2, u, a/L)$. Results are shown for the χSF with standard Wilson fermions and also for the SF with improved and standard Wilson fermions [96] at two values of the renormalization scale and for several values of the lattice spacing. $\vec{\theta} = (0.5, 0.5, 0.5)$.

$\Sigma_{\mathrm{P}}(2, u, a/L)$	
L/a	χSF
Intermediate scale: $\bar{g}^2 = 2.4484$	
8	0.9065 (23)
12	0.9048 (35)
16	0.8929 (39)
Perturbative scale: $\bar{g}^2 = 0.9944$	
8	0.9681 (12)
12	0.9644 (14)
16	0.9590 (23)

Table 8.3.: SSF of the pseudo-scalar density at finite lattice spacing, $\Sigma_{\mathrm{P}}(2, u, a/L)$. Results are shown for the χSF with standard Wilson fermions at two values of the renormalization scale and for several values of the lattice spacing. $\vec{\theta} = (1, 0, 0)$.

and it is linear in a/L for the SF with standard Wilson fermions,

$$\bar{y} = \bar{c}_0 + \bar{c}_1\Big(\frac{a}{L}\Big)\,. \tag{8.16}$$

The results of our fits are summarized in Tab. 8.4 for $\vec{\theta} = (0.5, 0.5, 0.5)$ and in Tab. 8.5 for $\vec{\theta} = (1, 0, 0)$. In both tables we show the results at the two values of the renormalization scale that have been considered, $\overline{g}^2 = 2.4484$ and $\overline{g}^2 = 0.9944$. For comparison, in Tab. 8.4 we also present the continuum limit results for the SF with improved and standard Wilson fermions. We have performed our own fits of the data obtained from the SF, since in [96] there are no tables with the final continuum limit values, where we could read the data from. Note the apparently big differences between the slope of the SF with Wilson fermions and the slopes of the two improved formulations, SF(Clover) and χSF (cf. Tab. 8.4). However, the slope for the Wilson case is not to be compared to those of the improved formulations, because different functions have been used to extrapolate the data to the continuum limit: linear fit in a/L for the SF(Wilson) and linear fit in $(a/L)^2$ for the SF(Clover) and χSF. A proper comparison may be performed e.g. from Fig. 8.1. Here we plot the data for $\Sigma_{\rm P}$ (cf. Tab. 8.2) as a function of a/L for the three formulations. The corresponding values in the continuum limit are also shown (cf. Tab. 8.4). From this figure it becomes clear that the slopes are consistent with zero in the three cases. In particular, the data from the three regularizations agree in the continuum limit at the two values of the renormalization scale. Moreover, at finite lattice spacing the data agree at $L/a = 16$ for the intermediate scale and at $L/a = 12, 16$ for the perturbative scale.

In Fig. 8.2 we show the extrapolation to the continuum limit of $\Sigma_{\rm P}$ as determined from the χSF, for the two values of $\vec{\theta}$ and the two values of $1/L$ that we have considered. The data are plotted as a function of $(a/L)^2$ and the corresponding values in the continuum limit, $\sigma_{\rm P}$, are also shown. The fitting curves are also plotted. Note that, although we show in this figure the χSF data for the two values of $\vec{\theta}$, employed in the definition of the renormalization prescription, the continuum limit values are not supposed to be compared. Different values of $\vec{\theta}$ give rise to different renormalization prescriptions and, as a consequence, the results are not expected to agree even in the continuum limit.

A similar plot is shown, Fig. 8.3, where we present the results of the extrapolation to the continuum limit for the χSF and the improved SF, for comparison. Results are shown at the two values of the renormalization scale and for $\vec{\theta} = (0.5, 0.5, 0.5)$. Since the same renormalization prescription is chosen in both formulations, the continuum limit values should agree, between the SF and the χSF. As shown in the plot, this is indeed the case. Note that the slopes for the two formulations have similar absolute values but opposite signs. This allows to perform a constraint fit to the continuum limit reducing the errors in the final results.

From all results presented here, we can conclude that the continuum limit of the SSF of the quark mass determined from the χSF, agrees with the corresponding value obtained using the standard formulation of the SF, with and without improvement. Furthermore, we observe that the results already agree at finite lattice spacing, at $L/a = 16$ for $\overline{g}^2 = 2.4484$ and at $L/a = 12, 16$ for $\overline{g}^2 = 0.9944$. These results are therefore a successful test of the universality of the continuum limit. Moreover, the approach to the continuum limit is consistent with leading $O(a^2)$ discretization effects in the χSF formulation. This result shows that the χSF is compatible with bulk automatic $O(a)$-improvement.

	χSF	SF (Clover)	SF (Wilson)
Intermediate scale: $\overline{g}^2 = 2.4484$			
$\sigma_{\rm P}(2,u)$	0.8981 (41)	0.8968 (28)	0.8993 (58)
slope	0.44 (34)	-0.22 (27)	-0.007 (56)
χ^2/dof	0.5349	6.4083	6.8156
Perturbative scale: $\overline{g}^2 = 0.9944$			
$\sigma_{\rm P}(2,u)$	0.9595 (21)	0.9602 (22)	0.9644 (37)
slope	0.59 (18)	0.19 (19)	-0.004 (35)
χ^2/dof	2.4748	1.1258	0.5129

Table 8.4.: Continuum limit of the SSF of the pseudo-scalar density. Results are shown for the χSF with standard Wilson fermions and also for the SF with improved and standard Wilson fermions at two values of the renormalization scale. $\vec{\theta} = (0.5, 0.5, 0.5)$. These results correspond to linear fits of the data in Tab. 8.2. The fit is linear in a/L for the SF(Wilson) formulation while it is linear in $(a/L)^2$ for the χSF and SF(Clover) formulations.

	χSF
Intermediate scale: $\overline{g}^2 = 2.4484$	
$\sigma_{\rm P}(2,u)$	0.8942 (42)
slope	0.82 (34)
χ^2/dof	3.3471
Perturbative scale: $\overline{g}^2 = 0.9944$	
$\sigma_{\rm P}(2,u)$	0.9591 (21)
slope	0.59 (17)
χ^2/dof	1.8644

Table 8.5.: Continuum limit of the SSF of the pseudo-scalar density. Results are shown for the χSF with standard Wilson fermions at two values of the renormalization scale. $\vec{\theta} = (1, 0, 0)$. These results correspond to linear fits in $(a/L)^2$ of the data in Tab. 8.3.

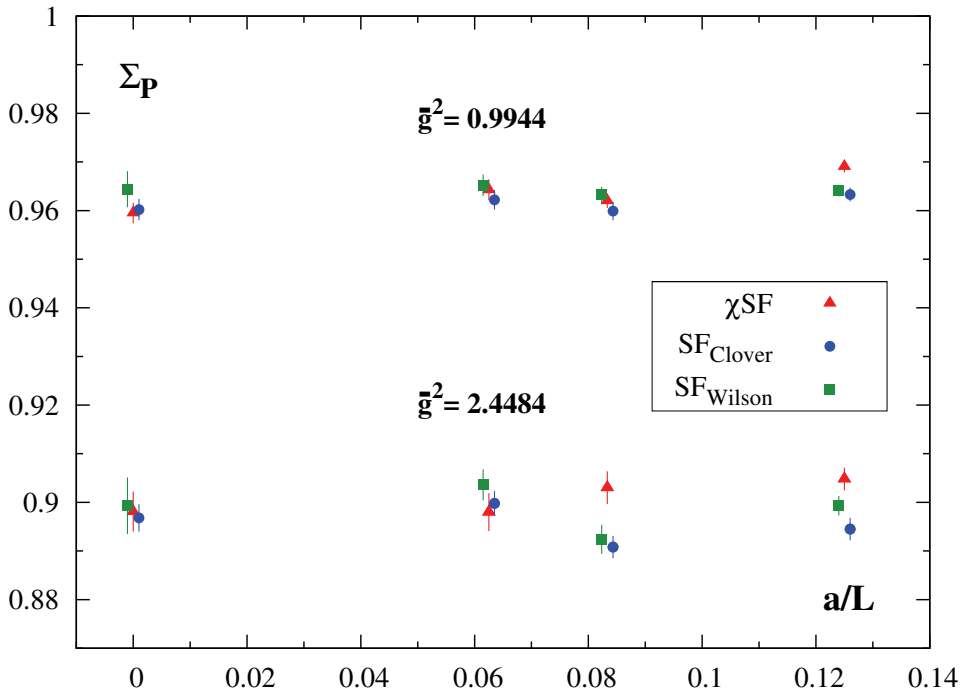

Figure 8.1.: Lattice SSF of the pseudo-scalar density and continuum limit values. Results are shown for the χSF with standard Wilson fermions and the SF with improved and standard Wilson fermions, at the intermediate and perturbative scales and for $\vec{\theta} = (0.5, 0.5, 0.5)$. The extrapolations to the continuum limit are performed according to Tab. 8.4: linear in $(a/L)^2$ for the χSF and the SF with improved fermions and linear in a/L for the SF with standard Wilson fermions. The data from the SF have been slightly displaced to the right and left, respectively, for the improved and unimproved formulations.

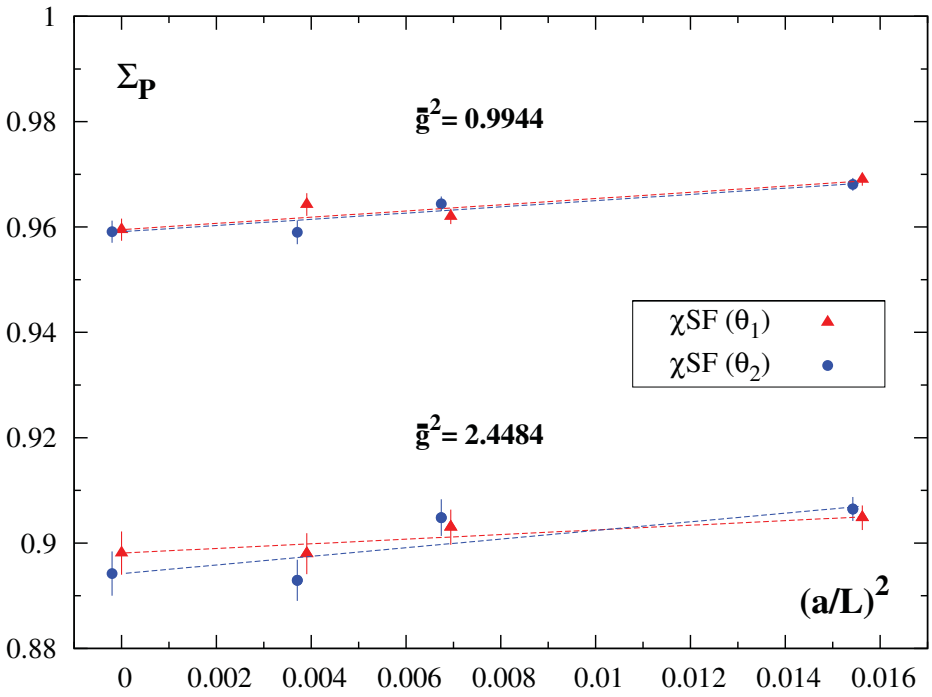

Figure 8.2.: Continuum limit extrapolation of the SSF of the pseudo-scalar density. Only χSF data are shown, both for $\theta_1 \equiv \vec{\theta} = (0.5, 0.5, 0.5)$ and $\theta_2 \equiv \vec{\theta} = (1, 0, 0)$, at the intermediate and perturbative scales. The extrapolations to the continuum limit are linear in $(a/L)^2$ as shown in Tab. 8.4 and Tab. 8.5. The values in the continuum limit are also plotted. The data from θ_2 have been slightly displaced to the left.

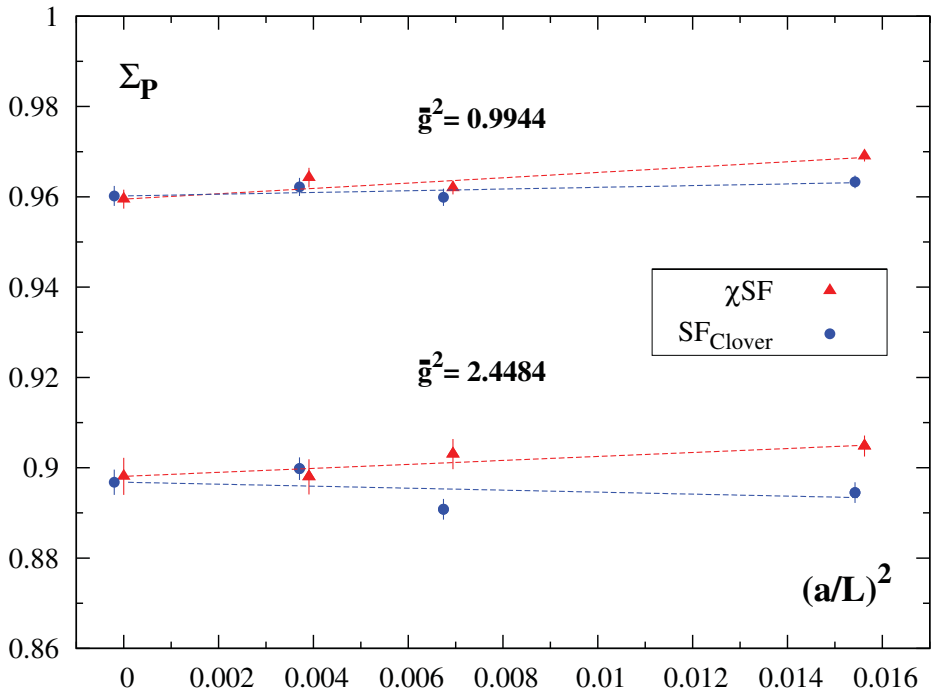

Figure 8.3.: Continuum limit extrapolation of the SSF of the pseudo-scalar density. Results are shown for the χSF with standard Wilson fermions and the SF with improved Wilson fermions, at the intermediate and perturbative scales and for $\vec{\theta} = (0.5, 0.5, 0.5)$. The extrapolations to the continuum limit are linear in $(a/L)^2$ for all cases. The results from the fits are presented in Tab. 8.4. The data from the SF have been slightly displaced to the left.

9. Computation of the RGI strange quark mass

In this chapter we compute the RGI strange quark mass, $M_{\rm s}$, in quenched QCD, using the χSF renormalization scheme and the bare data from large volume simulations with twisted mass fermions at maximal twist. As a byproduct, we also provide the value of the running strange quark mass, in physical units, for a 4-loop running in the $\overline{\rm MS}$-scheme at 2GeV, $\overline{\mu}_{\rm s}^{\overline{\rm MS}}(2\,{\rm GeV})$. The purpose of this computation is to perform another check of the χSF formulation, this time at the hadronic scale, $L = 1.436\,r_0$. In practice, we compute the quantity $r_0\,(M_{\rm s} + \hat{M})$, where $\hat{M} = (M_{\rm u} + M_{\rm d})/2$, and perform the continuum limit. The resulting continuum limit value, obtained from the χSF, is compared to the previously obtained value in [99], using the standard SF with improved Wilson fermions. We will show that the continuum limit value agrees with the one in [99], which is a numerical evidence of the universality of the continuum limit at the matching scale. Moreover, this quantity is expected to scale towards the continuum limit with leading $O(a^2)$ discretization effects, up to possible boundary effects. In fact, we will also show that the scaling behavior is consistent with leading $O(a^2)$ effects. This represents another test of bulk automatic $O(a)$-improvement and moreover it again indicates that the boundary effects coming from d_s are negligible, even at the large values of g_0 considered in this chapter. Furthermore, the discretization effects are so small that even a constant fit to the continuum limit is consistent with our data.

Before going into the details of the results, we briefly describe in Sec. 9.1 the main steps needed in the computation of the RGI quark mass, M. In the following sections we present our results at each of these steps. In Sec. 9.2 we determine $Z_{\rm P}$ at the matching scale, $L = 1.436\,r_0$. The bare reference quark mass, $\mu_{\rm ref}(g_0)$, is determined in Sec. 9.3. In Sec. 9.4 we compute the RGI reference mass, $M_{\rm s} + \hat{M}$, in the continuum limit and in units of r_0. From the continuum limit value of the reference quark mass and the values of ratios of light quark masses, obtained using theoretical predictions based on chiral perturbation theory [100–102], we eventually determine the RGI strange quark mass, $M_{\rm s}$, in units of r_0 in Sec. 9.5. In this section we also give the value, in physical units, of $M_{\rm s}$ and $\overline{\mu}_{\rm s}^{\overline{\rm MS}}(2\,{\rm GeV})$.

9.1. The RGI quark mass

The RG equation of the quark mass has been discussed in Sec. 8.1 of the previous chapter. The reader is referred to that section for notations and detailed explanations. The exact expression defining the RGI quark mass, M, was given in Eq. (8.5). As it has been argued, M is an universal quantity which is independent on the renormalization scheme. Therefore, as the SSFs, it is a good candidate to perform universality tests of the continuum limit.

In the following we will denote M the RGI quark mass, $\mu(g_0)$ the bare quark mass and $\overline{\mu}(L)$ the renormalized running quark mass at the value $1/L$ of the renormalization scale. Therefore, we can write

$$\overline{\mu}(L) = Z_{\rm P}^{-1}(g_0, L)\mu(g_0)\,, \tag{9.1}$$

with $Z_{\rm P}$ the renormalization factor of the pseudo-scalar density, as discussed in detail in Sec. 8.1.

The RGI quark mass, M, can be directly related to the bare quark mass, $\mu(g_0)$,

$$M = Z_{\rm M}(g_0)\mu(g_0)\,, \tag{9.2}$$

L/a	β	$Z_{\rm P}$
8	6.0219	0.5385 (12)
10	6.1628	0.5264 (12)
12	6.2885	0.5272 (16)
16	6.4956	0.5187 (22)

Table 9.1.: $Z_{\rm P}(g_0, L/a)$ at $L = 1.436\, r_0$ and for $\vec{\theta} = (0.5, 0.5, 0.5)$.

through a renormalization factor, $Z_{\rm M}(g_0)$, defined as the product of two terms as follows

$$Z_{\rm M}(g_0) = \left(\frac{M}{\overline{\mu}(L)}\right)\left(\frac{1}{Z_{\rm P}(g_0, L)}\right). \tag{9.3}$$

The first term, $M/\overline{\mu}(L)$, is regularization independent but depends on the renormalization scheme as well as on the matching scale $1/L$. The second term, $Z_{\rm P}^{-1}(g_0, L)$, depends on both the renormalization scheme and the regulator. The dependence is such that the total factor $Z_{\rm M}(g_0)$ does not depend on the renormalization scheme but only on the regularization. All dependence on the matching scale has also disappeared.

In the discussion above, all equations correspond to the continuum theory. When the lattice is used as regularization scheme, the correct relation would be

$$M = Z_{\rm M}(g_0)\mu(g_0) + O(a^n)\,, \tag{9.4}$$

with $n = 1$ in case of unimproved formulations and $n = 2$ if improvement is at work.

The regularization independent part of $Z_{\rm M}(g_0)$, $M/\overline{\mu}(L)$, has already been determined in [97]. The value is known in the *continuum theory* and at the matching scale $L = 1.436\, r_0$. Once the continuum limit is performed this factor is then universal (meant it is regulator independent) and therefore, we can use it for our calculations without the need of a new computation, since both the SF and the χSF are equivalent formulations in the continuum theory. The value obtained in [97] for this regularization independent term, in the continuum limit, is

$$M/\overline{\mu}(L) = 1.157\,(15) \quad \text{at} \quad L = 1.436\, r_0\,, \tag{9.5}$$

which has a relative error of 1.3%.

This means we are only left with the computation of two quantities. One is the regularization dependent part of the total renormalization factor, $Z_{\rm P}^{-1}(g_0, L)$, which is to be computed at the matching point for several values of β and within the χSF scheme (cf. Sec. 9.2). The other quantity is the bare quark mass, $\mu(g_0)$, which also has to be determined for a range of bare couplings as explained in detail below in Sec. 9.3.

9.2. Determination of $Z_{\rm P}$ at the matching scale

The determination of $Z_{\rm P}(g_0, L/a)$ from the χSF, at a certain value of the renormalization scale and for several values of the lattice spacing, has already been explained in the previous chapter and the results are given in Tab. 8.1, at three values of $1/L$ and two values of $\vec{\theta}$. Amongst the cases presented in Tab. 8.1, we are here interested only in the data corresponding to the matching scale, $L = 1.436\, r_0$, and $\vec{\theta} = (0.5, 0.5, 0.5)$. For such a choice of the parameters, we have computed $Z_{\rm P}(g_0, L/a)$ at several values of the lattice spacing in the β range $6.0 \leq \beta \leq 6.5$, which we recall in Tab. 9.1.

i	$z_i^{\rm P}$	$z_i^{\rm M}$
0	0.5394 (14)	2.1444 (55)
1	-0.077 (15)	0.321 (60)
2	0.078 (30)	-0.32 (12)

Table 9.2.: Coefficients of the beta dependence of $Z_{\rm P}(g_0, L/a)$ at the matching scale $L = 1.436\, r_0$ (cf. Eq. (9.6)) and $Z_{\rm M}(g_0)$ (cf. Eq. (9.7)). Results are shown for the χSF with standard Wilson fermions at $\vec{\theta} = (0.5, 0.5, 0.5)$.

L/a	β	$Z_{\rm P}^{-1}$	$Z_{\rm M}$
8	6.0219	1.8569 (41)	2.1484 (47)
10	6.1628	1.8995 (42)	2.1977 (49)
12	6.2885	1.8968 (59)	2.1946 (68)
16	6.4956	1.9279 (80)	2.2306 (93)

Table 9.3.: $Z_{\rm P}^{-1}(g_0, L/a)$ at $L = 1.436\, r_0$ and $Z_{\rm M}(g_0)$, for $\vec{\theta} = (0.5, 0.5, 0.5)$. Results are shown for the χSF formulation and for all the β values where simulations have been performed.

With these data we can now study the dependence of $Z_{\rm P}$ on β and determine a curve that describes this dependence in the range of β we have. The next polinomial fit describes our data

$$\begin{aligned} &Z_{\rm P}(g_0, L/a)_{L=1.436\, r_0} = \sum_{i=0}^{2} z_i^{\rm P} (\beta - 6.0)^i \,, \\ &\beta = 6/g_0^2, \qquad 6.0 \le \beta \le 6.5 \,, \end{aligned} \tag{9.6}$$

with the coefficients presented in the second column of Tab. 9.2. The data in Tab. 9.1 together with the fitting curve Eq. (9.6) are plotted in Fig. 9.1.

From these data we may also determine a curve for $Z_{\rm M}$. It is done by computing $Z_{\rm P}^{-1}$ and then multiplying the result by the regularization independent term $M/\overline{\mu}(L) = 1.157$, as given in Eq. (9.5). This value has an uncertainty of 1.3% which will be added in quadrature only at the end of all calculations, after the extrapolation to the continuum limit has been carried out. As argued in [97], this value corresponds to the continuum limit and therefore, it does not make sense to include the error already at finite value of the cutoff but only after the continuum extrapolation has been performed. The results for $Z_{\rm M}$ at each of the β values where we have performed simulations are summarized in Tab. 9.3 together with the values of $Z_{\rm P}^{-1}$.

The curve describing the dependence of $Z_{\rm M}$ with β is the following

$$\begin{aligned} &Z_{\rm M}(g_0) = \sum_{i=0}^{2} z_i^{\rm M} (\beta - 6.0)^i \,, \\ &\beta = 6/g_0^2, \quad 6.0 \le \beta \le 6.5 \,, \end{aligned} \tag{9.7}$$

with the coefficients presented in the third column of Tab. 9.2.

From the curves Eq. (9.6) and Eq. (9.7), it is now possible to compute $Z_{\rm P}$ and $Z_{\rm M}$ at any value of β within the range $6.0 \le \beta \le 6.5$. This is indeed the range of β where the bare quark masses, $\mu(g_0)$, have been chosen in the large volume simulations. In particular at the values $\beta = 6.00, 6.10, 6.20, 6.45$. The corresponding values of $Z_{\rm P}$ and $Z_{\rm M}$ at the chosen values of β, as obtained from the previous curves, are summarized in Tab. 9.4.

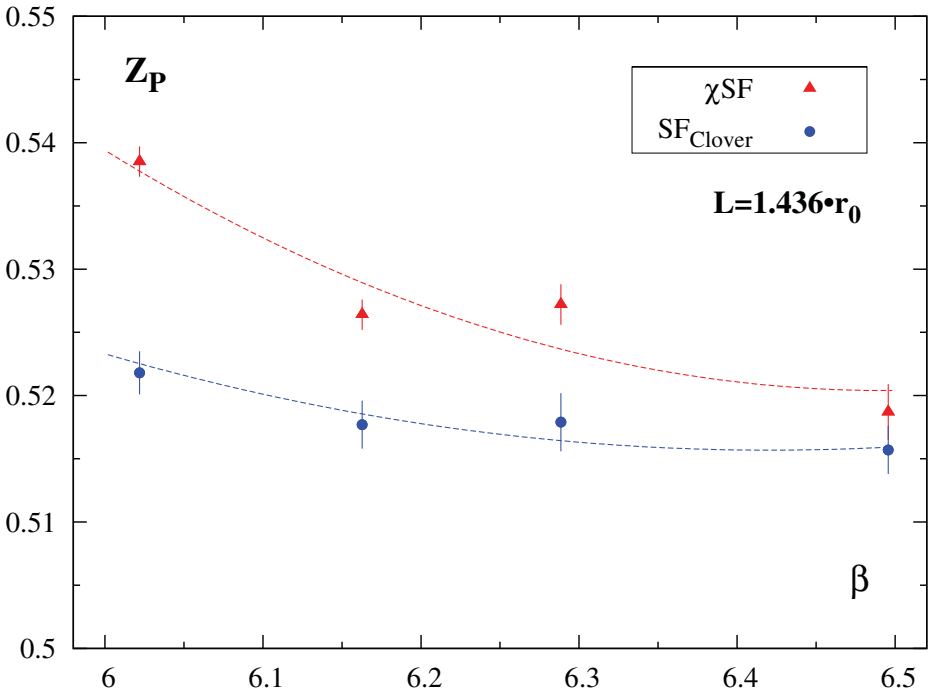

Figure 9.1.: Numerical results for $Z_{\mathrm{P}}(g_0, L/a)$ at scale $L = 1.436\, r_0$ and for several β values. $\vec{\theta} = (0.5, 0.5, 0.5)$. Results are shown for the χSF with standard Wilson fermions (cf. Tab. 9.1) and for the SF with improved Wilson fermions, as taken from [97]. The fitting curves are also plotted (cf. Eq. (9.6) and Tab. (9.2)).

β	Z_{P}	Z_{M}
6.00	0.5394 (14)	2.1444 (55)
6.10	0.53240 (82)	2.1733 (33)
6.20	0.5270 (10)	2.1957 (42)
6.45	0.5203 (17)	2.2236 (70)

Table 9.4.: $Z_{\mathrm{P}}(g_0, L/a)$ at $L = 1.436\, r_0$ and $Z_{\mathrm{M}}(g_0)$, for $\vec{\theta} = (0.5, 0.5, 0.5)$. Results are presented for the χSF formulation at several β values, as determined from the curves in Eq. (9.6) and Eq. (9.7).

β	5.70	5.85	6.00	6.10	6.20	6.45
a (fm)	0.171	0.123	0.093	0.079	0.068	0.048
r_0/a	2.930	4.067	5.368	6.324	7.360	10.458
L/a	12	16	16	20	24	32
T/a	32	32	32	40	48	64
	pion definition (κ_c^{pion})					
N_{meas}	600	378	387	300	260	182
$\mu_1 a$	0.0070	0.0050	0.0038	0.0032	0.0028	0.0020
$\mu_2 a$	0.0139	0.0100	0.0076	0.0064	0.0055	0.0039
$\mu_3 a$	0.0278	0.0200	0.0151	0.0128	0.0111	
$\mu_4 a$	0.0556	0.0400	0.0302	0.0257	0.0221	
$\mu_5 a$	0.0834	0.0600	0.0454	0.0385	0.0332	
$\mu_6 a$	0.1112	0.0800	0.0605	0.0514	0.0442	
$\mu_7 a$	0.1390	0.1000	0.0756	0.0642	0.0553	
	PCAC definition (κ_c^{PCAC})					
N_{meas}	600	500	400		300	
$\mu_1 a$	0.0070	0.0050	0.0038		0.0028	
$\mu_2 a$	0.0139	0.0100	0.0076		0.0055	
$\mu_3 a$	0.0278	0.0200	0.0151		0.0111	
$\mu_4 a$	0.0556	0.0400	0.0302		0.0221	
$\mu_5 a$	0.0834	0.0600	0.0454		0.0332	
$\mu_6 a$	0.1112	0.0800	0.0605		0.0442	
$\mu_7 a$	0.1390	0.1000	0.0756		0.0553	
$\mu_8 a$	0.0200	0.0144	0.0109		0.0080	
$\mu_9 a$	0.0420	0.0302	0.0228		0.0166	

Table 9.5.: Simulation parameters and statistics (N_{meas}). Table taken from [103].

9.3. Determination of the bare reference quark mass

In this section we determine the values of the bare reference quark mass, $\mu_{\text{ref}}(g_0)$, at the values of β which are available from the large volume simulations and which overlap with the range of β described by our data, $6.0 \leq \beta \leq 6.5$. The data from the large volume simulations are taken from [103], where the β values which overlap with our range are $\beta = 6.00, 6.10, 6.20, 6.45$. The definition of the reference quark mass will be given below in this section. In [103], the pseudo-scalar mass, m_{PS}, in lattice units was obtained at the aforementioned values of β and for several values of the twisted quark mass μ, also in lattice units, using twisted mass Wilson fermions at maximal twist. The pseudo-scalar masses were computed, at each chosen value of the quark masses, using two different definitions of the critical mass, m_c; the PION and the PCAC definitions. The differences between the two definitions are $O(a)$ effects which give rise to differences of only $O(a^2)$ in physical quantities. We are not concerned here with the different definitions employed and we refer the reader to [103] for further insights in this topic. The data as taken from [103] are presented in Tab. 9.5 for the simulation parameters and in Tab. 9.6 for the corresponding pseudo-scalar masses.

The pseudo-scalar mass range covered by these data is $270\text{MeV} < m_{\text{PS}} < 1180\text{MeV}$. Within this range, we may determine the curve describing the dependence of the pseudo-scalar mass, am_{PS}, on the quark mass, $a\mu$. Then, given the experimental value of the mass of a certain meson, within the previous range of masses, the corresponding quark mass can be obtained from the curve by an interpolation of the data. In particular we are interested here in determining the

β	5.70	5.85	6.00	6.10	6.20	6.45
	$m_{\rm PS}a$ $(\kappa_c^{\rm pion})$					
$\mu_1 a$	0.2455(23)	0.1682(26)	0.1385(66)	0.1129(41)	0.1004(27)	0.0720(28)
$\mu_2 a$	0.3237(16)	0.2256(22)	0.1764(42)	0.1482(27)	0.1298(23)	0.0914(27)
$\mu_3 a$	0.4434(11)	0.3122(19)	0.2373(32)	0.2030(21)	0.1768(17)	
$\mu_4 a$	0.6272(09)	0.4452(14)	0.3335(22)	0.2865(15)	0.2463(15)	
$\mu_5 a$	0.7767(09)	0.5535(12)	0.4134(17)	0.3534(13)	0.3037(13)	
$\mu_6 a$	0.9074(09)	0.6488(13)	0.4839(16)	0.4130(13)	0.3546(12)	
$\mu_7 a$	1.0255(08)	0.7358(12)	0.5491(14)	0.4676(12)	0.4021(11)	
	$m_{\rm PS}a$ $(\kappa_c^{\rm PCAC})$					
$\mu_1 a$	0.2323(18)	0.1640(23)	0.1217(66)		0.0934(24)	
$\mu_2 a$	0.3245(15)	0.2289(17)	0.1708(50)		0.1276(21)	
$\mu_3 a$	0.4598(12)	0.3232(13)	0.2396(33)		0.1779(18)	
$\mu_4 a$	0.6564(10)	0.4606(11)	0.3403(22)		0.2492(13)	
$\mu_5 a$	0.8114(10)	0.5701(10)	0.4214(17)		0.3071(12)	
$\mu_6 a$	0.9451(10)	0.6658(09)	0.4925(14)		0.3588(10)	
$\mu_7 a$	1.0647(09)	0.7530(09)	0.5579(14)		0.4062(09)	
$\mu_8 a$	0.3892(14)	0.2741(15)	0.2038(40)		0.1519(20)	
$\mu_9 a$	0.5678(11)	0.3984(12)	0.2948(26)		0.2160(16)	

Table 9.6.: Pseudo-Scalar meson masses $m_{\rm PS}a$ for all simulation points. Table taken from [103].

strange quark mass, $a\mu_{\rm s}$, for which we use as an input the experimental value of the Kaon mass, $m_{\rm K}$. Indeed, from the previous interpolation we do not directly obtain $a\mu_{\rm s}$ but the aforementioned reference mass, $a\mu_{\rm ref}$, as it will be made clear below.

9.3.1. Dependence of the pseudo-scalar mass on the quark mass

At each β value, the interpolation curve that describes the dependence of the pseudo-scalar mass, $am_{\rm PS}$, on the quark mass, $a\mu$, is the following

$$(am_{\rm PS})^2 = c_0 + c_1(a\mu) + c_2(a\mu)^2\,. \tag{9.8}$$

For the two definitions that we have for the critical mass and the β of interest, we summarize the results of the fit in Tab. 9.7. For comparison, we have added a second table, Tab. 9.8, with the results of a linear fit, where only the three points closest to the interpolation point (the Kaon mass) were considered. This can be done because in this small $a\mu$ range the behaviour is certainly linear in $a\mu$ and, moreover, our interest here is to describe the data in the region of the Kaon mass and not to perform a chiral extrapolation. From such a linear fit we obtained the same values, within statistical errors, as with the quadratic fit Eq. (9.8). This implies the fit Eq. (9.8) to be a valid choice. Values derived from this fit are used for all calculations in this section, while results from the linear fit just serve as a check. We present here also some figures containing the data points together with the fitting curves for both cases. These are Fig. 9.2 and Fig. 9.3 for the quadratic fits and for the PION and PCAC definitions, respectively, and Fig. 9.4 and Fig. 9.5 for the linear fits.

From these curves, once the value of $am_{\rm K}$ is known, we can directly compute the reference quark mass, $a\mu_{\rm ref}$. In the case of the K-meson, the reference mass is given by $2\mu_{\rm ref} = \mu_{\rm s} + \hat{\mu}$, where, $\hat{\mu} = (\mu_{\rm u} + \mu_{\rm d})/2$ (see [99] for discussion). For this purpose we first need to know the values of r_0 in lattice units at the β values of interest.

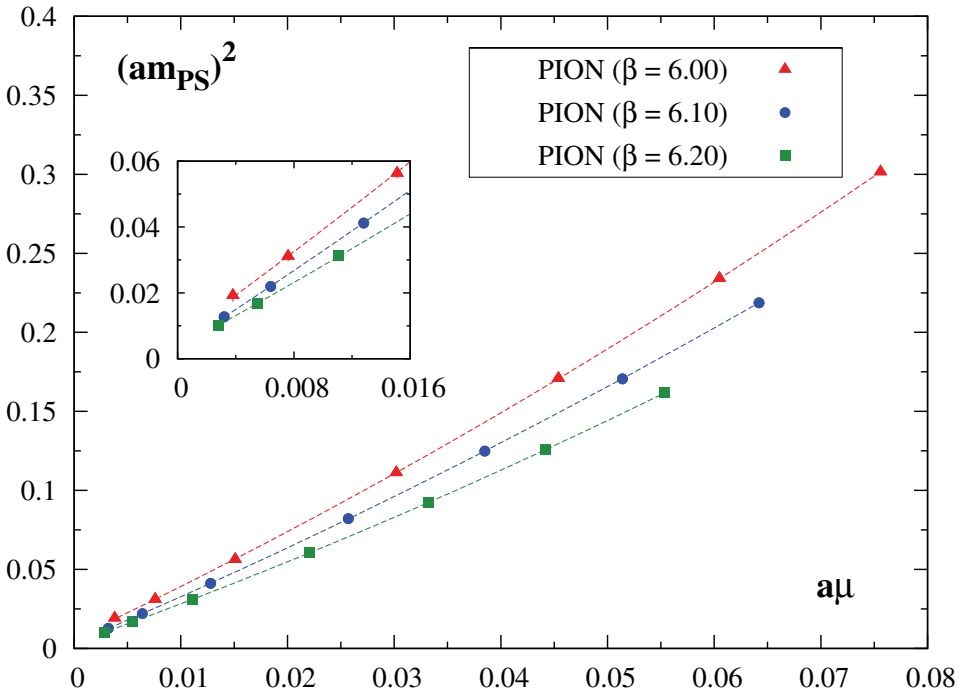

Figure 9.2.: $(am_{\rm PS})^2$ vs. $a\mu$ at three values of β. The data are obtained from Tab. 9.5 and Tab. 9.6, as taken from [103], and correspond to the PION definition of the critical mass. The interpolations are performed according to Eq. (9.8), considering all the points shown in the plot. The coefficients of the fits may be read off from Tab. 9.7. In the small box we zoom the area around the Kaon mass.

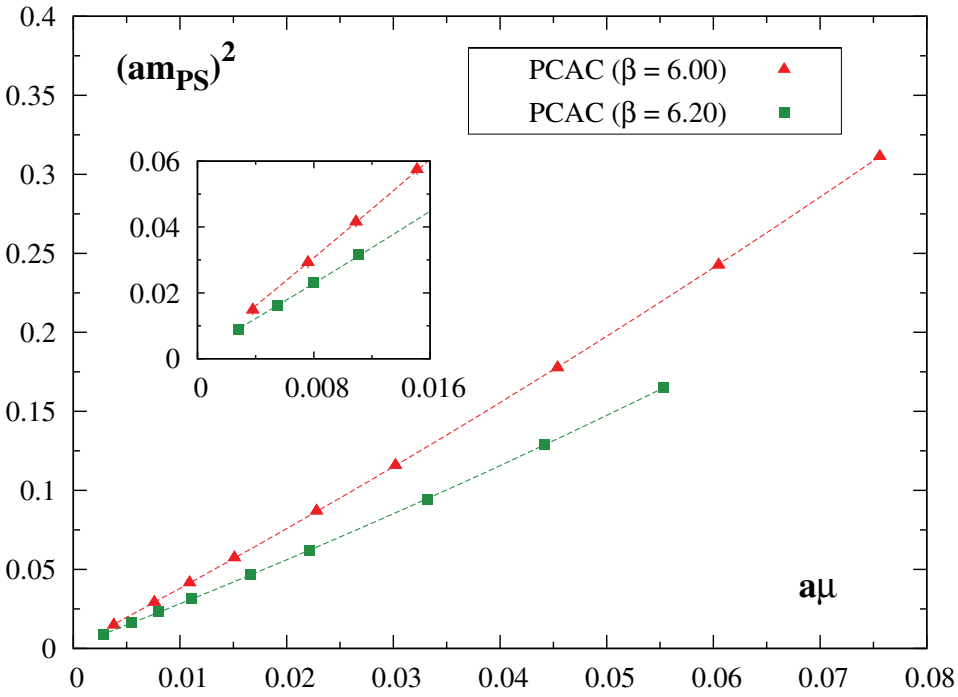

Figure 9.3.: $(am_{\rm PS})^2$ vs. $a\mu$ at two values of β. The data are obtained from Tab. 9.5 and Tab. 9.6, as taken from [103], and correspond to the PCAC definition of the critical mass. The interpolations are performed according to Eq. (9.8), considering all the points shown in the plot. The coefficients of the fits may be read off from Tab. 9.7. In the small box we zoom the area around the Kaon mass.

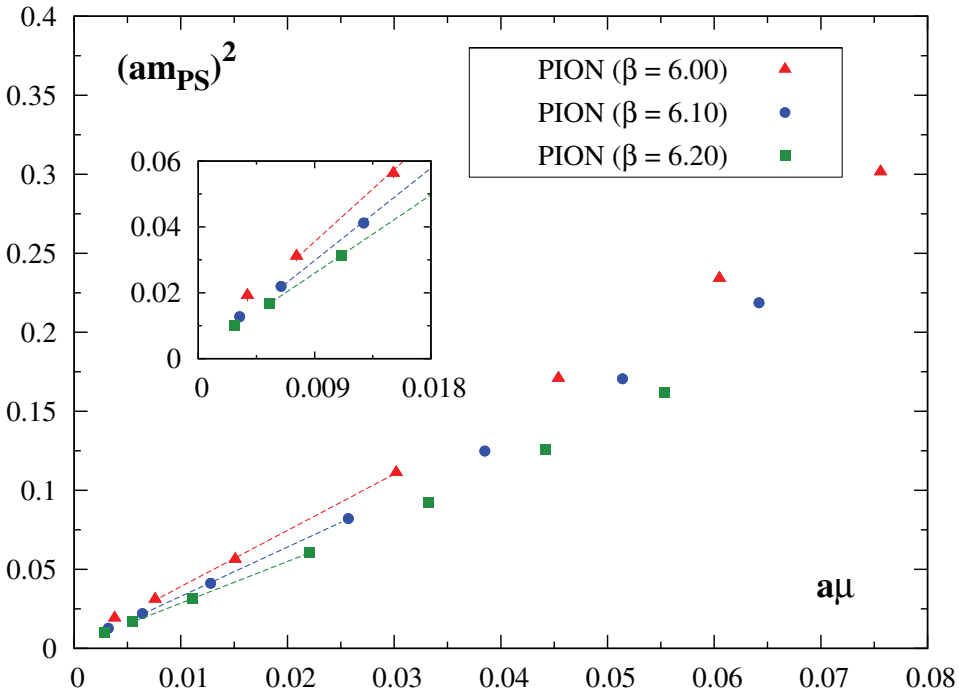

Figure 9.4.: $(am_{\mathrm{PS}})^2$ vs. $a\mu$ at three values of β. The data are obtained from Tab. 9.5 and Tab. 9.6, as taken from [103], and correspond to the PION definition of the critical mass. The interpolations are linear in $a\mu$ and only the three points closest to the interpolation value (cf. Tab. 9.10) have been considered in the fit. The coefficients of the fits may be read off from Tab. 9.8. In the small box we zoom the area around the Kaon mass.

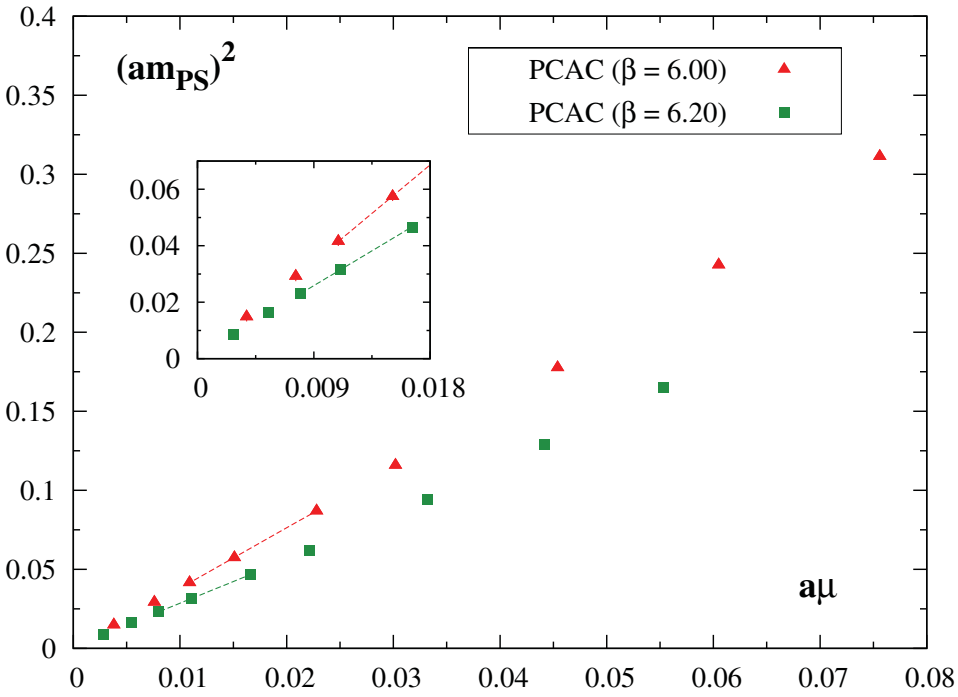

Figure 9.5.: $(am_{\mathrm{PS}})^2$ vs. $a\mu$ at two values of β. The data are obtained from Tab. 9.5 and Tab. 9.6, as taken from [103], and correspond to the PCAC definition of the critical mass. The interpolations are linear in $a\mu$ and only the three points closest to the interpolation value (cf. Tab. 9.10) have been considered in the fit. The coefficients of the fits may be read off from Tab. 9.8. In the small box we zoom the area around the Kaon mass.

β	6.00	6.10	6.20
	κ_c^{pion} definition		
c_0	0.0064 (14)	0.00341 (78)	0.00334 (53)
c_1	3.187 (95)	2.860 (67)	2.412 (59)
c_2	9.5 (1.2)	7.7 (1.0)	8.1 (1.1)
χ^2/dof	0.1964	0.0498	0.1395
	κ_c^{PCAC} definition		
c_0	0.0017 (13)		0.00174 (44)
c_1	3.566 (90)		2.587 (49)
c_2	7.0 (1.1)		6.54 (88)
χ^2/dof	0.3208		1.6965

Table 9.7.: Fit parameters for $(am_{\text{PS}})^2$ vs. $a\mu$. The fitting function is of the form given in Eq. (9.8).

β	6.00	6.10	6.20
	κ_c^{pion} definition		
c_0	0.0035 (18)	0.0017 (10)	0.00217 (76)
c_1	3.558 (91)	3.121 (60)	2.642 (57)
χ^2/dof	0.5477	0.4352	0.2373
	κ_c^{PCAC} definition		
c_0	-0.0001 (32)		0.0012 (13)
c_1	3.82 (18)		2.74 (11)
χ^2/dof	0.0050		0.0088

Table 9.8.: Fit parameters for $(am_{\text{PS}})^2$ vs. $a\mu$. This is a linear fit considering only the three closest points to the interpolation value.

9.3.2. Determination of r_0/a at several beta values

For the determination of r_0/a at the desired β values, we take [38] as our starting point (cf. App. C.3). In [38] the β dependence of r_0/a was determined in the range $5.7 \leq \beta \leq 6.57$, which certainly covers our range of interest. The curve determined in this reference is the following

$$\ln(a/r_0) = -1.6805 - 1.7139(\beta - 6) + 0.8155(\beta - 6)^2 - 0.6667(\beta - 6)^3 \,, \tag{9.9}$$

with a relative uncertainty in the determination of r_0/a of 0.3% at $\beta = 5.7$ which grows linearly up to 0.6% at $\beta = 6.57$.

From this information we can determine the curve describing the relative uncertainty in this β range

$$\Delta(r_0/a) = 0.3 + 0.345(\beta - 5.70) \,. \tag{9.10}$$

For the β values of Tab. 9.5 we summarize the values of r_0/a with the corresponding relative uncertainty in Tab. 9.9.

9.3.3. Determination of the Kaon mass in lattice units

In this section we follow [99], where they provide the QCD value of the Kaon mass, m_{K}, which is given by

$$m_{\text{K}}^2 = \frac{1}{2}(m_{\text{K}^+}^2 + m_{\text{K}^0}^2)_{\text{QCD}} = (495\,\text{MeV})^2 \,, \tag{9.11}$$

β	$\Delta(\%)$	r_0/a
5.70	0.30	2.9298 (88)
5.85	0.35	4.067 (14)
6.00	0.40	5.368 (22)
6.10	0.44	6.324 (28)
6.20	0.47	7.360 (35)
6.45	0.56	10.458 (58)

Table 9.9.: r_0/a and relative uncertainty, $\Delta(r_0/a)$, at several values of β.

β	$(am_{\rm K})^2$
5.70	0.1833 (14)
5.85	0.09511 (81)
6.00	0.05460 (52)
6.10	0.03934 (40)
6.20	0.02904 (31)
6.45	0.01438 (18)

Table 9.10.: $(am_{\rm K})^2$ at particular values of β.

with an accuracy of about 0.5% in $m_{\rm K}^2$. The subscript 'QCD' indicates that no electromagnetic interactions are considered but only pure QCD.

In order to determine $(am_{\rm K})^2$ we do it through the product

$$(am_{\rm K})^2 = (r_0^2 m_{\rm K}^2)(r_0/a)^{-2}\,. \tag{9.12}$$

Both terms of this product are known and we take for the Sommer parameter the value $r_0 = 0.5\,\text{fm}$. The first term is then $r_0^2 m_{\rm K}^2 = 1.5732(79)$. Using the values of r_0/a determined in Sec. 9.3.2 we obtain the values for $(am_{\rm K})^2$ shown in Tab. 9.10.

9.3.4. Determination of the reference quark mass in units of r_0

Now we have the ingredients to compute the reference quark mass in lattice units, $a\mu_{\rm ref}$. From Sec. 9.3.1 we know the relation between $am_{\rm PS}$ and $a\mu$ and from Sec. 9.3.3 we know $(am_{\rm PS})^2$ at the value of the Kaon mass, which we need to plug in as an input in the relation between $am_{\rm PS}$ and $a\mu$. The results are summarized in Tab. 9.11. The last column of the table contains the corresponding values obtained from the linear fit just to show that the values agree within errors, so this should not change our final result.

β	$(am_{\rm K})^2$	$a\mu_{\rm ref}$	$a\mu_{\rm ref}$(linear)
$\kappa_c^{\rm pion}$ definition			
6.00	0.05460 (52)	0.01450 (59)	0.01436 (64)
6.10	0.03934 (40)	0.01216 (40)	0.01206 (42)
6.20	0.02904 (31)	0.01030 (34)	0.01017 (38)
$\kappa_c^{\rm PCAC}$ definition			
6.00	0.05460 (52)	0.01443 (51)	0.0143 (11)
6.20	0.02904 (31)	0.01029 (27)	0.01016 (64)

Table 9.11.: $a\mu_{\rm ref}$ at the value of the Kaon mass and for particular values of β. Results are shown for the pion and the PCAC definitions of the critical mass.

β	r_0/a	$a\mu_{\rm ref}$	$\mu_{\rm ref}\, r_0$
$\kappa_c^{\rm pion}$ definition			
6.00	5.368 (22)	0.01450 (59)	0.0778 (32)
6.10	6.324 (28)	0.01216 (40)	0.0769 (26)
6.20	7.360 (35)	0.01030 (34)	0.0758 (25)
6.45	10.458 (58)		
$\kappa_c^{\rm PCAC}$ definition			
6.00	5.368 (22)	0.01443 (51)	0.0775 (28)
6.20	7.360 (35)	0.01029 (27)	0.0757 (20)

Table 9.12.: $\mu_{\rm ref}\, r_0$ at the value of the Kaon mass and for particular values of β. Results are shown for the pion and the PCAC definitions of the critical mass.

β	$Z_{\rm M}$	$r_0\,(M_{\rm s}+\hat{M})$
$\kappa_c^{\rm pion}$ definition		
6.00	2.1444 (55)	0.334 (14)
6.10	2.1733 (33)	0.334 (11)
6.20	2.1957 (42)	0.333 (11)
6.45	2.2236 (70)	
$\kappa_c^{\rm PCAC}$ definition		
6.00	2.1444 (55)	0.332 (12)
6.20	2.1957 (42)	0.3324 (88)

Table 9.13.: $r_0\,(M_{\rm s}+\hat{M}) = Z_{\rm M}(2\mu_{\rm ref}\, r_0)$ at several values of β. Results are shown for the pion and the PCAC definitions of the critical mass.

In order to compute the reference quark mass in units of the reference scale, $\mu_{\rm ref}\, r_0$, we have to multiply the values of r_0/a and $a\mu_{\rm ref}$. The final results for $\mu_{\rm ref}\, r_0$, together with the corresponding values of r_0/a and $a\mu_{\rm ref}$, are presented in Tab. 9.12.

9.4. Determination of the RGI reference mass

In this section we determine the RGI reference quark mass in units of the Sommer parameter and perform the continuum limit. The data at finite lattice spacing are summarized in Tab. 9.13.

In Fig. 9.6 we plot our data for $r_0\,(M_{\rm s}+\hat{M})$ vs. $(a/r_0)^2$ for the two methods employed in the determination of κ_c. The corresponding fitting curves and continuum limit values are also shown in the plot. These fits correspond to linear extrapolations in $(a/r_0)^2$. The data obtained from the SF with improved Wilson fermions [99] are also plotted for comparison.

The final values in the continuum limit, obtained from the linear extrapolations in $(a/r_0)^2$, are presented in Eq. (9.13) and Eq. (9.14) for the PION and PCAC definitions, respectively

$$\text{PION}: \quad r_0\,(M_{\rm s}+\hat{M})^{\chi{\rm SF}} = 0.332\,(28)\,, \tag{9.13}$$

$$\text{PCAC}: \quad r_0\,(M_{\rm s}+\hat{M})^{\chi{\rm SF}} = 0.333\,(23)\,. \tag{9.14}$$

The errors are obtained after adding in quadrature the 1.3% uncertainty in the factor $M/\mu(L)$. The value given in [99] is the following

$$r_0\,(M_{\rm s}+\hat{M})^{\rm SF} = 0.362\,(12)\,. \tag{9.15}$$

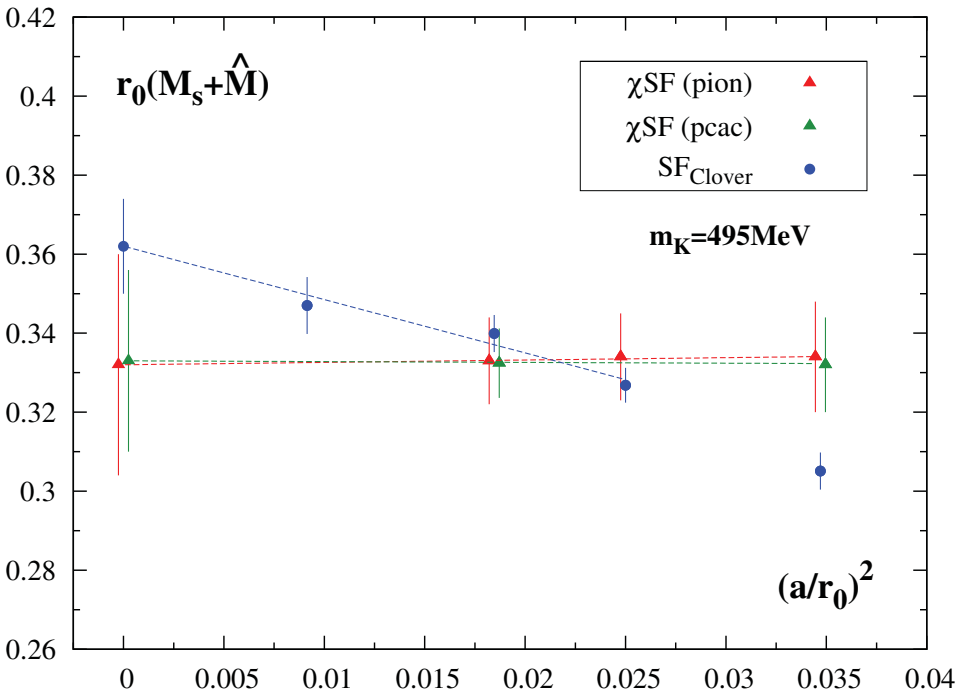

Figure 9.6.: $r_0(M_\mathrm{s} + \hat{M})$ vs. $(a/r_0)^2$, at the physical value of the Kaon mass, $m_\mathrm{K} = 495\mathrm{MeV}$. The extrapolations to the continuum limit are performed with linear fits in $(a/r_0)^2$. The values in the continuum limit are also plotted. Results are shown for the χSF with standard Wilson fermions, for the two definitions of the critical mass, and also for the SF with improved Wilson fermions [99]. The data for the χSF have been plotted slightly displaced to the right and left, respectively, for the PCAC and PION definitions of the critical mass.

Therefore, we can conclude that the results obtained using the χSF and the SF agree in the continuum limit. As it can be seen from the previous numbers and the data in Fig. 9.6, the SF data have relative errors which are about two times smaller than the errors obtained in our calculation using the χSF. Yet, this difference in the errors is not worrisome. The reason for that difference is the size of the statistical errors in the bare pseudo-scalar masses; if we compare the statistical errors in the bare pseudo-scalar masses from the large volume simulations using twisted mass fermions [103] with those of [99], we can see that the statistical errors in the last case are also about two times smaller than those of the former reference. It should be emphasized that such errors come from the large volume simulations and they are not related at all to the χSF formulation.

All previous results have been obtained from a continuum extrapolation linear in $(a/r_0)^2$. However, the χSF data show a constant behavior in the approach to the continuum limit and therefore, a constant fit would be also appropriate in this case. This flat behavior is an evidence of the small size of the $O(a^2)$ discretization effects in the χSF formulation. Performing a constant fit of the χSF data the results in the continuum limit are the following,

$$\text{PION (const):} \quad r_0\,(M_\mathrm{s} + \hat{M})^{\chi\mathrm{SF}} = 0.3336\,(81)\,, \tag{9.16}$$

$$\text{PCAC (const):} \quad r_0\,(M_\mathrm{s} + \hat{M})^{\chi\mathrm{SF}} = 0.3323\,(83)\,. \tag{9.17}$$

With the constant fit the relative errors in the continuum limit are substantially reduced. In this case, however, the continuum limit values differ in about 3.5σ from the SF value, Eq. (9.15). Nevertheless, this is not a problem, since the SF and the χSF data agree within statistical errors already at non-zero lattice spacing, for $\beta = 6.10$ and $\beta = 6.20$. In order to have a more precise comparison in this case, it would be interesting to have χSF results also at $\beta = 6.45$ and to reduce the statistical errors in the bare data.

We can conclude that the values of the RGI reference quark mass, and therefore the RGI strange quark mass itself, determined using the SF and the χSF agree in the continuum limit. This is another test of the universality of the continuum limit, this time at the matching scale, $L = 1.436\,r_0$. In particular, these results demonstrate that the χSF and twisted mass Wilson fermions at maximal twist are a valuable tool for the computation of quark masses.

9.5. Determination of the RGI strange quark mass

Even if not necessary for the universality test, we would like to close this chapter giving the value of the RGI strange quark mass, M_s, in physical units and the running strange quark mass in the $\overline{\mathrm{MS}}$-scheme. As discussed in [99], chiral perturbation theory allows for a precise determination of ratios of masses of the three lightest quarks, u, d, s [100–102]. Such determinations led to

$$M_\mathrm{u}/M_\mathrm{d} = 0.553 \pm 0.043\,, \qquad M_\mathrm{s}/\hat{M} = 24.4 \pm 1.5\,, \tag{9.18}$$

with

$$\hat{M} \equiv \frac{1}{2}\,(M_\mathrm{u} + M_\mathrm{d})\,. \tag{9.19}$$

Considering these relations together with Eq. (9.13) and Eq. (9.14), we can determine the value of the RGI strange quark mass, M_s. The final result in units of r_0 is thus,

$$\text{PION}: \quad r_0\,M_\mathrm{s}^{\chi\mathrm{SF}} = 0.319\,(27)\,, \tag{9.20}$$

$$\text{PCAC}: \quad r_0\,M_\mathrm{s}^{\chi\mathrm{SF}} = 0.320\,(22)\,, \tag{9.21}$$

for the PION and PCAC definitions of κ_c, respectively. Doing the same with the data in [99]

we obtain,

$$r_0\, M_{\rm s}^{\rm SF} = 0.348\,(12)\,. \tag{9.22}$$

The value of the RGI strange quark mass can be now given in physical units,

$$\text{PION}: \quad M_{\rm s}^{\chi{\rm SF}} = 126\,(11)\,\text{MeV}\,, \tag{9.23}$$

$$\text{PCAC}: \quad M_{\rm s}^{\chi{\rm SF}} = 126\,(9)\,\text{MeV}\,, \tag{9.24}$$

and for the SF,

$$M_{\rm s}^{\rm SF} = 137\,(5)\,\text{MeV}\,. \tag{9.25}$$

Using the conversion factor between the RGI mass and the running mass in the $\overline{\rm MS}$-scheme, the running strange quark mass in the $\overline{\rm MS}$-scheme can be directly determined. At a value of the energy scale of 2 GeV and up to 4-loop, the conversion factor is

$$\overline{m}^{\overline{\rm MS}}(2\,\text{GeV})/M = 0.72076\,. \tag{9.26}$$

As a result, the strange quark mass at 2 GeV with a 4-loop running in the $\overline{\rm MS}$-scheme is the following, as determined from the χSF and the SF,

$$\chi\text{SF (PION)}: \quad \overline{\mu}_{\rm s}^{\overline{\rm MS}}(2\,\text{GeV}) = 91\,(8)\,\text{MeV}\,, \tag{9.27}$$

$$\chi\text{SF (PCAC)}: \quad \overline{\mu}_{\rm s}^{\overline{\rm MS}}(2\,\text{GeV}) = 91\,(6)\,\text{MeV}\,, \tag{9.28}$$

$$\text{SF}: \quad \overline{m}_{\rm s}^{\overline{\rm MS}}(2\,\text{GeV}) = 99\,(4)\,\text{MeV}\,. \tag{9.29}$$

10. Z-factors and SSFs of twist-2 operators

In the present chapter, we compute the SSF of the non-singlet twist-2 local operator related to the first moment of the valence quark parton distribution function (PDF) in a hadron. Such computation is performed within the χSF scheme at two values of the renormalization scale, $1/L$, and for two choices of the kinematical parameter $\vec{\theta}$. In order to perform the continuum limit, we have evaluated the SSF on the lattice at several values of the lattice spacing, for each value of the renormalization scale and the kinematical parameters. The final results in the continuum limit are then compared to the corresponding results obtained from the SF scheme using two different regularizations of fermions, standard and non-perturbatively improved Wilson fermions. We will show that the SSFs, as obtained from the three different lattice formulations of fermions, agree within statistical errors in the continuum limit. These results are another numerical evidence of the universality of the continuum limit, which demonstrate that the χSF scheme gives rise to a well-defined continuum limit. We will also show that the scaling of the SSFs, obtained from the χSF formulation, is in all cases consistent with leading $O(a^2)$ discretization effects. This indicates that the scaling behavior of these SSFs is consistent with bulk automatic $O(a)$-improvement and is not affected by the boundary effects coming from d_s, as it was also the case of the pseudo-scalar density and the RGI strange quark mass at the hadronic scale. In addition, we have determined the β-dependence of the Z-factors of the twist-2 operators at the most non-perturbative coupling, which corresponds to the matching scale with the hadronic scheme, and the RGI Z-factors, relating the matrix elements of the bare operators to those of their RGI counterparts.

The chapter is structured in the following way. In Sec. 10.1 we briefly motivate the necessity of twist-2 local operators in QCD. In Sec. 10.2 the main definitions are collected, in the continuum and on the lattice. In Sec. 10.3 we define the SSF of the twist-2 operator and choose a renormalization prescription for such an operator. In Sec. 10.4 we present our results for the renormalization factors and SSFs at finite value of the cutoff for all the cases we have studied. Results for the SSFs in the continuum limit are summarized in Sec. 10.5, where we also perform a comparison of our results with those obtained from the standard formulation. Eventually in Sec. 10.6 we present our results on the Z-factors at the matching scale and the RGI Z-factors, which are compared to those obtained from the standard SF formulation.

10.1. Motivation of the twist-2 operators

From the theoretical point of view, the operator-product-expansion (OPE) arises as a tool for giving a meaningful definition of composite operators. A composite field, or composite operator, is a product of fields at the *same* space-time point (e.g. $j_\mu(x) = \overline{\psi}(x)\gamma_\mu\psi(x)$). Taking such a product in a naive way, a composite field is not a well defined object; its vacuum expectation value is divergent. It was Wilson [104, 105] who introduced the OPE, in order to have a meaningful definition of composite fields.

Given a product of (local) composite fields, $A(x)$ and $B(y)$, at space-time points x and y, respectively, such a product is not well-defined in the limit $x \to y$ [1]. However, the OPE states that this product may be expanded in a series of well-defined (regular or non-singular) local

[1] Note that A and B may just be the fields themselves, e.g. $\psi(x)$.

composite fields with singular c-coefficients (coefficient functions) as follows

$$A(x)B(y) = \sum_n C_n(x-y)O_n(\frac{x+y}{2})\,, \tag{10.1}$$

with C_n the singular c-coefficients and O_n the local regular composite fields. With regular field it is meant that when $x \to y$, where the singularities of the product of composite fields arise, the local composite fields of the expansion remain non-singular and all singularity is contained only in the c-coefficients. The OPE may then serve to define a regularized composite operator. Moreover, the OPE provides a clear separation of the short-distance from the long-distance effects. In particular, the singular coefficient functions characterize the short-distance behavior whilst the regular local composite fields of the expansion contain all the information of the long-distance properties, which are unimportant in the short-distance region. This implies that the singular parts may be treated in PT while the regular parts can only be studied using non-perturbative methods or experimental input. Although there is not a non-perturbative proof of the OPE relation, it was conjectured by Wilson and then proved in PT [106] using the BPHZ method and it is expected to hold beyond PT.

From the phenomenological point of view, we are interested here in *deep inelastic lepton-hadron scattering* (DIS) processes. DIS is a relevant experimental technique in QCD because, through the deep inelastic scattering of leptons off hadronic targets, it is possible to determine the quark and gluon structure of hadrons. On the one hand, in DIS processes, the invariant cross-section is proportional to the contraction of the leptonic and hadronic tensors, $L_{\mu\nu}W^{\mu\nu}$. In particular, the hadronic tensor is expressed in terms of the invariant hadronic structure functions, which provide information about the internal structure of hadrons, according to the parton model. On the other hand, the total cross section is expressed in terms of the (electromagnetic) current commutator which, in DIS processes implies the computation of the Green function of the product of two electromagnetic currents, $j_\mu(x)j_\nu(0)$, in the light-cone region, $x^2 \sim 0$, for which the OPE is applied.

What it is important here, is that the moments of the structure functions can be related to the OPE expansion through certain moment-sum-rules. In particular, the moment-sum-rules relate the moments of structure functions to products of the singular c-coefficients in the OPE expansion with matrix elements of the composite fields. While the c-coefficients may be treated in perturbation theory, the matrix elements are related to the long-distance properties. Therefore, the matrix elements may only be determined using experimental input or, theoretically, via non-perturbative methods. It is then here where the application of lattice QCD becomes important. The regular composite fields entering the matrix elements in DIS processes may be classified according to the twist number, τ_n, and they are denoted twist-n operators. The twist number is defined as the difference between the dimension of the operator and its spin, $\tau_n = \dim - \text{spin}$. At sufficiently large momentum transferred [2], the largest contribution comes from the composite operators with the lowest twist, twist-2, and higher twist contributions are rather small. Twist-2 operators are made of 2-fields (quark and/or gluon fields) and may be classified, according to their flavor structure, in *singlet* or *non-singlet* twist-2 composite operators.

In our particular case in this thesis, we only deal with non-singlet composite fields made up of quark and anti-quark fields. In this case, the relevant gauge-invariant composite operator, with $\tau_n = 2$, is

$$O^a_{\mu_1\cdots\mu_n}(x) = \mathrm{i}^{n-1}\, S\overline{\psi}(x)\gamma_{\mu_1} \overset{\leftrightarrow}{D}_{\mu_2} \cdots \overset{\leftrightarrow}{D}_{\mu_n} \frac{\tau^a}{2}\psi(x) + \text{`trace terms'}\,. \tag{10.2}$$

The symmetrization in the Lorentz indices, S, is required because we deal here with unpolarized

[2] The momentum transferred is defined as $Q^2 = -q^2$, where $q_\mu = p'_\mu - p_\mu$ with p_μ (p'_μ) the initial (final) momentum of the electron in the DIS processes.

scatterings and the 'trace terms' (terms with $g_{\mu_i\mu_j}$) in order to provide the composite field with a definite spin. The covariant derivative, $\overset{\leftrightarrow}{D}_{\mu_i}$, is defined as the combination

$$\overset{\leftrightarrow}{D}_{\mu_i} = \frac{\overrightarrow{D}_{\mu_i} - \overleftarrow{D}_{\mu_i}}{2}\,, \tag{10.3}$$

with $\overrightarrow{D}_{\mu_i}$ and $\overleftarrow{D}_{\mu_i}$ the covariant derivatives acting on right and left, respectively. (Note that here we define the derivative $\overset{\leftrightarrow}{D}_{\mu}$ with the opposite convention than in Eq. (5.59) of Chap. 5. During the present chapter the convention in Eq. (10.3) is employed).

In the case of the lowest moment, the first moment, Eq. (10.2) reduces to

$$O^a_{\mu\nu}(x) = \mathrm{i}\, S\overline{\psi}(x)\gamma_\mu \overset{\leftrightarrow}{D}_\nu \frac{\tau^a}{2}\psi(x) + \text{'trace terms'}\,. \tag{10.4}$$

These composite fields are scale-dependent quantities which need to be renormalized, $O_{\mathrm{R}} = Z_{\mathrm{O}}^{-1} O_{\mathrm{B}}$, with O_{B} the bare operator and Z_{O} its renormalization constant. In the present chapter we are interested in the renormalization of the non-singlet twist-2 quark operators related to the first moments of structure functions, Eq. (10.4). A detailed description of the operators and the renormalization prescription, together with our results for the Z-factors and SSFs are presented in all remaining sections of this chapter.

10.2. Twist-2 non-singlet quark operators

After the previous discussion of the main concepts, we may now give a precise definition of the non-singlet twist-2 quark local composite operator related to the first moment of unpolarized structure functions. Our starting point is the definition of the corresponding operator in Minkowski space. Then, performing a Wick's rotation we obtain the expression of the operator in Euclidean space. We will eventually give the definition in Euclidean space on the lattice, in the twisted basis.

Twist-2 operator in Minkowski space

The general expression for the twist-2 non-singlet quark operator in Minkowski space is given by [107]

$$O^a_{\mu_1\cdots\mu_n}(x) = \mathrm{i}^{n-1}\overline{\psi}(x)\,\gamma_{\{\mu_1} \overset{\leftrightarrow}{D}_{\mu_2} \cdots \overset{\leftrightarrow}{D}_{\mu_n\}} \frac{\tau^a}{2}\,\psi(x)\,. \tag{10.5}$$

The definition of the curly braket here is

$$f_{\{\mu_1\cdots\mu_n\}} = S(f_{\mu_1\cdots\mu_n}) + \text{'trace terms'} \tag{10.6}$$

with S denoting symmetrization in the Lorentz indices,

$$S(f_{\mu_1\cdots\mu_n}) \equiv \frac{1}{n!}\,(f_{\mu_1\cdots\mu_n} + \text{permutations})\,. \tag{10.7}$$

In our case, we consider the twist-2 non-singlet quark operator corresponding to the first moment, which is then given by

$$O^a_{\mu\nu}(x) = \mathrm{i}\overline{\psi}(x)\,\gamma_{\{\mu} \overset{\leftrightarrow}{D}_{\nu\}} \frac{\tau^a}{2}\,\psi(x)\,. \tag{10.8}$$

In this particular case,

$$f_{\{\mu\nu\}} = S(f_{\mu\,\nu}) + \text{'trace terms'} \tag{10.9}$$

with

$$S(f_{\mu\nu}) = \frac{1}{2}\,(f_{\mu\nu} + f_{\nu\mu})\,. \tag{10.10}$$

The trace terms are expressed as $g_{\mu\nu}O$ and are determined by imposing the condition,

$$g^{\mu\nu} f_{\{\mu\nu\}} = 0\,. \tag{10.11}$$

Developing this equation for our case then we have

$$g^{\mu\nu}\Big(\frac{1}{2!}(\gamma_\mu \overleftrightarrow{D}_\nu + \gamma_\nu \overleftrightarrow{D}_\mu) + g_{\mu\,\nu}O\Big) = 0\,, \tag{10.12}$$

which has as a result for the trace terms

$$O = -\frac{1}{4} g^{\alpha\beta}\,\gamma_\alpha \overleftrightarrow{D}_\beta = -\frac{1}{4} g^{\alpha\beta}\, S(\gamma_\alpha \overleftrightarrow{D}_\beta)\,. \tag{10.13}$$

Therefore, the final expression for the operator is

$$O^a_{\mu\nu}(x) = \mathrm{i}\overline{\psi}(x)\left[S(\gamma_\mu \overleftrightarrow{D}_\nu) - \frac{1}{4} g_{\mu\nu}\, g^{\alpha\beta}\, S(\gamma_\alpha \overleftrightarrow{D}_\beta)\right]\frac{\tau^a}{2}\,\psi(x)\,. \tag{10.14}$$

Note that, only if $\mu = \nu$ the trace terms contribute.

Twist-2 operator in Euclidean space

In Euclidean space the twist-2 non-singlet operator takes the form

$$O^a_{\mu\nu}(x) = \overline{\psi}(x)\,\gamma_{\{\mu} \overleftrightarrow{D}_{\nu\}} \frac{\tau^a}{2}\,\psi(x)\,, \tag{10.15}$$

where now the gamma matrices are expressed in Euclidean space and the Dirac operator is also expressed in Euclidean space. Expanding this expression as before, we obtain the Euclidean expression for the operator,

$$O^a_{\mu\nu}(x) = \overline{\psi}(x)\left[S(\gamma_\mu \overleftrightarrow{D}_\nu) - \frac{1}{4}\delta_{\mu\nu}\,\delta^{\alpha\beta}\, S(\gamma_\alpha \overleftrightarrow{D}_\beta)\right]\frac{\tau^a}{2}\,\psi(x)\,. \tag{10.16}$$

Twist-2 operator on the lattice

On the lattice, Eq. (10.16) takes the same form as in the continuum,

$$O^a_{\mu\nu}(x) = \overline{\psi}(x)\left[S(\gamma_\mu \overleftrightarrow{D}_\nu) - \frac{1}{4}\delta_{\mu\nu}\,\delta^{\alpha\beta}\, S(\gamma_\alpha \overleftrightarrow{D}_\beta)\right]\frac{\tau^a}{2}\,\psi(x)\,, \tag{10.17}$$

with the covariant derivative, $\overleftrightarrow{D}_\mu$, as defined in Eq. (10.3), but where now $\overrightarrow{D}_\mu$ and $\overleftarrow{D}_\mu$ are the lattice symmetric covariant derivatives acting on right and left, respectively, as defined in Eq. (A.28) and Eq. (A.29).

One important difference between the lattice and continuum formulations is that, on the lattice, 4-dimensional rotational invariance, $O(4)$, is broken into hypercubic symmetry, $H(4)$. Therefore, on the lattice there are more than one representations for a given continuum operator. In the case of the non-singlet twist-2 quark operator related to the first moment of the unpolarized structure functions, the two representations are those with $\mu \neq \nu$ or with $\mu = \nu$.

In particular, we consider here two cases: $\mu = 1, \nu = 2$ and $\mu = \nu = 0$. The corresponding expressions are then [3],

$$O^a_{12}(x) = \frac{1}{2}\,\overline{\psi}(x)\left[\gamma_1 \overleftrightarrow{D}_2 + \gamma_2 \overleftrightarrow{D}_1\right]\frac{\tau^a}{2}\,\psi(x) \tag{10.18}$$

and

$$O^a_{44}(x) = \frac{3}{4}\,\overline{\psi}(x)\left[\gamma_0 \overleftrightarrow{D}_0 - \frac{1}{3}\sum_{k=1}^{3}\gamma_k \overleftrightarrow{D}_k\right]\frac{\tau^a}{2}\,\psi(x)\,. \tag{10.19}$$

Twist-2 operator on the lattice in the twisted basis

Since we compute quantities within the χSF scheme and we work in the twisted basis, we give here the expressions of the twist-2 operators in the twisted basis. These can be obtained from the corresponding expressions in the physical basis, applying the rotation Eq. (2.97) in the continuum theory and then directly translating the fields and derivatives to the lattice, as it has been done above in the physical basis. Performing the rotation we obtain

$$O^a_{\mu\nu}(x) = \overline{\chi}(x)\, e^{\mathrm{i}\frac{\alpha}{2}\gamma_5\tau^3}\,\gamma_{\{\mu}\overleftrightarrow{D}_{\nu\}}\,\frac{\tau^a}{2}\,e^{\mathrm{i}\frac{\alpha}{2}\gamma_5\tau^3}\,\chi(x) \tag{10.20}$$

and depending on the flavor structure,

$$O^a_{\mu\nu}(x) = \begin{cases} \overline{\chi}(x)\,\gamma_{\{\mu}\overleftrightarrow{D}_{\nu\}}\left[\cos(\alpha)\,\frac{\tau^a}{2} + \epsilon_{ab3}\sin(\alpha)\,\gamma_5\,\frac{\tau^b}{2}\right]\chi(x) & (a=1,2)\,, \\ \overline{\chi}(x)\,\gamma_{\{\mu}\overleftrightarrow{D}_{\nu\}}\,\frac{\tau^a}{2}\,\chi(x) & (a=3)\,, \end{cases} \tag{10.21}$$

with ϵ_{abc} the totally anti-symmetric tensor and $\epsilon_{123} = 1$. In the particular case of maximal twist, $\alpha = \pi/2$, this expression reduces to

$$O^a_{\mu\nu}(x) = \begin{cases} \epsilon_{ab3}\,\overline{\chi}(x)\,\gamma_{\{\mu}\overleftrightarrow{D}_{\nu\}}\,\gamma_5\,\frac{\tau^b}{2}\,\chi(x) & (a=1,2)\,, \\ \overline{\chi}(x)\,\gamma_{\{\mu}\overleftrightarrow{D}_{\nu\}}\,\frac{\tau^a}{2}\,\chi(x) & (a=3)\,. \end{cases} \tag{10.22}$$

Eventually we will compute correlation functions boundary to bulk, with the twist-2 operators inserted in the bulk of the lattice at a certain space-time point x. The boundary interpolating fields at $x_0 = 0$ that we consider here are the following, expressed in the physical basis,

$$\mathcal{O}^a_{\gamma_k} = a^6 \sum_{\vec{y},\vec{z}} \overline{\zeta}(\vec{y})\gamma_k\frac{\tau^a}{2}\zeta(\vec{z})\,. \tag{10.23}$$

Performing a rotation to the twisted basis, with maximal twist angle, such boundary interpolating fields take the form

$$\mathcal{O}^a_{\gamma_k} = \begin{cases} \epsilon_{ab3}\,a^6\,\sum_{\vec{y},\vec{z}}\,\overline{\zeta}(\vec{y})\,\gamma_k\gamma_5\frac{\tau^b}{2}\,\widetilde{Q}_-\,\zeta(\vec{z}) & (a=1,2)\,, \\ a^6\,\sum_{\vec{y},\vec{z}}\,\overline{\zeta}(\vec{y})\,\gamma_k\frac{\tau^a}{2}\,\widetilde{Q}_-\,\zeta(\vec{z}) & (a=3)\,. \end{cases} \tag{10.24}$$

[3] Note that the operator with $\mu = \nu = 0$ is labelled with the subscript 44 instead of 00 which would be a more appropriate choice here. However, the 44 notation is the usual labeling in the literature for this operator. We therefore keep the 44 labeling in order to match the notation of previous publications.

In particular, we consider two cases for the gamma matrices at the boundaries, γ_k with $k = 1, 2$. The case $k = 1$ ($k = 2$) will be used when computing the correlation function of the operator O^a_{44} (O^a_{12}). Therefore, the correlation functions that we consider here are the following,

$$g_{12}(x_0,\theta) \equiv -\frac{a^9}{L^3} \sum_{\vec{x},\vec{y},\vec{z}} \langle \overline{\chi}(x)\, \gamma_{\{1} \overset{\leftrightarrow}{D}_{2\}}\, \gamma_5 \frac{\tau^1}{2}\, \chi(x)\, \overline{\zeta}(\vec{y})\, \gamma_2\gamma_5 \frac{\tau^1}{2}\, \widetilde{Q}_-\, \zeta(\vec{z})\rangle\,, \tag{10.25a}$$

$$g_{44}(x_0,\theta) \equiv -\frac{a^9}{L^3} \sum_{\vec{x},\vec{y},\vec{z}} \langle \overline{\chi}(x)\, \gamma_{\{0} \overset{\leftrightarrow}{D}_{0\}}\, \gamma_5 \frac{\tau^1}{2}\, \chi(x)\, \overline{\zeta}(\vec{y})\, \gamma_1\gamma_5 \frac{\tau^1}{2}\, \widetilde{Q}_-\, \zeta(\vec{z})\rangle\,. \tag{10.25b}$$

Note that we have chosen only the cases where the two flavor matrices, in the bulk and at the boundary, are the same and we have picked up only the component τ^1. The reason for choosing both matrices to be the same is that this is the only possibility for the correlation functions not to vanish, due to symmetry arguments. Amongst the three possibilites, $\tau^{1,2,3}$, all of them should provide the same value in the continuum limit. On the lattice, due to our particular setup where flavor symmetry is broken, there is a distinction between $\tau^{1,2}$ and τ^3. Even if in the case with τ^3 the expressions look simpler, because this correlation function does not rotate, the appearance of disconnected pieces, which are very costly from the numerical point of view, makes us to decide for the other cases $\tau^{1,2}$. Since these two cases are exactly equivalent, we choose just τ^1. For a detailed treatment of these correlation functions see App. H.

There is a remark to be made. Correlation functions of the operator for the first moment involve two directions. In order for the correlation functions not to vanish, the two directions must be provided by external vectors. One is provided here by the parameter $\vec{\theta}$, as it was discussed in detail in [73]. The other is given by the contraction matrix, γ_k, entering the definition of the boundary operators.

10.3. SSF and renormalization prescription

As in previous chapters, we define here the SSF of a scale-dependent operator, $O_{\rm R}(L)$, which in our particular case will be the non-singlet twist-2 local operator corresponding to the first moment of the unpolarized structure function, $O^a_{\mu\nu}(L)$. Variations of the renormalized operator, $O_{\rm R}(L)$, under changes in the renormalization scale, $1/L$, are described by the anomalous dimension of the operator, $\gamma_{\rm O}(\overline{g}(L))$, through the RG equations as follows

$$L\,\frac{\partial O_{\rm R}(L)}{\partial L} = -\,\gamma_{\rm O}(\overline{g}(L))\, O_{\rm R}(L)\,. \tag{10.26}$$

The operator is renormalized as follows,

$$O_{\rm R}(L) = Z_{\rm O}^{-1}(g_0, L)\, O_{\rm B}(g_0)\,, \tag{10.27}$$

with $Z_{\rm O}$ the renormalization constant and $O_{\rm B}$ the bare operator. It is then possible to rewrite the Eq. (10.26) in terms of $Z_{\rm O}$ as,

$$L\,\frac{\partial Z_{\rm O}(L)}{\partial L} = \gamma_{\rm O}(\overline{g}(L))\, Z_{\rm O}(L)\,. \tag{10.28}$$

The integrated form of Eq. (10.28) reads as follows,

$$Z_{\rm O}(sL) = \sigma_{\rm Z_O}(s, \overline{g}^2(L))\, Z_{\rm O}(L)\,, \qquad \sigma_{\rm Z_O}(s, \overline{g}^2(L)) = \exp\Big\{ -\int_{\overline{g}(L)}^{\overline{g}(sL)} dg\, \frac{\gamma_{\rm O}(g)}{\beta(g)} \Big\}\,. \tag{10.29}$$

In this expression, β is the Callan-Symanzik β-function describing the changes in the gauge coupling, $\overline{g}(L)$, with the renormalization scale. As the β- and τ-functions, $\gamma_{\rm O}$ is only known perturbatively. Its asymptotic expansion is given as,

$$\gamma_{\rm O}(\overline{g}) \overset{\overline{g}\to 0}{\sim} -\overline{g}^2 \sum_{n=0}^{\infty} \gamma_n \, \overline{g}^{2n} \,. \tag{10.30}$$

The 1-loop anomalous dimension,

$$\gamma_0 = \frac{16}{3} C_{\rm F} (4\pi)^{-2} \,, \qquad C_{\rm F} = \frac{N_{\rm C}^2 - 1}{2N_{\rm C}} \,, \tag{10.31}$$

is renormalization-scheme-independent while all other higher order coefficients are scheme-dependent.

The exact expression defining the RGI operator, $O_{\rm RGI}$, is

$$O_{\rm RGI} = O_{\rm R}(L) \, (\overline{g}^2(L))^{-\gamma_0/(2b_0)} \exp\left\{ -\int_0^{\overline{g}(L)} {\rm d}g \left[\frac{\gamma_{\rm O}(g)}{\beta(g)} - \frac{\gamma_0}{b_0 g} \right] \right\} . \tag{10.32}$$

As the RGI quark masses, RGI operators are not only scale-independent but also scheme-independent.

In the present chapter we are concerned with the SSF, $\sigma_{\rm Z_O}(s, \overline{g}^2(L))$, of the operator $O_{\rm R}$, or equivalently, of its renormalization constant. The SSF provides the evolution of the renormalization constant, $Z_{\rm O}(L)$, from a value of the renormalization scale $1/L$ to the value $1/sL$, where s is a certain scale factor. From the definition given in Eq. (10.29), the SSF in the continuum is the following,

$$\sigma_{\rm Z_O}(s, \overline{g}^2(L)) = \frac{Z_{\rm O}(g_0, sL)}{Z_{\rm O}(g_0, L)} \,. \tag{10.33}$$

Using a lattice as a regulator, lattice artifacts must be taken into account and therefore the renormalized operator is given as,

$$O_{\rm R}(L) = \lim_{a\to 0} Z_{\rm O}^{-1}(g_0, L/a) \, O_{\rm B}(g_0) \,, \tag{10.34}$$

with $O_{\rm B}(g_0)$ the bare operator and a the lattice spacing.

We can now choose a renormalization prescription for the twist-2 operator within the χSF scheme. In particular we impose the renormalization condition

$$Z_{\rm O}(g_0, L/a) = c(\theta, a/L) \, \frac{g_{\rm O}(L/2, \theta)}{\sqrt{g_1(\theta)}} \Big|_{m=0} \,. \tag{10.35}$$

In this expression, $m = 0$ indicates that the renormalization condition is imposed at zero quark mass which, as discussed in previous chapters, corresponds to set the bare quark mass to its critical value, $m_0 = m_c$. The factor $c(\theta, a/L)$ is chosen such that $Z_{\rm O}$ takes the correct value at tree-level, $Z_{\rm O}(0, L/a) = 1$. Therefore it is defined as

$$c(\theta, a/L) \equiv \frac{\sqrt{g_1(\theta)}}{g_{\rm O}(L/2, \theta)} \Big|_{m_0=0}^{\rm tree} \,. \tag{10.36}$$

In this expression, g_1 is the two-point function defined in previous chapters and given e.g. in Eq. (8.12). The other two-point function, $g_{\rm O}$, is either g_{12} or g_{44} (cf. Eq. (10.25)), depending if we consider the SSF of the operator O_{12}^a or O_{44}^a. In order to determine the renormalization prescription completely, a value of θ has to be chosen. In particular, we consider here two cases,

$\vec{\theta} = (0.5, 0.5, 0.5)$ and $\vec{\theta} = (1, 0, 0)$. The reason for studying the case with $\vec{\theta} = (1, 0, 0)$ is that this is the only choice with $\vec{\theta} \neq \vec{0}$ for which there are data available from the standard SF [73] which, thus, allows us to test the continuum limit of the χSF. Although there are no SF data available for the choice $\vec{\theta} = (0.5, 0.5, 0.5)$, we have also analyzed this setup, since this is the usual choice when computing quantities within the SF formulation, as it was shown with the results presented in Chap. 8 and Chap. 9. Moreover, this additional choice for the parameter $\vec{\theta}$ allows us to check the differences in the relative statistical errors when changing renormalization prescription through $\vec{\theta}$. All correlation functions are evaluated at $x_0 = T/2$, where $T = L$ is the time extent of the lattice. The scale factor is always set to $s = 2$.

Given a fixed value of the renormalization scale, defined through $\overline{g}^2(L) = u$, and a fixed value of the lattice spacing, L/a, the lattice SSF of O, defined in the chiral limit, is given as

$$\Sigma_{\mathrm{Z_O}}(s, u, a/L) = \frac{Z_{\mathrm{O}}(g_0, sL/a)}{Z_{\mathrm{O}}(g_0, L/a)}\Big|_{m=0,\, \overline{g}^2(L)=u} . \tag{10.37}$$

In the continuum limit the SSF is finite and takes the value

$$\sigma_{\mathrm{Z_O}}(s, u) = \lim_{a\to 0} \Sigma_{\mathrm{Z_O}}(s, u, a/L) = \frac{O_{\mathrm{R}}(L)}{O_{\mathrm{R}}(sL)}\Big|_{\overline{g}^2(L)=u} , \tag{10.38}$$

with $O_{\mathrm{R}}(L)$ the renormalized operator at a given value of the physical scale, $1/L$, and within the χSF renormalization scheme.

10.4. Renormalization factors and lattice SSFs

From the definitions given in the previous sections of this chapter and the chosen renormalization prescription, we determine the renormalization factors of the operators O^a_{12} and O^a_{44} within the χSF scheme, at finite lattice spacing. Results are presented for several β-values and at three values of the renormalization scale, $1/L$. In particular, at the values such that $\overline{g}^2 = 0.9944$, $\overline{g}^2 = 2.4484$ and $L = 1.436\, r_0$. These results are presented in Tab. 10.1 and Tab. 10.2 for O^a_{12} and O^a_{44}, respectively. In both cases we show results at $\vec{\theta} = (0.5, 0.5, 0.5)$ and $\vec{\theta} = (1, 0, 0)$.

At the two most perturbative couplings, $\overline{g}^2 = 0.9944$ and $\overline{g}^2 = 2.4484$, we have determined the lattice SSFs for both operators, whose values are shown in Tab. 10.3 for $\vec{\theta} = (0.5, 0.5, 0.5)$ and in Tab. 10.4 for $\vec{\theta} = (1, 0, 0)$. In Tab. 10.4 we have also added the values obtained for the lattice SSFs using the SF scheme with standard and non-perturbatively improved Wilson fermions. These values were taken from [73], with available data only at the intermediate coupling, $\overline{g}^2 = 2.4484$. From the data that we obtain for the SSFs within the χSF scheme, we conclude that the discretization effects are rather small, as it will be discussed in more detail below in Sec. 10.5, where we present our results for the extrapolation of the SSFs to the continuum limit.

Concerning our results for the Z-factors in the χSF scheme, Tab. 10.1 and Tab. 10.2, at the three values of the renormalization scale and for all values of the lattice spacing that we have analyzed, we conclude the following. For any of the two operators, O^a_{12} or O^a_{44}, the relative statistical errors in the renormalization constants, $\Delta Z_{\mathrm{O}}/Z_{\mathrm{O}}$, are always smaller for $\vec{\theta} = (1, 0, 0)$ than for $\vec{\theta} = (0.5, 0.5, 0.5)$ by nearly a factor of 2. Moreover, at fixed values of all parameters, the relative errors in $Z_{\mathrm{O}_{44}}$ are always slightly larger than those of $Z_{\mathrm{O}_{12}}$. These results are encouraging, since they are consistent with the pattern discussed previously in [73] within the standard SF setup. In that publication it was shown that the relative statistical errors in $Z_{\mathrm{O}_{12}}$ and $Z_{\mathrm{O}_{44}}$ increase when the value of $\vec{\theta}$ decreases in modulus, for values such that the modulus of $\vec{\theta}$ is smaller or equal than 1, as it is our case here. There it was also shown that the errors in

		$\vec{\theta} = (0.5, 0.5, 0.5)$		$\vec{\theta} = (1, 0, 0)$	
L/a	β	$Z_{\mathrm{O}_{12}}(g_0, L/a)$	$Z_{\mathrm{O}_{12}}(g_0, 2L/a)$	$Z_{\mathrm{O}_{12}}(g_0, L/a)$	$Z_{\mathrm{O}_{12}}(g_0, 2L/a)$
Hadronic scale: $L = 1.436\, r_0$					
8	6.0219	0.395 (12)		0.3746 (59)	
10	6.1628	0.374 (13)		0.3509 (59)	
12	6.2885	0.348 (15)		0.3547 (77)	
16	6.4956	0.353 (21)		0.341 (11)	
Intermediate scale: $\bar{g}^2 = 2.4484$					
8	7.0197	0.6077 (80)	0.482 (13)	0.5675 (41)	0.4498 (64)
12	7.3551	0.613 (11)	0.495 (16)	0.5634 (58)	0.4401 (84)
16	7.6101	0.611 (14)	0.460 (16)	0.5587 (70)	0.4383 (84)
Perturbative scale: $\bar{g}^2 = 0.9944$					
8	10.3000	0.7989 (44)	0.7570 (68)	0.7717 (25)	0.7287 (36)
12	10.6086	0.7800 (66)	0.7597 (62)	0.7530 (35)	0.7295 (34)
16	10.8910	0.7762 (83)	0.730 (11)	0.7511 (45)	0.7161 (68)

Table 10.1.: Renormalization factors $Z_{\mathrm{O}_{12}}$ for $\vec{\theta} = (0.5, 0.5, 0.5)$ and $\vec{\theta} = (1, 0, 0)$. Results are shown for the χSF with standard Wilson fermions at three values of the renormalization scale and for several values of the lattice spacing.

$Z_{\mathrm{O}_{44}}$ are slightly larger than those in $Z_{\mathrm{O}_{12}}$, which is consistent with what we observe from our χSF data.

10.5. Continuum limit of the SSF

In this section we present our results for the continuum extrapolation of the lattice SSFs discussed in Sec. 10.4. We have performed fits of the lattice data in Tab. 10.3 and Tab. 10.4, linear in $(a/L)^2$ for the χSF formulation and linear in a/L for the SF with standard and improved Wilson fermions. We have performed linear fits in a/L for the SF data even in the improved formulation because, although the action is improved in this setup, it is not the case for the twist-2 operators, for which no improvement counterterm has been taken into account. On the contrary, within the χSF it is not necessary to consider additional counterterms to the operators, since this formulation is expected to preserve bulk automatic $O(a)$-improvement, up to, possibly, small boundary effects. The results of the fits are presented in Tab. 10.5 and Tab. 10.6.

The data for the lattice SSFs, Tab. 10.3 and Tab. 10.4, are plotted in Fig. 10.1, Fig. 10.2, Fig. 10.3 and Fig. 10.4, where we show the continuum limit approach of all SSFs that we have computed. In these figures we have also plotted the corresponding values of the SSFs in the continuum limit and the fitting curves, as given in Tab. 10.5 and Tab. 10.6.

In Fig. 10.1 and Fig. 10.2 we show the continuum limit approach of the SSFs of the operators O^a_{12} and O^a_{44}, respectively, within the χSF scheme. In both figures we plot the results for both values of $\vec{\theta}$ and the two scales where we have computed the SSFs. Results are presented as a function of $(a/L)^2$, since only χSF data are considered. We can conclude, from these figures and the corresponding tables, that the cutoff effects in the χSF SSFs are consistent with $O(a^2)$ and are, indeed, very small. We can also see that the discretization effects are similar for different values of the renormalized coupling and $\vec{\theta}$. Note that the values in the continuum limit for different values of $\vec{\theta}$ are not expected to agree, since different $\vec{\theta}$ values correspond to different renormalization prescriptions.

In Fig. 10.3 and Fig. 10.4 we compare the results for the SSFs of O^a_{12} and O^a_{44} as obtained

		$\vec{\theta} = (0.5, 0.5, 0.5)$		$\vec{\theta} = (1, 0, 0)$	
L/a	β	$Z_{\mathrm{O}_{44}}(g_0, L/a)$	$Z_{\mathrm{O}_{44}}(g_0, 2L/a)$	$Z_{\mathrm{O}_{44}}(g_0, L/a)$	$Z_{\mathrm{O}_{44}}(g_0, 2L/a)$
Hadronic scale: $L = 1.436\, r_0$					
8	6.0219	0.319 (10)		0.3416 (62)	
10	6.1628	0.307 (10)		0.3305 (62)	
12	6.2885	0.280 (14)		0.3217 (86)	
16	6.4956	0.261 (19)		0.297 (12)	
Intermediate scale: $\overline{g}^2 = 2.4484$					
8	7.0197	0.5174 (75)	0.388 (12)	0.5382 (44)	0.4203 (71)
12	7.3551	0.532 (11)	0.404 (16)	0.5340 (64)	0.4189 (93)
16	7.6101	0.521 (14)	0.405 (17)	0.5236 (82)	0.4417 (86)
Perturbative scale: $\overline{g}^2 = 0.9944$					
8	10.3000	0.7369 (46)	0.6781 (71)	0.7529 (26)	0.7044 (39)
12	10.6086	0.7145 (64)	0.6882 (68)	0.7334 (37)	0.7068 (39)
16	10.8910	0.7114 (88)	0.686 (11)	0.7301 (51)	0.7135 (65)

Table 10.2.: Renormalization factors $Z_{\mathrm{O}_{44}}$ for $\vec{\theta} = (0.5, 0.5, 0.5)$ and $\vec{\theta} = (1, 0, 0)$. Results are shown for the χSF with standard Wilson fermions at three values of the renormalization scale and for several values of the lattice spacing.

χSF		
L/a	$\Sigma_{\mathrm{O}_{12}}(2, u, a/L)$	$\Sigma_{\mathrm{O}_{44}}(2, u, a/L)$
Intermediate scale: $\overline{g}^2 = 2.4484$		
8	0.793 (24)	0.751 (26)
12	0.809 (31)	0.761 (34)
16	0.752 (31)	0.777 (39)
Perturbative scale: $\overline{g}^2 = 0.9944$		
8	0.948 (10)	0.920 (11)
12	0.974 (11)	0.963 (13)
16	0.940 (18)	0.964 (20)

Table 10.3.: SSF of O_{12} and O_{44} at finite lattice spacing, $\Sigma_{\mathrm{O}_{12}}$ and $\Sigma_{\mathrm{O}_{44}}$. Results are shown for the χSF with standard Wilson fermions at two values of the renormalization scale and for several values of the lattice spacing. $\vec{\theta} = (0.5, 0.5, 0.5)$.

	$\Sigma_{\mathrm{O}_{12}}(2, u, a/L)$			$\Sigma_{\mathrm{O}_{44}}(2, u, a/L)$		
L/a	χSF	SF (Clover)	SF (Wilson)	χSF	SF (Clover)	SF (Wilson)
Intermediate scale: $\overline{g}^2 = 2.4484$						
8	0.793 (13)	0.8223 (77)	0.8811 (85)	0.781 (15)	0.7885 (91)	0.7935 (119)
12	0.781 (17)	0.8053 (77)	0.8589 (136)	0.784 (20)	0.7921 (94)	0.7942 (186)
16	0.785 (18)	0.8116 (107)	0.8519 (85)	0.844 (21)	0.8036 (127)	0.7823 (115)
Perturbative scale: $\overline{g}^2 = 0.9944$						
8	0.9443 (56)			0.9355 (62)		
12	0.9688 (64)			0.9637 (72)		
16	0.953 (11)			0.977 (11)		

Table 10.4.: SSF of O_{12} and O_{44} at finite lattice spacing, $\Sigma_{\mathrm{O}_{12}}$ and $\Sigma_{\mathrm{O}_{44}}$. Results are shown for the χSF with standard Wilson fermions and also for the SF [73] with improved and standard Wilson fermions at two values of the renormalization scale and for several values of the lattice spacing. $\vec{\theta} = (1, 0, 0)$.

χSF		
	O_{12}	O_{44}
Intermediate scale: $\overline{g}^2 = 2.4484$		
$\sigma_{\mathrm{O}}(2,u)$	0.766 (35)	0.779 (42)
slope	2 (3)	-2 (4)
χ^2/dof	1.4081	0.0421
Perturbative scale: $\overline{g}^2 = 0.9944$		
$\sigma_{\mathrm{O}}(2,u)$	0.970 (16)	0.989 (19)
slope	-1 (1)	-4 (2)
χ^2/dof	3.3364	0.2731

Table 10.5.: Continuum limit of the SSF, $\sigma_{\mathrm{O}_{12}}$ and $\sigma_{\mathrm{O}_{44}}$, of the operators O_{12} and O_{44}. Results are shown for the χSF with standard Wilson fermions at two values of the renormalization scale. $\vec{\theta} = (0.5, 0.5, 0.5)$. These results correspond to linear fits of the data in Tab. 10.3. The fits are linear in $(a/L)^2$.

from the three formulations, χSF and SF with standard and improved Wilson fermions. Only the data at the intermediate coupling and for $\vec{\theta} = (1, 0, 0)$ are plotted. For a comparison with the SF, the data are plotted here as a function of a/L, although the values in the continuum limit for the χSF have been obtained from linear fits in $(a/L)^2$. As stated above, although the lattice data for the SF have been taken from [73], in this thesis we have performed our own fits towards the continuum limit. These results, for the three formulations, may be seen in Tab. 10.6. Additionally in Tab. 10.5 we show the results at $\vec{\theta} = (0.5, 0.5, 0.5)$ only for the χSF formulation. From Fig. 10.3, Fig. 10.4 and Tab. 10.6 we conclude that the SF improved and χSF formulations show less cutoff effects than the SF with standard Wilson fermions. Moreover, there is a very good agreement within statistical errors between the χSF and the improved SF formulations in the continuum limit. There is also agreement between the improved and unimproved formulations of the standard SF, although the agreement is better in the former case. Between the χSF and the standard SF with unimproved Wilson fermions, the values in the continuum differ by about 2σ for O^a_{12} and 2.5σ for O^a_{44}. In the case of O^a_{44}, the disagreement seems to be driven by statistical fluctuations at $L/a = 16$. Note that at the coarser lattices, $L/a = 8, 12$, there is perfect agreement between the data from the three formulations. Therefore, we can be confident that the data agree in the continuum limit.

In summary, we can conclude that there is agreement, within statistical errors, in the continuum limit amongst the results from the three formulations and therefore, the universality of the continuum limit is confirmed also through the SSFs of the twist-2 operators. Additionally, we observe that the scaling behavior of the SSFs obtained from the χSF is consistent with leading $O(a^2)$ discretization effects, which, furthermore, turn out to be rather small.

10.6. Z-factors at the matching scale and RGI Z-factors

The aim of this section is to determine the RGI Z-factors of the operators O^a_{12} and O^a_{44} using the χSF formulation. These factors then relate the bare and the RGI matrix elements of the corresponding operator.

As we did for the case of the pseudo-scalar density, we first study the dependence of the Z-factors on β, at the matching scale $L = 1.436\, r_0$, and determine the curve describing such a

	O_{12}			O_{44}		
	χSF	SF (Clover)	SF (Wil)	χSF	SF (Clover)	SF (Wil)
Intermediate scale: $\overline{g}^2 = 2.4484$						
$\sigma_{\mathrm{O}}(2,u)$	0.778 (20)	0.790 (19)	0.822 (18)	0.837 (23)	0.812 (23)	0.774 (25)
slope	1 (2)	0.25 (19)	0.47 (19)	-4 (2)	-0.19 (23)	0.17 (26)
χ^2/dof	0.0772	0.8338	0.0332	2.9018	0.2471	0.1586
Perturbative scale: $\overline{g}^2 = 0.9944$						
$\sigma_{\mathrm{O}}(2,u)$	0.9752 (97)			0.988 (10)		
slope	-1.89 (82)			-3.40 (88)		
χ^2/dof	2.9783			0.0534		

Table 10.6.: Continuum limit of the SSF, $\sigma_{\mathrm{O}_{12}}$ and $\sigma_{\mathrm{O}_{44}}$, of the operators O_{12} and O_{44}. Results are shown for the χSF with standard Wilson fermions and also for the SF with improved and standard Wilson fermions at two values of the renormalization scale. $\vec{\theta} = (1,0,0)$. These results correspond to linear fits of the data in Tab. 10.4. The fits are linear in $(a/L)^2$ for the χSF formulation while they are linear in a/L for the SF.

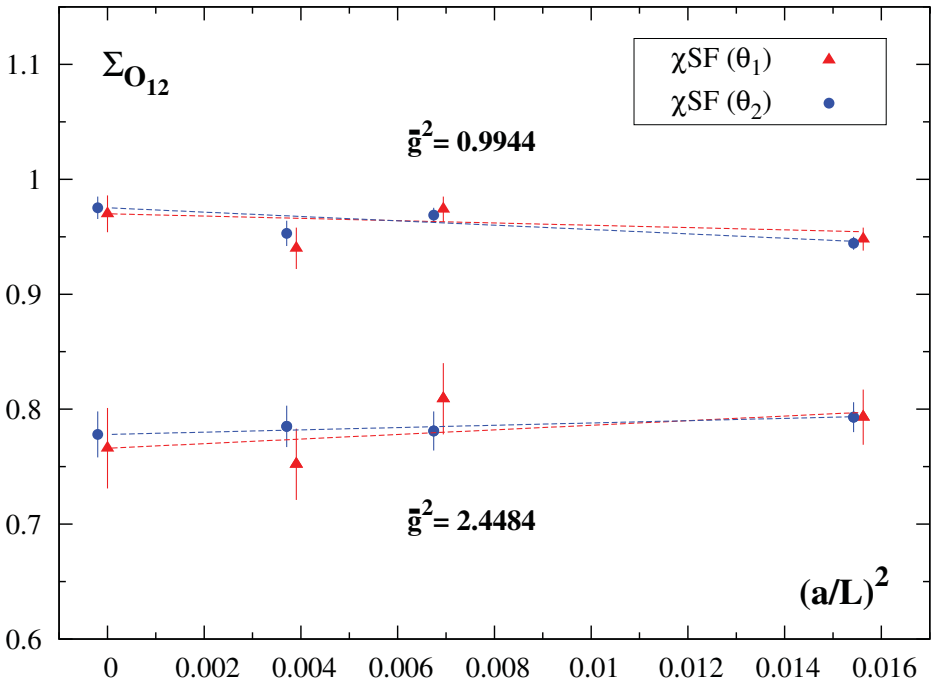

Figure 10.1.: Continuum limit extrapolation of the SSF of the operator O_{12}. Only χSF data are shown, both for $\theta_1 \equiv \vec{\theta} = (0.5, 0.5, 0.5)$ and $\theta_2 \equiv \vec{\theta} = (1,0,0)$, at the intermediate and perturbative scales. The extrapolations to the continuum limit are linear in $(a/L)^2$ as shown in Tab. 10.5 and Tab. 10.6. The values in the continuum limit are also plotted. The data from θ_2 have been plotted slightly displaced to the left.

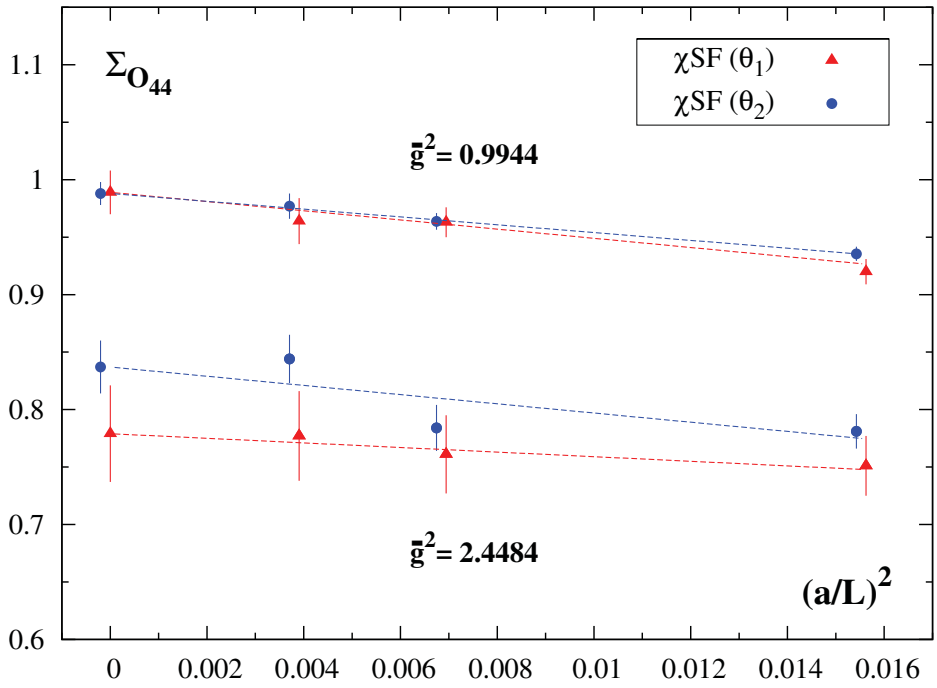

Figure 10.2.: Continuum limit extrapolation of the SSF of the operator O_{44}. Only χSF data are shown, both for $\theta_1 \equiv \vec{\theta} = (0.5, 0.5, 0.5)$ and $\theta_2 \equiv \vec{\theta} = (1, 0, 0)$, at the intermediate and perturbative scales. The extrapolations to the continuum limit are linear in $(a/L)^2$ as shown in Tab. 10.5 and Tab. 10.6. The values in the continuum limit are also plotted. The data from θ_2 have been plotted slightly displaced to the left.

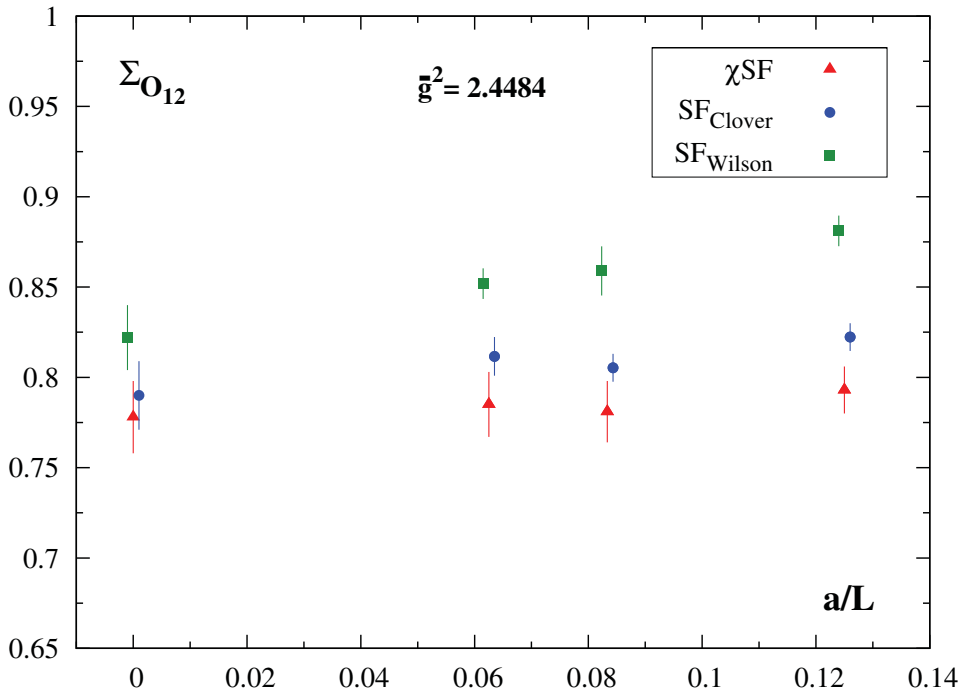

Figure 10.3.: Continuum limit approach of the SSF of the operator O_{12}. Data are shown for the χSF with standard Wilson fermions and for the SF with improved and standard Wilson fermions, at the intermediate scale and for $\vec{\theta} = (1, 0, 0)$. The continuum limit is performed according to Tab. 10.6: linear in $(a/L)^2$ for the χSF and linear in a/L for the SF with both regularizations. The continuum limit values are also plotted. The data from the SF have been plotted slightly displaced to the right and left, respectively, for the improved and unimproved formulations.

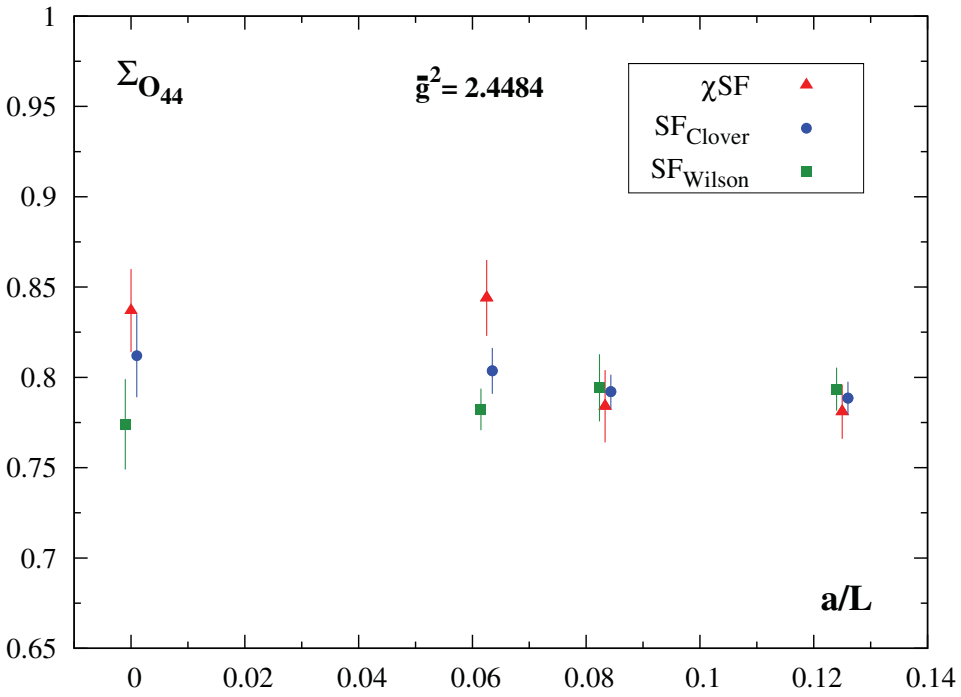

Figure 10.4.: Continuum limit approach of the SSF of the operator O_{44}. Data are shown for the χSF with standard Wilson fermions and for the SF with improved and standard Wilson fermions, at the intermediate scale and for $\vec{\theta} = (1, 0, 0)$. The continuum limit is performed according to Tab. 10.6: linear in $(a/L)^2$ for the χSF and linear in a/L for the SF with both regularizations. The continuum limit values are also plotted. The data from the SF have been plotted slightly displaced to the right and left, respectively, for the improved and unimproved formulations.

	$z_i(O_{12})$			$z_i(O_{44})$		
i	χSF	SF (Clover)	SF (Wilson)	χSF	SF (Clover)	SF (Wilson)
$\vec{\theta} = (0.5, 0.5, 0.5)$						
0	0.402 (14)			0.323 (12)		
1	-0.25 (15)			-0.12 (12)		
2	0.30 (29)			-0.02 (25)		
$\vec{\theta} = (1, 0, 0)$						
0	0.3761 (69)	0.3410 (31)	0.3659 (35)	0.3426 (73)	0.3450 (37)	0.3197 (44)
1	-0.151 (72)	-0.077 (31)	-0.102 (35)	-0.059 (77)	-0.180 (37)	-0.117 (44)
2	0.18 (15)	0.061 (62)	0.047 (70)	-0.07 (16)	0.196 (72)	0.105 (89)

Table 10.7.: Coefficients of the beta-dependence of $Z_{\mathrm{O}_{12}}$ and $Z_{\mathrm{O}_{44}}$ at the matching scale $L = 1.436\, r_0$. Results are shown for the χSF with standard Wilson fermions at $\vec{\theta} = (1, 0, 0)$ and $\vec{\theta} = (0.5, 0.5, 0.5)$ and also for the SF [74] with improved and standard Wilson fermions at $\vec{\theta} = (1, 0, 0)$.

dependence. Performing a fit of the data for the Z-factors (Tab. 10.1 and Tab. 10.2) of the form,

$$\begin{aligned} &Z_{\mathrm{O}}(g_0, L/a)_{L=1.436\, r_0} = \sum_{i=0}^{2} z_i^{\mathrm{REN}} (\beta - 6.0)^i \,, \\ &\beta = 6/g_0^2, \qquad 6.0 \leq \beta \leq 6.5 \,, \end{aligned} \tag{10.39}$$

we obtain the fitting coefficients presented in Tab. 10.7 for the χSF and the SF with standard and improved Wilson fermions. In Eq. (10.39), 'REN' stays for the particular setup chosen: χSF, SF with standard Wilson fermions or SF with improved Wilson fermions. We show results for O_{12}^a and O_{44}^a at $\vec{\theta} = (1, 0, 0)$ for all formulations and at $\vec{\theta} = (0.5, 0.5, 0.5)$ only for the χSF. These results are obtained from fits performed in this work for the three formulations, which for the SF are in agreement with the final results previously presented in [74]. We show the data together with the fitting curves, at $\vec{\theta} = (1, 0, 0)$ and for the three formulations, in Fig. 10.5 and Fig. 10.6 for $Z_{\mathrm{O}_{12}}$ and $Z_{\mathrm{O}_{44}}$, respectively.

From the knowledge of the Z-factors, $Z^{\mathrm{REN}}(g_0, L_{\mathrm{ref}}/a)$ at a given value of the renormalization scale, L_{ref}, and the corresponding ultraviolet (UV) invariant SSFs, $\sigma_{\mathrm{INV,O}}^{\mathrm{UV,REN}}(L_{\mathrm{ref}})$, at the same value of the renormalization scale, it is possible to determine the total RGI renormalization factor, $Z_{\mathrm{O}}^{\mathrm{RGI}}(g_0)$.

The UV invariant SSF of a certain operator is independent on the particular regularization but it depends on the renormalization scheme and the reference scale. In particular it is defined as,

$$\sigma_{\mathrm{INV,O}}^{\mathrm{UV,REN}}(L_{\mathrm{ref}}) = \frac{O^{\mathrm{RGI}}}{O_{\mathrm{R}}(L_{\mathrm{ref}})} \,, \tag{10.40}$$

with $O_{\mathrm{R}}(L_{\mathrm{ref}})$ the renormalized operator at scale L_{ref}, defined in Eq. (10.27) and O^{RGI} the corresponding RGI operator defined in Eq. (10.32).

The RGI renormalization factor is scale and scheme independent but it depends on the particular regularization. It relates any bare matrix element of the bare operator, $O_{\mathrm{B}}(g_0)$, with the corresponding RGI matrix element and it is defined as follows,

$$Z_{\mathrm{O}}^{\mathrm{RGI}}(g_0) = \frac{Z^{\mathrm{REN}}(g_0, L_{\mathrm{ref}}/a)}{\sigma_{\mathrm{INV,O}}^{\mathrm{UV,REN}}(L_{\mathrm{ref}})} \,. \tag{10.41}$$

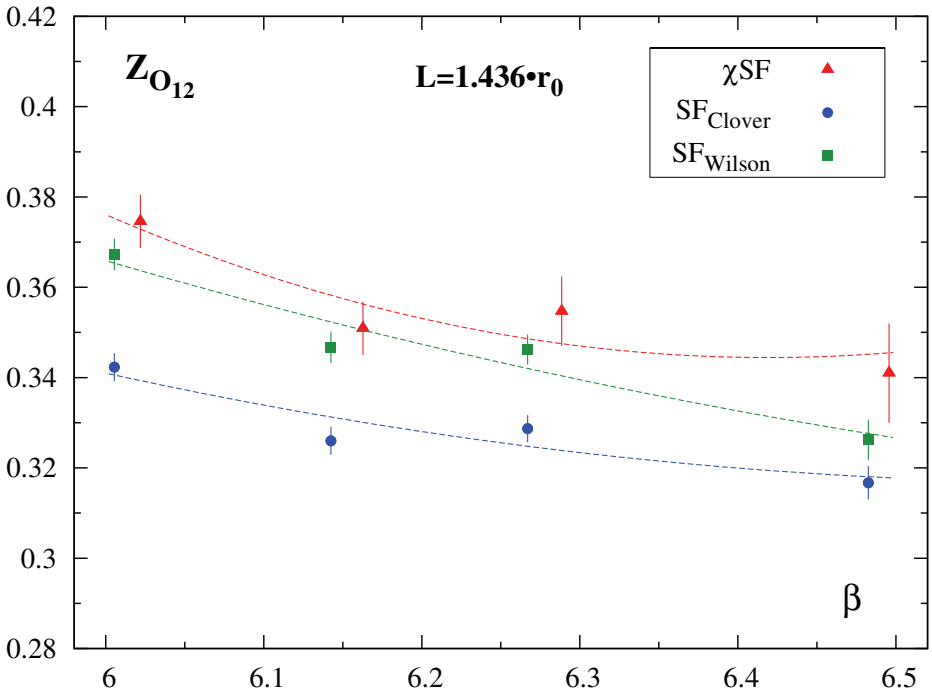

Figure 10.5.: Numerical results for $Z_{\mathrm{O}_{12}}(g_0, L/a)$ at scale $L = 1.436\, r_0$ and for several β values. $\vec{\theta} = (1, 0, 0)$. Results are shown for the χSF with standard Wilson fermions (cf. Tab. 10.1) and for the SF with standard and improved Wilson fermions, as taken from [74]. The fitting curves are also plotted (cf. Eq. (10.39) and Tab. (10.7)).

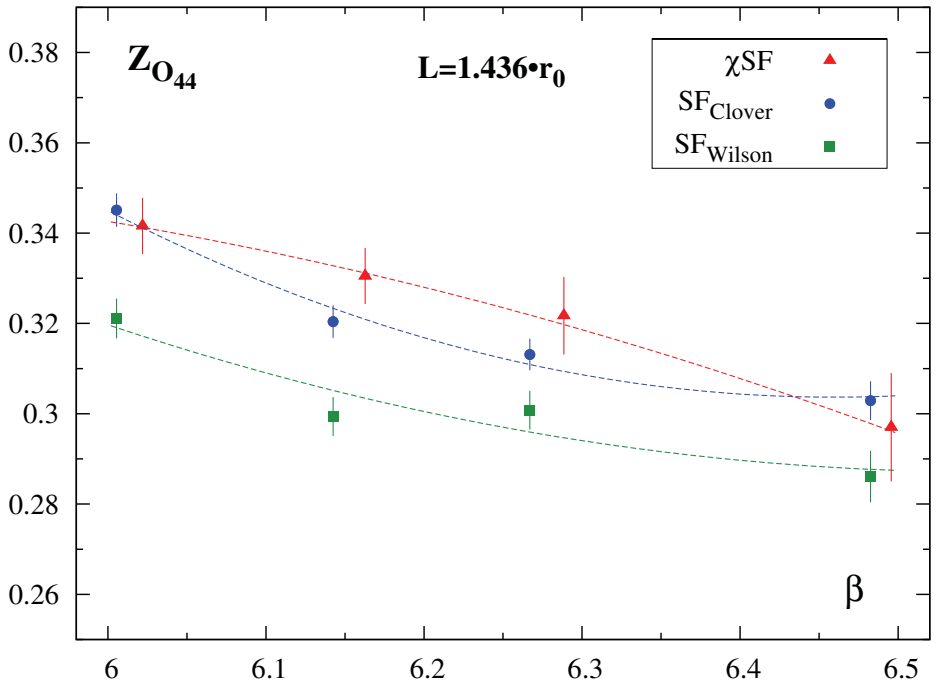

Figure 10.6.: Numerical results for $Z_{\mathrm{O}_{44}}(g_0, L/a)$ at scale $L = 1.436\, r_0$ and for several β values. $\vec{\theta} = (1, 0, 0)$. Results are shown for the χSF with standard Wilson fermions (cf. Tab. 10.2) and for the SF with standard and improved Wilson fermions, as taken from [74]. The fitting curves are also plotted (cf. Eq. (10.39) and Tab. (10.7)).

		$Z^{\rm RGI}_{\rm O_{12}}(g_0)$			$Z^{\rm RGI}_{\rm O_{44}}(g_0)$		
L/a	β	χSF	SF (Clo)	SF (Wil)	χSF	SF (Clo)	SF (Wil)
8	6.0219	1.548 (24)	1.414 (13)	1.518 (14)	1.546 (28)	1.562 (17)	1.453 (20)
10	6.1628	1.450 (24)	1.347 (13)	1.433 (14)	1.495 (28)	1.450 (16)	1.355 (19)
12	6.2885	1.466 (32)	1.358 (12)	1.431 (14)	1.456 (39)	1.417 (16)	1.361 (19)
16	6.4956	1.409 (45)	1.309 (15)	1.348 (18)	1.344 (54)	1.371 (19)	1.295 (26)

Table 10.8.: RGI renormalization factors, $Z^{\rm RGI}_{\rm O_{12}}(g_0)$ and $Z^{\rm RGI}_{\rm O_{44}}(g_0)$ for $\vec{\theta} = (1,0,0)$. Results are shown for the χSF with standard Wilson fermions and the SF with improved and standard Wilson fermions, for several values of the lattice spacing. We have determined in this work the RGI Z-factors for the SF from the Z-factors given in [74].

	$z_i^{\rm RGI}(O_{12})$			$z_i^{\rm RGI}(O_{44})$		
i	χSF	SF (Clover)	SF (Wilson)	χSF	SF (Clover)	SF (Wilson)
0	1.554 (29)	1.409 (13)	1.512 (14)	1.550 (33)	1.561 (17)	1.447 (20)
1	-0.62 (30)	-0.32 (13)	-0.42 (14)	-0.27 (35)	-0.81 (17)	-0.53 (20)
2	0.74 (62)	0.25 (26)	0.19 (29)	-0.32 (72)	0.89 (33)	0.48 (40)

Table 10.9.: Coefficients of the beta-dependence of $Z^{\rm RGI}_{\rm O_{12}}(g_0)$ and $Z^{\rm RGI}_{\rm O_{44}}(g_0)$. Results are shown for the χSF with standard Wilson fermions and the SF with improved and standard Wilson fermions at $\vec{\theta} = (1,0,0)$.

Note that all this discussion is similar to the one presented in Chap. 9, where we determined the RGI strange quark mass.

In [73], the value of the UV invariant SSF was given for the operators O^a_{12} and O^a_{44} at scale $L = 1.436\, r_0$ and for $\vec{\theta} = (1,0,0)$. The values quoted there are

$$\sigma^{\rm UV,SF}_{\rm INV,O_{12}} = 0.242\,(8)\,, \qquad \sigma^{\rm UV,SF}_{\rm INV,O_{44}} = 0.221\,(9)\,. \tag{10.42}$$

Substituting in Eq. (10.41) the values given in Eq. (10.42) and the Z-factors in Tab. 10.1-10.2, at the matching scale $L = 1.436\, r_0$, the RGI Z-factors of the operators O^a_{12} and O^a_{44} are obtained and presented in Tab. 10.8. Results are shown only for $\vec{\theta} = (1,0,0)$. Since the UV invariant SSFs are only known at $\vec{\theta} = (1,0,0)$, the case of $\vec{\theta} = (0.5,0.5,0.5)$ is not discussed any longer in the present section. In the determination of the RGI Z-factors, the error in the UV invariant SSF is not taken into account. This is a quantity in the continuum, and therefore its error is only considered at the end of all calculations, after the continuum limit has been performed. Its error is to be added in quadrature to the final value in the continuum limit.

A curve of $Z^{\rm RGI}_{\rm O}(g_0)$ as a function of β may be determined from the previous values in Tab. 10.8. The curve obtained is the following

$$\begin{aligned} &Z^{\rm RGI}_{\rm O}(g_0) = \sum_{i=0}^{2} z_i^{\rm RGI}(\beta - 6.0)^i\,, \\ &\beta = 6/g_0^2, \qquad 6.0 \le \beta \le 6.5\,, \end{aligned} \tag{10.43}$$

with the coefficients given in Tab. 10.9.

From the curves in Eq. (10.39) and Eq. (10.43) it is possible to determine, respectively, the Z-factors and the RGI Z-factors at any β-value within the range $6.0 \le \beta \le 6.5$. In particular, we show results for the Z-factors and RGI Z-factors in Tab. 10.10, at the β-values for which bare matrix elements have been evaluated in large volume simulations [108], keeping in mind a future

β	$Z_{\mathrm{O}_{12}}$	$Z^{\mathrm{RGI}}_{\mathrm{O}_{12}}$	$Z_{\mathrm{O}_{44}}$	$Z^{\mathrm{RGI}}_{\mathrm{O}_{44}}$
	χSF			
6.00	0.3761 (69)	1.554 (29)	0.3426 (73)	1.550 (33)
6.10	0.3627 (40)	1.499 (17)	0.3361 (43)	1.521 (19)
6.20	0.3529 (49)	1.458 (20)	0.3283 (53)	1.486 (24)
6.45	0.3436 (82)	1.420 (34)	0.3031 (90)	1.371 (41)
	SF (Clover)			
6.00	0.3410 (31)	1.409 (13)	0.3450 (37)	1.561 (17)
6.10	0.3338 (20)	1.3793 (83)	0.3290 (23)	1.489 (10)
6.20	0.3279 (23)	1.3550 (95)	0.3168 (27)	1.433 (12)
6.45	0.3186 (30)	1.317 (12)	0.3035 (35)	1.373 (16)
	SF (Wilson)			
6.00	0.3659 (35)	1.512 (14)	0.3197 (44)	1.447 (20)
6.10	0.3562 (22)	1.4719 (91)	0.3091 (28)	1.399 (13)
6.20	0.3474 (25)	1.436 (10)	0.3005 (32)	1.360 (14)
6.45	0.3296 (36)	1.362 (15)	0.2884 (46)	1.305 (21)

Table 10.10.: $Z_{\mathrm{O}}(g_0, L/a)$ at scale $L = 1.436\, r_0$ and $Z^{\mathrm{RGI}}_{\mathrm{O}}(g_0)$, for O_{12} and O_{44}. $\vec{\theta} = (1,0,0)$. Results are presented for the χSF with standard Wilson fermions and the SF with improved and standard Wilson fermions.

determination of the corresponding renormalized matrix elements. The results presented in Tab. 10.10 correspond to $Z_{\mathrm{O}_{12}}$, $Z^{\mathrm{RGI}}_{\mathrm{O}_{12}}$, $Z_{\mathrm{O}_{44}}$ and $Z^{\mathrm{RGI}}_{\mathrm{O}_{44}}$, at $\vec{\theta} = (1,0,0)$. We also show in Tab. 10.10 the corresponding results for the SF formulation with improved and standard Wilson fermions. Note that, these data for $Z_{\mathrm{O}}(g_0, L/a)$ and $Z^{\mathrm{RGI}}_{\mathrm{O}}(g_0)$ are not supposed to be compared amongst the three formulations. The Z-factors and the RGI Z-factors depend on the regularization and therefore, only a comparison of the corresponding renormalized matrix elements in the continuum limit or the RGI matrix elements, depending on the case, would make sense.

10.7. Conclusions on the universality tests

From the results that we have obtained in the last three chapters, Chap. 8-Chap. 10, where we have performed studies of several SSFs and also of the RGI strange quark mass, we provide a numerical demonstration that the χSF is a proper non-perturbative renormalization scheme with a well-defined continuum limit, provided the parameters κ and z_f are properly tuned to their critical values. We have also seen that all physically relevant quantities, obtained from the χSF formulation, are consistent with bulk automatic $O(a)$-improvement. The χSF is thus a promising renormalization scheme for using eventually in dynamical simulations, while maintaining bulk automatic $O(a)$-improvement, up to possible small discretization effects coming from the boundaries.

11. Topology of the ensembles

We discuss here the thermalization process and topological aspects of the ensembles of gauge configurations which we have generated during the present work. We have performed this investigation of topology because of inconsistencies observed, for few of our ensembles, in our initial results for fermionic observables. In particular, we observed these inconsistencies when comparing our data with results obtained using the standard SF formulation. With our results obtained in this thesis, within the quenched approximation to QCD and for the volumes that we have simulated, we show that the initial inconsistencies were related to thermalization issues. In fact, what we observed is that all ensembles with non-trivial values of the topological charge were not thermalized. Our investigation also shows that once an ensemble has reached the thermalization region, the algorithm remains in the trivial topological sector. These results are consistent with the theoretical discussion presented in [109] for the pure Yang-Mills theory, where it is shown that in small volumes, $L \leq 0.4\,\mathrm{fm}$, the probability of having an instanton is nearly zero. Numerical simulations with $N_\mathrm{f} = 2$ [110] further support our own experiences. Furthermore, our data suggest that the probability of having a non-trivial value of the topological charge is still negligible at the matching scale, $L \sim 0.7\,\mathrm{fm}$, even if L is in this case appreciably larger than the theoretical bound given in [109].

The chapter is structured in the following way. In Sec. 11.1 we summarize our simulation strategy. In Sec. 11.2 we show the behavior of our data during the thermalization process. In Sec. 11.3 we briefly recall the theoretical argument given in [109], which justifies the absence of instantons in small volumes. Here we also present our own results in small volumes, which are in agreement with the theoretical discussion in [109]. To conclude, in Sec. 11.4 we discuss our observations concerning the topology of the ensembles at the matching scale.

11.1. Simulation strategy

The gauge field configurations that we have generated during the present work have been produced using a modified version of the ETMC code [111], based on a HMC algorithm [112]. During this thesis, we have modified the gauge sector of the aforementioned code in order to implement the SF boundary conditions. We have employed the lattice gauge action discussed in detail in Chap. 3. The fermion sector of the code was not used, since only quenched simulations were performed here.

As it was discussed in previous chapters, we have performed simulations at five values of the renormalization scale, $1/L$, or equivalently the renormalized coupling, $\overline{g}^2(L)$. These values range from the very perturbative region, where contact with perturbation theory may be made, down to the matching scale with hadronic schemes. From the most perturbative to the hadronic scale, these were denoted in Chap. 6 as: PP, 2P, P (perturbative), I (intermediate) and NP (non-perturbative or matching) scale. At each of these values of the renormalization scale, simulations were performed at several values of β, each giving place to a different ensemble of gauge configurations. In particular, at the intermediate and perturbative scales we have computed SSFs of certain scale dependent observables. For that purpose, two kinds of ensembles were generated at these values of the renormalization scale. These correspond to simulations at a fixed value of the lattice spacing (or equivalently β or g_0) and for a number of lattice points

which are, respectively, N (single) and $2N$ (double). Since the lattice spacing remains fixed, this implies simulations at two values of the physical volume, L and $2L$, one double size with respect to the other.

Our simulation strategy was the following. For all points where we have performed simulations (either single or double lattices), such that $L/a \leq 20$, we have used hot starts, which means that the initial configuration of the ensemble is random. The runs were always prolonged beyond the thermalization region. Only then measurements of fermionic observables were performed.

A slight modification of these steps takes place in the case of all those lattices with $L/a = 24, 32$, which correspond to the largest number of points that we have simulated. For the lattices with $L/a = 24, 32$, the gauge configurations were generated using replicas. This procedure consists in starting a run (hot start in our case) at a certain value of β and then to split this initial run in several others which are thus 'replicas' of the former. The initial replica from which all others are obtained is what we denote here 'rep0'. The splitting of rep0 in all other replicas takes place only once rep0 has reached the thermalization region. At this point, we take the last configuration of rep0 and from it we start new sets of gauge fields generation (rep1, rep2, ...), using different random numbers for each of the replicas. Measurements of physical observables take place only after a number of MC steps large enough such that the different replicas of a certain run may be considered to be independent from each other. Eventually, the final results are obtained by an average over all the replicas (of a given run). The reason to use replicas for the largest lattices simulated is the high cost of these runs in comparison to the smaller lattices. Due to the lack of a parallel version of the code, for the SF boundary conditions, using replicas allowed us to increase statistics by a factor corresponding to the number of replicas, but using the same amount of time (not MC time but real time).

In all the runs, the quantity used initially to study thermalization was the plaquette, $P[U]$, defined as follows,

$$P[U] = \frac{2}{g_0^2} \sum_x \sum_{\mu<\nu} w(p) \operatorname{Re} \operatorname{tr}_c \left[U_{\mu\nu}(x) \right], \tag{11.1}$$

with the plaquette field, $U_{\mu\nu}(x)$, defined in Eq. (2.10) and recalled here for convenience [1],

$$U_{\mu\nu}(x) = U_\mu(x)\, U_\nu(x+\vec{\mu})\, U_\mu(x+\vec{\nu})^\dagger\, U_\nu(x)^\dagger . \tag{11.2}$$

The thermalization region is identified with a plateau in the MC history of the plaquette. As an example we plot in Fig. 11.1 the MC history of the plaquette for one particular ensemble: the lattice $2L/a = 32$ at the perturbative scale, $\bar{g}^2 = 0.9944$. From the figure we can see that the plateau is reached at about the trajectory number 500. This can be shown, for instance, computing the average value of the plaquette, $\langle P[U] \rangle_{\mathrm{G}}$, for different intervals in the MC history. We see that, independently on the interval taken, after the trajectory 500, the average value of the plaquette is always the same. However, as it is shown below in this chapter, the plaquette turned out to be the wrong quantity for us to look at.

11.2. Discussion of the data

We discuss here our results, some of which have already been presented in previous chapters, centering now our attention on the thermalization of the different ensembles of gauge configurations. In particular, we only discuss here results at two values of the renormalization scale, perturbative and intermediate scales.

During the first analysis of our data for fermionic observables, we observed an unexpected behavior in few of our ensembles. We noticed this behavior when comparing the values of the

[1] We refer the reader to Sec. 2.2, Sec. 3.2.1 and Sec. 3.2.2 for notations and detailed explanations.

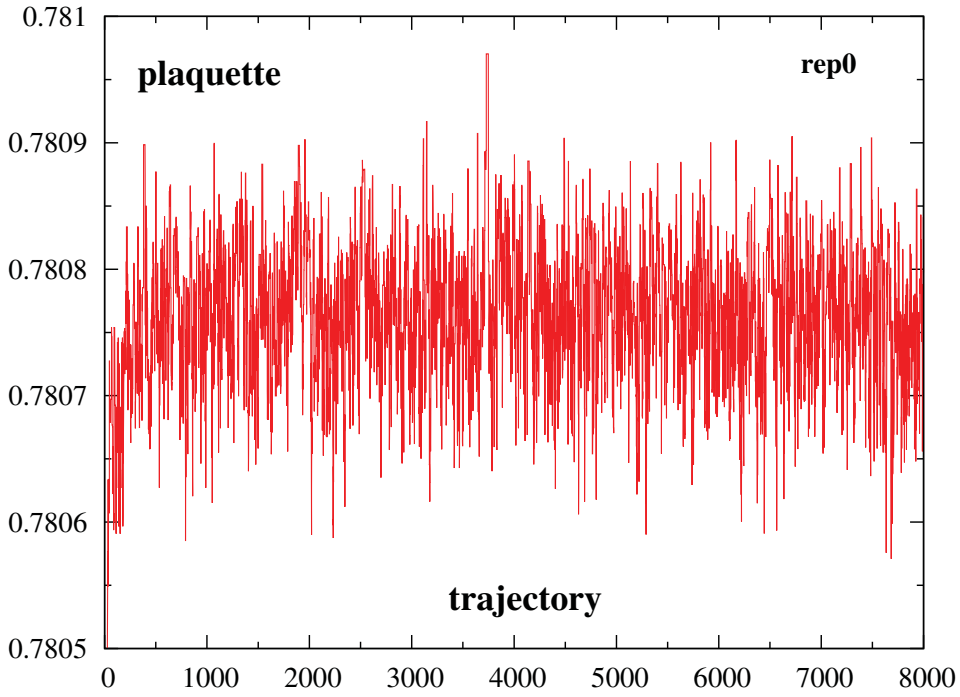

Figure 11.1.: MC history of the plaquette at the perturbative scale, $\overline{g}^2 = 0.9944$, and for a lattice with $2L/a = 32$ number of points. The thermalization region is identified with the plateau of the plaquette in MC time. The plaquette is clearly thermalized after the trajectory number 500.

L/a	β	$Z_{\rm P}^{\chi{\rm SF}}(g_0, L/a)$	$Z_{\rm P}^{\chi{\rm SF}}(g_0, 2L/a)$	$\Sigma_{\rm P}^{\chi{\rm SF}}$	$\Sigma_{\rm P}^{\rm SF}$(Clo)	$\Sigma_{\rm P}^{\rm SF}$(Wil)
Intermediate scale: $\overline{g}^2 = 2.4484$						
8	7.0197	0.68509 (95)	0.6199 (14)	0.9048 (23)	0.8945 (23)	0.8993 (20)
12	7.3551	0.6735 (13)	0.6000 (18)*	0.8909 (31)	0.8908 (23)	0.8924 (30)
16	7.6101	0.6672 (16)	*0.1585 (19)**	*0.2376 (30)*	0.8998 (25)	0.9036 (32)
Perturbative scale: $\overline{g}^2 = 0.9944$						
8	10.3000	0.82689 (56)	0.80129 (84)	0.9690 (12)	0.9633 (14)	0.9641 (12)
12	10.6086	0.81651 (88)	0.78549 (84)	0.9620 (15)	0.9599 (19)	0.9632 (17)
16	10.8910	0.8110 (10)	*0.7275 (34)**	*0.8971 (44)*	0.9622 (20)	0.9652 (22)

Table 11.1.: Renormalization factors, $Z_{\rm P}(g_0, L/a)$ and $Z_{\rm P}(g_0, 2L/a)$, and the corresponding lattice SSF, $\Sigma_{\rm P}(2, u, a/L)$, of the pseudo-scalar density for $\vec{\theta} = (0.5, 0.5, 0.5)$. We present results for the Z-factors only for the χSF. We show the SSF for χSF and the SF [96] with improved and standard Wilson fermions. Results are presented at two values of the renormalization scale, intermediate and perturbative scales. The emphasized data are the cases that brought as to understand that there was a problem. The data marked with a star correspond to the ensembles which indeed had problems.

Z-factors and lattice SSFs of the pseudo-scalar density, as obtained in this thesis from the χSF formulation, to those obtained using the SF [96] with both, standard and improved Wilson fermions. What we exactly observed was a lack of consistency in the values of the lattice SSFs between the χSF and the SF, at the intermediate and perturbative scales and for $L/a = 16$ in both cases. This discrepancy in the data may be seen in Tab. 11.1. Here we present the χSF results obtained for $Z_{\rm P}(g_0, L/a)$, $Z_{\rm P}(g_0, 2L/a)$ and its SSF on the lattice, $\Sigma_{\rm P}(2, u, a/L)$, at the intermediate and perturbative scales, corresponding, respectively, to $\overline{g}^2 = 2.4484$ and $\overline{g}^2 = 0.9944$. In the last two columns we show the corresponding SSFs obtained from the SF with improved and standard Wilson fermions, respectively. As we can see, the χSF SSFs look consistent with the SF data except for the largest lattices (which have been emphasized with italic characters in the table). Note that the SSFs at finite lattice spacing do not need to agree with each other but only in the continuum limit. Yet, the values are expected to be not far from each other. Therefore, a jump in the SSF from about 0.96 to 0.90 at the most perturbative coupling and from 0.90 to 0.24 at the intermediate coupling, clearly suggests that there is a problem. In the same table, looking at the Z-factors instead of the SSFs, it seems clear that the problem has its origin in the double (2L/a) lattices and not in the single (L/a) ones. The differences in the values of the Z-factors from the 2L/a=16 and 24 lattices to the 2L/a=32 are far too large.

In order to understand the problem we performed several checks. In particular, we considered the possibility that something went wrong with the generation of the replicas, since they were used only for the lattices where we have observed anomalies in the data. Therefore, we have also analyzed all the replicas independently. As a first check, we looked at the data for $Z_{\rm P}(g_0, 2L/a)$ and $\Sigma_{\rm P}(2, u, a/L)$ for each of the replicas. These results are shown in Tab. 11.2. The replicas are denoted with 'R' in the table. For comparison, the results considering the average over all the replicas are also presented and denoted as 'all'. In this table we only show those ensembles for which eventually problems were encountered. Indeed, we can see that there are discrepancies between results obtained from different replicas at $2L/a = 32$ for the perturbative coupling and at $2L/a = 24, 32$ at the intermediate coupling. All those replicas which present problems are marked with a star (also in Tab. 11.1). All others provide results which are consistent with the SF data.

L/a	β	R	$Z_{\mathrm{P}}(g_0, 2L/a)$	$\Sigma_{\mathrm{P}}(2, u, a/L)$
Intermediate scale: $\bar{g}^2 = 2.4484$				
12	7.3551	all*	0.6000 (18)	0.8909 (31)
12	7.3551	0	0.6068 (27)	0.9010 (44)
12	7.3551	1*	0.5825 (42)	0.8650 (65)
12	7.3551	2*	0.6013 (35)	0.8930 (55)
12	7.3551	3	0.6095 (28)	0.9051 (45)
16	7.6101	all*	0.1585 (19)	0.2376 (30)
16	7.6101	0*	0.1750 (55)	0.2624 (83)
16	7.6101	1*	0.1633 (54)	0.2447 (81)
16	7.6101	2*	0.1553 (56)	0.2327 (84)
16	7.6101	3*	0.1558 (35)	0.2336 (53)
16	7.6101	4*	0.1865 (74)	0.280 (11)
16	7.6101	5*	0.1656 (44)	0.2482 (67)
16	7.6101	6*	0.1507 (42)	0.2258 (63)
16	7.6101	7*	0.1237 (39)	0.1854 (58)
Perturbative scale: $\bar{g}^2 = 0.9944$				
16	10.8910	all*	0.7275 (34)	0.8971 (44)
16	10.8910	0*	0.6966 (77)	0.8589 (96)
16	10.8910	1	0.7825 (23)	0.9649 (31)
16	10.8910	2*	0.7706 (41)	0.9501 (52)
16	10.8910	3*	0.6678 (55)	0.8234 (69)
16	10.8910	4	0.7796 (28)	0.9612 (37)
16	10.8910	5*	0.7042 (98)	0.868 (12)
16	10.8910	6*	0.6611 (81)	0.815 (10)
16	10.8910	7*	0.7839 (22)	0.9666 (30)

Table 11.2.: Renormalization factors of the pseudo-scalar density, $Z_{\mathrm{P}}(g_0, 2L/a)$, and lattice SSF, $\Sigma_{\mathrm{P}}(2, u, a/L)$, for $\vec{\theta} = (0.5, 0.5, 0.5)$. Data are shown only for the χSF formulation at two values of the renormalization scale, intermediate and perturbative, and three values of β. We show the values obtained for each replica as well as the average over all the replicas, which is denoted as 'all' (cf. Tab. 11.1). The data marked with a star correspond to the ensembles which indeed had problems.

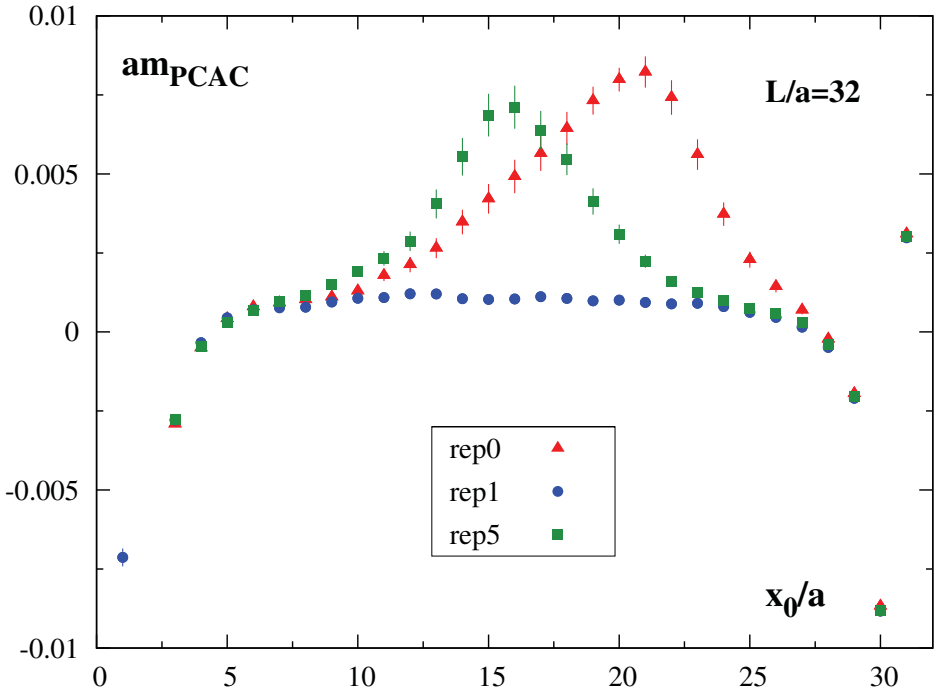

Figure 11.2.: Euclidean-time dependence of the PCAC mass for three different replicas (rep0, rep1 and rep5). These correspond to the perturbative value of the renormalization scale and the lattices $2L/a = 32$. $\vec{\theta} = (0.5, 0.5, 0.5)$. While the data from rep1 show the expected plateau behavior, the data form rep0 and rep5 deviate from the expected behavior.

For further checks, we have also looked at other fermionic observables. One is the PCAC mass, m_{PCAC}, which should actually be zero, according to the tuning condition of κ, and independent on the particular time-slice, x_0. The results for the PCAC mass follow the same line as in the previous discussion; all single lattices behave as expected while the $2L/a = 24, 32$ lattices follow an unexpected behavior. In particular, we plot in Fig. 11.2 the PCAC mass as a function of x_0 for three different replicas (rep0, rep1 and rep5) of the $2L/a = 32$ lattices at the perturbative coupling. As suggested from the results shown in Tab. 11.2 for the Z-factors and SSFs, rep1 corresponds to a PCAC mass which behaves as expected while rep0 and rep5 present problems; they deviate from the plateau at certain values of x_0. Note that for rep1 the m_{PCAC} is not exactly zero. These are just cutoff effects since, although the tuning has been performed at this β-value, it has been done for the single lattice and not for the double one, which is the case shown in the plot. Moreover, the tuning has been performed at $\vec{\theta} = (0, 0, 0)$ while the PCAC mass shown in the plot has been evaluated at $\vec{\theta} = (0.5, 0.5, 0.5)$, which results in further discretization effects.

As a last example, we plot in Fig. 11.3 the MC history of the correlation function $g^{11}_{\mathrm{A}_{0-}}$ for the same replicas as in the case of the PCAC mass (rep0, rep1 and rep5) and for a fixed value of $x_0 = T/2$. We show the history for the 50 gauge configurations which have been used to evaluate such quantities (50 configurations for each replica). In fact, we can see that the correlation

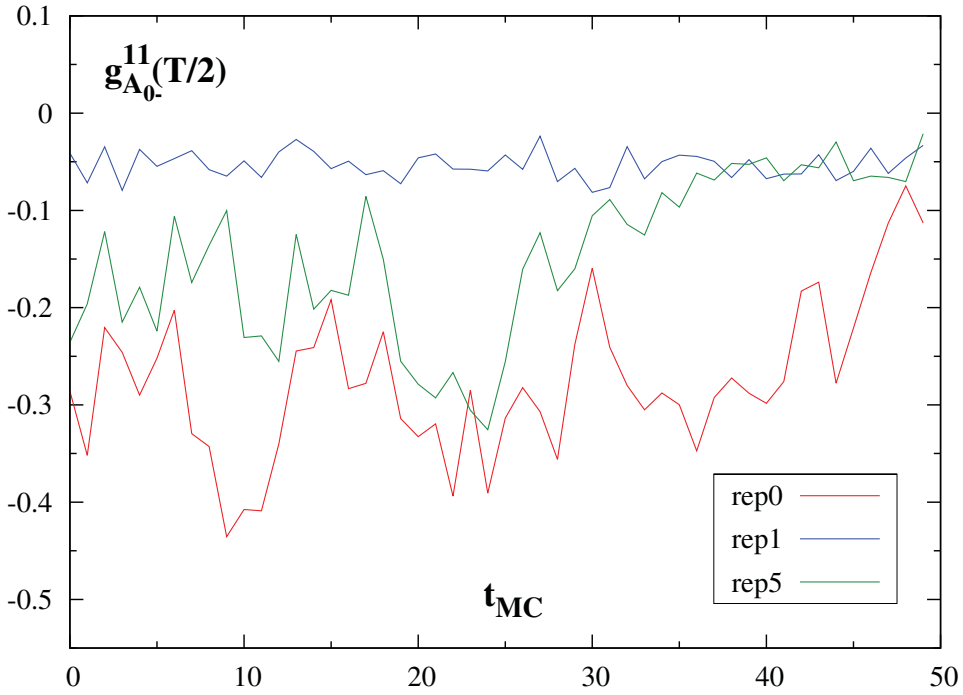

Figure 11.3.: MC-time history of the fermionic correlation function $g^{11}_{\mathrm{A}_{0-}}(T/2)$ for three different replicas (rep0, rep1 and rep5). These correspond to the perturbative value of the renormalization scale and the lattices $2L/a = 32$. $\vec{\theta} = (0.5, 0.5, 0.5)$. The MC-time interval shown in the plot corresponds to the 50 gauge configurations which were used in the analysis of the data.

function of rep1 seems to be in the thermalization region for the whole range of MC steps shown (it shows a plateau behavior), while the other two replicas do not look thermalized yet (they still show a trend to increasing values). For rep5 the correlation function seems to thermalize at about the configuration 38 (which corresponds to the trajectory 2400). The correlation function corresponding to rep0 does not reach thermalization in the whole range, although it seems to try to approach the value of rep1 at the end of the range shown. In fact, looking at the MC history of all other fermionic observables computed in this thesis we observe the same pattern as in the case of $g^{11}_{\mathrm{A}_{0-}}$. For instance, we also plot here the MC history of the correlation function $g^{11}_{\mathrm{P}_-}$ in Fig. 11.4. Besides the study of the MC history, our conclusions on the thermalization process of the different replicas is also supported by the results in Tab. 11.1 and Tab. 11.2. While the lattice SSF determined using only rep1 has a value which is consistent with the SSF determined using the SF with standard and improved Wilson fermions, the SSFs obtained from rep0 and rep5 are certainly not consistent with the SF data.

In contrast to all these results, the plaquette, which is a pure gauge observable, looks thermalized in all cases discussed here. As an example we plot the MC history of the plaquette, Fig. 11.5, for the same three replicas shown for the previous fermionic observables and for the same gauge configurations considered in Fig. 11.3 and Fig. 11.4. From Fig. 11.5 it is not possible to distinguish a special behavior in any of the three replicas indicating that any of them is not

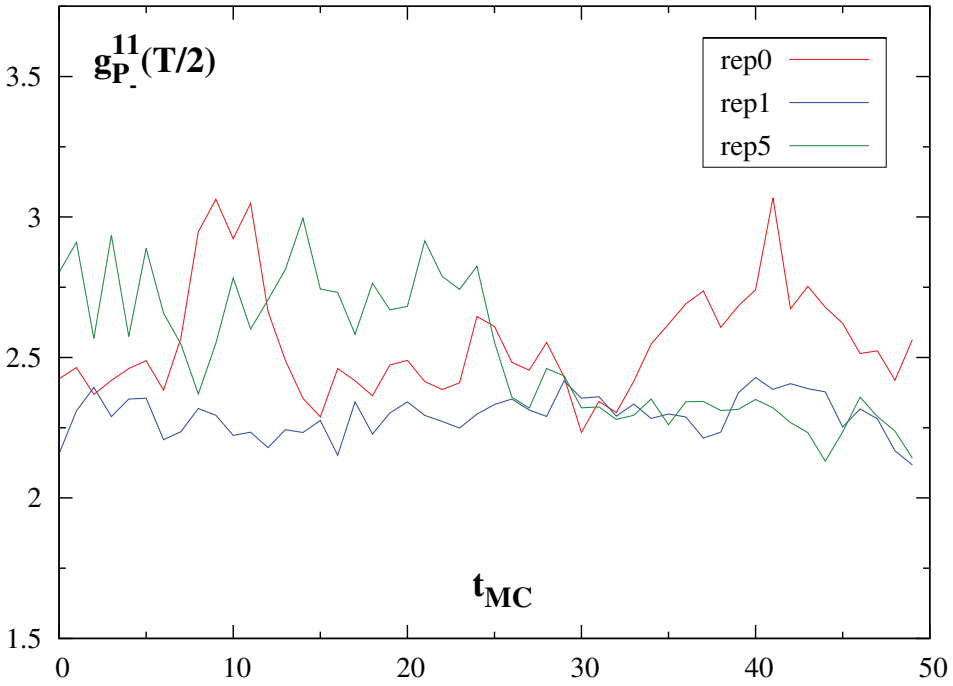

Figure 11.4.: Same caption as in Fig. 11.3 but for the fermionic correlation function $g^{11}_{\mathrm{P}_-}(T/2)$.

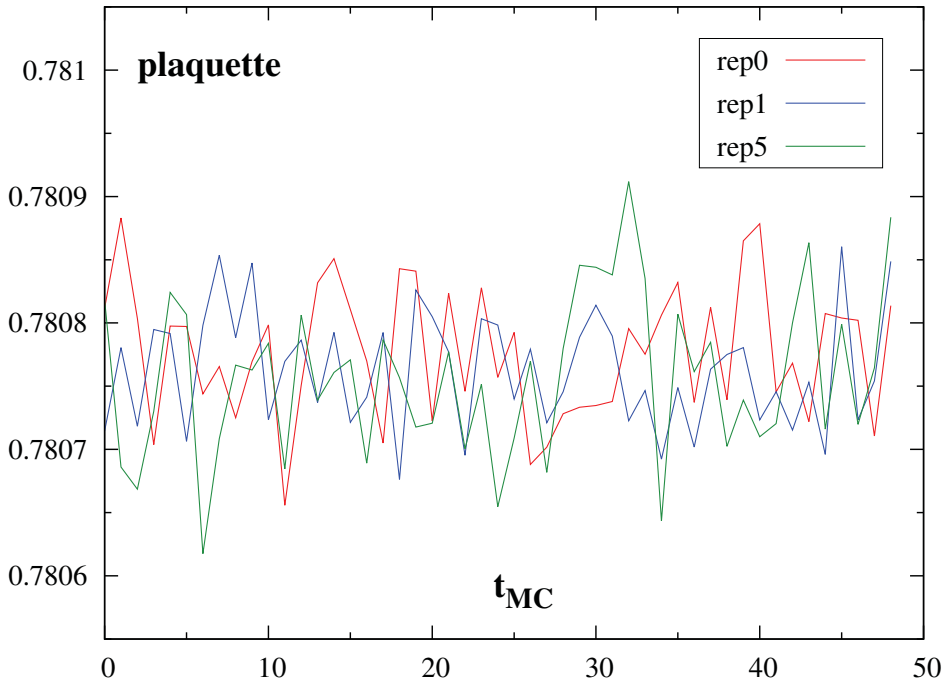

Figure 11.5.: MC-time history of the plaquette for three different replicas (rep0, rep1 and rep5). These correspond to the perturbative value of the renormalization scale and the lattices $2L/a = 32$. The MC-time interval shown in the plot corresponds to the 50 gauge configurations which were used in the analysis of the fermionic quantities.

thermalized yet. Moreover, the average values of the plaquette for the three replicas are in agreement with each other.

As we could confirm later on, all these results brought us to think that we were experiencing a thermalization problem and that the problematic ensembles may be stucked in some non-trivial topological sector. Therefore, we decided to look at the topology of all our ensembles, either if they looked thermalized or not. The topology study was performed via two observables; the (classical) gauge field action, $S_{\rm G}$, and the topological charge, $Q_{\rm top}$. On the lattice and within our setup, the gauge action corresponds to the expression given in Eq. (3.60) with the weight factors $w(p)$ defined in Eq. (3.64) and with the 2-loop value of c_t, given in Eq. (3.69). For the topological charge on the lattice we have employed the so called 'naive definition' of [113]. In measuring both quantities we have used a cooling procedure [114–116] with $O(100)$ cooling iterations. Cooling consists in a local minimization of the lattice gauge action and, therefore, it removes the ultraviolet quantum fluctuations. Note that, as it was argued in [116, 117], the cooling procedure removes the ultraviolet fluctuations but it does not modify the topological charge i.e. a plateau value in the cooling process can be identified. Therefore, the value of $Q_{\rm top}$ which is measured after smoothening (cooling) is the same as that of the initial gauge configuration. From the numerical point of view, we have cooled our gauge configurations using the Cabibbo-Marinari updating routine [118].

In the pure Yang-Mills theory in the continuum, the gauge field action is bounded by [119]

$$g_0^2 S_{\rm G} \geq 8\pi^2 |Q_{\rm top}| \,, \tag{11.3}$$

where $Q_{\rm top}$ is the topological charge of the gauge field configuration. On the lattice with SF boundary conditions and in the absence of a background field, as it is our case here, the bound in Eq. (11.3) holds up to discretization effects.

What we observed from our measurements of $Q_{\rm top}$ and $S_{\rm G}$ is the following: some of the ensembles were always at zero topological charge, $Q_{\rm top} = 0$, while other ensembles changed topological sectors during the MC history. Examples of these cases can be seen for instance in Fig. 11.6 and Fig. 11.7, where we plot, respectively, the classical gauge action and the absolute value of the topological charge, for the rep0, rep1 and rep5 discussed above. As we can see from these figures, rep1 has a gauge action which is $g_0^2 S_{\rm G} \geq 0$ and a value of the topological charge $Q_{\rm top} \simeq 0$. On the other hand, for rep0 and rep5 non-trivial values of the topological charge were measured. For instance in the case of rep5, the gauge action takes a value $g_0^2 S_{\rm G} \simeq 80$ and the topological charge is $|Q_{\rm top}| \simeq 1$ for the first 37 analyzed configurations and it reaches $Q_{\rm top} \simeq 0$ ($g_0^2 S_{\rm G} \geq 0$) at $t_{\rm MC} \simeq 38$ (trajectory 2400), where it remains from that moment on. The same is true for rep0 except that the $Q_{\rm top} \simeq 0$ configuration is reached at a larger value of the MC time ($t_{\rm MC} \simeq 60$, trajectory 2950). These results, in fact, agree with the behavior observed by studying the MC history of the different fermionic correlation functions. In particular for the behavior just described above and shown in Fig. 11.3 for $g^{11}_{\rm A_{0\_}}$ and Fig. 11.4 for $g^{11}_{\rm P\_}$. In contrast to these results, we can see in Fig. 11.1 and Fig. 11.5 the MC history of the plaquette for the same replicas, whose behavior does not show any particular anomaly.

After having the information about the topology of each ensemble we observe that only the ensembles at $Q_{\rm top} = 0$ give rise to consistent results, meaning they are consistent with those results obtained using the SF scheme with standard and improved Wilson fermions. In fact, this behavior has a well justified explanation which is provided below in Sec. 11.3. Moreover, all the results discussed here suggest that, while all fermionic observables that we have analyzed are very sensitive to changes of topological sectors, the plaquette is insensitive to these variations. Therefore, at least in our case, the plaquette is not a good observable to look at in order to study the thermalization process.

11.3. Topology in small volumes

In [109] it is theoretically shown, in the pure Yang-Mills theory, that in small volumes, V, the probability, P_ν, of being at $Q_{\rm top} = \nu$ with $\nu \neq 0$ is negligible, at least for values of the renormalized coupling, $\overline{g}^2(L)$, which are small enough [2]. In particular, it was shown there that in small volumes the topological susceptibility,

$$\chi_{\rm t}^V = \frac{\langle Q_{\rm top}^2 \rangle}{V} = V^{-1} \sum_{\nu=-\infty}^{\infty} \nu^2 P_\nu \,, \tag{11.4}$$

is dominated by the one instanton contribution

$$\chi_{\rm t}^V \sim \frac{2P_1}{V} \overset{V\to 0}{\longrightarrow} 0 \,, \tag{11.5}$$

[2] The author thanks R. Sommer for a very enlightening discussion on this topic.

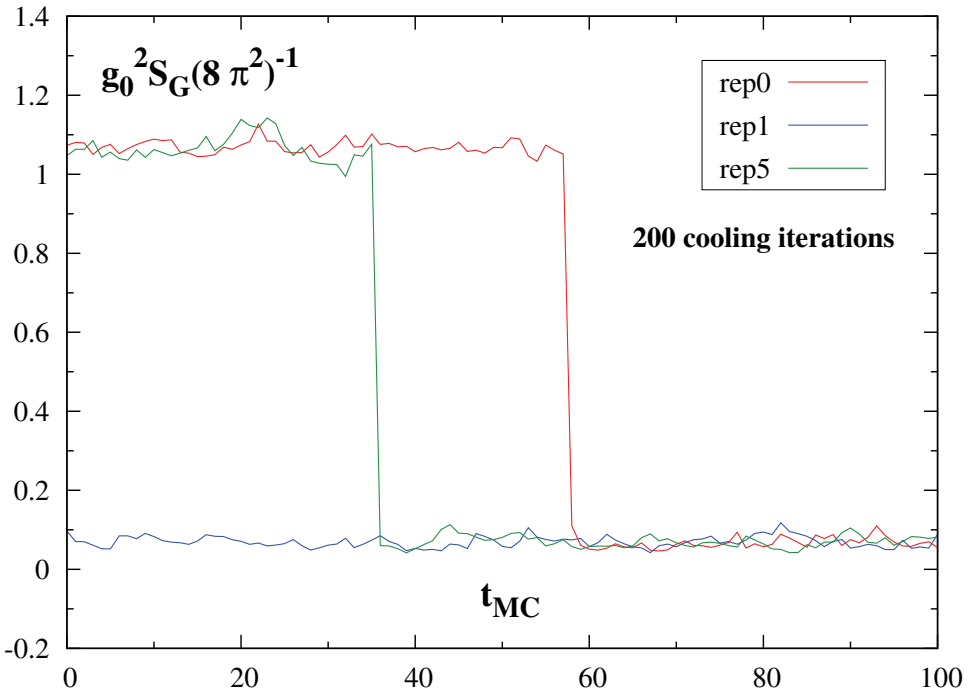

Figure 11.6.: MC-time history of the classical gauge action, S_{G}, for three different replicas (rep0, rep1 and rep5) and after 200 cooling iterations. The replicas correspond to the perturbative value of the renormalization scale and the lattices $2L/a = 32$. The MC-time interval shown in the plot contains the 50 gauge configurations which were used in the analysis of the fermionic quantities (corresponding in this plot to $0 \leq t_{\mathrm{MC}} \leq 49$).

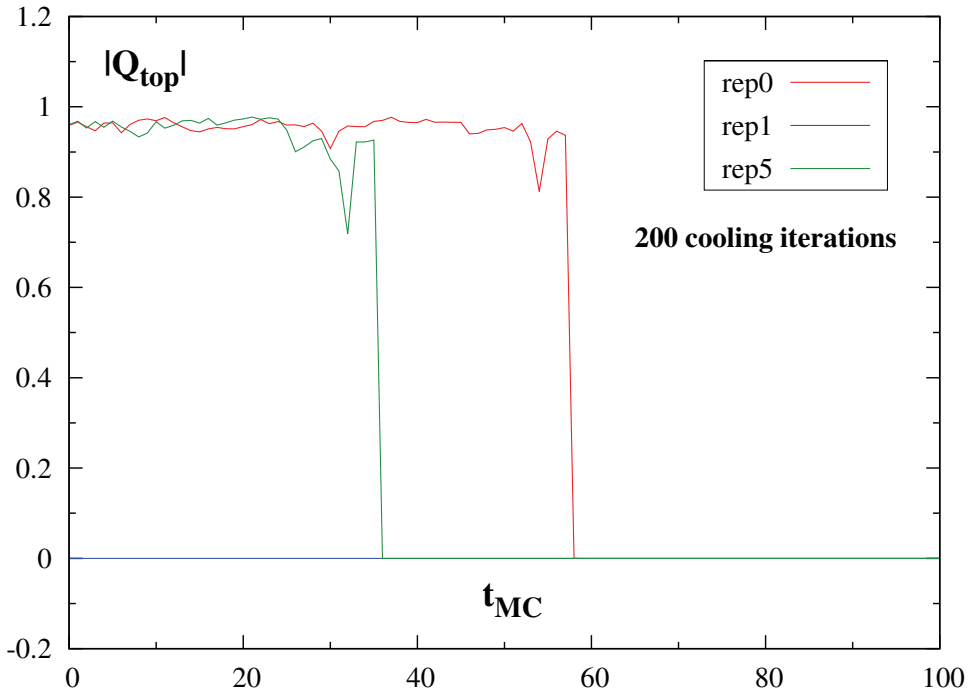

Figure 11.7.: Same caption as in Fig. 11.6 but plotting in the y-axis the absolute value of the topological charge, $|Q_{\mathrm{top}}|$.

whose probability, P_1, may be determined analytically. In particular, in terms of the renormalized gauge coupling, $\overline{g}$, and up to 2-loops it is given as

$$P_1 = K_1(n)(\overline{g}^2)^{-2n} e^{-8\pi^2/\overline{g}^2} \left\{1 + O(\overline{g}^2)\right\}, \quad \text{for SU}(n)\,. \tag{11.6}$$

In this expression, $K_1(n)$ is a constant whose value has been numerically determined in [109] for several values of n. In our case, SU(3), the value quoted there is $K_1(3) = 0.5101 \times 10^{13}$. Moreover, the renormalized coupling is a function of only the system size, ρ as denoted in [109], and the corresponding mass parameter, Λ, defining the energy scale, $\overline{g}^2(\Lambda\rho)$. This implies that also P_1 is only a function of $\Lambda\rho$, $P_1(\Lambda\rho)$. As it was discussed in that reference, in the small volume limit the renormalized coupling goes to zero,

$$\lim_{\rho\to 0} \overline{g}^2(\Lambda\rho) = 0\,. \tag{11.7}$$

This means that for small volumes (or $\overline{g}^2$), P_1 becomes small enough such as to guarantee that once the system is at $Q_{\text{top}} = 0$ it will not change topological sector.

The important point now is to understand what can be considered to be a small enough system size, ρ, so that the previous approximate expressions can be assumed to be accurate enough. Two criteria, one of perturbative and the other of non-perturbative nature, are considered in [109] in order to decide what is a small enough system size; (1) the $O(\overline{g}^2)$ corrections to P_1 should be small enough (perturbative nature). (2) $P_2 << P_1 << 1$ (non-perturbative nature).

Arguments are given in [109] to consider that the constrain (2) is fulfilled if P_1 is bounded such that $P_1 \leq 0.1$. With this bound in P_1, the renormalized coupling should thus be bounded by,

$$\overline{g}^2 \leq \overline{g}_c^2 \sim 3.22 \tag{11.8}$$

and, correspondingly, the system size

$$\rho \leq \rho_c \sim 0.19\,\Lambda_{\overline{\text{MS}}}^{-1}\,. \tag{11.9}$$

Considering the relation between Λ_{MS} and $\Lambda_{\overline{\text{MS}}}$ and for a value of $\Lambda_{\overline{\text{MS}}} \sim 250\,\text{MeV}$ (cf. Eq. (3.88)-(3.89)) the bound in the system size is thus

$$\rho_c \sim 0.4\,\text{fm}\,, \quad \text{for } \Lambda_{\overline{\text{MS}}} \sim 250\,\text{MeV}\,. \tag{11.10}$$

According to this discussion, it is expected that at least for all those systems whose size is below 0.4 fm, once an ensemble has reached $Q_{\text{top}} = 0$, the algorithm will not sample all topological sectors but, instead, it will remain at trivial topology. This proof, furthermore, provides a strong argument that all ensembles of gauge configurations which are at some non-trivial topological sector are not yet thermalized. The theoretical proof in [109] has been carried out in the pure Yang-Mills theory and, therefore, the same bounds should hold in the quenched approximation. In the case of dynamical fermions no theoretical proof is available, and, in principle, these bounds may be different. Yet, a numerical evidence has been given for $N_{\text{f}} = 2$ in [110], where they confirm these theoretical expectations for a value of $\overline{g}^2 \sim 2.5$ and lattice sizes $L/a = 8, 12$, using a PHMC algorithm.

All our ensembles at energies below the matching scale correspond to values of $\overline{g}^2$ and L which are below the bounds given above. For instance, the value of the renormalized coupling at the intermediate and perturbative scale, respectively, is $\overline{g}^2 = 2.4484$ and $\overline{g}^2 = 0.9944$, which is well below the bound $\overline{g}_c^2 \sim 3.22$. Equivalently, the corresponding lattice sizes are within the range, $0.123\,\text{fm} < L < 0.246\,\text{fm}$ for the intermediate scale and $L << 0.015\,\text{fm}$ for the perturbative coupling, which are also quite below $\rho_c \sim 0.4\,\text{fm}$. Therefore, all results that have been discussed

above in Sec. 11.2 are perfectly consistent with the expectations in these small volumes. To be concrete, it is natural that all those ensembles at $Q_{\rm top} \neq 0$ are not yet thermalized and that all those already at $Q_{\rm top} = 0$ will remain in this topological sector. As an outcome, all results presented in this thesis correspond to ensembles which have $Q_{\rm top} = 0$ and all those ensembles which were at $Q_{\rm top} \neq 0$ have not been considered in the analysis.

11.4. Topology at the matching scale

At the matching scale, the system size is $L = 0.718\,\text{fm}$, which is a value significantly larger than the theoretical bound $\rho_c \sim 0.4\,\text{fm}$. The value of the renormalized coupling at the matching scale may be read off from Fig.2 of [120], and it is $\overline{g}^2 \sim 7$, which is also quite above $\overline{g}_c^2 \sim 3.22$. Therefore, doubts may arise whether the natural status of an ensemble is still that of $Q_{\rm top} = 0$. At this scale, we can thus only judge using our own numerical data and not from a fully theoretical point of view. What we have observed is that, indeed, all the ensembles at the matching scale, for all the values of the lattice spacing which we have studied, $L/a = 8, 10, 12, 16, 20, 24, 32$, follow the same pattern as described for the small volumes. Namely, all those ensembles which at some stage were at $Q_{\rm top} = 0$ never took values outside the trivial topological sector later in MC time.

12. Summary and conclusions

In this thesis we have investigated several aspects of the chirally rotated Schrödinger functional (χSF) within the quenched approximation to QCD, using both analytical and numerical methods. The χSF has been proposed [26] as a tool to perform non-perturbative renormalization of physical observables while still being compatible with the property of automatic $O(a)$-improvement in the bulk of the lattice, when using massless Wilson fermions as a regulator of the fermion sector of QCD. This is achieved at the moderate expense of tuning non-perturbatively only two parameters. One is the bare quark mass, m_0, which has to be tuned to its critical value, m_c, in order to define a massless renormalization scheme. This additive renormalization of the quark mass is indeed necessary in any lattice formulation with Wilson fermions due to the breaking of chiral symmetry by the Wilson term. The other parameter, z_f, is the coefficient of a dimension three boundary counterterm, whose tuning is required in order to restore the $\gamma_5\tau^1$-symmetry which is broken by the lattice regulator. Contrary to the quark mass, the tuning of z_f is characteristic of the χSF formulation and it does not have an analogue in the standard formulation of the SF. In order to remove boundary $O(a)$ effects, an additional coefficient is required, d_s, which is the analogue of $\tilde{c}_t$ in the standard SF. As for $\tilde{c}_t$, a perturbative determination of d_s is expected to be enough for the cancellation of these $O(a)$ effects coming from the boundaries.

In the literature, there are two proposals to solve the incompatibility problem between standard SF boundary conditions and bulk automatic $O(a)$-improvement when using non-improved Wilson fermions as a regulator. One is the aforementioned χSF formulation and the other is what we denote here the γ_5SF [19] formulation. As an initial step in our investigation (cf. Chap. 4), we have analyzed, in the free continuum theory, aspects of these two different ways of implementing Schrödinger functional boundary conditions: the eigenvalue spectrum and the quark propagator. From this analytic study in the continuum theory we could infer that the χSF formulation gives rise to a well defined QCD spectrum, with a minimal eigenvalue which is bounded from below even in the massless theory, due to the presence of the boundary conditions. As it is the case in the standard formulation of the SF, this bound in the spectrum of the Dirac operator is provided by the finite extent of the system in the time direction. Moreover, we have also derived the explicit analytic expression of the quark propagator satisfying the χSF boundary conditions in the continuum theory. With the γ_5SF boundary conditions, we have noticed that the eigenvalue problem has either a trivial solution or, in the massless case, an infinite number of solutions. The reason is the lack of additional conditions on the normal derivatives of the fields at the boundaries. This result is a consequence of the fact that there is no distinction between the normal (γ_0) and the tangential (γ_k) components of the fields at the time boundaries with respect to the projectors here considered. For the quark propagator we find a similar pattern, that is, in order to satisfy all the boundary conditions the quark propagator has to vanish. We still found an analytic expression for the quark propagator, which satisfies the boundary conditions with the projectors applied on the left, but this solution does not satisfy the boundary conditions with the projectors applied on the right side. We showed that this quark propagator actually satisfies different boundary conditions on the right side, which are obtained from the ones on the left via charge conjugation. Therefore, a non vanishing solution can only be found changing the boundary conditions, such that charge conjugation is a preserved symmetry amongst the boundary conditions. Yet, given the fact that the γ_5SF

boundary conditions violate parity and preserve time reversal, this would correspond to a theory which violates $\mathcal{P}$ and $\mathcal{CPT}$. It is important to emphasize that for the χSF boundary conditions the situation is completely different. It is enough to consider parity and time-reversal symmetries in the twisted basis to see that the χSF boundary conditions actually preserve separately $\mathcal{C}$, $\mathcal{P}$ and $\mathcal{T}$. If one is interested in the lattice formulation of the χSF with Wilson fermions, then the Wilson term will certainly break the twisted parity $\mathcal{P}_{\frac{\pi}{2}}$ and twisted time reversal $\mathcal{T}_{\frac{\pi}{2}}$. Though, separately $\mathcal{C}$ and $\mathcal{PT}$, and thus $\mathcal{CPT}$, remain symmetries of the lattice theory with Wilson fermions. Our conclusion from this analytic study in the continuum theory is that the standard and χSF boundary conditions are a sound definition of QCD with SF boundaries, while the γ_5SF formulation has still issues which need to be further investigated. With the current picture, we have performed studies beyond the formal continuum theory only within the χSF formulation. In particular, we have also determined the analytic expression of the free quark propagator on the lattice satisfying χSF boundary conditions (cf. Sec. 5.1.1), which has been numerically cross-checked with the propagator obtained from a numerical inversion of the free lattice Dirac operator given in Eq. (5.2) and also with the corresponding propagator in [26].

Having decided to explore the χSF beyond the tree-level approximation, we then proceeded towards our main target, namely to compute renormalization factors and investigate the universality of the continuum limit with the example of step scaling functions (SSFs) and selected physical quantities such as the strange quark mass. After the initial analysis of the χSF in the free theory, the first step towards a non-perturbative determination of renormalization factors is to define non-perturbatively the χSF renormalization scheme. This means to perform the non-perturbative tuning of the bare quark mass, m_0, or equivalently the hopping parameter, $\kappa = (8 + 2am_0)^{-1}$, and of the boundary coefficient z_f. In Chap. 6 we have presented the results of the non-perturbative tuning of κ and z_f for the χSF at several physical scales and for a range of lattice spacings, using 7 different definitions of z_f^c. This demonstrates that the tuning of these two coefficients is indeed feasible, at least in the quenched approximation. Moreover, we observe that the tuning of z_f and κ are nearly independent. This observation is important keeping in mind dynamical fermion simulations; if this behavior persists with dynamical calculations, it may ease the numerical effort necessary to perform the tuning, thus reducing the number of required simulations. We have also shown that, as expected, different tuning conditions give rise to values of z_f^c which differ amongst themselves by $O(a)$ discretization effects. In fact, different values of z_f^c give rise to different regularizations of the theory differing by discretization effects. Therefore, our demonstration that the differences in z_f^c, amongst the different tuning conditions, vanish in the continuum limit, represents a numerical evidence of the universality of the continuum limit. As we have also shown in this thesis, the $O(a)$ uncertainties in the determination of z_f^c affect physical quantities, at most, at $O(a^2)$. We remark again that even with non-improved Wilson fermions in the bulk, κ and z_f are the only parameters that must be tuned non-perturbatively within the χSF setup, in order to guarantee bulk automatic $O(a)$-improvement, thus eliminating the need for the bulk counterterm to the action, $c_{\rm sw}$, and for the many operator improvement coefficients necessary in the standard SF. The boundary improvement coefficients, c_t and d_s, are still required in this formulation, as in any lattice regularization with SF-like boundary conditions. However, for the boundary improvement coefficients, a perturbative determination is expected to be enough for the cancellation of these residual $O(a)$ discretization effects.

The realization of automatic $O(a)$-improvement means that all those quantities which are even under $\gamma_5\tau^1$-symmetry are free from $O(a)$ discretization effects, while all odd quantities are not $O(a)$-improved. These last are unphysical quantities which should vanish in the continuum limit, while all the physical content is contained only in the even quantities. In order to check that the χSF is compatible with bulk automatic $O(a)$-improvement, we have studied the scaling behavior of several even and odd quantities towards the continuum limit and the results were

discussed in Chap. 7. From these studies we have derived several conclusions. The first one is that the massless free quark χSF is $O(a)$-improved, provided the boundary coefficient, d_s, is set to its correct tree-level value. Moreover, the quantities computed within the χSF, in the tree approximation, converge in the continuum limit to the results computed in the continuum theory with χSF boundaries. These results are a numerical evidence of the universality of the continuum limit in the free theory. With these tree-level studies, we have also shown that it is justified to impose tuning conditions, at each value of the lattice spacing, by assuming those $\gamma_5\tau^1$-odd correlation functions which are used to define z_f^c, to vanish. From the analysis in the interacting theory, we found that the lattice spacing scaling of all quantities which are expected to vanish in the continuum limit, either by boundary conditions or by symmetry arguments, shows a very strong dependence on z_f^c. Concerning the quantities which should vanish due to boundary conditions, we see that they decrease towards the continuum limit independently on the chosen tuning condition and, when computed from different values of z_f^c, the spread in the results tends to vanish in the continuum limit approach. A vanishing value is a numerical evidence that, indeed, the correct boundary conditions are recovered in the continuum. Yet, we have not found how exactly the continuum limit is reached and further investigations are still required for these quantities. It would be important to perform simulations using significantly smaller values of the lattice spacing and, preferably, also with a determination of d_s beyond tree-level. Nevertheless, at the moment there is little doubt that the correct boundary conditions are recovered. From the results presented in several chapters in this thesis, we obtain numerical evidences of the existence of a universal continuum limit and we show that $\gamma_5\tau^1$-symmetry is restored in the continuum limit. These results strongly suggest that the χSF provides a correct and non-perturbative renormalization scheme (on and off the lattice). In the case of those correlation functions which vanish due to symmetry arguments ($\gamma_5\tau^1$-odd quantities), we have shown that they go to zero in the continuum limit with leading $O(a)$ discretization effects for all the tuning conditions employed. This is a numerical evidence of the restoration of $\gamma_5\tau^1$-symmetry in the continuum limit and the independence of the continuum limit values on the particular tuning condition. All quantities with a finite continuum limit i.e. the only physically relevant quantities, agree within statistical errors for all the methods to tune z_f, already at non-zero lattice spacing. This result is very encouraging. Of course, it needs to be tested in future simulations whether the same is true for other observables, but our results here provide strong indications that this is the case.

This expectation is further supported by the results shown in Chap. 8, Chap. 9 and Chap. 10. We have demonstrated that the χSF gives rise to a well-defined continuum limit. This has been achieved through studies of the universality of the continuum limit, via the computation of several physical observables. In particular, we have computed the RGI mass of the strange quark and the SSFs of the pseudo-scalar density and the twist-2 operators, O_{12} and O_{44}, as derived from the χSF. These observables have been determined at several values of the renormalization scale. The corresponding values in the continuum limit have been compared to those of the same observables determined using the standard SF, with two different regularizations of fermions. We have shown that all the observables computed from the χSF take the expected values in the continuum limit. We demonstrate, therefore, that the χSF leads to a well-defined and universal continuum limit. Moreover, all physical quantities computed in this thesis show small discretization effects which are consistent with $O(a^2)$. The χSF with massless Wilson fermions is thus a promising non-perturbative renormalization scheme, which can be applied in the computation of renormalization constants using dynamical simulations, while still maintaining bulk automatic $O(a)$-improvement.

In addition to all previous results, we have also investigated topological aspects of our ensembles of gauge configurations (cf. Chap. 11). This investigation was motivated by the fact that

we observed inconsistencies in our data for fermionic quantities, such as the SSFs, in few of our ensembles. We have shown that such inconsistencies where related to thermalization problems. From our numerical results we observed that all ensembles with a topological charge different from zero, $Q_{\rm top} \neq 0$, were not thermalized. Moreover, we have also observed that thermalized ensembles, those with $Q_{\rm top} = 0$, do not abandon the trivial topological sector. As we have discussed, these results can be theoretically justified [109], at least for the lattices with $L \leq 0.4\,\text{fm}$. Note that for our largest volume, $L = 0.718\,\text{fm}$, there is, a priori, no theoretical expectation that the natural status of the ensembles is also that of $Q_{\rm top} = 0$. Yet, as an interesting aspect, we have observed the same pattern as for the smaller volumes.

In summary, in this thesis we have tested the χSF scheme with massless Wilson fermions in quenched QCD. As a first step we have defined the scheme through the non-perturbative tuning of all required parameters. After the scheme has been properly defined we have performed several checks. We have determined the continuum limit of physically relevant quantities, which have then been compared against results obtained using the standard formulation of the SF. In particular, we have computed the strange quark mass and the step scaling function of the pseudo-scalar density and of the operators O_{12} and O_{44}, as relevant for interpreting results of deep inelastic scattering experiments. We have found that all results obtained from the χSF formulation are consistent with those obtained using the SF in its standard form. With this agreement we have provided another numerical evidence of the universality of the continuum limit and, therefore, we have demonstrated that the χSF is a well-defined renormalization scheme. We have also shown that cutoff effects are rather small and that the scaling behavior of physical observables is consistent with leading $O(a^2)$ effects. These results directly open the possibility to use the χSF scheme in dynamical simulations of QCD. In particular, it becomes very important for the computation of renormalization factors of quantities determined using maximally twisted mass simulations with four flavors (u,d,s,c) of quarks, due to the compatibility of the χSF with bulk automatic $O(a)$-improvement.

Acknowledgments

I first want to thank my direct supervisor, Dr. habil. Karl Jansen, for offering me the possibility to do my Ph.D thesis within his research group. I specially appreciate his very involved and constant supervision and the many important discussions, from which I have learned so much and which have guided me in the completion of this work. I am also extremely thankful to him for supporting my participation in several schools, conferences and meetings of the ETM collaboration, which have been so important for my scientific development. I also want to thank his support and understanding in the difficult moments of this work, as well as the careful and critical reading of a first version of this manuscript.

I am also greatly thankful and indebted to my official supervisor, Prof. Dr. Michael Müller-Preussker, who has given me the opportunity of doing my Ph.D thesis within his research group, at the Humboldt–Universität zu Berlin. I want to thank the many useful discussions as well as his guidance and help in all bureaucratic part of the Ph.D project. I am really thankful to him as otherwise the realization of this Ph.D within the Humboldt–Universität zu Berlin would not have been possible.

Many thanks to the SFB-TR9 for the financial support during all these years and the NIC and theory groups in DESY-Zeuthen for providing me with a place to work.

The numerical part of this work has been carried out between the PC Farm in DESY-Zeuthen and the supercomputer JUROPA located in the Supercomputing Center in Jülich, Germany. I am particularly thankful for the opportunity of using these resources and for the professional and efficient support provided by both places.

I want to make a special mention of Dr. Dru B. Renner and Dr. Andrea Shindler, for following closely the supervision of this Ph.D thesis and encouraging me when I needed it most. I want to express my gratitude for the many long and enlightening discussions which have contributed so much to my own development as a scientist. I finally want to thank them for cross-checking the analytical and numerical results presented in this thesis.

I would also like to acknowledge, in alphabetic order, crucial discussions with Dr. Roberto Frezzotti, Dr. Gregorio Herdoiza, Dr. Björn Leder, Prof. Dr. Giancarlo Rossi, Dr. Stefan Sint and Dr. Rainer Sommer.

Thanks a lot, also alphabetically, to Marion Götsch and Sylvia Richter for all the help with the bureaucratic part of this thesis.

I am very much thankful to all my colleagues at DESY-Zeuthen, the ones who are still there and also those who have already found their way in some other place. All of them have contributed to my personal development and have made my stay in DESY very warm and enjoyable. I thank them for being much more than just colleagues, for all the moral support and the great moments that we have spent together. In particular I would like to mention, in alphabetic order, Simon Dinter, Dr. Philipp Gerhold, Isaac Hailperin and Andreas Nube for useful hints in the numerical side of my work. Thanks also to Dr. Xu Feng and Jim Kallarackal for the nice discussions at the whiteboard and to Pan Kessel for the reading of some chapters of this manuscript. I also want to thank Attila Nagy for helping me with his experience and the German language while I was teaching at the Humboldt–Universität zu Berlin.

I want to acknowledge my former teachers at the University of Salamanca, Dr. Fernando Atrio Barandela and Dr. Alfredo Valcarce Mejía. Thanks to Fernando for his nice lectures and all conversations which taught me a lot. Thanks to Alfredo, thanks to whom I have discovered

the beauty of particle physics and whose lectures and discussions have helped me to choose my scientific way.

I make a special mention of my very close friends, who have contributed to make these last years a much better time. Thanks very much, Camino Lamiel Puente, Ana Belén Raimóndez Yebra, Yesica Rodríguez González and Lucía Santamaría Lara for being such good friends, especially during the most difficult moments of the development of this thesis.

I really want to thank my boyfriend, Andrea Shindler, for being there every second of these years, giving me all his support and great understanding.

Eventually, I want to say 'thanks very much' to my family, all of whom are great and have supported me so much in one way or another. In particular, I want to mention my aunt, Carmen López Martínez, for being always there. Of course I want to thank my parents the most, Margarita López Martínez and Isidro González López, which ever since I was born have been by my side, besides the physical distances. I want to thank them for the unmeasurable love they have ever given to me, for having always supported my choices in life and for giving me all the courage that many times I did not have.

A. Conventions

A.1. Index conventions and general notation

- Components of spatial vectors: $k, l, \ldots$ running from 1 to 3
- Lorentz indices: $\mu, \nu, \ldots$ running from 0 to 3
- Dirac indices: $\alpha, \beta, \ldots$ running from 1 to 4
- Color vectors in the fundamental representation of SU(N_c): $A, B, \ldots$ from 1 to N_c
- Color vectors in the adjoint representation: $a, b, \ldots$ from 1 to $N_c^2 - 1$
- Flavor vectors in the fundamental representation of SU(N_f): $i, j, \ldots$ from 1 to N_f
- Flavor vectors in the adjoint representation: $a, b, \ldots$ from 1 to $N_f^2 - 1$
- In general sums over indices are explicitly written. In case they are omitted, repeated indices are always summed over, unless the opposite is stated
- Scalar products are always taken in Euclidean space (E) and all notation in general refers to Euclidean space. In case a reference to Minkowski space (M) is needed it will be made explicit
- The vectors $\vec{\mu} = a\hat{\mu}$ denote vectors on the lattice of length a and direction of the unitary vector $\hat{\mu}$
- $x = an$ denote discrete coordinates on the lattice, with a the lattice spacing and n the lattice points

A.2. Relation Minkowski-Euclidean space

Given the metric $g^{\mu\nu} = \mathrm{diag}\,(-1, 1, 1, 1)$ in Minkowski space, the relations satisfied by the Dirac matrices are

$$(\gamma^\mu_{\mathrm{M}})^\dagger = \gamma^0_{\mathrm{M}}\,\gamma^\mu_{\mathrm{M}}\,\gamma^0_{\mathrm{M}}\,, \qquad \{\gamma^\mu_{\mathrm{M}}, \gamma^\nu_{\mathrm{M}}\} = 2\,g^{\mu\nu}\,, \tag{A.1}$$

together with

$$(\gamma^0_{\mathrm{M}})^2 = -1\,, \qquad (\gamma^k_{\mathrm{M}})^2 = 1\,. \tag{A.2}$$

Also the relation between the contra- and co-variant matrices as given by the metric is

$$\gamma^0_{\mathrm{M}} = -\,\gamma^{\mathrm{M}}_0 \qquad \gamma^k_{\mathrm{M}} = \gamma^{\mathrm{M}}_k\,. \tag{A.3}$$

With this metric, the scalar product of two vectors in Dirac space, $x = (ct, \vec{x})$ and $p = (E/c, \vec{p})$ is defined by

$$p \cdot x = p^\mu x_\mu = g_{\mu\nu} p^\mu x^\nu = -Et + \vec{p} \cdot \vec{x}\,. \tag{A.4}$$

The rotation from Minkowski to Euclidean space, Wick's rotation, amounts to a transformation of the time coordinate from being real to purely imaginary

$$x_0^E \equiv -\mathrm{i}\, x_0^M \quad \Rightarrow \quad p_0^E \equiv -\mathrm{i}\, p_0^M \,, \tag{A.5}$$

where the metric is now the Euclidean metric $g_{\mu\nu} = \delta_{\mu\nu}$ and the contra- and co-variant indices behave equally.

The definition of the Dirac matrices in Euclidean space is then

$$\gamma_0^{\mathrm{E}} = -\mathrm{i}\,\gamma_0^{\mathrm{M}} \,, \qquad \gamma_k^{\mathrm{E}} = \gamma_k^{\mathrm{M}} \,, \tag{A.6}$$

which have the properties given in App. A.3. The expression of the Dirac matrices in Euclidean space and in the chiral representation are also collected in App. A.3.

Correlation functions in Minkowski space (Wightman functions) can be analytically continued to Euclidean space giving the corresponding Euclidean correlation functions (Schwinger functions) and viceversa. Therefore, results obtained in one space or the other do provide the same physical answer. In particular, this implies that all results obtained from simulations on the lattice, and thus in Euclidean space, can be traced back to Minkowski space recovering all the physical content of the theory. However, this statement is true *only* if the so called Osterwalder-Schrader conditions [48, 49] are fulfilled, which are not only necessary but also sufficient conditions to guarantee the equivalence between both spaces. The discussion of this topic goes beyond the scope of this work, but for all considerations here performed, the Osterwalder-Schrader conditions are fulfilled.

A.3. Dirac matrices

A chiral representation is chosen for the Dirac matrices, where

$$\gamma_\mu = \begin{pmatrix} 0 & e_\mu \\ e_\mu^\dagger & 0 \end{pmatrix} .$$

The 2×2 matrices e_μ are

$$e_0 = -1 \,, \quad e_k = -\mathrm{i}\,\sigma_k \,, \tag{A.7}$$

with σ_k the Pauli matrices[1]

$$\sigma_1 = \begin{pmatrix} 0 & 1 \\ 1 & 0 \end{pmatrix} , \qquad \sigma_2 = \begin{pmatrix} 0 & -i \\ i & 0 \end{pmatrix} , \qquad \sigma_3 = \begin{pmatrix} 1 & 0 \\ 0 & -1 \end{pmatrix} ,$$

satisfying the relations

$$\{\sigma_i \,, \sigma_j\} = 2\,\delta_{ij} \,, \qquad [\sigma_i \,, \sigma_j] = \mathrm{i}2\,\epsilon_{ijk}\,\sigma_k \,. \tag{A.8}$$

ϵ_{ijk} is the totally antisymmetric tensor with $\epsilon_{123} = 1$.

The Dirac matrices satisfy

$$\gamma_\mu = \gamma_\mu^\dagger = \gamma_\mu^{-1} \,, \qquad \{\gamma_\mu, \gamma_\nu\} = 2\delta_{\mu\nu} \,. \tag{A.9}$$

The γ_5 matrix is defined as

$$\gamma_5 \equiv \gamma_0\,\gamma_1\,\gamma_2\,\gamma_3 \qquad \Longrightarrow \qquad \gamma_5 = \begin{pmatrix} 1 & 0 \\ 0 & -1 \end{pmatrix}$$

[1] Pauli matrices specifying the flavor group are denoted τ^a $(a = 1, 2, 3)$ instead of σ_k.

thus

$$\gamma_5 = \gamma_5^\dagger\,, \qquad \gamma_5^2 = 1\,, \qquad \{\gamma_\mu\,,\gamma_5\} = 0\,. \tag{A.10}$$

The hermitian matrices

$$\sigma_{\mu\nu} = \frac{i}{2}\,[\gamma_\mu\,,\gamma_\nu]\,, \qquad \sigma_{\mu\nu}^\dagger = \sigma_{\nu\mu} \tag{A.11}$$

are explicitly given by

$$\sigma_{0k} = \begin{pmatrix} \sigma_k & 0 \\ 0 & -\sigma_k \end{pmatrix}\,, \qquad \sigma_{ij} = -\epsilon_{ijk} \begin{pmatrix} \sigma_k & 0 \\ 0 & \sigma_k \end{pmatrix}\,.$$

A.4. Group theory

The following notation is used here; SU(N) represents a special unitary Lie group and su(N) its corresponding Lie algebra. The elements of the group are $N \times N$, complex, unitary matrices, U, with $\det[U] = 1$. SU(N) is a non-abelian group, which means that the group operation is not commutative. The group operation is in this case the matrix multiplication.

Given a $N \times N$ unitary matrix, U, it can always be represented by the exponential of a $N \times N$ anti-hermitian (thus diagonalizable) matrix, A, as

$$U = e^A \quad \Rightarrow \quad U^\dagger U = 1 \quad \Rightarrow \quad U^\dagger = U^{-1}\,, \text{unitarity guaranteed}\,. \tag{A.12}$$

Due to the anti-hermiticity of A, N^2 independent real parameters are needed to describe a $N \times N$ unitary matrix. Due to the condition on the determinant (equivalent to $\mathrm{tr}[A] = 0$, module 2π), the SU(N) matrices, U, can then be described by only $N^2 - 1$ independent real parameters.

The most general form of the $N \times N$, complex, anti-hermitian, traceless matrices A is

$$A = \sum_{a=1}^{N^2-1} \omega^a\, T_a\,, \tag{A.13}$$

thus the group elements can be written in their final form

$$U = \exp\Big(\sum_{a=1}^{N^2-1} \omega^a\, T_a\Big)\,, \tag{A.14}$$

with ω^a the $N^2 - 1$ real independent parameters needed to parametrize the group elements U and T_a the $N^2 - 1$ generators of SU(N), which are $N \times N$, complex, anti-hermitian, traceless matrices.

The group generators verify the properties

$$[T_a\,,T_b] = f_{abc}\,T_c\,, \qquad \mathrm{tr}[T_a\,T_b] = -\frac{1}{2}\,\delta_{ab}\,, \tag{A.15}$$

with f_{abc} totally anti-symmetric coefficients named structure constants, since they provide the structure of the Lie algebra of the group, su(N). In this case, the Lie algebra is given by the linear combinations of the group generators given in Eq. (A.13). With the conventions chosen here, the elements of the Lie algebra, A, are anti-hermitian.

In case $N = 2$ the standard representation for the SU(2) generators is

$$T_a = \frac{1}{2\mathrm{i}}\,\sigma_a\,, \tag{A.16}$$

with σ_a the Pauli matrices defined in App. A.3 and $f_{abc} = \epsilon_{abc}$ the completely anti-symmetric tensor.

In case $N = 3$ the standar representation for the SU(3) generators is

$$T_a = \frac{1}{2\mathrm{i}}\,\lambda_a\,, \tag{A.17}$$

with λ_a the Gell-Mann matrices. When representing the color group SU(N_c) with $N_c = 3$, the algebra of the group, su(N_c) is usually denoted

$$A_\mu(x) = \sum_{a=1}^{N_c^2-1} A_\mu^a(x)\,T^a\,. \tag{A.18}$$

Here the elements of the algebra are the gauge fields with Lorentz indices μ and the real-valued fields $A_\mu^a(x)$ are the color components of the gauge fields.

A.5. Lattice derivatives

A.5.1. Ordinary lattice derivatives

The ordinary lattice derivatives act on color singlet functions, $f(x)$, and are defined by

$$\partial_\mu f(x) = \frac{1}{a}\,[\,f(x+\vec{\mu}) - f(x)\,]\,, \tag{A.19}$$

$$\partial_\mu^* f(x) = \frac{1}{a}\,[\,f(x) - f(x-\vec{\mu})\,]\,. \tag{A.20}$$

The lattice symmetric derivative and the lattice d'Alambert operator can be defined as well,

$$\frac{1}{2}\Big(\partial_\mu + \partial_\mu^*\Big) f(x) = \frac{1}{2a}\,[\,f(x+\vec{\mu}) - f(x-\vec{\mu})\,]\,, \tag{A.21}$$

$$\partial_\mu^*\,\partial_\mu f(x) = \frac{1}{a^2}\,[\,f(x+\vec{\mu}) + f(x-\vec{\mu}) - 2f(x)\,]\,. \tag{A.22}$$

The next relation holds

$$\partial_\mu^*\,\partial_\mu = \partial_\mu\,\partial_\mu^* = \frac{1}{a}\,\Big(\partial_\mu - \partial_\mu^*\Big)\,. \tag{A.23}$$

A.5.2. Covariant lattice derivatives

The gauge covariant derivative operators act on the quark fields $\psi(x)$. Due to the presence of the lattice gauge fields $U_\mu(x)$, there is a non-trivial color structure.

The action on the right of forward and backward drivatives is defined, respectively,

$$\overrightarrow{\nabla}_\mu \psi(x) = \frac{1}{a}\,[\,\lambda_\mu\,U_\mu(x)\,\psi(x+\vec{\mu}) - \psi(x)\,]\,, \tag{A.24}$$

$$\overrightarrow{\nabla}_\mu^* \psi(x) = \frac{1}{a}\,[\,\psi(x) - \lambda_\mu^\dagger\,U_\mu(x-\vec{\mu})^\dagger\,\psi(x-\vec{\mu})\,]\,, \tag{A.25}$$

and the action on the left as

$$\overline{\psi}(x)\overleftarrow{\nabla}_\mu = \frac{1}{a}\,[\,\overline{\psi}(x+\vec{\mu})\,U_\mu(x)^\dagger\,\lambda_\mu^\dagger - \overline{\psi}(x)\,]\,, \tag{A.26}$$

$$\overline{\psi}(x)\overleftarrow{\nabla}_\mu^* = \frac{1}{a}\,[\,\overline{\psi}(x) - \overline{\psi}(x-\vec{\mu})\,U_\mu(x-\vec{\mu})\,\lambda_\mu\,]\,. \tag{A.27}$$

The lattice covariant symmetric derivatives acting on right and left are thus

$$\frac{1}{2}\Big(\overrightarrow{\nabla}_\mu + \overrightarrow{\nabla}^*_\mu\Big)\psi(x) = \frac{1}{2a}\left[\,\lambda_\mu\, U_\mu(x)\,\psi(x+\vec{\mu}) - \lambda^\dagger_\mu\, U_\mu(x-\vec{\mu})^\dagger\,\psi(x-\vec{\mu})\,\right], \tag{A.28}$$

$$\overline{\psi}(x)\frac{1}{2}\Big(\overleftarrow{\nabla}_\mu + \overleftarrow{\nabla}^*_\mu\Big) = \frac{1}{2a}\left[\,\overline{\psi}(x+\vec{\mu})\, U_\mu(x)^\dagger\,\lambda^\dagger_\mu - \overline{\psi}(x-\vec{\mu})\, U_\mu(x-\vec{\mu})\,\lambda_\mu\,\right]. \tag{A.29}$$

The covariant lattice d'Alambert operator is

$$\overrightarrow{\nabla}^*_\mu\,\overrightarrow{\nabla}_\mu\psi(x) = \frac{1}{a^2}\left[\,\lambda_\mu\, U_\mu(x)\,\psi(x+\vec{\mu}) + \lambda^\dagger_\mu\, U_\mu(x-\vec{\mu})^\dagger\,\psi(x-\vec{\mu}) - 2\psi(x)\,\right], \tag{A.30}$$

$$\overline{\psi}(x)\overleftarrow{\nabla}_\mu\,\overleftarrow{\nabla}^*_\mu = \frac{1}{a^2}\left[\,\overline{\psi}(x+\vec{\mu})\, U_\mu(x)^\dagger\,\lambda^\dagger_\mu + \overline{\psi}(x-\vec{\mu})\, U_\mu(x-\vec{\mu})\,\lambda_\mu - 2\psi(x)\,\right], \tag{A.31}$$

which verifies

$$\overrightarrow{\nabla}^*_\mu\,\overrightarrow{\nabla}_\mu = \overrightarrow{\nabla}_\mu\,\overrightarrow{\nabla}^*_\mu = \frac{1}{a}\left(\overrightarrow{\nabla}_\mu - \overrightarrow{\nabla}^*_\mu\right), \qquad \overleftarrow{\nabla}^*_\mu\,\overleftarrow{\nabla}_\mu = \overleftarrow{\nabla}_\mu\,\overleftarrow{\nabla}^*_\mu = \frac{1}{a}\left(\overleftarrow{\nabla}_\mu - \overleftarrow{\nabla}^*_\mu\right). \tag{A.32}$$

The phase factors in these expressions are defined as

$$\lambda_\mu = e^{\mathrm{i}\,a\,\theta_\mu/L}, \qquad \theta_0 = 0\,, \quad -\pi < \theta_k \leq \pi\,, \tag{A.33}$$

where L denotes the spatial extent of the lattice. In particular, in the infinite volume limit these phase factors take the value one.

The phase factors are directly related to the boundary conditions in the spatial directions as follows. Assuming periodic boundary conditions in the spatial directions

$$\psi(x+L\hat{k}) = \psi(x)\,, \qquad \overline{\psi}(x+L\hat{k}) = \overline{\psi}(x)\,, \tag{A.34}$$

and having the definitions for the derivatives given above, is equivalent to define the derivatives without the phase factors but with periodic boundary conditions up to a phase, the so called generalized periodic boundary conditions, given by

$$\psi(x+L\hat{k}) = e^{\mathrm{i}\theta_k}\,\psi(x)\,, \qquad \overline{\psi}(x+L\hat{k}) = \overline{\psi}(x)\,e^{-\mathrm{i}\theta_k}\,. \tag{A.35}$$

Although both formulations are equivalent, it is technically simpler to keep the phase factors in the definition of the derivatives. The equivalence can be demonstrated by the application of an abelian gauge transformation. The angles θ_k parametrize a family of admisible boundary conditions and give more opportunities to probe the quark dynamics.

B. Symmetries

The convention used for the transformations is as follows; given a transformation, t, acting on a certain field, $M(x)$, $M(x)^t$ means that the corresponding transformation affects all indices of the field $M(x)$ and also the space-time coordinates, x, while if $M^t(x)$ is written, the space-time coordinates are not transformed.

B.1. Discrete symmetries

B.1.1. Hermiticity and γ_5-hermiticity

An operator D which is γ_5-hermitian must verify

$$\gamma_5 \, D \, \gamma_5 = D^\dagger \, . \tag{B.1}$$

From a γ_5-hermitian operator, an operator Q can be constructed

$$Q := \gamma_5 \, D \tag{B.2}$$

which is then hermitian

$$Q = Q^\dagger \, . \tag{B.3}$$

γ_5-*hermiticity* implies that the eigenvalues of the operator D are either real or complex conjugate pairs and its determinant is real. This condition on the determinant is of maximal importance in MC simulations of QCD, where D is a Dirac operator on the lattice. *Hermiticity* implies that the eigenvalues of the operator Q are always real and its determinant is real.

There is still another possibility, the so called γ_5-*hermiticity times flavor exchange*,

$$\tau^{1,2} \gamma_5 \, D \, \gamma_5 \, \tau^{1,2} = D^\dagger \, , \tag{B.4}$$

which gives rise to the same properties of the Dirac operator as indicated above for γ_5-hermiticity.

B.1.2. Charge conjugation, parity and time reversal in the standard basis

In the chiral representation of the Dirac matrices (cf. App. A.3), a possible choice for the charge conjugation matrix is

$$C = \mathrm{i} \, \gamma_0 \, \gamma_2 \, , \tag{B.5}$$

with the properties

$$C \, \gamma_\mu \, C^{-1} = -\gamma_\mu^T \, , \quad C \, \gamma_5 \, C^{-1} = \gamma_5 \, , \quad C = C^\dagger = C^{-1} = -C^T \, . \tag{B.6}$$

Charge conjugation symmetry is defined

$$\mathcal{C} \, : \, \begin{cases} U_\mu(x) \, \rightarrow \, U_\mu(x)^* \\ \psi(x) \, \rightarrow \, C^{-1} \, \overline{\psi}(x)^T \\ \overline{\psi}(x) \, \rightarrow \, -\psi(x)^T \, C \end{cases} \tag{B.7}$$

Parity and time reversal transformations are defined, respectively,

$$\mathcal{P}\,:\,\begin{cases} U_0(x_0,\vec{x})\;\to\;U_0(x_0,-\vec{x})\,, \quad U_k(x_0,\vec{x})\;\to\;U_k^\dagger(x_0,-\vec{x}-\vec{k}) \\ \psi(x_0,\vec{x})\;\to\;\gamma_0\,\psi(x_0,-\vec{x}) \\ \overline{\psi}(x_0,\vec{x})\;\to\;\overline{\psi}(x_0,-\vec{x})\,\gamma_0 \end{cases} \tag{B.8}$$

$$\mathcal{T}\,:\,\begin{cases} U_0(x_0,\vec{x})\;\to\;U_0^\dagger(-x_0-a,\vec{x})\,, \quad U_k(x_0,\vec{x})\;\to\;U_k(-x_0,\vec{x}) \\ \psi(x_0,\vec{x})\;\to\;\mathrm{i}\,\gamma_0\,\gamma_5\,\psi(-x_0,\vec{x}) \\ \overline{\psi}(x_0,\vec{x})\;\to\;\overline{\psi}(-x_0,\vec{x})\,\mathrm{i}\,\gamma_0\,\gamma_5 \end{cases} \tag{B.9}$$

When considering ψ to be a flavor doublet, also the symmetries $\mathcal{P}$, $\mathcal{T}$ and $\mathcal{C}$ with a flavor exchange can be defined,

$$\mathcal{P}_F^{1,2}\,:\,\begin{cases} U_0(x_0,\vec{x})\;\to\;U_0(x_0,-\vec{x})\,, \quad U_k(x_0,\vec{x})\;\to\;U_k^\dagger(x_0,-\vec{x}-\vec{k}) \\ \psi(x_0,\vec{x})\;\to\;\mathrm{i}\,\gamma_0\,\tau^{1,2}\,\psi(x_0,-\vec{x}) \\ \overline{\psi}(x_0,\vec{x})\;\to\;-\overline{\psi}(x_0,-\vec{x})\,\mathrm{i}\,\gamma_0\,\tau^{1,2} \end{cases} \tag{B.10}$$

$$\mathcal{T}_F^{1,2}\,:\,\begin{cases} U_0(x_0,\vec{x})\;\to\;U_0^\dagger(-x_0-a,\vec{x})\,, \quad U_k(x_0,\vec{x})\;\to\;U_k(-x_0,\vec{x}) \\ \psi(x_0,\vec{x})\;\to\;\gamma_0\,\gamma_5\,\tau^{1,2}\,\psi(-x_0,\vec{x}) \\ \overline{\psi}(x_0,\vec{x})\;\to\;-\overline{\psi}(-x_0,\vec{x})\,\gamma_0\,\gamma_5\,\tau^{1,2} \end{cases} \tag{B.11}$$

$$\mathcal{C}_F^{1,2}\,:\,\begin{cases} \psi(x)\to i\tau^{1,2}C^{-1}\,\overline{\psi}(x)^T \\ \overline{\psi}(x)\to\psi(x)^T\,i\tau^{1,2}C \end{cases} \tag{B.12}$$

B.1.3. Charge conjugation, parity and time reversal in the twisted basis

The twisted basis $\{\chi\,,\overline{\chi}\}$ and the standard basis $\{\psi\,,\overline{\psi}\}$ are related by the axial non-anomalous transformation

$$\psi(x)=e^{\mathrm{i}\,\frac{\alpha}{2}\,\gamma_5\,\tau^3}\,\chi(x)\,,\qquad \overline{\psi}(x)=\overline{\chi}(x)\,e^{\mathrm{i}\,\frac{\alpha}{2}\,\gamma_5\,\tau^3}\,. \tag{B.13}$$

While charge conjugation stays invariant, parity and time reversal are affected by the rotation and take a different form in the twisted basis. In this basis they are denoted $\mathcal{P}_\alpha$ and $\mathcal{T}_\alpha$, respectively, and have the expressions

$$\mathcal{P}_\alpha\,:\,\begin{cases} U_0(x_0,\vec{x})\;\to\;U_0(x_0,-\vec{x})\,, \quad U_k(x_0,\vec{x})\;\to\;U_k^\dagger(x_0,-\vec{x}-\vec{k}) \\ \chi(x_0,\vec{x})\;\to\;\gamma_0\,e^{\mathrm{i}\,\alpha\,\gamma_5\,\tau^3}\,\chi(x_0,-\vec{x}) \\ \overline{\chi}(x_0,\vec{x})\;\to\;\overline{\chi}(x_0,-\vec{x})\,e^{\mathrm{i}\,\alpha\,\gamma_5\,\tau^3}\,\gamma_0 \end{cases} \tag{B.14}$$

$$\mathcal{T}_\alpha\,:\,\begin{cases} U_0(x_0,\vec{x})\;\to\;U_0^\dagger(-x_0-a,\vec{x})\,, \quad U_k(x_0,\vec{x})\;\to\;U_k(-x_0,\vec{x}) \\ \chi(x_0,\vec{x})\;\to\;\mathrm{i}\,\gamma_0\,\gamma_5\,e^{\mathrm{i}\,\alpha\,\gamma_5\,\tau^3}\,\chi(-x_0,\vec{x}) \\ \overline{\chi}(x_0,\vec{x})\;\to\;\overline{\chi}(-x_0,\vec{x})\,e^{\mathrm{i}\,\alpha\,\gamma_5\,\tau^3}\,\mathrm{i}\,\gamma_0\,\gamma_5 \end{cases} \tag{B.15}$$

B.2. Continuous chiral symmetry with $N_f = 2$

In this section, the definitions of Tab. 2.1 are particularized for $N_f = 2$. The Pauli matrices are denoted τ^a when referring to flavor space (see App. A.3 for definitions). The matrix $\mathbb{1}$ denotes the identity matrix of dimension 2×2.

Note that, with abuse of notation, we denote here $\mathrm{SU}(2)_A$ the non-singlet axial-vector transformations. Such transformations, however, do not have a group structure. As indicated above in Chap. 2, this notation is employed in order to make the discussion of the standard and twisted basis more clear.

B.2.1. Symmetries in the standard basis

$$\mathrm{SU}(2)_V : \begin{cases} \psi(x) \;\to\; e^{\mathrm{i}\,\frac{\alpha_V^a}{2}\,\tau^a}\,\psi(x) \\ \overline{\psi}(x) \;\to\; \overline{\psi}(x)\,e^{-\mathrm{i}\,\frac{\alpha_V^a}{2}\,\tau^a} \end{cases} \tag{B.16}$$

$$\mathrm{SU}(2)_A : \begin{cases} \psi(x) \;\to\; e^{\mathrm{i}\,\frac{\alpha_A^a}{2}\,\gamma_5\,\tau^a}\,\psi(x) \\ \overline{\psi}(x) \;\to\; \overline{\psi}(x)\,e^{\mathrm{i}\,\frac{\alpha_A^a}{2}\,\gamma_5\,\tau^a} \end{cases} \tag{B.17}$$

$$\mathrm{U}(1)_V : \begin{cases} \psi(x) \;\to\; e^{\mathrm{i}\,\alpha_V^0\,\mathbb{1}}\,\psi(x) \\ \overline{\psi}(x) \;\to\; \overline{\psi}(x)\,e^{-\mathrm{i}\,\alpha_V^0\,\mathbb{1}} \end{cases} \tag{B.18}$$

$$\mathrm{U}(1)_A : \begin{cases} \psi(x) \;\to\; e^{\mathrm{i}\,\alpha_A^0\,\gamma_5\,\mathbb{1}}\,\psi(x) \\ \overline{\psi}(x) \;\to\; \overline{\psi}(x)\,e^{\mathrm{i}\,\alpha_A^0\,\gamma_5\,\mathbb{1}} \end{cases} \tag{B.19}$$

B.2.2. Symmetries in the twisted basis

Under the rotation Eq. (B.13), which brings the transformations from the physical to the twisted basis, only the non-singlet transformations change form. Indeed, only the charged sector ($\tau^{1,2}$) transforms, while the neutral sector (τ^3) remains invariant.

In the twisted basis, for a general rotation angle α, these transformations read as follows

$$[\mathrm{SU}(2)_V]_\alpha : \begin{cases} \chi(x) \;\to\; e^{-\mathrm{i}\,\frac{\alpha}{2}\,\gamma_5\,\tau^3}\,e^{\mathrm{i}\,\frac{\alpha_V^a}{2}\,\tau^a}\,e^{\mathrm{i}\,\frac{\alpha}{2}\,\gamma_5\,\tau^3}\,\chi(x) \\ \overline{\chi}(x) \;\to\; \overline{\chi}(x)\,e^{\mathrm{i}\,\frac{\alpha}{2}\,\gamma_5\,\tau^3}\,e^{-\mathrm{i}\,\frac{\alpha_V^a}{2}\,\tau^a}\,e^{-\mathrm{i}\,\frac{\alpha}{2}\,\gamma_5\,\tau^3} \end{cases} \tag{B.20}$$

$$[\mathrm{SU}(2)_A]_\alpha : \begin{cases} \chi(x) \;\to\; e^{-\mathrm{i}\,\frac{\alpha}{2}\,\gamma_5\,\tau^3}\,e^{\mathrm{i}\,\frac{\alpha_A^a}{2}\,\gamma_5\,\tau^a}\,e^{\mathrm{i}\,\frac{\alpha}{2}\,\gamma_5\,\tau^3}\,\chi(x) \\ \overline{\chi}(x) \;\to\; \overline{\chi}(x)\,e^{\mathrm{i}\,\frac{\alpha}{2}\,\gamma_5\,\tau^3}\,e^{\mathrm{i}\,\frac{\alpha_A^a}{2}\,\gamma_5\,\tau^a}\,e^{-\mathrm{i}\,\frac{\alpha}{2}\,\gamma_5\,\tau^3} \end{cases} \tag{B.21}$$

which at the so called maximal twist condition, $\alpha = \pi/2$, and for $a = 1, 2$ become

$$[\mathrm{SU}(2)_V^{1,2}]_{\frac{\pi}{2}} : \begin{cases} \chi(x) \;\to\; e^{\pm\mathrm{i}\,\frac{\alpha_V^{1,2}}{2}\,\gamma_5\,\tau^{2,1}}\,\chi(x) \\ \overline{\chi}(x) \;\to\; \overline{\chi}(x)\,e^{\pm\mathrm{i}\,\frac{\alpha_V^{1,2}}{2}\,\gamma_5\,\tau^{2,1}} \end{cases} \tag{B.22}$$

$$[\mathrm{SU}(2)_A^{1,2}]_{\frac{\pi}{2}} : \begin{cases} \chi(x) \;\to\; e^{\pm \mathrm{i}\, \frac{\alpha_A^{1,2}}{2}\, \tau^{2,1}}\, \chi(x) \\ \overline{\chi}(x) \;\to\; \overline{\chi}(x)\, e^{\mp \mathrm{i}\, \frac{\alpha_A^{1,2}}{2}\, \tau^{2,1}} \end{cases} \tag{B.23}$$

B.3. Symmetries of the QCD action

The QCD action is always invariant under local gauge transformations and Poincaré transformations. The last are the space-time translations and the Lorentz transformations (boosts and spatial rotations).

The chiral group of the QCD *action* in a theory with N_f flavors of fermion fields which are degenerate in mass is

$$\mathrm{SU}(N_f)_V \times \mathrm{U}(1)_V \times \mathrm{U}(1)_A \,, \tag{B.24}$$

while for mass non-degenerate quarks it reduces to

$$\mathrm{U}(1)_V^{\,(1)} \times \mathrm{U}(1)_V^{\,(2)} \times \cdots \overset{(N_f-1)}{\times} \mathrm{U}(1)_V \times \mathrm{U}(1)_A \,. \tag{B.25}$$

Note however, that the chiral group of the QCD action is not that of QCD itself. The chiral group of QCD is reduced with respect to that of the action by the anomaly and the spontaneous symmetry breaking. For a detailed discussion of the chiral group of QCD and of the transformations of the chiral group see Sec. 2.4.

Additionally, the QCD action is invariant under the discrete symmetries; charge conjugation $\mathcal{C}$, parity $\mathcal{P}$ and time reversal $\mathcal{T}$ and thus also $\mathcal{CP}$, $\mathcal{CT}$, $\mathcal{PT}$ and $\mathcal{CPT}$.

Local gauge invariance:

Let us denote x the space-time coordinates and $\psi(x)$ the fermion (matter) fields. Invariance under local gauge transformations means that, given an internal degree of freedom of the matter field (color in QCD), it should be possible to choose a basis to describe this degree of freedom independently on the space-time point. In order for this to happen it is required a coupling between the matter field and a gauge field which accounts for the basis transformation between different (infinitesimally close) points. In practice, this is done replacing the normal derivative with the covariant derivative. This replacement is the so-called *minimal coupling prescription.*

With this prescription, the QCD action is invariant under local transformations generated by elements of the non-abelian special unitary group of 3×3 matrices, SU(3). The group elements, $\Omega(x)$, are 3×3 complex unitary matrices, $\Omega(x)^\dagger = \Omega(x)^{-1}$, with $\det[\Omega(x)] = 1$.

The transformation has the form,

$$\psi(x) \to \psi'(x) = \Omega(x)\psi(x) \;,\; \overline{\psi}(x) \to \overline{\psi}'(x) = \overline{\psi}(x)\Omega(x)^\dagger \tag{B.26}$$

for the fermion and anti-fermion fields and

$$A_\mu(x) \to A'_\mu(x) = \Omega(x)A_\mu(x)\Omega(x)^\dagger + \Omega(x)\partial_\mu\Omega(x)^\dagger \tag{B.27}$$

for the gauge fields.

These transformations ensure that $\psi(x)$ and $D_\mu\psi(x)$ transform in the same way. In particular,

$$D_\mu \to D'_\mu = \Omega(x)D_\mu\Omega(x)^\dagger \tag{B.28}$$

$$F_{\mu\nu}(x) \to F'_{\mu\nu}(x) = \Omega(x)F_{\mu\nu}(x)\Omega(x)^\dagger \,. \tag{B.29}$$

B.4. Hermiticity of Wilson-type fermions

B.4.1. Standard Wilson fermions

The standard Wilson operator defined in Sec. 2.7.2 can also be written in the form (we treat in this section the free quark theory)

$$K_{\rm W}(x,y) = \frac{1}{2a}\sum_{\mu}\Big\{\,\gamma_\mu\,\Delta^{\mu}_{xy} - r\,\Box^{\mu}_{xy}\,\Big\} + m_0\,\delta_{xy} \tag{B.30}$$

with

$$\Delta^{\mu}_{xy} = \delta_{x+a\hat{\mu},y} - \delta_{x-a\hat{\mu},y}\,, \tag{B.31}$$

$$\Box^{\mu}_{xy} = \delta_{x+a\hat{\mu},y} + \delta_{x-a\hat{\mu},y} - 2\delta_{xy}\,. \tag{B.32}$$

So, the hermitian conjugate of the Wilson operator is

$$K^{\dagger}_{\rm W}(x,y) = \frac{1}{2a}\sum_{\mu}\Big\{\,\gamma_\mu\,(\Delta^{\dagger})^{\mu}_{xy} - r\,(\Box^{\dagger})^{\mu}_{xy}\,\Big\} + m_0\,(\delta^{\dagger})_{xy} \tag{B.33}$$

which using translation invariance and the relations

$$\begin{aligned}(\Delta^{\dagger})^{\mu}_{xy} &= \delta_{y,x+a\hat{\mu}} - \delta_{y,x-a\hat{\mu}}\\ &= \delta_{y-a\hat{\mu},x} - \delta_{y+a\hat{\mu},x}\\ &= -\Delta_{yx}\,,\end{aligned} \tag{B.34}$$

$$\begin{aligned}(\Box^{\dagger})^{\mu}_{xy} &= \delta_{y,x+a\hat{\mu}} + \delta_{y,x-a\hat{\mu}} - 2\,\delta_{yx}\\ &= \delta_{y-a\hat{\mu},x} + \delta_{y+a\hat{\mu},x} - 2\,\delta_{yx}\\ &= \Box_{yx}\,,\end{aligned} \tag{B.35}$$

$$(\delta^{\dagger})_{xy} = \delta_{yx}\,, \tag{B.36}$$

is reduced to

$$K^{\dagger}_{\rm W}(x,y) = \frac{1}{2a}\sum_{\mu}\Big\{\,-\gamma_\mu\,\Delta^{\mu}_{yx} - r\,\Box^{\mu}_{yx}\,\Big\} + m_0\,\delta_{yx}\,. \tag{B.37}$$

Multiplying both sides of Eq. (B.37) by γ_5 and using the anti-commutation property of the gamma matrices, $\{\gamma_\mu\,,\gamma_5\} = 0$, as well as $\gamma_5^2 = 1$, it becomes clear the γ_5-*hermiticity* relation for the Wilson operator

$$\gamma_5\,K^{\dagger}_{\rm W}(x,y)\,\gamma_5 = K_{\rm W}(y,x)\,. \tag{B.38}$$

The next step is to use the relation between the Wilson operator and the quark propagator $S_{\rm W}(x,y)$[1]

$$K_{\rm W}(x,y)\,S_{\rm W}(y,z) = \delta_{xz}\,, \tag{B.39}$$

its transpose

$$S_{\rm W}(z,y)\,K_{\rm W}(y,x) = \delta_{zx}\,, \tag{B.40}$$

and its transpose hermitian conjugate

$$K^{\dagger}_{\rm W}(y,x)\,S^{\dagger}_{\rm W}(z,y) = (\delta^{\dagger})_{zx}. \tag{B.41}$$

[1] The relations are written in lattice units and Einstein convention is used.

Replacing in Eq. (B.39) the Wilson operator by its hermitian conjugate, by using the hermiticity property Eq. (B.38) derived above, then

$$\gamma_5\, K_{\rm W}^{\dagger}(y,x)\,\gamma_5\, S_{\rm W}(y,z) = \delta_{xz}\,. \tag{B.42}$$

On the other hand, introducing the γ_5 matrix into Eq. (B.41) the next relation is obtained

$$\gamma_5\, K_{\rm W}^{\dagger}(y,x)\,\gamma_5\,\gamma_5\, S_{\rm W}^{\dagger}(z,y)\,\gamma_5 = \delta_{xz}\,. \tag{B.43}$$

Comparing now Eq. (B.42) and Eq. (B.43), the γ_5-*hermiticity* relation is demonstrated for the quark propagator of Wilson fermions

$$\gamma_5\, S_{\rm W}^{\dagger}(z,y)\,\gamma_5 = S_{\rm W}(y,z)\,. \tag{B.44}$$

B.4.2. Twisted mass Wilson fermions

The fermionic operator for two flavors of mass-degenerate twisted mass Wilson fermions, described in Sec. 2.7.3 can also be expressed as (in the free quark theory)

$$K(x,y) = K_{\rm W}(x,y) + \mathrm{i}\,\mu_q\,\gamma_5\,\tau^3\,\delta_{xy}\,. \tag{B.45}$$

Making explicit the flavor content of the spinors

$$\chi = \begin{pmatrix} u \\ d \end{pmatrix}, \qquad \overline{\chi} = (\overline{u}, \overline{d})\,, \tag{B.46}$$

the twisted mass Wilson operator can be written separately for each flavor

$$K^u(x,y) = K_{\rm W}(x,y) + \mathrm{i}\,\mu_q\,\gamma_5\,\delta_{xy} \tag{B.47a}$$

$$K^d(x,y) = K_{\rm W}(x,y) - \mathrm{i}\,\mu_q\,\gamma_5\,\delta_{xy}\,. \tag{B.47b}$$

Performing the hermitian conjugation of Eq. (B.47), multiplying both sides by γ_5 and using the γ_5-hermiticity relation for the Wilson operator, Eq. (B.38), the γ_5-*hermiticity with flavor exchange* property of the twisted mass Wilson fermion operator is obtained

$$\gamma_5\, K^{\dagger\, u}(x,y)\,\gamma_5 = K_{\rm W}(y,x) - \mathrm{i}\,\mu_q\,\gamma_5\,\delta_{yx} = K^d(y,x) \tag{B.48a}$$

$$\gamma_5\, K^{\dagger\, d}(x,y)\,\gamma_5 = K_{\rm W}(y,x) + \mathrm{i}\,\mu_q\,\gamma_5\,\delta_{yx} = K^u(y,x)\,. \tag{B.48b}$$

As in the Wilson case, the next relations are needed

$$K^u(x,y)\,S^u(y,z) = \delta_{xz} \tag{B.49a}$$

$$K^d(x,y)\,S^d(y,z) = \delta_{xz}\,, \tag{B.49b}$$

and their hermitian transpose

$$K^{\dagger\, u}(y,x)\,S^{\dagger\, u}(z,y) = \delta_{xz} \tag{B.50a}$$

$$K^{\dagger\, d}(y,x)\,S^{\dagger\, d}(z,y) = \delta_{xz}\,. \tag{B.50b}$$

Substituting Eq. (B.48) in Eq. (B.49) the next relations are obtained

$$\gamma_5 \, K^{\dagger\, d}(y,x)\, \gamma_5 S^u(y,z) = \delta_{xz} \tag{B.51a}$$
$$\gamma_5 \, K^{\dagger\, u}(y,x)\, \gamma_5 S^d(y,z) = \delta_{xz}\,. \tag{B.51b}$$

Introducing γ_5 in Eq. (B.50)

$$\gamma_5 \, K^{\dagger\, u}(y,x)\, \gamma_5 \, \gamma_5 \, S^{\dagger\, u}(z,y)\, \gamma_5 = \delta_{xz} \tag{B.52a}$$
$$\gamma_5 \, K^{\dagger\, d}(y,x)\, \gamma_5 \, \gamma_5 \, S^{\dagger\, d}(z,y)\, \gamma_5 = \delta_{xz}\,. \tag{B.52b}$$

Comparing now Eq. (B.51) and Eq. (B.52) the γ_5-*hermiticity with flavor exchange* property of the propagator of twisted mass Wilson fermions is obtained for each flavor

$$\gamma_5 \, S^{\dagger\, u}(z,y)\, \gamma_5 = S^d(y,z) \tag{B.53a}$$
$$\gamma_5 \, S^{\dagger\, d}(z,y)\, \gamma_5 = S^u(y,z)\,. \tag{B.53b}$$

Eventually, Eq. (B.48) and Eq. (B.53) can be written in a more compact form. They are, respectively,

$$\tau^{1,2}\gamma_5 \, K^{\dagger}(x,y)\, \gamma_5 \, \tau^{1,2} = K(y,x) \tag{B.54}$$
$$\tau^{1,2}\gamma_5 \, S^{\dagger}(x,y)\, \gamma_5 \, \tau^{1,2} = S(y,x)\,. \tag{B.55}$$

C. Useful notions in lattice QCD

C.1. Doublers

Given the free naive lattice Dirac operator in coordinate space[1]

$$K(x,y) = \sum_{\mu} \frac{1}{2a}\,\gamma_\mu\,[\delta_{x+\hat{\mu},y} - \delta_{x-\hat{\mu},y}] + m_0\,\delta_{x,y}\,, \tag{C.1}$$

it is related to the quark propagator, $S(x,y)$, by the matrix relation

$$a^4 \sum_{z} K(x,z)S(z,y) = \delta_{x,y}\,. \tag{C.2}$$

In momentum space, however, an algebraic relation holds

$$\widetilde{K}(p)\,\widetilde{S}(p) = 1 \implies \widetilde{S}(p) = \widetilde{K}(p)^{-1}\,, \tag{C.3}$$

with the Dirac operator in momentum space given by

$$\widetilde{K}(p) = \mathrm{i}\,\gamma_\mu\,\mathring{p}_\mu + m_0\,, \quad \mathring{p}_\mu = \frac{1}{a}\sin\left(ap_\mu\right). \tag{C.4}$$

Performing the inversion of $\widetilde{K}(p)$, as indicated by Eq. (C.3), the quark propagator in momentum space reads

$$\widetilde{S}(p) = \frac{-\mathrm{i}\,\gamma_\mu\,\mathring{p}_\mu + m_0}{\mathring{p}^2 + m_0^2}\,. \tag{C.5}$$

In the finite-volume lattice (L^3T) the propagator in coordinate space in the continuum limit can be obtained performing the naive continuum limit of the expression

$$S(x,y) = \lim_{a\to 0} \frac{1}{L^3T} \sum_{p_\mu} \widetilde{S}(p)\,e^{\mathrm{i}\,p\,(x-y)}\,. \tag{C.6}$$

The continuum limit of Eq. (C.5) at a fixed value of the momentum gives as a result the usual free quark propagator in momentum space in the continuum

$$\lim_{a\to 0} \widetilde{S}(p)|_{p\,\text{fixed}} = \frac{-\mathrm{i}\,\gamma_\mu\,p_\mu + m_0}{p^2 + m_0^2}\,, \tag{C.7}$$

which, as expected, has a pole at $p_\mu = 0\;\forall\,\mu$ in the massless limit, $m_0 = 0$.

However, from the expression at finite lattice spacing, Eq. (C.5), it is evident that the quark propagator also has poles ($\mathring{p}$ vanishes) at all values of p such that $p_\mu = 0$ and/or $p_\mu = \pi/a$. Thus, at non-zero lattice spacing there are 15 additional poles (doublers) which do not have a continuum analogue and are not physical. In fact, the doublers remain even after the continuum limit has been performed giving place to a wrong continuum limit.

[1] Matrix/vector convention is used for all indices non-relevant in the discussion and $\delta_{x,y}$ is the dimensionless Kronocker delta.

The name doubling has its origin in the fact that for each dimension of the space-time the number of contributions is doubled (2^d). This problem can be seen as an excess of symmetries of the discretized action and its origin resides in the use of the anti-hermitian symmetric lattice derivative, which involves twice the lattice scale. The problem can not be cured by the use of the left or right derivatives (which would be the initial candidates to think of) because in this case problems concerning the covariance and renormalizability of the theory would arise when interactions are taken into account.

C.2. Exceptional configurations

The existence of exceptional configurations is a phenomenon related to lattice regularizations which break chiral symmetry e.g. Wilson fermions. The exceptional configurations are certain fluctuations of the gauge fields which induce very small eigenvalues in the spectrum of the lattice Dirac operator. This happens because the fluctuations of the eigenvalues, of chiral symmetry breaking regularizations, are coupled to the fluctuations of the gauge fields.

Numerically, the quark propagator needs to be computed for each gauge configuration, in order to evaluate vacuum expectation values of certain composite fields. In practice, the quark propagator is obtained via a numerical inversion of the lattice Dirac operator for a particular gauge configuration. As a result, if the Dirac operator has to be inverted for an exceptional configuration, this causes a numerical problem. However, due to the coupling between the fluctuations of the eigenvalues and the fluctuations of the gauge fields some methods can be applied to remove these fluctuations.

Getting rid of the fluctuations is yet not so easy in the quenched approximation. In this case, the fermion determinant entering the functional integral is neglected and it does not compensate anymore the small eigenvalues of the Dirac operator. Therefore, in the quenched setup the quark massess are limited to relatively high values in order to avoid this problem. This is true unless a non-zero bound in the spectrum of the Dirac operator is provided by other means. Such is for instance the case in a finite volume with SF-like boundary conditions, where a bound in the spectrum is provided by the particular form of the boundary conditions in the time direction (see Chap. 3, Chap. 4 and Chap. 5). In the following discussion, however, we assume a volume where no infrared cutoff is provided by the boundary conditions.

C.2.1. Wilson fermions

The massive Wilson operator can be written as

$$D = D_{\mathrm{W}} + m_0 \tag{C.8}$$

and its eigenvalues are given by the sum

$$\lambda[U] = \lambda_{\mathrm{W}}[U] + m_0\,, \tag{C.9}$$

with $\lambda_{\mathrm{W}}[U]$ the eigenvalues of D_{W} for a certain gauge configuration U.

Due to the γ_5-hermiticity of the Wilson operator (cf. App. B.1.1), its eigenvalues can be either real or complex conjugate pairs. This allows the possibility of having negative real eigenvalues which can give a very small $\lambda[U]$. The only way out is then to have a value of the quark mass high enough to compensate the negative real $\lambda_{\mathrm{W}}[U]$. However, this excludes computations close to the chiral point and even close to the physical massess of light hadrons, like the pion mass.

C.2.2. Twisted mass Wilson fermions

Using a twisted mass formulation of fermions and working at non-vanishing values of the twisted quark mass, μ_q, eliminates the problem of exceptional configurations.

The twisted mass Wilson Dirac operator can be expressed in terms of the Wilson operator as follows

$$D = D_\mathrm{W} + m_0 + \mathrm{i}\,\mu_\mathrm{q}\,\gamma_5\,\tau^3\,. \tag{C.10}$$

A common way of writing the inverse Dirac operator is

$$D^{-1} = (D^\dagger D)^{-1}\,D^\dagger\,, \tag{C.11}$$

which means that the expression to be inverted is now $D^\dagger D$. In the case of the twisted mass Wilson operator, this can be seen as

$$D^\dagger D = (D_\mathrm{W} + m_0)^\dagger\,(D_\mathrm{W} + m_0) + \mu_\mathrm{q}^2 = Q^2 + \mu_\mathrm{q}^2\,, \tag{C.12}$$

where Q is the hermitian operator defined as $Q = \gamma_5(D_\mathrm{W} + m_0)$. Due to the hermiticity of Q, its eigenvalues can only be real. This implies that the smallest eigenvalue that Q^2 can have is zero. Then it again shows the problem of exceptional configurations in simulations with standard Wilson fermions. In the twisted mass formulation, however, even if Q^2 has a zero mode, it is avoided by the presence of the twisted mass, as seen in Eq. (C.12), which provides a positive infrared cutoff in the spectrum.

C.3. Setting the scale with the static $q\overline{q}$ potential

The static QCD potential, $V(r)$, represents the energy of a quark-antiquark pair separated by a distance $r = |\vec{r}| = |\vec{x} - \vec{y}|$. Its derivative is the force between the two quarks $F(r) = dV(r)/dr$. The potential is assumed to have the form (at least in the quenched approximation)

$$V(r) = A + \frac{B}{r} + \sigma\,r. \tag{C.13}$$

B is the strength of the Coulomb interaction (similar to QED) which becomes the dominant term in the weak coupling, g_0, limit. In the strong coupling limit the dominant term is the linearly rising term (which does not have a QED counter part) with the real constant σ being the string tension. A is just a normalization of the energy.

In lattice calculations, the static QCD potential is also interesting from a practical point of view. A hadronic length scale r_0 is introduced. It is called the Sommer scale and it was first discussed in [37]. This scale is introduced via the force $F(r)$ between two static quarks at intermediate distances as the value of r such that

$$r_0^2\,F(r_0) = 1.65, \tag{C.14}$$

which it is known to be $r_0 \simeq 0.5\,\mathrm{fm}$. In lattice calculations r_0 is a very good quantity to set the scale, at least in quenched simulations, and also to perform scaling studies, since it can be obtained from Monte Carlo simulations in a very accurate way.

The dimensionless quantity r_0/a, at a certain value of β, can be obtained from a lattice computation of $r^2\,F(r)$ at the value of 1.65. From the result obtained for r_0/a it is straightforward to determine the lattice spacing in physical units using the value of $r_0 = 0.5\,\mathrm{fm}$.

If this procedure is repeated at several values of β, a parametrization of r_0/a as a function of β is possible. This has been performed for the Wilson gauge action, first in [38], which is the

parametrization that we have used in the computation of $M_{\rm S}$, and later in [39].

The parametrization corresponding to [38] gives

$$\ln(a/r_0) = -1.6805 - 1.7139\,(\beta-6) + 0.8155\,(\beta-6)^2 - 0.6667\,(\beta-6)^3\ ,\ 5.7 \le \beta \le 6.57\,, \quad \text{(C.15)}$$

and the one in [39]

$$\ln(a/r_0) = -1.6804 - 1.7331\,(\beta-6) + 0.7849\,(\beta-6)^2 - 0.4428\,(\beta-6)^3\ ,\ 5.7 \le \beta \le 6.92\,. \quad \text{(C.16)}$$

Eq. (C.16) covers a larger range of β than the one given in Eq. (C.15), but it is less precise in the low β range [39].

C.4. Symanzik improvement for Wilson-like fermions

C.4.1. Improvement of standard Wilson fermions

The $O(a)$ effective Lagrangian, $\mathcal{L}_1(x)$, is a linear combination of the fields

$$\mathcal{L}_1^1(x) = \overline{\psi}(x)\,\sigma_{\mu\nu}\,F_{\mu\nu}(x)\,\psi(x)\,, \quad \text{(C.17)}$$
$$\mathcal{L}_1^2(x) = \overline{\psi}(x)\,[\overrightarrow{D}_\mu\,\overrightarrow{D}_\mu + \overleftarrow{D}_\mu\,\overleftarrow{D}_\mu]\,\psi(x)\,, \quad \text{(C.18)}$$
$$\mathcal{L}_1^3(x) = m\,\mathrm{tr}\,\{F_{\mu\nu}(x)\,F_{\mu\nu}(x)\}\,, \quad \text{(C.19)}$$
$$\mathcal{L}_1^4(x) = m\,\overline{\psi}(x)\,\gamma_\mu\,[\overrightarrow{D}_\mu - \overleftarrow{D}_\mu]\,\psi(x)\,, \quad \text{(C.20)}$$
$$\mathcal{L}_1^5(x) = m^2\,\overline{\psi}(x)\,\psi(x)\,, \quad \text{(C.21)}$$

where $F_{\mu\nu}$ is the field strength tensor and D_μ the covariant derivative. Applying the classical field equation, $\gamma_\mu\partial_\mu + m = 0$, the terms $\mathcal{L}_1^2(x)$ and $\mathcal{L}_1^4(x)$ can be related to the others. Adding the lattice representation of the remaining fields to the QCD lattice action (where the Wilson gauge action is assumed in the gauge sector), it can be seen that only the term $\mathcal{L}_1^1(x)$ is needed. The reason is that the terms $\mathcal{L}_1^3(x)$ and $\mathcal{L}_1^5(x)$ amount to a renormalization of the bare coupling and mass, respectively ($b_{\rm g}$ in Eq. (2.87) and $b_{\rm m}$ in Eq. (2.88)).

The $O(a)$ effective axial-vector current, $(\mathcal{A}_1)_\mu^a(x)$, is a linear combination of the fields

$$(\mathcal{A}_1^1)_\mu^a(x) = \overline{\psi}(x)\,\gamma_5\,\frac{\tau^a}{2}\,\sigma_{\mu\nu}\,[\overrightarrow{D}_\nu - \overleftarrow{D}_\nu]\,\psi(x)\,, \quad \text{(C.22)}$$
$$(\mathcal{A}_1^2)_\mu^a(x) = \overline{\psi}(x)\,\gamma_5\,\frac{\tau^a}{2}\,[\overrightarrow{D}_\mu + \overleftarrow{D}_\mu]\,\psi(x)\,, \quad \text{(C.23)}$$
$$(\mathcal{A}_1^3)_\mu^a(x) = m\,\overline{\psi}(x)\,\gamma_\mu\,\gamma_5\,\frac{\tau^a}{2}\,\psi(x)\,. \quad \text{(C.24)}$$

Using the field equations, $(\mathcal{A}_1^1)_\mu^a(x)$ can be eliminated. Also $(\mathcal{A}_1^3)_\mu^a(x)$ can be dropped because it can be reabsorbed in the renormalization of the vector-axial current ($b_{\rm A}$ in Eq. (2.92)).

The possible improvement counterterms to the vector current are

$$(\mathcal{V}_1^1)_\mu^a(x) = \overline{\psi}(x)\,\frac{\tau^a}{2}\,\sigma_{\mu\nu}\,[\overrightarrow{D}_\nu + \overleftarrow{D}_\nu]\,\psi(x)\,, \quad \text{(C.25)}$$
$$(\mathcal{V}_1^2)_\mu^a(x) = m\,\overline{\psi}(x)\,\gamma_\mu\,\frac{\tau^a}{2}\,\psi(x)\,, \quad \text{(C.26)}$$

which are reduced to only $(\mathcal{V}_1^1)_\mu^a(x)$ because the other counterterm corresponds to a renormalization of the vector current ($b_{\rm V}$ in Eq. (2.93)).

The pseudo-scalar density does not have any counterterm at $O(a)$, since the only possibility would be

$$(\mathcal{P}_1^1)^a(x) = m\,\overline{\psi}(x)\,\gamma_5\frac{\tau^a}{2}\,\psi(x)\,, \tag{C.27}$$

which again can be reabsorbed in the renormalization of $\mathcal{P}^a(x)$ ($b_{\rm P}$ in Eq. (2.91)).

C.4.2. Improvement of twisted mass Wilson fermions

In this section all notation refers to the twisted basis. The $O(a)$ effective Lagrangian, $\mathcal{L}_1(x)$, is a linear combination of the fields

$$\mathcal{L}_1^1(x) = \overline{\chi}(x)\,\mathrm{i}\sigma_{\mu\nu}\,F_{\mu\nu}(x)\,\chi(x)\,, \tag{C.28}$$
$$\mathcal{L}_1^2(x) = \overline{\chi}(x)\,[\overrightarrow{D}_\mu\,\overrightarrow{D}_\mu + \overleftarrow{D}_\mu\,\overleftarrow{D}_\mu]\,\chi(x)\,, \tag{C.29}$$
$$\mathcal{L}_1^3(x) = m_{\rm q}\,\mathrm{tr}\,\{F_{\mu\nu}(x)\,F_{\mu\nu}(x)\}\,, \tag{C.30}$$
$$\mathcal{L}_1^4(x) = m_{\rm q}\,\overline{\chi}(x)\,\gamma_\mu\,[\overrightarrow{D}_\mu - \overleftarrow{D}_\mu]\,\chi(x)\,, \tag{C.31}$$
$$\mathcal{L}_1^5(x) = m_{\rm q}^2\,\overline{\chi}(x)\,\chi(x)\,, \tag{C.32}$$
$$\mathcal{L}_1^6(x) = m_{\rm q}\mu_{\rm q}\,\overline{\chi}(x)\,\mathrm{i}\gamma_5\tau^3\,\chi(x)\,, \tag{C.33}$$
$$\mathcal{L}_1^7(x) = \mu_{\rm q}^2\,\overline{\chi}(x)\,\chi(x)\,. \tag{C.34}$$

Applying the classical field equations, the following relations are obtained

$$0 = \mathcal{L}_1^1(x) - \mathcal{L}_1^2(x) + 2\mathcal{L}_1^5(x) + 2\mathcal{L}_1^7(x)\,, \tag{C.35}$$
$$0 = \mathcal{L}_1^4(x) + 2\mathcal{L}_1^5(x) + 2\mathcal{L}_1^6(x)\,, \tag{C.36}$$

which allow to eliminate $\mathcal{L}_1^2(x)$ and $\mathcal{L}_1^4(x)$. Adding the lattice representation of the remaining fields to the QCD lattice action, it can be seen that only the term $\mathcal{L}_1^1(x)$ is needed, as with standard Wilson fermions. The reason is that the term $\mathcal{L}_1^3(x)$ amounts to a renormalization of the bare coupling ($b_{\rm g}$ in Eq. (2.112)), $\mathcal{L}_1^6(x)$ is reabsorbed in a renormalization of the bare twisted quark mass (b_μ in Eq. (2.114)) and the terms $\mathcal{L}_1^5(x)$ and $\mathcal{L}_1^7(x)$ amount to a renormalization of the bare untwisted quark mass ($b_{\rm m}$ and $\tilde{b}_{\rm m}$ in Eq. (2.113)).

The $O(a)$ effective axial-vector current, $(\mathcal{A}_1)_\mu^a(x)$, is a linear combination of the fields

$$(\mathcal{A}_1^1)_\mu^a(x) = \overline{\chi}(x)\,\gamma_5\,\frac{\tau^a}{2}\,\sigma_{\mu\nu}\,[\overrightarrow{D}_\nu - \overleftarrow{D}_\nu]\,\chi(x)\,, \tag{C.37}$$
$$(\mathcal{A}_1^2)_\mu^a(x) = \overline{\chi}(x)\,\gamma_5\,\frac{\tau^a}{2}\,[\overrightarrow{D}_\mu + \overleftarrow{D}_\mu]\,\chi(x)\,, \tag{C.38}$$
$$(\mathcal{A}_1^3)_\mu^a(x) = m_{\rm q}\,\overline{\chi}(x)\,\gamma_\mu\,\gamma_5\,\frac{\tau^a}{2}\,\chi(x)\,, \tag{C.39}$$
$$(\mathcal{A}_1^4)_\mu^a(x) = \mu_{\rm q}\,\epsilon^{3ab}\,\overline{\chi}(x)\,\gamma_\mu\,\frac{\tau^b}{2}\,\chi(x)\,. \tag{C.40}$$

Using the field equations, $(\mathcal{A}_1^1)_\mu^a(x)$ can be eliminated. Also $(\mathcal{A}_1^3)_\mu^a(x)$ can be dropped because it can be reabsorbed in the renormalization of the axial-vector current. The $O(a)$-improved axial-vector current is then given (in the continuum effective theory) by

$$(A_{\rm I})_\mu^a(x) = A_\mu^a(x) + a\,c_{\rm A}\,\partial_\mu\,P^a(x) + a\,\mu_{\rm q}\,\widetilde{b}_{\rm A}\,\epsilon^{3ab}\,V_\mu^b(x)\,. \tag{C.41}$$

The possible improvement counterterms to the vector current are

$$(\mathcal{V}_1^1)_\mu^a(x) = \overline{\chi}(x)\,\frac{\tau^a}{2}\,\sigma_{\mu\nu}\,[\overrightarrow{D}_\nu + \overleftarrow{D}_\nu]\,\chi(x)\,, \tag{C.42}$$

$$(\mathcal{V}_1^2)_\mu^a(x) = m_{\rm q}\,\overline{\chi}(x)\,\gamma_\mu\,\frac{\tau^a}{2}\,\chi(x)\,, \tag{C.43}$$

$$(\mathcal{V}_1^3)_\mu^a(x) = \mu_{\rm q}\,\epsilon^{3ab}\,\overline{\chi}(x)\,\gamma_\mu\,\gamma_5\,\frac{\tau^b}{2}\,\chi(x)\,. \tag{C.44}$$

The counterterm $(\mathcal{V}_1^2)_\mu^a(x)$ corresponds to a renormalization of the vector current. Thus, the $O(a)$-improved vector current in the effective continuum theory is

$$(V_{\rm I})_\mu^a(x) = V_\mu^a(x) + a\,c_{\rm V}\,\partial_\nu\,T_{\mu\nu}^a(x) + a\,\mu_{\rm q}\,\widetilde{b}_{\rm V}\,\epsilon^{3ab}\,A_\mu^b(x)\,. \tag{C.45}$$

The pseudo-scalar density does not have any counterterm at $O(a)$, since the only possibility would be

$$(\mathcal{P}_1^1)^a(x) = m_{\rm q}\,\overline{\chi}(x)\,\gamma_5\frac{\tau^a}{2}\,\chi(x)\,, \tag{C.46}$$

which again can be reabsorbed in the renormalization of $P^a(x)$.

C.5. Proof of automatic $O(a)$-improvement

Following Symanzik improvement programme (cf. Sec. 2.6), the improvement of twisted mass Wilson fermions can be achieved [67]. It takes place in the same way as discussed in detail in the case of standard Wilson fermions (cf. Sec. 2.7.2 and App. C.4.1). The improvement programme for twisted mass fermions is sketched in App. C.4.2 for the action and fields of interest. However, as it was first shown in [24], the application of the improvement programme with twisted mass fermions can be circumvented. In [24] it was shown for the first time that at maximal twist all $O(a^{\rm odd})$ counterterms to the action and to the expectation values of physical quantities are irrelevant; their contribution in this cases is at most an $O(a^2)$ effect. This property of twisted mass Wilson fermions at maximal twist is referred to as automatic $O(a)$-improvement. Automatic improvement can be shown in different manners. After the original proof in [24], alternative demonstrations were discussed in [18, 68–70]. Automatic $O(a)$-improvement is presented here following the argumentation given in [18], which is based on Symanzik programme and the discrete transformation $\mathcal{R}_5^{1,2}$ [24] defined in Eq. (C.50). In order to avoid any problem concerning phase transitions with Wilson-like fermions, a *finite volume* without boundaries is assumed in the discussion here presented. In this case, no spontaneous symmetry breaking takes place and analyticity on the quark mass is guaranteed. The lack of phase transitions avoids problems in the application of Symanzik programme, which implicitly assumes to work in a regime of continuum QCD where cutoff effects are asymptotically small corrections and can, thus, be treated as operator insertions (expectation values of operators evaluated in the continuum).

As described in Sec. 2.6, in Symanzik's continuum effective theory the effective action is given by

$$S_{\rm eff} = S_0 + a\,\mathcal{S}_1 + O(a^2) \tag{C.47}$$

and a renormalized connected correlation function is expressed as

$$\langle \mathbf{O} \rangle_{\rm eff} = \langle \mathbf{O}_0 \rangle_0 - a\,\langle \mathcal{S}_1 \mathbf{O}_0 \rangle_0 + a\,\langle \mathbf{O}_1 \rangle_0 + O(a^2)\,, \tag{C.48}$$

up to corrections of $O(a^2)$.

In order to show automatic $O(a)$-improvement, the following discrete symmetry of the con-

tinuum QCD action is considered,

$$\psi(x) \longrightarrow \mp \mathrm{i}\tau^{2,1}\,\psi(x)\,, \quad \overline{\psi}(x) \longrightarrow \pm\,\overline{\psi}(x)\,\mathrm{i}\tau^{2,1}\,. \tag{C.49}$$

This transformation is part of the vector symmetry of two flavor QCD. If a rotation of the quark fields to maximal twist is performed, the continuum QCD action is given in its twisted mass form at maximal twist. In the twisted basis, the discrete transformation Eq. (C.49) becomes the chiral transformation,

$$\chi(x) \longrightarrow \mathrm{i}\gamma_5\tau^{1,2}\,\chi(x)\,, \quad \overline{\chi}(x) \longrightarrow \overline{\chi}(x)\,\mathrm{i}\gamma_5\tau^{1,2}\,, \tag{C.50}$$

which is referred to as $\mathcal{R}_5^{1,2}$-transformation, and it is thus a symmetry of QCD in the continuum at maximal twist (where all contribution to the mass comes only from the twisted mass).

Considering gauge invariant fields, the transformation squares to the identity. This allows to define a parity associated to that transformation, $\mathcal{R}_5^{1,2}$-parity, and thus, composite fields can be classified according to it.

Since two flavor QCD is invariant under the $\mathcal{R}_5^{1,2}$-transformation, the continuum action S_0 is invariant and therefore,

$$S_0 \xrightarrow{\mathcal{R}_5^{1,2}} +\,S_0\,. \tag{C.51}$$

Also, given a field in the continuum, $\mathbf{O}_0$, with a definite chirality, it transforms under $\mathcal{R}_5^{1,2}$ as follows,

$$\mathbf{O}_0 \xrightarrow{\mathcal{R}_5^{1,2}} \pm\,\mathbf{O}_0\,, \tag{C.52}$$

where the $\pm$ indicates that the field has either even or odd chirality, respectively.

The key point in the demonstration is that all operator insertions of one dimension higher than the quantity to be described have the *opposite* chirality as the corresponding continuum quantity. That is,

$$\mathcal{S}_1 \xrightarrow{\mathcal{R}_5^{1,2}} -\,\mathcal{S}_1\,, \tag{C.53}$$

$$\mathbf{O}_1 \xrightarrow{\mathcal{R}_5^{1,2}} \mp\,\mathbf{O}_1\,. \tag{C.54}$$

In order to demonstrate the last statement, the definition of another transformation is needed, $\mathcal{D}_d$, which basically counts the dimension, d, of the fields [24],

$$\mathcal{D}_d\,:\,\begin{cases} U_\mu(x) & \to\; U_\mu^\dagger(-x-\vec{\mu}) \\ \chi(x) & \to\; e^{\mathrm{i}3\pi/2}\,\chi(-x)\,. \\ \overline{\chi}(x) & \to\; \overline{\chi}(-x)\,e^{\mathrm{i}3\pi/2} \end{cases} \tag{C.55}$$

$\mathcal{D}_d$ is a symmetry of the *lattice* gauge action but it is not a symmetry of the fermion action. All terms in the fermion action which are chirally symmetric are even under the $\mathcal{D}_d$-transformation, while all terms which break chiral symmetry are odd under $\mathcal{D}_d$. On the other hand $\mathcal{R}_5^{1,2}\times\mathcal{D}_d$ is a symmetry of the lattice QCD action. This therefore implies that all operator insertions, $\mathbf{O}_1$, with one dimension higher than the original field, $\mathbf{O}_0$, must have the opposite chirality, $\mathcal{R}_5^{1,2}$.

After these considerations, the transformation properties of expectation values with respect to the $\mathcal{R}_5^{1,2}$-transformation can be derived by applying the transformation to the integration variables in the functional integral. Due to the invariance of the functional integral under such transformation, together with the invariance of the measure and the continuum action, the following properties can be deduced.

If $\mathbf{O}_0$ is an *even* operator under $\mathcal{R}_5^{1,2}$-parity,

$$\mathbf{O}_0 \xrightarrow{\mathcal{R}_5^{1,2}} +\mathbf{O}_0\,, \tag{C.56}$$

it is automatically verified that

$$\langle \mathbf{O}_0\rangle_0 = +\langle \mathbf{O}_0\rangle_0\,, \tag{C.57}$$
$$\langle \mathbf{O}_1\rangle_0 = -\langle \mathbf{O}_1\rangle_0 \quad\Longrightarrow\quad \langle \mathbf{O}_1\rangle_0 = 0\,, \tag{C.58}$$
$$\langle \mathcal{S}_1\mathbf{O}_0\rangle_0 = -\langle \mathcal{S}_1\mathbf{O}_0\rangle_0 \quad\Longrightarrow\quad \langle \mathcal{S}_1\mathbf{O}_0\rangle_0 = 0\,. \tag{C.59}$$

If $\mathbf{O}_0$ is an *odd* operator under $\mathcal{R}_5^{1,2}$-parity,

$$\mathbf{O}_0 \xrightarrow{\mathcal{R}_5^{1,2}} -\mathbf{O}_0\,, \tag{C.60}$$

then

$$\langle \mathbf{O}_0\rangle_0 = -\langle \mathbf{O}_0\rangle_0 \quad\Longrightarrow\quad \langle \mathbf{O}_0\rangle_0 = 0\,, \tag{C.61}$$
$$\langle \mathbf{O}_1\rangle_0 = +\langle \mathbf{O}_1\rangle_0\,, \tag{C.62}$$
$$\langle \mathcal{S}_1\mathbf{O}_0\rangle_0 = +\langle \mathcal{S}_1\mathbf{O}_0\rangle_0\,. \tag{C.63}$$

Therefore, the conclusion drawn from this discussion is that

$$\text{Even:}\quad \mathbf{O}_0 \xrightarrow{\mathcal{R}_5^{1,2}} +\mathbf{O}_0 \quad\Longrightarrow\quad \langle \mathbf{O}\rangle_{\text{eff}} = \langle \mathbf{O}_0\rangle_0 + O(a^2)\,, \tag{C.64}$$
$$\text{Odd:}\quad \mathbf{O}_0 \xrightarrow{\mathcal{R}_5^{1,2}} -\mathbf{O}_0 \quad\Longrightarrow\quad \langle \mathbf{O}\rangle_{\text{eff}} = -a\,\langle \mathcal{S}_1\mathbf{O}_0\rangle_0 + a\,\langle \mathbf{O}_1\rangle_0 + O(a^2)\,. \tag{C.65}$$

In words, these equations say that correlation functions of $\mathcal{R}_5^{1,2}$-even interpolating fields have a finite continuum limit and are automatically $O(a)$-improved, whilst, correlation functions of $\mathcal{R}_5^{1,2}$-odd interpolating fields vanish in the continuum limit up to $O(a)$-effects. Indeed, automatic $O(a)$-improvement does not only mean that all $O(a)$ effects cancel in $\mathcal{R}_5^{1,2}$-even correlation functions but, furthermore, it means that all counterterms with odd powers of a vanish. In the same way, given a $\mathcal{R}_5^{1,2}$-odd correlation function, only terms with odd powers of a appear [24, 70].

This result can be generalized even further; since standard Wilson and twisted mass Wilson fermions are equivalent in the chiral limit, it can be concluded that massless standard Wilson fermions in a finite volume without boundaries are automatic $O(a)$-improved [24]. Indeed, in order to show automatic $O(a)$-improvement for massless Wilson fermions it would have been enough to consider, instead of $\mathcal{R}_5^{1,2}$, the less restrictive chiral transformation $\mathcal{R}_5$,

$$\psi(x) \longrightarrow \mathrm{i}\gamma_5\,\psi(x)\,,\quad \overline{\psi}(x) \longrightarrow \overline{\psi}(x)\,\mathrm{i}\gamma_5\,. \tag{C.66}$$

D. Notes on the tuning

Guess values for the tuning Hadronic scale: $L = 1.436\, r_0$							
L/a	β	N_{conf}	z_f	κ	N_{conf}	z_f	κ
8	6.0219	1000	1.74	0.1534	1000	1.79	0.1530
			1.77	0.1537		1.80	0.1534
			1.80			1.81	0.1537
			1.83			1.82	0.1540
			1.86				
10	6.1628	1000	1.73	0.1521	1000	1.78	0.1520
			1.76	0.1522		1.79	0.1521
			1.79			1.80	0.1522
			1.82			1.81	0.1523
12	6.2885	500	1.71	0.15050	300	1.70	0.15025
			1.74	0.15100		1.73	0.15050
			1.77			1.77	0.15100
			1.80			1.80	0.15125
16	6.4956	300	1.64	0.1489	100	1.70	0.1488
			1.67	0.1490		1.71	0.1489
			1.70			1.73	0.1490
			1.73			1.74	0.1491
			1.76				
20	6.6790	112	1.66	0.1473			
			1.68	0.1474			
			1.70	0.1475			
			1.72	0.1476			
24	6.8187	100	1.60	0.1463			
			1.63	0.1464			
			1.66	0.1465			
			1.69	0.1466			

Table D.1.: Values of κ and z_f used as guess for the tuning and number of configurations, N_{conf}, used in all calculations at the corresponding value of β. Scale NP. The data of the last three columns have been used only for a separate analysis with method (1), which we denote here as method (1*).

Guess values for the tuning Intermediate scale: $\overline{g}^2 = 2.4484$							
L/a	β	N_{conf}	z_f	κ	N_{conf}	z_f	κ
8	7.0197	1000	1.51	0.14445	1000	1.35	0.14440
			1.54	0.14450		1.45	0.14445
			1.57			1.55	0.14450
			1.60			1.65	0.14455
12	7.3551	500	1.46	0.1431	300	1.50	0.1430
			1.49	0.1432		1.51	0.1431
			1.52			1.52	0.1432
			1.55			1.53	0.1433
16	7.6101	300	1.44	0.1421	100	1.48	0.1420
			1.47	0.1422		1.49	0.1421
			1.50			1.50	0.1422
			1.53			1.51	0.1423

Table D.2.: Same caption as in Tab. D.1 but at scale I.

Guess values for the tuning Perturbative scale: $\overline{g}^2 = 0.9944$							
L/a	β	N_{conf}	z_f	κ	N_{conf}	z_f	κ
8	10.3000				1000	1.2955	0.13541
						1.2965	0.13544
						1.2975	0.13547
						1.2985	0.13550
12	10.6086				300	1.292	0.13514
						1.294	0.13517
						1.297	0.13520
						1.299	0.13523
16	10.8910	300	1.23	0.13484	100	1.285	0.13482
			1.26	0.13487		1.286	0.13484
			1.29			1.287	0.13487
			1.32			1.288	0.13489

Table D.3.: Same caption as in Tab. D.1 but at scale P.

Guess values for the tuning 2P scale				
L/a	β	N_{conf}	z_f	κ
16	12.0000	100	1.23	0.1335
			1.24	0.1336
			1.25	0.1337
			1.26	0.1338

Table D.4.: Same caption as in Tab. D.1 but at scale 2P. Here no separate tuning was performed for method (1).

Guess values for the tuning PP scale				
L/a	β	N_{conf}	z_f	κ
16	24.0000	80	1.11	0.1287
			1.12	0.1288
			1.13	0.1289
			1.14	0.1290

Table D.5.: Same caption as in Tab. D.1 but at scale PP. Here no separate tuning was performed for method (1).

Tuning results Hadronic scale: $L = 1.436\, r_0$				
L/a	β	m	z_f^c	κ_c
8	6.0219	1*	1.8090 (32)	0.153530 (24)
		1	1.8091 (32)	0.15353 (66)
		2	1.7946 (34)	0.15354 (66)
		3	1.8434 (37)	0.15352 (67)
		4	1.7656 (27)	0.15354 (66)
		5	1.7597 (27)	0.15354 (66)
		6	1.7835 (40)	0.15354 (66)
		7	1.7980 (17)	0.15353 (66)
10	6.1628	1*	1.7920 (30)	0.152134 (17)
		1	1.7923 (29)	0.15213 (66)
		2	1.7820 (31)	0.15214 (66)
		3	1.8175 (33)	0.15213 (67)
		4	1.7541 (25)	0.15214 (66)
		5	1.7497 (25)	0.15214 (66)
		6	1.7687 (38)	0.15214 (66)
12	6.2885	1*	1.7664 (51)	0.150815 (22)
		1	1.7658 (38)	0.15082 (66)
		2	1.7573 (40)	0.15082 (66)
		3	1.7869 (46)	0.15082 (66)
		4	1.7312 (34)	0.15082 (65)
		5	1.7283 (32)	0.15082 (65)
		6	1.7408 (56)	0.15082 (65)
		7	1.7509 (22)	0.15082 (66)
16	6.4956	1*	1.7212 (83)	0.148945 (25)
		1	1.7201 (41)	0.14894 (34)
		2	1.7132 (44)	0.14894 (33)
		3	1.7377 (46)	0.14893 (34)
		4	1.6929 (35)	0.14894 (33)
		5	1.6894 (34)	0.14894 (33)
		6	1.7053 (63)	0.14894 (33)
		7	1.7076 (21)	0.14894 (33)
20	6.6790	1	1.6841 (56)	0.14748 (74)
		2	1.6789 (59)	0.14748 (74)
		3	1.6973 (65)	0.14748 (74)

Table D.6.: (continuing on the next page, caption below)

Tuning results Hadronic scale: $L = 1.436\, r_0$				
L/a	β	m	z_f^c	κ_c
		4	1.6582 (52)	0.14748 (73)
		5	1.6577 (52)	0.14748 (73)
		6	1.6600 (90)	0.14748 (73)
24	6.8187	1	1.6427 (56)	0.14645 (41)
		2	1.6381 (60)	0.14645 (41)
		3	1.6529 (60)	0.14645 (42)
		4	1.6253 (51)	0.14645 (41)
		5	1.6201 (50)	0.14645 (41)
		6	1.6421 (88)	0.14645 (41)
		7	1.6366 (27)	0.14645 (41)

Table D.6.: Final results of the tuning of κ and z_f at the NP scale. Results for all the methods (1) to (7) are shown (see Sec. 6.1 for a description of all the methods). The results of method (1*) are obtained from method (1) but using slightly different simulation parameters (see Tab. D.1).

Tuning results Intermediate scale: $\overline{g}^2 = 2.4484$				
L/a	β	m	z_f^c	κ_c
8	7.0197	1*	1.5467 (15)	0.144501 (13)
		1	1.5404 (16)	0.14450 (41)
		2	1.5296 (17)	0.14450 (41)
		3	1.5597 (18)	0.14450 (41)
		4	1.5156 (14)	0.14450 (41)
		5	1.5126 (14)	0.14450 (41)
		6	1.5229 (21)	0.14450 (41)
		7	1.5392 (12)	0.14450 (41)
12	7.3551	1*	1.5126 (23)	0.143113 (12)
		1	1.5139 (18)	0.14311 (29)
		2	1.5088 (19)	0.14311 (29)
		3	1.5233 (19)	0.14311 (29)
		4	1.4955 (16)	0.14311 (29)
		5	1.4945 (15)	0.14311 (29)
		6	1.4981 (23)	0.14311 (29)
		7	1.5120 (12)	0.14311 (29)
16	7.6101	1*	1.4942 (37)	0.142112 (13)
		1	1.4943 (20)	0.14212 (23)
		2	1.4908 (21)	0.14212 (23)
		3	1.5007 (23)	0.14212 (23)
		4	1.4800 (18)	0.14212 (23)
		5	1.4789 (17)	0.14212 (23)
		6	1.4827 (28)	0.14212 (23)
		7	1.4916 (13)	0.14212 (23)

Table D.7.: Same caption as in Tab. D.6 but at scale I.

Tuning results Perturbative scale: $\bar{g}^2 = 0.9944$				
L/a	β	m	z_f^c	κ_c
8	10.3000	1*	1.29730 (67)	0.1354609 (54)
12	10.6086	1*	1.2954 (11)	0.1351758 (56)
16	10.8910	1*	1.2858 (15)	0.1348440 (61)
		1	1.28692 (88)	0.134844 (93)
		2	1.28487 (91)	0.134844 (93)
		3	1.28984 (99)	0.134844 (93)
		4	1.27999 (83)	0.134844 (93)
		5	1.27976 (75)	0.134844 (93)
		6	1.2805 (13)	0.134844 (93)
		7	1.28619 (67)	0.134844 (93)

Table D.8.: Same caption as in Tab. D.6 but at scale P.

Tuning results 2P scale				
L/a	β	m	z_f^c	κ_c
16	12.0000	1	1.2493 (14)	0.13363 (41)
		2	1.2481 (14)	0.13363 (41)
		3	1.2510 (15)	0.13363 (41)
		4	1.2438 (13)	0.13363 (41)
		5	1.2443 (12)	0.13363 (41)
		6	1.2428 (20)	0.13363 (41)
		7	1.2494 (10)	0.13363 (41)

Table D.9.: Same caption as in Tab. D.6 but at scale 2P.

Tuning results PP scale				
L/a	β	m	z_f^c	κ_c
16	24.0000	1	1.11268 (57)	0.12877 (15)
		2	1.11162 (58)	0.12877 (15)
		3	1.11391 (65)	0.12877 (15)
		4	1.11013 (54)	0.12877 (15)
		5	1.11003 (48)	0.12877 (15)
		6	1.11030 (87)	0.12877 (15)
		7	1.11269 (50)	0.12877 (15)

Table D.10.: Same caption as in Tab. D.6 but at scale PP.

Intermediate step in the tuning Hadronic scale: $L = 1.436\, r_0$						
L/a	β	z_f	$g^*_{A_{0-}}$	$\frac{dg_{A_{0-}}}{dm_{\mathrm{PCAC}}}$	κ^*	$\frac{dm_{\mathrm{PCAC}}}{d\kappa}$
8	6.0219	1.79	0.0562 (97)	-22.62 (11)	0.153535 (25)	-20.479 (45)
		1.80	0.0263 (96)	-22.50 (11)	0.153533 (25)	-20.468 (45)
		1.81	-0.0032 (95)	-22.36 (11)	0.153530 (25)	-20.458 (45)
		1.82	-0.0323 (95)	-22.20 (11)	0.153528 (25)	-20.448 (44)
10	6.1628	1.78	0.0338 (85)	-27.63 (12)	0.152135 (18)	-20.958 (37)
		1.79	0.0054 (85)	-27.54 (12)	0.152134 (18)	-20.947 (37)
		1.80	-0.0227 (84)	-27.43 (12)	0.152132 (18)	-20.936 (37)
		1.81	-0.0504 (84)	-27.29 (13)	0.152131 (18)	-20.925 (37)
12	6.2885	1.70	0.179 (14)	-31.67 (26)	0.150821 (23)	-21.555 (57)
		1.73	0.096 (14)	-31.64 (26)	0.150818 (22)	-21.520 (57)
		1.77	-0.011 (14)	-31.14 (27)	0.150814 (22)	-21.479 (57)
		1.80	-0.088 (13)	-30.46 (27)	0.150812 (22)	-21.452 (56)
16	6.4956	1.70	0.055 (21)	-40.48 (49)	0.148946 (25)	-22.361 (72)
		1.71	0.029 (21)	-40.45 (50)	0.148946 (25)	-22.351 (72)
		1.73	-0.023 (21)	-40.27 (50)	0.148945 (25)	-22.332 (72)
		1.74	-0.048 (21)	-40.11 (50)	0.148944 (25)	-22.322 (71)

Table D.11.: Tuning parameters and results for the intermediate step of the tuning at $L = 1.436\, r_0$. These data are obtained from a linear interpolation of $g_{A_{0-}}$ and κ, in either case, in the PCAC mass. We have denoted with $*$ the value of the corresponding quantity, $g_{A_{0-}}$ or κ, at which the PCAC mass vanishes. These data correspond to method (1*) (see caption in Tab. D.1). See also Sec. 6.2.

Tuning results Hadronic scale: $L = 1.436\, r_0$					
L/a	β	$\frac{dg^*_{A_{0-}}}{dz_f}$	$\frac{d\kappa^*}{dz_f}$	κ_c	z_f^c
8	6.0219	-2.951 (14)	-0.000235 (11)	0.153530 (24)	1.8090 (32)
10	6.1628	-2.808 (13)	-0.0001453 (68)	0.152134 (17)	1.7920 (30)
12	6.2885	-2.667 (24)	-0.0000859 (83)	0.150815 (22)	1.7664 (51)
16	6.4956	-2.574 (36)	-0.0000472 (78)	0.148945 (25)	1.7212 (83)

Table D.12.: Tuning parameters and final results at $L = 1.436\, r_0$. These data are obtained from a linear interpolation of $g^*_{A_{0-}}$ and κ^*, as taken from Tab. D.11, in z_f. First the critical value of z_f, z_f^c, is obtained by an interpolation to $g^*_{A_{0-}} = 0$. Then, κ_c is determined by interpolating to the previously determined z_f^c. These data correspond to method (1*) (see caption in Tab. D.1). See also Sec. 6.2.

Intermediate step in the tuning Intermediate scale: $\bar{g}^2 = 2.4484$						
L/a	β	z_f	$g^*_{A_{0-}}$	$\frac{dg_{A_{0-}}}{dm_{\rm PCAC}}$	κ^*	$\frac{dm_{\rm PCAC}}{d\kappa}$
8	7.0197	1.35	0.7853 (61)	-20.088 (65)	0.144515 (13)	-24.859 (28)
		1.45	0.3665 (64)	-23.007 (68)	0.144508 (13)	-24.674 (28)
		1.55	-0.0397 (61)	-22.384 (71)	0.144500 (13)	-24.526 (28)
		1.65	-0.3866 (55)	-19.248 (70)	0.144494 (13)	-24.414 (26)
12	7.3551	1.50	0.0471 (88)	-33.12 (17)	0.143113 (12)	-25.033 (37)
		1.51	0.0094 (88)	-33.03 (17)	0.143113 (12)	-25.022 (37)
		1.52	-0.0279 (87)	-32.89 (17)	0.143113 (12)	-25.012 (37)
		1.53	-0.0647 (87)	-32.72 (17)	0.143113 (12)	-25.002 (37)
16	7.6101	1.48	0.052 (14)	-43.37 (39)	0.142112 (13)	-25.349 (49)
		1.49	0.015 (13)	-43.32 (39)	0.142112 (13)	-25.341 (49)
		1.50	-0.021 (13)	-43.22 (39)	0.142112 (13)	-25.334 (49)
		1.51	-0.058 (13)	-43.06 (39)	0.142112 (13)	-25.326 (49)

Table D.13.: Same as in caption of Tab. D.11 but at $\bar{g}^2 = 2.4484$.

Tuning results Intermediate scale: $\bar{g}^2 = 2.4484$					
L/a	β	$\frac{dg^*_{A_{0-}}}{dz_f}$	$\frac{d\kappa^*}{dz_f}$	κ_c	z_f^c
8	7.0197	-3.909 (12)	-0.0000702 (66)	0.144501 (13)	1.5467 (15)
12	7.3551	-3.729 (21)	-0.0000247 (62)	0.143113 (12)	1.5126 (23)
16	7.6101	-3.668 (36)	-0.0000209 (61)	0.142112 (13)	1.4942 (37)

Table D.14.: Same as in caption of Tab. D.12 but at $\bar{g}^2 = 2.4484$. The values $*$ which are used in the interpolation, are here taken from Tab. D.13.

Intermediate step in the tuning Perturbative scale: $\bar{g}^2 = 0.9944$						
L/a	β	z_f	$g^*_{A_{0-}}$	$\frac{dg_{A_{0-}}}{dm_{\rm PCAC}}$	κ^*	$\frac{dm_{\rm PCAC}}{d\kappa}$
8	10.3000	1.2955	0.0086 (32)	-24.065 (46)	0.1354609 (54)	-28.086 (15)
		1.2965	0.0038 (32)	-24.047 (46)	0.1354609 (54)	-28.085 (15)
		1.2975	-0.0010 (32)	-24.028 (46)	0.1354609 (54)	-28.084 (15)
		1.2985	-0.0057 (32)	-24.009 (46)	0.1354609 (54)	-28.084 (15)
12	10.6086	1.292	0.0158 (51)	-34.86 (12)	0.1351758 (56)	-28.162 (21)
		1.294	0.0064 (51)	-34.83 (12)	0.1351758 (56)	-28.161 (21)
		1.297	-0.0076 (51)	-34.78 (12)	0.1351758 (56)	-28.159 (21)
		1.299	-0.0169 (51)	-34.74 (12)	0.1351758 (56)	-28.157 (21)
16	10.8910	1.285	0.0039 (71)	-45.62 (23)	0.1348440 (61)	-28.294 (28)
		1.286	-0.0007 (71)	-45.60 (23)	0.1348440 (61)	-28.293 (28)
		1.287	-0.0054 (71)	-45.59 (23)	0.1348440 (61)	-28.293 (28)
		1.288	-0.0100 (71)	-45.57 (23)	0.1348440 (61)	-28.292 (28)

Table D.15.: Same as in caption of Tab. D.11 but at $\bar{g}^2 = 0.9944$.

Tuning results Perturbative scale: $\overline{g}^2 = 0.9944$					
L/a	β	$\frac{dg^*_{A_{0-}}}{dz_f}$	$\frac{d\kappa^*}{dz_f}$	κ_c	z_f^c
8	10.3000	-4.7907 (96)	-0.0000095 (35)	0.1354609 (54)	1.29730 (67)
12	10.6086	-4.661 (17)	0.0000008 (34)	0.1351758 (56)	1.2954 (11)
16	10.8910	-4.624 (26)	0.0000013 (35)	0.1348440 (61)	1.2858 (15)

Table D.16.: Same as in caption of Tab. D.12 but at $\bar{g}^2 = 0.9944$. The values $*$ which are used in the interpolation, are here taken from Tab. D.15.

β	$\kappa_c(1^*)$	$\kappa_c(1)$	$\kappa_c(2)$	$\kappa_c(3)$	$\kappa_c(4)$	$\kappa_c(5)$	$\kappa_c(6)$	$\kappa_c(7)$
Hadronic scale: $L = 1.436\, r_0$								
6.0219	0.153530 (24)	0.15353 (66)	0.15354 (66)	0.15352 (67)	0.15354 (66)	0.15354 (66)	0.15354 (66)	0.15353 (66)
6.1628	0.152134 (17)	0.15213 (66)	0.15214 (66)	0.15213 (67)	0.15214 (66)	0.15214 (66)	0.15214 (66)	
6.2885	0.150815 (22)	0.15082 (66)	0.15082 (66)	0.15082 (66)	0.15082 (65)	0.15082 (65)	0.15082 (65)	0.15082 (66)
6.4956	0.148945 (25)	0.14894 (34)	0.14894 (33)	0.14893 (34)	0.14894 (33)	0.14894 (33)	0.14894 (33)	0.14894 (33)
6.6790		0.14748 (74)	0.14748 (74)	0.14748 (74)	0.14748 (73)	0.14748 (73)	0.14748 (73)	
6.8187		0.14645 (41)	0.14645 (41)	0.14645 (42)	0.14645 (41)	0.14645 (41)	0.14645 (41)	0.14645 (41)
Intermediate scale: $\overline{g}^2 = 2.4484$								
7.0197	0.144501 (13)	0.14450 (41)	0.14450 (41)	0.14450 (41)	0.14450 (41)	0.14450 (41)	0.14450 (41)	0.14450 (41)
7.3551	0.143113 (12)	0.14311 (29)	0.14311 (29)	0.14311 (29)	0.14311 (29)	0.14311 (29)	0.14311 (29)	0.14311 (29)
7.6101	0.142112 (13)	0.14212 (23)	0.14212 (23)	0.14212 (23)	0.14212 (23)	0.14212 (23)	0.14212 (23)	0.14212 (23)
Perturbative scale: $\overline{g}^2 = 0.9944$								
10.3000	0.1354609 (54)							
10.6086	0.1351758 (56)							
10.8910	0.1348440 (61)	0.134844 (93)	0.134844 (93)	0.134844 (93)	0.134844 (93)	0.134844 (93)	0.134844 (93)	0.134844 (93)
2P scale								
12.0000		0.13363 (41)	0.13363 (41)	0.13363 (41)	0.13363 (41)	0.13363 (41)	0.13363 (41)	0.13363 (41)
PP scale								
24.0000		0.12877 (15)	0.12877 (15)	0.12877 (15)	0.12877 (15)	0.12877 (15)	0.12877 (15)	0.12877 (15)

Table D.17.: Summary table of κ_c for all beta values and tuning conditions, (1) to (7) (see Sec. 6.1 for a description of all the methods). The data of column (1*) correspond to a separate analysis with method (1), using slightly different simulation parameters (cf. Tab. D.1, Tab. D.2 and Tab. D.3).

β	$z_f^c(1^*)$	$z_f^c(1)$	$z_f^c(2)$	$z_f^c(3)$	$z_f^c(4)$	$z_f^c(5)$	$z_f^c(6)$	$z_f^c(7)$
Hadronic scale: $L = 1.436\, r_0$								
6.0219	1.8090 (32)	1.8091 (32)	1.7946 (34)	1.8434 (37)	1.7656 (27)	1.7597 (27)	1.7835 (40)	1.7980 (17)
6.1628	1.7920 (30)	1.7923 (29)	1.7820 (31)	1.8175 (33)	1.7541 (25)	1.7497 (25)	1.7687 (38)	
6.2885	1.7664 (51)	1.7658 (38)	1.7573 (40)	1.7869 (46)	1.7312 (34)	1.7283 (32)	1.7408 (56)	1.7509 (22)
6.4956	1.7212 (83)	1.7201 (41)	1.7132 (44)	1.7377 (46)	1.6929 (35)	1.6894 (34)	1.7053 (63)	1.7076 (21)
6.6790		1.6841 (56)	1.6789 (59)	1.6973 (65)	1.6582 (52)	1.6577 (52)	1.6600 (90)	
6.8187		1.6427 (56)	1.6381 (60)	1.6529 (60)	1.6253 (51)	1.6201 (50)	1.6421 (88)	1.6366 (27)
Intermediate scale: $\overline{g}^2 = 2.4484$								
7.0197	1.5467 (15)	1.5404 (16)	1.5296 (17)	1.5597 (18)	1.5156 (14)	1.5126 (14)	1.5229 (21)	1.5392 (12)
7.3551	1.5126 (23)	1.5139 (18)	1.5088 (19)	1.5233 (19)	1.4955 (16)	1.4945 (15)	1.4981 (23)	1.5120 (12)
7.6101	1.4942 (37)	1.4943 (20)	1.4908 (21)	1.5007 (23)	1.4800 (18)	1.4789 (17)	1.4827 (28)	1.4916 (13)
Perturbative scale: $\overline{g}^2 = 0.9944$								
10.3000	1.29730 (67)							
10.6086	1.2954 (11)							
10.8910	1.2858 (15)	1.28692 (88)	1.28487 (91)	1.28984 (99)	1.27999 (83)	1.27976 (75)	1.2805 (13)	1.28619 (67)
2P scale								
12.0000		1.2493 (14)	1.2481 (14)	1.2510 (15)	1.2438 (13)	1.2443 (12)	1.2428 (20)	1.2494 (10)
PP scale								
24.0000		1.11268 (57)	1.11162 (58)	1.11391 (65)	1.11013 (54)	1.11003 (48)	1.11030 (87)	1.11269 (50)

Table D.18.: Summary table of z_f^c for all beta values and tuning conditions, (1) to (7) (see Sec. 6.1 for a description of all the methods). The data of column (1*) correspond to a separate analysis with method (1), using slightly different simulation parameters (cf. Tab. D.1, Tab. D.2 and Tab. D.3).

$\Delta z_f^c(m)$ for different methods Hadronic scale: $L = 1.436\, r_0$						
L/a	2	3	4	5	6	7
8	0.0145 (47)	-0.0343 (49)	0.0435 (42)	0.0494 (42)	0.0256 (51)	0.0111 (36)
10	0.0103 (42)	-0.0252 (44)	0.0382 (38)	0.0426 (38)	0.0236 (48)	
12	0.0085 (55)	-0.0211 (60)	0.0346 (51)	0.0375 (50)	0.0250 (68)	0.0149 (44)
16	0.0069 (60)	-0.0176 (62)	0.0272 (54)	0.0307 (53)	0.0148 (75)	0.0125 (46)
20	0.0052 (81)	-0.0132 (86)	0.0259 (76)	0.0264 (76)	0.024 (11)	
24	0.0046 (82)	-0.0102 (82)	0.0174 (76)	0.0226 (75)	0.001 (10)	0.0061 (62)

Table D.19.: Differences of z_f^c, $\Delta z_f^c(m)$, determined from different methods. The differences are always $z_f^c(1)$ minus $z_f^c(m)$, obtained from any other method $m = 2 \ldots 7$. Scale NP.

Continuum limit of $\Delta z_f^c(m)$. Hadronic scale: $L = 1.436\, r_0$		
Fit: $\Delta z_f^c = b_0 + b_1 \frac{a}{L}$		
m	b_0	b_1
2	0.0006 (99)	0.10 (12)
3	-0.001 (10)	-0.24 (13)
4	0.0076 (91)	0.31 (11)
5	0.0096 (91)	0.33 (11)
6	-0.000 (12)	0.25 (15)
7	-0.001 (12)	0.20 (18)

Table D.20.: Continuum limit of the data presented in Tab. D.19. We have performed a linear fit in a/L. The point $L/a = 8$ is not included in the fit.

E. Notes on the scaling analysis. Free theory

$\|\|S(x_0, y_0; \vec{p}^{+})\|\|$ $\quad \vec{\theta} = (1,1,1)$			
L/a	$(T/4, 2T/4)$	$(T/4, 3T/4)$	$(2T/4, 3T/4)$
4	9.297016e-02	6.546853e-02	9.297016e-02
8	9.818017e-02	6.834657e-02	9.818017e-02
16	9.954480e-02	6.905485e-02	9.954479e-02
32	9.988739e-02	6.922735e-02	9.988742e-02
64	9.997282e-02	6.926972e-02	9.997281e-02
cont	1.000012e-01	6.928372e-02	1.000012e-01

Table E.1.: Continuum limit of the norm of the quark propagator, S, at fixed time slices, (x_0, y_0), and $\vec{\theta} = (1,1,1)$. The line with 'cont' refers to the numbers obtained by directly evaluating the analytic expression in the continuum. See Sec. 7.1 for explanations.

$\|\|(S - S^{\dagger})(x_0, y_0; \vec{p}^{+})\|\|$ $\quad \vec{\theta} = (1,1,1)$			
L/a	$(T/4, 2T/4)$	$(T/4, 3T/4)$	$(2T/4, 3T/4)$
4	1.858798e-01	1.308836e-01	1.858798e-01
8	1.963571e-01	1.366901e-01	1.963571e-01
16	1.990894e-01	1.381095e-01	1.990895e-01
32	1.997748e-01	1.384547e-01	1.997748e-01
64	1.999456e-01	1.385394e-01	1.999456e-01
cont	2.000024e-01	1.385674e-01	2.000024e-01

Table E.2.: Continuum limit of the norm of the even operator $S - S^{\dagger}$, at fixed time slices, (x_0, y_0), and $\vec{\theta} = (1,1,1)$. The line with 'cont' refers to the numbers obtained by directly evaluating the analytic expression in the continuum. See Sec. 7.1 for explanations.

$\|\|S(x_0, y_0; \vec{p}^{+})\|\|$ $\quad \vec{\theta} = (1,1,0)$			
L/a	$(T/4, 2T/4)$	$(T/4, 3T/4)$	$(2T/4, 3T/4)$
4	1.044163e-01	8.023310e-02	1.044163e-01
8	1.084303e-01	8.272696e-02	1.084304e-01
16	1.094612e-01	8.333614e-02	1.094612e-01
32	1.097188e-01	8.348463e-02	1.097188e-01
64	1.097830e-01	8.352121e-02	1.097830e-01
cont	1.098043e-01	8.353326e-02	1.098043e-01

Table E.3.: Same caption as in Tab. E.1 but with $\vec{\theta} = (1,1,0)$.

$\|\|(S - S^\dagger)(x_0, y_0; \vec{p}^+)\|\|$ $\quad \vec{\theta} = (1,1,0)$			
L/a	$(T/4, 2T/4)$	$(T/4, 3T/4)$	$(2T/4, 3T/4)$
4	2.087964e-01	1.604331e-01	2.087964e-01
8	2.168587e-01	1.654520e-01	2.168587e-01
16	2.189223e-01	1.666722e-01	2.189222e-01
32	2.194376e-01	1.669693e-01	2.194376e-01
64	2.195659e-01	1.670423e-01	2.195659e-01
cont	2.196086e-01	1.670665e-01	2.196086e-01

Table E.4.: Same caption as in Tab. E.2 but with $\vec{\theta} = (1,1,0)$.

$\|\|S(x_0, y_0; \vec{p}^+)\|\|$ $\quad \vec{\theta} = (1,0,0)$			
L/a	$(T/4, 2T/4)$	$(T/4, 3T/4)$	$(2T/4, 3T/4)$
4	1.202059e-01	1.032210e-01	1.202059e-01
8	1.225857e-01	1.049242e-01	1.225857e-01
16	1.231868e-01	1.053407e-01	1.231868e-01
32	1.233367e-01	1.054429e-01	1.233367e-01
64	1.233741e-01	1.054682e-01	1.233741e-01
cont	1.233865e-01	1.054765e-01	1.233865e-01

Table E.5.: Same caption as in Tab. E.1 but with $\vec{\theta} = (1,0,0)$.

$\|\|(S - S^\dagger)(x_0, y_0; \vec{p}^+)\|\|$ $\quad \vec{\theta} = (1,0,0)$			
L/a	$(T/4, 2T/4)$	$(T/4, 3T/4)$	$(2T/4, 3T/4)$
4	2.403987e-01	2.064296e-01	2.403987e-01
8	2.451708e-01	2.098477e-01	2.451707e-01
16	2.463735e-01	2.106814e-01	2.463736e-01
32	2.466733e-01	2.108858e-01	2.466734e-01
64	2.467482e-01	2.109364e-01	2.467482e-01
cont	2.467730e-01	2.109530e-01	2.467730e-01

Table E.6.: Same caption as in Tab. E.2 but with $\vec{\theta} = (1,0,0)$.

$\|\|S(x_0, y_0; \vec{p}^+)\|\|$ $\quad \vec{\theta} = (1,0,0)$			
fit : $y = a_0 + a_1(\frac{a}{L})^2 + a_2(\frac{a}{L})^4$			
	$(T/4, 2T/4)$	$(T/4, 3T/4)$	$(2T/4, 3T/4)$
cont	1.233865e-01	1.054765e-01	1.233865e-01
a_0	1.23387e-01	1.05477e-01	1.23387e-01
a_1	-5.1395e-02	-3.51445e-02	-5.1395e-02
a_2	7.97061e-03	-1.53116e-02	7.97061e-03

Table E.7.: Fit of the data presented in Tab. E.5. Continuum limit of the norm of the quark propagator, S, at fixed time slices, (x_0, y_0), and $\vec{\theta} = (1,0,0)$. The line with 'cont' refers to the numbers obtained by directly evaluating the analytic expression in the continuum. This line is to be compared to the line of a_0. The data are plotted in Fig. 7.1 for the time slices $(T/4, 2T/4)$.

$\|\|S(x_0, y_0; \vec{p}^{+})\|\|$ $\quad \vec{\theta} = (1,0,0)$			
fit : $y = b_0 + b_1(\frac{a}{L}) + b_2(\frac{a}{L})^2$			
	$(T/4, 2T/4)$	$(T/4, 3T/4)$	$(2T/4, 3T/4)$
cont	1.233865e-01	1.054765e-01	1.233865e-01
b_0	1.23386e-01	1.05477e-01	1.23386e-01
b_1	9.6e-06	3.2e-05	9.6e-06
b_2	-5.12683e-02	-3.52256e-02	-5.12683e-02

Table E.8.: Fit of the data presented in Tab. E.5. Continuum limit of the norm of the quark propagator, S, at fixed time slices, (x_0, y_0), and $\vec{\theta} = (1,0,0)$. The line with 'cont' refers to the numbers obtained by directly evaluating the analytic expression in the continuum. This line is to be compared to the line of b_0.

$\|\|(S - S^{\dagger})(x_0, y_0; \vec{p}^{+})\|\|$ $\quad \vec{\theta} = (1,0,0)$			
fit : $y = a_0 + a_1(\frac{a}{L})^2 + a_2(\frac{a}{L})^4$			
	$(T/4, 2T/4)$	$(T/4, 3T/4)$	$(2T/4, 3T/4)$
cont	2.467730e-01	2.109530e-01	2.467730e-01
a_0	2.46774e-01	2.10955e-01	2.46774e-01
a_1	-1.02766e-01	-7.02825e-02	-1.02766e-01
a_2	1.22319e-02	-3.39024e-02	1.22319e-02

Table E.9.: Fit of the data presented in Tab. E.6. Continuum limit of the norm of the even operator $S - S^{\dagger}$, at fixed time slices, (x_0, y_0), and $\vec{\theta} = (1,0,0)$. The line with 'cont' refers to the numbers obtained by directly evaluating the analytic expression in the continuum. This line is to be compared to the line of a_0. The data are plotted in Fig. 7.2 for the time slices $(T/4, 2T/4)$.

$\|\|(S - S^{\dagger})(x_0, y_0; \vec{p}^{+})\|\|$ $\quad \vec{\theta} = (1,0,0)$			
fit : $y = b_0 + b_1(\frac{a}{L}) + b_2(\frac{a}{L})^2$			
	$(T/4, 2T/4)$	$(T/4, 3T/4)$	$(2T/4, 3T/4)$
cont	2.467730e-01	2.109530e-01	2.467730e-01
b_0	2.46773e-01	2.10953e-01	2.46773e-01
b_1	6.4e-06	6.4e-05	6.4e-06
b_2	-1.024e-01	-7.04512e-02	-1.024e-01

Table E.10.: Fit of the data presented in Tab. E.6. Continuum limit of the norm of the even operator $S - S^{\dagger}$, at fixed time slices, (x_0, y_0), and $\vec{\theta} = (1,0,0)$. The line with 'cont' refers to the numbers obtained by directly evaluating the analytic expression in the continuum. This line is to be compared to the line of b_0.

$\|\|S(T/4, 2T/4; \vec{p}^{+})\|\|$ $\quad \vec{\theta} = (1,1,1)$							
L/a	$z_f = 0.9$	$z_f = 0.99$	$z_f = 0.999$	$z_f = 1.0$	$z_f = 1.001$	$z_f = 1.01$	$z_f = 1.1$
4	9.345086e-02	9.301113e-02	9.297421e-02	9.297018e-02	9.296617e-02	9.293072e-02	9.263724e-02
8	9.846726e-02	9.820507e-02	9.818263e-02	9.818018e-02	9.817773e-02	9.815611e-02	9.797488e-02
12	9.938613e-02	9.920673e-02	9.919127e-02	9.918958e-02	9.918789e-02	9.917297e-02	9.904727e-02
16	9.969336e-02	9.955781e-02	9.954608e-02	9.954480e-02	9.954352e-02	9.953220e-02	9.943655e-02
20	9.982852e-02	9.971978e-02	9.971035e-02	9.970932e-02	9.970829e-02	9.969919e-02	9.962213e-02
24	9.989811e-02	9.980739e-02	9.979952e-02	9.979865e-02	9.979780e-02	9.979018e-02	9.972571e-02
28	9.993779e-02	9.985999e-02	9.985323e-02	9.985249e-02	9.985175e-02	9.984521e-02	9.978981e-02
32	9.996206e-02	9.989398e-02	9.988805e-02	9.988741e-02	9.988676e-02	9.988103e-02	9.983248e-02
36	9.997770e-02	9.991718e-02	9.991191e-02	9.991133e-02	9.991076e-02	9.990566e-02	9.986245e-02
40	9.998817e-02	9.993370e-02	9.992896e-02	9.992844e-02	9.992792e-02	9.992333e-02	9.988440e-02
44	9.999539e-02	9.994588e-02	9.994156e-02	9.994109e-02	9.994062e-02	9.993645e-02	9.990103e-02
48	1.000005e-01	9.995510e-02	9.995114e-02	9.995071e-02	9.995028e-02	9.994645e-02	9.991397e-02
52	1.000041e-01	9.996224e-02	9.995859e-02	9.995819e-02	9.995779e-02	9.995426e-02	9.992426e-02
56	1.000068e-01	9.996789e-02	9.996450e-02	9.996413e-02	9.996376e-02	9.996048e-02	9.993261e-02
60	1.000087e-01	9.997243e-02	9.996926e-02	9.996891e-02	9.996857e-02	9.996551e-02	9.993949e-02
64	1.000102e-01	9.997612e-02	9.997316e-02	9.997283e-02	9.997251e-02	9.996964e-02	9.994524e-02
cont	1.00001e-01	1.00001e-01	1.00001e-01	1.00001e-01	1.00001e-01	1.00001e-01	1.00001e-01
fit: $y = b_0 + b_1(\frac{a}{L}) + b_2(\frac{a}{L})^2 + b_3(\frac{a}{L})^3$ (without $L/a = 4$)							
b_0	1.0e-01	1.0e-01	1.0e-01	1.0e-01	1.0e-01	1.0e-01	1.0e-01
b_1	0.24874e-02	3.19133e-04	1.28794e-04	1.08157e-04	8.74622e-05	-9.71133e-05	-1.66321e-03
b_2	-1.18747e-01	-1.19307e-01	-1.19308e-01	-1.19311e-01	-1.19314e-01	-1.19301e-01	-1.19085e-01
b_3	5.92176e-03	1.49554e-02	1.56568e-02	1.57473e-02	1.58369e-02	1.64733e-02	0.22192e-01
fit: $y = a_0 + a_1(\frac{a}{L})^2$ (without $L/a = 4$)							
a_0	1.00055e-01	1.00006e-01	1.00002e-01	1.00001e-01	1.00001e-01	0.999965e-01	0.999614e-01
a_1	-0.100045	-0.11517	-0.116461	-0.116602	-0.116743	-0.117986	-0.128389

Table E.11.: Continuum limit of the norm of the quark propagator, S, at fixed time slices, $(T/4, 2T/4)$, and $\vec{\theta} = (1,1,1)$, for several values of z_f. We have performed two fits of the data, excluding the pont $L/a = 4$: a cubic fit in a/L and a linear fit in $(\frac{a}{L})^2$. The line with 'cont' refers to the numbers obtained by directly evaluating the analytic expression in the continuum. This line is to be compared to the line of a_0 or b_0, depending on the fit. See Sec. 7.1.2 for more explanations.

$\|\|S(T/4, 2T/4; \vec{p}^{+})\|\|$ $\quad \vec{\theta} = (1,1,1)$						
L/a	$z_f = 0.995$	$z_f = 0.996$	$z_f = 0.997$	$z_f = 0.998$	$z_f = 0.999$	$z_f = 1.0$
4	9.299047e-02	9.298638e-02	9.298231e-02	9.297825e-02	9.297421e-02	9.297018e-02
8	9.819252e-02	9.819003e-02	9.818756e-02	9.818509e-02	9.818263e-02	9.818018e-02
12	9.919809e-02	9.919637e-02	9.919467e-02	9.919296e-02	9.919127e-02	9.918958e-02
16	9.955126e-02	9.954996e-02	9.954866e-02	9.954737e-02	9.954608e-02	9.954480e-02
20	9.971451e-02	9.971347e-02	9.971242e-02	9.971139e-02	9.971035e-02	9.970932e-02
24	9.980299e-02	9.980212e-02	9.980125e-02	9.980038e-02	9.979952e-02	9.979865e-02
28	9.985621e-02	9.985546e-02	9.985471e-02	9.985397e-02	9.985323e-02	9.985249e-02
32	9.989067e-02	9.989001e-02	9.988936e-02	9.988870e-02	9.988805e-02	9.988741e-02
36	9.991423e-02	9.991365e-02	9.991307e-02	9.991249e-02	9.991191e-02	9.991133e-02
40	9.993105e-02	9.993052e-02	9.993000e-02	9.992948e-02	9.992896e-02	9.992844e-02
44	9.994346e-02	9.994299e-02	9.994251e-02	9.994204e-02	9.994156e-02	9.994109e-02
48	9.995289e-02	9.995245e-02	9.995201e-02	9.995158e-02	9.995114e-02	9.995071e-02
52	9.996020e-02	9.995980e-02	9.995939e-02	9.995899e-02	9.995859e-02	9.995819e-02
56	9.996599e-02	9.996562e-02	9.996524e-02	9.996487e-02	9.996450e-02	9.996413e-02
60	9.997066e-02	9.997031e-02	9.996996e-02	9.996961e-02	9.996926e-02	9.996891e-02
64	9.997447e-02	9.997414e-02	9.997381e-02	9.997348e-02	9.997316e-02	9.997283e-02
cont	1.00001e-01	1.00001e-01	1.00001e-01	1.00001e-01	1.00001e-01	1.00001e-01
fit: $y = a_0 + a_1(\frac{a}{L})^2$ (without $L/a = 4$)						
a_0	1.00003e-01	1.00003e-01	1.00003e-01	1.00002e-01	1.00002e-01	1.00001e-01
a_1	-0.115892	-0.116035	-0.116177	-0.11632	-0.116461	-0.116602

Table E.12.: Continuum limit of the norm of the quark propagator, S, at fixed time slices, $(T/4, 2T/4)$, and $\vec{\theta} = (1,1,1)$, for several values of z_f. We have fitted the data using a linear fit in $(\frac{a}{L})^2$ and the point $L/a = 4$ has been neglected. The line with 'cont' refers to the numbers obtained by directly evaluating the analytic expression in the continuum. This line is to be compared to the line of a_0. See Sec. 7.1.2 for more explanations.

F. Notes on the scaling analysis. Interacting theory

$\gamma_5\tau^1$-even correlation functions NP scale: $L = 1.436\, r_0$ and $\vec{\theta} = (0,0,0)$							
L/a	β	m	$g^{11}_{\mathrm{P}_-}$	$g^{11}_{\mathrm{P}_+}$	$g^{12}_{\mathrm{V}_{0-}}$	$g^{12}_{\mathrm{V}_{0+}}$	g^{11}_{1}
8	6.0219	1	3.637 (14)	0.02609 (25)	1.9779 (85)	0.01279 (16)	1.1857 (53)
		2	3.643 (14)	0.02249 (19)	1.9839 (85)	0.01090 (12)	1.1883 (52)
		3	3.619 (14)	0.03956 (38)	1.9568 (87)	0.01990 (24)	1.1767 (54)
		4	3.652 (13)	0.01903 (13)	1.9907 (83)	0.009143 (79)	1.1915 (51)
		5	3.653 (13)	0.01893 (14)	1.9912 (83)	0.009112 (80)	1.1918 (51)
		6	3.647 (13)	0.02057 (15)	1.9873 (84)	0.00991 (10)	1.1899 (52)
		7	3.642 (14)	0.02322 (20)	1.9827 (85)	0.01128 (13)	1.1878 (52)
10	6.1628	1	3.605 (13)	0.02081 (22)	1.8788 (84)	0.01028 (13)	1.1136 (51)
		2	3.607 (13)	0.01738 (18)	1.8815 (84)	0.00852 (11)	1.1143 (51)
		3	3.598 (14)	0.03178 (29)	1.8685 (85)	0.01592 (17)	1.1104 (52)
		4	3.610 (13)	0.011182 (99)	1.8843 (83)	0.005342 (60)	1.1144 (50)
		5	3.610 (13)	0.010616 (88)	1.8842 (82)	0.005053 (53)	1.1142 (50)
		6	3.609 (13)	0.01386 (14)	1.8836 (83)	0.006714 (85)	1.1147 (50)
12	6.2885	1	3.528 (19)	0.01809 (24)	1.808 (12)	0.00900 (14)	1.0660 (70)
		2	3.530 (19)	0.01510 (22)	1.810 (11)	0.00748 (13)	1.0663 (69)
		3	3.524 (19)	0.02724 (30)	1.801 (12)	0.01363 (18)	1.0644 (71)
		4	3.531 (18)	0.00836 (13)	1.811 (11)	0.004065 (76)	1.0657 (68)
		5	3.531 (18)	0.00784 (12)	1.811 (11)	0.003801 (71)	1.0655 (68)
		6	3.531 (19)	0.01041 (16)	1.811 (11)	0.005104 (94)	1.0662 (69)
		7	3.530 (19)	0.01310 (20)	1.810 (11)	0.00647 (11)	1.0663 (69)
16	6.4956	1	3.458 (22)	0.01423 (18)	1.702 (13)	0.00691 (10)	0.9921 (77)
		2	3.458 (22)	0.01179 (16)	1.702 (13)	0.005714 (90)	0.9919 (77)
		3	3.456 (22)	0.02169 (22)	1.698 (13)	0.01057 (13)	0.9918 (78)
		4	3.456 (21)	0.00620 (11)	1.702 (13)	0.002974 (59)	0.9905 (76)
		5	3.456 (21)	0.005474 (99)	1.702 (13)	0.002620 (54)	0.9902 (76)
		6	3.457 (21)	0.00933 (14)	1.703 (13)	0.004510 (78)	0.9915 (77)
		7	3.457 (21)	0.01001 (15)	1.703 (13)	0.004842 (82)	0.9917 (77)
20	6.6790	1	3.377 (35)	0.01356 (22)	1.628 (22)	0.00650 (13)	0.948 (13)
		2	3.377 (35)	0.01172 (20)	1.628 (22)	0.00561 (12)	0.948 (13)
		3	3.377 (35)	0.01886 (27)	1.626 (22)	0.00903 (16)	0.948 (14)
		4	3.375 (34)	0.00571 (13)	1.627 (22)	0.002713 (72)	0.946 (13)
		5	3.375 (34)	0.00559 (13)	1.627 (22)	0.002656 (71)	0.946 (13)
		6	3.375 (34)	0.00614 (14)	1.628 (22)	0.002925 (76)	0.946 (13)
24	6.8187	1	3.346 (38)	0.00805 (14)	1.643 (21)	0.003932 (81)	0.950 (13)
		2	3.346 (37)	0.00679 (13)	1.643 (21)	0.003318 (73)	0.950 (13)
		3	3.345 (38)	0.01125 (18)	1.642 (21)	0.00549 (10)	0.951 (13)

Table F.1.: (continuing on the next page, caption below)

$\gamma_5\tau^1$-even correlation functions NP scale: $L = 1.436\, r_0$ and $\vec{\theta} = (0,0,0)$							
L/a	β	m	$g^{11}_{\mathrm{P}_-}$	$g^{11}_{\mathrm{P}_+}$	$g^{12}_{\mathrm{V}_{0-}}$	$g^{12}_{\mathrm{V}_{0+}}$	g^{11}_{1}
		4	3.345 (37)	0.003896 (90)	1.643 (21)	0.001900 (50)	0.950 (13)
		5	3.344 (37)	0.002970 (75)	1.643 (21)	0.001447 (42)	0.949 (13)
		6	3.346 (38)	0.00788 (14)	1.643 (21)	0.003849 (80)	0.950 (13)
		7	3.345 (37)	0.00641 (12)	1.643 (21)	0.003129 (70)	0.950 (13)

Table F.1.: Results for the $\gamma_5\tau^1$-even correlation functions, $g^{11}_{\mathrm{P}_\pm}$, $g^{12}_{\mathrm{V}_{0\pm}}$ and g^{11}_{1}, at scale $L = 1.436\, r_0$ and for $\vec{\theta} = (0,0,0)$. The data have been obtained via linear interpolations to the critical values of κ and quadratic interpolations to the critical values of z_f for all the tuning methods (1) to (7). See Sec. 7.2.1 and Sec. 7.2.2 for explanations.

$\gamma_5\tau^1$-even correlation functions I scale: $\overline{g}^2 = 2.4484$ and $\vec{\theta} = (0,0,0)$							
L/a	β	m	$g^{11}_{\mathrm{P}_-}$	$g^{11}_{\mathrm{P}_+}$	$g^{12}_{\mathrm{V}_{0-}}$	$g^{12}_{\mathrm{V}_{0+}}$	g^{11}_{1}
8	7.0197	1	3.2342 (83)	0.010013 (72)	2.2115 (68)	0.006152 (52)	1.5371 (48)
		2	3.2391 (82)	0.010043 (76)	2.2170 (68)	0.006203 (54)	1.5412 (48)
		3	3.2240 (85)	0.011667 (97)	2.1987 (69)	0.007214 (71)	1.5286 (49)
		4	3.2446 (81)	0.01110 (10)	2.2222 (67)	0.006959 (69)	1.5456 (47)
		5	3.2456 (81)	0.01148 (11)	2.2231 (67)	0.007222 (74)	1.5464 (47)
		6	3.2418 (82)	0.010407 (86)	2.2197 (67)	0.006468 (59)	1.5434 (47)
		7	3.2348 (83)	0.009982 (72)	2.2121 (68)	0.006135 (52)	1.5376 (48)
12	7.3551	1	3.219 (11)	0.003185 (35)	2.1342 (89)	0.001976 (25)	1.4657 (61)
		2	3.220 (11)	0.002968 (32)	2.1358 (89)	0.001835 (22)	1.4668 (61)
		3	3.216 (11)	0.004005 (48)	2.1305 (89)	0.002514 (35)	1.4633 (61)
		4	3.223 (10)	0.003154 (40)	2.1386 (88)	0.001966 (26)	1.4691 (61)
		5	3.224 (10)	0.003212 (42)	2.1387 (88)	0.002005 (27)	1.4693 (61)
		6	3.223 (10)	0.003032 (37)	2.1382 (88)	0.001884 (24)	1.4688 (61)
		7	3.220 (11)	0.003085 (34)	2.1348 (89)	0.001911 (24)	1.4662 (61)
16	7.6101	1	3.203 (13)	0.001786 (30)	2.094 (11)	0.001123 (21)	1.4314 (76)
		2	3.204 (13)	0.001526 (25)	2.095 (11)	0.000954 (18)	1.4319 (75)
		3	3.202 (13)	0.002454 (40)	2.092 (11)	0.001559 (28)	1.4303 (76)
		4	3.206 (13)	0.001195 (17)	2.096 (11)	0.000741 (12)	1.4331 (75)
		5	3.206 (13)	0.001201 (18)	2.096 (11)	0.000745 (12)	1.4332 (75)
		6	3.205 (13)	0.001211 (18)	2.096 (11)	0.000750 (12)	1.4329 (75)
		7	3.204 (13)	0.001579 (26)	2.095 (11)	0.000988 (18)	1.4318 (75)

Table F.2.: Same caption as in Tab. F.1 but at scale $\overline{g}^2 = 2.4484$.

$\gamma_5\tau^1$-even correlation functions P scale: $\overline{g}^2 = 0.9944$ and $\vec{\theta} = (0,0,0)$							
L/a	β	m	$g^{11}_{\mathrm{P}_-}$	$g^{11}_{\mathrm{P}_+}$	$g^{12}_{\mathrm{V}_{0-}}$	$g^{12}_{\mathrm{V}_{0+}}$	g^{11}_{1}
16	10.8910	1	3.0565 (76)	0.0006071 (87)	2.4403 (81)	0.0004638 (70)	1.9652 (65)
		2	3.0568 (76)	0.0006251 (90)	2.4407 (81)	0.0004782 (72)	1.9656 (65)
		3	3.0560 (76)	0.0006260 (90)	2.4396 (81)	0.0004787 (73)	1.9646 (65)
		4	3.0574 (75)	0.000772 (11)	2.4414 (81)	0.0005952 (88)	1.9663 (65)
		5	3.0574 (75)	0.000782 (11)	2.4414 (81)	0.0006035 (89)	1.9663 (65)
		6	3.0573 (75)	0.000750 (11)	2.4414 (81)	0.0005775 (86)	1.9662 (65)
		7	3.0566 (76)	0.0006105 (88)	2.4405 (81)	0.0004665 (70)	1.9653 (65)

Table F.3.: Same caption as in Tab. F.1 but at scale $\overline{g}^2 = 0.9944$.

$\gamma_5\tau^1$-even correlation functions 2P scale and $\vec{\theta} = (0,0,0)$							
L/a	β	m	$g^{11}_{\mathrm{P}_-}$	$g^{11}_{\mathrm{P}_+}$	$g^{12}_{\mathrm{V}_{0-}}$	$g^{12}_{\mathrm{V}_{0+}}$	g^{11}_{1}
16	12.0000	1	3.049 (11)	0.000537 (16)	2.527 (13)	0.000429 (13)	2.089 (11)
		2	3.049 (11)	0.000569 (17)	2.527 (13)	0.000455 (14)	2.089 (11)
		3	3.048 (11)	0.000508 (15)	2.526 (13)	0.000404 (12)	2.088 (11)
		4	3.049 (11)	0.000754 (21)	2.527 (13)	0.000609 (18)	2.090 (11)
		5	3.049 (11)	0.000726 (21)	2.527 (13)	0.000586 (17)	2.090 (11)
		6	3.049 (11)	0.000813 (23)	2.527 (13)	0.000658 (19)	2.090 (11)
		7	3.049 (11)	0.000535 (16)	2.526 (13)	0.000427 (13)	2.089 (11)

Table F.4.: Same caption as in Tab. F.1 but at scale 2P.

$\gamma_5\tau^1$-even correlation functions PP scale and $\vec{\theta} = (0,0,0)$							
L/a	β	m	$g^{11}_{\mathrm{P}_-}$	$g^{11}_{\mathrm{P}_+}$	$g^{12}_{\mathrm{V}_{0-}}$	$g^{12}_{\mathrm{V}_{0+}}$	g^{11}_{1}
16	24.0000	1	3.0201 (56)	0.0002171 (50)	2.7853 (73)	0.0001936 (46)	2.5652 (67)
		2	3.0201 (56)	0.0002289 (52)	2.7854 (73)	0.0002045 (48)	2.5653 (67)
		3	3.0200 (56)	0.0002117 (50)	2.7852 (73)	0.0001885 (46)	2.5651 (67)
		4	3.0202 (56)	0.0002566 (56)	2.7855 (73)	0.0002301 (51)	2.5655 (67)
		5	3.0202 (56)	0.0002589 (56)	2.7855 (73)	0.0002322 (51)	2.5655 (67)
		6	3.0202 (56)	0.0002528 (55)	2.7855 (73)	0.0002266 (50)	2.5654 (67)
		7	3.0201 (56)	0.0002171 (50)	2.7853 (73)	0.0001935 (46)	2.5652 (67)

Table F.5.: Same caption as in Tab. F.1 but at scale PP.

$\gamma_5\tau^1$-even correlation functions NP scale: $L = 1.436\, r_0$ and $\vec{\theta} = (0.5, 0.5, 0.5)$							
L/a	β	m	$g^{11}_{\mathrm{P}_-}$	$g^{11}_{\mathrm{P}_+}$	$g^{12}_{\mathrm{V}_{0-}}$	$g^{12}_{\mathrm{V}_{0+}}$	g^{11}_{1}
8	6.0219	1*	2.9412 (86)	0.04976 (16)	1.4129 (64)	0.02207 (12)	0.8461 (39)
		1	2.937 (10)	0.04978 (21)	1.4098 (64)	0.02206 (14)	0.8443 (39)
		2	2.9421 (98)	0.04653 (17)	1.4150 (63)	0.02060 (12)	0.8466 (39)
		3	2.920 (10)	0.06126 (30)	1.3929 (65)	0.02729 (19)	0.8371 (40)
		4	2.9510 (95)	0.04291 (15)	1.4218 (62)	0.01900 (10)	0.8498 (38)
		5	2.9524 (95)	0.04264 (16)	1.4226 (62)	0.01889 (10)	0.8502 (38)
		6	2.9459 (97)	0.04469 (15)	1.4182 (62)	0.01978 (11)	0.8480 (39)
		7	2.9409 (99)	0.04721 (18)	1.4139 (63)	0.02090 (13)	0.8461 (39)
10	6.1628	1*	2.9218 (85)	0.03592 (12)	1.3452 (61)	0.015758 (78)	0.7946 (36)
		1	2.9199 (94)	0.03600 (18)	1.3442 (60)	0.01579 (11)	0.7940 (36)
		2	2.9223 (93)	0.03308 (16)	1.3467 (60)	0.014474 (99)	0.7948 (36)
		3	2.9122 (96)	0.04519 (23)	1.3354 (61)	0.01991 (14)	0.7910 (37)
		4	2.9267 (91)	0.02758 (10)	1.3506 (59)	0.012006 (71)	0.7958 (35)
		5	2.9271 (90)	0.027036 (96)	1.3508 (59)	0.011761 (68)	0.7958 (35)
		6	2.9248 (92)	0.03002 (13)	1.3491 (59)	0.013099 (85)	0.7955 (36)
12	6.2885	1*	2.867 (13)	0.02844 (13)	1.3043 (80)	0.012551 (83)	0.7656 (48)
		1	2.857 (14)	0.02820 (20)	1.2953 (80)	0.01239 (12)	0.7602 (47)
		2	2.859 (13)	0.02569 (18)	1.2969 (79)	0.01127 (11)	0.7606 (47)
		3	2.852 (14)	0.03579 (25)	1.2894 (81)	0.01577 (14)	0.7585 (48)
		4	2.861 (13)	0.01992 (12)	1.2997 (78)	0.008694 (75)	0.7610 (46)
		5	2.862 (13)	0.01946 (12)	1.2998 (78)	0.008488 (72)	0.7609 (46)
		6	2.861 (13)	0.02170 (14)	1.2991 (79)	0.009491 (86)	0.7610 (47)
		7	2.860 (13)	0.02400 (17)	1.2979 (79)	0.010519 (98)	0.7609 (47)
16	6.4956	1*	2.817 (15)	0.01967 (11)	1.2317 (93)	0.008430 (65)	0.7138 (55)
		1	2.814 (15)	0.01926 (16)	1.2301 (92)	0.008238 (89)	0.7129 (55)
		2	2.815 (15)	0.01723 (14)	1.2310 (92)	0.007364 (81)	0.7129 (55)
		3	2.812 (15)	0.02540 (19)	1.2268 (93)	0.01090 (11)	0.7122 (55)
		4	2.815 (15)	0.012555 (99)	1.2320 (92)	0.005338 (59)	0.7125 (55)
		5	2.815 (15)	0.011940 (93)	1.2319 (92)	0.005071 (56)	0.7124 (55)
		6	2.815 (15)	0.01519 (12)	1.2316 (92)	0.006478 (72)	0.7129 (55)
		7	2.815 (15)	0.01575 (13)	1.2315 (92)	0.006723 (75)	0.7129 (55)
20	6.6790	1	2.709 (24)	0.01578 (18)	1.166 (15)	0.00672 (11)	0.6748 (92)
		2	2.709 (24)	0.01427 (16)	1.166 (15)	0.00608 (10)	0.6747 (92)
		3	2.708 (24)	0.02009 (21)	1.164 (15)	0.00856 (14)	0.6746 (92)
		4	2.709 (23)	0.00934 (11)	1.167 (15)	0.003954 (70)	0.6741 (92)
		5	2.709 (23)	0.00924 (11)	1.167 (15)	0.003911 (69)	0.6741 (92)
		6	2.709 (23)	0.00970 (12)	1.167 (15)	0.004110 (73)	0.6742 (92)

Table F.6.: (continuing on the next page, caption below)

$\gamma_5\tau^1$-even correlation functions NP scale: $L = 1.436\, r_0$ and $\vec{\theta} = (0.5, 0.5, 0.5)$							
L/a	β	m	$g^{11}_{\mathrm{P}_-}$	$g^{11}_{\mathrm{P}_+}$	$g^{12}_{\mathrm{V}_{0-}}$	$g^{12}_{\mathrm{V}_{0+}}$	g^{11}_1
24	6.8187	1	2.675 (27)	0.00976 (13)	1.136 (16)	0.004107 (75)	0.6529 (93)
		2	2.675 (27)	0.00875 (12)	1.136 (16)	0.003678 (68)	0.6529 (93)
		3	2.675 (27)	0.01234 (16)	1.135 (16)	0.005194 (92)	0.6528 (94)
		4	2.675 (27)	0.006389 (88)	1.136 (16)	0.002683 (50)	0.6526 (93)
		5	2.675 (27)	0.005632 (76)	1.136 (16)	0.002363 (44)	0.6524 (93)
		6	2.675 (27)	0.00963 (13)	1.136 (16)	0.004049 (74)	0.6529 (93)
		7	2.675 (27)	0.00843 (12)	1.136 (16)	0.003546 (66)	0.6529 (93)

Table F.6.: Same caption as in Tab. F.1 but at $\vec{\theta} = (0.5, 0.5, 0.5)$. The values denoted with (1*) have been obtained by direct simulations at the critical values of κ and z_f. See Chap. 6 for explanation of (1*).

$\gamma_5\tau^1$-even correlation functions I scale: $\overline{g}^2 = 2.4484$ and $\vec{\theta} = (0.5, 0.5, 0.5)$							
L/a	β	m	$g^{11}_{\mathrm{P}_-}$	$g^{11}_{\mathrm{P}_+}$	$g^{12}_{\mathrm{V}_{0-}}$	$g^{12}_{\mathrm{V}_{0+}}$	g^{11}_1
8	7.0197	1*	2.5142 (48)	0.003341 (79)	1.4348 (43)	0.017953 (66)	1.0006 (30)
		1	2.5143 (55)	0.003306 (79)	1.4358 (44)	0.017784 (65)	1.0013 (31)
		2	2.5186 (54)	0.003279 (86)	1.4399 (44)	0.017680 (66)	1.0042 (31)
		3	2.5056 (56)	0.003480 (85)	1.4265 (45)	0.018668 (71)	0.9953 (31)
		4	2.5235 (53)	0.00332 (10)	1.4442 (43)	0.017964 (72)	1.0075 (31)
		5	2.5245 (53)	0.00334 (11)	1.4450 (43)	0.018086 (74)	1.0081 (30)
		6	2.5210 (54)	0.003288 (93)	1.4421 (44)	0.017757 (68)	1.0058 (31)
		7	2.5148 (55)	0.003300 (79)	1.4363 (44)	0.017759 (65)	1.0016 (31)
12	7.3551	1*	2.5015 (62)	0.014097 (43)	1.3856 (53)	0.007547 (35)	0.9509 (37)
		1	2.5003 (65)	0.014158 (43)	1.3847 (52)	0.007568 (36)	0.9504 (36)
		2	2.5016 (65)	0.013931 (42)	1.3859 (52)	0.007449 (35)	0.9512 (36)
		3	2.4976 (66)	0.014895 (47)	1.3819 (53)	0.007964 (40)	0.9486 (36)
		4	2.5044 (65)	0.013914 (50)	1.3883 (52)	0.007454 (36)	0.9530 (36)
		5	2.5046 (65)	0.013947 (51)	1.3884 (52)	0.007473 (36)	0.9531 (36)
		6	2.5039 (65)	0.013852 (48)	1.3879 (52)	0.007417 (35)	0.9527 (36)
		7	2.5008 (65)	0.014059 (42)	1.3852 (52)	0.007516 (36)	0.9507 (36)
16	7.6101	1*	2.4864 (82)	0.008178 (31)	1.3483 (67)	0.004364 (25)	0.9199 (46)
		1	2.4868 (84)	0.008141 (33)	1.3484 (67)	0.004335 (27)	0.9200 (46)
		2	2.4875 (84)	0.007918 (31)	1.3490 (67)	0.004217 (26)	0.9204 (46)
		3	2.4855 (85)	0.008695 (38)	1.3469 (67)	0.004631 (30)	0.9191 (46)
		4	2.4893 (84)	0.007593 (29)	1.3505 (67)	0.004047 (23)	0.9214 (46)
		5	2.4895 (84)	0.007591 (29)	1.3506 (67)	0.004047 (23)	0.9215 (46)
		6	2.4889 (84)	0.007623 (29)	1.3502 (67)	0.004062 (23)	0.9212 (46)
		7	2.4874 (84)	0.007964 (31)	1.3489 (67)	0.004241 (26)	0.9203 (46)

Table F.7.: Same caption as in Tab. F.6 but at scale $\overline{g}^2 = 2.4484$.

$\gamma_5\tau^1$-even correlation functions P scale: $\overline{g}^2 = 0.9944$ and $\vec{\theta} = (0.5, 0.5, 0.5)$							
L/a	β	m	$g^{11}_{\mathrm{P}_-}$	$g^{11}_{\mathrm{P}_+}$	$g^{12}_{\mathrm{V}_{0-}}$	$g^{12}_{\mathrm{V}_{0+}}$	g^{11}_1
8	10.3000	1*	2.2985 (23)	0.028122 (36)	1.4760 (25)	0.017520 (35)	1.2182 (21)
12	10.6086	1*	2.2970 (34)	0.012289 (22)	1.4514 (34)	0.007613 (21)	1.1786 (27)
16	10.8910	1*	2.2924 (43)	0.006800 (15)	1.4342 (44)	0.004191 (14)	1.1555 (35)
		1	2.2921 (44)	0.006796 (15)	1.4340 (44)	0.004181 (14)	1.1553 (35)
		2	2.2924 (44)	0.006796 (16)	1.4343 (44)	0.004182 (14)	1.1556 (35)
		3	2.2916 (45)	0.006830 (15)	1.4334 (44)	0.004202 (14)	1.1549 (35)
		4	2.2931 (44)	0.006872 (17)	1.4350 (44)	0.004230 (15)	1.1562 (35)
		5	2.2931 (44)	0.006878 (17)	1.4350 (44)	0.004234 (15)	1.1563 (35)
		6	2.2930 (44)	0.006859 (17)	1.4349 (44)	0.004222 (15)	1.1562 (35)
		7	2.2922 (44)	0.006794 (15)	1.4341 (44)	0.004180 (14)	1.1554 (35)

Table F.8.: Same caption as in Tab. F.6 but at scale $\overline{g}^2 = 0.9944$.

$\gamma_5\tau^1$-even correlation functions 2P scale and $\vec{\theta} = (0.5, 0.5, 0.5)$							
L/a	β	m	$g^{11}_{\mathrm{P}_-}$	$g^{11}_{\mathrm{P}_+}$	$g^{12}_{\mathrm{V}_{0-}}$	$g^{12}_{\mathrm{V}_{0+}}$	g^{11}_1
16	12.0000	1	2.2686 (65)	0.006722 (22)	1.4486 (62)	0.004247 (19)	1.1988 (52)
		2	2.2688 (65)	0.006737 (22)	1.4488 (62)	0.004257 (19)	1.1990 (52)
		3	2.2683 (66)	0.006712 (21)	1.4483 (62)	0.004240 (19)	1.1985 (52)
		4	2.2694 (65)	0.006845 (25)	1.4494 (62)	0.004327 (21)	1.1996 (51)
		5	2.2693 (65)	0.006828 (25)	1.4493 (62)	0.004316 (20)	1.1995 (51)
		6	2.2695 (65)	0.006882 (26)	1.4495 (62)	0.004351 (21)	1.1997 (51)
		7	2.2686 (65)	0.006721 (22)	1.4486 (62)	0.004246 (19)	1.1988 (52)

Table F.9.: Same caption as in Tab. F.1 but at scale 2P and $\vec{\theta} = (0.5, 0.5, 0.5)$.

$\gamma_5\tau^1$-even correlation functions PP scale and $\vec{\theta} = (0.5, 0.5, 0.5)$							
L/a	β	m	$g^{11}_{\mathrm{P}_-}$	$g^{11}_{\mathrm{P}_+}$	$g^{12}_{\mathrm{V}_{0-}}$	$g^{12}_{\mathrm{V}_{0+}}$	g^{11}_1
16	24.0000	1	2.1966 (29)	0.006459 (11)	1.5009 (31)	0.004391 (10)	1.3851 (28)
		2	2.1967 (29)	0.006459 (11)	1.5011 (31)	0.004392 (10)	1.3853 (28)
		3	2.1964 (29)	0.006464 (10)	1.5007 (31)	0.004395 (11)	1.3850 (28)
		4	2.1968 (29)	0.006468 (11)	1.5013 (31)	0.004398 (10)	1.3855 (28)
		5	2.1969 (29)	0.006469 (11)	1.5013 (31)	0.004399 (10)	1.3855 (28)
		6	2.1968 (29)	0.006467 (11)	1.5012 (31)	0.004397 (10)	1.3854 (28)
		7	2.1966 (29)	0.006459 (11)	1.5009 (31)	0.004391 (10)	1.3851 (28)

Table F.10.: Same caption as in Tab. F.1 but at scale PP and $\vec{\theta} = (0.5, 0.5, 0.5)$.

$\gamma_5\tau^1$-odd correlation functions NP scale: $L = 1.436\, r_0$ and $\vec{\theta} = (0,0,0)$				
L/a	β	m	$g^{11}_{\mathrm{A}_{0-}}$	$\overline{g}^{12}_{\mathrm{V}_{k-}}$
8	6.0219	1	———	-0.171 (10)
		2	0.0434 (97)	-0.114 (10)
		3	-0.1031 (95)	-0.306 (10)
		4	0.1305 (98)	———
		5	0.1482 (98)	0.023 (11)
		6	0.0767 (97)	-0.070 (11)
		7	0.0332 (97)	-0.127 (10)
10	6.1628	1	———	-0.1449 (93)
		2	0.0296 (84)	-0.1058 (93)
		3	-0.0724 (84)	-0.2405 (92)
		4	0.1098 (85)	———
		5	0.1224 (85)	0.0167 (95)
		6	0.0678 (85)	-0.0554 (94)
12	6.2885	1	———	-0.124 (12)
		2	0.023 (11)	-0.093 (12)
		3	-0.058 (10)	-0.199 (12)
		4	0.094 (11)	———
		5	0.102 (11)	0.010 (12)
		6	0.068 (11)	-0.034 (12)
		7	0.041 (11)	-0.071 (12)
16	6.4956	1	———	-0.095 (12)
		2	0.018 (11)	-0.071 (12)
		3	-0.047 (11)	-0.156 (12)
		4	0.072 (11)	———
		5	0.082 (11)	0.012 (12)
		6	0.039 (11)	-0.043 (12)
		7	0.033 (11)	-0.051 (12)
20	6.6790	1	———	-0.084 (17)
		2	0.013 (14)	-0.067 (17)
		3	-0.033 (14)	-0.128 (16)
		4	0.065 (14)	———
		5	0.066 (14)	0.002 (17)
		6	0.061 (14)	-0.006 (17)
24	6.8187	1	———	-0.058 (17)
		2	0.012 (15)	-0.043 (17)
		3	-0.027 (15)	-0.092 (17)
		4	0.045 (15)	———
		5	0.059 (15)	0.017 (17)
		6	0.001 (15)	-0.056 (17)
		7	0.016 (15)	-0.038 (17)

Table F.11.: Results for the $\gamma_5\tau^1$-odd correlation functions, $g^{11}_{\mathrm{A}_{0-}}$ and $\overline{g}^{12}_{\mathrm{V}_{k-}}$, at scale $L = 1.436\, r_0$ and for $\vec{\theta} = (0,0,0)$. The data have been obtained via linear interpolations to the critical values of κ and z_f for all the tuning methods (1) to (7). The lines represent the cases where the corresponding quantity has been used as tuning condition. See Sec. 7.2.3 for explanations.

$\gamma_5\tau^1$-odd correlation functions I scale: $\overline{g}^2 = 2.4484$ and $\vec{\theta} = (0,0,0)$				
L/a	β	m	$g^{11}_{\mathrm{A}_{0-}}$	$\overline{g}^{12}_{\mathrm{V}_{k-}}$
8	7.0197	1	———	-0.1134 (64)
		2	0.0406 (61)	-0.0640 (65)
		3	-0.0730 (60)	-0.2015 (62)
		4	0.0935 (62)	———
		5	0.1048 (63)	0.0137 (66)
		6	0.0659 (62)	-0.0334 (65)
		7	0.0044 (61)	-0.1079 (64)
12	7.3551	1	———	-0.0845 (72)
		2	0.0192 (67)	-0.0610 (72)
		3	-0.0355 (67)	-0.1277 (71)
		4	0.0695 (68)	———
		5	0.0732 (68)	0.0048 (73)
		6	0.0597 (68)	-0.0118 (72)
		7	0.0072 (67)	-0.0757 (72)
16	7.6101	1	———	-0.0645 (80)
		2	0.0131 (75)	-0.0487 (80)
		3	-0.0236 (74)	-0.0933 (80)
		4	0.0531 (75)	———
		5	0.0572 (75)	0.0048 (81)
		6	0.0431 (75)	-0.0123 (80)
		7	0.0101 (75)	-0.0523 (80)

Table F.12.: Same caption as in Tab. F.11 but at scale $\overline{g}^2 = 2.4484$.

$\gamma_5\tau^1$-odd correlation functions P scale: $\overline{g}^2 = 0.9944$ and $\vec{\theta} = (0,0,0)$				
L/a	β	m	$g^{11}_{\mathrm{A}_{0-}}$	$\overline{g}^{12}_{\mathrm{V}_{k-}}$
16	10.8910	1	———	-0.0363 (43)
		2	0.0096 (41)	-0.0255 (43)
		3	-0.0136 (41)	-0.0516 (43)
		4	0.0323 (41)	———
		5	0.0334 (41)	0.0012 (44)
		6	0.0299 (41)	-0.0027 (44)
		7	0.0034 (41)	-0.0325 (43)

Table F.13.: Same caption as in Tab. F.11 but at scale $\overline{g}^2 = 0.9944$.

$\gamma_5\tau^1$-odd correlation functions 2P scale and $\vec{\theta} = (0,0,0)$				
L/a	β	m	$g^{11}_{\mathrm{A}_{0-}}$	$\overline{g}^{12}_{\mathrm{V}_{k-}}$
16	12.0000	1	———	-0.0292 (70)
		2	0.0059 (67)	-0.0228 (70)
		3	-0.0081 (67)	-0.0382 (70)
		4	0.0266 (67)	———
		5	0.0242 (67)	-0.0026 (70)
		6	0.0315 (67)	0.0054 (70)
		7	-0.0004 (67)	-0.0297 (70)

Table F.14.: Same caption as in Tab. F.11 but at scale 2P.

$\gamma_5\tau^1$-odd correlation functions PP scale and $\vec{\theta} = (0,0,0)$				
L/a	β	m	$g^{11}_{\mathrm{A}_{0-}}$	$\overline{g}^{12}_{\mathrm{V}_{k-}}$
16	24.0000	1	———	-0.0144 (31)
		2	0.0057 (31)	-0.0084 (31)
		3	-0.0066 (31)	-0.0213 (31)
		4	0.0137 (31)	———
		5	0.0143 (31)	0.0005 (31)
		6	0.0128 (31)	-0.0010 (31)
		7	-0.0001 (31)	-0.0144 (31)

Table F.15.: Same caption as in Tab. F.11 but at scale PP.

$\gamma_5\tau^1$-odd correlation functions NP scale: $L = 1.436\, r_0$ and $\vec{\theta} = (0.5,0.5,0.5)$				
L/a	β	m	$g^{11}_{\mathrm{A}_{0-}}$	$\overline{g}^{12}_{\mathrm{V}_{k-}}$
8	6.0219	1*	-0.0270 (59)	
		1	-0.0307 (71)	-0.1465 (75)
		2	———	-0.1034 (76)
		3	-0.1031 (70)	-0.2482 (73)
		4	0.0612 (73)	-0.0174 (78)
		5	0.0736 (73)	———
		6	0.0234 (72)	-0.0705 (77)
		7	-0.0072 (71)	-0.1135 (76)
10	6.1628	1*	-0.0173 (50)	
		1	-0.0210 (64)	-0.1239 (70)
		2	———	-0.0939 (70)
		3	-0.0724 (64)	-0.1971 (69)
		4	0.0570 (65)	-0.0129 (71)
		5	0.0659 (65)	———
		6	0.0272 (64)	-0.0553 (70)

Table F.16.: (continuing on the next page, caption below)

$\gamma_5\tau^1$-odd correlation functions NP scale: $L = 1.436\, r_0$ and $\vec{\theta} = (0.5, 0.5, 0.5)$				
L/a	β	m	$g^{11}_{\mathrm{A}_{0-}}$	$\overline{g}^{12}_{\mathrm{V}_{k-}}$
12	6.2885	1*	-0.0215 (58)	
		1	-0.0165 (77)	-0.1035 (87)
		2	———	-0.0800 (87)
		3	-0.0576 (77)	-0.1617 (85)
		4	0.0508 (78)	-0.0079 (89)
		5	0.0564 (78)	———
		6	0.0321 (78)	-0.0344 (88)
		7	0.0125 (78)	-0.0623 (88)
16	6.4956	1*	-0.0072 (50)	
		1	-0.0132 (84)	-0.0837 (91)
		2	———	-0.0648 (91)
		3	-0.0471 (84)	-0.1316 (91)
		4	0.0391 (84)	-0.0095 (92)
		5	0.0458 (84)	———
		6	0.0152 (84)	-0.0433 (92)
		7	0.0108 (84)	-0.0496 (92)
20	6.6790	1	-0.009 (10)	-0.067 (13)
		2	———	-0.054 (13)
		3	-0.033 (10)	-0.100 (13)
		4	0.037 (11)	-0.001 (13)
		5	0.038 (11)	———
		6	0.034 (11)	-0.006 (13)
24	6.8187	1	-0.008 (11)	-0.057 (13)
		2	———	-0.046 (13)
		3	-0.027 (11)	-0.083 (13)
		4	0.023 (11)	-0.013 (13)
		5	0.032 (11)	———
		6	-0.007 (11)	-0.056 (13)
		7	0.003 (11)	-0.042 (13)

Table F.16.: Same caption as in Tab. F.11 but at $\vec{\theta} = (0.5, 0.5, 0.5)$. The values denoted with (1*) have been obtained by direct simulations at the critical values of κ and z_f. See Chap. 6 for explanation of (1*).

$\gamma_5\tau^1$-odd correlation functions I scale: $\overline{g}^2 = 2.4484$ and $\vec{\theta} = (0.5, 0.5, 0.5)$				
L/a	β	m	$g^{11}_{\mathrm{A}_{0-}}$	$\overline{g}^{12}_{\mathrm{V}_{k-}}$
8	7.0197	1*	-0.0378 (31)	
		1	-0.0263 (41)	-0.0898 (43)
		2	———	-0.0550 (43)
		3	-0.0730 (40)	-0.1521 (41)
		4	0.0338 (42)	-0.0098 (44)
		5	0.0411 (42)	———
		6	0.0161 (41)	-0.0334 (44)
		7	-0.0234 (41)	-0.0860 (43)
12	7.3551	1*	-0.0083 (31)	
		1	-0.0125 (47)	-0.0640 (50)
		2	———	-0.0472 (50)
		3	-0.0355 (47)	-0.0951 (49)
		4	0.0324 (47)	-0.0032 (50)
		5	0.0348 (47)	———
		6	0.0260 (47)	-0.0118 (50)
		7	-0.0079 (47)	-0.0577 (50)
16	7.6101	1*	-0.0137 (30)	
		1	-0.0084 (50)	-0.0500 (54)
		2	———	-0.0386 (54)
		3	-0.0236 (50)	-0.0708 (54)
		4	0.0257 (50)	-0.0035 (54)
		5	0.0283 (50)	———
		6	0.0193 (50)	-0.0123 (54)
		7	-0.0019 (50)	-0.0412 (54)

Table F.17.: Same caption as in Tab. F.16 but at scale $\overline{g}^2 = 2.4484$.

$\gamma_5\tau^1$-odd correlation functions P scale: $\overline{g}^2 = 0.9944$ and $\vec{\theta} = (0.5, 0.5, 0.5)$				
L/a	β	m	$g^{11}_{\mathrm{A}_{0-}}$	$\overline{g}^{12}_{\mathrm{V}_{k-}}$
8	10.3000	1*	-0.0146 (14)	
12	10.6086	1*	-0.0063 (14)	
16	10.8910	1*	-0.0034 (15)	
		1	-0.0056 (25)	-0.0256 (27)
		2	———	-0.0183 (27)
		3	-0.0136 (25)	-0.0360 (27)
		4	0.0134 (25)	-0.0008 (27)
		5	0.0140 (25)	———
		6	0.0120 (25)	-0.0027 (27)
		7	-0.0036 (25)	-0.0230 (27)

Table F.18.: Same caption as in Tab. F.16 but at scale $\overline{g}^2 = 0.9944$.

$\gamma_5\tau^1$-odd correlation functions 2P scale and $\vec{\theta} = (0.5, 0.5, 0.5)$				
L/a	β	m	$g^{11}_{\mathrm{A}_{0-}}$	$\overline{g}^{12}_{\mathrm{V}_{k-}}$
16	12.0000	1	-0.0034 (40)	-0.0178 (42)
		2	———	-0.0135 (42)
		3	-0.0081 (40)	-0.0239 (42)
		4	0.0118 (40)	0.0019 (42)
		5	0.0104 (40)	———
		6	0.0146 (40)	0.0055 (42)
		7	-0.0037 (40)	-0.0181 (42)

Table F.19.: Same caption as in Tab. F.11 but at scale 2P and $\vec{\theta} = (0.5, 0.5, 0.5)$.

$\gamma_5\tau^1$-odd correlation functions PP scale and $\vec{\theta} = (0.5, 0.5, 0.5)$				
L/a	β	m	$g^{11}_{\mathrm{A}_{0-}}$	$\overline{g}^{12}_{\mathrm{V}_{k-}}$
16	24.0000	1	-0.0031 (17)	-0.0097 (17)
		2	———	-0.0058 (17)
		3	-0.0066 (17)	-0.0141 (17)
		4	0.0043 (17)	-0.0004 (17)
		5	0.0046 (17)	———
		6	0.0038 (17)	-0.0010 (17)
		7	-0.0031 (17)	-0.0097 (17)

Table F.20.: Same caption as in Tab. F.11 but at scale PP and $\vec{\theta} = (0.5, 0.5, 0.5)$.

Continuum limit of $g^{11}_{\mathrm{A}_{0-}}$. NP scale				
	$\vec{\theta} = (0, 0, 0)$		$\vec{\theta} = (0.5, 0.5, 0.5)$	
m	b_0	b_1	b_0	b_1
1	———	———	0.001 (14)	-0.22 (17)
2	-0.001 (18)	0.31 (23)	———	———
3	0.003 (18)	-0.75 (23)	0.004 (14)	-0.76 (17)
4	0.008 (18)	1.02 (23)	0.007 (14)	0.51 (17)
5	0.013 (18)	1.09 (23)	0.010 (14)	0.56 (17)
6	-0.006 (18)	0.79 (23)	-0.003 (14)	0.34 (17)
7	-0.005 (29)	0.57 (42)	-0.005 (21)	0.22 (31)

Table F.21.: Continuum limit of $g^{11}_{\mathrm{A}_{0-}}$ for all definitions of z_f^c from (1) to (7). Scale NP. Results are shown for $\vec{\theta} = (0, 0, 0)$ and $\vec{\theta} = (0.5, 0.5, 0.5)$, as obtained from linear fits of the data in Tab. F.11 and Tab. F.16, respectively. The fits are linear in a/L and the point $L/a = 8$ is excluded in all cases. The lines represent the cases where the corresponding quantity has been used as tuning condition. See Sec. 7.2.3 for more explanations.

Continuum limit of $\overline{g}^{12}_{\mathrm{V}_{k-}}$. NP scale				
	$\vec{\theta} = (0,0,0)$		$\vec{\theta} = (0.5,0.5,0.5)$	
m	b_0	b_1	b_0	b_1
1	-0.008 (21)	-1.37 (26)	-0.012 (16)	-1.12 (20)
2	-0.011 (21)	-0.96 (26)	-0.013 (16)	-0.81 (20)
3	-0.002 (20)	-2.39 (26)	-0.008 (16)	-1.89 (19)
4	———	———	-0.004 (16)	-0.07 (20)
5	0.005 (21)	0.10 (26)	———	———
6	-0.018 (21)	-0.32 (26)	-0.020 (16)	-0.31 (20)
7	-0.002 (33)	-0.81 (48)	-0.019 (25)	-0.51 (36)

Table F.22.: Same caption as in Tab. F.21 but for $\overline{g}^{12}_{\mathrm{V}_{k-}}$.

G. Notes on Z_{P}

$Z_{\mathrm{P}}(g_0, L/a)$ Hadronic scale: $L = 1.436\, r_0$ and $\theta = 0.5$					
L/a	β	m	z_f^c	κ_c	Z_{P}
8	6.0219	1*	1.8090 (32)	0.153530 (24)	0.5385 (12)
		1	1.8091 (32)	0.15353 (66)	0.5388 (14)
		2	1.7946 (34)	0.15354 (66)	0.5385 (14)
		3	1.8434 (37)	0.15352 (67)	0.5395 (14)
		4	1.7656 (27)	0.15354 (66)	0.5379 (14)
		5	1.7597 (27)	0.15354 (66)	0.5378 (13)
		6	1.7835 (40)	0.15354 (66)	0.5383 (14)
		7	1.7980 (17)	0.15353 (66)	0.5386 (14)
10	6.1628	1*	1.7920 (30)	0.152134 (17)	0.5264 (12)
		1	1.7923 (29)	0.15213 (66)	0.5266 (13)
		2	1.7820 (31)	0.15214 (66)	0.5264 (13)
		3	1.8175 (33)	0.15213 (67)	0.5270 (13)
		4	1.7541 (25)	0.15214 (66)	0.5260 (13)
		5	1.7497 (25)	0.15214 (66)	0.5259 (13)
		6	1.7687 (38)	0.15214 (66)	0.5262 (13)
12	6.2885	1*	1.7664 (51)	0.150815 (22)	0.5272 (16)
		1	1.7658 (38)	0.15082 (66)	0.5272 (17)
		2	1.7573 (40)	0.15082 (66)	0.5271 (17)
		3	1.7869 (46)	0.15082 (66)	0.5275 (18)
		4	1.7312 (34)	0.15082 (65)	0.5267 (17)
		5	1.7283 (32)	0.15082 (65)	0.5266 (17)
		6	1.7408 (56)	0.15082 (65)	0.5268 (17)
		7	1.7509 (22)	0.15082 (66)	0.5270 (17)
16	6.4956	1*	1.7212 (83)	0.148945 (25)	0.5187 (22)
		1	1.7201 (41)	0.14894 (34)	0.5189 (22)
		2	1.7132 (44)	0.14894 (33)	0.5188 (22)
		3	1.7377 (46)	0.14893 (34)	0.5191 (22)
		4	1.6929 (35)	0.14894 (33)	0.5187 (22)
		5	1.6894 (34)	0.14894 (33)	0.5186 (22)
		6	1.7053 (63)	0.14894 (33)	0.5188 (22)
		7	1.7076 (21)	0.14894 (33)	0.5188 (22)
20	6.6790	1	1.6841 (56)	0.14748 (74)	0.5247 (38)
		2	1.6789 (59)	0.14748 (74)	0.5246 (38)
		3	1.6973 (65)	0.14748 (74)	0.5248 (38)
		4	1.6582 (52)	0.14748 (73)	0.5244 (37)
		5	1.6577 (52)	0.14748 (73)	0.5244 (37)
		6	1.6600 (90)	0.14748 (73)	0.5244 (38)

Table G.1.: (continuing on the next page, caption below)

$Z_{\rm P}(g_0, L/a)$ Hadronic scale: $L = 1.436\, r_0$ and $\theta = 0.5$					
L/a	β	m	z_f^c	κ_c	$Z_{\rm P}$
24	6.8187	1	1.6427 (56)	0.14645 (41)	0.5228 (42)
		2	1.6381 (60)	0.14645 (41)	0.5228 (42)
		3	1.6529 (60)	0.14645 (42)	0.5229 (42)
		4	1.6253 (51)	0.14645 (41)	0.5227 (42)
		5	1.6201 (50)	0.14645 (41)	0.5227 (42)
		6	1.6421 (88)	0.14645 (41)	0.5228 (42)
		7	1.6366 (27)	0.14645 (41)	0.5228 (42)

Table G.1.: Results for $Z_{\rm P}(g_0, L/a)$ at scale $L = 1.436\, r_0$ and for $\vec{\theta} = (0.5, 0.5, 0.5)$. The data have been obtained via interpolations to the critical values of κ and z_f for all the tuning methods (1) to (7). The values denoted with (1*) have been obtained by direct simulations at the critical values of κ and z_f. See Chap. 6 for explanations on the tuning conditions and Chap. 8 for definition and discussion of $Z_{\rm P}$.

$Z_{\rm P}(g_0, L/a)$ Intermediate scale: $\overline{g}^2 = 2.4484$ and $\theta = 0.5$					
L/a	β	m	z_f^c	κ_c	$Z_{\rm P}$
8	7.0197	1*	1.5467 (15)	0.144501 (13)	0.68509 (95)
		1	1.5404 (16)	0.14450 (41)	0.6853 (10)
		2	1.5296 (17)	0.14450 (41)	0.6851 (10)
		3	1.5597 (18)	0.14450 (41)	0.6856 (10)
		4	1.5156 (14)	0.14450 (41)	0.6849 (10)
		5	1.5126 (14)	0.14450 (41)	0.6849 (10)
		6	1.5229 (21)	0.14450 (41)	0.6850 (10)
		7	1.5392 (12)	0.14450 (41)	0.6853 (10)
12	7.3551	1*	1.5126 (23)	0.143113 (12)	0.6735 (13)
		1	1.5139 (18)	0.14311 (29)	0.6736 (13)
		2	1.5088 (19)	0.14311 (29)	0.6735 (13)
		3	1.5233 (19)	0.14311 (29)	0.6737 (13)
		4	1.4955 (16)	0.14311 (29)	0.6734 (13)
		5	1.4945 (15)	0.14311 (29)	0.6734 (13)
		6	1.4981 (23)	0.14311 (29)	0.6734 (13)
		7	1.5120 (12)	0.14311 (29)	0.6736 (13)
16	7.6101	1*	1.4942 (37)	0.142112 (13)	0.6672 (16)
		1	1.4943 (20)	0.14212 (23)	0.6671 (16)
		2	1.4908 (21)	0.14212 (23)	0.6670 (16)
		3	1.5007 (23)	0.14212 (23)	0.6671 (16)
		4	1.4800 (18)	0.14212 (23)	0.6669 (16)
		5	1.4789 (17)	0.14212 (23)	0.6669 (16)
		6	1.4827 (28)	0.14212 (23)	0.6669 (16)
		7	1.4916 (13)	0.14212 (23)	0.6670 (16)

Table G.2.: Same caption as in Tab. G.1 but at scale $\overline{g}^2 = 2.4484$.

$Z_{\rm P}(g_0, L/a)$ Perturbative scale: $\overline{g}^2 = 0.9944$ and $\theta = 0.5$					
L/a	β	m	z_f^c	κ_c	$Z_{\rm P}$
8	10.3000	1*	1.29730 (67)	0.1354609 (54)	0.82689 (56)
12	10.6086	1*	1.2954 (11)	0.1351758 (56)	0.81651 (88)
16	10.8910	1*	1.2858 (15)	0.1348440 (61)	0.8110 (10)
		1	1.28692 (88)	0.134844 (93)	0.8110 (11)
		2	1.28487 (91)	0.134844 (93)	0.8110 (11)
		3	1.28984 (99)	0.134844 (93)	0.8111 (11)
		4	1.27999 (83)	0.134844 (93)	0.8110 (11)
		5	1.27976 (75)	0.134844 (93)	0.8110 (11)
		6	1.2805 (13)	0.134844 (93)	0.8110 (11)
		7	1.28619 (67)	0.134844 (93)	0.8110 (11)

Table G.3.: Same caption as in Tab. G.1 but at scale $\overline{g}^2 = 0.9944$.

$Z_{\rm P}(g_0, L/a)$ 2P scale and $\theta = 0.5$					
L/a	β	m	z_f^c	κ_c	$Z_{\rm P}$
16	12.0000	1	1.2493 (14)	0.13363 (41)	0.8347 (17)
		2	1.2481 (14)	0.13363 (41)	0.8347 (17)
		3	1.2510 (15)	0.13363 (41)	0.8347 (17)
		4	1.2438 (13)	0.13363 (41)	0.8347 (17)
		5	1.2443 (12)	0.13363 (41)	0.8347 (17)
		6	1.2428 (20)	0.13363 (41)	0.8347 (17)
		7	1.2494 (10)	0.13363 (41)	0.8347 (17)

Table G.4.: Same caption as in Tab. G.1 but at scale 2P.

$Z_{\rm P}(g_0, L/a)$ PP scale and $\theta = 0.5$					
L/a	β	m	z_f^c	κ_c	$Z_{\rm P}$
16	24.0000	1	1.11268 (57)	0.12877 (15)	0.92667 (81)
		2	1.11162 (58)	0.12877 (15)	0.92667 (81)
		3	1.11391 (65)	0.12877 (15)	0.92667 (81)
		4	1.11013 (54)	0.12877 (15)	0.92666 (81)
		5	1.11003 (48)	0.12877 (15)	0.92666 (81)
		6	1.11030 (87)	0.12877 (15)	0.92666 (81)
		7	1.11269 (50)	0.12877 (15)	0.92667 (81)

Table G.5.: Same caption as in Tab. G.1 but at scale PP.

H. Notes on 2-point functions

In the present appendix we define and give explicit expressions for all 2-point functions which have been computed along this thesis. We provide expressions in the standard SF and the χSF formulations and give the relation between the 2-point functions in both formulations.

In all the cases discussed here we treat the 2-point functions in the time-momentum representation. Therefore, all correlation functions depend on the time coordinate, x_0, the spatial momenta, $\vec{p}$, and the angles $\vec{\theta}$, entering the definitions of the lattice derivatives. However, in order to render the expressions more simple, the explicit dependence on $\vec{p}$ and $\vec{\theta}$ is not written as an argument of the correlation functions, yet it should be understood. Nevertheless, all 2-point functions that we compute are always evaluated at zero spatial momenta, $\vec{p} = (0, 0, 0)$, so they only depend on x_0 and $\vec{\theta}$. On the one hand, in all basic 2-point functions (those without derivatives), the dependence on $\vec{\theta}$ is implicitly contained in the quark propagator. On the other hand, the 2-point functions containing derivatives (those of the twist-2 operators), depend on $\vec{\theta}$ implicitly through the quark propagator but also explicitly through the derivative appearing in the definition of the bulk operators, which results in additional phase factors.

The appendix is structured as follows. In App. H.1 we provide general definitions of the boundary to bulk and boundary to boundary 2-point functions, in the standard SF and χSF formulations. We determine the basic boundary to bulk and boundary to boundary 2-point functions in the χSF formulation in App. H.2 and eventually particularize the general expressions for those cases computed in this thesis. In App. H.3 we define and compute the boundary to bulk 2-point functions of the non-singlet twist-2 operators in the standard SF formulation. A the end of the calculations we also give expressions for the particular cases computed in this thesis. In App. H.4 we perform a rotation of the 2-point functions of the twist-2 operators, from the physical to the twisted basis. This provides the relation between the correlation functions in the standard SF and χSF schemes. We determine the 2-point functions of the twist-2 operators in the χSF formulation in App. H.5.

H.1. Definition of the 2-point functions in SF-like schemes

In this section we collect the main definitions needed in the computation of boundary to bulk and boundary to boundary 2-point functions within SF-like schemes. We give the definitions in the standard SF and the χSF formulations.

H.1.1. Standard SF formulation

In the SF formulation, the quark and antiquark fields at the time boundaries of the lattice are defined as

$$\zeta(\vec{x}) = U_0(x_0 - a, \vec{x}) P_- \psi(x)|_{x_0=a} \qquad \zeta'(\vec{x}) = U_0(x_0, \vec{x})^\dagger P_+ \psi(x)|_{x_0=T-a} \tag{H.1}$$

$$\overline{\zeta}(\vec{x}) = \overline{\psi}(x) P_+ U_0(x_0 - a, \vec{x})^\dagger|_{x_0=a} \qquad \overline{\zeta}'(\vec{x}) = \overline{\psi}(x) P_- U_0(x_0, \vec{x})|_{x_0=T-a}\,. \tag{H.2}$$

From these expressions we can define operators at the time boundaries $x_0 = 0$ and $x_0 = T$,

respectively, as

$$\mathcal{O}^a = a^6 \sum_{\vec{y},\vec{z}} \overline{\zeta}(\vec{y})\, \Gamma_{\mathrm{O}} \frac{\tau^a}{2}\, \zeta(\vec{z})\, e^{\mathrm{i}\vec{p}(\vec{y}-\vec{z})}\,, \tag{H.3}$$

$$\mathcal{O}'^a = a^6 \sum_{\vec{y},\vec{z}} \overline{\zeta}'(\vec{y})\, \Gamma_{\mathrm{O}} \frac{\tau^a}{2}\, \zeta'(\vec{z})\, e^{\mathrm{i}\vec{p}(\vec{y}-\vec{z})}\,. \tag{H.4}$$

Here a denotes the flavor index and Γ_{O} is a particular combination of γ-matrices containing the Dirac structure of the interpolating field, $\mathcal{O}^a$ or $\mathcal{O}'^a$.

A correlation function from the boundary at $x_0 = 0$ to a certain point $x = (x_0, \vec{x})$ in the bulk of the lattice is defined as

$$f_{\mathrm{X}}^{ab}(x_0) = -\frac{a^3}{L^3} \sum_{\vec{x}} \left\langle X^a(x) \mathcal{O}^b \right\rangle, \tag{H.5}$$

where $X^a(x)$ is a local operator in the bulk of the lattice, at the space-time point x, and a and b are the flavor indices of the bulk and boundary interpolating fields, respectively. Similar expressions can be defined for the other boundary at $x_0 = T$, but such correlation functions have not been considered in this work and thus, are not mentioned any longer.

Concerning the 2-point functions boundary to boundary, we only consider here one case. This is

$$f_1^{ab} = -\frac{1}{L^6} \left\langle \mathcal{O}'^a \mathcal{O}^b \right\rangle, \tag{H.6}$$

where $a = b$ and $\Gamma_{\mathrm{O}} = \gamma_5$ for both operators, $\mathcal{O}^a$ and $\mathcal{O}'^a$.

H.1.2. χSF formulation

In the χSF formulation, where we work in the twisted basis, the quark and antiquark fields at the time boundaries are defined as

$$\zeta(\vec{x}) = U_0(x_0 - a, \vec{x}) \chi(x)|_{x_0 = a} \qquad \zeta'(\vec{x}) = U_0(x_0, \vec{x})^\dagger \chi(x)|_{x_0 = T - a} \tag{H.7}$$

$$\overline{\zeta}(\vec{x}) = \overline{\chi}(x) U_0(x_0 - a, \vec{x})^\dagger|_{x_0 = a} \qquad \overline{\zeta}'(\vec{x}) = \overline{\chi}(x) U_0(x_0, \vec{x})|_{x_0 = T - a}\,. \tag{H.8}$$

In the same way as in the standard setup, we can define operators at the boundaries $x_0 = 0$ and $x_0 = T$, respectively, as

$$\widetilde{\mathcal{O}}^a_{\pm} = a^6 \sum_{\vec{y},\vec{z}} \overline{\zeta}(\vec{y})\, \Gamma_{\mathrm{O}} \frac{\tau^a}{2} \widetilde{Q}_{\pm}\, \zeta(\vec{z})\, e^{\mathrm{i}\vec{p}(\vec{y}-\vec{z})}\,, \tag{H.9}$$

$$\widetilde{\mathcal{O}'}^a_{\pm} = a^6 \sum_{\vec{y},\vec{z}} \overline{\zeta}'(\vec{y})\, \Gamma_{\mathrm{O}} \frac{\tau^a}{2} \widetilde{Q}_{\pm}\, \zeta'(\vec{z})\, e^{\mathrm{i}\vec{p}(\vec{y}-\vec{z})}\,. \tag{H.10}$$

The projectors $\widetilde{Q}_{\pm}$ are the χSF projectors defined earlier in the text, e.g. in Eq. (3.105).

A correlation function boundary to bulk, from the boundary at $x_0 = 0$ to the bulk point x, may be generically defined as

$$g_{\mathrm{X}_{\pm}}^{ab}(x_0) = -\frac{a^3}{L^3} \sum_{\vec{x}} \left\langle X^a(x) \widetilde{\mathcal{O}}^b_{\pm} \right\rangle. \tag{H.11}$$

In the same way, the boundary to boundary correlation function which is considered in this work is the following,

$$g_1^{ab} = -\frac{1}{L^6} \left\langle \widetilde{\mathcal{O}'}^a_{+} \widetilde{\mathcal{O}}^b_{-} \right\rangle \quad \forall \quad a, b \neq 3\,. \tag{H.12}$$

Note that this is the only possible combination which can be different from zero. All the others,

$++, --, -+$ for all flavor combinations or $+-$ with $a, b = 3$ vanish in the continuum limit because of boundary conditions. In particular, we only consider the cases when $a = b$ and $\Gamma_{\rm O} = \gamma_5$ for both operators, $\widetilde{\mathcal{O}}^a_-$ and $\widetilde{\mathcal{O}'}^a_+$.

Note that all correlation functions in the χSF formulation may be related to correlation functions in the standard SF via the non-anomalous axial transformation relating the physical and the twisted basis, Eq. (2.97).

H.2. Determination of basic 2-point functions in the χSF

Here we determine the basic boundary to bulk and boundary to boundary 2-point functions defined in the previous section in the χSF formulation. In particular, we give the explicit final expressions which are then numerically evaluated. All calculations are carried out assuming general boundary and bulk interpolating fields and particularized for the cases of interest only at the end of the calculations.

H.2.1. Determination of boundary to bulk 2-point functions

Writing the bulk operator generically as $X^a(x)$, where $X^a(x) = \overline{\chi}(x)\Gamma_{\rm X}\frac{\tau^a}{2}\chi(x)$, the most general expression of a boundary to bulk 2-point function has the following form

$$\begin{aligned} g^{ab}_{{\rm X}_\pm}(x_0) &= -\frac{a^3}{L^3}\sum_{\vec{x}}\left\langle X^a(x)\widetilde{\mathcal{O}}^b_\pm\right\rangle \\ &= -\frac{a^9}{L^3}\sum_{\vec{x},\vec{y},\vec{z}} e^{{\rm i}\vec{p}(\vec{y}-\vec{z})}\left\langle\,\overline{\chi}(x)\,\Gamma_{\rm X}\frac{\tau^a}{2}\,\chi(x)\,\overline{\zeta}(\vec{y})\,\Gamma_{\rm O}\frac{\tau^b}{2}\widetilde{Q}_\pm\,\zeta(\vec{z})\,\right\rangle . \end{aligned} \tag{H.13}$$

The momentum dependence in Eq. (H.13) originates from the definition of the boundary interpolating fields. Such dependence is kept in the expressions at the moment but the evaluation of the correlation functions is always performed at $\vec{p} = (0,0,0)$.

Reordering the quark fields and performing all fermionic contractions, which are denoted here as $[\cdot]_{\rm F}$, the previous expression takes the form

$$\begin{aligned} g^{ab}_{{\rm X}_\pm}(x_0) =& \frac{a^9}{L^3}\sum_{\vec{x},\vec{y},\vec{z}} e^{{\rm i}\vec{p}(\vec{y}-\vec{z})}\left\langle\,{\rm Tr}\Big\{\,[\zeta(\vec{z})\overline{\chi}(x)]_{\rm F}\,\Gamma_{\rm X}\frac{\tau^a}{2}\,[\chi(x)\overline{\zeta}(\vec{y})]_{\rm F}\,\Gamma_{\rm O}\frac{\tau^b}{2}\widetilde{Q}_\pm\,\Big\}\,\right\rangle_{\rm G} \\ &-\frac{a^9}{L^3}\sum_{\vec{x},\vec{y},\vec{z}} e^{{\rm i}\vec{p}(\vec{y}-\vec{z})}\left\langle\,{\rm Tr}\Big\{\,[\chi(x)\overline{\chi}(x)]_{\rm F}\,\Gamma_{\rm X}\frac{\tau^a}{2}\,\Big\}\,{\rm Tr}\Big\{\,[\zeta(\vec{z})\overline{\zeta}(\vec{y})]_{\rm F}\,\Gamma_{\rm O}\frac{\tau^b}{2}\widetilde{Q}_\pm\,\Big\}\,\right\rangle_{\rm G} . \end{aligned} \tag{H.14}$$

Using the γ_5-*hermiticity with flavor exchange* property of the quark propagator in the χSF formulation,

$$[\chi(x)\overline{\chi}(y)]_{\rm F} = \gamma_5\tau^1\,[\chi(y)\overline{\chi}(x)]^\dagger_{\rm F}\,\gamma_5\tau^1\,, \tag{H.15}$$

Eq. (H.14) becomes

$$\begin{aligned} g^{ab}_{{\rm X}_\pm}(x_0) =& \frac{a^9}{L^3}\sum_{\vec{x},\vec{y},\vec{z}} e^{{\rm i}\vec{p}(\vec{y}-\vec{z})}\left\langle\,{\rm Tr}\Big\{\,\gamma_5\tau^1\,[\chi(x)\overline{\zeta}(\vec{z})]^\dagger_{\rm F}\,\gamma_5\tau^1\,\Gamma_{\rm X}\frac{\tau^a}{2}\,[\chi(x)\overline{\zeta}(\vec{y})]_{\rm F}\,\Gamma_{\rm O}\frac{\tau^b}{2}\widetilde{Q}_\pm\,\Big\}\,\right\rangle_{\rm G} \\ &-\frac{a^9}{L^3}\sum_{\vec{x},\vec{y},\vec{z}} e^{{\rm i}\vec{p}(\vec{y}-\vec{z})}\left\langle\,{\rm Tr}\Big\{\,[\chi(x)\overline{\chi}(x)]_{\rm F}\,\Gamma_{\rm X}\frac{\tau^a}{2}\,\Big\}\,{\rm Tr}\Big\{\,[\zeta(\vec{z})\overline{\zeta}(\vec{y})]_{\rm F}\,\Gamma_{\rm O}\frac{\tau^b}{2}\widetilde{Q}_\pm\,\Big\}\,\right\rangle_{\rm G} . \end{aligned} \tag{H.16}$$

In the following we will use the definitions

$$H(x;\vec{p}) \equiv a^3 \sum_{\vec{y}} e^{\mathrm{i}\vec{p}\,\vec{y}}\,[\chi(x)\overline{\zeta}(\vec{y})]_{\mathrm{F}} = a^3 \sum_{\vec{y}} e^{\mathrm{i}\vec{p}\,\vec{y}}\,S(x,y)U_0(y-a\hat{0})^\dagger|_{y_0=a}\,, \tag{H.17a}$$

$$H(x;\vec{p})^\dagger \equiv a^3 \sum_{\vec{y}} e^{-\mathrm{i}\vec{p}\,\vec{y}}\,[\chi(x)\overline{\zeta}(\vec{y})]^\dagger_{\mathrm{F}} = a^3 \sum_{\vec{y}} e^{-\mathrm{i}\vec{p}\,\vec{y}}\,U_0(y-a\hat{0})S(x,y)^\dagger|_{y_0=a}\,, \tag{H.17b}$$

$$\overline{H}(x;\vec{p}) \equiv a^3 \sum_{\vec{y}} e^{-\mathrm{i}\vec{p}\,\vec{y}}\,[\zeta(\vec{y})\overline{\chi}(x)]_{\mathrm{F}} = a^3 \sum_{\vec{y}} e^{-\mathrm{i}\vec{p}\,\vec{y}}\,U_0(y-a\hat{0})S(y,x)|_{y_0=a}\,, \tag{H.17c}$$

with the relation

$$\overline{H}(x;\vec{p}) = \gamma_5\tau^1\,H(x;\vec{p})^\dagger\,\gamma_5\tau^1\,. \tag{H.18}$$

Note that these quark propagators also depend upon the gauge links and the angles $\vec{\theta}$, although the dependence is not explicitly written in order to render the expressions simpler.

Since, eventually, we will only consider the cases $a, b \neq 3$, the disconnected part of the correlation functions in which we are interested vanishes. Therefore in order to make the expressions more clear, from now on, we will only write the contributing piece of the correlation functions (the connected piece). Using the definitions in Eq. (H.17) and neglecting the disconnected piece, the expression we have to evaluate is

$$g^{ab}_{\mathrm{X}_\pm}(x_0) = \frac{a^3}{L^3}\sum_{\vec{x}} \Big\langle\, \mathrm{Tr}\Big\{\,\gamma_5\tau^1\,H(x;\vec{p})^\dagger\,\gamma_5\tau^1\,\Gamma_{\mathrm{X}}\frac{\tau^a}{2}\,H(x;\vec{p})\,\Gamma_{\mathrm{O}}\frac{\tau^b}{2}\widetilde{Q}_\pm\,\Big\}\,\Big\rangle_{\mathrm{G}}\,. \tag{H.19}$$

Now we define projectors in flavor space

$$T_\pm = \frac{1}{2}(1 \pm \tau^3) \tag{H.20}$$

and redefine the chirally rotated projectors without the flavor structure,

$$Q_\pm = \frac{1}{2}(1 \pm \mathrm{i}\gamma_0\gamma_5)\,, \tag{H.21}$$

such that

$$\widetilde{Q}_\pm = Q_\pm T_+ + Q_\mp T_-\,. \tag{H.22}$$

Also the fermionic contractions may be decomposed in the two flavor components as

$$H(x;\vec{p}) = H_+(x;\vec{p})\,T_+ + H_-(x;\vec{p})\,T_-\,. \tag{H.23}$$

With this flavor decomposition, the flavor structure can completely factor out in the expression of the correlation function, thus giving

$$\begin{aligned} g^{ab}_{\mathrm{X}_\pm}(x_0) = \frac{a^3}{L^3}\sum_{\vec{x}}\sum_{i,j,k=\pm} \mathrm{Tr}\Big\{\,\tau^1 T_i \tau^1 \frac{\tau^a}{2} T_j \frac{\tau^b}{2} T_{\pm k}\,\Big\}\times \\ \Big\langle\, \mathrm{Tr}\Big\{\,\gamma_5\,H_i(x;\vec{p})^\dagger\,\gamma_5\,\Gamma_{\mathrm{X}}\,H_j(x;\vec{p})\,\Gamma_{\mathrm{O}}Q_k\,\Big\}\,\Big\rangle_{\mathrm{G}}\,. \end{aligned} \tag{H.24}$$

Reordering the flavor part we find that (provided $a, b \neq 3$)

$$g^{ab}_{\mathrm{X}_\pm}(x_0) = \frac{a^3}{L^3}\sum_{\vec{x}}\sum_{i=\pm} \mathrm{Tr}\Big\{\,\frac{\tau^a}{2}\frac{\tau^b}{2}T_{-i}\,\Big\}\Big\langle\, \mathrm{Tr}\Big\{\,\gamma_5\,H_i(x;\vec{p})^\dagger\,\gamma_5\,\Gamma_{\mathrm{X}}\,H_i(x;\vec{p})\,\Gamma_{\mathrm{O}}Q_{\mp i}\,\Big\}\,\Big\rangle_{\mathrm{G}}\,. \tag{H.25}$$

Writing all sums explicitly,

$$\begin{aligned} g^{ab}_{\mathrm{X}_\pm}(x_0) &= \frac{a^3}{L^3}\sum_{\vec{x}} \mathrm{Tr}\Big\{ \frac{\tau^a}{2}\frac{\tau^b}{2} T_- \Big\}\Big\langle \mathrm{Tr}\Big\{ \gamma_5\, H_+(x;\vec{p})^\dagger\, \gamma_5\, \Gamma_{\mathrm{X}}\, H_+(x;\vec{p})\, \Gamma_{\mathrm{O}} Q_\mp \Big\}\Big\rangle_{\mathrm{G}} \\ &+ \frac{a^3}{L^3}\sum_{\vec{x}} \mathrm{Tr}\Big\{ \frac{\tau^a}{2}\frac{\tau^b}{2} T_+ \Big\}\Big\langle \mathrm{Tr}\Big\{ \gamma_5\, H_-(x;\vec{p})^\dagger\, \gamma_5\, \Gamma_{\mathrm{X}}\, H_-(x;\vec{p})\, \Gamma_{\mathrm{O}} Q_\pm \Big\}\Big\rangle_{\mathrm{G}} \\ &= \frac{a^3}{L^3}\sum_{\vec{x}} \mathrm{Tr}\Big\{ \frac{\tau^a}{2}\frac{\tau^b}{2} T_- \Big\}\Big\langle \mathrm{Tr}\Big\{ H_+(x;\vec{p})^\dagger\, \gamma_5\, \Gamma_{\mathrm{X}}\, H_+(x;\vec{p})\, \Gamma_{\mathrm{O}}\gamma_5 Q_\pm \Big\}\Big\rangle_{\mathrm{G}} \\ &+ \frac{a^3}{L^3}\sum_{\vec{x}} \mathrm{Tr}\Big\{ \frac{\tau^a}{2}\frac{\tau^b}{2} T_+ \Big\}\Big\langle \mathrm{Tr}\Big\{ H_-(x;\vec{p})^\dagger\, \gamma_5\, \Gamma_{\mathrm{X}}\, H_-(x;\vec{p})\, \Gamma_{\mathrm{O}}\gamma_5 Q_\mp \Big\}\Big\rangle_{\mathrm{G}} . \end{aligned} \tag{H.26}$$

As it is written Eq. (H.26), it is expressed in terms of the plus and minus components of the quark propagators, $H_\pm$, with respect to flavor space. Yet, the numerical cost is reduced by a factor of two if the expression is evaluated in terms of only one of the flavor components of the quark propagator, either H_+ or H_-. This indeed can be done by using parity symmetry, $P^{1,2}_{\mathrm{F}}$, defined in Eq. (B.10). In the following, we use $P^{1,2}_{\mathrm{F}}$ in order to rewrite Eq. (H.26) in terms of only H_+. In particular, $P^{1,2}_{\mathrm{F}}$ transforms the gauge links, the angles $\vec{\theta}$, the spatial momenta and the spatial coordinates upon which the quark propagators, H, depend. These variables transform as follows; $\vec{\theta} \to -\vec{\theta}$, $\vec{p} \to -\vec{p}$ and $\vec{x} \to -\vec{x}$. Therefore, the quark propagators, $H(x;\vec{p};\vec{\theta};U)$, transform as

$$H_\pm(x;\vec{p};\vec{\theta};U) \to \gamma_0\, H_\mp(\tilde{x};-\vec{p};-\vec{\theta};\tilde{U})\,\gamma_0\,, \tag{H.27}$$

with $\tilde{x} = (x_0, -\vec{x})$ and $\tilde{U}$ the transformed gauge field. Defining the quark propagator as a function of the transformed fields as follows,

$$\widetilde{H}_\pm(x;\vec{p};\vec{\theta};U) \equiv H_\pm(\tilde{x};-\vec{p};-\vec{\theta};\tilde{U})\,, \tag{H.28}$$

Eq. (H.26) can be expressed as

$$\begin{aligned} g^{ab}_{\mathrm{X}_\pm}(x_0) &= \frac{a^3}{L^3}\sum_{\vec{x}} \mathrm{Tr}\Big\{ \frac{\tau^a}{2}\frac{\tau^b}{2} T_- \Big\}\Big\langle \mathrm{Tr}\Big\{ H_+(x;\vec{p})^\dagger\, \gamma_5\, \Gamma_{\mathrm{X}}\, H_+(x;\vec{p})\, \Gamma_{\mathrm{O}}\gamma_5 Q_\pm \Big\}\Big\rangle_{\mathrm{G}} \\ &+ \frac{a^3}{L^3}\sum_{\vec{x}} \mathrm{Tr}\Big\{ \frac{\tau^a}{2}\frac{\tau^b}{2} T_+ \Big\}\Big\langle \mathrm{Tr}\Big\{ \widetilde{H}_+(x;\vec{p})^\dagger\, \gamma_0\gamma_5\, \Gamma_{\mathrm{X}}\gamma_0\, \widetilde{H}_+(x;\vec{p})\, \gamma_0\Gamma_{\mathrm{O}}\gamma_5\gamma_0 Q_\pm \Big\}\Big\rangle_{\mathrm{G}} , \end{aligned} \tag{H.29}$$

where we have again removed the explicit dependences on $\vec{\theta}$ and U in order to render the expressions simpler.

Now, defining

$$\begin{aligned} \eta(X) &= +1 \quad \text{if } \{\gamma_0, \Gamma_{\mathrm{X}}\} = 0 \\ &= -1 \quad \text{if } [\gamma_0, \Gamma_{\mathrm{X}}] = 0 \end{aligned} \tag{H.30}$$

we have

$$\begin{aligned} g^{ab}_{\mathrm{X}_\pm}(x_0) = \frac{a^3}{L^3}\sum_{\vec{x}} \Bigg\{ & \mathrm{Tr}\Big\{ \frac{\tau^a}{2}\frac{\tau^b}{2} T_- \Big\}\Big\langle \mathrm{Tr}\Big\{ H_+(x;\vec{p})^\dagger\, \gamma_5\, \Gamma_{\mathrm{X}}\, H_+(x;\vec{p})\, \Gamma_{\mathrm{O}}\gamma_5 Q_\pm \Big\}\Big\rangle_{\mathrm{G}} \\ & + \eta(X)\eta(O)\, \mathrm{Tr}\Big\{ \frac{\tau^a}{2}\frac{\tau^b}{2} T_+ \Big\}\Big\langle \mathrm{Tr}\Big\{ \widetilde{H}_+(x;\vec{p})^\dagger\, \gamma_5\, \Gamma_{\mathrm{X}}\, \widetilde{H}_+(x;\vec{p})\, \Gamma_{\mathrm{O}}\gamma_5 Q_\pm \Big\}\Big\rangle_{\mathrm{G}} \Bigg\} . \end{aligned} \tag{H.31}$$

Taking into account the fact that after averaging over the gauge fields and due to the invariance of the effective gauge action under $P_{\rm F}^{1,2}$, the next relation holds [67]

$$\Big\langle \mathrm{Tr}\Big\{ \widetilde{H}_{\pm}(x;\vec{p})^{\dagger}\gamma_5\Gamma_{\rm X}\widetilde{H}_{\pm}(x;\vec{p})\Gamma_{\rm O}\gamma_5 Q_{\pm}\Big\}\Big\rangle_{\rm G} = \Big\langle \mathrm{Tr}\Big\{ H_{\pm}(x;\vec{p})^{\dagger}\gamma_5\Gamma_{\rm X}H_{\pm}(x;\vec{p})\Gamma_{\rm O}\gamma_5 Q_{\pm}\Big\}\Big\rangle_{\rm G} \tag{H.32}$$

we can rewrite the correlator in Eq. (H.31) as

$$\begin{aligned} g^{ab}_{{\rm X}_{\pm}}(x_0) = \frac{a^3}{L^3}\sum_{\vec{x}}\Big[\mathrm{Tr}\Big\{\frac{\tau^a}{2}\frac{\tau^b}{2}T_-\Big\} + \eta(X)\eta(O)\,\mathrm{Tr}\Big\{\frac{\tau^a}{2}\frac{\tau^b}{2}T_+\Big\}\Big]\times \\ \Big\langle \mathrm{Tr}\Big\{ H_+(x;\vec{p})^{\dagger}\gamma_5\Gamma_{\rm X}H_+(x;\vec{p})\Gamma_{\rm O}\gamma_5 Q_{\pm}\Big\}\Big\rangle_{\rm G}\,. \end{aligned} \tag{H.33}$$

The two possible signs of $\eta(X)$ and $\eta(O)$ constrain the flavor strucuture in the next manner:

if $\eta(X)\eta(O) = +1$ then

$$\mathrm{Tr}\Big\{\,\frac{\tau^a}{2}\frac{\tau^b}{2}T_-\,\Big\} + \eta(X)\eta(O)\,\mathrm{Tr}\Big\{\,\frac{\tau^a}{2}\frac{\tau^b}{2}T_+\,\Big\} = \frac{1}{2}\delta^{ab} \tag{H.34}$$

and if $\eta(X)\eta(O) = -1$

$$\mathrm{Tr}\Big\{\,\frac{\tau^a}{2}\frac{\tau^b}{2}T_-\,\Big\} + \eta(X)\eta(O)\,\mathrm{Tr}\Big\{\,\frac{\tau^a}{2}\frac{\tau^b}{2}T_+\,\Big\} = -\frac{\mathrm{i}}{2}\epsilon^{ab3}\,. \tag{H.35}$$

Therefore, the most simplified expressions that we have now for the correlaton functions are:

if $\eta(X) = \eta(O)$,

$$g^{ab}_{{\rm X}_{\pm}}(x_0) = \delta^{ab}\frac{a^3}{2L^3}\sum_{\vec{x}}\Big\langle\,\mathrm{Tr}\Big\{\,H_+(x;\vec{p})^{\dagger}\,\gamma_5\,\Gamma_{\rm X}\,H_+(x;\vec{p})\,\Gamma_{\rm O}\gamma_5 Q_{\pm}\,\Big\}\Big\rangle_{\rm G}\,, \tag{H.36}$$

while if $\eta(X) = -\eta(O)$,

$$g^{ab}_{{\rm X}_{\pm}}(x_0) = -\mathrm{i}\epsilon^{ab3}\frac{a^3}{2L^3}\sum_{\vec{x}}\Big\langle\,\mathrm{Tr}\Big\{\,H_+(x;\vec{p})^{\dagger}\,\gamma_5\,\Gamma_{\rm X}\,H_+(x;\vec{p})\,\Gamma_{\rm O}\gamma_5 Q_{\pm}\,\Big\}\Big\rangle_{\rm G}\,. \tag{H.37}$$

As particular cases we may have

$$\eta(P) = \eta(A_0) = \eta(V_k) = +1\,, \tag{H.38a}$$

$$\eta(A_k) = \eta(V_0) = -1\,. \tag{H.38b}$$

In this thesis, the boundary to bulk 2-point functions that we compute are the following. Amongst those with $\eta(X) = \eta(O)$ we compute correlation functions with the pairs ($\Gamma_{\rm O} = \gamma_5$, $\Gamma_{\rm X} = \gamma_5, \gamma_0\gamma_5$). Amongst the ones with $\eta(X) = -\eta(O)$ we have the pairs ($\Gamma_{\rm O} = \gamma_5$, $\Gamma_{\rm X} = \gamma_0$) and ($\Gamma_{\rm O} = \gamma_k\gamma_5$, $\Gamma_{\rm X} = \gamma_k$). All these cases were defined in Chap. 6 and Chap. 7. Following the notation there (where we refer the reader for more explanations) we have the 2-point functions,

$$g^{11}_{\mathrm{P}_\pm}(x_0) = -\frac{a^3}{L^3}\sum_{\vec{x}}\left\langle P^1(x)\widetilde{\mathcal{P}}^1_\pm\right\rangle = \frac{a^3}{2L^3}\sum_{\vec{x}}\left\langle \mathrm{Tr}\Big\{ H_+(x;\vec{p})^\dagger H_+(x;\vec{p})Q_\pm \Big\}\right\rangle_{\mathrm{G}}, \tag{H.39a}$$

$$g^{11}_{\mathrm{A}_{0\pm}}(x_0) = -\frac{a^3}{L^3}\sum_{\vec{x}}\left\langle A^1_0(x)\widetilde{\mathcal{P}}^1_\pm\right\rangle = -\frac{a^3}{2L^3}\sum_{\vec{x}}\left\langle \mathrm{Tr}\Big\{ H_+(x;\vec{p})^\dagger\gamma_0 H_+(x;\vec{p})Q_\pm \Big\}\right\rangle_{\mathrm{G}}, \tag{H.39b}$$

$$g^{12}_{\mathrm{V}_{0\pm}}(x_0) = -\frac{a^3}{L^3}\sum_{\vec{x}}\left\langle V^1_0(x)\widetilde{\mathcal{P}}^2_\pm\right\rangle = \frac{\mathrm{i}a^3}{2L^3}\sum_{\vec{x}}\left\langle \mathrm{Tr}\Big\{ H_+(x;\vec{p})^\dagger\gamma_0\gamma_5 H_+(x;\vec{p})Q_\pm \Big\}\right\rangle_{\mathrm{G}}, \tag{H.39c}$$

$$\overline{g}^{12}_{\mathrm{V}_{k\pm}}(x_0) = -\frac{a^3}{L^3}\sum_{\vec{x}}\left\langle V^1_k(x)\widetilde{\mathcal{A}}^2_{k\pm}\right\rangle = \frac{\mathrm{i}a^3}{2L^3}\sum_{\vec{x}}\left\langle \mathrm{Tr}\Big\{ H_+(x;\vec{p})^\dagger\gamma_k\gamma_5 H_+(x;\vec{p})\gamma_k Q_\pm \Big\}\right\rangle_{\mathrm{G}}. \tag{H.39d}$$

Note that we only compute the cases above but, using the exact U(1) flavor symmetry, each of these cases would be equivalent to

$$g^{22}_{\mathrm{X}_\pm}(x_0) = g^{11}_{\mathrm{X}_\pm}(x_0), \qquad g^{21}_{\mathrm{X}_\pm}(x_0) = -g^{12}_{\mathrm{X}_\pm}(x_0). \tag{H.40}$$

In the case of the correlation function $\overline{g}^{12}_{\mathrm{V}_{k\pm}}(x_0)$, what we actually compute is the average over the three spatial directions $k = 1, 2, 3$.

H.2.2. Determination of boundary to boundary 2-point functions

Here we consider the correlation function boundary to boundary g_1^{ab} defined in Eq. (H.12), which reads as follows,

$$\begin{aligned} g_1^{ab} &= -\frac{1}{L^6}\left\langle \widetilde{\mathcal{O}'}^a_+ \widetilde{\mathcal{O}}^b_- \right\rangle \\ &= -\frac{a^{12}}{L^6}\sum_{\vec{u},\vec{v},\vec{y},\vec{z}} e^{\mathrm{i}\vec{p}(\vec{u}-\vec{v})}\, e^{\mathrm{i}\vec{q}(\vec{y}-\vec{z})}\left\langle \overline{\zeta}'(\vec{u})\,\gamma_5\frac{\tau^a}{2}\widetilde{Q}_+\,\zeta'(\vec{v})\,\overline{\zeta}(\vec{y})\,\gamma_5\frac{\tau^b}{2}\widetilde{Q}_-\,\zeta(\vec{z})\right\rangle. \end{aligned} \tag{H.41}$$

As with the boundary to bulk correlation functions, we keep the general indices until the end of the calculation, although this 2-point function takes a non-zero value in the continuum limit provided $a, b \neq 3$. Using the definitions of the boundary fields given by Eq. (H.7)-(H.8) we can write Eq. (H.41) as

$$\begin{aligned} g_1^{ab} = -\frac{a^{12}}{L^6}\sum_{\vec{u},\vec{v},\vec{y},\vec{z}} & e^{\mathrm{i}\vec{p}(\vec{u}-\vec{v})}\, e^{\mathrm{i}\vec{q}(\vec{y}-\vec{z})} \\ & \Big\langle \overline{\chi}(T-a,\vec{u})U_0(T-a,\vec{u})\gamma_5\frac{\tau^a}{2}\widetilde{Q}_+ U_0(T-a,\vec{v})^\dagger\chi(T-a,\vec{v}) \\ & \overline{\chi}(a,\vec{y})U_0(0,\vec{y})^\dagger\gamma_5\frac{\tau^b}{2}\widetilde{Q}_- U_0(0,\vec{z})\chi(a,\vec{z})\Big\rangle. \end{aligned} \tag{H.42}$$

Writing explicitly the fermion contractions

$$\begin{aligned} g_1^{ab} = -\frac{a^{12}}{L^6} \sum_{\vec{u},\vec{v},\vec{y},\vec{z}} e^{\mathrm{i}\vec{p}(\vec{u}-\vec{v})}\, e^{\mathrm{i}\vec{q}(\vec{y}-\vec{z})} \Big\{ \\ - \Big\langle \mathrm{Tr}\Big\{ U_0(0,\vec{z})[\chi(a,\vec{z})\overline{\chi}(T-a,\vec{u})]_{\mathrm{F}} U_0(T-a,\vec{u})\,\gamma_5 \frac{\tau^a}{2}\widetilde{Q}_+ \\ \times U_0(T-a,\vec{v})^\dagger [\chi(T-a,\vec{v})\overline{\chi}(a,\vec{y})]_{\mathrm{F}} U_0(0,\vec{y})^\dagger\,\gamma_5 \frac{\tau^b}{2}\widetilde{Q}_- \Big\} \Big\rangle_{\mathrm{G}} \\ + \Big\langle \mathrm{Tr}\Big\{ U_0(T-a,\vec{v})^\dagger [\chi(T-a,\vec{v})\overline{\chi}(T-a,\vec{u})]_{\mathrm{F}} U_0(T-a,\vec{u})\,\gamma_5 \frac{\tau^a}{2}\widetilde{Q}_+ \Big\} \\ \times \mathrm{Tr}\Big\{ U_0(0,\vec{z})[\chi(a,\vec{z})\overline{\chi}(a,\vec{y})]_{\mathrm{F}} U_0(0,\vec{y})^\dagger\,\gamma_5 \frac{\tau^b}{2}\widetilde{Q}_- \Big\} \Big\rangle_{\mathrm{G}} \Big\}. \end{aligned} \tag{H.43}$$

Since we only consider here the case $a, b \neq 3$, the disconnected contribution vanishes and we get the simpler expression

$$\begin{aligned} g_1^{ab} = \frac{a^{12}}{L^6} \sum_{\vec{u},\vec{v},\vec{y},\vec{z}} e^{\mathrm{i}\vec{p}(\vec{u}-\vec{v})}\, e^{\mathrm{i}\vec{q}(\vec{y}-\vec{z})} \\ \Big\langle \mathrm{Tr}\Big\{ U_0(0,\vec{z})[\chi(a,\vec{z})\overline{\chi}(T-a,\vec{u})]_{\mathrm{F}} U_0(T-a,\vec{u})\,\gamma_5 \frac{\tau^a}{2}\widetilde{Q}_+ \\ \times U_0(T-a,\vec{v})^\dagger [\chi(T-a,\vec{v})\overline{\chi}(a,\vec{y})]_{\mathrm{F}} U_0(0,\vec{y})^\dagger\,\gamma_5 \frac{\tau^b}{2}\widetilde{Q}_- \Big\} \Big\rangle_{\mathrm{G}}. \end{aligned} \tag{H.44}$$

Considering the definitions of $H(x;\vec{p})$ and $H(x;\vec{p})^\dagger$ given above in Eq. (H.17)

$$g_1^{ab} = \frac{a^6}{L^6} \sum_{\vec{u},\vec{v}} e^{\mathrm{i}\vec{p}(\vec{u}-\vec{v})} \Big\langle \mathrm{Tr}\Big\{ \gamma_5\tau^1 H(u;\vec{q})^\dagger \gamma_5\tau^1 U_0(u)\gamma_5 \frac{\tau^a}{2}\widetilde{Q}_+\, U_0(v)^\dagger H(v;\vec{q})\gamma_5 \frac{\tau^b}{2}\widetilde{Q}_- \Big\} \Big\rangle_{\mathrm{G}} \tag{H.45}$$

where $u_0 = v_0 = T - a$.

Using the definitions

$$K(\vec{p},\vec{q}) \equiv \frac{a^3}{L^3} \sum_{\vec{x}} e^{-\mathrm{i}\vec{p}\vec{x}}\, U_0(x)^\dagger H(x;\vec{q})|_{x_0=T-a}\,, \tag{H.46a}$$

$$K(\vec{p},\vec{q})^\dagger \equiv \frac{a^3}{L^3} \sum_{\vec{x}} e^{\mathrm{i}\vec{p}\vec{x}}\, H(x;\vec{q})^\dagger U_0(x)|_{x_0=T-a}\,, \tag{H.46b}$$

the correlation function can be written as

$$g_1^{ab} = \Big\langle \mathrm{Tr}\Big\{ \gamma_5\tau^1 K(\vec{p},\vec{q})^\dagger \tau^1 \frac{\tau^a}{2}\widetilde{Q}_+\, K(\vec{p},\vec{q})\,\gamma_5 \frac{\tau^b}{2}\widetilde{Q}_- \Big\} \Big\rangle_{\mathrm{G}}. \tag{H.47}$$

In the particular case $\vec{p} = \vec{q} = \vec{0}$, as it is the case in this thesis, we define

$$K \equiv \frac{a^3}{L^3} \sum_{\vec{x}} U_0(x)^\dagger H(x)|_{x_0=T-a}\,, \tag{H.48a}$$

$$K^\dagger \equiv \frac{a^3}{L^3} \sum_{\vec{x}} H(x)^\dagger U_0(x)|_{x_0=T-a}\,, \tag{H.48b}$$

with

$$H(x) \equiv a^3 \sum_{\vec{y}} [\chi(x)\overline{\zeta}(\vec{y})]_{\rm F} = a^3 \sum_{\vec{y}} S(x,y) U_0(y - a\hat{0})^\dagger|_{y_0=a}\,, \tag{H.49a}$$

$$H(x)^\dagger \equiv a^3 \sum_{\vec{y}} [\chi(x)\overline{\zeta}(\vec{y})]^\dagger_{\rm F} = a^3 \sum_{\vec{y}} U_0(y - a\hat{0}) S(x,y)^\dagger|_{y_0=a}\,, \tag{H.49b}$$

and

$$g_1^{ab} = \Big\langle \, {\rm Tr}\Big\{ \, \gamma_5 \tau^1 K^\dagger \tau^1 \frac{\tau^a}{2} \widetilde{Q}_+ K \gamma_5 \frac{\tau^b}{2} \widetilde{Q}_- \, \Big\} \Big\rangle_{\rm G}\,. \tag{H.50}$$

The flavor structure of K is the same as that of H and therefore we can also decompose K in the two flavor components as

$$K = K_+ T_+ + K_- T_-\,. \tag{H.51}$$

Using this flavor decomposition, the flavor structure in g_1^{ab} may be factored out in the following manner

$$g_1^{ab} = \sum_{i,j,k,l=\pm} {\rm Tr}\Big\{ \, \tau^1 T_i \tau^1 \frac{\tau^a}{2} T_j T_k \frac{\tau^b}{2} T_{-l} \, \Big\} \Big\langle \, {\rm Tr}\Big\{ \, \gamma_5 K_i^\dagger Q_j K_k \gamma_5 Q_l \, \Big\} \Big\rangle_{\rm G}\,. \tag{H.52}$$

For $a, b \neq 3$,

$$g_1^{ab} = \sum_{i=\pm} {\rm Tr}\Big\{ \, T_{-i} \frac{\tau^a}{2} \frac{\tau^b}{2} \, \Big\} \Big\langle \, {\rm Tr}\Big\{ \, \gamma_5 K_i^\dagger Q_i K_i \gamma_5 Q_i \, \Big\} \Big\rangle_{\rm G}\,, \tag{H.53}$$

or more explicitly

$$\begin{aligned} g_1^{ab} = {} & {\rm Tr}\Big\{ \, T_- \frac{\tau^a}{2} \frac{\tau^b}{2} \, \Big\} \Big\langle \, {\rm Tr}\Big\{ \, \gamma_5 K_+^\dagger Q_+ K_+ \gamma_5 Q_+ \, \Big\} \Big\rangle_{\rm G} \\ & + {\rm Tr}\Big\{ \, T_+ \frac{\tau^a}{2} \frac{\tau^b}{2} \, \Big\} \Big\langle \, {\rm Tr}\Big\{ \, \gamma_5 K_-^\dagger Q_- K_- \gamma_5 Q_- \, \Big\} \Big\rangle_{\rm G}\,. \end{aligned} \tag{H.54}$$

We may use again $P_{\rm F}^{1,2}$ symmetry in order to rewrite g_1^{ab} in terms of only K_+. In the same way as H, the transformation in K is $K_\pm(x) \to \gamma_0 \widetilde{K}_\mp(x) \gamma_0$, where we use the same notation as in Eq. (H.28). In this case,

$$\begin{aligned} g_1^{ab} = {} & {\rm Tr}\Big\{ \, T_- \frac{\tau^a}{2} \frac{\tau^b}{2} \, \Big\} \Big\langle \, {\rm Tr}\Big\{ \, \gamma_5 K_+^\dagger Q_+ K_+ \gamma_5 Q_+ \, \Big\} \Big\rangle_{\rm G} \\ & + {\rm Tr}\Big\{ \, T_+ \frac{\tau^a}{2} \frac{\tau^b}{2} \, \Big\} \Big\langle \, {\rm Tr}\Big\{ \, \gamma_5 \gamma_0 \widetilde{K}_+^\dagger \gamma_0 Q_- \gamma_0 \widetilde{K}_+ \gamma_0 \gamma_5 Q_- \, \Big\} \Big\rangle_{\rm G}\,. \end{aligned} \tag{H.55}$$

Since $\gamma_0 \gamma_5 Q_\pm \gamma_5 \gamma_0 = Q_\pm$ and $\gamma_5 Q_\pm \gamma_5 = \gamma_0 Q_\pm \gamma_0 = Q_\mp$ then

$$\begin{aligned} g_1^{ab} = {} & {\rm Tr}\Big\{ \, T_- \frac{\tau^a}{2} \frac{\tau^b}{2} \, \Big\} \Big\langle \, {\rm Tr}\Big\{ \, K_+^\dagger Q_+ K_+ Q_- \, \Big\} \Big\rangle_{\rm G} \\ & + {\rm Tr}\Big\{ \, T_+ \frac{\tau^a}{2} \frac{\tau^b}{2} \, \Big\} \Big\langle \, {\rm Tr}\Big\{ \, \widetilde{K}_+^\dagger Q_+ \widetilde{K}_+ Q_- \, \Big\} \Big\rangle_{\rm G}\,. \end{aligned} \tag{H.56}$$

Using again the invariance of the effective gauge action under $P_{\rm F}^{1,2}$ symmetry and averaging over the gauge fields, Eq. (H.56) is simplified to

$$\begin{aligned} g_1^{ab} &= {\rm Tr}\Big\{ \, \frac{\tau^a}{2} \frac{\tau^b}{2} \, \Big\} \Big\langle \, {\rm Tr}\Big\{ \, K_+^\dagger Q_+ K_+ Q_- \, \Big\} \Big\rangle_{\rm G} \\ &= \frac{1}{2} \delta^{ab} \Big\langle \, {\rm Tr}\Big\{ \, K_+^\dagger Q_+ K_+ Q_- \, \Big\} \Big\rangle_{\rm G}\,. \end{aligned} \tag{H.57}$$

As a result, we eventually compute the expression

$$g_1^{11} = g_1^{22} = \frac{1}{2}\left\langle \mathrm{Tr}\Big\{ K_+^\dagger Q_+ K_+ Q_- \Big\}\right\rangle_{\mathrm{G}}. \tag{H.58}$$

H.3. Correlators of twist-2 operators from the standard SF

In this section $X^a(x) = O^a_{\mu\nu}(x)$ and thus, the most generic expression of the 2-point function is in this case

$$f^{ab}_{\mathrm{O}^a_{\mu\nu}}(x_0) = -\frac{a^3}{L^3}\sum_{\vec{x}}\left\langle O^a_{\mu\nu}(x)\mathcal{O}^b\right\rangle. \tag{H.59}$$

Note that this expression refers to the physical basis, since through this section we determine the 2-point functions in the standard SF formulation.

According to the discussion in Sec. 10.2, to which we refer the reader for a complete explanation, the operator $O^a_{\mu\nu}(x)$ may be written as the sum of two terms as follows,

$$O^a_{\mu\nu}(x) = \overline{\psi}(x)\, S(\gamma_\mu \overset{\leftrightarrow}{D}_\nu)\, \frac{\tau^a}{2}\,\psi(x) - \frac{1}{4}\delta_{\mu\nu}\,\delta^{\alpha\beta}\,\overline{\psi}(x)\, S(\gamma_\alpha \overset{\leftrightarrow}{D}_\beta)\,\frac{\tau^a}{2}\,\psi(x)\,, \tag{H.60}$$

for general values of the Lorentz indices μ and ν. In particular, if $\mu \neq \nu$ only the first term on the r.h.s. of Eq. (H.60) contributes. In the following discussion, we refer to this term as 'the piece of the operator without the delta'. We denote this piece with a superscript 'S', indicating the symmetrization in the Lorentz indices. If $\mu = \nu$, also the second term on the r.h.s. of Eq. (H.60) contributes. We refer to this term as 'the delta piece of the operator'.

In the following sections, we will employ the more compact notation for the operator,

$$O^a_{\mu\nu}(x) = O^{S,a}_{\mu\nu}(x) - \delta_{\mu\nu}\,\frac{1}{4}\sum_{\alpha=0}^{3} O^{S,a}_{\alpha\alpha}(x)\,. \tag{H.61}$$

Note that the delta term is just a particular case of the term without the delta with $\alpha = \beta$. Therefore, in the following we only expand the expression of the correlation function, Eq. (H.59), for the non-delta piece and we sum up the two pieces only at the end. General values of μ, ν and a are used and we treat the particular cases at the end of the calculations. In this case, the correlation function corresponding to only the piece of the operator without the delta is the following

$$\begin{aligned}
f^{ab}_{O^{S,a}_{\mu\nu}}(x_0) &= -\frac{a^3}{L^3}\sum_{\vec{x}}\left\langle O^{S,a}_{\mu\nu}(x)\mathcal{O}^b\right\rangle \\
&= -\frac{a^3}{L^3}\sum_{\vec{x}}\left\langle \overline{\psi}(x)\frac{1}{2!}\left[\gamma_\mu \overset{\leftrightarrow}{D}_\nu + \gamma_\nu \overset{\leftrightarrow}{D}_\mu\right]\frac{\tau^a}{2}\,\psi(x)\mathcal{O}^b\right\rangle \\
&= -\frac{a^9}{L^3}\sum_{\vec{x},\vec{y},\vec{z}} e^{\mathrm{i}\vec{p}(\vec{y}-\vec{z})}\left\langle \frac{1}{2}\overline{\psi}(x)\left[\gamma_\mu \overset{\leftrightarrow}{D}_\nu + \gamma_\nu \overset{\leftrightarrow}{D}_\mu\right]\frac{\tau^a}{2}\,\psi(x)\overline{\zeta}(\vec{y})\,\Gamma_{\mathrm{O}}\frac{\tau^b}{2}\,\zeta(\vec{z})\right\rangle \\
&= -\frac{a^9}{16L^3}\sum_{\vec{x},\vec{y},\vec{z}} e^{\mathrm{i}\vec{p}(\vec{y}-\vec{z})}\left\langle \overline{\psi}(x)\left[\gamma_\mu(\overrightarrow{D}_\nu - \overleftarrow{D}_\nu) + \gamma_\nu(\overrightarrow{D}_\mu - \overleftarrow{D}_\mu)\right]\tau^a\psi(x)\overline{\zeta}(\vec{y})\,\Gamma_{\mathrm{O}}\tau^b\,\zeta(\vec{z})\right\rangle.
\end{aligned} \tag{H.62}$$

We can write

$$f^{ab}_{O^{S,a}_{\mu\nu}}(x_0) = A^{ab}_{\mu\nu}(x_0) - B^{ab}_{\mu\nu}(x_0) + C^{ab}_{\mu\nu}(x_0) - D^{ab}_{\mu\nu}(x_0)\,, \tag{H.63}$$

with the definitions

$$A^{ab}_{\mu\nu}(x_0) = -\frac{a^9}{16L^3}\sum_{\vec{x},\vec{y},\vec{z}} e^{\mathrm{i}\vec{p}(\vec{y}-\vec{z})}\left\langle \overline{\psi}(x)\,\gamma_\mu\,\overrightarrow{D}_\nu\,\tau^a\,\psi(x)\overline{\zeta}(\vec{y})\,\Gamma_{\mathrm{O}}\tau^b\,\zeta(\vec{z})\right\rangle, \tag{H.64a}$$

$$B^{ab}_{\mu\nu}(x_0) = -\frac{a^9}{16L^3}\sum_{\vec{x},\vec{y},\vec{z}} e^{\mathrm{i}\vec{p}(\vec{y}-\vec{z})}\left\langle \overline{\psi}(x)\,\gamma_\mu\,\overleftarrow{D}_\nu\,\tau^a\,\psi(x)\overline{\zeta}(\vec{y})\,\Gamma_{\mathrm{O}}\tau^b\,\zeta(\vec{z})\right\rangle, \tag{H.64b}$$

$$C^{ab}_{\mu\nu}(x_0) = -\frac{a^9}{16L^3}\sum_{\vec{x},\vec{y},\vec{z}} e^{\mathrm{i}\vec{p}(\vec{y}-\vec{z})}\left\langle \overline{\psi}(x)\,\gamma_\nu\,\overrightarrow{D}_\mu\,\tau^a\,\psi(x)\overline{\zeta}(\vec{y})\,\Gamma_{\mathrm{O}}\tau^b\,\zeta(\vec{z})\right\rangle = A^{ab}_{\nu\mu}(x_0), \tag{H.64c}$$

$$D^{ab}_{\mu\nu}(x_0) = -\frac{a^9}{16L^3}\sum_{\vec{x},\vec{y},\vec{z}} e^{\mathrm{i}\vec{p}(\vec{y}-\vec{z})}\left\langle \overline{\psi}(x)\,\gamma_\nu\,\overleftarrow{D}_\mu\,\tau^a\,\psi(x)\overline{\zeta}(\vec{y})\,\Gamma_{\mathrm{O}}\tau^b\,\zeta(\vec{z})\right\rangle = B^{ab}_{\nu\mu}(x_0). \tag{H.64d}$$

With these relations we can write

$$f^{ab}_{O^{S,a}_{\mu\nu}}(x_0) = \Big(A^{ab}_{\mu\nu}(x_0) + A^{ab}_{\nu\mu}(x_0)\Big) - \Big(B^{ab}_{\mu\nu}(x_0) + B^{ab}_{\nu\mu}(x_0)\Big). \tag{H.65}$$

Now we proceed to the calculation of $A^{ab}_{\mu\nu}(x_0)$ and $B^{ab}_{\mu\nu}(x_0)$. In the case of $A^{ab}_{\mu\nu}(x_0)$,

$$\begin{aligned} A^{ab}_{\mu\nu}(x_0) = -\frac{a^9}{2a16L^3}\sum_{\vec{x},\vec{y},\vec{z}} e^{\mathrm{i}\vec{p}(\vec{y}-\vec{z})}\Bigg\{&\left\langle \overline{\psi}(x)\,\gamma_\mu\,\lambda_\nu\,U_\nu(x)\,\tau^a\,\psi(x+a\hat{\nu})\overline{\zeta}(\vec{y})\,\Gamma_{\mathrm{O}}\tau^b\,\zeta(\vec{z})\right\rangle \\ &-\left\langle \overline{\psi}(x)\,\gamma_\mu\,\lambda^*_\nu\,U_\nu(x-a\hat{\nu})^\dagger\,\tau^a\,\psi(x-a\hat{\nu})\overline{\zeta}(\vec{y})\,\Gamma_{\mathrm{O}}\tau^b\,\zeta(\vec{z})\right\rangle\Bigg\}, \end{aligned} \tag{H.66}$$

which after carrying out the fermionic contractions becomes

$$\begin{aligned} A^{ab}_{\mu\nu}(x_0) = \frac{a^9}{2a16L^3}\sum_{\vec{x},\vec{y},\vec{z}} e^{\mathrm{i}\vec{p}(\vec{y}-\vec{z})}\Bigg\{&\\ &\left\langle \mathrm{Tr}\Big\{\,[\zeta(\vec{z})\overline{\psi}(x)]_{\mathrm{F}}\,\gamma_\mu\,\lambda_\nu\,U_\nu(x)\,\tau^a\,[\psi(x+a\hat{\nu})\overline{\zeta}(\vec{y})]_{\mathrm{F}}\,\Gamma_{\mathrm{O}}\tau^b\,\Big\}^{c,f,s}\right\rangle_G \\ -&\left\langle \mathrm{Tr}\Big\{\,[\psi(x+a\hat{\nu})\overline{\psi}(x)]_{\mathrm{F}}\,\gamma_\mu\,\lambda_\nu\,U_\nu(x)\,\tau^a\,\Big\}^{c,f,s}\,\mathrm{Tr}\Big\{\,[\zeta(\vec{z})\overline{\zeta}(\vec{y})]_{\mathrm{F}}\,\Gamma_{\mathrm{O}}\tau^b\,\Big\}^{c,f,s}\right\rangle_G \\ &-\left\langle \mathrm{Tr}\Big\{\,[\zeta(\vec{z})\overline{\psi}(x)]_{\mathrm{F}}\,\gamma_\mu\,\lambda^*_\nu\,U_\nu(x-a\hat{\nu})^\dagger\,\tau^a\,[\psi(x-a\hat{\nu})\overline{\zeta}(\vec{y})]_{\mathrm{F}}\,\Gamma_{\mathrm{O}}\tau^b\,\Big\}^{c,f,s}\right\rangle_G \\ &+\left\langle \mathrm{Tr}\Big\{\,[\psi(x-a\hat{\nu})\overline{\psi}(x)]_{\mathrm{F}}\,\gamma_\mu\,\lambda^*_\nu\,U_\nu(x-a\hat{\nu})^\dagger\,\tau^a\,\Big\}^{c,f,s}\,\mathrm{Tr}\Big\{\,[\zeta(\vec{z})\overline{\zeta}(\vec{y})]_{\mathrm{F}}\,\Gamma_{\mathrm{O}}\tau^b\,\Big\}^{c,f,s}\right\rangle_G\Bigg\}. \end{aligned} \tag{H.67}$$

Since the propagator does not have a flavor structure (note that we work in the standard setup at the moment), all terms containing the trace of only one flavor matrix will vanish. So is the case of all disconnected pieces. Therefore, after performing the flavor trace we can write

$$\begin{aligned} A^{ab}_{\mu\nu}(x_0) =&\delta_{ab}\,\frac{a^9}{a16L^3}\sum_{\vec{x},\vec{y},\vec{z}} e^{\mathrm{i}\vec{p}(\vec{y}-\vec{z})}\Bigg\{\\ &\lambda_\nu\left\langle \mathrm{Tr}\Big\{\,[\zeta(\vec{z})\overline{\psi}(x)]_{\mathrm{F}}\,\gamma_\mu\,U_\nu(x)\,[\psi(x+a\hat{\nu})\overline{\zeta}(\vec{y})]_{\mathrm{F}}\,\Gamma_{\mathrm{O}}\,\Big\}^{c,s}\right\rangle_G \\ &-\lambda^*_\nu\left\langle \mathrm{Tr}\Big\{\,[\zeta(\vec{z})\overline{\psi}(x)]_{\mathrm{F}}\,\gamma_\mu\,U_\nu(x-a\hat{\nu})^\dagger\,[\psi(x-a\hat{\nu})\overline{\zeta}(\vec{y})]_{\mathrm{F}}\,\Gamma_{\mathrm{O}}\,\Big\}^{c,s}\right\rangle_G\Bigg\}. \end{aligned} \tag{H.68}$$

Proceeding with $B^{ab}_{\mu\nu}(x_0)$ in the same way,

$$B^{ab}_{\mu\nu}(x_0) = -\frac{a^9}{2a16L^3}\sum_{\vec{x},\vec{y},\vec{z}} e^{\mathrm{i}\vec{p}(\vec{y}-\vec{z})}\left\{\left\langle\overline{\psi}(x+a\hat{\nu})\,\gamma_\mu\,\lambda^*_\nu\,U_\nu(x)^\dagger\,\tau^a\,\psi(x)\overline{\zeta}(\vec{y})\,\Gamma_{\mathrm{O}}\tau^b\,\zeta(\vec{z})\right\rangle\right. \\ \left. -\left\langle\overline{\psi}(x-a\hat{\nu})\,\gamma_\mu\,\lambda_\nu\,U_\nu(x-a\hat{\nu})\,\tau^a\,\psi(x)\overline{\zeta}(\vec{y})\,\Gamma_{\mathrm{O}}\tau^b\,\zeta(\vec{z})\right\rangle\right\}, \tag{H.69}$$

which eventually reduces to

$$B^{ab}_{\mu\nu}(x_0) =\delta_{ab}\,\frac{a^9}{a16L^3}\sum_{\vec{x},\vec{y},\vec{z}} e^{\mathrm{i}\vec{p}(\vec{y}-\vec{z})}\left\{\right. \\ \lambda^*_\nu\left\langle\mathrm{Tr}\Big\{\,[\zeta(\vec{z})\overline{\psi}(x+a\hat{\nu})]_{\mathrm{F}}\,\gamma_\mu\,U_\nu(x)^\dagger\,[\psi(x)\overline{\zeta}(\vec{y})]_{\mathrm{F}}\,\Gamma_{\mathrm{O}}\,\Big\}^{c,s}\right\rangle_G \\ \left. -\,\lambda_\nu\left\langle\mathrm{Tr}\Big\{\,[\zeta(\vec{z})\overline{\psi}(x-a\hat{\nu})]_{\mathrm{F}}\,\gamma_\mu\,U_\nu(x-a\hat{\nu})\,[\psi(x)\overline{\zeta}(\vec{y})]_{\mathrm{F}}\,\Gamma_{\mathrm{O}}\,\Big\}^{c,s}\right\rangle_G\right\}. \tag{H.70}$$

Considering the definition of the boundary to bulk quark propagator in the physical basis, $\mathcal{H}(x;\vec{p})$ and $\mathcal{H}(x;\vec{p})^\dagger$, as given by

$$\mathcal{H}(x;\vec{p}) \equiv a^3\sum_{\vec{y}} e^{\mathrm{i}\vec{p}\,\vec{y}}\,[\psi(x)\overline{\zeta}(\vec{y})]_{\mathrm{F}} = a^3\sum_{\vec{y}} e^{\mathrm{i}\vec{p}\,\vec{y}}\,S(x,y)U_0(y-a\hat{0})^\dagger|_{y_0=a}\,P_+\,, \tag{H.71a}$$

$$\mathcal{H}(x;\vec{p})^\dagger \equiv a^3\sum_{\vec{y}} e^{-\mathrm{i}\vec{p}\,\vec{y}}\,[\psi(x)\overline{\zeta}(\vec{y})]^\dagger_{\mathrm{F}} = a^3\sum_{\vec{y}} e^{-\mathrm{i}\vec{p}\,\vec{y}}\,P_+\,U_0(y-a\hat{0})S(x,y)^\dagger|_{y_0=a}\,, \tag{H.71b}$$

it is possible to write these expressions in terms of those of $H(x;\vec{p})$ and $H(x;\vec{p})^\dagger$ (cf. Eq. (H.17)) as follows,

$$\mathcal{H}(x;\vec{p}) \equiv H(x;\vec{p})\,P_+\,, \tag{H.72a}$$

$$\mathcal{H}(x;\vec{p})^\dagger \equiv P_+\,H(x;\vec{p})^\dagger\,. \tag{H.72b}$$

Note that here $H(x;\vec{p})$ and $H(x;\vec{p})^\dagger$ refer to the physical basis. This is an abuse of notation, since $H(x;\vec{p})$ and $H(x;\vec{p})^\dagger$ have been previously defined in the twisted basis. In this case, we adopt these expressions in order to denote the general form of the corresponding propagator, but during all this section the physical basis is considered. Therefore, all following expressions in the present section are written in terms of $H(x;\vec{p})$ and $H(x;\vec{p})^\dagger$, expressed in the physical basis, and the projectors $P_\pm$, which appear thus explicitly. Using the definitions in Eq. (H.71)-(H.72), the expressios for $A^{ab}_{\mu\nu}(x_0)$ and $B^{ab}_{\mu\nu}(x_0)$ can be rewritten, respectively, as

$$A^{ab}_{\mu\nu}(x_0) =\delta_{ab}\,\frac{a^3}{a16L^3}\sum_{\vec{x}}\left\{\right. \\ \lambda_\nu\left\langle\mathrm{Tr}\Big\{\,P_+\Gamma_{\mathrm{O}}P_-\gamma_5 H(x;\vec{p})^\dagger\gamma_5\,\gamma_\mu\,U_\nu(x)\,H(x+a\hat{\nu};\vec{p})\,\Big\}^{c,s}\right\rangle_G \\ \left. -\,\lambda^*_\nu\left\langle\mathrm{Tr}\Big\{\,P_+\Gamma_{\mathrm{O}}P_-\gamma_5 H(x;\vec{p})^\dagger\gamma_5\,\gamma_\mu\,U_\nu(x-a\hat{\nu})^\dagger\,H(x-a\hat{\nu};\vec{p})\,\Big\}^{c,s}\right\rangle_G\right\} \tag{H.73}$$

and

$$
\begin{aligned}
B^{ab}_{\mu\nu}(x_0) =& \delta_{ab}\,\frac{a^3}{a16L^3}\sum_{\vec{x}}\Bigg\{ \\
&\lambda^*_\nu\left\langle \mathrm{Tr}\Big\{\, P_+\Gamma_{\mathrm{O}}P_-\gamma_5 H(x+a\hat{\nu};\vec{p})^\dagger\gamma_5\,\gamma_\mu\,U_\nu(x)^\dagger\,H(x;\vec{p})\,\Big\}^{c,s}\right\rangle_G \\
&-\lambda_\nu\left\langle \mathrm{Tr}\Big\{\, P_+\Gamma_{\mathrm{O}}P_-\gamma_5 H(x-a\hat{\nu};\vec{p})^\dagger\gamma_5\,\gamma_\mu\,U_\nu(x-a\hat{\nu})\,H(x;\vec{p})\,\Big\}^{c,s}\right\rangle_G\Bigg\}.
\end{aligned}
\tag{H.74}
$$

As it can be seen from the expressions of $A^{ab}_{\mu\nu}(x_0)$ and $B^{ab}_{\mu\nu}(x_0)$ in Eq. (H.73)-Eq. (H.74), all choices of Γ_{O} such that $\Gamma_{\mathrm{O}}P_\pm = P_\pm\Gamma_{\mathrm{O}}$ give raise to a vanishing correlation function because $P_\pm$ are projectors. Therefore, we assume from now on that Γ_{O} is such that $\Gamma_{\mathrm{O}}P_\pm = P_\mp\Gamma_{\mathrm{O}}$ and thus $P_+\Gamma_{\mathrm{O}}P_- = \Gamma_{\mathrm{O}}P_-$. In this case, the final expression is

$$
\begin{aligned}
f^{ab}_{O^{S,a}_{\mu\nu}}(x_0) = \delta_{ab}\,\frac{a^3}{a16L^3}\sum_{\vec{x}}\Bigg\{ \\
&\lambda_\nu\Big[\left\langle \mathrm{Tr}\Big\{\,\Gamma_{\mathrm{O}}P_-\gamma_5 H(x;\vec{p})^\dagger\gamma_5\,\gamma_\mu\,U_\nu(x)\,H(x+a\hat{\nu};\vec{p})\,\Big\}^{c,s}\right\rangle_G \\
&\quad+\left\langle \mathrm{Tr}\Big\{\,\Gamma_{\mathrm{O}}P_-\gamma_5 H(x-a\hat{\nu};\vec{p})^\dagger\gamma_5\,\gamma_\mu\,U_\nu(x-a\hat{\nu})\,H(x;\vec{p})\,\Big\}^{c,s}\right\rangle_G\Big] \\
&+\lambda_\mu\Big[\left\langle \mathrm{Tr}\Big\{\,\Gamma_{\mathrm{O}}P_-\gamma_5 H(x;\vec{p})^\dagger\gamma_5\,\gamma_\nu\,U_\mu(x)\,H(x+a\hat{\mu};\vec{p})\,\Big\}^{c,s}\right\rangle_G \\
&\quad+\left\langle \mathrm{Tr}\Big\{\,\Gamma_{\mathrm{O}}P_-\gamma_5 H(x-a\hat{\mu};\vec{p})^\dagger\gamma_5\,\gamma_\nu\,U_\mu(x-a\hat{\mu})\,H(x;\vec{p})\,\Big\}^{c,s}\right\rangle_G\Big] \\
&-\lambda^*_\nu\Big[\left\langle \mathrm{Tr}\Big\{\,\Gamma_{\mathrm{O}}P_-\gamma_5 H(x;\vec{p})^\dagger\gamma_5\,\gamma_\mu\,U_\nu(x-a\hat{\nu})^\dagger\,H(x-a\hat{\nu};\vec{p})\,\Big\}^{c,s}\right\rangle_G \\
&\quad+\left\langle \mathrm{Tr}\Big\{\,\Gamma_{\mathrm{O}}P_-\gamma_5 H(x+a\hat{\nu};\vec{p})^\dagger\gamma_5\,\gamma_\mu\,U_\nu(x)^\dagger\,H(x;\vec{p})\,\Big\}^{c,s}\right\rangle_G\Big] \\
&-\lambda^*_\mu\Big[\left\langle \mathrm{Tr}\Big\{\,\Gamma_{\mathrm{O}}P_-\gamma_5 H(x;\vec{p})^\dagger\gamma_5\,\gamma_\nu\,U_\mu(x-a\hat{\mu})^\dagger\,H(x-a\hat{\mu};\vec{p})\,\Big\}^{c,s}\right\rangle_G \\
&\quad+\left\langle \mathrm{Tr}\Big\{\,\Gamma_{\mathrm{O}}P_-\gamma_5 H(x+a\hat{\mu};\vec{p})^\dagger\gamma_5\,\gamma_\nu\,U_\mu(x)^\dagger\,H(x;\vec{p})\,\Big\}^{c,s}\right\rangle_G\Big]\Bigg\}.
\end{aligned}
\tag{H.75}
$$

H.3.1. Particular cases

We write here the expressions for the particular cases that we compute in this thesis, namely the operators O^a_{12} and O^a_{44}, whose respective correlation functions are $f^{ab}_{O^a_{12}}(x_0)$ and $f^{ab}_{O^a_{44}}(x_0)$.

Determination of the O_{12} 2-point function

In this case only the non-delta part contributes and therefore, $f^{ab}_{O^a_{12}}(x_0) = f^{ab}_{O^{S,a}_{12}}(x_0)$. For our choice of the gamma matrix, $\Gamma_O = \gamma_2$, the correlation function may be written as follows

$$\begin{aligned}
f^{ab}_{O^a_{12}}(x_0) = \delta_{ab}\,\frac{a^3}{a16L^3}\sum_{\vec{x}}\Bigg\{ & \\
& \lambda_2\Big[\Big\langle \mathrm{Tr}\Big\{\,\gamma_2 P_-\gamma_5 H(x;\vec{p})^\dagger\gamma_5\,\gamma_1\,U_2(x)\,H(x+a\hat{2};\vec{p})\,\Big\}^{c,s}\Big\rangle_G \\
& \quad +\Big\langle \mathrm{Tr}\Big\{\,\gamma_2 P_-\gamma_5 H(x-a\hat{2};\vec{p})^\dagger\gamma_5\,\gamma_1\,U_2(x-a\hat{2})\,H(x;\vec{p})\,\Big\}^{c,s}\Big\rangle_G\Big] \\
& +\lambda_1\Big[\Big\langle \mathrm{Tr}\Big\{\,\gamma_2 P_-\gamma_5 H(x;\vec{p})^\dagger\gamma_5\,\gamma_2\,U_1(x)\,H(x+a\hat{1};\vec{p})\,\Big\}^{c,s}\Big\rangle_G \\
& \quad +\Big\langle \mathrm{Tr}\Big\{\,\gamma_2 P_-\gamma_5 H(x-a\hat{1};\vec{p})^\dagger\gamma_5\,\gamma_2\,U_1(x-a\hat{1})\,H(x;\vec{p})\,\Big\}^{c,s}\Big\rangle_G\Big] \\
& -\lambda_2^*\Big[\Big\langle \mathrm{Tr}\Big\{\,\gamma_2 P_-\gamma_5 H(x;\vec{p})^\dagger\gamma_5\,\gamma_1\,U_2(x-a\hat{2})^\dagger\,H(x-a\hat{2};\vec{p})\,\Big\}^{c,s}\Big\rangle_G \\
& \quad +\Big\langle \mathrm{Tr}\Big\{\,\gamma_2 P_-\gamma_5 H(x+a\hat{2};\vec{p})^\dagger\gamma_5\,\gamma_1\,U_2(x)^\dagger\,H(x;\vec{p})\,\Big\}^{c,s}\Big\rangle_G\Big] \\
& -\lambda_1^*\Big[\Big\langle \mathrm{Tr}\Big\{\,\gamma_2 P_-\gamma_5 H(x;\vec{p})^\dagger\gamma_5\,\gamma_2\,U_1(x-a\hat{1})^\dagger\,H(x-a\hat{1};\vec{p})\,\Big\}^{c,s}\Big\rangle_G \\
& \quad +\Big\langle \mathrm{Tr}\Big\{\,\gamma_2 P_-\gamma_5 H(x+a\hat{1};\vec{p})^\dagger\gamma_5\,\gamma_2\,U_1(x)^\dagger\,H(x;\vec{p})\,\Big\}^{c,s}\Big\rangle_G\Big]\Bigg\}.
\end{aligned} \tag{H.76}$$

Determination of the O_{44} 2-point function

If $\mu = \nu$ the delta part also contributes to the correlation function. In this case we have that

$$O^a_{\mu\mu}(x) = O^{S,a}_{\mu\mu}(x) - \frac{1}{4}\sum_{\alpha=0}^{3} O^{S,a}_{\alpha\alpha}(x) = \frac{3}{4}\Big[\,O^{S,a}_{\mu\mu}(x) - \frac{1}{3}\sum_{\alpha\neq\mu} O^{S,a}_{\alpha\alpha}(x)\,\Big]. \tag{H.77}$$

According to Eq. (H.75), the non-delta part with $\mu = \nu$ is given by

$$\begin{aligned}
f^{ab}_{O^{S,a}_{\mu\mu}}(x_0) = \delta_{ab}\,\frac{2a^3}{a16L^3}\sum_{\vec{x}}\Bigg\{ & \\
& \lambda_\mu\Big[\Big\langle \mathrm{Tr}\Big\{\,\Gamma_O P_-\gamma_5 H(x;\vec{p})^\dagger\gamma_5\,\gamma_\mu\,U_\mu(x)\,H(x+a\hat{\mu};\vec{p})\,\Big\}^{c,s}\Big\rangle_G \\
& \quad +\Big\langle \mathrm{Tr}\Big\{\,\Gamma_O P_-\gamma_5 H(x-a\hat{\mu};\vec{p})^\dagger\gamma_5\,\gamma_\mu\,U_\mu(x-a\hat{\mu})\,H(x;\vec{p})\,\Big\}^{c,s}\Big\rangle_G\Big] \\
& -\lambda_\mu^*\Big[\Big\langle \mathrm{Tr}\Big\{\,\Gamma_O P_-\gamma_5 H(x;\vec{p})^\dagger\gamma_5\,\gamma_\mu\,U_\mu(x-a\hat{\mu})^\dagger\,H(x-a\hat{\mu};\vec{p})\,\Big\}^{c,s}\Big\rangle_G \\
& \quad +\Big\langle \mathrm{Tr}\Big\{\,\Gamma_O P_-\gamma_5 H(x+a\hat{\mu};\vec{p})^\dagger\gamma_5\,\gamma_\mu\,U_\mu(x)^\dagger\,H(x;\vec{p})\,\Big\}^{c,s}\Big\rangle_G\Big]\Bigg\}.
\end{aligned} \tag{H.78}$$

The total contribution is then

$$f^{ab}_{O^a_{\mu\mu}}(x_0) = \frac{3}{4}\Big[\,f^{ab}_{O^{S,a}_{\mu\mu}}(x_0) - \frac{1}{3}\sum_{\alpha\neq\mu} f^{ab}_{O^{S,a}_{\alpha\alpha}}(x_0)\Big], \tag{H.79}$$

which explicitly reads as follows

$$
\begin{aligned}
f^{ab}_{O^a_{\mu\mu}}(x_0) = \delta_{ab}\,\frac{2a^3}{a16L^3}\,\frac{3}{4}\sum_{\vec{x}}\Bigg\{ & \\
& \lambda_\mu\Big[\Big\langle \mathrm{Tr}\Big\{\,\Gamma_{\mathrm{O}}P_-\gamma_5 H(x;\vec{p})^\dagger\gamma_5\,\gamma_\mu\,U_\mu(x)\,H(x+a\hat{\mu};\vec{p})\,\Big\}^{c,s}\Big\rangle_G \\
& \quad +\Big\langle \mathrm{Tr}\Big\{\,\Gamma_{\mathrm{O}}P_-\gamma_5 H(x-a\hat{\mu};\vec{p})^\dagger\gamma_5\,\gamma_\mu\,U_\mu(x-a\hat{\mu})\,H(x;\vec{p})\,\Big\}^{c,s}\Big\rangle_G\Big] \\
& -\lambda^*_\mu\Big[\Big\langle \mathrm{Tr}\Big\{\,\Gamma_{\mathrm{O}}P_-\gamma_5 H(x;\vec{p})^\dagger\gamma_5\,\gamma_\mu\,U_\mu(x-a\hat{\mu})^\dagger\,H(x-a\hat{\mu};\vec{p})\,\Big\}^{c,s}\Big\rangle_G \\
& \quad +\Big\langle \mathrm{Tr}\Big\{\,\Gamma_{\mathrm{O}}P_-\gamma_5 H(x+a\hat{\mu};\vec{p})^\dagger\gamma_5\,\gamma_\mu\,U_\mu(x)^\dagger\,H(x;\vec{p})\,\Big\}^{c,s}\Big\rangle_G\Big] \\
-\frac{1}{3}\sum_{\alpha\neq\mu}\Big\{ & \lambda_\alpha\Big[\Big\langle \mathrm{Tr}\Big\{\,\Gamma_{\mathrm{O}}P_-\gamma_5 H(x;\vec{p})^\dagger\gamma_5\,\gamma_\alpha\,U_\alpha(x)\,H(x+a\hat{\alpha};\vec{p})\,\Big\}^{c,s}\Big\rangle_G \\
& \quad +\Big\langle \mathrm{Tr}\Big\{\,\Gamma_{\mathrm{O}}P_-\gamma_5 H(x-a\hat{\alpha};\vec{p})^\dagger\gamma_5\,\gamma_\alpha\,U_\alpha(x-a\hat{\alpha})\,H(x;\vec{p})\,\Big\}^{c,s}\Big\rangle_G\Big] \\
& -\lambda^*_\alpha\Big[\Big\langle \mathrm{Tr}\Big\{\,\Gamma_{\mathrm{O}}P_-\gamma_5 H(x;\vec{p})^\dagger\gamma_5\,\gamma_\alpha\,U_\alpha(x-a\hat{\alpha})^\dagger\,H(x-a\hat{\alpha};\vec{p})\,\Big\}^{c,s}\Big\rangle_G \\
& \quad +\Big\langle \mathrm{Tr}\Big\{\,\Gamma_{\mathrm{O}}P_-\gamma_5 H(x+a\hat{\alpha};\vec{p})^\dagger\gamma_5\,\gamma_\alpha\,U_\alpha(x)^\dagger\,H(x;\vec{p})\,\Big\}^{c,s}\Big\rangle_G\Big]\Big\}\Bigg\}.
\end{aligned}
\tag{H.80}
$$

For our choice of gamma matrices, $\Gamma_{\mathrm{O}} = \gamma_1$, and indices, $\mu = \nu = 0$, it becomes

$$
\begin{aligned}
f^{ab}_{O^a_{44}}(x_0) = \delta_{ab}\,\frac{2a^3}{a16L^3}\,\frac{3}{4}\sum_{\vec{x}}\Bigg\{ & \\
& \Big[\Big\langle \mathrm{Tr}\Big\{\,\gamma_1 P_-\gamma_5 H(x;\vec{p})^\dagger\gamma_5\,\gamma_0\,U_0(x)\,H(x+a\hat{0};\vec{p})\,\Big\}^{c,s}\Big\rangle_G \\
& \quad +\Big\langle \mathrm{Tr}\Big\{\,\gamma_1 P_-\gamma_5 H(x-a\hat{0};\vec{p})^\dagger\gamma_5\,\gamma_0\,U_0(x-a\hat{0})\,H(x;\vec{p})\,\Big\}^{c,s}\Big\rangle_G\Big] \\
& -\Big[\Big\langle \mathrm{Tr}\Big\{\,\gamma_1 P_-\gamma_5 H(x;\vec{p})^\dagger\gamma_5\,\gamma_0\,U_0(x-a\hat{0})^\dagger\,H(x-a\hat{0};\vec{p})\,\Big\}^{c,s}\Big\rangle_G \\
& \quad +\Big\langle \mathrm{Tr}\Big\{\,\gamma_1 P_-\gamma_5 H(x+a\hat{0};\vec{p})^\dagger\gamma_5\,\gamma_0\,U_0(x)^\dagger\,H(x;\vec{p})\,\Big\}^{c,s}\Big\rangle_G\Big] \\
-\frac{1}{3}\sum_{\alpha=1}^{3}\Big\{ & \lambda_\alpha\Big[\Big\langle \mathrm{Tr}\Big\{\,\gamma_1 P_-\gamma_5 H(x;\vec{p})^\dagger\gamma_5\,\gamma_\alpha\,U_\alpha(x)\,H(x+a\hat{\alpha};\vec{p})\,\Big\}^{c,s}\Big\rangle_G \\
& \quad +\Big\langle \mathrm{Tr}\Big\{\,\gamma_1 P_-\gamma_5 H(x-a\hat{\alpha};\vec{p})^\dagger\gamma_5\,\gamma_\alpha\,U_\alpha(x-a\hat{\alpha})\,H(x;\vec{p})\,\Big\}^{c,s}\Big\rangle_G\Big] \\
& -\lambda^*_\alpha\Big[\Big\langle \mathrm{Tr}\Big\{\,\gamma_1 P_-\gamma_5 H(x;\vec{p})^\dagger\gamma_5\,\gamma_\alpha\,U_\alpha(x-a\hat{\alpha})^\dagger\,H(x-a\hat{\alpha};\vec{p})\,\Big\}^{c,s}\Big\rangle_G \\
& \quad +\Big\langle \mathrm{Tr}\Big\{\,\gamma_1 P_-\gamma_5 H(x+a\hat{\alpha};\vec{p})^\dagger\gamma_5\,\gamma_\alpha\,U_\alpha(x)^\dagger\,H(x;\vec{p})\,\Big\}^{c,s}\Big\rangle_G\Big]\Big\}\Bigg\},
\end{aligned}
\tag{H.81}
$$

where we have already assumed that $\theta_0 = 0$ and therefore $\lambda_0 = 1$.

H.4. Rotation of the twist-2 correlators to the twisted basis

We have to compute the physical quantity

$$f^{ab}_{O^a_{\mu\nu}}(x_0) = -\frac{a^3}{L^3}\sum_{\vec{x}}\left\langle O^a_{\mu\nu}(x)\,\mathcal{O}^b\right\rangle_\psi, \tag{H.82}$$

as discussed in detail in the previous section, and want to find out how it looks like if we write it in the twisted basis $\{\chi,\overline{\chi}\}$. In Eq. (H.82) we have added the subscript ψ in order to indicate that this expression is written in the physical basis. Expressions in the twisted basis will be in the following denoted with the subscript χ.

In order to find the expressions in the twisted basis, we have to perform the non-anomalous axial transformation of the quark fields,

$$\psi(x) = e^{\mathrm{i}\frac{\alpha}{2}\gamma_5\tau^3}\,\chi(x)\,, \qquad \overline{\psi}(x) = \overline{\chi}(x)\,e^{\mathrm{i}\frac{\alpha}{2}\gamma_5\tau^3}\,, \tag{H.83}$$

and find the expressions of $O^a_{\mu\nu}(x)$ and $\mathcal{O}^a$ in the twisted basis.

H.4.1. Rotation of $O^a_{\mu\nu}(x)$ to the twisted basis

Applying the transformation Eq. (H.83) to the quark fields entering the definition of $O^a_{\mu\nu}(x)$, in the physical basis, it is expressed in the twisted basis as

$$O^a_{\mu\nu}(x) = \overline{\psi}(x)\,\gamma_{\{\mu}\overset{\leftrightarrow}{D}_{\nu\}}\,\frac{\tau^a}{2}\,\psi(x) = \overline{\chi}(x)\,e^{\mathrm{i}\frac{\alpha}{2}\gamma_5\tau^3}\,\gamma_{\{\mu}\overset{\leftrightarrow}{D}_{\nu\}}\,\frac{\tau^a}{2}\,e^{\mathrm{i}\frac{\alpha}{2}\gamma_5\tau^3}\,\chi(x)\,. \tag{H.84}$$

Depending on the flavor structure, we have the cases

$$O^a_{\mu\nu}(x) = \begin{cases} \overline{\chi}(x)\,\gamma_{\{\mu}\overset{\leftrightarrow}{D}_{\nu\}}\left[\cos(\alpha)\,\frac{\tau^a}{2} + \epsilon_{ab3}\sin(\alpha)\,\gamma_5\,\frac{\tau^b}{2}\right]\chi(x) & (a=1,2)\,, \\ \overline{\chi}(x)\,\gamma_{\{\mu}\overset{\leftrightarrow}{D}_{\nu\}}\,\frac{\tau^a}{2}\,\chi(x) & (a=3)\,, \end{cases} \tag{H.85}$$

with ϵ_{abc} the totally anti-symmetric tensor and $\epsilon_{123}=1$. In the particular case of maximal twist, $\alpha=\pi/2$, this expression reduces to

$$O^a_{\mu\nu}(x) = \begin{cases} \epsilon_{ab3}\,\overline{\chi}(x)\,\gamma_{\{\mu}\overset{\leftrightarrow}{D}_{\nu\}}\,\gamma_5\,\frac{\tau^b}{2}\,\chi(x) & (a=1,2)\,, \\ \overline{\chi}(x)\,\gamma_{\{\mu}\overset{\leftrightarrow}{D}_{\nu\}}\,\frac{\tau^a}{2}\,\chi(x) & (a=3)\,. \end{cases} \tag{H.86}$$

H.4.2. Rotation of $\mathcal{O}^a$ to the twisted basis

In the case of the boudary operator we have the expression

$$\begin{aligned} \mathcal{O}^a &= a^6\sum_{\vec{y},\vec{z}}\overline{\zeta}(\vec{y})\,\Gamma_{\mathrm{O}}\frac{\tau^a}{2}\,\zeta(\vec{z})\,e^{\mathrm{i}\vec{p}(\vec{y}-\vec{z})} \\ &= a^6\sum_{\vec{y},\vec{z}}\overline{\psi}(y)P_+U_0(0,\vec{y})^\dagger\,\Gamma_{\mathrm{O}}\frac{\tau^a}{2}\,U_0(0,\vec{z})P_-\psi(z)|_{y_0=z_0=a}\,e^{\mathrm{i}\vec{p}(\vec{y}-\vec{z})} \end{aligned} \tag{H.87}$$

in the physical basis. We now perform the rotation to the twisted basis (cf. Eq. (H.83)) and write the final expression in terms of $\widetilde{Q}_\pm$. For that, we perform the rotation and insert the

identity matrix in the following manner,

$$\mathcal{O}^a = a^6 \sum_{\vec{y},\vec{z}} \overline{\chi}(y)\, e^{\mathrm{i}\frac{\alpha}{2}\gamma_5\tau^3}\, P_+\, 1\, U_0(0,\vec{y})^\dagger\, \Gamma_{\mathrm{O}} \frac{\tau^a}{2}\, U_0(0,\vec{z})\, 1\, P_-\, e^{\mathrm{i}\frac{\alpha}{2}\gamma_5\tau^3}\, \chi(z)|_{y_0=z_0=a}\, e^{\mathrm{i}\vec{p}(\vec{y}-\vec{z})}\,, \quad \text{(H.88)}$$

where we consider that

$$1 = e^{-\mathrm{i}\frac{\alpha}{2}\gamma_5\tau^3}\, e^{\mathrm{i}\frac{\alpha}{2}\gamma_5\tau^3} \qquad \text{in the first insertion}\,, \quad \text{(H.89a)}$$

$$1 = e^{\mathrm{i}\frac{\alpha}{2}\gamma_5\tau^3}\, e^{-\mathrm{i}\frac{\alpha}{2}\gamma_5\tau^3} \qquad \text{in the second insertion}\,. \quad \text{(H.89b)}$$

Taking into account the relations

$$e^{\mathrm{i}\frac{\alpha}{2}\gamma_5\tau^3}\, P_+\, e^{-\mathrm{i}\frac{\alpha}{2}\gamma_5\tau^3} = \frac{1}{2}(1+\gamma_0\, e^{-\mathrm{i}\alpha\gamma_5\tau^3})\,, \quad \text{(H.90a)}$$

$$e^{-\mathrm{i}\frac{\alpha}{2}\gamma_5\tau^3}\, P_-\, e^{\mathrm{i}\frac{\alpha}{2}\gamma_5\tau^3} = \frac{1}{2}(1-\gamma_0\, e^{\mathrm{i}\alpha\gamma_5\tau^3})\,, \quad \text{(H.90b)}$$

we can write

$$\begin{aligned}\mathcal{O}^a = a^6 \sum_{\vec{y},\vec{z}}\, & e^{\mathrm{i}\vec{p}(\vec{y}-\vec{z})} \\ & \overline{\chi}(y)\, \widetilde{P}_+(-\alpha)\, U_0(0,\vec{y})^\dagger\, e^{\mathrm{i}\frac{\alpha}{2}\gamma_5\tau^3}\, \Gamma_{\mathrm{O}} \frac{\tau^a}{2}\, e^{\mathrm{i}\frac{\alpha}{2}\gamma_5\tau^3}\, U_0(0,\vec{z})\, \widetilde{P}_-(\alpha)\, \chi(z)|_{y_0=z_0=a}\,,\end{aligned} \quad \text{(H.91)}$$

where we have used the definition

$$\widetilde{P}_\pm(\alpha) = \frac{1}{2}\,(1 \pm \gamma_0\, e^{\mathrm{i}\alpha\gamma_5\tau^3})\,. \quad \text{(H.92)}$$

In the case of maximal twist, $\alpha = \pi/2$, Eq. (H.91) reduces to

$$\mathcal{O}^a = a^6 \sum_{\vec{y},\vec{z}} \overline{\chi}(y)\, \widetilde{Q}_-\, U_0(0,\vec{y})^\dagger\, e^{\mathrm{i}\frac{\pi}{4}\gamma_5\tau^3}\, \Gamma_{\mathrm{O}} \frac{\tau^a}{2}\, e^{\mathrm{i}\frac{\pi}{4}\gamma_5\tau^3}\, U_0(0,\vec{z})\, \widetilde{Q}_-\, \chi(z)|_{y_0=z_0=a}\, e^{\mathrm{i}\vec{p}(\vec{y}-\vec{z})}\,. \quad \text{(H.93)}$$

This is the most general expression for the boundary operator in the twisted basis. Depending on the chosen flavor and Dirac structure we can discuss several cases. In particular in this thesis, only the cases $\Gamma_{\mathrm{O}} = \gamma_k$ are considered in the computation of correlators of the twist-2 operators. In this case, the boundary interpolating field takes the following form in the twisted basis,

$$\mathcal{O}^a_{\gamma_k} \equiv \mathcal{O}^a(\Gamma_{\mathrm{O}} = \gamma_k) = \begin{cases} \epsilon_{ab3}\, a^6 \sum_{\vec{y},\vec{z}}\, \overline{\zeta}(\vec{y})\, \gamma_k\gamma_5 \frac{\tau^b}{2}\, \widetilde{Q}_-\, \zeta(\vec{z}) & (a=1,2)\,, \\ a^6 \sum_{\vec{y},\vec{z}}\, \overline{\zeta}(\vec{y})\, \gamma_k \frac{\tau^a}{2}\, \widetilde{Q}_-\, \zeta(\vec{z}) & (a=3)\,. \end{cases} \quad \text{(H.94)}$$

H.4.3. Rotation of the 2-point functions to the twisted basis

In this section we provide the form of the correlation functions that we compute in this thesis, which are given in the twisted basis. These expressions can be directly deduced from the rotation of the bulk and boundary fields as discussed in the previous two sections. In particular, we only consider correlation functions with $a = b$, as imposed by the factor δ_{ab} in the expressions of the correlation functions in the physical basis, discussed in previous sections.

In this case,

$$f^{11}_{O^1_{\mu\nu}}(x_0) = -\frac{a^3}{L^3}\sum_{\vec{x}}\left\langle O^1_{\mu\nu}(x)\,\mathcal{O}^1_{\gamma_k}\right\rangle_\psi = -\frac{a^3}{L^3}\sum_{\vec{x}}\left\langle \widetilde{O}^2_{\mu\nu}(x)\,\widetilde{\mathcal{O}}^2_{\gamma_k-}\right\rangle_\chi = g^{22}_{O^2_{\mu\nu}-}(x_0)\,, \tag{H.95a}$$

$$f^{22}_{O^2_{\mu\nu}}(x_0) = -\frac{a^3}{L^3}\sum_{\vec{x}}\left\langle O^2_{\mu\nu}(x)\,\mathcal{O}^2_{\gamma_k}\right\rangle_\psi = -\frac{a^3}{L^3}\sum_{\vec{x}}\left\langle \widetilde{O}^1_{\mu\nu}(x)\,\widetilde{\mathcal{O}}^1_{\gamma_k-}\right\rangle_\chi = g^{11}_{O^1_{\mu\nu}-}(x_0)\,, \tag{H.95b}$$

$$f^{33}_{O^3_{\mu\nu}}(x_0) = -\frac{a^3}{L^3}\sum_{\vec{x}}\left\langle O^3_{\mu\nu}(x)\,\mathcal{O}^3_{\gamma_k}\right\rangle_\psi = -\frac{a^3}{L^3}\sum_{\vec{x}}\left\langle \widetilde{O}^3_{\mu\nu}(x)\,\widetilde{\mathcal{O}}^3_{\gamma_k-}\right\rangle_\chi = g^{33}_{O^3_{\mu\nu}-}(x_0)\,. \tag{H.95c}$$

We have used the notation with the 'tilde' in order to denote the operators in the twisted basis. In particular, according to the rotations discussed above, these correspond to

$$\widetilde{O}^1_{\mu\nu}(x) \equiv \overline{\chi}(x)\,\gamma_{\{\mu}\,\overset{\leftrightarrow}{D}_{\nu\}}\,\gamma_5\,\frac{\tau^1}{2}\,\chi(x)\,, \tag{H.96a}$$

$$\widetilde{O}^2_{\mu\nu}(x) \equiv \overline{\chi}(x)\,\gamma_{\{\mu}\,\overset{\leftrightarrow}{D}_{\nu\}}\,\gamma_5\,\frac{\tau^2}{2}\,\chi(x)\,, \tag{H.96b}$$

$$\widetilde{O}^3_{\mu\nu}(x) \equiv \overline{\chi}(x)\,\gamma_{\{\mu}\,\overset{\leftrightarrow}{D}_{\nu\}}\,\frac{\tau^3}{2}\,\chi(x)\,, \tag{H.96c}$$

for the bulk operators and

$$\widetilde{\mathcal{O}}^1_{\gamma_k-} \equiv a^6\sum_{\vec{y},\vec{z}}\overline{\zeta}(\vec{y})\,\gamma_k\gamma_5\frac{\tau^1}{2}\,\widetilde{Q}_-\,\zeta(\vec{z})\,, \tag{H.97a}$$

$$\widetilde{\mathcal{O}}^2_{\gamma_k-} \equiv a^6\sum_{\vec{y},\vec{z}}\overline{\zeta}(\vec{y})\,\gamma_k\gamma_5\frac{\tau^2}{2}\,\widetilde{Q}_-\,\zeta(\vec{z})\,, \tag{H.97b}$$

$$\widetilde{\mathcal{O}}^3_{\gamma_k-} \equiv a^6\sum_{\vec{y},\vec{z}}\overline{\zeta}(\vec{y})\,\gamma_k\frac{\tau^3}{2}\,\widetilde{Q}_-\,\zeta(\vec{z})\,, \tag{H.97c}$$

for the ones at the boundaries. The correlation functions in the twisted basis are denoted with 'g' instead of 'f'.

In particular, the only two cases computed in this thesis are

$$g_{12}(x_0) \equiv g^{11}_{O^1_{12}-}(x_0) = -\frac{a^9}{L^3}\sum_{\vec{x},\vec{y},\vec{z}}\left\langle\overline{\chi}(x)\,\gamma_{\{1}\,\overset{\leftrightarrow}{D}_{2\}}\,\gamma_5\,\frac{\tau^1}{2}\,\chi(x)\,\overline{\zeta}(\vec{y})\,\gamma_2\gamma_5\frac{\tau^1}{2}\,\widetilde{Q}_-\,\zeta(\vec{z})\right\rangle, \tag{H.98a}$$

$$g_{44}(x_0) \equiv g^{11}_{O^1_{44}-}(x_0) = -\frac{a^9}{L^3}\sum_{\vec{x},\vec{y},\vec{z}}\left\langle\overline{\chi}(x)\,\gamma_{\{0}\,\overset{\leftrightarrow}{D}_{0\}}\,\gamma_5\,\frac{\tau^1}{2}\,\chi(x)\,\overline{\zeta}(\vec{y})\,\gamma_1\gamma_5\frac{\tau^1}{2}\,\widetilde{Q}_-\,\zeta(\vec{z})\right\rangle, \tag{H.98b}$$

where we have chosen $\gamma_k = \gamma_2$ for the correlation function of O^a_{12} and $\gamma_k = \gamma_1$ for O^a_{44}, as indicated in previous sections and justified in Chap. 10.

H.5. Correlators of twist-2 operators from the χSF

We provide here the explicit expressions of the 2-point functions $g_{12}(x_0)$ and $g_{44}(x_0)$, which are to be evaluated numerically. For general a and $\mu\nu$ indices (assuming $a = 1, 2$), the correlation function we want to compute is

$$g^{aa}_{O^a_{\mu\nu}-}(x_0) = -\frac{a^3}{L^3}\sum_{\vec{x}}\left\langle\widetilde{O}^a_{\mu\nu}(x)\widetilde{\mathcal{O}}^a_{\gamma_k-}\right\rangle_\chi. \tag{H.99}$$

As before, we develop only the expressions for the non-delta part. The delta terms cancel for O^a_{12}. For O^a_{44} they do not cancel but we know how to compute them from the non-delta pieces, as it was done before for the standard setup. From now on, we do not write anymore the subscript χ, since it is clear that we are working in the twisted basis. Writing explicitly the form of the operators, the non-delta part becomes

$$\begin{aligned} g^{aa}_{O^{S,a}_{\mu\nu}-}(x_0) &= -\frac{a^3}{L^3}\sum_{\vec{x}}\left\langle \widetilde{O}^{S,a}_{\mu\nu}(x)\widetilde{\mathcal{O}}^a_{\gamma_k-}\right\rangle \\ &= -\frac{a^9}{L^3}\sum_{\vec{x},\vec{y},\vec{z}} e^{\mathrm{i}\vec{p}(\vec{y}-\vec{z})}\Big\langle \frac{1}{2}\overline{\chi}(x)\left[\gamma_\mu \overleftrightarrow{D}_\nu + \gamma_\nu \overleftrightarrow{D}_\mu\right]\gamma_5\frac{\tau^a}{2}\chi(x)\overline{\zeta}(\vec{y})\,\gamma_k\gamma_5\frac{\tau^a}{2}\widetilde{Q}_-\,\zeta(\vec{z})\Big\rangle\,. \end{aligned} \tag{H.100}$$

Performing all the fermionic contractions and considering the definitions of $H(x;\vec{p})$, $H(x;\vec{p})^\dagger$ and $\overline{H}(x;\vec{p})$ given in Eq. (H.17), we can then write the correlation functions as

$$\begin{aligned} g^{aa}_{O^a_{12}-}(x_0) = \frac{a^3}{2a16L^3}\sum_{\vec{x}}\Bigg\{ & \\ \lambda_2\Big[& \Big\langle \mathrm{Tr}\Big\{\gamma_5\tau^1 H(x;\vec{p})^\dagger\gamma_5\tau^1\,\gamma_1\gamma_5\,U_2(x)\,\tau^a H(x+a\hat{2};\vec{p})\,\gamma_2\gamma_5\tau^a\widetilde{Q}_-\Big\}^{c,s,f}\Big\rangle_G \\ & +\Big\langle \mathrm{Tr}\Big\{\gamma_5\tau^1 H(x-a\hat{2};\vec{p})^\dagger\gamma_5\tau^1\,\gamma_1\gamma_5\,U_2(x-a\hat{2})\,\tau^a H(x;\vec{p})\,\gamma_2\gamma_5\tau^a\widetilde{Q}_-\Big\}^{c,s,f}\Big\rangle_G\Big] \\ +\lambda_1\Big[& \Big\langle \mathrm{Tr}\Big\{\gamma_5\tau^1 H(x;\vec{p})^\dagger\gamma_5\tau^1\,\gamma_2\gamma_5\,U_1(x)\,\tau^a H(x+a\hat{1};\vec{p})\,\gamma_2\gamma_5\tau^a\widetilde{Q}_-\Big\}^{c,s,f}\Big\rangle_G \\ & +\Big\langle \mathrm{Tr}\Big\{\gamma_5\tau^1 H(x-a\hat{1};\vec{p})^\dagger\gamma_5\tau^1\,\gamma_2\gamma_5\,U_1(x-a\hat{1})\,\tau^a H(x;\vec{p})\,\gamma_2\gamma_5\tau^a\widetilde{Q}_-\Big\}^{c,s,f}\Big\rangle_G\Big] \\ -\lambda_2^*\Big[& \Big\langle \mathrm{Tr}\Big\{\gamma_5\tau^1 H(x;\vec{p})^\dagger\gamma_5\tau^1\,\gamma_1\gamma_5\,U_2(x-a\hat{2})^\dagger\,\tau^a H(x-a\hat{2};\vec{p})\,\gamma_2\gamma_5\tau^a\widetilde{Q}_-\Big\}^{c,s,f}\Big\rangle_G \\ & +\Big\langle \mathrm{Tr}\Big\{\gamma_5\tau^1 H(x+a\hat{2};\vec{p})^\dagger\gamma_5\tau^1\,\gamma_1\gamma_5\,U_2(x)^\dagger\,\tau^a H(x;\vec{p})\,\gamma_2\gamma_5\tau^a\widetilde{Q}_-\Big\}^{c,s,f}\Big\rangle_G\Big] \\ -\lambda_1^*\Big[& \Big\langle \mathrm{Tr}\Big\{\gamma_5\tau^1 H(x;\vec{p})^\dagger\gamma_5\tau^1\,\gamma_2\gamma_5\,U_1(x-a\hat{1})^\dagger\,\tau^a H(x-a\hat{1};\vec{p})\,\gamma_2\gamma_5\tau^a\widetilde{Q}_-\Big\}^{c,s,f}\Big\rangle_G \\ & +\Big\langle \mathrm{Tr}\Big\{\gamma_5\tau^1 H(x+a\hat{1};\vec{p})^\dagger\gamma_5\tau^1\,\gamma_2\gamma_5\,U_1(x)^\dagger\,\tau^a H(x;\vec{p})\,\gamma_2\gamma_5\tau^a\widetilde{Q}_-\Big\}^{c,s,f}\Big\rangle_G\Big]\Bigg\}, \end{aligned} \tag{H.101}$$

$$
\begin{aligned}
g^{aa}_{O^a_{44}-}(x_0) = \frac{a^3}{a16L^3}\,\frac{3}{4}\sum_{\vec{x}}\Bigg\{ & \\
& \Big\langle \mathrm{Tr}\Big\{\,\gamma_5\tau^1 H(x;\vec{p})^\dagger\gamma_5\tau^1\,\gamma_0\gamma_5\,U_0(x)\tau^a\,H(x+a\hat{0};\vec{p})\,\gamma_1\gamma_5\tau^a\widetilde{Q}_-\,\Big\}^{c,s,f}\Big\rangle_G \\
& +\Big\langle \mathrm{Tr}\Big\{\,\gamma_5\tau^1 H(x-a\hat{0};\vec{p})^\dagger\gamma_5\tau^1\,\gamma_0\gamma_5\,U_0(x-a\hat{0})\tau^a\,H(x;\vec{p})\,\gamma_1\gamma_5\tau^a\widetilde{Q}_-\,\Big\}^{c,s,f}\Big\rangle_G \\
& -\Big\langle \mathrm{Tr}\Big\{\,\gamma_5\tau^1 H(x;\vec{p})^\dagger\gamma_5\tau^1\,\gamma_0\gamma_5\,U_0(x-a\hat{0})^\dagger\tau^a\,H(x-a\hat{0};\vec{p})\,\gamma_1\gamma_5\tau^a\widetilde{Q}_-\,\Big\}^{c,s,f}\Big\rangle_G \\
& -\Big\langle \mathrm{Tr}\Big\{\,\gamma_5\tau^1 H(x+a\hat{0};\vec{p})^\dagger\gamma_5\tau^1\,\gamma_0\gamma_5\,U_0(x)^\dagger\tau^a\,H(x;\vec{p})\,\gamma_1\gamma_5\tau^a\widetilde{Q}_-\,\Big\}^{c,s,f}\Big\rangle_G \\
-\frac{1}{3}\sum_{\alpha=1}^{3}\Big\{ & \lambda_\alpha\Big\langle \mathrm{Tr}\Big\{\,\gamma_5\tau^1 H(x;\vec{p})^\dagger\gamma_5\tau^1\,\gamma_\alpha\gamma_5\,U_\alpha(x)\tau^a\,H(x+a\hat{\alpha};\vec{p})\,\gamma_1\gamma_5\tau^a\widetilde{Q}_-\,\Big\}^{c,s,f}\Big\rangle_G \\
& +\lambda_\alpha\Big\langle \mathrm{Tr}\Big\{\,\gamma_5\tau^1 H(x-a\hat{\alpha};\vec{p})^\dagger\gamma_5\tau^1\,\gamma_\alpha\gamma_5\,U_\alpha(x-a\hat{\alpha})\tau^a\,H(x;\vec{p})\,\gamma_1\gamma_5\tau^a\widetilde{Q}_-\,\Big\}^{c,s,f}\Big\rangle_G \\
& -\lambda^*_\alpha\Big\langle \mathrm{Tr}\Big\{\,\gamma_5\tau^1 H(x;\vec{p})^\dagger\gamma_5\tau^1\,\gamma_\alpha\gamma_5\,U_\alpha(x-a\hat{\alpha})^\dagger\tau^a\,H(x-a\hat{\alpha};\vec{p})\,\gamma_1\gamma_5\tau^a\widetilde{Q}_-\,\Big\}^{c,s,f}\Big\rangle_G \\
& -\lambda^*_\alpha\Big\langle \mathrm{Tr}\Big\{\,\gamma_5\tau^1 H(x+a\hat{\alpha};\vec{p})^\dagger\gamma_5\tau^1\,\gamma_\alpha\gamma_5\,U_\alpha(x)^\dagger\tau^a\,H(x;\vec{p})\,\gamma_1\gamma_5\tau^a\widetilde{Q}_-\,\Big\}^{c,s,f}\Big\rangle_G\Big\}\Bigg\}\,.
\end{aligned}
\tag{H.102}
$$

Now we eliminate the flavor structure from these expressions. In order to do that we make use of the flavor projectors $T_\pm$ defined in Eq. (H.20) and the chirally rotated projectors without flavor structure $Q_\pm$ given in Eq. (H.21). The resulting expressions are,

$$
\begin{aligned}
g^{aa}_{O^a_{12}-}(x_0) = \frac{a^3}{2a16L^3}\sum_{\vec{x}}\sum_{i=\pm}\Bigg\{ & \\
& -\lambda_2\Big[\Big\langle \mathrm{Tr}\Big\{\,H_i(x;\vec{p})^\dagger\,\gamma_1\,U_2(x)\,H_i(x+a\hat{2};\vec{p})\,\gamma_2 Q_{-i}\,\Big\}^{c,s}\Big\rangle_G \\
& \quad +\Big\langle \mathrm{Tr}\Big\{\,H_i(x-a\hat{2};\vec{p})^\dagger\,\gamma_1\,U_2(x-a\hat{2})\,H_i(x;\vec{p})\,\gamma_2 Q_{-i}\,\Big\}^{c,s}\Big\rangle_G\Big] \\
& -\lambda_1\Big[\Big\langle \mathrm{Tr}\Big\{\,H_i(x;\vec{p})^\dagger\,\gamma_2\,U_1(x)\,H_i(x+a\hat{1};\vec{p})\,\gamma_2 Q_{-i}\,\Big\}^{c,s}\Big\rangle_G \\
& \quad +\Big\langle \mathrm{Tr}\Big\{\,H_i(x-a\hat{1};\vec{p})^\dagger\,\gamma_2\,U_1(x-a\hat{1})\,H_i(x;\vec{p})\,\gamma_2 Q_{-i}\,\Big\}^{c,s}\Big\rangle_G\Big] \\
& +\lambda^*_2\Big[\Big\langle \mathrm{Tr}\Big\{\,H_i(x;\vec{p})^\dagger\,\gamma_1\,U_2(x-a\hat{2})^\dagger\,H_i(x-a\hat{2};\vec{p})\,\gamma_2 Q_{-i}\,\Big\}^{c,s}\Big\rangle_G \\
& \quad +\Big\langle \mathrm{Tr}\Big\{\,H_i(x+a\hat{2};\vec{p})^\dagger\,\gamma_1\,U_2(x)^\dagger\,H_i(x;\vec{p})\,\gamma_2 Q_{-i}\,\Big\}^{c,s}\Big\rangle_G\Big] \\
& +\lambda^*_1\Big[\Big\langle \mathrm{Tr}\Big\{\,H_i(x;\vec{p})^\dagger\,\gamma_2\,U_1(x-a\hat{1})^\dagger\,H_i(x-a\hat{1};\vec{p})\,\gamma_2 Q_{-i}\,\Big\}^{c,s}\Big\rangle_G \\
& \quad +\Big\langle \mathrm{Tr}\Big\{\,H_i(x+a\hat{1};\vec{p})^\dagger\,\gamma_2\,U_1(x)^\dagger\,H_i(x;\vec{p})\,\gamma_2 Q_{-i}\,\Big\}^{c,s}\Big\rangle_G\Big]\Bigg\}\,,
\end{aligned}
\tag{H.103}
$$

$$
\begin{aligned}
g^{aa}_{O^a_{44}-}(x_0) = \frac{a^3}{a16L^3}\,\frac{3}{4}\sum_{\vec{x}}\sum_{i=\pm}\Bigg\{ & \\
& -\Big\langle \mathrm{Tr}\Big\{\, H_i(x;\vec{p})^\dagger\,\gamma_0\,U_0(x)\,H_i(x+a\hat{0};\vec{p})\,\gamma_1 Q_{-i}\,\Big\}^{c,s}\Big\rangle_G \\
& -\Big\langle \mathrm{Tr}\Big\{\, H_i(x-a\hat{0};\vec{p})^\dagger\,\gamma_0\,U_0(x-a\hat{0})\,H_i(x;\vec{p})\,\gamma_1 Q_{-i}\,\Big\}^{c,s}\Big\rangle_G \\
& +\Big\langle \mathrm{Tr}\Big\{\, H_i(x;\vec{p})^\dagger\,\gamma_0\,U_0(x-a\hat{0})^\dagger\,H_i(x-a\hat{0};\vec{p})\,\gamma_1 Q_{-i}\,\Big\}^{c,s}\Big\rangle_G \\
& +\Big\langle \mathrm{Tr}\Big\{\, H_i(x+a\hat{0};\vec{p})^\dagger\,\gamma_0\,U_0(x)^\dagger\,H_i(x;\vec{p})\,\gamma_1 Q_{-i}\,\Big\}^{c,s}\Big\rangle_G \\
+\frac{1}{3}\sum_{\alpha=1}^{3}\Big\{ & \lambda_\alpha\Big\langle \mathrm{Tr}\Big\{\, H_i(x;\vec{p})^\dagger\,\gamma_\alpha\,U_\alpha(x)\,H_i(x+a\hat{\alpha};\vec{p})\,\gamma_1 Q_{-i}\,\Big\}^{c,s}\Big\rangle_G \\
& +\lambda_\alpha\Big\langle \mathrm{Tr}\Big\{\, H_i(x-a\hat{\alpha};\vec{p})^\dagger\,\gamma_\alpha\,U_\alpha(x-a\hat{\alpha})\,H_i(x;\vec{p})\,\gamma_1 Q_{-i}\,\Big\}^{c,s}\Big\rangle_G \\
& -\lambda^*_\alpha\Big\langle \mathrm{Tr}\Big\{\, H_i(x;\vec{p})^\dagger\,\gamma_\alpha\,U_\alpha(x-a\hat{\alpha})^\dagger\,H_i(x-a\hat{\alpha};\vec{p})\,\gamma_1 Q_{-i}\,\Big\}^{c,s}\Big\rangle_G \\
& -\lambda^*_\alpha\Big\langle \mathrm{Tr}\Big\{\, H_i(x+a\hat{\alpha};\vec{p})^\dagger\,\gamma_\alpha\,U_\alpha(x)^\dagger\,H_i(x;\vec{p})\,\gamma_1 Q_{-i}\,\Big\}^{c,s}\Big\rangle_G\Big\}\Bigg\}\,.
\end{aligned}
\tag{H.104}
$$

These correlation functions can be now rewritten in terms of only the + component of the quark propagators, as we did before for the basic two-point functions. Proceeding as in previous sections we have the final expressions,

$$
\begin{aligned}
g^{aa}_{O^a_{12}-}(x_0) = \frac{a^3}{a16L^3}\sum_{\vec{x}}\Bigg\{ & \\
& -\lambda_2\Big[\Big\langle \mathrm{Tr}\Big\{\, H_+(x;\vec{p})^\dagger\,\gamma_1\,U_2(x)\,H_+(x+a\hat{2};\vec{p})\,\gamma_2 Q_-\,\Big\}^{c,s}\Big\rangle_G \\
& \quad +\Big\langle \mathrm{Tr}\Big\{\, H_+(x-a\hat{2};\vec{p})^\dagger\,\gamma_1\,U_2(x-a\hat{2})\,H_+(x;\vec{p})\,\gamma_2 Q_-\,\Big\}^{c,s}\Big\rangle_G\Big] \\
& -\lambda_1\Big[\Big\langle \mathrm{Tr}\Big\{\, H_+(x;\vec{p})^\dagger\,\gamma_2\,U_1(x)\,H_+(x+a\hat{1};\vec{p})\,\gamma_2 Q_-\,\Big\}^{c,s}\Big\rangle_G \\
& \quad +\Big\langle \mathrm{Tr}\Big\{\, H_+(x-a\hat{1};\vec{p})^\dagger\,\gamma_2\,U_1(x-a\hat{1})\,H_+(x;\vec{p})\,\gamma_2 Q_-\,\Big\}^{c,s}\Big\rangle_G\Big] \\
& +\lambda^*_2\Big[\Big\langle \mathrm{Tr}\Big\{\, H_+(x;\vec{p})^\dagger\,\gamma_1\,U_2(x-a\hat{2})^\dagger\,H_+(x-a\hat{2};\vec{p})\,\gamma_2 Q_-\,\Big\}^{c,s}\Big\rangle_G \\
& \quad +\Big\langle \mathrm{Tr}\Big\{\, H_+(x+a\hat{2};\vec{p})^\dagger\,\gamma_1\,U_2(x)^\dagger\,H_+(x;\vec{p})\,\gamma_2 Q_-\,\Big\}^{c,s}\Big\rangle_G\Big] \\
& +\lambda^*_1\Big[\Big\langle \mathrm{Tr}\Big\{\, H_+(x;\vec{p})^\dagger\,\gamma_2\,U_1(x-a\hat{1})^\dagger\,H_+(x-a\hat{1};\vec{p})\,\gamma_2 Q_-\,\Big\}^{c,s}\Big\rangle_G \\
& \quad +\Big\langle \mathrm{Tr}\Big\{\, H_+(x+a\hat{1};\vec{p})^\dagger\,\gamma_2\,U_1(x)^\dagger\,H_+(x;\vec{p})\,\gamma_2 Q_-\,\Big\}^{c,s}\Big\rangle_G\Big]\Bigg\}\,,
\end{aligned}
\tag{H.105}
$$

$$
\begin{aligned}
g^{aa}_{O^a_{44}-}(x_0) =& \frac{2a^3}{a16L^3}\,\frac{3}{4}\,\sum_{\vec{x}}\,\Bigg\{ \\
&-\Big\langle \mathrm{Tr}\Big\{\, H_+(x;\vec{p})^\dagger\,\gamma_0\,U_0(x)\,H_+(x+a\hat{0};\vec{p})\,\gamma_1 Q_-\,\Big\}^{c,s}\Big\rangle_G \\
&-\Big\langle \mathrm{Tr}\Big\{\, H_+(x-a\hat{0};\vec{p})^\dagger\,\gamma_0\,U_0(x-a\hat{0})\,H_+(x;\vec{p})\,\gamma_1 Q_-\,\Big\}^{c,s}\Big\rangle_G \\
&+\Big\langle \mathrm{Tr}\Big\{\, H_+(x;\vec{p})^\dagger\,\gamma_0\,U_0(x-a\hat{0})^\dagger\,H_+(x-a\hat{0};\vec{p})\,\gamma_1 Q_-\,\Big\}^{c,s}\Big\rangle_G \\
&+\Big\langle \mathrm{Tr}\Big\{\, H_+(x+a\hat{0};\vec{p})^\dagger\,\gamma_0\,U_0(x)^\dagger\,H_+(x;\vec{p})\,\gamma_1 Q_-\,\Big\}^{c,s}\Big\rangle_G \\
&+\frac{1}{3}\sum_{\alpha=1}^{3}\,\Big\{\lambda_\alpha\Big\langle \mathrm{Tr}\Big\{\, H_+(x;\vec{p})^\dagger\,\gamma_\alpha\,U_\alpha(x)\,H_+(x+a\hat{\alpha};\vec{p})\,\gamma_1 Q_-\,\Big\}^{c,s}\Big\rangle_G \\
&\quad+\lambda_\alpha\Big\langle \mathrm{Tr}\Big\{\, H_+(x-a\hat{\alpha};\vec{p})^\dagger\,\gamma_\alpha\,U_\alpha(x-a\hat{\alpha})\,H_+(x;\vec{p})\,\gamma_1 Q_-\,\Big\}^{c,s}\Big\rangle_G \\
&\quad-\lambda^*_\alpha\Big\langle \mathrm{Tr}\Big\{\, H_+(x;\vec{p})^\dagger\,\gamma_\alpha\,U_\alpha(x-a\hat{\alpha})^\dagger\,H_+(x-a\hat{\alpha};\vec{p})\,\gamma_1 Q_-\,\Big\}^{c,s}\Big\rangle_G \\
&\quad-\lambda^*_\alpha\Big\langle \mathrm{Tr}\Big\{\, H_+(x+a\hat{\alpha};\vec{p})^\dagger\,\gamma_\alpha\,U_\alpha(x)^\dagger\,H_+(x;\vec{p})\,\gamma_1 Q_-\,\Big\}^{c,s}\Big\rangle_G\Big\}\Bigg\}\,.
\end{aligned}
\tag{H.106}
$$

List of Figures

3.1 The strategy for a non-perturbative renormalization via the SF. The scaling factor 's' is typically chosen to be s=2. 33

3.2 Schrödinger functional boundary conditions. 41

6.1 $g_{\mathrm{A}_{0-}}$ vs. am_{PCAC} at four values of z_f (open symbols). All fits are linear in am_{PCAC}. The values of $g_{\mathrm{A}_{0-}}$ at $am_{\mathrm{PCAC}} = 0$, denoted $g^*_{\mathrm{A}_{0-}}$, are also plotted (filled symbols). See data in Tab. D.11. 96

6.2 $g^*_{\mathrm{A}_{0-}}$ vs. z_f (red). The fit is linear in z_f. The value of z_f^c, $z_f(g^*_{\mathrm{A}_{0-}} = 0)$, is also plotted (blue). See data in Tab. D.12. 97

6.3 am_{PCAC} vs. κ at four values of z_f (open symbols). All fits are linear in κ. The values of κ at $am_{\mathrm{PCAC}} = 0$, denoted κ^*, are also plotted (filled symbols). See data in Tab. D.11. 98

6.4 κ^* vs. z_f (red). The fit is linear in z_f. The value of z_f^c (cf. Fig. 6.2) and of κ_c, defined as $\kappa^*(z_f = z_f^c)$, are also plotted (blue). See data in Tab. D.12. 99

6.5 Differences of z_f^c, $\Delta z_f^c(m)$, as determined from different methods (cf. Eq. (6.19)). The differences are always $z_f^c(1)$ minus $z_f^c(m)$, determined from any other method $m = 2 \ldots 7$. The data are presented in Tab. D.19. All extrapolations to the continuum limit are linear in a/L and the point $L/a = 8$ is excluded from all the fits. The results from the fits are presented in Tab. D.20. The points have been plotted slightly displaced from each other amongst the different methods. 101

7.1 Continuum limit of the norm of the quark propagator, $S(x_0, y_0)$, at fixed time slices $(x_0, y_0) = (T/4, T/2)$ and fixed $\vec{\theta} = (1, 0, 0)$. Fit: $y = a_0 + a_1\left(\frac{a}{L}\right)^2 + a_2\left(\frac{a}{L}\right)^4$ (cf. Tab. E.7). All parameters are set to their critical values at tree-level of perturbation theory. The blue point represents the value in the continuum limit, as obtained from the fit. 106

7.2 Continuum limit of the norm of the even operator, $S^{\mathrm{even}}(x_0, y_0) \equiv (S - S^\dagger)(x_0, y_0)$, at fixed time slices $(x_0, y_0) = (T/4, T/2)$ and fixed $\vec{\theta} = (1, 0, 0)$. Fit: $y = a_0 + a_1\left(\frac{a}{L}\right)^2 + a_2\left(\frac{a}{L}\right)^4$ (cf. Tab. E.9). All parameters are set to their critical values at tree-level of perturbation theory. The blue point represents the value in the continuum limit, as obtained from the fit. 107

7.3 Continuum limit of the norm of the quark propagator, $S(x_0, y_0)$, at fixed time slices $(x_0, y_0) = (T/4, T/2)$ and fixed $\vec{\theta} = (1, 1, 1)$. The parameters m_0 and d_s are set to their critical tree-level values, while several values of z_f are considered. The range in the values of z_f is $[0.995, 1.000]$. All fits are of the form: $y = a_0 + a_1\left(\frac{a}{L}\right)^2$ (cf. Tab. E.12). 110

7.4 Same caption as in Fig. 7.3, except that in the present plot the chosen range of z_f is wider than in Fig. 7.3. The range in the values of z_f is now $[0.900, 1.100]$. All fits are of the form: $y = a_0 + a_1\left(\frac{a}{L}\right)^2$ (cf. Tab. E.11). 111

7.5 Same caption as in Fig. 7.4, except that the fits performed in the present plot are of the form: $y = b_0 + b_1\left(\frac{a}{L}\right) + b_2\left(\frac{a}{L}\right)^2 + b_3\left(\frac{a}{L}\right)^3$ (cf. Tab. E.11). 112
7.6 Comparison between different tuning conditions using the $\gamma_5\tau^1$-even quantity $g^{11}_{\mathrm{P}_-}$. Scale NP and $\vec{\theta} = (0,0,0)$. Data for all methods (1) to (7) are presented (cf. Tab. F.1). No continuum limit is performed, since this quantity takes a finite value in the continuum limit only after renormalization. Instead, the purpose of the plot is to compare the results from the different tuning conditions at non-zero lattice spacing. The data from the different methods have been plotted slightly displaced from each other. 115
7.7 Comparison between different tuning conditions using the $\gamma_5\tau^1$-even quantity $g^{12}_{\mathrm{V}_{0-}}$. Scale NP and $\vec{\theta} = (0.5,0.5,0.5)$. Data for all methods (1) to (7) are presented (cf. Tab. F.6). No continuum limit is performed, since this quantity takes a finite value in the continuum limit only after renormalization. Instead, the purpose of the plot is to compare the results from the different tuning conditions at non-zero lattice spacing. The data from the different methods have been plotted slightly displaced from each other. 116
7.8 Approach to the continuum limit of the $\gamma_5\tau^1$-even quantity $g^{11}_{\mathrm{P}_+}$. Scale NP and $\vec{\theta} = (0,0,0)$. Data for all methods (1) to (7) are presented (cf. Tab. F.1). $g^{11}_{\mathrm{P}_+}$ is plotted here as a function of a/L. 117
7.9 Approach to the continuum limit of the $\gamma_5\tau^1$-even quantity $g^{11}_{\mathrm{P}_+}$. Scale NP and $\vec{\theta} = (0.5,0.5,0.5)$. Data for all methods (1) to (7) are presented (cf. Tab. F.6). $g^{11}_{\mathrm{P}_+}$ is plotted as a function of $(a/L)^2$. 118
7.10 Same caption as in Fig. 7.8, except that we plot in this case the $\gamma_5\tau^1$-even quantity $g^{12}_{\mathrm{V}_{0+}}$. 119
7.11 Same caption as in Fig. 7.9, except that we plot in this case the $\gamma_5\tau^1$-even quantity $g^{12}_{\mathrm{V}_{0+}}$. 120
7.12 Extrapolation to the continuum limit of the $\gamma_5\tau^1$-odd quantity $g^{11}_{\mathrm{A}_{0-}}$. Scale NP and $\vec{\theta} = (0,0,0)$. Data for methods (2) to (7) are presented (cf. Tab. F.11). The fits are all linear in a/L (cf. Tab. F.21). The point $L/a = 8$ has been excluded from all the fits. We show the data for all tuning conditions except condition (1) because it corresponds to imposing $g^{11}_{\mathrm{A}_{0-}} = 0$. The continuum limit values obtained from the different tuning conditions have been plotted slightly displaced from each other. 121
7.13 Extrapolation to the continuum limit of the $\gamma_5\tau^1$-odd quantity $g^{11}_{\mathrm{A}_{0-}}$. Scale NP and $\vec{\theta} = (0.5,0.5,0.5)$. Data for methods (1) and (3) to (7) are presented (cf. Tab. F.16). The fits are all linear in a/L (cf. Tab. F.21). The point $L/a = 8$ has been excluded from all the fits. We show the data for all tuning conditions except condition (2) because it corresponds to imposing $g^{11}_{\mathrm{A}_{0-}} = 0$. The continuum limit values obtained from the different tuning conditions have been plotted slightly displaced from each other. 122
7.14 Extrapolation to the continuum limit of the $\gamma_5\tau^1$-odd quantity $\overline{g}^{12}_{\mathrm{V}_{k-}}$. Scale NP and $\vec{\theta} = (0,0,0)$. Data for methods (1) to (3) and (5) to (7) are presented (cf. Tab. F.11). The fits are all linear in a/L (cf. Tab. F.22). The point $L/a = 8$ has been excluded from all the fits. We show the data for all tuning conditions except condition (4) because it corresponds to imposing $\overline{g}^{12}_{\mathrm{V}_{k-}} = 0$. The continuum limit values obtained from the different tuning conditions have been plotted slightly displaced from each other. 123

7.15 Extrapolation to the continuum limit of the $\gamma_5\tau^1$-odd quantity $\overline{g}^{12}_{\mathrm{V}_{k-}}$. Scale NP and $\vec{\theta} = (0.5, 0.5, 0.5)$. Data for methods (1) to (4) and (6) to (7) are presented (cf. Tab. F.16). The fits are all linear in a/L (cf. Tab. F.22). The point $L/a = 8$ has been excluded from all the fits. We show the data for all tuning conditions except condition (5) because it corresponds to imposing $\overline{g}^{12}_{\mathrm{V}_{k-}} = 0$. The continuum limit values obtained from the different tuning conditions have been plotted slightly displaced from each other. 124

8.1 Lattice SSF of the pseudo-scalar density and continuum limit values. Results are shown for the χSF with standard Wilson fermions and the SF with improved and standard Wilson fermions, at the intermediate and perturbative scales and for $\vec{\theta} = (0.5, 0.5, 0.5)$. The extrapolations to the continuum limit are performed according to Tab. 8.4: linear in $(a/L)^2$ for the χSF and the SF with improved fermions and linear in a/L for the SF with standard Wilson fermions. The data from the SF have been slightly displaced to the right and left, respectively, for the improved and unimproved formulations. 134

8.2 Continuum limit extrapolation of the SSF of the pseudo-scalar density. Only χSF data are shown, both for $\theta_1 \equiv \vec{\theta} = (0.5, 0.5, 0.5)$ and $\theta_2 \equiv \vec{\theta} = (1, 0, 0)$, at the intermediate and perturbative scales. The extrapolations to the continuum limit are linear in $(a/L)^2$ as shown in Tab. 8.4 and Tab. 8.5. The values in the continuum limit are also plotted. The data from θ_2 have been slightly displaced to the left. 135

8.3 Continuum limit extrapolation of the SSF of the pseudo-scalar density. Results are shown for the χSF with standard Wilson fermions and the SF with improved Wilson fermions, at the intermediate and perturbative scales and for $\vec{\theta} = (0.5, 0.5, 0.5)$. The extrapolations to the continuum limit are linear in $(a/L)^2$ for all cases. The results from the fits are presented in Tab. 8.4. The data from the SF have been slightly displaced to the left. 136

9.1 Numerical results for $Z_{\mathrm{P}}(g_0, L/a)$ at scale $L = 1.436\, r_0$ and for several β values. $\vec{\theta} = (0.5, 0.5, 0.5)$. Results are shown for the χSF with standard Wilson fermions (cf. Tab. 9.1) and for the SF with improved Wilson fermions, as taken from [97]. The fitting curves are also plotted (cf. Eq. (9.6) and Tab. (9.2)). 140

9.2 $(am_{\mathrm{PS}})^2$ vs. $a\mu$ at three values of β. The data are obtained from Tab. 9.5 and Tab. 9.6, as taken from [103], and correspond to the PION definition of the critical mass. The interpolations are performed according to Eq. (9.8), considering all the points shown in the plot. The coefficients of the fits may be read off from Tab. 9.7. In the small box we zoom the area around the Kaon mass. 143

9.3 $(am_{\mathrm{PS}})^2$ vs. $a\mu$ at two values of β. The data are obtained from Tab. 9.5 and Tab. 9.6, as taken from [103], and correspond to the PCAC definition of the critical mass. The interpolations are performed according to Eq. (9.8), considering all the points shown in the plot. The coefficients of the fits may be read off from Tab. 9.7. In the small box we zoom the area around the Kaon mass. 144

9.4 $(am_{\mathrm{PS}})^2$ vs. $a\mu$ at three values of β. The data are obtained from Tab. 9.5 and Tab. 9.6, as taken from [103], and correspond to the PION definition of the critical mass. The interpolations are linear in $a\mu$ and only the three points closest to the interpolation value (cf. Tab. 9.10) have been considered in the fit. The coefficients of the fits may be read off from Tab. 9.8. In the small box we zoom the area around the Kaon mass. 145

9.5 $(am_{\rm PS})^2$ vs. $a\mu$ at two values of β. The data are obtained from Tab. 9.5 and Tab. 9.6, as taken from [103], and correspond to the PCAC definition of the critical mass. The interpolations are linear in $a\mu$ and only the three points closest to the interpolation value (cf. Tab. 9.10) have been considered in the fit. The coefficients of the fits may be read off from Tab. 9.8. In the small box we zoom the area around the Kaon mass. 146

9.6 $r_0(M_{\rm s}+\hat{M})$ vs. $(a/r_0)^2$, at the physical value of the Kaon mass, $m_{\rm K}=495$MeV. The extrapolations to the continuum limit are performed with linear fits in $(a/r_0)^2$. The values in the continuum limit are also plotted. Results are shown for the χSF with standard Wilson fermions, for the two definitions of the critical mass, and also for the SF with improved Wilson fermions [99]. The data for the χSF have been plotted slightly displaced to the right and left, respectively, for the PCAC and PION definitions of the critical mass. 150

10.1 Continuum limit extrapolation of the SSF of the operator O_{12}. Only χSF data are shown, both for $\theta_1\equiv\vec{\theta}=(0.5,0.5,0.5)$ and $\theta_2\equiv\vec{\theta}=(1,0,0)$, at the intermediate and perturbative scales. The extrapolations to the continuum limit are linear in $(a/L)^2$ as shown in Tab. 10.5 and Tab. 10.6. The values in the continuum limit are also plotted. The data from θ_2 have been plotted slightly displaced to the left. 164

10.2 Continuum limit extrapolation of the SSF of the operator O_{44}. Only χSF data are shown, both for $\theta_1\equiv\vec{\theta}=(0.5,0.5,0.5)$ and $\theta_2\equiv\vec{\theta}=(1,0,0)$, at the intermediate and perturbative scales. The extrapolations to the continuum limit are linear in $(a/L)^2$ as shown in Tab. 10.5 and Tab. 10.6. The values in the continuum limit are also plotted. The data from θ_2 have been plotted slightly displaced to the left. 165

10.3 Continuum limit approach of the SSF of the operator O_{12}. Data are shown for the χSF with standard Wilson fermions and for the SF with improved and standard Wilson fermions, at the intermediate scale and for $\vec{\theta}=(1,0,0)$. The continuum limit is performed according to Tab. 10.6: linear in $(a/L)^2$ for the χSF and linear in a/L for the SF with both regularizations. The continuum limit values are also plotted. The data from the SF have been plotted slightly displaced to the right and left, respectively, for the improved and unimproved formulations. 166

10.4 Continuum limit approach of the SSF of the operator O_{44}. Data are shown for the χSF with standard Wilson fermions and for the SF with improved and standard Wilson fermions, at the intermediate scale and for $\vec{\theta}=(1,0,0)$. The continuum limit is performed according to Tab. 10.6: linear in $(a/L)^2$ for the χSF and linear in a/L for the SF with both regularizations. The continuum limit values are also plotted. The data from the SF have been plotted slightly displaced to the right and left, respectively, for the improved and unimproved formulations. 167

10.5 Numerical results for $Z_{\rm O_{12}}(g_0,L/a)$ at scale $L=1.436\,r_0$ and for several β values. $\vec{\theta}=(1,0,0)$. Results are shown for the χSF with standard Wilson fermions (cf. Tab. 10.1) and for the SF with standard and improved Wilson fermions, as taken from [74]. The fitting curves are also plotted (cf. Eq. (10.39) and Tab. (10.7)). . 169

10.6 Numerical results for $Z_{\rm O_{44}}(g_0,L/a)$ at scale $L=1.436\,r_0$ and for several β values. $\vec{\theta}=(1,0,0)$. Results are shown for the χSF with standard Wilson fermions (cf. Tab. 10.2) and for the SF with standard and improved Wilson fermions, as taken from [74]. The fitting curves are also plotted (cf. Eq. (10.39) and Tab. (10.7)). . 170

11.1 MC history of the plaquette at the perturbative scale, $\overline{g}^2 = 0.9944$, and for a lattice with $2L/a = 32$ number of points. The thermalization region is identified with the plateau of the plaquette in MC time. The plaquette is clearly thermalized after the trajectory number 500. 175
11.2 Euclidean-time dependence of the PCAC mass for three different replicas (rep0, rep1 and rep5). These correspond to the perturbative value of the renormalization scale and the lattices $2L/a = 32$. $\vec{\theta} = (0.5, 0.5, 0.5)$. While the data from rep1 show the expected plateau behavior, the data form rep0 and rep5 deviate from the expected behavior. 178
11.3 MC-time history of the fermionic correlation function $g^{11}_{\mathrm{A}_{0-}}(T/2)$ for three different replicas (rep0, rep1 and rep5). These correspond to the perturbative value of the renormalization scale and the lattices $2L/a = 32$. $\vec{\theta} = (0.5, 0.5, 0.5)$. The MC-time interval shown in the plot corresponds to the 50 gauge configurations which were used in the analysis of the data. 179
11.4 Same caption as in Fig. 11.3 but for the fermionic correlation function $g^{11}_{\mathrm{P}_-}(T/2)$. 180
11.5 MC-time history of the plaquette for three different replicas (rep0, rep1 and rep5). These correspond to the perturbative value of the renormalization scale and the lattices $2L/a = 32$. The MC-time interval shown in the plot corresponds to the 50 gauge configurations which were used in the analysis of the fermionic quantities. 181
11.6 MC-time history of the classical gauge action, S_{G}, for three different replicas (rep0, rep1 and rep5) and after 200 cooling iterations. The replicas correspond to the perturbative value of the renormalization scale and the lattices $2L/a = 32$. The MC-time interval shown in the plot contains the 50 gauge configurations which were used in the analysis of the fermionic quantities (corresponding in this plot to $0 \leq t_{\mathrm{MC}} \leq 49$). 183
11.7 Same caption as in Fig. 11.6 but plotting in the y-axis the absolute value of the topological charge, $|Q_{\mathrm{top}}|$. 184

List of Tables

2.1 Definition of the transformations of the chiral group. Note that, with abuse of notation, we denote here $\mathrm{SU}(N_f)_A$ the non-singlet axial-vector transformations. Such transformations, however, do not have a group structure. 12

2.2 Symmetries of Wilson and twisted mass Wilson fermions, with mass degeneracy. For notation and definition of the symmetries see App. B.1 and App. B.2. 28

6.1 Fixed parameters during the tuning. 91

6.2 Results from the tuning at a hadronic, intermediate and perturbative scale. We give the critical values, z_f^c and κ_c, calculated in this work for the χSF. These results have been obtained using method (1*) (see Tab. D.1, Tab. D.2 and Tab. D.3). For reference, we also give κ_c for the SF [73, 95, 96]. 95

6.3 Summary of all the points where the tuning was performed. The references in the last column correspond to the tables where all results are presented. 100

8.1 Renormalization factors of the pseudo-scalar density, Z_{P}, at $\vec{\theta} = (0.5, 0.5, 0.5)$ and $\vec{\theta} = (1, 0, 0)$. Results are shown for the χSF with standard Wilson fermions at three values of the renormalization scale and for several values of the lattice spacing. 131

8.2 SSF of the pseudo-scalar density at finite lattice spacing, $\Sigma_{\mathrm{P}}(2, u, a/L)$. Results are shown for the χSF with standard Wilson fermions and also for the SF with improved and standard Wilson fermions [96] at two values of the renormalization scale and for several values of the lattice spacing. $\vec{\theta} = (0.5, 0.5, 0.5)$. 131

8.3 SSF of the pseudo-scalar density at finite lattice spacing, $\Sigma_{\mathrm{P}}(2, u, a/L)$. Results are shown for the χSF with standard Wilson fermions at two values of the renormalization scale and for several values of the lattice spacing. $\vec{\theta} = (1, 0, 0)$. 131

8.4 Continuum limit of the SSF of the pseudo-scalar density. Results are shown for the χSF with standard Wilson fermions and also for the SF with improved and standard Wilson fermions at two values of the renormalization scale. $\vec{\theta} = (0.5, 0.5, 0.5)$. These results correspond to linear fits of the data in Tab. 8.2. The fit is linear in a/L for the SF(Wilson) formulation while it is linear in $(a/L)^2$ for the χSF and SF(Clover) formulations. 133

8.5 Continuum limit of the SSF of the pseudo-scalar density. Results are shown for the χSF with standard Wilson fermions at two values of the renormalization scale. $\vec{\theta} = (1, 0, 0)$. These results correspond to linear fits in $(a/L)^2$ of the data in Tab. 8.3. 133

9.1 $Z_{\mathrm{P}}(g_0, L/a)$ at $L = 1.436\, r_0$ and for $\vec{\theta} = (0.5, 0.5, 0.5)$. 138

9.2 Coefficients of the beta dependence of $Z_{\mathrm{P}}(g_0, L/a)$ at the matching scale $L = 1.436\, r_0$ (cf. Eq. (9.6)) and $Z_{\mathrm{M}}(g_0)$ (cf. Eq. (9.7)). Results are shown for the χSF with standard Wilson fermions at $\vec{\theta} = (0.5, 0.5, 0.5)$. 139

9.3 $Z_{\mathrm{P}}^{-1}(g_0, L/a)$ at $L = 1.436\, r_0$ and $Z_{\mathrm{M}}(g_0)$, for $\vec{\theta} = (0.5, 0.5, 0.5)$. Results are shown for the χSF formulation and for all the β values where simulations have been performed. 139

9.4 $Z_{\rm P}(g_0, L/a)$ at $L = 1.436\, r_0$ and $Z_{\rm M}(g_0)$, for $\vec{\theta} = (0.5, 0.5, 0.5)$. Results are presented for the χSF formulation at several β values, as determined from the curves in Eq. (9.6) and Eq. (9.7). 140
9.5 Simulation parameters and statistics ($N_{\rm meas}$). Table taken from [103]. 141
9.6 Pseudo-Scalar meson masses $m_{\rm PS}a$ for all simulation points. Table taken from [103]. 142
9.7 Fit parameters for $(am_{\rm PS})^2$ vs. $a\mu$. The fitting function is of the form given in Eq. (9.8). 147
9.8 Fit parameters for $(am_{\rm PS})^2$ vs. $a\mu$. This is a linear fit considering only the three closest points to the interpolation value. 147
9.9 r_0/a and relative uncertainty, $\Delta(r_0/a)$, at several values of β. 148
9.10 $(am_{\rm K})^2$ at particular values of β. 148
9.11 $a\mu_{\rm ref}$ at the value of the Kaon mass and for particular values of β. Results are shown for the pion and the PCAC definitions of the critical mass. 148
9.12 $\mu_{\rm ref}\, r_0$ at the value of the Kaon mass and for particular values of β. Results are shown for the pion and the PCAC definitions of the critical mass. 149
9.13 $r_0\,(M_{\rm s} + \hat{M}) = Z_{\rm M}(2\mu_{\rm ref}\, r_0)$ at several values of β. Results are shown for the pion and the PCAC definitions of the critical mass. 149

10.1 Renormalization factors $Z_{\rm O_{12}}$ for $\vec{\theta} = (0.5, 0.5, 0.5)$ and $\vec{\theta} = (1, 0, 0)$. Results are shown for the χSF with standard Wilson fermions at three values of the renormalization scale and for several values of the lattice spacing. 161
10.2 Renormalization factors $Z_{\rm O_{44}}$ for $\vec{\theta} = (0.5, 0.5, 0.5)$ and $\vec{\theta} = (1, 0, 0)$. Results are shown for the χSF with standard Wilson fermions at three values of the renormalization scale and for several values of the lattice spacing. 162
10.3 SSF of O_{12} and O_{44} at finite lattice spacing, $\Sigma_{\rm O_{12}}$ and $\Sigma_{\rm O_{44}}$. Results are shown for the χSF with standard Wilson fermions at two values of the renormalization scale and for several values of the lattice spacing. $\vec{\theta} = (0.5, 0.5, 0.5)$. 162
10.4 SSF of O_{12} and O_{44} at finite lattice spacing, $\Sigma_{\rm O_{12}}$ and $\Sigma_{\rm O_{44}}$. Results are shown for the χSF with standard Wilson fermions and also for the SF [73] with improved and standard Wilson fermions at two values of the renormalization scale and for several values of the lattice spacing. $\vec{\theta} = (1, 0, 0)$. 162
10.5 Continuum limit of the SSF, $\sigma_{\rm O_{12}}$ and $\sigma_{\rm O_{44}}$, of the operators O_{12} and O_{44}. Results are shown for the χSF with standard Wilson fermions at two values of the renormalization scale. $\vec{\theta} = (0.5, 0.5, 0.5)$. These results correspond to linear fits of the data in Tab. 10.3. The fits are linear in $(a/L)^2$. 163
10.6 Continuum limit of the SSF, $\sigma_{\rm O_{12}}$ and $\sigma_{\rm O_{44}}$, of the operators O_{12} and O_{44}. Results are shown for the χSF with standard Wilson fermions and also for the SF with improved and standard Wilson fermions at two values of the renormalization scale. $\vec{\theta} = (1, 0, 0)$. These results correspond to linear fits of the data in Tab. 10.4. The fits are linear in $(a/L)^2$ for the χSF formulation while they are linear in a/L for the SF. 164
10.7 Coefficients of the beta-dependence of $Z_{\rm O_{12}}$ and $Z_{\rm O_{44}}$ at the matching scale $L = 1.436\, r_0$. Results are shown for the χSF with standard Wilson fermions at $\vec{\theta} = (1, 0, 0)$ and $\vec{\theta} = (0.5, 0.5, 0.5)$ and also for the SF [74] with improved and standard Wilson fermions at $\vec{\theta} = (1, 0, 0)$. 168
10.8 RGI renormalization factors, $Z^{\rm RGI}_{\rm O_{12}}(g_0)$ and $Z^{\rm RGI}_{\rm O_{44}}(g_0)$ for $\vec{\theta} = (1, 0, 0)$. Results are shown for the χSF with standard Wilson fermions and the SF with improved and standard Wilson fermions, for several values of the lattice spacing. We have determined in this work the RGI Z-factors for the SF from the Z-factors given in [74]. 171

10.9 Coefficients of the beta-dependence of $Z^{\mathrm{RGI}}_{\mathrm{O}_{12}}(g_0)$ and $Z^{\mathrm{RGI}}_{\mathrm{O}_{44}}(g_0)$. Results are shown for the χSF with standard Wilson fermions and the SF with improved and standard Wilson fermions at $\vec{\theta} = (1, 0, 0)$. 171
10.10 $Z_{\mathrm{O}}(g_0, L/a)$ at scale $L = 1.436\, r_0$ and $Z^{\mathrm{RGI}}_{\mathrm{O}}(g_0)$, for O_{12} and O_{44}. $\vec{\theta} = (1, 0, 0)$. Results are presented for the χSF with standard Wilson fermions and the SF with improved and standard Wilson fermions. 172

11.1 Renormalization factors, $Z_{\mathrm{P}}(g_0, L/a)$ and $Z_{\mathrm{P}}(g_0, 2L/a)$, and the corresponding lattice SSF, $\Sigma_{\mathrm{P}}(2, u, a/L)$, of the pseudo-scalar density for $\vec{\theta} = (0.5, 0.5, 0.5)$. We present results for the Z-factors only for the χSF. We show the SSF for χSF and the SF [96] with improved and standard Wilson fermions. Results are presented at two values of the renormalization scale, intermediate and perturbative scales. The emphasized data are the cases that brought as to understand that there was a problem. The data marked with a star correspond to the ensembles which indeed had problems. 176
11.2 Renormalization factors of the pseudo-scalar density, $Z_{\mathrm{P}}(g_0, 2L/a)$, and lattice SSF, $\Sigma_{\mathrm{P}}(2, u, a/L)$, for $\vec{\theta} = (0.5, 0.5, 0.5)$. Data are shown only for the χSF formulation at two values of the renormalization scale, intermediate and perturbative, and three values of β. We show the values obtained for each replica as well as the average over all the replicas, which is denoted as 'all' (cf. Tab. 11.1). The data marked with a star correspond to the ensembles which indeed had problems. 177

D.1 Values of κ and z_f used as guess for the tuning and number of configurations, N_{conf}, used in all calculations at the corresponding value of β. Scale NP. The data of the last three columns have been used only for a separate analysis with method (1), which we denote here as method (1*). 215
D.2 Same caption as in Tab. D.1 but at scale I. 216
D.3 Same caption as in Tab. D.1 but at scale P. 216
D.4 Same caption as in Tab. D.1 but at scale 2P. Here no separate tuning was performed for method (1). 216
D.5 Same caption as in Tab. D.1 but at scale PP. Here no separate tuning was performed for method (1). 217
D.6 Final results of the tuning of κ and z_f at the NP scale. Results for all the methods (1) to (7) are shown (see Sec. 6.1 for a description of all the methods). The results of method (1*) are obtained from method (1) but using slightly different simulation parameters (see Tab. D.1). 218
D.7 Same caption as in Tab. D.6 but at scale I. 218
D.8 Same caption as in Tab. D.6 but at scale P. 219
D.9 Same caption as in Tab. D.6 but at scale 2P. 219
D.10 Same caption as in Tab. D.6 but at scale PP. 219
D.11 Tuning parameters and results for the intermediate step of the tuning at $L = 1.436\, r_0$. These data are obtained from a linear interpolation of $g_{A_{0-}}$ and κ, in either case, in the PCAC mass. We have denoted with $*$ the value of the corresponding quantity, $g_{A_{0-}}$ or κ, at which the PCAC mass vanishes. These data correspond to method (1*) (see caption in Tab. D.1). See also Sec. 6.2. . . . 220
D.12 Tuning parameters and final results at $L = 1.436\, r_0$. These data are obtained from a linear interpolation of $g^*_{A_{0-}}$ and κ^*, as taken from Tab. D.11, in z_f. First the critical value of z_f, z_f^c, is obtained by an interpolation to $g^*_{A_{0-}} = 0$. Then, κ_c is determined by interpolating to the previously determined z_f^c. These data correspond to method (1*) (see caption in Tab. D.1). See also Sec. 6.2. 220

D.13 Same as in caption of Tab. D.11 but at $\bar{g}^2 = 2.4484$. 221
D.14 Same as in caption of Tab. D.12 but at $\bar{g}^2 = 2.4484$. The values $*$ which are used in the interpolation, are here taken from Tab. D.13. 221
D.15 Same as in caption of Tab. D.11 but at $\bar{g}^2 = 0.9944$. 221
D.16 Same as in caption of Tab. D.12 but at $\bar{g}^2 = 0.9944$. The values $*$ which are used in the interpolation, are here taken from Tab. D.15. 222
D.17 Summary table of κ_c for all beta values and tuning conditions, (1) to (7) (see Sec. 6.1 for a description of all the methods). The data of column (1*) correspond to a separate analysis with method (1), using slightly different simulation parameters (cf. Tab. D.1, Tab. D.2 and Tab. D.3). 223
D.18 Summary table of z_f^c for all beta values and tuning conditions, (1) to (7) (see Sec. 6.1 for a description of all the methods). The data of column (1*) correspond to a separate analysis with method (1), using slightly different simulation parameters (cf. Tab. D.1, Tab. D.2 and Tab. D.3). 224
D.19 Differences of z_f^c, $\Delta z_f^c(m)$, determined from different methods. The differences are always $z_f^c(1)$ minus $z_f^c(m)$, obtained from any other method $m = 2 \ldots 7$. Scale NP. 225
D.20 Continuum limit of the data presented in Tab. D.19. We have performed a linear fit in a/L. The point $L/a = 8$ is not included in the fit. 225

E.1 Continuum limit of the norm of the quark propagator, S, at fixed time slices, (x_0, y_0), and $\vec{\theta} = (1, 1, 1)$. The line with 'cont' refers to the numbers obtained by directly evaluating the analytic expression in the continuum. See Sec. 7.1 for explanations. 227
E.2 Continuum limit of the norm of the even operator $S - S^\dagger$, at fixed time slices, (x_0, y_0), and $\vec{\theta} = (1, 1, 1)$. The line with 'cont' refers to the numbers obtained by directly evaluating the analytic expression in the continuum. See Sec. 7.1 for explanations. 227
E.3 Same caption as in Tab. E.1 but with $\vec{\theta} = (1, 1, 0)$. 227
E.4 Same caption as in Tab. E.2 but with $\vec{\theta} = (1, 1, 0)$. 228
E.5 Same caption as in Tab. E.1 but with $\vec{\theta} = (1, 0, 0)$. 228
E.6 Same caption as in Tab. E.2 but with $\vec{\theta} = (1, 0, 0)$. 228
E.7 Fit of the data presented in Tab. E.5. Continuum limit of the norm of the quark propagator, S, at fixed time slices, (x_0, y_0), and $\vec{\theta} = (1, 0, 0)$. The line with 'cont' refers to the numbers obtained by directly evaluating the analytic expression in the continuum. This line is to be compared to the line of a_0. The data are plotted in Fig. 7.1 for the time slices $(T/4, 2T/4)$. 228
E.8 Fit of the data presented in Tab. E.5. Continuum limit of the norm of the quark propagator, S, at fixed time slices, (x_0, y_0), and $\vec{\theta} = (1, 0, 0)$. The line with 'cont' refers to the numbers obtained by directly evaluating the analytic expression in the continuum. This line is to be compared to the line of b_0. 229
E.9 Fit of the data presented in Tab. E.6. Continuum limit of the norm of the even operator $S - S^\dagger$, at fixed time slices, (x_0, y_0), and $\vec{\theta} = (1, 0, 0)$. The line with 'cont' refers to the numbers obtained by directly evaluating the analytic expression in the continuum. This line is to be compared to the line of a_0. The data are plotted in Fig. 7.2 for the time slices $(T/4, 2T/4)$. 229
E.10 Fit of the data presented in Tab. E.6. Continuum limit of the norm of the even operator $S - S^\dagger$, at fixed time slices, (x_0, y_0), and $\vec{\theta} = (1, 0, 0)$. The line with 'cont' refers to the numbers obtained by directly evaluating the analytic expression in the continuum. This line is to be compared to the line of b_0. 229

E.11 Continuum limit of the norm of the quark propagator, S, at fixed time slices, $(T/4, 2T/4)$, and $\vec{\theta} = (1,1,1)$, for several values of z_f. We have performed two fits of the data, excluding the pont $L/a = 4$: a cubic fit in a/L and a linear fit in $(\frac{a}{L})^2$. The line with 'cont' refers to the numbers obtained by directly evaluating the analytic expression in the continuum. This line is to be compared to the line of a_0 or b_0, depending on the fit. See Sec. 7.1.2 for more explanations. 230

E.12 Continuum limit of the norm of the quark propagator, S, at fixed time slices, $(T/4, 2T/4)$, and $\vec{\theta} = (1,1,1)$, for several values of z_f. We have fitted the data using a linear fit in $(\frac{a}{L})^2$ and the point $L/a = 4$ has been neglected. The line with 'cont' refers to the numbers obtained by directly evaluating the analytic expression in the continuum. This line is to be compared to the line of a_0. See Sec. 7.1.2 for more explanations. 231

F.1 Results for the $\gamma_5\tau^1$-even correlation functions, $g^{11}_{\mathrm{P}_\pm}$, $g^{12}_{\mathrm{V}_{0\pm}}$ and g^{11}_1, at scale $L = 1.436\, r_0$ and for $\vec{\theta} = (0,0,0)$. The data have been obtained via linear interpolations to the critical values of κ and quadratic interpolations to the critical values of z_f for all the tuning methods (1) to (7). See Sec. 7.2.1 and Sec. 7.2.2 for explanations. 234

F.2 Same caption as in Tab. F.1 but at scale $\overline{g}^2 = 2.4484$. 234

F.3 Same caption as in Tab. F.1 but at scale $\overline{g}^2 = 0.9944$. 235

F.4 Same caption as in Tab. F.1 but at scale 2P. 235

F.5 Same caption as in Tab. F.1 but at scale PP. 235

F.6 Same caption as in Tab. F.1 but at $\vec{\theta} = (0.5, 0.5, 0.5)$. The values denoted with (1*) have been obtained by direct simulations at the critical values of κ and z_f. See Chap. 6 for explanation of (1*). 237

F.7 Same caption as in Tab. F.6 but at scale $\overline{g}^2 = 2.4484$. 237

F.8 Same caption as in Tab. F.6 but at scale $\overline{g}^2 = 0.9944$. 238

F.9 Same caption as in Tab. F.1 but at scale 2P and $\vec{\theta} = (0.5, 0.5, 0.5)$. 238

F.10 Same caption as in Tab. F.1 but at scale PP and $\vec{\theta} = (0.5, 0.5, 0.5)$. 238

F.11 Results for the $\gamma_5\tau^1$-odd correlation functions, $g^{11}_{\mathrm{A}_{0-}}$ and $\overline{g}^{12}_{\mathrm{V}_{k-}}$, at scale $L = 1.436\, r_0$ and for $\vec{\theta} = (0,0,0)$. The data have been obtained via linear interpolations to the critical values of κ and z_f for all the tuning methods (1) to (7). The lines represent the cases where the corresponding quantity has been used as tuning condition. See Sec. 7.2.3 for explanations. 240

F.12 Same caption as in Tab. F.11 but at scale $\overline{g}^2 = 2.4484$. 240

F.13 Same caption as in Tab. F.11 but at scale $\overline{g}^2 = 0.9944$. 240

F.14 Same caption as in Tab. F.11 but at scale 2P. 241

F.15 Same caption as in Tab. F.11 but at scale PP. 241

F.16 Same caption as in Tab. F.11 but at $\vec{\theta} = (0.5, 0.5, 0.5)$. The values denoted with (1*) have been obtained by direct simulations at the critical values of κ and z_f. See Chap. 6 for explanation of (1*). 242

F.17 Same caption as in Tab. F.16 but at scale $\overline{g}^2 = 2.4484$. 243

F.18 Same caption as in Tab. F.16 but at scale $\overline{g}^2 = 0.9944$. 243

F.19 Same caption as in Tab. F.11 but at scale 2P and $\vec{\theta} = (0.5, 0.5, 0.5)$. 244

F.20 Same caption as in Tab. F.11 but at scale PP and $\vec{\theta} = (0.5, 0.5, 0.5)$. 244

F.21 Continuum limit of $g^{11}_{\mathrm{A}_{0-}}$ for all definitions of z_f^c from (1) to (7). Scale NP. Results are shown for $\vec{\theta} = (0,0,0)$ and $\vec{\theta} = (0.5,0.5,0.5)$, as obtained from linear fits of the data in Tab. F.11 and Tab. F.16, respectively. The fits are linear in a/L and the point $L/a = 8$ is excluded in all cases. The lines represent the cases where the corresponding quantity has been used as tuning condition. See Sec. 7.2.3 for more explanations. 244
F.22 Same caption as in Tab. F.21 but for $\overline{g}^{12}_{\mathrm{V}_{k-}}$. 245

G.1 Results for $Z_{\mathrm{P}}(g_0, L/a)$ at scale $L = 1.436\, r_0$ and for $\vec{\theta} = (0.5,0.5,0.5)$. The data have been obtained via interpolations to the critical values of κ and z_f for all the tuning methods (1) to (7). The values denoted with (1*) have been obtained by direct simulations at the critical values of κ and z_f. See Chap. 6 for explanations on the tuning conditions and Chap. 8 for definition and discussion of Z_{P}. 248
G.2 Same caption as in Tab. G.1 but at scale $\overline{g}^2 = 2.4484$. 248
G.3 Same caption as in Tab. G.1 but at scale $\overline{g}^2 = 0.9944$. 249
G.4 Same caption as in Tab. G.1 but at scale 2P. 249
G.5 Same caption as in Tab. G.1 but at scale PP. 249

Bibliography

[1] H. Fritzsch, M. Gell-Mann, and H. Leutwyler. Advantages of the color octet gluon picture. *Phys. Lett.*, B47:365–368, 1973. doi: 10.1016/0370-2693(73)90625-4.

[2] C.-N. Yang and R. L. Mills. Conservation of isotopic spin and isotopic gauge invariance. *Phys. Rev.*, 96:191–195, 1954.

[3] M. Gell-Mann. A schematic model of baryons and mesons. *Phys. Lett.*, 8:214–215, 1964. doi: 10.1016/S0031-9163(64)92001-3.

[4] G. Zweig. An SU(3) model for strong interaction symmetry and its breaking. *CERN-TH-401*, 1981.

[5] G. 't Hooft. The renormalization procedure for Yang-Mills fields. *Unpublished*, 1972.

[6] D. J. Gross and F. Wilczek. Ultraviolet behavior of non-abelian gauge theories. *Phys. Rev. Lett.*, 30:1343–1346, 1973. doi: 10.1103/PhysRevLett.30.1343.

[7] H. D. Politzer. Reliable perturbative results for strong interactions? *Phys. Rev. Lett.*, 30: 1346–1349, 1973. doi: 10.1103/PhysRevLett.30.1346.

[8] R. P. Feynman. Space-time approach to nonrelativistic quantum mechanics. *Rev. Mod. Phys.*, 20:367–387, 1948.

[9] M. Creutz. Monte Carlo study of quantized SU(2) gauge theory. *Phys. Rev.*, D21:2308–2315, 1980. doi: 10.1103/PhysRevD.21.2308.

[10] K. G. Wilson. Confinement of quarks. *Phys. Rev.*, D10:2445–2459, 1974.

[11] M. Lüscher, P. Weisz, and U. Wolff. A numerical method to compute the running coupling in asymptotically free theories. *Nucl. Phys.*, B359:221–243, 1991. doi: 10.1016/0550-3213(91)90298-C.

[12] M. Lüscher, R. Narayanan, P. Weisz, and U. Wolff. The Schrödinger functional: a renormalizable probe for nonabelian gauge theories. *Nucl. Phys.*, B384:168–228, 1992.

[13] M. Lüscher, R. Sommer, U. Wolff, and P. Weisz. Computation of the running coupling in the SU(2) Yang- Mills theory. *Nucl. Phys.*, B389:247–264, 1993. doi: 10.1016/0550-3213(93)90292-W.

[14] M. Lüscher, R. Sommer, P. Weisz, and U. Wolff. A precise determination of the running coupling in the SU(3) Yang-Mills theory. *Nucl. Phys.*, B413:481–502, 1994. doi: 10.1016/0550-3213(94)90629-7.

[15] S. Sint. On the Schrödinger functional in QCD. *Nucl. Phys.*, B421:135–158, 1994.

[16] S. Sint. One loop renormalization of the QCD Schrödinger functional. *Nucl. Phys.*, B451: 416–444, 1995.

[17] S. Sint and R. Sommer. The running coupling from the QCD Schrödinger functional: a one loop analysis. *Nucl. Phys.*, B465:71–98, 1996. doi: 10.1016/0550-3213(96)00020-X.

[18] S. Sint. The Schrödinger functional with chirally rotated boundary conditions. *PoS*, LAT2005:235, 2006.

[19] R. Frezzotti and G. C. Rossi. Chirally improving Wilson fermions III. The Schrödinger functional. *hep-lat/0507030*, 2005.

[20] K. G. Wilson. The renormalization group: Critical phenomena and the kondo problem. *Rev. Mod. Phys.*, 47:773, 1975.

[21] K. Symanzik. Some topics in quantum field theory. *Presented at 6th Int. Conf. on Mathematical Physics, Berlin, West Germany, Aug 11-21, 1981*, 1981.

[22] K. Symanzik. Continuum limit and improved action in lattice theories. 1. principles and phi**4 theory. *Nucl. Phys.*, B226:187, 1983.

[23] K. Symanzik. Continuum limit and improved action in lattice theories. 2. o(n) nonlinear sigma model in perturbation theory. *Nucl. Phys.*, B226:205, 1983.

[24] R. Frezzotti and G. C. Rossi. Chirally improving wilson fermions. 1. o(a) improvement. *JHEP*, 08:007, 2004.

[25] J. González López, K. Jansen, and A. Shindler. Analysis of the Schrödinger functional with chirally rotated boundary conditions. *POS*, LATTICE2008:242, 2008.

[26] Stefan Sint. The chirally rotated Schródinger functional with Wilson fermions and automatic O(a) improvement. *Nucl. Phys.*, B847:491–531, 2011. doi: 10.1016/j.nuclphysb.2011.02.002.

[27] C. Gattringer and C. B. Lang. Quantum chromodynamics on the lattice. *Lect. Notes Phys.*, 788:1–211, 2010. doi: 10.1007/978-3-642-01850-3.

[28] J. Gasser and H. Leutwyler. Chiral perturbation theory to one loop. *Ann. Phys.*, 158:142, 1984. doi: 10.1016/0003-4916(84)90242-2.

[29] H. B. Nielsen and M. Ninomiya. Absence of neutrinos on a lattice. 1. proof by homotopy theory. *Nucl. Phys.*, B185:20, 1981.

[30] H. B. Nielsen and M. Ninomiya. No go theorem for regularizing chiral fermions. *Phys. Lett.*, B105:219, 1981.

[31] H. B. Nielsen and M. Ninomiya. Absence of neutrinos on a lattice. 2. intuitive topological proof. *Nucl. Phys.*, B193:173, 1981.

[32] M. Lüscher. Exact chiral symmetry on the lattice and the ginsparg-wilson relation. *Phys. Lett.*, B428:342–345, 1998.

[33] P. H. Ginsparg and K. G. Wilson. A remnant of chiral symmetry on the lattice. *Phys. Rev.*, D25:2649, 1982.

[34] H. Neuberger. Exactly massless quarks on the lattice. *Phys. Lett.*, B417:141–144, 1998.

[35] H. Neuberger. More about exactly massless quarks on the lattice. *Phys. Lett.*, B427: 353–355, 1998.

[36] P. Hasenfratz. Prospects for perfect actions. *Nucl. Phys. Proc. Suppl.*, 63:53–58, 1998. doi: 10.1016/S0920-5632(97)00696-8.

[37] R. Sommer. A new way to set the energy scale in lattice gauge theories and its applications to the static force and alpha-s in su(2) yang-mills theory. *Nucl. Phys.*, B411:839–854, 1994.

[38] M. Guagnelli, R. Sommer, and H. Wittig. Precision computation of a low-energy reference scale in quenched lattice qcd. *Nucl. Phys.*, B535:389–402, 1998.

[39] S. Necco and R. Sommer. The $N_f = 0$ heavy quark potential from short to intermediate distances. *Nucl. Phys.*, B622:328–346, 2002. doi: 10.1016/S0550-3213(01)00582-X.

[40] F. Niedermayer. Exact chiral symmetry, topological charge and related topics. *Nucl. Phys. Proc. Suppl.*, 73:105–119, 1999. doi: 10.1016/S0920-5632(99)85011-7.

[41] M. Lüscher and P. Weisz. On-shell improved lattice gauge theories. *Commun. Math. Phys.*, 97:59, 1985.

[42] B. Sheikholeslami and R. Wohlert. Improved continuum limit lattice action for QCD with Wilson fermions. *Nucl. Phys.*, B259:572, 1985.

[43] P. Weisz. Continuum limit improved lattice action for pure yang-mills theory. 1. *Nucl. Phys.*, B212:1, 1983.

[44] M. Lüscher, S. Sint, R. Sommer, and P. Weisz. Chiral symmetry and O(a) improvement in lattice QCD. *Nucl. Phys.*, B478:365–400, 1996.

[45] R. Wohlert. Improved continuum limit lattice action for quarks. *DESY 87/069*, 1987.

[46] G. Heatlie, G. Martinelli, C. Pittori, G. C. Rossi, and C. T. Sachrajda. The improvement of hadronic matrix elements in lattice QCD. *Nucl. Phys.*, B352:266–288, 1991.

[47] M. Lüscher. Construction of a selfadjoint, strictly positive transfer matrix for euclidean lattice gauge theories. *Commun. Math. Phys.*, 54:283, 1977.

[48] K. Osterwalder and R. Schräder. Axioms for Euclidean Green's functions. *Commun. Math. Phys.*, 31:83–112, 1973.

[49] K. Osterwalder and R. Schräder. Axioms for Euclidean Green's functions. 2. *Commun. Math. Phys.*, 42:281, 1975.

[50] T. Reisz. A power counting theorem for feynman integrals on the lattice. *Commun. Math. Phys.*, 116:81, 1988.

[51] T. Reisz. A convergence theorem for lattice feynman integrals with massless propagators. *Commun. Math. Phys.*, 116:573, 1988.

[52] T. Reisz. Renormalization of feynman integrals on the lattice. *Commun. Math. Phys.*, 117:79, 1988.

[53] T. Reisz. Renormalization of lattice feynman integrals with massless propagators. *Commun. Math. Phys.*, 117:639, 1988.

[54] T. Reisz. Lattice gauge theory: renormalization to all orders in the loop expansion. *Nucl. Phys.*, B318:417, 1989.

[55] K. Jansen et al. Non-perturbative renormalization of lattice QCD at all scales. *Phys. Lett.*, B372:275–282, 1996. doi: 10.1016/0370-2693(96)00075-5.

[56] M. Lüscher, S. Sint, R. Sommer, and H. Wittig. Non-perturbative determination of the axial current normalization constant in O(a) improved lattice QCD. *Nucl. Phys.*, B491: 344–364, 1997. doi: 10.1016/S0550-3213(97)00087-4.

[57] S. Sint and P. Weisz. Further results on O(a) improved lattice QCD to one-loop order of perturbation theory. *Nucl. Phys.*, B502:251–268, 1997. doi: 10.1016/S0550-3213(97)00372-6.

[58] A. Shindler. Twisted mass lattice QCD. *Phys. Rept.*, 461:37–110, 2008. doi: 10.1016/j.physrep.2008.03.001.

[59] S. Sint. Lattice QCD with a chiral twist. Lectures given at Workshop on Perspectives in Lattice QCD, Nara, Japan, 31 Oct - 11 Nov 2005. *hep-lat/0702008*, 2007.

[60] R. Frezzotti, P. A. Grassi, S. Sint, and P. Weisz. Lattice QCD with a chirally twisted mass term. *JHEP*, 08:058, 2001.

[61] R. Frezzotti and G. C. Rossi. Twisted-mass lattice QCD with mass non-degenerate quarks. *Nucl. Phys. Proc. Suppl.*, 128:193–202, 2004.

[62] P. Dimopoulos, R. Frezzotti, C. Michael, G. C. Rossi, and C. Urbach. $O(a^2)$ cut-off effects in lattice Wilson fermion simulations. *Phys. Rev.*, D81:034509, 2010. doi: 10.1103/PhysRevD.81.034509.

[63] S. Aoki. New phase structure for lattice QCD with Wilson fermions. *Phys. Rev.*, D30: 2653, 1984.

[64] W. A. Bardeen, A. Duncan, E. Eichten, G. Hockney, and H. Thacker. Light quarks, zero modes, and exceptional configurations. *Phys. Rev.*, D57:1633–1641, 1998.

[65] W. A. Bardeen, A. Duncan, E. Eichten, and H. Thacker. Quenched chiral artifacts for Wilson-Dirac fermions. *Phys. Rev.*, D59:014507, 1999. doi: 10.1103/PhysRevD.59.014507.

[66] R. Frezzotti, P. A. Grassi, S. Sint, and P. Weisz. A local formulation of lattice QCD without unphysical fermion zero modes. *Nucl. Phys. Proc. Suppl.*, 83:941–946, 2000.

[67] R. Frezzotti, S. Sint, and P. Weisz. O(a) improved twisted mass lattice QCD. *JHEP*, 07: 048, 2001.

[68] R. Frezzotti, G. Martinelli, M. Papinutto, and G. C. Rossi. Reducing cutoff effects in maximally twisted lattice QCD close to the chiral limit. *JHEP*, 04:038, 2006.

[69] A. Shindler. Twisted mass lattice QCD: recent developments and results. *PoS*, LAT2005: 014, 2006.

[70] S. Aoki and O. Bär. Automatic $O(a)$-improvement for twisted-mass QCD in the presence of spontaneous symmetry breaking. *Phys. Rev.*, D74:034511, 2006.

[71] A. Bucarelli, F. Palombi, R. Petronzio, and A. Shindler. Moments of parton evolution probabilities on the lattice within the Schrödinger functional scheme. *Nucl. Phys.*, B552: 379–391, 1999. doi: 10.1016/S0550-3213(99)00176-5.

[72] A. Shindler et al. Non-perturbative renormalization of moments of parton distribution functions. *Nucl. Phys. Proc. Suppl.*, 129:278–280, 2004. doi: 10.1016/S0920-5632(03)02555-6.

[73] M. Guagnelli et al. Continuous external momenta in nonperturbative lattice simulations: A computation of renormalization factors. *Nucl. Phys.*, B664:276–298, 2003.

[74] M. Guagnelli et al. Non-perturbative pion matrix element of a twist-2 operator from the lattice. *Eur. Phys. J.*, C40:69–80, 2005.

[75] M. Bochicchio, L. Maiani, G. Martinelli, G. C. Rossi, and M. Testa. Chiral symmetry on the lattice with Wilson fermions. *Nucl. Phys.*, B262:331, 1985.

[76] F. Tekin, R. Sommer, and U. Wolff. The running coupling of QCD with four flavors. *Nucl. Phys.*, B840:114–128, 2010. doi: 10.1016/j.nuclphysb.2010.07.002.

[77] M. Della Morte et al. Non-perturbative quark mass renormalization in two-flavor QCD. *Nucl. Phys.*, B729:117–134, 2005. doi: 10.1016/j.nuclphysb.2005.09.028.

[78] R. Narayanan and U. Wolff. Two loop computation of a running coupling lattice Yang-Mills theory. *Nucl. Phys.*, B444:425–446, 1995. doi: 10.1016/0550-3213(95)00170-W.

[79] A. Bode. Two loop expansion of the Schrödinger functional coupling $\alpha_{\rm SF}$ in SU(3) lattice gauge theory. *Nucl. Phys. Proc. Suppl.*, 63:796–798, 1998. doi: 10.1016/S0920-5632(97)00903-1.

[80] G. de Divitiis et al. Universality and the approach to the continuum limit in lattice gauge theory. *Nucl. Phys.*, B437:447–470, 1995. doi: 10.1016/0550-3213(94)00019-B.

[81] R. Sommer. Non-perturbative renormalization of QCD. Talk given at the 36th Internationale Universitatswochen Für Kernphysik und Teilchenphysik, Schladming, Austria, 1-8 Mar 1997. *hep-ph/9711243*, 1997.

[82] M. Lüscher. The Schrödinger functional in lattice QCD with exact chiral symmetry. *JHEP*, 05:042, 2006.

[83] K. Symanzik. Schrödinger representation and casimir effect in renormalizable quantum field theory. *Nucl. Phys.*, B190:1, 1981. doi: 10.1016/0550-3213(81)90482-X.

[84] M. Lüscher. Schrödinger representation in quantum field theory. *Nucl. Phys.*, B254:52–57, 1985. doi: 10.1016/0550-3213(85)90210-X.

[85] A. Bode, U. Wolff, and P. Weisz. Two-loop computation of the Schrödinger functional in pure SU(3) lattice gauge theory. *Nucl. Phys.*, B540:491–499, 1999. doi: 10.1016/S0550-3213(98)00772-X.

[86] A. Bode, P. Weisz, and U. Wolff. Two loop computation of the Schrödinger functional in lattice QCD. *Nucl. Phys.*, B576:517–539, 2000. doi: 10.1016/S0550-3213(00)00187-5.

[87] M. Lüscher and P. Weisz. $O(a)$-improvement of the axial current in lattice QCD to one-loop order of perturbation theory. *Nucl. Phys.*, B479:429–458, 1996. doi: 10.1016/0550-3213(96)00448-8.

[88] M. Lüscher. Advanced lattice QCD. Talk given at Les Houches Summer School in Theoretical Physics, Session 68: Probing the Standard Model of Particle Interactions, Les Houches, France, 28 Jul - 5 Sep 1997. *hep-lat/9802029*, 1998.

[89] M. Lüscher and P. Weisz. Two loop relation between the bare lattice coupling and the MS coupling in pure SU(N) gauge theories. *Phys. Lett.*, B349:165–169, 1995. doi: 10.1016/0370-2693(95)00250-O.

[90] S. Capitani et al. Non-perturbative quark mass renormalization. *Nucl. Phys. Proc. Suppl.*, 63:153–158, 1998. doi: 10.1016/S0920-5632(97)00707-X.

[91] M. Lüscher, S. Sint, R. Sommer, P. Weisz, and U. Wolff. Non-perturbative O(a) improvement of lattice QCD. *Nucl. Phys.*, B491:323–343, 1997.

[92] B. Leder and S. Sint. Testing universality and automatic $O(a)$-improvement in massless lattice QCD with Wilson quarks. *PoS*, LATTICE2010:265, 2010.

[93] J. González López, K. Jansen, D. B. Renner, and A. Shindler. Chirally rotated Schrödinger functional: non-perturbative tuning in the quenched approximation. *PoS*, LAT2009:199, 2009.

[94] Y. Taniguchi. Schrödinger functional formalism with Ginsparg-Wilson fermion. *JHEP*, 12:037, 2005. doi: 10.1088/1126-6708/2005/12/037.

[95] M. Guagnelli, J. Heitger, C. Pena, S. Sint, and A. Vladikas. Non-perturbative renormalization of left-left four-fermion operators in quenched lattice QCD. *JHEP*, 03:088, 2006.

[96] M. Guagnelli, J. Heitger, F. Palombi, C. Pena, and A. Vladikas. The continuum limit of the quark mass step scaling function in quenched lattice QCD. *JHEP*, 05:001, 2004.

[97] S. Capitani, M. Lüscher, R. Sommer, and H. Wittig. Non-perturbative quark mass renormalization in quenched lattice QCD. *Nucl. Phys.*, B544:669–698, 1999. doi: 10.1016/S0550-3213(98)00857-8.

[98] M. Lüscher et al. Some new results in $O(a)$-improved lattice QCD. *Nucl. Phys. Proc. Suppl.*, 53:905–913, 1997. doi: 10.1016/S0920-5632(96)00815-8.

[99] J. Garden, J. Heitger, R. Sommer, and H. Wittig. Precision computation of the strange quark's mass in quenched QCD. *Nucl. Phys.*, B571:237–256, 2000.

[100] J. Gasser and H. Leutwyler. Quark masses. *Phys. Rept.*, 87:77–169, 1982.

[101] H. Leutwyler. Principles of chiral perturbation theory. Lectures given at the Hadrons 94 Workshop, Gramado, Brazil, 10-14 Apr 1994. *hep-ph/9406283*, 1994.

[102] H. Leutwyler. The ratios of the light quark masses. *Phys. Lett.*, B378:313–318, 1996. doi: 10.1016/0370-2693(96)00386-3.

[103] K. Jansen, M. Papinutto, A. Shindler, C. Urbach, and I. Wetzorke. Quenched scaling of Wilson twisted mass fermions. *JHEP*, 09:071, 2005.

[104] K. G. Wilson. On products of quantum field operators at short distances. *Unpublished*, 1964.

[105] K. G. Wilson. Nonlagrangian models of current algebra. *Phys. Rev.*, 179:1499–1512, 1969. doi: 10.1103/PhysRev.179.1499.

[106] W. Zimmermann. Normal products and the short distance expansion in the perturbation theory of renormalizable interactions. *Ann. Phys.*, 77:570–601, 1973. doi: 10.1016/0003-4916(73)90430-2.

[107] T. Muta. Foundations of quantum chromodynamics. Second edition. *World Sci. Lect. Notes Phys.*, 57:1–409, 1998.

[108] S. Capitani et al. Parton distribution functions with twisted mass fermions. *Phys. Lett.*, B639:520–526, 2006. doi: 10.1016/j.physletb.2006.02.047.

[109] M. Lüscher. A semiclassical formula for the topological susceptibility in a finite space-time volume. *Nucl. Phys.*, B205:483, 1982. doi: 10.1016/0550-3213(82)90371-6.

[110] M. Della Morte et al. Computation of the strong coupling in QCD with two dynamical flavors. *Nucl. Phys.*, B713:378–406, 2005.

[111] K. Jansen and C. Urbach. tmLQCD: a program suite to simulate Wilson twisted mass lattice QCD. *Comput. Phys. Commun.*, 180:2717–2738, 2009. doi: 10.1016/j.cpc.2009.05.016.

[112] S. Duane, A. D. Kennedy, B. J. Pendleton, and D. Roweth. Hybrid Monte Carlo. *Phys. Lett.*, B195:216–222, 1987.

[113] P. Di Vecchia, K. Fabricius, G. C. Rossi, and G. Veneziano. Numerical checks of the lattice definition independence of topological charge fluctuations. *Phys. Lett.*, B108:323, 1982. doi: 10.1016/0370-2693(82)91203-5.

[114] M. Teper. The mass gap, the confining string and the physics of (lattice) topology. *Invited talk given at Conf. on Quark Confinement and Liberation, Berkeley, CA, May 22-24, 1985*, 1985.

[115] M. Teper. Instantons in the quantized SU(2) vacuum: a lattice Monte Carlo investigation. *Phys. Lett.*, B162:357, 1985. doi: 10.1016/0370-2693(85)90939-6.

[116] M. Teper. The topological susceptibility in SU(2) lattice gauge theory: an exploratory study. *Phys. Lett.*, B171:86, 1986. doi: 10.1016/0370-2693(86)91004-X.

[117] M. Teper. Large instantons in a lattice gauge theory and their stability under 'cooling'. *OXFORD-TP-59/88*, 1988.

[118] N. Cabibbo and E. Marinari. A new method for updating SU(N) matrices in computer simulations of gauge theories. *Phys. Lett.*, B119:387–390, 1982. doi: 10.1016/0370-2693(82)90696-7.

[119] A. A. Belavin, A. M. Polyakov, A. S. Schwartz, and Y. S. Tyupkin. Pseudoparticle solutions of the Yang-Mills equations. *Phys. Lett.*, B59:85–87, 1975. doi: 10.1016/0370-2693(75)90163-X.

[120] J. Heitger, H. Simma, R. Sommer, and U. Wolff. The Schrödinger functional coupling in quenched QCD at low energies. *Nucl. Phys. Proc. Suppl.*, 106:859–861, 2002. doi: 10.1016/S0920-5632(01)01867-9.

Selbständigkeitserklärung

Ich erkläre, dass ich die vorliegende Arbeit selbständig und nur unter Verwendung der angegebenen Literatur und Hilfsmittel angefertigt habe.

Berlin, den 25.03.2011 Jenifer González López